Mathematical Analysis of Boundary Integral Equations and Domain Decomposition Methods with Applications in Polarisable Electrostatics

Von der Fakultät für Mathematik, Informatik und Naturwissenschaften der RWTH Aachen University zur Erlangung des akademischen Grades eines Doktors der Naturwissenschaften genehmigte Dissertation

vorgelegt von

Muhammad Hassan, M.Sc.

aus Peshawar, Pakistan

Berichter: Prof. Dr. Eric Cancès
Prof. Dr. Ralf Hiptmair
Prof. Dr. Benjamin Stamm

Tag der mündlichen Prüfung: 15.06.2020

To the human spirit exemplified by my hero Noam Avram Chomsky and the selfless courage of the countless participants of emancipatory movements who continue to believe that a better world is possible.

Acknowledgements

This dissertation represents work accomplished in bursts of creative energy interspersed with long periods of procrastination, self-loathing, and existential despair (in that precise order). I think I can safely claim credit for all the time I spent ruminating on the meaninglessness of existence and similarly cheery avenues of thought (although repeat watches of Bojack Horseman certainly did help) but the dissertation itself would not have been possible without the efforts of several people, some of whom I simply have to mention.

I'm immensely grateful to my supervisor, Benjamin, for everything he has taught me, for always having time for a discussion, for his patience in answering questions (some of which were so idiotic, they make me wish I had access to the Neuralyzer from Men in Black), and for making my Ph.D. a wonderful experience. Every dissertation acknowledgement I've ever read makes it a point to thank the supervisor, which is strange since the law of large numbers would suggest that at least *some* of these supervisors must be doing a bad job, but I really do have to say that without Benjamin's advice, suggestions and help, this document would be suitable only as kindling. *Merci vielmal Ben!*

Additionally, I wish to acknowledge two people who've had an enormous influence on my growth as a mathematician: Arnulf Jentzen, who taught me the value of rigour and precision when it comes to writing formally correct mathematics, and Xavier Claeys who gave me a wonderful introduction to functional analysis for PDEs and boundary integral equations, who hosted me in Paris and who has always been exceedingly generous in sharing his expertise and time with me. Furthermore, I would like to thank Yvon Maday for taking an interest in my work, for sharing his immense experience, and for very generously hosting me at UPMC. Thanks are also due to Gabriele Ciaramella for inviting me several times to Konstanz, which has resulted in a fruitful collaboration, to Bérenger Bramas for his help on adapting the ScalFMM library, to Julien Toulouse for organising (twice!) the GDR CORREL workshops and inviting me to attend, and to David Gontier and Michael Herbst for many useful comments. Finally, I wish to thank Eric Cancès and Ralf Hiptmair for very kindly agreeing to review my dissertation.

On a personal level, I wish to thank my friends and family who, despite my eccentricities and general self-centredness, have been a wonderful source of support. To shamelessly plagiarize Wes Anderson, they remind me that "there are still faint glimmers of civilization left in this barbaric slaughterhouse that was once known as humanity". Finally, I would be remiss if I didn't mention my parents. It takes a special kind of courage for a middle-class family in the third world to encourage their son to study *mathematics*, and I'll always be grateful for their support.

Zusammenfassung

Diese Dissertation befasst sich in erster Linie mit der Analyse von mathematischen Modellen, die bei der Untersuchung der polarisierbaren Elektrostatik entstehen, entweder im Zusammenhang mit dielektrischen Teilchen, die sich gegenseitig polarisieren, oder mit impliziten Solvationsmodellen in der theoretischen Chemie. Das Hauptziel unserer Arbeit ist es zu verstehen, wie die Genauigkeit und der Rechenaufwand der numerischen Methoden, die zur Lösung der leitenden Gleichungen in beiden Fällen verwendet werden, mit der Anzahl der Objekte im Problem skalieren. Um den Leser zu unterstützen, haben wir die Dissertation in drei weitgehend unabhängige Teile gegliedert:

Im ersten Teil dieser Dissertation (Kapitel $2-5$) analysieren wir eine Randintegralgleichung, die die elektrostatische Wechselwirkung zwischen N dielektrischen kugelförmigen Teilchen modelliert, die sich gegenseitig polarisieren. Unser Hauptergebnis ist der Nachweis, dass unter geeigneten geometrischen Annahmen die drei wichtigsten Größen, die für dieses Problem von Interesse sind, nämlich die induzierte Oberflächenladung auf jedem Teilchen, die gesamte elektrostatische Energie des Systems und die auf jedes Teilchen wirkenden elektrostatischen Kräfte, mit linearer Skalierung in der Genauigkeit berechnet werden können, d.h. es sind nur $\mathcal{O}(N)$ Operationen erforderlich, um Näherungen dieser Größen mit einem gegebenen und festen relativen Fehler zu berechnen.

Im zweiten Teil dieser Dissertation (Kapitel $6-8$) führen wir eine Skalierbarkeitsanalyse der parallelen Schwarz-Methode durch, die zur Lösung des impliziten Solvationsmodells von COSMO für das Reaktionspotential verwendet wird, das von einem gelösten Molekül mit einer gegebenen Ladungsverteilung, das in ein polarisierbares Medium eingebettet ist, erzeugt wird. Unser Hauptergebnis ist die Konstruktion eines neuen, systematischen Rahmens, der es uns erlaubt, die Norm des Schwarz-Operators für Gebiete zu charakterisieren, die gelöste Moleküle repräsentieren, in denen mehrere Atome eine gemeinsame Überlappung haben und Atome vollständig im Inneren des Moleküls ohne Zugang zum äußeren Medium eingebettet sein können.

Der dritte Teil dieser Dissertation (Kapitel 9) stellt eine Abkehr von den Themen der polarisierbaren Elektrostatik und der Skalierbarkeitsanalyse dar, die sich auf die Teile I und II beziehen, aber sowohl mit den Integraloperatoren als auch mit der Gebietszerlegung in einem allgemeinen Sinn verbunden sind. Unser Hauptergebnis ist hier die Etablierung einer fundamentalen Kontinuitätseigenschaft für Riesz-Potentiale auf polygonalen Rändern in zwei räumlichen Dimensionen. Als schwach singuläre Integraloperatoren können Riesz-Potentiale verwendet werden, um exponentiell konvergente, nicht überlappende Gebietszerlegungsmethoden für die Helmholtz-Gleichung zu konstruieren, und unser Ergebnis füllt eine Lücke in der Analyse solcher Methoden.

Abstract

This dissertation is primarily concerned with the analysis of mathematical models that arise in the study of polarisable electrostatics, either in the context of dielectric particles undergoing mutual polarisation or implicit solvation modelling in theoretical chemistry. The main objective of our work is to understand how the accuracy and computational cost of the numerical methods used to solve the governing equations in both cases scale with the number of objects in the problem. To aid the reader, we have divided the dissertation into three broadly independent parts:

In the first part of this dissertation (Chapters 2-5), we analyse a boundary integral equation that models the electrostatic interaction between N dielectric spherical particles undergoing mutual polarisation. Our main result is to prove that under appropriate geometrical assumptions, the three key quantities of interest in this problem, namely, the induced surface charge on each particle, the total electrostatic energy of system, and the electrostatic forces acting on each particle can be computed with linear scaling in accuracy, i.e., it requires only $\mathcal{O}(N)$ operations to compute approximations of these quantities with a given and fixed relative error.

In the second part of this dissertation (Chapters 6-8), we perform a scalability analysis of the parallel Schwarz method which is used to solve the COSMO implicit solvation model for the reaction potential generated by a solute molecule with a given charge distribution embedded in a polarisable medium. Our main result is to construct a new, systematic framework that allows us to characterise the norm of the Schwarz operator for domains representing solute molecules in which multiple atoms have a common overlap and atoms can be completely buried in the interior of the molecule with no access to the external medium.

The third part of this dissertation (Chapter 9) is a departure from the themes of polarisable electrostatics and scalability analysis that relate Parts I and II but is connected to both integral operators and domain decomposition in a general sense. Our main result here is to establish a fundamental continuity property for Riesz potentials on polygonal boundaries in two spatial dimensions. As weakly singular integral operators, Riesz potentials can be used to construct exponentially convergent, non-overlapping domain decomposition methods for the Helmholtz equation, and our result fills a gap in the analysis of such methods.

Contents

1

General Introduction

1.1 Overview

Many problems in the natural sciences involve the solution of equations posed on domains that can be viewed as the unions of a large number of simple subdomains (see Figures 1.1 and 1.2). From this viewpoint, a natural solution strategy consists of solving 'local' problems on each of these subdomains and then recovering the global solution by means of appropriate coupling conditions which link the solutions on different subdomains. For the numerical analyst, this 'divide and conquer' approach raises an obvious question, namely, how do such algorithms behave when applied to systems composed of an increasingly larger number of subdomains? More precisely, we can ask

1. If the number of degrees of freedom per subdomain is fixed, how does the *accuracy* of a given numerical method change as the number N of subdomains increases?
2. If the number of degrees of freedom per subdomain is fixed, how does the *computational cost* of solving the full, global problem grow as the number N of subdomains increases?

This dissertation is, largely, an attempt to answer these questions for two different numerical methods that are used to solve two different physical problems. In the first part of the dissertation (Chapters 2-5), we consider a boundary integral equation (BIE) that is used to model the electrostatic interaction between charged dielectric particles undergoing mutual polarisation. In this situation, the subdomains are disjoint spheres with each sphere representing a particular dielectric particle, and the global domain is simply the union of these subdomains. In the second part of this thesis (Chapters 6-8), we study the so-called parallel Schwarz domain decomposition method which is used to solve for the electrostatic interaction between a solute molecule and the surrounding solvent as approximated by the COSMO solvation model. Here, each subdomain is an open ball representing a given atomic cavity whereas the global domain, which represents the molecular cavity, is the union of such overlapping spherical subdomains. The third part of this dissertation (Chapter 9) is a departure from these themes of scalability and contains a mathematical result that is of importance in domain decomposition methods for the wave (Helmholtz) equation.

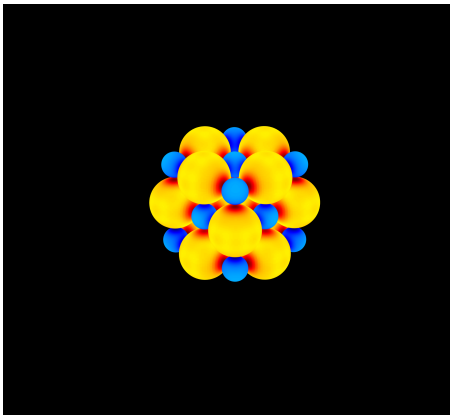

(a) Unit Cell of a lattice structure with $N = 27$ particles.

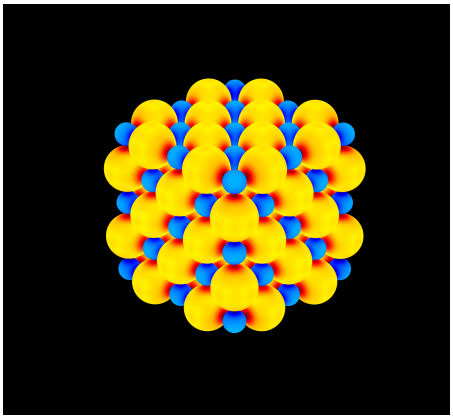

(b) Unit cell of a lattice structure with $N = 125$ particles.

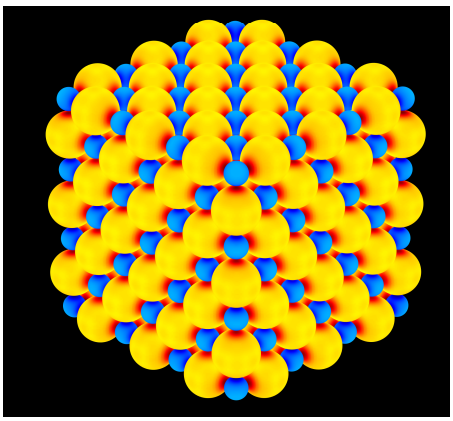

(c) Unit cell of a lattice structure with $N = 343$ particles.

Figure 1.1: Lattice structures composed of charged dielectric spherical particles. Practitioners are, for instance, interested in computing the surface charge on each particle.

It is important to emphasise that the scalability analysis we present in this dissertation involves geometrical settings wherein the degrees of freedom per subdomain are typically fixed, and it is the number of subdomains that grows. These situations arise precisely when we consider systems consisting of an increasing number of dielectric particles (see Figure 1.1), or solute molecules composed of an increasing number of atoms (see Figure 1.2). This is to be contrasted with the usual setting of, for instance, finite element analysis, where the computational domain is fixed and it is the number of degrees of freedom that increases. Although these two settings may appear superficially similar, in the sense that both involve problems with an increasing number of *total* degrees of freedom, the behaviour of the underlying numerical methods need not be the same.

Outline of this Dissertation

The remainder of Chapter 1 is organised as follows: A large part of this dissertation concerns mathematical models that arise in the study of polarisable electrostatics, either in the context of dielectric particles undergoing mutual polarisation or implicit solvation

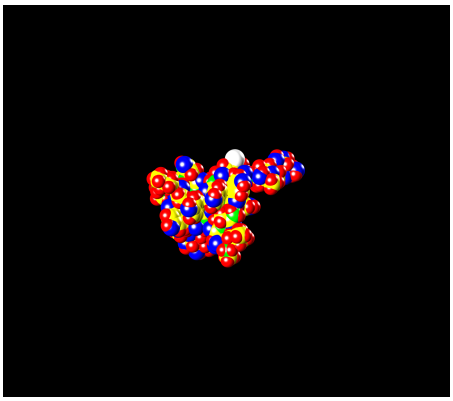

(a) A molecule of the antibiotic Vancomycin composed of $N = 377$ atoms.

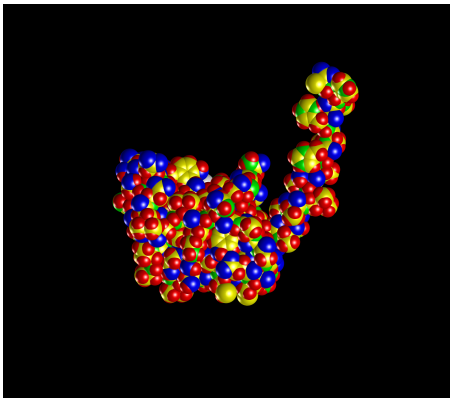

(b) The redox enzyme Glutaredoxin composed of $N = 1277$ atoms.

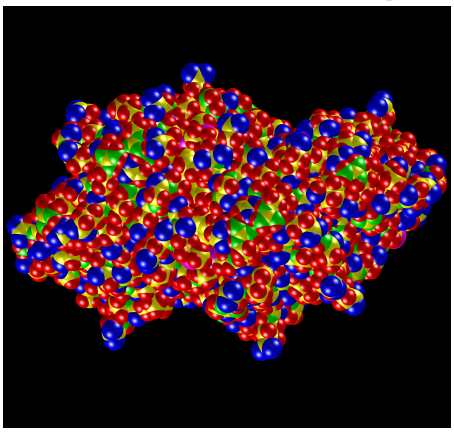

(c) A molecule of the enzyme Pyruvate carboxylase composed of $N = 6609$ atoms.

Figure 1.2: Atomic structures of three increasingly large biological molecules. The molecules are represented as unions of intersecting spherical cavities with each cavity corresponding to one atom. A common problem in chemical physics is to compute the electric potential on the surface of the molecular cavity in the presence of a polarisable solvent.

modelling in theoretical chemistry. Consequently, we present in Section 1.2 a semi-formal introduction to electrostatics in dielectric media. Subsequently, in Section 1.3 we recall some key tools from the theory of partial differential equations and establish standard notation that will be used throughout this dissertation. Finally, in Section 1.4, we provide a concise, self-contained introduction to boundary integral operators which, as we shall see, are natural tools to study the types of electrostatics problems we consider in this work.

To aid the reader, we have divided the main content of the dissertation into three broadly independent parts, the first (Chapters 2-5) dealing with the boundary integral equation formalism for polarisable electrostatics, the second (Chapters 6-8) concerning the parallel Schwarz domain decomposition method for implicit solvation modelling, and the third (Chapter 9) pertaining to properties of a certain boundary integral operator that has applications in non-overlapping domain decomposition methods for the Helmholtz

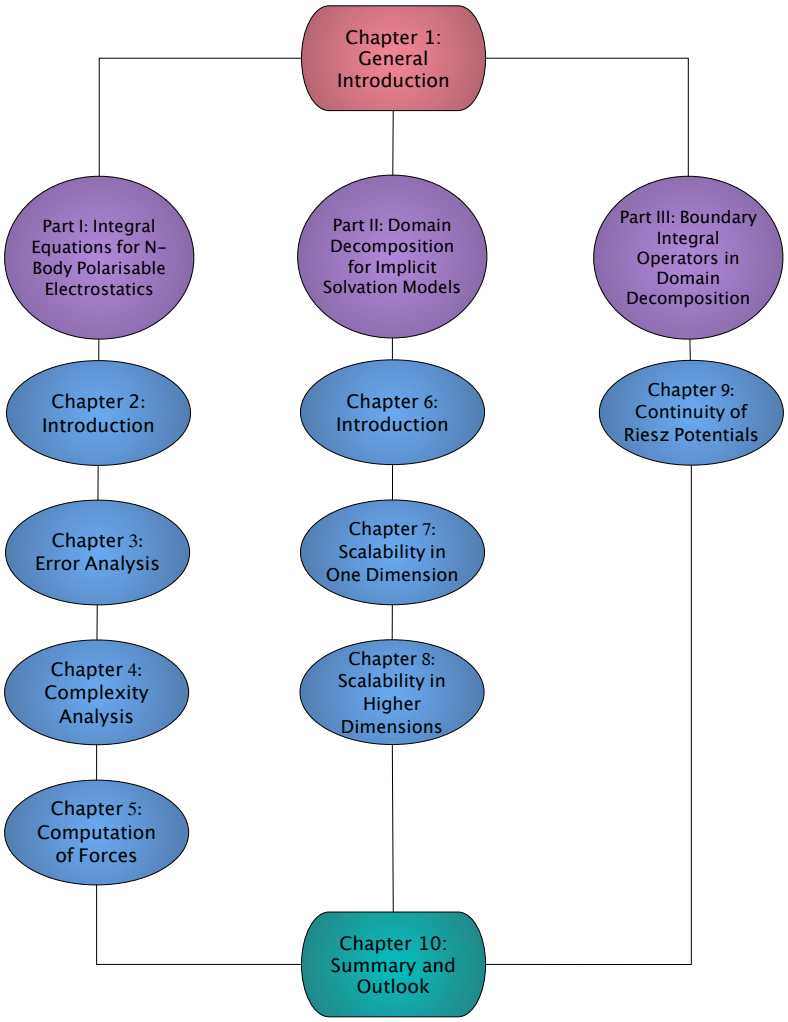

Figure 1.3: Organisation of this dissertation.

equation. Finally, Chapter 10 contains an outlook and summary of the dissertation. A schematic presentation of the dissertation organisation is given in Figure 1.3.

Chapter 2 serves as an in-depth introduction to Part I of this dissertation. We first state the so-called abstract dielectric spheres electrostatic interaction problem as a PDE-based transmission problem in the entire space $\mathbb{R}^3$. Next, we use the integral equation formalism stated in Section 1.4 to reformulate this PDE-based transmission problem as a so-called boundary integral equation of the second kind posed on the boundaries of the N dielectric spherical particles. Finally, we give an overview of the state-of-the-art for such integral equation formulations.

In Chapter 3, we develop a new a priori error analysis that demonstrates N-independent stability of the continuous and discrete formulations of the boundary integral equation introduced in Chapter 2. In particular, we obtain convergence rates for the induced surface charge on these particles and the total electrostatic energy that do

not explicitly depend on N. This allows us to deduce N-independent error estimates for these two quantities of interest under appropriate geometrical assumptions.

In Chapter 4, we provide a convergence analysis of the iterative method used to solve the linear system associated with the Galerkin discretisation of the underlying BIE, and we show that the number of liner solver iterations required to obtain an approximate solution is independent of N. In conjunction with the fast multipole method (FMM), this allows us to present two linear scaling (in N) solution strategies for the computation of the approximate induced surface charges and electrostatic energy. Finally, we consider a series of numerical experiments designed to validate our theoretical results and explore the dependence of the numerical errors and computational cost of solving the underlying linear system on different system parameters.

In Chapter 5, using the preceding analysis, we propose a linear scaling (in N) algorithm for the computation of the approximate electrostatic forces between these N dielectric particles. We establish exponential convergence of the approximate forces and derive error estimates for the approximate forces that, again, do not explicitly depend on the number of dielectric particles N. We deduce therefore that under appropriate geometrical assumptions, our proposed method requires only $\mathcal{O}(N)$ operations to compute the electrostatic forces acting on N dielectric particles up to any given and fixed average error. This chapter concludes the first part of the dissertation.

Chapter 6 serves as an in-depth introduction to Part II of this dissertation. We begin with an introduction to the phenomenon of implicit solvation and the so-called COnductor-like Screening MOdel (COSMO). Next, we provide an overview of the classical parallel Schwarz method (PSM) with a particular emphasis on its use to solve the COSMO equations, an algorithm which is known in this context as ddCOSMO. Once again, we provide an overview of the state-of-the-art in the scalability analysis of this class of domain decomposition methods.

In Chapter 7, we consider as a first step, the parallel Schwarz method applied to the one-dimensional Laplace equation. Although heuristic explanations indicate that the PSM applied to the Laplace equation in one dimension does not scale with the number of subintervals in the domain decomposition, a systematic analysis is still missing in the literature. We provide a rigorous result that precisely quantifies the lack of scalability of the PSM in such cases. The key novelty of our analysis technique is that it suggests a possible roadmap for a systematic extension to more realistic problems in higher dimensions.

Subsequently, in Chapter 8, we analyse the convergence behaviour and scalability properties of the PSM for higher dimensional domain decomposition problems in which many subdomains may be completely embedded in the interior of the global domain and an arbitrary number of subdomains may have a common overlap. Extending the ideas of Chapter 7, we develop a new systematic framework that allows us to bound the norm of the Schwarz iteration operator for such geometrical configurations. We provide numerical experiments that support our main results, and we consider concrete biological molecules that have been studied in solvation models in computational chemistry and understand the consequences of our analysis as it pertains to these complex bio-molecules. This

chapter concludes the second part of this dissertation.

Chapter 9 is a departure from the broad theme of scalability that links Parts I and II of this dissertation but is related, in a general sense, to both the study of boundary integral operators and domain decomposition methods. Here, we introduce the so-called Riesz potential in two dimensions and establish some continuity properties of this integral operator on polygonal boundaries $\partial\Omega$. More specifically, we prove that the Riesz potential extends as a bounded linear map from $L^2(\partial\Omega)$ to $H^{\frac{1}{2}}(\partial\Omega)$. This result has applications in the analysis of non-overlapping domain decomposition methods for the Helmholtz equation on polygonal subdomains.

1.2 Electrostatics in Dielectric Media

The aim of this section is to present a brief discussion of the phenomenon of electrostatics in dielectric materials with the goal of understanding how to model the electrostatic potential generated by a charged dielectric object embedded in a polarisable medium. We emphasise that our aim is not a rigorous, axiomatic derivation of the underlying partial differential equation (PDE), rather we simply wish to provide some basic physical background for how such a PDE can be derived. We will assume throughout this section that the reader is familiar with basic vector calculus.

Classical electromagnetism consists of the study of electric and magnetic fields generated by electrical charges under non-relativistic settings, at length scales and field intensities where quantum mechanical effects are not felt. The equations of classical electromagnetism were first arrived at, in their complete form, by the great 19$^{\text{th}}$ century physicist James Clerk Maxwell in his treatise [144]. Using these equations, Maxwell was able to deduce that ordinary light was simply a manifestation of electromagnetic fields, a discovery that has been called the second great unification in Physics [157] (after Newton's unification of celestial and terrestrial mechanics).

Title	Equation
Gauss' Law	$\nabla \cdot \boldsymbol{E} = \frac{\rho}{\boldsymbol{\epsilon_0}}$
Gauss' Law for Magnetism	$\nabla \cdot \boldsymbol{B} = 0$
Maxwell-Faraday Equation	$\nabla \times \boldsymbol{E} = -\frac{\partial \boldsymbol{B}}{\partial t}$
Ampère's Law (with Correction)	$\nabla \times \boldsymbol{B} = \boldsymbol{\mu_0}(\boldsymbol{J} + \boldsymbol{\epsilon_0}\frac{\partial \boldsymbol{E}}{\partial t})$

Table 1.1: The differential form of Maxwell's equations in SI units. Here, $\boldsymbol{E}$ and $\boldsymbol{B}$ denote the electric and magnetic fields respectively, ρ is the electric charge density, $\boldsymbol{\epsilon_0}$ and $\boldsymbol{\mu_0}$ are physical constants and denote the so-called permittivity and permeability of free space respectively, and $\boldsymbol{J}$ is the electric current density.

In this dissertation, we are concerned with the phenomenon of electrostatics, i.e., the behaviour of the electric field when the electric charges either do not move or do so sufficiently slowly so that the induced magnetic field may be considered negligible. In

this situation, we obtain the stationary form of Maxwell's equations:

$$\begin{aligned} \nabla \cdot \boldsymbol{E} &= \frac{\rho}{\boldsymbol{\epsilon_0}} \\ \nabla \times \boldsymbol{E} &= 0. \end{aligned} \tag{1.1}$$

The study of Equation (1.1) amounts to the mathematical analysis of a curl-free vector field $\boldsymbol{E}$ with a given divergence, which is a prototypical example of a problem in vector calculus. Indeed, if the charge density ρ is *known*, then (under assumptions of sufficient regularity) one may apply the Helmholtz decomposition theorem from vector calculus (in physics terminology: use the fact that the electric field is *conservative*) to deduce the existence of a scalar potential field Φ, known as the electric potential, such that $\boldsymbol{E} = -\nabla\Phi$. Equation (1.1) then reduces to the standard Poisson problem

$$-\Delta\Phi = \frac{\rho}{\boldsymbol{\epsilon_0}}, \tag{1.2}$$

which can be uniquely solved by supplying appropriate auxiliary conditions (such as boundary or decay conditions).

Obviously, the above calculations do not tell the entire story. Indeed, the biggest difficulty lies in the fact that in most physical problems, the charge density ρ is *not known a priori* (or at least not *fully* known a priori). This problem is illustrated very well if one studies electrostatics in dielectric media.

Maxwell's equations in dielectric media

The following discussion is taken from the Feynman lecture notes on physics [66, Chapter 10]. Let us consider a parallel-plate capacitor with some charges on the surfaces of the conductors as shown in Figure 1.4. Without loss of generality, we assume that the top plate of the capacitor carries a negative charge $-Q$ and the bottom plate carries a positive charge Q, and we further assume that the area of each plate is $A > 0$. Our goal now is to determine the electric field in the interior of this capacitor, i.e., inside the insulating dielectric material that fills the spacing of the plates.

Since the material filling the capacitor is assumed to be insulating, one might initially be tempted to conclude that there are no (net) additional charges on this material, and therefore Maxwell's equations (1.1) should hold with right hand side determined purely by the charge Q. Pursuing this line of reasoning yields that the electric field $\boldsymbol{E}$ inside the capacitor has constant magnitude $|\boldsymbol{E}| = \frac{Q}{\boldsymbol{\epsilon_0} A}$ and points from the bottom to the top plate. One of the seminal discoveries of the English scientist Michael Faraday was that this is not precisely the case, and the following reasoning explains why.

Consider an arbitrary atom composing the dielectric material. In a semi-classical physical model, the atom consists of a positively charged nucleus surrounded by an electron cloud. Under the influence of the electric field $\boldsymbol{E}$ generated by the charge Q on the capacitor plates, the electron cloud will be displaced relative to the nucleus, in a direction that is anti-parallel to the electric field, and therefore, from a distance, the

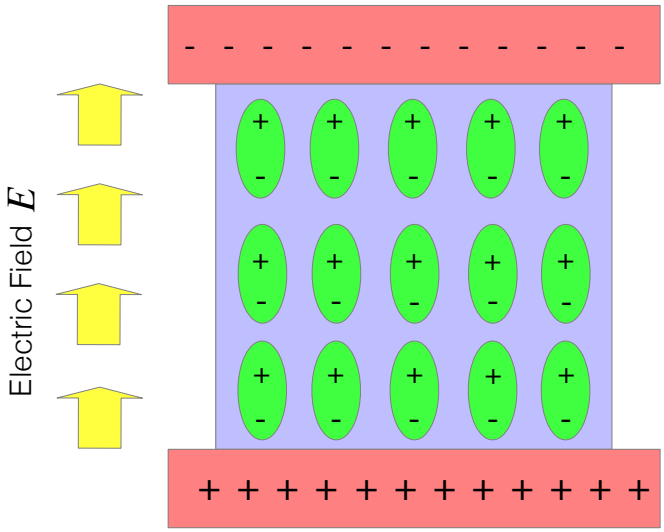

Figure 1.4: A visual representation of a parallel-plate capacitor. At the top and bottom (in red) are the conducting plates of the capacitor carrying charge $\pm Q$. This charge on the conducting plates results in an electric field $\boldsymbol{E}$. The insulating dielectric material inside the capacitor is shown in blue. As we shall see, the electric field $\boldsymbol{E}$ produces tiny dipoles (shown in green) in the dielectric medium.

formally neutral atom appears as a dipole to first approximation. A visual representation of the situation is given in Figure 1.5.

The question we now face is how to describe the resulting dipole moment of the dielectric material. Let $\boldsymbol{P}$ denote the so-called polarisation vector, i.e., the dipole moment per unit volume. Under the assumption that each nucleus carries a charge q and the relative displacement of the electron cloud is $\boldsymbol{\delta}$, we obtain that

$$\boldsymbol{P} = Nq\boldsymbol{\delta},$$

where N is the number of atoms per unit volume. Of course, this construction tells us nothing about how the polarisation vector $\boldsymbol{P}$ relates to $\boldsymbol{E}$, i.e., the *net* electric field generated by the charge Q on the capacitor plates. It seems reasonable to assume however that the relative displacement of the electron cloud at every point of the dielectric medium should be proportional to $\boldsymbol{E}$, and consequently we can write

$$\boldsymbol{P} = \chi \boldsymbol{\epsilon_0} \boldsymbol{E}, \tag{1.3}$$

where χ is a proportionality constant that depends on the material properties of the dielectric and is known in the physics literature as the electric susceptibility.

The next task is to determine the so-called *bound* charge density ρ_{bound} inside the dielectric material. This is precisely the charge density that creates the polarisation vector $\boldsymbol{P}$. To this end, we consider an arbitrary closed surface Σ of unit volume in the interior of the dielectric. In the absence of any polarisation effects, the net charge Q_Σ enclosed by Σ is zero. The polarisation mechanism described above however implies that

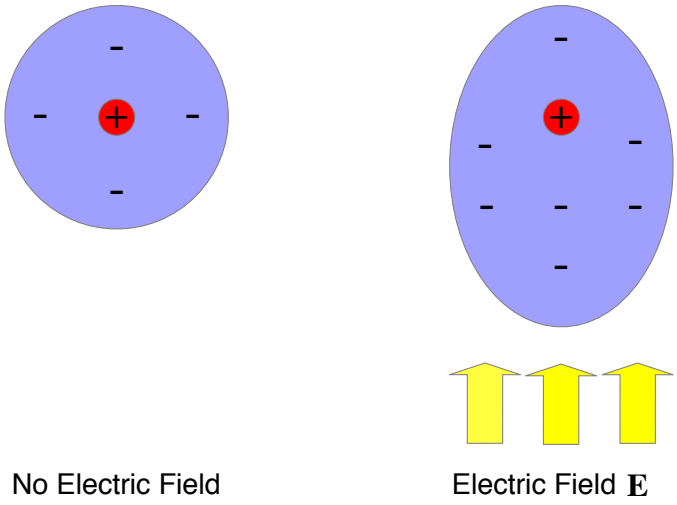

Figure 1.5: A semi-classical model of an atom consisting of a positively charged nucleus (in red) surrounded by a negatively charged electron cloud (in blue). In the presence of an electric field $\boldsymbol{E}$, the position of the electron cloud is displaced relative to the position of the nucleus.

a charge $(Nq\boldsymbol{\delta}) \cdot \boldsymbol{\eta} dA$ is displaced across any infinitesimal surface element dA of Σ. Thus, the net charge enclosed by Σ is given as the surface integral

$$Q_\Sigma = -\oint_\Sigma (Nq\boldsymbol{\delta}) \cdot \boldsymbol{\eta} dA = -\oint_\Sigma \boldsymbol{P} \cdot \boldsymbol{\eta} dA,$$

from which we conclude, using the divergence theorem, that the bound charge density is given by

$$\rho_{\text{bound}} := -\nabla \cdot \boldsymbol{P}.$$

Let us now consider Maxwell's equations (1.1) as they apply to this dielectric material. We have the pair of equations

$$\nabla \cdot \boldsymbol{E} = \frac{\rho}{\boldsymbol{\epsilon_0}} \qquad \text{and} \qquad \nabla \times \boldsymbol{E} = 0,$$

where ρ denotes the *net* charge density and $\boldsymbol{E}$ denotes the *net* electric field. Let us focus on the first equation. For simplicity, we may write $\rho = \rho_{\text{bound}} + \rho_{\text{free}}$ where ρ_{bound} is the bound charge density and ρ_{free} is the so-called free-charge density defined as $\rho_{\text{free}} := \rho - \rho_{\text{bound}}$. Intuitively, we may consider ρ_{free} as the charge density in the absence of polarisation effects. Using the above computations, we conclude that

$$\nabla \cdot \boldsymbol{E} = \frac{\rho_{\text{bound}} + \rho_{\text{free}}}{\boldsymbol{\epsilon_0}} = \frac{-\nabla \cdot \boldsymbol{P} + \rho_{\text{free}}}{\boldsymbol{\epsilon_0}},$$

which yields

$$\nabla \cdot \left(\boldsymbol{E} + \frac{\boldsymbol{P}}{\boldsymbol{\epsilon_0}} \right) = \frac{\rho_{\text{free}}}{\boldsymbol{\epsilon_0}}.$$

Using Equation (1.3) and introducing the constant $\kappa = 1 + \chi$, which is known in the physics literature as the *relative permittivity*, we finally obtain Maxwell's equations in a dielectric medium:

$$\nabla \cdot (\kappa \boldsymbol{E}) = \frac{\rho_{\text{free}}}{\boldsymbol{\epsilon_0}} \qquad \text{and} \qquad \nabla \times \boldsymbol{E} = 0. \tag{1.4}$$

Several remarks are now in order:

- We recall that the main assumption used to derive Equations (1.4) was the proportionality of the polarisation vector and the electric field, i.e, $\boldsymbol{P} = \chi \boldsymbol{\epsilon_0} \boldsymbol{E}$ with a spatially independent constant χ. Materials that obey this property are known as linear, homogeneous, isotropic dielectrics.
- Equations (1.4) do not explicitly contain the bound charge density ρ_{bound} and are formulated purely in terms of the free-charge ρ_{free}. In many physical problems, ρ_{free} can be taken as a known quantity.
- Using once again the Helmholtz decomposition, we can write Equations (1.4) as a single generalised Poisson equation for the electrostatic potential Φ:

$$-\nabla \cdot \big(\kappa \nabla \Phi\big) = \frac{\rho_{\text{free}}}{\boldsymbol{\epsilon_0}}. \tag{1.5}$$

  We remark here that in the case of linear, homogeneous, isotropic dielectrics, the factor κ is simply a constant so Equation (1.5) reduces to a simple Poisson problem. This is to be contrasted with the case of non-homogenous dielectrics in which κ is a spatially dependent function.
- The phenomenon we have described here is known as dielectric polarisation. In many physical situations, there can be other sources of polarisation as well.

Interface conditions at the boundary of dielectric media

The discussion thus far has been limited to the behaviour of the electric field in the interior of a dielectric medium which led us to Equations (1.4) or the equivalent generalised Poisson problem given by Equation (1.5). We now study what happens at the interface of a dielectric medium. To this end, we consider a bounded object Ω^- composed of a dielectric material with relative permittivity κ_-, embedded in a different dielectric medium, denoted $\Omega^+ := \mathbb{R}^3 \setminus \overline{\Omega^-}$, with relative permittivity κ_+. We assume that the boundary $\partial\Omega$ of the object Ω^- carries a so-called free surface charge density σ_f, i.e., a surface charge density that would be present in the absence of any polarisation effects. Our goal is now to determine how the electric field varies across the boundary $\partial\Omega$.

We denote by $\boldsymbol{\eta}$ the unit normal vector on the surface $\partial\Omega$ that points from Ω^- towards the exterior Ω^+. Additionally, we denote by $\boldsymbol{E}^{\pm}$ the values of the electric field $\boldsymbol{E}$ as one approaches the boundary $\partial\Omega$ from $\Omega^{\pm}$ respectively. We assume that all functions we consider here are sufficiently regular so that the following calculations are valid.

Let Σ denote an oriented surface in $\mathbb{R}^3$ with rectangular boundary $\partial\Sigma$ of height $\delta > 0$ that intersects part of the boundary $\partial\Omega$ as shown in Figure 1.6. We recall from Equation (1.4) that the electric field $\boldsymbol{E}$ is curl-free. Thus, Stokes' Theorem implies that

$$\oint_{\partial\Sigma} \boldsymbol{E} \cdot d\boldsymbol{\tau} = \iint_{\Sigma} \nabla \times \boldsymbol{E} \cdot d\mathbf{A} = 0.$$

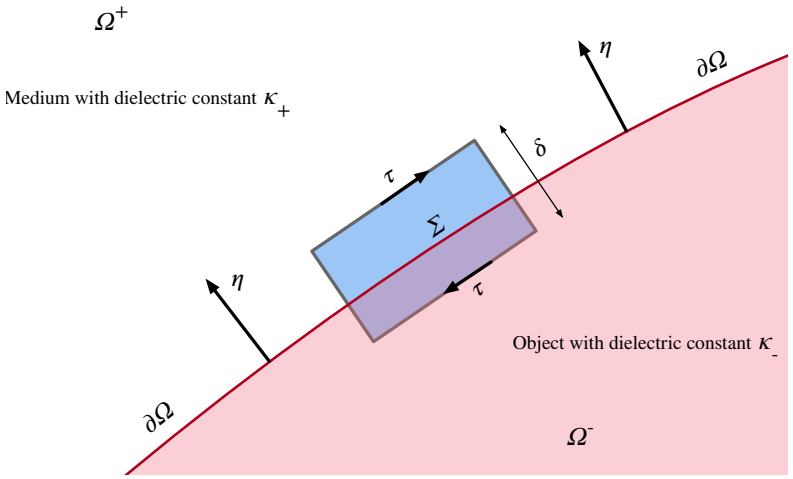

Figure 1.6: The geometric setting used to derive *tangential* jump conditions for the electric field across a dielectric interface.

Keeping the length of the rectangular boundary $\partial\Sigma$ fixed, and taking the limit $\delta \to 0$, $\partial\Sigma$ flattens to an infinitesimally thin rectangle whose non-negligible opposite sides coincide (arbitrarily closely) with a curve C on the boundary $\partial\Omega$. Consequently, we have

$$\begin{aligned} 0 = \oint_{\partial\Sigma} \boldsymbol{E}(\boldsymbol{\tau}) \cdot d\boldsymbol{\tau} &= \int_C \mathbf{E}^+(\boldsymbol{\tau}) \cdot d\boldsymbol{\tau} - \int_C \mathbf{E}^-(\boldsymbol{\tau}) \cdot d\boldsymbol{\tau} \\ &= \int_C \big(\mathbf{E}^+(\boldsymbol{\tau}) - \mathbf{E}^-(\boldsymbol{\tau})\big) \cdot d\boldsymbol{\tau}. \end{aligned}$$

Since a similar construction works for any curve C on $\partial\Omega$, we conclude that

$$\mathbf{E}^+(\boldsymbol{\tau}) \cdot \boldsymbol{\tau} = \mathbf{E}^-(\boldsymbol{\tau}) \cdot \boldsymbol{\tau} \qquad \text{on } \partial\Omega \quad \text{for any tangent vector } \boldsymbol{\tau}.$$

In other words, there is *no jump in the tangential component of the electric field* $\boldsymbol{E}$ *across the dielectric interface* $\partial\Omega$.

On the other hand, it can be shown that there is a jump in the *normal* component of the electric field. Indeed, let $\Sigma \subset \mathbb{R}^3$ be a *cuboid* of height $\delta > 0$ that intersects part of the boundary $\partial\Omega$ as shown in Figure 1.7. Let Q_Σ denote the charge enclosed in this cuboid. Gauss' Law from Equation (1.4) then implies that

$$\frac{Q_\Sigma}{\boldsymbol{\epsilon_0}} = \iiint_{\Sigma} \nabla \cdot \kappa \boldsymbol{E}\, dV = \iint_{\partial\Sigma} \kappa \boldsymbol{E} \cdot d\boldsymbol{A},$$

where the last step follows from the divergence theorem. Here κ is piecewise constant function that takes value κ_- in Ω^- and κ^+ in Ω^+ and $d\boldsymbol{A}$ denotes a vector surface element that points towards the exterior of Σ, i.e, in the direction of the unit normal vector $\boldsymbol{\eta}_\Sigma$ on the cuboid's boundary.

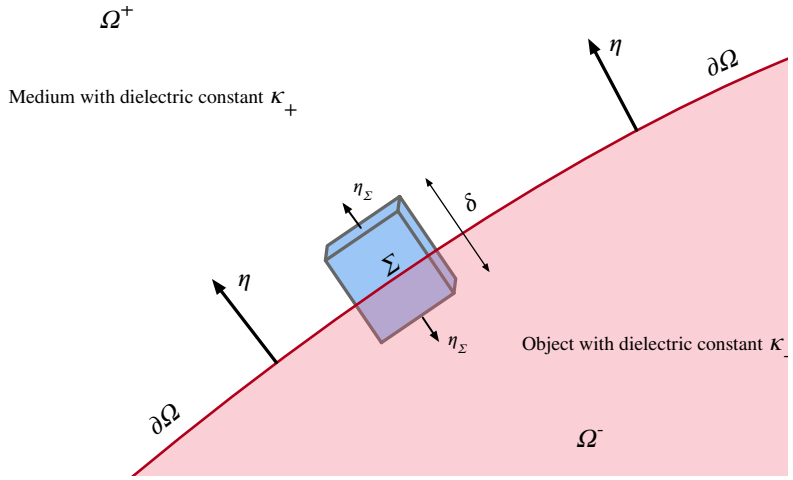

Figure 1.7: The geometric setting used to derive *normal* jump conditions for the electric field across a dielectric interface.

We now use the same geometrical argument as before, i.e., we take the limit $\delta \to 0$ whilst keeping the length and width of the cuboid constant. We thus obtain

$$\begin{aligned}\frac{Q_\Sigma}{\boldsymbol{\epsilon_0}} &= \iint_{\partial\Sigma} \kappa \boldsymbol{E} \cdot \, d\boldsymbol{A} = \iint_{\partial\Sigma\cap\partial\Omega} \kappa_+ \boldsymbol{E}^+ \cdot \boldsymbol{\eta} \, dA - \iint_{\partial\Sigma\cap\partial\Omega} \kappa_- \boldsymbol{E}^- \cdot \boldsymbol{\eta} \, dA \\ &= \iint_{\partial\Sigma\cap\partial\Omega} \left(\kappa_+ \boldsymbol{E}^+ - \kappa_- \boldsymbol{E}^-\right) \cdot \boldsymbol{\eta} \, dA.\end{aligned}$$

On the other hand, we know that the charge Q_Σ enclosed by the cuboid Σ is given as a surface integral involving the free-charge density σ_f:

$$Q_\sigma = \iint_{\partial\Sigma\cap\partial\Omega} \sigma_f \, dA.$$

Since the above calculations hold for any cuboid Σ, it follows that

$$\frac{\sigma_f}{\boldsymbol{\epsilon_0}} = \kappa_+ \boldsymbol{E}^+ \cdot \boldsymbol{\eta} - \kappa_- \boldsymbol{E}^- \cdot \boldsymbol{\eta}. \tag{1.6}$$

In other words, there is a jump in the normal component of the *weighted* electric field across the dielectric interface, governed by the free surface charge density σ_f.

We have therefore determined jump conditions for both the tangential component and the normal component of the electric field on the boundary of the dielectric. We conclude this discussion by highlighting an important consequence of these conditions. Recall that we introduced the notion of the electrostatic potential Φ such that $\boldsymbol{E} = -\nabla\Phi$, which

allowed us to write Maxwell's equation in a dielectric medium (1.4) as the generalised Poisson equation (1.5). One may therefore ask how the potential behaves across the dielectric interface. To answer this question, let us first observe that by definition, for any point $\boldsymbol{a} \in \Omega^-$ and $\boldsymbol{b} \in \Omega^+$ it holds that

$$\Phi(\boldsymbol{b}) - \Phi(\boldsymbol{a}) = \int_\gamma \boldsymbol{E} \cdot d\ell,$$

where γ is any path in $\mathbb{R}^3$ that connects the point $\boldsymbol{b}$ to the point $\boldsymbol{a}$. Since the electric field $\boldsymbol{E}$ is bounded in Ω^- and Ω^+, and there is, at most, a finite jump in $\boldsymbol{E}$ across the interface boundary $\partial\Omega$, we may take the limits $\boldsymbol{a} \to \boldsymbol{x} \in \partial\Omega$ and $\boldsymbol{b} \to \boldsymbol{x} \in \partial\Omega$ to deduce that the above line integral converges to zero. Consequently, we have

$$\Phi^+ = \Phi^- \qquad \text{on } \partial\Omega. \tag{1.7}$$

Here, $\Phi^\pm$ denote the values of the potential Φ as one approaches the boundary $\partial\Omega$ from $\Omega^\pm$ respectively. Additionally, the jump condition (1.6) can also be rephrased in terms of the electrostatic potential Φ to obtain

$$\frac{\sigma_f}{\boldsymbol{\epsilon_0}} = \kappa_- \nabla\Phi^- \cdot \boldsymbol{\eta} - \kappa_+ \nabla\Phi^+ \cdot \boldsymbol{\eta}. \tag{1.8}$$

Combining therefore the generalised Poisson equation (1.5) with the interface conditions (1.7) and (1.8), we have a description of how the electrostatic potential Φ behaves both inside and on the interface boundary of any dielectric medium. Unfortunately, these three equations do not yet describe a *unique* potential function Φ. Indeed, a straightforward calculation shows that if any function Φ is a solution to Equations (1.5), (1.7) and (1.8), then $\Phi + c$ is also a solution for any constant $c \in \mathbb{R}$. This non-uniqueness is not surprising if we recall that the electric field $\boldsymbol{E}$ relates to the electric potential only as $\boldsymbol{E} = -\nabla\Phi$.

Decay conditions at infinity

In view of the preceding discussion, we must impose an additional condition in order to guarantee the existence and uniqueness of an electrostatic potential Φ that satisfies the generalised Poisson equation (1.5) and the interface conditions (1.7) and (1.8). If we are interested in determining the potential on an *unbounded* spatial domain due to a charge distribution with *bounded* support, then we look for so-called decay conditions that describe how the potential behaves at infinity. The usual convention in the physics literature is to set the potential at infinity to be zero. More precisely, we will assume that

$$\exists C > 0 \colon |\Phi(\mathbf{x})| \leq C|\mathbf{x}|^{-1} \qquad \text{for } |\mathbf{x}| \to \infty. \tag{1.9}$$

To summarise, we have derived equations that describe the electrostatic potential inside a dielectric medium (Equation (1.5)) and at the interface boundaries (Equations (1.7) and (1.8)), and we have imposed the decay condition (1.9) as an admissibility

criterion. Together, these three equations and admissibility condition are sufficient to write a well-posed mathematical model for the electrostatic potential generated by a charged dielectric object embedded in a polarisable medium. We conclude this section by remarking that while the preceding arguments are informal, they can be made completely rigorous by imposing suitable regularity assumptions on the problem geometry and physical quantities of interest.

1.3 Mathematical Preliminaries

The discussion in Section 1.2 was focused on explaining the physics behind polarisable electrostatics and relied primarily on heuristic, mathematically informal explanations. In order to introduce mathematical rigour and precision in the subsequent exposition, we will now establish basic notation and recall some key results from the theory of partial differential equations. The content of this section is largely classical and can be found in any standard textbook on functional analysis and PDE theory (see, e.g., [21, 64, 68, 82]). We will primarily follow the more focused presentation of [185] but we will also use some results from [50, 147]. We will also assume that the reader is familiar with differential calculus of several variables, the rudiments of measure theory, and basic point-set topology. In particular, the notions of classical differentiability, measurability and integrability (in the sense of Lebesgue) as well as ideas of compactness will be used without prior introduction.

1.3.1 Basic notation

Sets of numbers: We denote by $\mathbb{N} := \{1, 2, 3, \ldots\}$ and by $\mathbb{Z} := \mathbb{N} \cup \{0\} \cup -\mathbb{N}$ the set of natural numbers and the set of integers respectively, and we define $\mathbb{N}_0 := \{0, 1, 2, \ldots, \}$ as the set of non-negative integers. In addition, we write $\mathbb{R}$ and $\mathbb{C}$ for the set of real numbers and the set of complex numbers respectively. Finally, we denote by $\mathbb{R}_+$ and $\mathbb{R}_-$ the set of positive real numbers and the set of negative real numbers respectively.

Euclidean norm and scalar product: Let $n \in \mathbb{N}$. Then we denote by $|\cdot| \colon \mathbb{R}^n \to \mathbb{R}_+ \cup \{0\}$ and $(\cdot, \cdot)_{\mathbb{R}^n} \colon \mathbb{R}^n \times \mathbb{R}^n \to \mathbb{R}$ the mappings with the property that for all $u = (u_1, u_2, \ldots, u_n) \in \mathbb{R}^n$ and all $v = (v_1, v_2, \ldots, v_n) \in \mathbb{R}^n$ it holds that

$$|u|^2 := \sum_{j=1}^{n} u_j^2, \qquad \text{and} \qquad (u, v)_{\mathbb{R}^n} := \sum_{j=1}^{n} u_j v_j,$$

and we say that $|\cdot|$ and $(\cdot, \cdot)_{\mathbb{R}^n}$ are the Euclidean norm and Euclidean inner product on $\mathbb{R}^n$ respectively. Notice that the Euclidean norm is induced by the Euclidean inner product.

Essential mappings: Given a set A we denote by $I_A \colon A \to A$ the identity map on A, i.e., the map with the property that for all $a \in A$ it holds that $I_A(a) = a$ with the

convention that we drop the subscript A if the context is clear.

Next, given a set Ω, a subset $\Sigma \subset \Omega$ and a mapping $f\colon \Omega \to \mathbb{R}$, we define the restriction map $f|_\Sigma\colon \Sigma \to \mathbb{R}$ as $f|_\Sigma(\sigma) = f(\sigma)$ for all $\sigma \in \Sigma$.

Moreover, we denote by $\lfloor\cdot\rfloor\colon \mathbb{R} \to \mathbb{Z}$ the usual floor function, i.e., the mapping with the property that for any $s \in \mathbb{R}$, $\lfloor s \rfloor$ is the largest integer less than or equal to s. In a similar fashion, we denote by $\lceil\cdot\rceil\colon \mathbb{R} \to \mathbb{Z}$ the usual ceiling function, i.e., the mapping with the property that for any $s \in \mathbb{R}$, $\lceil s \rceil$ is the smallest integer greater than or equal to s.

Multi-indices: For any natural number $k \in \mathbb{N}$, we will frequently denote by $\alpha \in \mathbb{N}_0^k$ a generic multi-index with the convention that

$$\alpha! := \Pi_{j=1}^k \alpha_j! \qquad \text{and} \qquad |\alpha| := \sum_{j=1}^k \alpha_j.$$

In addition, given $k \in \mathbb{N}$, a multi-index $\alpha \in \mathbb{N}_0^k$, an open set $\Omega \subset \mathbb{R}^k$, $\mathbf{x} = (x_1, x_2, \ldots, x_k) \in \Omega$ and a function $f\colon \Omega \to \mathbb{R}$ we define

$$\partial^\alpha f(\mathbf{x}) := \partial_{\mathbf{x}}^\alpha f(\mathbf{x}) := \frac{\partial^{|\alpha|} f(\mathbf{x})}{\partial_{x_1}^{\alpha_1} \partial_{x_2}^{\alpha_2} \ldots \partial_{x_k}^{\alpha_k}}.$$

Miscellaneous: Given a Fréchet space E, i.e., a locally convex vector space that is complete with respect to a translation-invariant metric, we will frequent use the notation E^* to denote the topological dual space of E, and we write $\langle\cdot,\cdot\rangle_{E^*\times E}$ to denote the duality pairing, i.e., the action of an element of E^* on an element of E. Additionally, if $\big(E, \|\cdot\|_E\big)$ is a Banach space, then we equip the dual space E^* with the canonical dual norm $\|\cdot\|_{E^*}$, which is as defined as

$$\|\phi\|_{E^*} := \sup_{0\neq f\in E} \frac{\langle \phi, f\rangle_{E^*\times E}}{\|f\|_E} \qquad \forall \phi \in E^*.$$

Within this framework, we introduce the notion of the so-called adjoint operator: Let $\big(X, \|\cdot\|_X\big)$ and $\big(Y, \|\cdot\|_Y\big)$ be Banach spaces, and let $T\colon X \to Y$ be a bounded linear operator. Then we define the bounded linear operator $T^*\colon Y^* \to X^*$ as the mapping with the property that for each $y^* \in Y^*$, T^*y^* is the unique element in X^* such that for all $x \in X$ it holds that

$$\langle T^*y^*, x\rangle_{X^*\times X} = \langle y^*, Tx\rangle_{Y^*\times Y},$$

and we say that T^* is the adjoint operator of T. We remark that in some literature, the map T^* is known as the *dual* operator of T.

1.3.2 Function spaces on domains

Throughout this section, we assume that $n \in \mathbb{N}$, $k \in \mathbb{N}_0$, and $\Omega \subset \mathbb{R}^n$ is an open set. Additionally, given a continuous function $f\colon \Omega \to \mathbb{R}$ we define the set $\operatorname{supp}(f) \subset \Omega$ as the closure in Ω of the set $\{x \in \Omega\colon f(x) \neq 0\}$, and we say that $\operatorname{supp}(f)$ is the support of f.

Spaces of continuous functions We introduce the following classical function spaces:

$$\begin{aligned}
C^k(\Omega) &:= \{u\colon \Omega \to \mathbb{R}\colon \forall |\alpha| \leq k,\ \partial^\alpha u \text{ is continuous}\}, \\
C^k(\overline{\Omega}) &:= \left\{u \in C^k(\Omega)\colon \forall |\alpha| \leq k,\ \partial^\alpha u \text{ can be continuously extended to } \overline{\Omega}\right\}, \\
C^\infty(\Omega) &:= \bigcap_{k\in\mathbb{N}_0} C^k(\Omega), \qquad C^\infty(\overline{\Omega}) = \bigcap_{k\in\mathbb{N}_0} C^k(\overline{\Omega}), \\
C_0^\infty(\Omega) &:= \{u \in C^\infty(\Omega)\colon \operatorname{supp}(u) \text{ is a compact subset of } \Omega\}, \\
C_{\text{comp}}^\infty(\Omega) &:= \{u|_\Omega\colon u \in C_0^\infty(\mathbb{R}^n)\}.
\end{aligned}$$

We remark that the above spaces can all be equipped with locally convex topologies, and it is therefore possible to define the topological dual spaces $\left(C^\infty(\Omega)\right)^*$ and $\left(C_0^\infty(\Omega)\right)^*$. Note that it is common practice in the literature to use the notation of Laurent Schwartz [188] and write $\mathcal{E}(\Omega)$ for $C^\infty(\Omega)$ and $\mathcal{D}(\Omega)$ for $C_0^\infty(\Omega)$ but we do not follow this convention here.

Square integrable functions and weak derivatives We denote by $L^2(\Omega)$ the space of all Lebesgue measurable functions $f\colon \Omega \to \mathbb{R}$ that satisfy $\int_\Omega |f(\mathbf{x})|^2\, d\mathbf{x} < \infty$ with the convention that we do not distinguish between two functions $u, v \in L^2(\Omega)$ if they differ on a set of measure of zero. We equip $L^2(\Omega)$ with the usual inner product

$$(u, v)_{L^2(\Omega)} := \int_\Omega u(\mathbf{x})v(\mathbf{x})\, d\mathbf{x} \qquad \forall u, v \in L^2(\Omega),$$

and we write the norm induced by this inner product as $\|\cdot\|_{L^2(\Omega)}$. Notice that the space $L^2(\Omega \times \Omega)$ can be defined analogously.

Next, given a multi-index $\alpha \in \mathbb{N}_0^k$ and a function $u \in L^2(\Omega)$, if there exists another function $v \in L^2(\Omega)$ with the property that

$$(v, \phi)_{L^2(\Omega)} = -1^{|\alpha|}(u, \partial^\alpha \phi)_{L^2(\Omega)} \qquad \forall \phi \in C_0^\infty(\Omega),$$

then we write $v := \partial^\alpha u$. If such a function $v \in L^2(\Omega)$ exists, then it is unique, and we therefore say that v is the α^{th} weak derivative of u.

Convention: In this dissertation, we adopt the convention that derivatives of square integrable functions are always understood in the weak sense.

Sobolev spaces We define the Sobolev space $H^k(\Omega)$ of non-negative integer order as the vector space

$$H^k(\Omega) := \{u \in L^2(\Omega) \colon \forall |\alpha| \leq k,\ \partial^\alpha u \in L^2(\Omega)\},$$

equipped with the inner product

$$(u,v)_{H^k(\Omega)} := \sum_{|\alpha|<k} (\partial^\alpha u, \partial^\alpha v)_{L^2(\Omega)} + \sum_{|\alpha|=k} (\partial^\alpha u, \partial^\alpha v)_{L^2(\Omega)} \qquad \forall u, v \in H^k(\Omega) \tag{1.10}$$

and associated norm $\|u\|_{H^k(\Omega)} := (u,u)^{\frac{1}{2}}_{H^k(\Omega)} \quad \forall u \in H^k(\Omega)$. Additionally, we will frequently refer to the second sum in Equation (1.10) (i.e., the sum over multi-indices $|\alpha| = k$) as the $H^k(\Omega)$ semi-norm of u, denoted $|u|_{H^k(\Omega)}$.

Next, given a non-integer real number $s > 0$ with $s = \lfloor s \rfloor + \sigma$ we define the Sobolev space $H^s(\Omega)$ of non-negative fractional order as the vector space

$$H^s(\Omega) := \left\{ u \in H^{\lfloor s \rfloor}(\Omega) \colon \int_\Omega \int_\Omega \frac{|\partial^\alpha u(\mathbf{x}) - \partial^\alpha u(\mathbf{y})|^2}{|\mathbf{x}-\mathbf{y}|^{n+2\sigma}}\, d\mathbf{x} d\mathbf{y} < \infty \quad \text{for all } |\alpha| = \lfloor s \rfloor \right\},$$

equipped with the inner product

$$(u,v)_{H^s(\Omega)} := (u,v)_{H^{\lfloor s \rfloor}(\Omega)} + \sum_{|\alpha|=\lfloor s \rfloor} \int_\Omega \int_\Omega \frac{(\partial^\alpha u(\mathbf{x}) - \partial^\alpha u(\mathbf{y}))(\partial^\alpha v(\mathbf{x}) - \partial^\alpha v(\mathbf{y}))}{|\mathbf{x}-\mathbf{y}|^{n+2\sigma}}\, d\mathbf{x} d\mathbf{y}. \tag{1.11}$$

and associated norm $\|u\|_{H^s(\Omega)} := (u,u)^{\frac{1}{2}}_{H^s(\Omega)}$. We will frequently refer to the double integral in Equation (1.11) as the Sobolev-Slobodeckij semi-norm of u, denoted $|u|_{\sigma,\lfloor s \rfloor,\Omega}$.

Moreover, for any real number $s > 0$ we define the Sobolev space $H^s_0(\Omega)$ as the completion of $C^\infty_0(\Omega)$ with respect to the $\|\cdot\|_{H^s(\Omega)}$ norm defined through Equation (1.11). Finally, for any $s > 0$, we define the Sobolev space $H^{-s}(\Omega)$ of negative order as the topological dual space of $H^s_0(\Omega)$, i.e.,

$$\begin{aligned} H^{-s}(\Omega) &:= (H^s_0(\Omega))^* \\ &:= \left\{ f \colon H^s_0(\Omega) \to \mathbb{R} \colon \exists C > 0 \text{ such that } \forall u \in H^s_0(\Omega) \colon |f(u)| \leq C \|u\|_{H^s(\Omega)} \right\}, \end{aligned}$$

equipped with the canonical dual norm

$$\|f\|_{H^{-s}(\Omega)} := \sup_{0 \neq u \in H^s_0(\Omega)} \frac{\langle f, u \rangle_{H^{-s}(\Omega) \times H^s(\Omega)}}{\|u\|_{H^s(\Omega)}},$$

where we use the notation $\langle f, u \rangle_{H^{-s}(\Omega) \times H^s(\Omega)} := f(u)$. We remark that we will frequently use an abuse of notation to identify functions $u \in H^s_0(\Omega),\ s > 0$ as elements of $H^{-s}(\Omega)$. This should be understood in the sense of the Riesz representation theorem, i.e., when we say that a square-integrable function $u \in H^s_0(\Omega)$ is an element of $H^{-s}(\Omega)$, we are identifying u with the unique distribution $\phi_u \in H^{-s}(\Omega)$ such that $\phi_u(v) = (u,v)_{H^s(\Omega)}$ for all $v \in H^s_0(\Omega)$. Similar considerations also apply to other, general dual spaces.

1.3.3 Function spaces on surfaces

Let $n \in \mathbb{N}$, $k \in \mathbb{N}_0$, and $\Omega \subset \mathbb{R}^n$ be an open set. We denote by $\partial\Omega := \overline{\Omega} \cap (\mathbb{R}^n \setminus \Omega)$ the boundary of the open set Ω. The goal of this section is to introduce certain Sobolev spaces on the surface $\partial\Omega$. To this end, we require appropriate regularity assumptions on $\partial\Omega$.

Lipschitz domains We say that the open set Ω is a Lipschitz domain if $\partial\Omega$ is compact and there exist two countable families of sets $\{W_j\}_{j\in\mathbb{N}}, \{\Omega_j\}_{j\in\mathbb{N}}$ such that the following holds

1. The family $\{W_j\}$ is a finite open cover of $\partial\Omega$, i.e., each $W_j \subset \mathbb{R}^n$ is open and $\partial\Omega \subset \bigcup_j W_j$.
2. Each $\Omega_j \subset \mathbb{R}^n$ can be transformed to a Lipschitz hypograph, i.e., a set that consists of all points that lie below the graph of a Lipschitz function, through a rigid transformation consisting of only a rotation plus a translation.
3. We have for all j the relationship $\Omega \cap W_j = \Omega_j \cap W_j$.

Additionally, if, in condition (2) above, each $\Omega_j \subset \mathbb{R}^n$ can be transformed to a C^k hypograph, i.e., a set that consists of all points that lie below the graph of a C^k function with bounded derivatives of all orders less than or equal to k, then we say that Ω is a C^k domain. From these definitions, we see that the unit sphere in $\mathbb{R}^3$, denoted $\mathbb{S}^2$, is a C^∞ domain, i.e., it is a C^k domain for every $k \in \mathbb{N}$. Similar considerations apply to a general open ball $U \subset \mathbb{R}^n$.

Sobolev spaces on surfaces Assume now that Ω is a Lipschitz domain. To begin with, we denote by $L^2(\partial\Omega)$ the space of all Lebesgue integrable functions $f\colon \partial\Omega \to \mathbb{R}$ that satisfy $\int_{\partial\Omega} |f(\mathbf{x})|^2 \, d\mathbf{x} < \infty$ with the convention that we do not distinguish between two functions $u, v \in L^2(\partial\Omega)$ if they differ on a set of measure of zero. We equip $L^2(\partial\Omega)$ with the natural inner product

$$(u, v)_{L^2(\partial\Omega)} := \int_{\partial\Omega} u(\mathbf{x}) v(\mathbf{x}) \, d\mathbf{x} \qquad \forall u, v \in L^2(\partial\Omega),$$

and we write the norm induced by this inner product as $\|\cdot\|_{L^2(\partial\Omega)}$. Once again, we observe that the space $L^2(\partial\Omega \times \partial\Omega)$ can be defined analogously.

For connected sets Ω, given $s \in (0, 1)$ we define the fractional Sobolev space $H^s(\partial\Omega)$ as the vector space

$$H^s(\partial\Omega) := \left\{ u \in L^2(\partial\Omega) \colon \int_{\partial\Omega} \int_{\partial\Omega} \frac{|u(\mathbf{x}) - u(\mathbf{y})|^2}{|\mathbf{x} - \mathbf{y}|^{n-1+2s}} \, d\mathbf{x} d\mathbf{y} < \infty \right\},$$

equipped with the inner product

$$(u, v)_{H^s(\partial\Omega)} := (u, v)_{L^2(\partial\Omega)} + \int_{\partial\Omega} \int_{\partial\Omega} \frac{(u(\mathbf{x}) - u(\mathbf{y}))(v(\mathbf{x}) - v(\mathbf{y}))}{|\mathbf{x} - \mathbf{y}|^{n-1+2s}} \, d\mathbf{x} d\mathbf{y} \tag{1.12}$$

and associated norm $\|u\|_{H^s(\partial\Omega)} := (u,u)^{\frac{1}{2}}_{H^s(\partial\Omega)}$. If, on the other hand, the set Ω is the union of disjoint bounded sets, say $\Omega := \cup_{j=1}^N \Omega_i$, then we define the inner-product $(\cdot,\cdot)_{H^s(\partial\Omega)}$ in a *local* manner by setting for all $u, v \in H^s(\partial\Omega)$

$$(u,v)_{H^s(\partial\Omega)} := \sum_{j=1}^N (u,v)_{L^2(\partial\Omega_j)} + \sum_{j=1}^N \int_{\partial\Omega_j}\int_{\partial\Omega_j} \frac{(u(\mathbf{x})-u(\mathbf{y}))(v(\mathbf{x})-v(\mathbf{y}))}{|\mathbf{x}-\mathbf{y}|^{n-1+2s}}\, d\mathbf{x}d\mathbf{y},$$

where $\partial\Omega_j$ denotes the boundary of Ω_j for all $j = 1,\dots,N$.

In addition, we define the Sobolev spaces of negative fractional order $H^{-s}(\partial\Omega) := \big(H^s(\partial\Omega)\big)^*$, and we equip them with the canonical dual norms. Once again, we will frequently use an abuse of notation to identify functions $u \in H^s(\partial\Omega),\ s > 0$ as elements of $H^{-s}(\partial\Omega)$. We also remark that although we do not present this construction here, similar ideas can be used to define fractional Sobolev space $H^s(\partial\Omega)$ for any real $s \notin (0,1)$.

1.3.4 Trace operators

Throughout this section, let $n \in \mathbb{N}$, $k \in \mathbb{N}_0$, and $\Omega \subset \mathbb{R}^n$ be an open set with boundary $\partial\Omega$. We would now like to introduce the notion of the restriction of a function $u \in H^s(\Omega),\ s \in \mathbb{R}$ to the boundary $\partial\Omega$. Such restrictions can also be defined for functions that are only locally (in an appropriate sense) in $H^s(\Omega)$, the relevant space in this case being called $H^s_{\text{loc}}(\Omega)$. Since the necessary notions are slightly less standard, we provide formal definitions.

Dirichlet traces and the interior Dirichlet problem

Definition 1.1. Let $r > 0$ and $s \in \mathbb{R}$. We define the vector space $H^r_{\text{loc}}(\Omega)$ as

$$H^r_{\text{loc}}(\Omega) := \Big\{ u \in L^2_{\text{loc}}(\Omega) \text{ such that } \forall \chi \in C^\infty_{\text{comp}}(\Omega)\colon \chi u \in H^r(\Omega) \Big\}.$$

Here, $L^2_{\text{loc}}(\Omega)$ denotes the set of functions that are square integrable on all compact subsets of Ω. Moreover, we define the vector space $H^{-r}_{\text{loc}}(\Omega)$ as

$$H^{-r}_{\text{loc}}(\Omega) := \Big\{ \phi \in \big(C^\infty_{\text{comp}}(\Omega)\big)^* \text{ such that } \forall v \in C^\infty_{\text{comp}}(\Omega)\colon v\phi \in H^{-r}(\Omega) \Big\},$$

where for an arbitrary $\phi \in \big(C^\infty_{\text{comp}}(\Omega)\big)^*$ and $v \in C^\infty_{\text{comp}}(\Omega)$, the product $v\phi$ is understood as a distribution in $\big(C^\infty_{\text{comp}}(\Omega)\big)^*$ satisfying $\big(v\phi\big)(f) = \phi\big(v \cdot f\big)\ \forall f \in C^\infty_{\text{comp}}(\Omega)$. Additionally, we set $H^0_{\text{loc}}(\Omega) := L^2_{\text{loc}}(\Omega)$.

Next, we define the subspace $H^s_\Delta(\Omega) \subset H^s_{\text{loc}}(\Omega)$ as

$$H^s_\Delta(\Omega) := \Big\{ u \in H^s_{\text{loc}}(\Omega)\colon \Delta u = 0 \text{ in } \Omega \Big\}.$$

Moreover, if the set Ω is bounded, then we define the vector space $H^s_\Delta(\mathbb{R}^n \setminus \partial\Omega)$ as

$$H^s_\Delta(\mathbb{R}^n \setminus \partial\Omega) := \Big\{ u \in L^2_{\text{loc}}(\mathbb{R}^n)\colon u|_\Omega \in H^s_\Delta(\Omega) \quad \text{and} \quad u|_{\mathbb{R}^n\setminus\overline{\Omega}} \in H^s_\Delta\big(\mathbb{R}^n \setminus \overline{\Omega}\big) \Big\}.$$

Remark 1.2. Definition 1.1 is based on the exposition presented in [185, Section 2.6]. We emphasise in particular that in much of the functional analysis literature, in the definition of the space $H^r_{\mathrm{loc}}(\Omega), r > 0$, the condition $\chi \in C^\infty_{\mathrm{comp}}(\Omega)$ is replaced with $\chi \in C^\infty_0(\Omega)$, the latter choice being considered the standard approach for defining $H^r_{\mathrm{loc}}(\Omega)$.

Definition 1.3 (Support of non-continuous functions)**.**
Let $s \in \mathbb{R}$ and let $u \in H^s(\Omega)$. If $s \geq 0$, then the support of u, denoted $\mathrm{supp}(u)$ is the largest relatively closed set $V \subset \Omega$ such that $(u, f)_{H^s(\Omega)} = 0$ for all $f \in C^\infty(\Omega)$ satisfying $\mathrm{supp}(f) \subset \Omega \setminus V$. If $s < 0$, then supp (u) is the largest relatively closed set $V \subset \mathbb{R}^n$ such that $u(f) = 0$ for all $f \in C^\infty(\Omega)$ satisfying $\mathrm{supp}(f) \subset \Omega \setminus V$.

Definition 1.4.
Let $s \in \mathbb{R}$. We define the vector space $H^s_{\mathrm{comp}}(\Omega)$ as

$$H^s_{\mathrm{comp}}(\Omega) := \bigcup_{\substack{K \subset \Omega \\ K \text{ is compact}}} \left\{ u \in H^s_{\mathrm{loc}}(\Omega) \colon \mathrm{supp}(u) \subset K \right\}.$$

One can easily show that the spaces $H^s_{\mathrm{loc}}(\Omega), H^s_{\mathrm{comp}}(\Omega)$, and $H^s(\Omega)$ all coincide if Ω is a bounded set. Unfortunately, in the general case of an unbounded Ω, it is not possible to define norms on the vector space $H^s_{\mathrm{loc}}(\Omega)$ and $H^s_{\mathrm{comp}}(\Omega)$ for any $s \in \mathbb{R}$. It is, however, possible to define a metric and therefore a topology on these spaces. This development is outside the scope of this dissertation; for our purposes, we require only the following two theorems, the first of which establishes the notion of bounded linear operators on these spaces and the second of which describes the restrictions of these functions on surfaces.

Theorem 1.5 ([185, Theorem 2.6.7])**.**
Let $s, t \in \mathbb{R}$ and let $\left(E, \|\cdot\|_E\right)$ be a normed space. Then the following hold

1. *The bilinear form $\langle \cdot, \cdot \rangle \colon C^\infty(\Omega) \times C^\infty_{\mathrm{comp}}(\Omega) \to \mathbb{R}$ defined as*

$$\langle u, v \rangle := \int_\Omega u(\mathbf{x}) v(\mathbf{x}) \, d\mathbf{x},$$

extends to a duality pairing $\langle \cdot, \cdot \rangle_{H^s_{\mathrm{loc}}(\Omega) \times H^{-s}_{\mathrm{comp}}(\Omega)} \colon H^s_{\mathrm{loc}}(\Omega) \times H^{-s}_{\mathrm{comp}}(\Omega) \to \mathbb{R}$.

2. *A linear map $A \colon H^s_{\mathrm{comp}}(\Omega) \to E$ is bounded if and only if the restriction $A \colon \left\{ u \in H^s_{\mathrm{loc}}(\Omega) \colon \mathrm{supp}(u) \subset K \right\} \to E$ is bounded for every compact set $K \subset \Omega$. A linear map $A \colon H^s_{\mathrm{loc}}(\Omega) \to E$ is bounded if and only if there exists a function $\phi \in C^\infty_{\mathrm{comp}}(\Omega)$ and a constant $C_A > 0$ such that for all $u \in H^s_{\mathrm{loc}}(\Omega)$ it holds that*

$$\|Au\|_E \leq C_A \|\phi u\|_{H^s(\Omega)}.$$

3. *A linear map $A \colon E \to H^s_{\mathrm{loc}}(\Omega)$ is bounded if and only if for all $\phi \in C^\infty_{\mathrm{comp}}(\Omega)$ there exists a constant $C_A > 0$ such that for all $u \in E$ it holds that*

$$\|\phi(Au)\|_{H^s(\Omega)} \leq C_A \|u\|_E.$$

4. *A linear map* $A\colon H^s_{\mathrm{comp}}(\Omega) \to H^t_{\mathrm{loc}}(\Omega)$ *is bounded if and only if for all compact sets* $K \subset \Omega$ *and all* $\phi \in C^\infty_{\mathrm{comp}}(\Omega)$ *there exists a constant* $C_A > 0$ *such that for all* $u \in H^s_{\mathrm{comp}}(\Omega)$ *with* $\operatorname{supp}(u) \subset K$ *it holds that*

$$\|\phi(Au)\|_{H^t(\Omega)} \leq C_A \|u\|_{H^s(\Omega)}.$$

5. *A linear map* $A\colon H^s_{\mathrm{loc}}(\Omega) \to H^t_{\mathrm{comp}}(\Omega)$ *is compact if and only if for all cutoff functions* $\phi, \psi \in C^\infty_{\mathrm{comp}}(\Omega)$*, the restriction* $u \mapsto \phi\big(A(\psi u)\big)\colon H^s(\Omega) \to H^t(\Omega)$ *is compact.*

Theorem 1.6 ([185, Theorem 2.6.8])**.**
Let $\Omega^- \subset \mathbb{R}^n$ *be a bounded Lipschitz domain with boundary* $\partial\Omega$ *and let* $\Omega^+ := \mathbb{R}^n \setminus \overline{\Omega^-}$*. Then the following hold:*

1. *For every real number* $\ell \in \left(\frac{1}{2}, \frac{3}{2}\right)$ *there exists a bounded linear trace operator* $\gamma\colon H^\ell_{\mathrm{loc}}\big(\mathbb{R}^n\big) \to H^{\ell-\frac{1}{2}}(\partial\Omega)$ *such that*

$$\gamma\phi = \phi|_{\partial\Omega} \qquad \forall \phi \in C^0\big(\mathbb{R}^n\big).$$

2. *For* $s \in \{-, +\}$ *and every real number* $\ell \in \left(\frac{1}{2}, \frac{3}{2}\right)$ *there exist bounded linear trace operators* $\gamma^s\colon H^\ell_{\mathrm{loc}}\big(\Omega^s\big) \to H^{\ell-\frac{1}{2}}(\partial\Omega)$ *such that*

$$\gamma^s\phi = \phi|_{\partial\Omega} \qquad \forall \phi \in C^0\big(\overline{\Omega^s}\big).$$

   Additionally, for any $\phi \in H^\ell_{\mathrm{loc}}\big(\mathbb{R}^n\big)$ *it holds that*

$$\gamma^-\phi = \gamma^+\phi = \gamma\phi \qquad \text{in the sense of } H^{\ell-\frac{1}{2}}(\partial\Omega).$$

Remark 1.7. Consider the setting of Theorem 1.6. If the set Ω^- is assumed to be a C^k domain rather than simply Lipschitz, then the range of the index ℓ can be extended from $\ell \in \left(\frac{1}{2}, \frac{3}{2}\right)$ to $\ell \in \left(\frac{1}{2}, k\right]$ (see, e.g., [185, Theorem 2.6.9]). Notice that this may require the introduction of the surface Sobolev spaces $H^s(\partial\Omega)$ of order $s \geq 1$. Moreover, identical results hold for functions that are vector-valued rather than scalar-valued, in which case the trace operator is applied component-wise. Finally, we remark that the one-sided trace operators can also be applied to functions of appropriate regularity that are defined globally on $\mathbb{R}^n$.

Convention: In the sequel, we will frequently refer to the trace mappings defined through Theorem 1.6 as the so-called "Dirichlet" trace operators.

The next theorem is a standard result on the unique solvability of the interior Laplace problem with Dirichlet data (IDP) and will be used several times in this dissertation.

Theorem 1.8 (Unique solvability of the interior Laplace problem with Dirichlet data)**.**

Let $\ell \in \left(\frac{1}{2}, \frac{3}{2}\right)$ *be a real number and let* $\Omega^- \subset \mathbb{R}^n$ *be a bounded Lipschitz domain with boundary* $\partial\Omega$*. Then the restriction of the Dirichlet trace operator* $\gamma^-\colon H^\ell_\Delta(\Omega^-) \to H^{\ell-\frac{1}{2}}(\partial\Omega)$ *has a bounded inverse which we denote* $\mathcal{E}_{\Delta,\Omega^-}$*. Additionally, if the set* Ω^- *is a* C^k *domain, then this result also holds for all* $\ell \in \left(\frac{1}{2}, k\right]$*.*

The following theorem concerns the existence of a right-inverse to the Dirichlet trace operator in the general case.

Theorem 1.9 ([185, Theorem 2.6.11])**.**
Let $\Omega^- \subset \mathbb{R}^n$ be a bounded Lipschitz domain with boundary $\partial\Omega$ and let $\Omega^+ := \mathbb{R}^n \setminus \overline{\Omega^-}$. Then for all $\ell \in \left(\frac{1}{2}, \frac{3}{2}\right)$ there exists a bounded linear extension operator $Z_{\mathbb{R}^n} \colon H^{\ell-\frac{1}{2}}(\partial\Omega) \to H^\ell_{\mathrm{comp}}(\mathbb{R}^n)$ such that for all $\psi \in H^{\ell-\frac{1}{2}}(\partial\Omega)$ it holds that $(\gamma \circ Z_{\mathbb{R}^n})(\psi) = \psi$. Additionally, for each $s \in \{-,+\}$, if $R_{\Omega^s} \colon H^\ell_{\mathrm{comp}}(\mathbb{R}^n) \to H^\ell_{\mathrm{comp}}(\Omega^s)$ denotes the restriction operator, then the linear mapping $Z_{\Omega^s} \colon H^{\ell-\frac{1}{2}}(\partial\Omega) \to H^\ell_{\mathrm{comp}}(\Omega^s)$ defined as $Z_{\Omega^s} := R_{\Omega^s} \circ Z_{\mathbb{R}^n}$ is also bounded.

Neumann traces and the Dirichlet-to-Neumann map

Notation: Throughout this dissertation, we will frequently use the following notation. For a bounded Lipschitz domain $\Omega^- \subset \mathbb{R}^n$ with boundary $\partial\Omega$, we denote by $\boldsymbol{\eta} \colon \partial\Omega \to \mathbb{S}^{n-1}$ the so-called unit normal vector on the boundary $\partial\Omega$ with the convention that $\boldsymbol{\eta}$ always points towards the exterior of Ω^-. The (almost everywhere) existence of such a unit normal vector for an arbitrary bounded Lipschitz domain is a consequence of a well known result of Rademacher (see, e.g., [185, Theorem 2.7.1]).

Definition 1.10 (Neumann Traces)**.**
Let $\Omega^- \subset \mathbb{R}^n$ be a bounded Lipschitz domain with boundary $\partial\Omega$ and let $\Omega^+ := \mathbb{R}^n \setminus \overline{\Omega^-}$. Then we define the interior Neumann trace operator $\gamma_N^- \colon H^1_\Delta(\Omega^-) \to H^{-\frac{1}{2}}(\partial\Omega)$ and the exterior Neumann trace operator $\gamma_N^+ \colon H^1_\Delta(\Omega^+) \to H^{-\frac{1}{2}}(\partial\Omega)$ as the linear mappings with the property that for all $u^- \in H^1_\Delta(\Omega^-), u^+ \in H^1_\Delta(\Omega^+)$ and all $\psi \in H^{\frac{1}{2}}(\partial\Omega)$ it holds that

$$\langle \gamma_N^- u^-, \psi \rangle_{H^{-\frac{1}{2}}(\partial\Omega)\times H^{\frac{1}{2}}(\partial\Omega)} := \int_{\Omega^-} \nabla u^-(\mathbf{x}) \cdot \nabla\big(Z_{\Omega^-}\psi\big)(\mathbf{x})\, d\mathbf{x},$$
$$\langle \gamma_N^+ u^+, \psi \rangle_{H^{-\frac{1}{2}}(\partial\Omega)\times H^{\frac{1}{2}}(\partial\Omega)} := -\int_{\Omega^+} \nabla u^+(\mathbf{x}) \cdot \nabla\big(Z_{\Omega^+}\psi\big)(\mathbf{x})\, d\mathbf{x}.$$

Consider Definition 1.10 of the Neumann trace operators. Several remarks are now in order. First, it can be shown that this definition is independent of the exact choice of extension operator Z_{Ω^s}, $s \in \{-,+\}$, i.e., one can replace Z_{Ω^s} with a different extension operator $\tilde{Z}_{\Omega^s}$. Second, for smooth functions u^-, u^+ the Neumann trace operators $\gamma_N^- u^-, \gamma_N^+ u^+$ coincide with $\boldsymbol{\eta} \cdot \nabla u^-$ and $\boldsymbol{\eta} \cdot \nabla u^+$ respectively. This can be seen through Green's first identity (see, e.g., [185, Theorem 2.7.4]). Third, we observe that the one-sided Neumann trace operators $\gamma_N^\pm$ can also be applied to functions of appropriate regularity that are defined globally on $\mathbb{R}^n$.

The next theorem should be read together with Definition 1.10 of the Neumann traces.

Theorem 1.11 ([185, Theorem 2.7.7])**.**
Let $\Omega^- \subset \mathbb{R}^n$ be a bounded Lipschitz domain with boundary $\partial\Omega$ and let $\Omega^+ := \mathbb{R}^n \setminus \overline{\Omega^-}$.

Then for each $s \in \{-,+\}$ the Neumann trace operator $\gamma_N^s \colon H^1_\Delta(\Omega^s) \to H^{-\frac{1}{2}}(\partial\Omega)$ is bounded. Additionally, for each $s \in \{-,+\}$, any $u^s \in H^1_\Delta(\Omega^s)$ and any $v^s \in H^1_{\mathrm{loc}}(\Omega^s)$ such that either u^s or v^s has compact support, we have the relation

$$\langle \gamma_N^s u^s, \gamma^s v^s \rangle_{H^{-\frac{1}{2}}(\partial\Omega)\times H^{\frac{1}{2}}(\partial\Omega)} := \sigma_\eta(s) \int_{\Omega^s} \nabla u^s(\mathbf{x}) \cdot \nabla v^s(\mathbf{x})\, d\mathbf{x}, \tag{1.13}$$

where $\sigma_\eta(-) = 1$ and $\sigma_\eta(+) = -1$.

Consider the setting of Theorem 1.11. Two remarks are in order: First, the relation (1.13) can be shown to hold for more general functions that need not have compact support (see, e.g., [185, Theorem 2.9.6]). Second, it is possible to show that the Neumann trace operator can be extended to a bounded mapping from the Sobolev space $H^{\ell+1}_\Delta(\Omega^s)$ to $H^{\ell-\frac{1}{2}}(\partial\Omega)$ for every real number $\ell \in \big(-\frac{1}{2}, \frac{1}{2}\big)$. Additionally, if the set Ω^- is a C^∞ domain, then this result holds for all $\ell > -\frac{1}{2}$.

The next theorem is a simple consequence of the unique solvability of the interior Laplace problem with Neumann data.

Theorem 1.12 (Unique solvability of the interior Laplace problem with Neumann data)**.**

Let $\ell \in \big(-\frac{1}{2}, \frac{1}{2}\big)$, let $\Omega^- \subset \mathbb{R}^n$ be a bounded, connected Lipschitz domain with boundary $\partial\Omega$ and let the subspaces $\breve{H}^{\ell-\frac{1}{2}}(\partial\Omega) \subset H^{\ell-\frac{1}{2}}(\partial\Omega)$ and $\breve{H}^{\ell+1}_\Delta(\Omega^-) \subset H^{\ell+1}_\Delta(\Omega^-)$ be defined as

$$\begin{aligned}
\breve{H}^{\ell-\frac{1}{2}}(\partial\Omega) &:= \big\{\psi \in H^{\ell-\frac{1}{2}}(\partial\Omega) \colon \langle \psi, 1\rangle_{H^{\ell-\frac{1}{2}}(\partial\Omega)\times H^{-\ell+\frac{1}{2}}(\partial\Omega)} = 0\big\},\\
\breve{H}^{\ell+1}_\Delta(\Omega^-) &:= \big\{u \in H^{\ell+1}_\Delta(\Omega^-) \colon \int_{\partial\Omega} \gamma u = 0\big\}.
\end{aligned}$$

Then the restriction of the Neumann trace operator $\gamma_N^- \colon \breve{H}^{\ell+1}_\Delta(\Omega^-) \to \breve{H}^{\ell-\frac{1}{2}}(\partial\Omega)$ has a bounded inverse which we denote $\mathcal{E}^N_{\Delta,\Omega^-}$. Additionally, if the set Ω^- is a C^∞ domain, then this result also holds for all $\ell > -\frac{1}{2}$.

We conclude this section by defining one additional linear operator on the trace spaces which will be of fundamental importance in the first part of the dissertation.

Definition 1.13 (Dirichlet-to-Neumann map)**.**
Let $\ell \in \big(\frac{1}{2}, \frac{3}{2}\big)$ be a real number, let $\Omega^- \subset \mathbb{R}^n$ be a bounded Lipschitz domain with boundary $\partial\Omega$, and let the inverse Dirichlet trace operator $\mathcal{E}_{\Delta,\Omega^-} \colon H^{\ell-\frac{1}{2}}(\partial\Omega) \to H^\ell_\Delta(\Omega^-)$ be defined as in Theorem 1.8. Then we define the so-called (interior) Dirichlet-to-Neumann map $\mathrm{DtN} \colon H^{\ell-\frac{1}{2}}(\partial\Omega) \to H^{\ell-\frac{3}{2}}(\partial\Omega)$ as

$$\mathrm{DtN} := \gamma_N^- \circ \mathcal{E}_{\Delta,\Omega^-}.$$

Remark 1.14. Consider the setting of Definition 1.13. In view of Theorems 1.8 and 1.11, we see that the Dirichlet-to-Neumann map $\mathrm{DtN} \colon H^{\ell-\frac{1}{2}}(\partial\Omega) \to H^{\ell-\frac{3}{2}}(\partial\Omega)$ is bounded. Additionally, if Ω^- is a C^∞ domain, then this result holds for all indices $\ell > -\frac{1}{2}$.

Remark 1.15. Consider the setting of Definition 1.13. If the Lipschitz domain Ω^- is the union of disjoint bounded sets, say $\Omega^- := \cup_{j=1}^N \Omega_i$, then the Dirichlet-to-Neumann map can be viewed as a *local* operator in the following sense: Given $\lambda \in H^{\frac{1}{2}}(\partial\Omega)$, the output $\mathrm{DtN}\lambda|_{\partial\Omega_i}$ depends only on $\lambda|_{\partial\Omega_i}$. This fact will be used repeatedly in Part I of this dissertation.

1.4 Introduction to Boundary Integral Operators

The goal of this section is to provide a concise, self-contained introduction to potential theory and boundary integral operators. There is a vast literature on the integral equation formalism for general elliptic systems of second-order partial differential equations, and the interested reader can, for instance, refer to the textbooks [7, 105, 118, 147, 185, 195]. In view of the governing equations for polarisable electrostatics derived in Section 1.2 however, we will restrict our attention to the case of the Laplace operator. Moreover, we will follow the variational approach presented in [185].

Throughout this section, we will assume that $\Omega^- \subset \mathbb{R}^3$ is a bounded Lipschitz domain with boundary denoted $\partial\Omega$, and we define $\Omega^+ := \mathbb{R}^3 \setminus \overline{\Omega^-}$. Furthermore, we will adopt the notation and definitions introduced in Section 1.3. To begin with, we introduce the notion of the fundamental solution to the Laplace equation in three spatial dimensions.

Definition 1.16 (Fundamental Solution)**.** Let $G\colon \mathbb{R}^3\backslash\{0\} \to \mathbb{R}$ be defined as the function with the property that for all $\mathbf{x} \in \mathbb{R}^3 \setminus \{0\}$ it holds that

$$G(\mathbf{x}) = \frac{1}{4\pi|\mathbf{x}|}.$$

Then we say that G is the fundamental solution of the Laplace equation in $\mathbb{R}^3$.

The following property explains why the mapping G defined through Definition 1.16 is known as the fundamental solution of the Laplace equation.

Lemma 1.17. *Let $\delta_0 \in \big(C_0^\infty(\mathbb{R}^3)\big)^*$ denote the so-called Dirac delta distribution located at the origin $0 \in \mathbb{R}^3$, and let $G\colon \mathbb{R}^3 \setminus \{0\} \to \mathbb{R}$ be the fundamental solution of the Laplace equation in $\mathbb{R}^3$ as defined in Definition 1.16. Then G satisfies*

$$-\Delta G(\mathbf{x}) = 0 \qquad \forall \mathbf{x} \in \mathbb{R}^3 \setminus \{0\},$$

and

$$-\int_{\mathbb{R}^3} f(\mathbf{x})\Delta G(\mathbf{x})\, dx = f(0) \qquad \forall f \in C_0^\infty(\mathbb{R}^3),$$

i.e., $-\Delta G = \delta_0$ in the sense of distributions on $C_0^\infty(\mathbb{R}^3)$.

Convolutions of the fundamental solution G play an important role in the subsequent analysis. Indeed, we have the following definition.

Definition 1.18 (Newton Potential)**.** Let $G\colon \mathbb{R}^3 \setminus \{0\} \to \mathbb{R}$ be the fundamental solution of the Laplace equation in $\mathbb{R}^3$ as defined in Definition 1.16. We define the linear mapping $\mathcal{N}\colon C_0^\infty(\mathbb{R}^3) \to C^\infty(\mathbb{R}^3)$ as the function with the property that

$$(\mathcal{N}f)(\mathbf{x}) := \int_{\mathbb{R}^3} G(\mathbf{x}-\mathbf{y})f(\mathbf{y})\,d\mathbf{y} \qquad \forall \mathbf{x} \in \mathbb{R}^3,\ \forall f \in C_0^\infty(\mathbb{R}^3),$$

and we say that $\mathcal{N}$ is the Newton potential.

The Newton potential is the basic building block for constructing the volumic and boundary integral operators which will be the objects of our study. Before proceeding further, let us point out that it is possible to substantially extend the domain of definition of the Newton potential.

Lemma 1.19. *The Newton potential defined through Definition 1.18 can be extended through duality as a linear mapping* $\mathcal{N}\colon \big(C^\infty(\mathbb{R}^3)\big)^* \to \big(C_0^\infty(\mathbb{R}^3)\big)^*$*. Moreover, for any* $s \in \mathbb{R}$ *the Newton potential extends to a bounded linear operator* $\mathcal{N}\colon H^s_{\mathrm{comp}}(\mathbb{R}^3) \to H^{s+2}_{\mathrm{loc}}(\mathbb{R}^3)$*.*

In order to define the so-called layer potentials, we require the notion of certain adjoint operators.

Definition 1.20. We define the linear operators $\gamma^*\colon H^{-\frac{1}{2}}(\partial\Omega) \to \big(C^\infty(\mathbb{R}^3)\big)^*$ and $\gamma_N^*\colon H^{\frac{1}{2}}(\partial\Omega) \to \big(C^\infty(\mathbb{R}^3)\big)^*$ as mappings with the property that for all $\nu \in H^{-\frac{1}{2}}(\partial\Omega)$, all $\psi \in H^{\frac{1}{2}}(\partial\Omega)$ and all $\phi \in C^\infty(\mathbb{R}^3)$ it holds that

$$\begin{aligned}\langle \gamma^*\nu, \phi\rangle_{C^\infty(\mathbb{R}^3)^*\times C^\infty(\mathbb{R}^3)} &:= \langle \nu, \gamma\phi\rangle_{H^{-\frac{1}{2}}(\partial\Omega)\times H^{\frac{1}{2}}(\partial\Omega)},\\ \langle \gamma_N^*\psi, \phi\rangle_{C^\infty(\mathbb{R}^3)^*\times C^\infty(\mathbb{R}^3)} &:= \langle \psi, \boldsymbol{\eta}\cdot\nabla\phi\rangle_{H^{\frac{1}{2}}(\partial\Omega)\times H^{-\frac{1}{2}}(\partial\Omega)}.\end{aligned}$$

Here, γ denotes the Dirichlet trace operator as defined in Theorem 1.6, and $\boldsymbol{\eta}$ denotes the unit normal vector on the boundary $\partial\Omega$ that points towards the exterior, i.e., Ω^+.

Equipped with Lemma 1.19 and Definition 1.20, we can now define the single layer and double layer potentials.

Definition 1.21 (Layer Potentials)**.**
Let $\mathcal{N}\colon \big(C^\infty(\mathbb{R}^3)\big)^* \to \big(C_0^\infty(\mathbb{R}^3)\big)^*$ denote the Newton potential defined through Definition 1.18 and let the adjoint operators $\gamma^*\colon H^{-\frac{1}{2}}(\partial\Omega) \to \big(C^\infty(\mathbb{R}^3)\big)^*$ and $\gamma_N^*\colon H^{\frac{1}{2}}(\partial\Omega) \to \big(C^\infty(\mathbb{R}^3)\big)^*$ be defined through Definition 1.20. We define the linear mappings $\mathcal{S}\colon H^{-\frac{1}{2}}(\partial\Omega) \to \big(C_0^\infty(\mathbb{R}^3)\big)^*$ and $\mathcal{D}\colon H^{\frac{1}{2}}(\partial\Omega) \to \big(C_0^\infty(\mathbb{R}^3)\big)^*$ as

$$\mathcal{S} := \mathcal{N}\gamma^* \qquad \text{and} \qquad \mathcal{D} := \mathcal{N}\gamma_N^*,$$

and we say that $\mathcal{S}$ is the single layer potential and $\mathcal{D}$ is the double layer potential.

Consider the layer potentials defined through Definition 1.21. One may suspect that, similar to the Newton potential, it is possible to extend the single and double layer potentials as bounded mappings between Sobolev spaces. Indeed, we have the following result.

Theorem 1.22. *Let $s \in \left(-\frac{1}{2}, \frac{1}{2}\right)$ be a real number. Then the single and double layer potentials defined through Definition 1.21 extend to bounded linear operators*

$$\mathcal{S}\colon H^{-\frac{1}{2}+s}(\partial\Omega) \to H^{1+s}_{\mathrm{loc}}(\mathbb{R}^3) \quad \text{and} \quad \mathcal{D}\colon H^{\frac{1}{2}+s}(\partial\Omega) \to H^{1+s}_{\Delta}(\mathbb{R}^3 \setminus \partial\Omega).$$

Additionally, if the set Ω^- is a C^∞ domain, then the above mapping properties hold for all $s > -\frac{1}{2}$.

The single and double layer potentials have several important properties which we state in the form of the following theorem.

Theorem 1.23 (Properties of Single and Double Layer Potentials)**.**
Let $s \in \left(-\frac{1}{2}, \frac{1}{2}\right)$ be a real number, and let the single layer potential $\mathcal{S}\colon H^{-\frac{1}{2}+s}(\partial\Omega) \to H^{1+s}_{\mathrm{loc}}(\mathbb{R}^3)$ and double layer potential $\mathcal{D}\colon H^{\frac{1}{2}+s}(\partial\Omega) \to H^{1+s}_{\Delta}(\mathbb{R}^3 \setminus \partial\Omega)$ be defined as in Definition 1.21. Then the following hold:

1. *For functions $u \in L^1(\partial\Omega)$ we have the explicit representations*

$$(\mathcal{S}u)(\mathbf{x}) := \int_{\partial\Omega} u(\mathbf{y})\, \frac{1}{4\pi|\mathbf{x}-\mathbf{y}|}\, d\mathbf{y} \qquad \forall \mathbf{x} \in \mathbb{R}^3 \setminus \partial\Omega,$$
$$(\mathcal{D}u)(\mathbf{x}) := \int_{\partial\Omega} u(\mathbf{y})\, \boldsymbol{\eta} \cdot \nabla_{\mathbf{y}} \frac{1}{4\pi|\mathbf{x}-\mathbf{y}|}\, d\mathbf{y} \qquad \forall \mathbf{x} \in \mathbb{R}^3 \setminus \partial\Omega,$$

   where $\nabla_{\mathbf{y}}$ denotes the usual gradient with respect to the variable $\mathbf{y}$.

2. *For all $\nu \in H^{-\frac{1}{2}+s}(\partial\Omega)$ it holds that*

$$\Delta \mathcal{S}\nu = 0 \quad \text{on } \mathbb{R}^3 \setminus \partial\Omega,$$

   i.e., the single layer potential maps into the space of harmonic functions on $\mathbb{R}^3 \setminus \partial\Omega$.

3. *For all $\nu \in H^{-\frac{1}{2}+s}(\partial\Omega)$ and all $\psi \in H^{\frac{1}{2}+s}(\partial\Omega)$ we have the jump relations*

$$\gamma^+(S\nu) - \gamma^-(S\nu) = 0 \quad \text{and} \quad \gamma^+(D\psi) - \gamma^-(D\psi) = \psi,$$
$$\gamma_N^+(S\nu) - \gamma_N^-(S\nu) = -\nu \quad \text{and} \quad \gamma_N^+(D\psi) - \gamma_N^-(D\psi) = 0.$$

4. *If the set Ω^- is a C^∞ domain, then the above results can be extended to the range of indices $s > -\frac{1}{2}$.*

5. *The following mapping property holds: For all $\nu \in H^{-\frac{1}{2}}(\partial\Omega)$ and $\psi \in H^{\frac{1}{2}}(\partial\Omega)$ it holds that*

$$\mathcal{S}\nu|_{\Omega^+} \in H^1(\Delta;\Omega^+), \qquad \text{and} \qquad \mathcal{D}\psi|_{\Omega^+} \in H^1(\Delta;\Omega^+),$$

   where the Sobolev space $H^1(\Delta;\Omega^+)$ is the space of harmonic functions in $H^1_{\mathrm{loc}}(\Omega^+)$ that satisfy the exterior decay condition associated with the Laplace problem (see Definition 2.2 for a formal definition).

Remark 1.24. Consider Definition 1.21 of the single and double layer potentials. Theorems 1.22 and 1.23 imply in particular that the layer potential of any arbitrary function of appropriate regularity is harmonic on $\mathbb{R}^3 \setminus \partial\Omega$ and satisfies the correct decay condition associated with charge distributions of bounded support. This simple observation forms the core of the boundary integral equation formalism.

Using the single and double layer potentials and the Dirichlet and Neumann mappings introduced in Section 1.3, we now introduce four key boundary integral operators.

Definition 1.25. Let $s \in \left(-\frac{1}{2}, \frac{1}{2}\right)$ be a real number and let the single layer potential $\mathcal{S}\colon H^{-\frac{1}{2}+s}(\partial\Omega) \to H^{1+s}_{\text{loc}}(\mathbb{R}^3)$ and double layer potential $\mathcal{D}\colon H^{\frac{1}{2}+s}(\partial\Omega) \to H^{1+s}_{\Delta}(\mathbb{R}^3 \setminus \partial\Omega)$ be defined as in Definition 1.21. Then we define the bounded linear operators

$$\begin{aligned}
\mathcal{V} &:= \left(\gamma^- \circ \mathcal{S}\right) && : H^{-\frac{1}{2}+s}(\partial\Omega) \to H^{\frac{1}{2}+s}(\partial\Omega),\\
\mathcal{K} &:= \left(\gamma^- \circ \mathcal{D} + \frac{1}{2}I\right) && : H^{\frac{1}{2}+s}(\partial\Omega) \to H^{\frac{1}{2}+s}(\partial\Omega),\\
\mathcal{K}^* &:= \left(\gamma_N^- \circ \mathcal{S} - \frac{1}{2}I\right) && : H^{-\frac{1}{2}+s}(\partial\Omega) \to H^{-\frac{1}{2}+s}(\partial\Omega),\\
\mathcal{W} &:= -\left(\gamma_N^- \circ \mathcal{D}\right) && : H^{\frac{1}{2}+s}(\partial\Omega) \to H^{-\frac{1}{2}+s}(\partial\Omega).
\end{aligned}$$

Here, I denotes the identity operator on the relevant trace space, and we say that the mapping $\mathcal{V}$ is the single layer boundary operator, the mapping $\mathcal{K}$ is the double layer boundary operator, the mapping $\mathcal{K}^*$ is the adjoint double layer boundary operator, and the mapping $\mathcal{W}$ is the hypersingular boundary operator.

Remark 1.26. Consider Definition 1.25 of the boundary integral operators $\mathcal{V}, \mathcal{K}, \mathcal{K}^*$ and $\mathcal{W}$. As usual, if the set Ω^- is a C^∞ domain, then these mappings can be defined as bounded linear operators on the relevant Sobolev trace spaces for the range of indices $s > -\frac{1}{2}$.

The boundary integral operators defined through Definition 1.25 are the subject of a detailed analysis in the literature and we direct the interested read to the previously mentioned textbooks [7, 105, 118, 147, 185, 195] for a comprehensive discussion. Here, we focus our attention on some of the main properties that will be used in the sequel.

Theorem 1.27 (Properties of the Single Layer Boundary Operator)**.**
Let the single layer boundary operator $\mathcal{V}\colon H^{-\frac{1}{2}}(\partial\Omega) \to H^{\frac{1}{2}}(\partial\Omega)$ be defined as in Definition 1.25. Then the following hold:

1. *For any function $\nu \in L^\infty(\partial\Omega)$ we have the explicit representation*

$$(\mathcal{V}\nu)(\mathbf{x}) = \int_{\partial\Omega} G(\mathbf{x}-\mathbf{y})\nu(\mathbf{x})\,d\mathbf{x} \qquad \forall \mathbf{x} \in \partial\Omega.$$

2. *The operator $\mathcal{V}$ is Hermitian and coercive, i.e., there exists a constant $c_{\mathcal{V}} > 0$ such that for all functions $\sigma \in H^{-\frac{1}{2}}(\partial\Omega)$ it holds that*

$$\langle \sigma, \mathcal{V}\sigma \rangle_{H^{-\frac{1}{2}}(\partial\Omega)\times H^{\frac{1}{2}}(\partial\Omega)} \geq c_{\mathcal{V}} \|\sigma\|^2_{H^{-\frac{1}{2}}(\partial\Omega)}.$$

Theorem 1.27 has two important consequences:

a) Existence of inverse: We deduce that the inverse $\mathcal{V}^{-1}\colon H^{\frac{1}{2}}(\partial\Omega) \to H^{-\frac{1}{2}}(\partial\Omega)$ is also a Hermitian, coercive and bounded linear operator with continuity constant $\frac{1}{c_{\mathcal{V}}}$. We emphasise here that the coercivity constant $c_{\mathcal{V}}$ a priori depends on the geometry of Ω^-. The precise dependence of $c_{\mathcal{V}}$ on Ω^- which is the union of non-intersecting open balls is a key point in our analysis and will be the subject of further discussion in Chapter 3.

b) Induced norms: It follows that $\mathcal{V}$ induces a norm $\|\cdot\|_{\mathcal{V}}$ and associated inner product $(\cdot,\cdot)_{\mathcal{V}}$ on $H^{-\frac{1}{2}}(\partial\Omega)$, and the inverse $\mathcal{V}^{-1}$ induces a norm $\|\cdot\|_{\mathcal{V}^{-1}}$ and associated inner product $(\cdot,\cdot)_{\mathcal{V}^{-1}}$ on $H^{\frac{1}{2}}(\partial\Omega)$. It can be shown that the norm $\|\cdot\|_{\mathcal{V}^{-1}}$ is equivalent to the usual Sobolev-Slobodeckij norm $\|\cdot\|_{H^{\frac{1}{2}}(\partial\Omega)}$ on $H^{\frac{1}{2}}(\partial\Omega)$ and that the norm $\|\cdot\|_{\mathcal{V}}$ is equivalent to the usual dual norm $\|\cdot\|_{H^{-\frac{1}{2}}(\partial\Omega)}$ on $H^{-\frac{1}{2}}(\partial\Omega)$.

A similar theorem can be proven for the hypersingular boundary operator.

Theorem 1.28 (Properties of the Hypersingular Boundary Operator)**.**
Assume that the Lipschitz domain Ω^- is connected. The hypersingular boundary operator $\mathcal{W}\colon H^{\frac{1}{2}}(\partial\Omega) \to H^{-\frac{1}{2}}(\partial\Omega)$ is Hermitian, non-negative, and coercive on a subspace of $H^{\frac{1}{2}}(\partial\Omega)$, i.e., there exists a constant $c_{\mathcal{W}} > 0$ such that for all functions $\lambda \in H^{\frac{1}{2}}(\partial\Omega)$ with $\int_{\partial\Omega}\lambda(\mathbf{x})\,d\mathbf{x} = 0$, it holds that

$$\langle \mathcal{W}\lambda, \lambda\rangle_{H^{-\frac{1}{2}}(\partial\Omega)\times H^{\frac{1}{2}}(\partial\Omega)} \geq c_{\mathcal{W}}\|\lambda\|^2_{H^{\frac{1}{2}}(\partial\Omega)}. \tag{1.14}$$

Additionally, if the domain Ω^- is the union of disjoint bounded sets, say $\Omega^- := \cup_{i=1}^N \Omega_i$, then $\mathcal{W}$ is Hermitian and non-negative, and coercivity in the sense of Inequality (1.14) holds for all $\lambda \in H^{\frac{1}{2}}(\partial\Omega)$ such that $\sum_{i=1}^N \left|\int_{\partial\Omega_i}\lambda(\mathbf{x})\,d\mathbf{x}\right| = 0$.

Remark 1.29. Consider the setting of Theorem 1.28. Henceforth, we denote by $\breve{H}^{\frac{1}{2}}(\partial\Omega) \subset H^{\frac{1}{2}}(\partial\Omega)$ the subspace on which the hypersingular boundary operator is coercive. As noted in Theorem 1.28, the precise definition of this subspace depends on whether the Lipschitz domain Ω^- is connected or is the union of disjoint sets. We remark that this subspace will be the subject of further discussion in Chapter 3.

The next lemma establishes some conditions on the coercivity constants of the single layer and hypersingular boundary operator.

Lemma 1.30. *The coercivity constants of the single layer and hypersingular boundary operators satisfy $c_{\mathcal{V}}c_{\mathcal{W}} \leq \frac{1}{4}$. Therefore the constant*

$$c_{\mathcal{K}} := \frac{1}{2} + \sqrt{\frac{1}{4} - c_{\mathcal{V}}c_{\mathcal{W}}},$$

is well-defined and $c_{\mathcal{K}} \in \left[\frac{1}{2}, 1\right)$.

One of the core results in the theory of integral equations are the so-called Calderón identities, which relate the various boundary integral operators defined through Definition 1.25. For the purpose of this dissertation, we require only one consequence of these identities, which relates the boundary integral operators defined here to the Dirichlet-to-Neumann map introduced in Section 1.3.

Lemma 1.31. *Let the interior Dirichlet-to-Neumann map* $\mathrm{DtN}\colon H^{\frac{1}{2}}(\partial\Omega) \to H^{-\frac{1}{2}}(\partial\Omega)$ *be defined as in Definition 1.13, let* $I\colon H^{\frac{1}{2}}(\partial\Omega) \to H^{\frac{1}{2}}(\partial\Omega)$ *denote the identity map, and let the boundary integral operators* $\mathcal{V}\colon H^{-\frac{1}{2}}(\partial\Omega) \to H^{\frac{1}{2}}(\partial\Omega)$, $\mathcal{K}\colon H^{\frac{1}{2}}(\partial\Omega) \to H^{\frac{1}{2}}(\partial\Omega)$, $\mathcal{K}^*\colon H^{-\frac{1}{2}}(\partial\Omega) \to H^{-\frac{1}{2}}(\partial\Omega)$, *and* $\mathcal{W}\colon H^{\frac{1}{2}}(\partial\Omega) \to H^{-\frac{1}{2}}(\partial\Omega)$ *be defined as in Definition 1.25. Then it holds that*

$$\mathrm{DtN} = \mathcal{V}^{-1}\left(\frac{1}{2}I + \mathcal{K}\right) = \mathcal{W} + \left(\frac{1}{2}I + \mathcal{K}^*\right)\mathcal{V}^{-1}\left(\frac{1}{2}I + \mathcal{K}\right).$$

The next result concerns the boundedness of the boundary integral operator $\frac{1}{2}I + \mathcal{K}$ which appears in Lemma 1.31. This result can be found, for instance, in [185, Theorem 3.8.7] or [105, Theorem 3.1].

Lemma 1.32. *Let the constant* $c_{\mathcal{K}} > 0$ *be defined as in Lemma 1.30, let* $I\colon H^{\frac{1}{2}}(\partial\Omega) \to H^{\frac{1}{2}}(\partial\Omega)$ *denote the identity map, let the boundary integral operator* $\mathcal{K}\colon H^{\frac{1}{2}}(\partial\Omega) \to H^{\frac{1}{2}}(\partial\Omega)$ *be defined as in Definition 1.25, and let* $\|\cdot\|_{\mathcal{V}^{-1}}$ *denote the norm induced by the inverse single layer boundary* $\mathcal{V}^{-1}$ *as stated after Theorem 1.27. Then for all* $\lambda \in H^{\frac{1}{2}}(\partial\Omega)$ *it holds that*

$$\left\|\left(\frac{1}{2}I + \mathcal{K}\right)\lambda\right\|_{\mathcal{V}^{-1}} \leq c_{\mathcal{K}}\|\lambda\|_{\mathcal{V}^{-1}}.$$

We conclude this section by stating some fundamental nomenclature from the theory of integral equations that we will use throughout this dissertation.

Nomenclature 1. Let $f \in H^{\frac{1}{2}}(\partial\Omega)$ and $g \in H^{-\frac{1}{2}}(\partial\Omega)$ be given, let the boundary integral operators $\mathcal{V}\colon H^{-\frac{1}{2}}(\partial\Omega) \to H^{\frac{1}{2}}(\partial\Omega)$ and $\mathcal{W}\colon H^{\frac{1}{2}}(\partial\Omega) \to H^{-\frac{1}{2}}(\partial\Omega)$ be defined as in Definition 1.25, and consider the following boundary integral equations:

BIE F1) Find $\sigma \in H^{-\frac{1}{2}}(\partial\Omega)$ such that

$$\mathcal{V}\sigma = f.$$

BIE F2) Find $\lambda \in H^{\frac{1}{2}}(\partial\Omega)$ such that

$$\mathcal{W}\lambda = g.$$

The boundary integral equations **F1)** and **F2)** are known as integral equations of the first kind. Intuitively, first kind integral equations are characterised by the fact that the unknown function appears only in the integrand associated with the underlying boundary integral operator.

Nomenclature 2. Let $f \in H^{\frac{1}{2}}(\partial\Omega)$ and $g \in H^{-\frac{1}{2}}(\partial\Omega)$ be given, let $\alpha \in (0,1)$ be a real number, let the boundary integral operators $\mathcal{K}\colon H^{\frac{1}{2}}(\partial\Omega) \to H^{\frac{1}{2}}(\partial\Omega)$ and $\mathcal{K}^*\colon H^{-\frac{1}{2}}(\partial\Omega) \to H^{-\frac{1}{2}}(\partial\Omega)$ be defined as in Definition 1.25, and consider the following equations:

BIE S1) Find $\lambda \in H^{\frac{1}{2}}(\partial\Omega)$ such that

$$\frac{1}{2}\lambda \pm \alpha\mathcal{K}\lambda = f.$$

BIE S2) Find $\sigma \in H^{-\frac{1}{2}}(\partial\Omega)$ such that

$$\frac{1}{2}\sigma \pm \alpha\mathcal{K}^*\sigma = g.$$

The boundary integral equations **S1)** and **S2)** are known as integral equations of the second kind. Intuitively, second kind integral equations are characterised by the fact that the unknown function appears both inside and outside the integrand associated with the underlying boundary integral operator.

Part I

Integral Equations for N-Body Polarisable Electrostatics

2

Introduction

2.1 Overview and Motivation

The so-called *N-body problem* is a general term used to describe a vast category of physical problems involving the interaction of a large number of objects. Such problems arise in a variety of contexts in fields as diverse as quantum mechanics, molecular dynamics, astrophysics and electrostatics but the problem originated from attempts of early astronomers to explain the motion of celestial objects interacting due to gravity. Indeed, one of the first references to the N-body problem can be traced to the Principia Mathematica wherein Newton considered the motion of celestial bodies in the solar system [159]. Beginning with the work of Henri Poincaré [166], which incidentally led to the development of chaos theory, a significant amount of evidence has been accumulated that obtaining an analytic solution to the N-body gravitational problem in a tractable manner is not possible (see, e.g., [171, 197]). As a consequence, there has been a great deal of interest in developing numerical methods that can efficiently compute approximate solutions to the N-body gravitational problem. These attempts have led to the development of extremely efficient numerical algorithms such as tree codes (see, e.g., [3, 9, 15, 48, 81, 122]) including the so-called Fast Multipole method (see, e.g., [26, 85, 86, 87]), or particle mesh and P3M methods (see, e.g., [57, 100, 113])

The N-body problem is also ubiquitous in the discipline of chemical physics when one considers phenomena involving large-scale electrostatic interactions. Indeed, understanding the behaviour of charged colloidal particles (see, e.g., [10, 52, 106, 124, 139, 151, 152, 203]) or the fabrication of binary nanoparticle superlattices and so-called Coulombic crystals (see, e.g., [12, 16, 91, 116, 146, 177, 190]), or the assembly of proteins and other cellular structures (see, e.g., [53, 60, 107, 164, 184, 202, 210]) all require knowledge of Coulomb interactions between a large number of physical objects.

Many such electrostatic phenomena involve interactions between charged, spherical dielectric particles embedded in a dielectric medium, undergoing mutual polarisation. One is then typically interested in either the total electrostatic energy of the system or the electrostatic force acting on each particle, both of which can be derived from knowl-

edge of the electric potential generated by these particles. Knowledge of the forces in particular is required if one wishes to perform time-dynamic simulations or study assembly processes of charged particles (see, e.g., [47, 123, 168, 212] as well as the references on superlattices given above). In contrast to the much simpler case of the gravitational attraction between masses or the electrostatic interaction between point-charges however, a full description of the electric potential generated by such polarisable particles cannot be obtained as simply the sum of pairwise interactions. Instead, the potential is realised as the solution to a PDE, posed on the full three-dimensional space with interface conditions on the boundaries of the spherical particles (see, e.g., [16, 127]). Since this PDE cannot generally be solved analytically, it becomes necessary to use some numerical method to first compute the *approximate* electric potential and then use this to obtain *approximations* to either the total energy or the force acting on each particle. It is therefore of great interest to develop efficient numerical algorithms that can yield approximations to the energy and the forces with an acceptable accuracy.

A number of different approaches to this so-called *N-body dielectric spheres electrostatic interaction* problem have been proposed in the literature (see, e.g., [11, 39, 70, 130, 138, 152, 170, 209]). Unfortunately, many of these methods suffer from the handicap that they may become computationally prohibitive if the number of particles is very large. Additionally, these method have typically been formulated in a manner that makes them unsuitable for a systematic numerical analysis. As a consequence, it is usually not possible to theoretically evaluate the accuracy of these methods and, in particular, to explore the dependence of the accuracy on the number of dielectric particles N.

A natural measure of the quality of an N-body numerical method is the scaling of the accuracy and computational cost of the algorithm with N. To fix terminology

- We say that an N-body numerical method is *N-error stable* if, for a fixed number of degrees of freedom per object and assuming other properties such as the minimum inter-sphere separation are kept constant, the relative error in the approximate solution does not increase with N. Establishing that a numerical method is N-error stable requires a rigorous numerical analysis of the algorithm in question, which immediately rules out many of the existing algorithms cited above.

- We say that an N-body numerical method is *linear scaling in cost* if, for a fixed number of degrees of freedom per object and assuming other properties such as the minimum inter-sphere separation are kept constant, the numerical method requires $\mathcal{O}(N)$ operations to compute an approximate solution with a given and fixed tolerance. Typically, linear scaling in cost requires the use of fast summation methods such as tree codes, the FMM, or particle-mesh and P3M methods (see the references cited above). If the N-body numerical method also requires the solution of a linear system (which is indeed the case for the dielectric spheres problem), then one would additionally have to show that the number of linear solver iterations required to obtain an approximate solution does not grow with N. Again, this requires a systematic numerical analysis of the algorithm in question which is difficult for many of the existing numerical methods in the literature.

- Finally, we say that an N-body numerical method is *linear scaling in accuracy* if it is both N-error stable and linear scaling in cost. Thus, linear scaling in accuracy methods can be viewed as the gold-standard for N-body problems since these methods require only $\mathcal{O}(N)$ operations to compute an approximate solution with a given average error (the total error scaled by N) or relative error.

E. Lindgren and coworkers recently proposed in [127], a computational method based on a Galerkin discretisation of a second kind boundary integral equation that describes the so-called *induced surface charge* resulting on the surface of charged dielectric spherical particles embedded in a homogenous dielectric medium and undergoing mutual polarisation. Numerical experiments indicated that this algorithm displayed some promising behaviour:

O1) For a fixed number of degrees of freedom per sphere, the relative and average error (the total error scaled by N) in the approximate induced surface charge remained bounded when increasing the number of dielectric spheres;

O2) For a fixed number of dielectric spheres, the total error in the approximate induced surface decayed exponentially when increasing the degrees of freedom per sphere;

O3) Through the use of a modified FMM, the numerical method achieved computational complexity that scaled linearly with respect to the number of dielectric spheres.

O1) and O2) deal with the accuracy of the method and O3) gives a measure of the computational scalability of the numerical algorithm. Taken together, these numerical observations suggest empirically that the method proposed in [127] is *linear scaling in accuracy*, i.e., in order to obtain the approximate induced surface charge with a fixed average or relative error, the computational cost of the algorithm scales as $\mathcal{O}(N)$. Consequently, the integral equation-based approach proposed by Lindgren at al. represented a significant advance in the state-of-the-art for the computation of the electrostatic interactions between a large number of charged particles undergoing mutual polarisation.

It is now natural to ask if one can provide a rigorous mathematical justification for the behaviour O1)-O3) exhibited by this numerical method. Moreover, assuming that the answer is yes, can one also extend such mathematical results for the induced surface charge to other physical quantities of interest including the total electrostatic energy of the system and the electrostatic forces acting on each dielectric particle? Chapters 3-5 of this dissertation deal precisely with these questions. More specifically,

- In **Chapter 3** of this dissertation, we will show that the computational method proposed in [127] is N-error stable for the computation of the induced surface charge and total electrostatic energy in the system. More precisely, we will prove that

  (a) For any fixed geometrical configuration of non-intersecting spherical dielectric particles, the integral equation formulation of the second kind proposed in

[127] that describes the induced surface charges resulting on these dielectric spheres undergoing mutual polarisation is well-posed;

(b) For any fixed geometrical configuration of non-intersecting spherical dielectric particles, the Galerkin discretisation of this second-kind integral equation is also well-posed;

(c) For any fixed geometrical configuration of non-intersecting spherical dielectric particles, there exists an upper bound on the relative error of the approximate solution that does not explicitly depend on the number N of dielectric spheres in the system. As a consequence, we will deduce N-independent error estimates for any family of geometrical configurations that satisfies certain geometrical assumptions which are described in detail later;

(d) For any fixed geometrical configuration of non-intersecting spherical dielectric particles, given certain assumptions on the regularity of the exact solution, the total error of the approximate solution decays exponentially as the degrees of freedom per sphere are increased.

The content of this chapter is based on [96].

- In **Chapter 4** of this dissertation, we will present a detailed complexity analysis of the Galerkin method proposed by Lindgren and coworkers with the goal of showing that the method is also linear scaling in cost for the computation of the induced surface charge and total electrostatic energy in the system. Our main result will show that– under mild assumptions– the number of linear solver iterations required to solve the linear system obtained from the Galerkin discretisation up to a given tolerance is independent of N. Since the FMM allows us to compute approximate matrix-vector products involving the solution matrix using $\mathcal{O}(N)$ operations, it will follow that, under appropriate geometrical assumptions, an approximate solution with a given and fixed relative error can indeed be constructed by means of an iterative solver using only $\mathcal{O}(N)$ operations and thus the numerical method is linear scaling in cost. We will thus prove that the Galerkin method proposed by E. Lindgren and coworkers is linear scaling in accuracy for the computation of the induced surface charge and total electrostatic energy in the system. The content of this chapter is based on [97].

- Finally, in **Chapter 5** of this dissertation, we will propose and systematically analyse an efficient numerical method, based on the Galerkin BIE framework of Lindgren et al. and using the FMM, for the computation of the electrostatic forces acting on charged, dielectric spherical particles embedded in a homogenous dielectric medium undergoing mutual polarisation. Using the analysis of **Chapters 3** and **4**, we will prove that, under suitable geometrical assumptions, this numerical method achieves linear scaling in accuracy for the computation of the forces. In order to demonstrate this claim, we will first derive convergence rates for the approximate electrostatic forces that are explicitly independent of N, and we will then present a linear scaling in cost solution strategy for the computation of the approximate forces. The content of this chapter is based on [98].

The remainder of Chapter 2 is organised as follows: In Section 2.2, we state the N-body dielectric spheres electrostatic interaction problem as a partial differential equation on the full space $\mathbb{R}^3$ with suitable transmission conditions on the boundaries of the spherical particles respectively. Next, using the integral equation formalism stated in Section 1.4, we formulate in Section 2.3, the N-body dielectric spheres electrostatic interaction problem as an integral equation of the second kind posed on the boundaries of the spherical dielectric particles. Finally, in Section 2.4, we review the literature on boundary integral equations for N-body problems with a special emphasis on second kind integral equations. Moreover, we discuss the limitations of the existing analysis of such integral equations which prevents us from using the classical well-posedness theory to perform our analysis.

2.2 PDE-based Formulation of the N-Body Dielectric Spheres Problem

The goal of this section is to state a PDE-based transmission problem that describes the electrostatic potential generated by a collection of dielectric particles undergoing mutual polarisation. Guided by the exposition in Section 1.2, we will first state the *modelling assumptions* under which the PDE is derived. Next, we will anticipate the mathematical analysis in Chapters 3-5 by stating precise conditions on the types of geometrical configurations we will consider.

Model assumptions:

Consider the discussion on polarisable electrostatics in Section 1.2. Since we wish to model the electrostatic interaction between dielectric particles, a number of 'pre-modelling' questions must first be answered. In particular, we must state how the geometry of the particles is described mathematically and specify the types of dielectric materials that constitute both the particles as well as the background medium. Additionally, we require assumptions on the free charge distributions that reside on each dielectric particle.

For the purpose of this dissertation, we impose the following modelling assumptions (**MA**):

MA1) We will model the dielectric particles as perfect spheres that can be represented mathematically by open balls in $\mathbb{R}^3$.

MA2) We will model each dielectric particle as being composed of a linear, homogenous, isotropic dielectric material, although we will allow different particles to have different constitutent materials. Thus, the relative permittivity of each particle can be described by a single scalar quantity and we will refer to this as the dielectric constant of each particle.

MA3) We will model the background medium as a linear, homogenous isotropic dielectric with dielectric constant that is different from the dielectric constants of the spherical particles.

MA4) We will assume (in the terminology of Chapter 1.2) that a free *surface* charge density σ_f resides on the *surface* of the spherical dielectric particles. Moreover, we will assume that there is no free charge density ρ_f in the *interior* of the particles.

MA5) We will model each spherical particle as a uniform, rigid body that undergoes no deformation under the action of electrostatic forces.

Each of the modelling assumptions **MA1)-MA5)** can be weakened, and this is the subject of on-going work. We will see in Chapters 3-5 however, that even with these assumptions in place, the model problem we consider leads to interesting physics and possesses a rich mathematical structure.

Geometric assumptions:

Next, we describe precisely the geometrical assumptions we impose on our model problem. As indicated at the start of this section, we are interested in studying geometrical configurations that are the unions of an arbitrary number N of non-intersecting spherical dielectric particles in three spatial dimensions. More specifically, our aim is to analyse the properties of the proposed numerical algorithm as the number N of particles in the system increases. In order to draw the correct conclusions from the mathematical analysis we perform in Chapters 3-5 however, we must impose certain assumptions on the types of geometries we consider. To this end, let $\mathcal{I}$ denote a countable indexing set. We consider a so-called family of geometries $\{\Omega_{\mathcal{F}}\}_{\mathcal{F}\in\mathcal{I}}$. Each element $\Omega_{\mathcal{F}} \subset \mathbb{R}^3$ in this family is the (set) union of a fixed number of non-intersecting open balls of varying locations and radii with associated dielectric constants, and therefore represents a particular physical geometric situation. It is easy to see that each element $\Omega_{\mathcal{F}}$ of this family of geometries is uniquely determined by the following four parameters:

- A non-zero number $N_{\mathcal{F}} \in \mathbb{N}$, which represents the total number of dielectric spherical particles that compose the geometry $\Omega_{\mathcal{F}}$;
- A collection of points $\{\mathbf{x}_i^{\mathcal{F}}\}_{i=1}^{N_{\mathcal{F}}} \in \mathbb{R}^3$, which represent the centres of the spherical particles composing the geometry $\Omega_{\mathcal{F}}$;
- A collection of positive real numbers $\{r_i^{\mathcal{F}}\}_{i=1}^{N_{\mathcal{F}}} \in \mathbb{R}$, which represent the radii of the spherical particles composing the geometry $\Omega_{\mathcal{F}}$;
- A collection of positive real numbers $\{\kappa_i^{\mathcal{F}}\}_{i=0}^{N} \in \mathbb{R}$. Here, $\kappa_0^{\mathcal{F}}$ denotes the dielectric constant of the external medium while $\{\kappa_i^{\mathcal{F}}\}_{i=1}^{N}$ represent the dielectric constants of each dielectric sphere.

Indeed, using the first three parameters we can define the open balls $\Omega_i^{\mathcal{F}} := \mathcal{B}_{r_i}(\mathbf{x}_i) \subset \mathbb{R}^3$, $i \in \{1, \dots, N_{\mathcal{F}}\}$ which represent the spherical dielectric particles composing the geometry $\Omega_{\mathcal{F}}$, i.e., $\Omega_{\mathcal{F}} = \cup_{i=1}^{N_{\mathcal{F}}} \Omega_i^{\mathcal{F}}$. Moreover, the fourth parameter $\{\kappa_i^{\mathcal{F}}\}_{i=0}^{N}$ denotes the dielectric constants associated with this geometry.

We now impose the following three assumptions on the above parameters:

GA1) [**Uniformly bounded radii**] There exist constants $r_-^\infty > 0$ and $r_+^\infty > 0$ such that

$$\inf_{\mathcal{F}\in\mathcal{J}} \min_{i=1,\dots,N_{\mathcal{F}}} r_i^{\mathcal{F}} > r_-^\infty \quad \text{and} \quad \sup_{\mathcal{F}\in\mathcal{J}} \max_{i=1,\dots,N_{\mathcal{F}}} r_i^{\mathcal{F}} < r_+^\infty.$$

GA2) [**Uniformly bounded minimal separation**] There exists a constant $\epsilon^\infty > 0$ such that

$$\inf_{\mathcal{F}\in\mathcal{J}} \min_{\substack{i,j=1,\dots,N_{\mathcal{F}} \\ i\neq j}} \left(|\mathbf{x}_i^{\mathcal{F}} - \mathbf{x}_j^{\mathcal{F}}| - r_i^{\mathcal{F}} - r_j^{\mathcal{F}}\right) > \epsilon^\infty.$$

GA3) [**Uniformly bounded dielectric constants**] There exist constants $\kappa_-^\infty > 0$ and $\kappa_+^\infty > 0$ such that

$$\inf_{\mathcal{F}\in\mathcal{J}} \min_{i=1,\dots,N_{\mathcal{F}}} \kappa^{\mathcal{F}} > \kappa_-^\infty \quad \text{and} \quad \sup_{\mathcal{F}\in\mathcal{J}} \max_{i=1,\dots,N_{\mathcal{F}}} \kappa^{\mathcal{F}} < \kappa_+^\infty.$$

In other words we assume that the family of geometries $\{\Omega_{\mathcal{F}}\}_{\mathcal{F}\in\mathcal{J}}$ we consider in this article describe physical situations where the radii of the dielectric spherical particles, the minimum inter-sphere separation distance and the dielectric constants are all uniformly bounded. These assumptions are necessary because, as we will show in Chapters 3-5, the mathematical bounds we derive, while explicitly independent of the number of dielectric particles $N_{\mathcal{F}}$, do depend on other geometrical parameters, and we would thus like to avoid situations where these geometric parameters degrade with increasing $N_{\mathcal{F}}$. We remark that from a practical perspective, these assumptions do not greatly limit the scope of our results. Indeed, in many physical applications one typically considers non-metallic dielectric particles which neither have vanishing or exploding dielectric constants nor vanishing or exploding radii (see, e.g., [91, 121, 128, 146, 192]).

Classical formulation of the PDE-based model problem

We are now ready to state the electrostatic interaction problem for dielectric spheres in terms of a classical PDE, i.e., a PDE involving continuous and smooth functions. We will assume that the modelling assumptions **MA1)-MA5)** hold. Moreover, for the remainder of this dissertation we will always consider a *fixed* geometry from the family of geometries $\{\Omega_{\mathcal{F}}\}_{\mathcal{F}\in\mathcal{J}}$ satisfying the assumptions **GA1)-GA3)**. To avoid bulky notation we will drop the superscript and subscript $\mathcal{F}$ and denote this geometry by Ω^-. The geometry is constructed as follows: Let $N \in \mathbb{N}$, let $\{\mathbf{x}_i\}_{i=1}^N \in \mathbb{R}^3$ be a collection of points in $\mathbb{R}^3$ and let $\{r_i\}_{i=1}^N \in \mathbb{R}$ be a collection of positive real numbers, and for each

$i \in \{1, \dots, N\}$ let $\Omega_i := \mathcal{B}_{r_i}(\mathbf{x}_i) \subset \mathbb{R}^3$ be the open ball of radius $r_i > 0$ centred at the point $\mathbf{x}_i$. Then $\Omega^- \subset \mathbb{R}^3$ is defined as $\Omega^- := \cup_{i=1}^N \Omega_i$. Furthermore, we define $\Omega^+ := \mathbb{R}^3 \setminus \overline{\Omega^-}$, and we write $\partial\Omega$ for the boundary of Ω^- and $\eta(\mathbf{x})$ for the unit normal vector at $\mathbf{x} \in \partial\Omega$ pointing towards the exterior of Ω^-. Moreover, we denote by $\{\kappa_i\}_{i=0}^N \in \mathbb{R}$ a collection of positive real numbers such that each κ_i, $i \in \{1, \dots, N\}$ is the dielectric constant of the particle represented by the open ball Ω_i, and κ_0 is the dielectric constant of the background medium. Notice that for each $i \in \{1, \dots, N\}$, either $\frac{\kappa_i - \kappa_0}{\kappa_0} \geq 0$ or $\frac{\kappa_i - \kappa_0}{\kappa_0} \in (-1, 0]$. An example of a typical geometrical configuration is displayed in Figure 2.1.

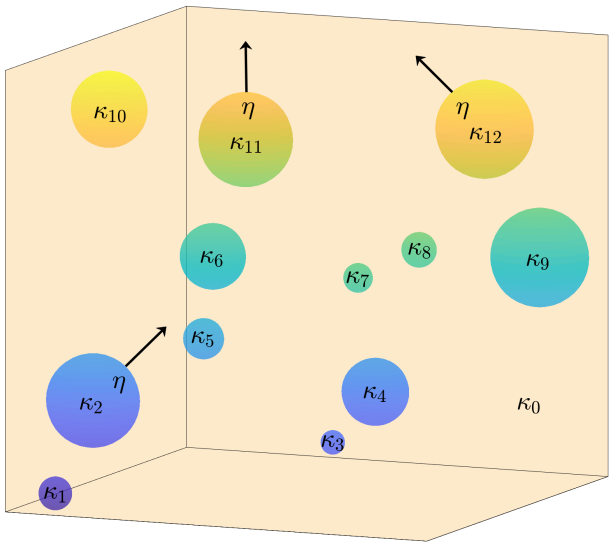

Figure 2.1: A geometrical configuration consisting of 12 spherical dielectric particles with different dielectric constants and radii.

Recalling now the calculations presented in Section 1.2 and using the modelling assumptions **MA1)-MA5)**, we arrive at the following model problem:

Let $\sigma_f \in C^0(\partial\Omega)$ be a free charge distribution. Find the electrostatic potential functions $\Phi^s \in C^2(\Omega^s) \cap C^1(\overline{\Omega^s})$, $s \in \{-, +\}$ such that for all $i \in \{1, \dots, N\}$ it holds that

$$\begin{aligned} -\Delta\Phi^s &= 0 && \text{in } \Omega^s, \\ \Phi^- - \Phi^+ &= 0 && \text{on } \partial\Omega_i, \\ \left(\kappa_i \nabla\Phi^- - \kappa_0 \nabla\Phi^+\right) \cdot \eta &= \frac{\sigma}{\boldsymbol{\epsilon_0}} && \text{on } \partial\Omega_i, \\ |\Phi^+(\mathbf{x})| &\leq C|\mathbf{x}|^{-1} && \text{for } |\mathbf{x}| \to \infty. \end{aligned} \tag{2.1}$$

Remark 2.1. Consider the boundary value problem (2.1). For simplicity, we will assume in the remainder of this dissertation that $\boldsymbol{\epsilon_0} \equiv 1$. This results in no loss of generality.

Unfortunately, the classical formulation (2.1) of the electrostatic interaction problem for dielectric spheres is unsatisfactory from a theoretical point-of-view. Indeed, it is well known that questions of existence and uniqueness of solutions for such classical formulations are not easy to answer. As a consequence, we will formulate the classical PDE (2.1) as a *weak* problem on suitable Sobolev spaces.

Weak formulation of the PDE-based model problem

We have already introduced Sobolev spaces on open sets and surfaces in $\mathbb{R}^3$ as well as Dirichlet and Neumann trace operators in Section 1.3. In order to write the weak formulation of the classical PDE (2.1) however, we must also take into account the decay condition of the electrostatic potential. The difficulty is that a function $\Phi \in C^\infty(\Omega^+)$ that satisfies the decay condition $|\Phi(\mathbf{x})| \leq C|\mathbf{x}|^{-1}$ for $|\mathbf{x}| \to \infty$ will, in general, *not* be an element of $L^2(\Omega^+)$. The usual approach to overcoming this problem is to equip Sobolev spaces on unbounded domains with weighted norms.

Definition 2.2 (Weighted Sobolev Space for the Exterior Laplace Problem)**.**
Let $\Omega \subset \mathbb{R}^3$ be an open set. We define the Hilbert space $H^1(\Delta;\Omega)$ as the completion of $C^\infty_{\text{comp}}(\Omega)$ with respect to the norm $\|\cdot\|_{H^1(\Delta;\Omega)}$ induced by the inner product

$$(u,v)_{H^1(\Delta;\Omega)} := \int_\Omega \frac{u(\mathbf{x})v(\mathbf{x})}{1+|\mathbf{x}|^2}\,d\mathbf{x} + \int_\Omega \nabla u(\mathbf{x})\cdot\nabla v(\mathbf{x})\,d\mathbf{x}.$$

It can readily be seen that the spaces $H^1(\Omega)$ and $H^1(\Delta;\Omega)$ coincide for any bounded open set Ω. If Ω is an unbounded open set however, we have $H^1(\Omega) \subset H^1(\Delta;\Omega)$.

Remark 2.3. Consider Definition 2.2 of the weighted Sobolev spaces. It can be shown (see, e.g., [185, Theorem 2.9.6]) that for any function $u \in H^1_\Delta(\Omega^s)$ and $v \in H^1(\Delta;\Omega)$, the relation 1.13 in Theorem 1.11 from Section 1.3 holds.

For ease of exposition, we introduce the following additional notation: Let the function $\kappa\colon \partial\Omega \to \mathbb{R}$ be defined as $\kappa(\mathbf{x}) := \kappa_i$ for $\mathbf{x} \in \partial\Omega_i$. Thus, κ is a piecewise constant function that takes constant positive values on the boundary of each open ball $\partial\Omega_i$, $i = 1,\ldots,N$. Physically, this function represents the dielectric constant of each of these open balls while the constant κ_0 represents the dielectric constant of the surrounding medium. Recalling now the notation and definitions introduced in Section 1.3, we obtain the following weak formulation of electrostatic interaction problem for dielectric spheres:

Let $\sigma_f \in H^{-\frac{1}{2}}(\partial\Omega)$ be a free charge distribution. Find the electrostatic potential functions $\left(\Phi^-,\Phi^+\right) \in H^1(\Omega^-)\times H^1(\Delta;\Omega^+)$ such that for all $i \in \{1,\ldots,N\}$ it holds that

$$\begin{aligned} -\Delta\Phi^s &= 0 && \text{on } \Omega^s,\\ \gamma^+\Phi^+ - \gamma^-\Phi^- &= 0 && \text{in } H^{\frac{1}{2}}(\partial\Omega),\\ \kappa\gamma_N^-\Phi^- - \kappa_0\gamma_N^+\Phi^+ &= \sigma_f && \text{in } H^{-\frac{1}{2}}(\partial\Omega),\\ |\Phi^+(\mathbf{x})| &\leq C|\mathbf{x}|^{-1} && \text{for } |\mathbf{x}| \to \infty. \end{aligned} \tag{2.2}$$

The key shortcoming of Equation (2.2) is that it is posed on the full space $\mathbb{R}^3$ which leads to considerable computational challenges if one wishes to use standard numerical algorithms such as the finite element method for solving this PDE. Indeed, since the electrostatic potential Φ^+ decays, a priori, only as $|\mathbf{x}|^{-1}$ for large $|\mathbf{x}|$, a naive truncation of the computational domain leads to significant numerical errors. The usual approach in the literature to circumventing this difficulty is to appeal to the theory of integral equations and reformulate Equation (2.2) as a so-called *boundary integral equation* (BIE) posed on the interface $\partial\Omega$. Consequently, in the next Section 2.3, we will reformulate the boundary value problem (2.2) as a boundary integral equation.

2.3 Integral Equation Formulation of the N-Body Dielectric Spheres Problem

There is a well established literature on the reformulation of elliptic boundary value problems such as Equation (2.2) as an integral equation involving the boundary integral operators introduced in Section 1.4 and we refer the interested reader to the previously cited textbooks [7, 105, 118, 147, 185, 195]. Such a reformulation is always possible if the underlying differential operator, say, $\mathcal{L}$ has a fundamental solution, i.e., a function $G_{\mathcal{L}} : \mathbb{R}^3 \setminus \{0\} \to \mathbb{R}$ such that $\mathcal{L}G_{\mathcal{L}} = G_{\mathcal{L}}\mathcal{L} = \delta_0$ in the sense of distributions (c.f., Lemma 1.17). Indeed, using the existence of such a fundamental solution, one can mimic the construction we have presented in Section 1.4 for the case of the Laplace equation, i.e., the case $\mathcal{L} = -\Delta$ to deduce the existence of boundary integral operators corresponding to more general differential operators $\mathcal{L}$.

Once these boundary integral operators have been constructed, there are two approaches that can be pursued to transform the underlying elliptic boundary value problem into an integral equation. These are known as the direct method and the indirect method respectively. In the direct approach, one takes the given boundary data, inserts this into the well-known Green's representation theorem (see, e.g., [185, Theorem 3.1.6]) and applies either the Dirichlet or Neumann trace operator. Depending on the choice of trace operator, this results in the construction of a Fredholm integral equation of the first or second kind that is posed only on the boundary of the geometry. In contrast, the indirect approach consists of proposing an ansatz potential, i.e., proposing that the solution to the elliptic boundary value problem is the layer potential generated by some unknown density function supported on the boundary of the geometry, and then using the boundary data to construct a boundary integral equation that the unknown density function must satisfy. Depending on the ansatz potential (single layer or double layer), the indirect approach also leads to a Fredholm equation of the first or second kind. A comprehensive discussion of both approaches including advantages and disadvantages of each, as well as the resulting boundary integral equations can, for instance, be found in [185, Chapter 3.4].

Let us now state the integral equation formulation of the dielectric spheres electrostatic interaction problem. The integral equation we state is essentially a second-kind Fredholm equation and is derived from the boundary value problem (2.2) using the in-

direct approach with a single layer potential ansatz.

Integral Equation Formulation for the Induced Surface Charge

Let $\sigma_f \in H^{-\frac{1}{2}}(\partial\Omega)$ be a free charge distribution. Find the *induced* surface charge $\nu \in H^{-\frac{1}{2}}(\partial\Omega)$ such that

$$\nu - \frac{\kappa_0 - \kappa}{\kappa_0}(\mathrm{DtN}\mathcal{V})\nu = \frac{\sigma_f}{\kappa_0}. \tag{2.3}$$

Remark 2.4. From a physical point of view, the *induced* surface charge $\nu \in H^{-\frac{1}{2}}(\partial\Omega)$ in the integral equation (2.3) is the charge (up to scaling) that results on the surface of each dielectric particle after polarisation effects are included. Thus, it is (up to scaling) the sum of the known free-charge σ_f and the unknown bound surface charge σ_b.

Remark 2.5. Consider the setting of the integral equation (2.3). Suppose there is some open ball Ω_j, $j \in \{1, \ldots, N\}$ such that $\kappa = \kappa_0$ on $\partial\Omega_j$. Then it follows that the induced surface charge ν_j on sphere $\partial\Omega_j$ is simply given by $\nu_j = \frac{\sigma_{f,j}}{\kappa_0}$ where $\sigma_{f,j}$ denotes the free charge on $\partial\Omega_j$. This justifies the model assumption **MA3)** which states that the dielectric constant of the background medium is different from the dielectric constants of the spherical particles. Note that physically, the situation $\kappa = \kappa_0$ on $\partial\Omega_j$ corresponds to no polarisation on the sphere $\partial\Omega_j$.

Before proceeding further, let us justify two of our prior claims, namely, that the BIE (2.3) can be derived from the boundary value problem (2.2) using a single layer ansatz and that the BIE (2.3) has the structure of a second kind Fredholm equation.

Lemma 2.6 (Derivation of the BIE (2.3))**.** *Let* $\mathbf{\Phi} := (\Phi^-, \Phi^+) \in H^1(\Omega^-) \times H^1(\Delta; \Omega^+)$ *be a solution to the boundary value problem* (2.2)*. Then* $\nu := \mathcal{V}^{-1}\left(\gamma^-\Phi^-\right)$ *is a solution to the boundary integral equation* (2.3)*. Conversely, let* $\nu \in H^{-\frac{1}{2}}(\partial\Omega)$ *be a solution to the BIE* (2.3)*. Then* $(\Phi^-, \Phi^+) := \left(\mathcal{S}\nu|_{\Omega^-}, \mathcal{S}\nu|_{\Omega^+}\right)$ *is a solution to the BVP* (2.2)*.*

Proof. Let $\mathbf{\Phi} := (\Phi^-, \Phi^+) \in H^1(\Omega^-) \times H^1(\Delta; \Omega^+)$ be a solution to the boundary value problem (2.2). It follows from Green's representation theorem (see, e.g., [185, Theorem 3.1.6]) that for each $s \in \{+, -\}$ it holds that

$$\Phi^s = \mathcal{S}\left(\gamma_N^-\Phi^- - \gamma_N^+\Phi^+\right)|_{\Omega^s}.$$

Due to the hypotheses of the BVP (2.2) we further have

$$-\gamma_N^+\Phi^+ = \frac{\sigma_f}{\kappa_0} - \frac{\kappa}{\kappa_0}\gamma_N^-\Phi^-,$$

so that

$$\begin{aligned}\gamma^-\Phi^- &= \gamma^-\mathcal{S}\left(\gamma_N^-\Phi^- + \frac{\sigma_f}{\kappa_0} - \frac{\kappa}{\kappa_0}\gamma_N^-\Phi^-\right)\\ &= \mathcal{V}\left(\frac{1}{\kappa_0}\left(\kappa_0\gamma_N^-\Phi^- - \kappa\gamma_N^-\Phi^-\right) + \frac{\sigma_f}{\kappa_0}\right)\end{aligned}$$

$$= \mathcal{V}\left(\frac{\kappa_0 - \kappa}{\kappa_0}\gamma_N^- \Phi^-\right) + \frac{1}{\kappa_0}\mathcal{V}\sigma_f$$
$$= \mathcal{V}\left(\frac{\kappa_0 - \kappa}{\kappa_0}\mathrm{DtN}\gamma^- \Phi^-\right) + \frac{1}{\kappa_0}\mathcal{V}\sigma_f.$$

We define $\nu := \mathcal{V}^{-1}\gamma^-\Phi^-$ and use the fact that $\mathcal{V}^{-1}\colon H^{\frac{1}{2}}(\partial\Omega) \to H^{-\frac{1}{2}}(\partial\Omega)$ is a bijection to obtain that

$$\nu = \left(\frac{\kappa_0 - \kappa}{\kappa_0}\mathrm{DtN}\mathcal{V}\nu\right) + \frac{1}{\kappa_0}\sigma_f.$$

This completes the first part of the proof.

For the converse, let $\nu \in H^{-\frac{1}{2}}(\partial\Omega)$ be a solution to the BIE (2.3). It follows from the jump properties of the single layer potential (see, e.g., [185, Theorem 3.3.1]) that

$$\nu = \gamma_N^- \mathcal{S}\nu - \gamma_N^+ \mathcal{S}\nu.$$

Define $(\Phi^-, \Phi^+) = \left(\mathcal{S}\nu|_{\Omega^-}, \mathcal{S}\nu|_{\Omega^+}\right)$. The properties of the single layer potential (see, e.g., Remark 1.24) imply that we need only check the jump condition for the normal derivative. We observe that

$$\begin{aligned}\kappa\gamma_N^-\Phi^- - \kappa_0\gamma_N^+\Phi^+ = \kappa\mathrm{DtN}\gamma^-\Phi^- + \kappa_0\nu - \kappa_0\mathrm{DtN}\gamma^-\Phi^- &= (\kappa - \kappa_0)\mathrm{DtN}\gamma^-\Phi^- + \kappa_0\nu \\ &= (\kappa - \kappa_0)\mathrm{DtN}\mathcal{V}\nu + \kappa_0\nu.\end{aligned}$$

From the hypotheses of BIE (2.3) we therefore obtain that

$$\kappa\gamma_N^-\Phi^- - \kappa_0\gamma_N^+\Phi^+ = (\kappa - \kappa_0)\mathrm{DtN}\mathcal{V}\nu + \kappa_0\nu = \sigma_f.$$

This completes the proof. □

Lemma 2.7 (Second kind structure of BIE (2.3))**.** *The boundary integral equation* (2.3) *can be written as an integral equation of the second kind.*

Proof. From Lemma 1.31 concerning the Calderón identities we have that

$$\mathrm{DtN}\mathcal{V} = (\mathcal{V}\mathrm{DtN})^* = \left(\frac{1}{2}I + \mathcal{K}\right)^* = \frac{1}{2}I + \mathcal{K}^*,$$

where $I\colon H^{-\frac{1}{2}}(\partial\Omega) \to H^{-\frac{1}{2}}(\partial\Omega)$ is the identity operator. Substituting in BIE (2.3) yields

$$\frac{\sigma_f}{\kappa_0} = \nu - \frac{\kappa_0 - \kappa}{\kappa_0}(\mathrm{DtN}\mathcal{V})\nu = \nu - \frac{\kappa_0 - \kappa}{\kappa_0}\left(\frac{1}{2}I + \mathcal{K}^*\right)\nu = \frac{\kappa_0 + \kappa}{2\kappa_0}\nu - \frac{\kappa_0 - \kappa}{\kappa_0}\mathcal{K}^*\nu.$$

The claim now follows since we obtain

$$\frac{\sigma_f}{\kappa_0 + \kappa} = \frac{1}{2}\nu - \frac{\kappa_0 - \kappa}{\kappa_0 + \kappa}\mathcal{K}^*\nu = \left(\frac{1}{2}I - \frac{\kappa_0 - \kappa}{\kappa_0 + \kappa}\mathcal{K}^*\right)\nu. \tag{2.4}$$

□

2.3.1 Weak formulation and Galerkin discretisation of the boundary integral equation

For clarity of exposition, we first define the relevant boundary integral operator.

Definition 2.8. We define the linear operator $\mathcal{A}\colon H^{\frac{1}{2}}(\partial\Omega) \to H^{\frac{1}{2}}(\partial\Omega)$ as the mapping with the property that for all $\lambda \in H^{\frac{1}{2}}(\partial\Omega)$ it holds that

$$\mathcal{A}\lambda := \lambda - \mathcal{V}\mathrm{DtN}\Big(\frac{\kappa_0 - \kappa}{\kappa_0}\lambda\Big).$$

In addition, we denote by $\mathcal{A}^*\colon H^{-\frac{1}{2}}(\partial\Omega) \to H^{-\frac{1}{2}}(\partial\Omega)$ the adjoint operator of $\mathcal{A}$.

The BIE (2.3) now has a straightforward weak formulation.

Weak Formulation of the Integral Equation (2.3)

Let $\sigma_f \in H^{-\frac{1}{2}}(\partial\Omega)$ and let $\mathcal{A}^*\colon H^{-\frac{1}{2}}(\partial\Omega) \to H^{-\frac{1}{2}}(\partial\Omega)$ denote the adjoint of the operator $\mathcal{A}$ given by Definition 2.8. Find $\nu \in H^{-\frac{1}{2}}(\partial\Omega)$ such that for all $\lambda \in H^{\frac{1}{2}}(\partial\Omega)$ it holds that

$$\langle \mathcal{A}^*\nu, \lambda\rangle_{H^{-\frac{1}{2}}(\partial\Omega)\times H^{\frac{1}{2}}(\partial\Omega)} = \frac{1}{\kappa_0}\langle \sigma_f, \lambda\rangle_{H^{-\frac{1}{2}}(\partial\Omega)\times H^{\frac{1}{2}}(\partial\Omega)}. \tag{2.5}$$

The next step is to state the Galerkin discretisation of the boundary integral equation (2.3). We first define the relevant approximation spaces.

Definition 2.9 (Spherical Harmonics)**.** Let $\ell \in \mathbb{N}_0$ and $m \in \{-\ell, \dots, \ell\}$ be integers. Then we define the function $\mathcal{Y}_\ell^m\colon \mathbb{S}^2 \to \mathbb{R}$ as

$$\mathcal{Y}_\ell^m(\theta,\phi) := \begin{cases} (-1)^m\sqrt{2}\sqrt{\frac{2\ell+1}{4\pi}\frac{(\ell-|m|)!}{(\ell+|m|)!}}P_\ell^{|m|}\big(\cos(\theta)\big)\sin\big(|m|\phi\big) & \text{if } m<0,\\ \sqrt{\frac{2\ell+1}{4\pi}}P_\ell^m\big(\cos(\theta)\big) & \text{if } m=0,\\ (-1)^m\sqrt{2}\sqrt{\frac{2\ell+1}{4\pi}\frac{(\ell-m)!}{(\ell+m)!}}P_\ell^m\big(\cos(\theta)\big)\cos\big(m\phi\big) & \text{if } m>0, \end{cases}$$

where P_ℓ^m denotes the associated Legendre polynomial of degree ℓ and order m. The function $\mathcal{Y}_\ell^m$ is known as the real-valued L^2-orthonormal spherical harmonic of degree ℓ and order m.

Definition 2.10 (Approximation Space on a Sphere)**.** Let $\mathcal{O}_{\mathbf{x}_0} \subset \mathbb{R}^3$ be an open ball of radius $r > 0$ centred at the point $\mathbf{x}_0 \in \mathbb{R}^3$ and let $\ell_{\max} \in \mathbb{N}$. We define the finite-dimensional Hilbert space $W^{\ell_{\max}}(\partial\mathcal{O}_{\mathbf{x}_0}) \subset H^{\frac{1}{2}}(\partial\mathcal{O}_{\mathbf{x}_0}) \subset H^{-\frac{1}{2}}(\partial\mathcal{O}_{\mathbf{x}_0})$ as the vector space

$$W^{\ell_{\max}}(\partial\mathcal{O}_{\mathbf{x}_0}) := \Big\{u\colon \partial\mathcal{O}_{\mathbf{x}_0} \to \mathbb{R} \text{ such that } u(\mathbf{x}) = \sum_{\ell=0}^{\ell_{\max}}\sum_{m=-\ell}^{m=+\ell}[u]_\ell^m\mathcal{Y}_\ell^m\left(\frac{\mathbf{x}-\mathbf{x}_0}{|\mathbf{x}-\mathbf{x}_0|}\right) \text{ where all } [u]_\ell^m \in \mathbb{R}\Big\},$$

equipped with the inner product

$$(u,v)_{W^{\ell_{\max}}(\partial\mathcal{O}_{\mathbf{x}_0})} := r^2[u]_0^0[v]_0^0 + r^2\sum_{\ell=1}^{\ell_{\max}}\sum_{m=-\ell}^{m=+\ell}\frac{\ell}{r}[u]_\ell^m[v]_\ell^m \qquad \forall u,v\in W^{\ell_{\max}}(\partial\mathcal{O}_{\mathbf{x}_0}). \quad (2.6)$$

It is now straightforward to extend the Hilbert space defined in Definition 2.10 to the domain $\partial\Omega$.

Definition 2.11 (Global Approximation Space)**.** We define the finite-dimensional Hilbert space $W^{\ell_{\max}} \subset H^{\frac{1}{2}}(\partial\Omega) \subset H^{-\frac{1}{2}}(\partial\Omega)$ as the vector space

$$W^{\ell_{\max}} := \Big\{u\colon \partial\Omega\to\mathbb{R} \text{ such that } \forall i\in\{1,\dots,N\}\colon u|_{\partial\Omega_i}\in W^{\ell_{\max}}(\partial\Omega_i)\Big\},$$

equipped with the inner product

$$(u,v)_{W^{\ell_{\max}}} := \sum_{i=1}^{N}(u,v)_{W^{\ell_{\max}}(\partial\Omega_i)} \qquad \forall u,v\in W^{\ell_{\max}}. \quad (2.7)$$

Galerkin Discretisation of the Integral Equation (2.3)

Let $\sigma_f\in H^{-\frac{1}{2}}(\partial\Omega)$ and let $\ell_{\max}\in\mathbb{N}$. Find $\nu_{\ell_{\max}}\in W^{\ell_{\max}}$ such that for all $\psi_{\ell_{\max}}\in W^{\ell_{\max}}$ it holds that

$$(\mathcal{A}^*\nu_{\ell_{\max}},\psi_{\ell_{\max}})_{L^2(\partial\Omega)} = \frac{1}{\kappa_0}(\sigma_f,\psi_{\ell_{\max}})_{L^2(\partial\Omega)}. \quad (2.8)$$

The weak formulation (2.5) and the Galerkin discretisation (2.8) of the second kind boundary integral equation (2.3) will be the key objects of study in Chapters 3-5 of this dissertation. Briefly, our plan is to

1. First perform a standard well-posedness for the infinite-dimensional weak formulation (2.5) and the finite-dimensional Galerkin discretisation (2.8). We will then derive a priori error estimates and convergence rates for two important physical quantities, namely, the induced surface charge and total electrostatic energy of the system. This is the subject of Chapter 3.

2. Propose solution strategies for solving the Galerkin discretisation (2.8) and perform a complexity analysis of these solution strategies. This is the subject of Chapter 4

3. Finally, use the results of Chapters 3 and 4 to propose a solution strategy for computing the *electrostatic forces* acting on the dielectric particles, and perform an error analysis and complexity analysis for these forces. This is the subject of Chapter 5

In order to highlight the novelty of our subsequent work, we present in the next Section 2.4, a brief overview of the existing literature on boundary integral equations of the second kind and discuss the limitations of the existing analysis.

2.4 Existing Literature on Integral Equations for N-Body Problems and its Limitations

N-body problems have been widely studied in the literature in the context of electromagnetic or acoustic scattering by a large number of obstacles (see, e.g., [2, 35, 36, 77, 78, 93, 206]). Such scattering problems are significantly more complicated to analyse than the electrostatic interaction problem we consider here because the underlying differential operator in wave phenomena is indefinite, which causes many technical difficulties. Consequently, it is already a significant challenge to design a computationally efficient numerical algorithm that is stable with respect to a large regime of wave numbers and obstacle sizes and placements, let alone perform a comprehensive numerical analysis of the algorithm and derive rigorous convergence rates. Thus, articles such as [2, 78, 93] quoted above focus mostly on the design of efficient computational methods and use numerical tests to validate their proposals. On the other hand while articles such as [45, 77] do establish convergence rates with respect to the degrees of freedom, these rates are not shown to be independent of the number of obstacles N. Incidentally, several of the articles mentioned above propose algorithms that are based on integral equations of the first kind (see [35, 36, 45, 206] quoted above). This framework, while suitable for numerical analysis, suffers from a well-known problem: Galerkin discretisations of integral equations of the first kind typically lead to dense, ill-conditioned solution matrices which causes slow convergence of the iterative solvers. As a remedy, several of these articles have proposed efficient preconditioners (see e.g., the article [35]) but the introduction of preconditioning techniques further complicates questions of scalability. Since the boundary integral equation (2.3) that we analyse in this dissertation is a Fredholm equation of the *second kind* however, we will face difficulties of a different nature in our analysis.

There is a significant literature on integral equations of the second kind (see, e.g., the books [6, 7, 105, 185] or the articles [4, 5, 62, 63, 145, 196]). In particular, the well-posedness theory of second kind integral equations (prior to introducing discretisation, i.e., in the infinite dimensional case) is fairly well established. It is also understood that, in contrast to first kind equations, Galerkin discretisations of second kind integral equations typically lead to well conditioned solution matrices. As a consequence, second kind integral equations have been constructed for the solutions of a variety of problems. More recently, such formulations have also been proposed for problems very similar to the N-body dielectric sphere problem including, for instance, acoustic and electromagnetic scattering by composite structures (see, e.g., [34, 37, 155, 178]) and multi-subdomain diffusion [38]. One disadvantage of second kind integral equation formulations is that stability estimates for the discretisation– and thus also error estimates– are difficult to establish except in special cases.

With access to such an abundance of literature, and in view of Lemma 2.7, the obvious starting point for the numerical analysis of the boundary integral equation (2.3) should be to appeal to the classical well-posedness analysis of second kind integral equations. Unfortunately, given our final goal, such a line of action is not very feasible. The key issue is that the existing integral equation formalism is typically applied in situations

where the size of the domain is considered *fixed* so the classical analysis in the literature focuses on establishing the existence of stability and continuity constants of the boundary integral operators that are independent of the *degrees of freedom* (such as the mesh width or the boundary element size). On the other hand, our aim is to derive error estimates for physical quantities of interest that do not depend on the number of objects N in the problem setting. Since the stability and continuity constants appear in the error estimates, it is therefore crucial to establish that these constants are explicitly independent of N. Unfortunately, this is not a priori clear and, in some cases, is not even true for the classical well-posedness analysis as we explain below.

Broadly speaking, there are two popular approaches in the literature to establishing the well-posedness of second kind integral equations. The traditional well-posedness analysis for second kind boundary integral equations is based on recognising that the boundary integral operator $\mathcal{K}\colon L^2(\partial\Omega) \to L^2(\partial\Omega)$ is compact if Ω is a C^1 domain (which is indeed the case for the current problem). It follows that the BIE (2.3) can be viewed as an operator equation on $L^2(\partial\Omega)$ involving a Fredholm operator of index zero, and well-posedness can be established by proving that the underlying operator is injective and then using the so-called Fredholm alternative. This approach was first developed by E. B. Fabes, M. Jodeit, Jr., and N. M. Rivière in 1978 [65]. Incidentally, in the general case when the domain Ω^- is only Lipschitz, the operator $\mathcal{K}$ is no longer compact on $L^2(\partial\Omega)$ but invertibility of the operator $\frac{1}{2}I - \frac{\kappa_0-\kappa}{\kappa_0+\kappa}\mathcal{K}$ on $L^2(\partial\Omega)$ can still be established as proven by Gregory Verchota in 1984 [204]. These results can then be extended to the Sobolev spaces $H^s(\partial\Omega)$ (see, e.g., the work of Johannes Elschner [62]). From the perspective of our work, the primary issue with this approach is that invertibility of the underlying boundary integral operator is established *indirectly*, i.e., by showing that the operator is injective. Thus, we are unable to obtain closed-form expressions for the stability constants which means that we are unable to determine precisely how these constants depend on the geometry Ω^- including the number of dielectric particles N. In the absence of such knowledge, there is no way to determine how the approximation error will depend on the geometry and, in particular, on N.

A second approach due to Steinbach and Wendland [105, 196] (see also the book of Sauter and Schwab [185]) is based on variational techniques. Using their results, it is possible to establish that the operator $\frac{1}{2}I - \frac{\kappa_0-\kappa}{\kappa_0+\kappa}\mathcal{K}$ is both bounded below and a contraction on $H^{\frac{1}{2}}(\partial\Omega)$ with respect to the inner product induced by the inverse single layer boundary operator $\mathcal{V}^{-1}$. This approach is based on the classical work of C. Neumann from the early 20^{th} century. Martin Costabel has written an interesting article on the historical development of C. Neumann's work which also contains the core idea of the proof [43].

There are three fundamental issues that prevent us from utilising the approach of Steinbach and Wendland to suit our needs. First, the lower bound constant for the operator $\frac{1}{2}I - \frac{\kappa_0-\kappa}{\kappa_0+\kappa}\mathcal{K}$ depends– amongst others– on the coercivity constant of the hypersingular boundary operator, and it is a priori unclear how this coercivity constant depends as the number of spherical particles N. Second, the analysis takes place in the Sobolev space $H^{\frac{1}{2}}(\partial\Omega)$ equipped with the inner-product induced by the inverse single

layer boundary operator $\mathcal{V}^{-1}$, and this inner-product is completely *non-local*. On the other hand, relative errors in approximate solutions for different values of N can only be compared to each other if the underlying norms are *local*. Consequently, in order to qualitatively compare relative approximation errors for different values of N, it becomes necessary to introduce norm equivalence constants and switch to the $H^{\frac{1}{2}}(\partial\Omega)$ norm, which is local in the sense that it involves a sphere-by-sphere sum (see Section 1.3). Unfortunately, these equivalence constants involve the continuity constant of $\mathcal{V}$, which increases as the number of objects N increases, thus resulting in error estimates that a priori depend on N. Such an error estimate is something we strongly wish to avoid. Finally, given our choice of approximation space for the Galerkin discretisation (2.8), discrete inf-sup stability is not directly inherited from the infinite-dimensional case.

In view of the preceding discussion, we felt it necessary to develop a new well-posedness analysis for the BIE (2.3) and its Galerkin discretisation (2.8). This new well-posedness analysis is the main subject of Chapter 3, and we shall see that it allows us to quantify precisely the dependence of the approximation errors on the geometry of our model problem.

3

Error Analysis of the Integral Equation Formulation of the N-Body Dielectric Spheres Problem

Throughout this chapter, we will assume the setting of Chapters 1 and 2. As emphasised in Section 2.3, the key objects of study in this chapter are the weak formulation (2.5) and the Galerkin discretisation (2.8) of the second kind boundary integral equation (BIE) (2.3) which describes the induced surface charge resulting on dielectric spherical particles undergoing mutual polarisation.

3.1 Main Theoretical Results

We begin this section by introducing a key quantity of interest in physical applications. This is the so-called total electrostatic energy associated with the free charge $\sigma_f \in H^{-\frac{1}{2}}(\partial\Omega)$ and the resulting induced surface charge $\nu \in H^{-\frac{1}{2}}(\partial\Omega)$, which is the solution to the BIE (2.3).

Definition 3.1 (Energy Functional and Total Electrostatic Energy)**.** Let $\sigma_f \in H^{-\frac{1}{2}}(\partial\Omega)$. Then we define the electrostatic energy functional $\mathcal{E}_{\sigma_f} \colon H^{-\frac{1}{2}}(\partial\Omega) \to \mathbb{R}$ as the bounded linear mapping with the property that for all $\sigma \in H^{-\frac{1}{2}}(\partial\Omega)$ it holds that

$$\mathcal{E}_{\sigma_f}(\sigma) := \frac{1}{2}\langle \sigma_f, \mathcal{V}\sigma \rangle_{H^{-\frac{1}{2}}(\partial\Omega)\times H^{\frac{1}{2}}(\partial\Omega)} = \frac{1}{2}\langle \sigma, \mathcal{V}\sigma_f \rangle_{H^{-\frac{1}{2}}(\partial\Omega)\times H^{\frac{1}{2}}(\partial\Omega)}, \tag{3.1}$$

and we define the total electrostatic energy of the system as $\mathcal{E}_{\sigma_f}(\nu)$ where $\nu \in H^{-\frac{1}{2}}(\partial\Omega)$ is the solution to the integral equation (2.3).

Next, we fix some additional notation and introduce a new norm and inner product on the space $H^{\frac{1}{2}}(\partial\Omega)$ that will be a key element in our subsequent analysis.

Notation: In an effort to avoid tedious notation, when there is no possibility of confusion, we will frequent write $\langle \cdot, \cdot \rangle_{\partial\Omega}$ to denote the duality pairing $\langle \cdot, \cdot \rangle_{H^{-\frac{1}{2}}(\partial\Omega)\times H^{\frac{1}{2}}(\partial\Omega)}$.

Notation: We define $\mathcal{C}(\partial\Omega)$ as the set of functions given by

$$\mathcal{C}(\partial\Omega) := \{u\colon \partial\Omega \to \mathbb{R}\colon \forall i = 1, \ldots, N \text{ the restriction } u|_{\partial\Omega_i} \text{ is a constant function}\},$$

and we observe that $\mathcal{C}(\partial\Omega)$ is a closed subspace of dimension N of $H^{\frac{1}{2}}(\partial\Omega)$ under the $L^2(\partial\Omega)$ norm (since the Slobodeckij semi-norm of constant functions is zero).

Notation: We define the function spaces $\breve{H}^{\frac{1}{2}}(\partial\Omega)$ and $\breve{H}^{-\frac{1}{2}}(\partial\Omega)$ as

$$\breve{H}^{\frac{1}{2}}(\partial\Omega) := \left\{u \in H^{\frac{1}{2}}(\partial\Omega)\colon (u, v)_{L^2(\partial\Omega)} = 0 \ \forall v \in \mathcal{C}(\partial\Omega)\right\},$$
$$\breve{H}^{-\frac{1}{2}}(\partial\Omega) := \left\{\phi \in H^{-\frac{1}{2}}(\partial\Omega)\colon \langle \phi, v\rangle_{\partial\Omega} = 0 \ \forall v \in \mathcal{C}(\partial\Omega)\right\},$$

and we observe that both sets are Banach spaces under the Sobolev-Slobodeckij norms introduced earlier. Intuitively, the spaces $\breve{H}^{\frac{1}{2}}(\partial\Omega)$ and $\breve{H}^{-\frac{1}{2}}(\partial\Omega)$ are trace spaces that do not contain any piecewise constant functions. We remark that the space $\breve{H}^{\frac{1}{2}}(\partial\Omega)$ is precisely the subspace of $H^{\frac{1}{2}}(\partial\Omega)$ on which the hypersingular boundary operator $\mathcal{W}\colon H^{\frac{1}{2}}(\partial\Omega) \to H^{-\frac{1}{2}}(\partial\Omega)$ is coercive (see Remark 1.29).

Lemma 3.2. *There exist complementary decompositions (in the sense of Brezis [21, Section 2.4]) of the spaces $H^{\frac{1}{2}}(\partial\Omega)$ and $H^{-\frac{1}{2}}(\partial\Omega)$ given by*

$$H^{\frac{1}{2}}(\partial\Omega) = \breve{H}^{\frac{1}{2}}(\partial\Omega) \oplus \mathcal{C}(\partial\Omega), \tag{3.2}$$
$$H^{-\frac{1}{2}}(\partial\Omega) = \breve{H}^{-\frac{1}{2}}(\partial\Omega) \oplus \mathcal{C}(\partial\Omega).$$

Moreover, the projection operators $\mathbb{P}_0^{\perp}\colon H^{\frac{1}{2}}(\partial\Omega) \to \breve{H}^{\frac{1}{2}}(\partial\Omega)$ and $\mathbb{P}_0\colon H^{\frac{1}{2}}(\partial\Omega) \to \mathcal{C}(\partial\Omega)$, $\mathbb{Q}_0^{\perp}\colon H^{-\frac{1}{2}}(\partial\Omega) \to \breve{H}^{-\frac{1}{2}}(\partial\Omega)$, and $\mathbb{Q}_0\colon H^{-\frac{1}{2}}(\partial\Omega) \to \mathcal{C}(\partial\Omega)$ associated with these complementary decompositions are all bounded.

The complementary decomposition introduced through Lemma 3.2 is at the heart of our well-posedness analysis as will become clear in Section 3.3.

Remark 3.3. Consider the complementary decomposition introduced through Lemma 3.2. It is a simple exercise to show that for all $\lambda \in H^{\frac{1}{2}}(\partial\Omega)$ and all $\sigma \in H^{-\frac{1}{2}}(\partial\Omega)$ the following relations hold:

$$\left\langle \mathbb{Q}_0\sigma, \mathbb{P}_0^{\perp}\lambda \right\rangle_{\partial\Omega} = 0 \quad \text{and} \quad \left\langle \mathbb{Q}_0^{\perp}\sigma, \mathbb{P}_0\lambda \right\rangle_{\partial\Omega} = 0.$$

In order to take full advantage of this decomposition of $H^{\frac{1}{2}}(\partial\Omega)$, it is necessary to introduce a new norm on $H^{\frac{1}{2}}(\partial\Omega)$.

Definition 3.4. We define on $H^{\frac{1}{2}}(\partial\Omega)$ a new norm $|||\cdot|||\colon H^{\frac{1}{2}}(\partial\Omega) \to \mathbb{R}$ given by

$$\forall \lambda \in H^{\frac{1}{2}}(\partial\Omega)\colon \ |||\lambda|||^2 := \|\mathbb{P}_0\lambda\|^2_{L^2(\partial\Omega)} + \langle \mathrm{DtN}\lambda, \lambda\rangle_{\partial\Omega}\,.$$

Remark 3.5. It is a straightforward exercise to prove that the norm $|||\cdot|||$ is equivalent to the $\|\cdot\|_{H^{\frac{1}{2}}(\partial\Omega)}$ norm introduced in Section 1.3 (see, for instance, the discussion in [96]). Consequently, there exists a constant $c_{\mathrm{equiv}} > 1$ such that for all $\lambda \in H^{\frac{1}{2}}(\partial\Omega)$ it holds that $\frac{1}{c_{\mathrm{equiv}}}|||\lambda||| \leq \|\lambda\|_{H^{\frac{1}{2}}(\partial\Omega)} \leq c_{\mathrm{equiv}}|||\lambda|||$. It is important to note that the equivalence constant c_{equiv} is independent of N.

Henceforth, we adopt the convention that the Hilbert space $H^{\frac{1}{2}}(\partial\Omega)$ is equipped with the $|||\cdot|||$ norm defined through Definition 3.4. The main advantage of using the new $|||\cdot|||$ norm is that it preserves the structure of the complementary decomposition of $H^{\frac{1}{2}}(\partial\Omega)$. Indeed, for any function $\lambda \in H^{\frac{1}{2}}(\partial\Omega)$, we have

$$|||\lambda|||^2 = \|\mathbb{P}_0\lambda\|^2_{L^2(\partial\Omega)} + \langle \mathrm{DtN}\lambda, \lambda\rangle_{\partial\Omega} = |||\mathbb{P}_0\lambda|||^2 + |||\mathbb{P}_0^{\perp}\lambda|||^2.$$

Remark 3.6. We remark that under this convention, due to the equivalence of norms, the definitions of the dual space $H^{-\frac{1}{2}}(\partial\Omega)$ and the associated duality pairing $\langle\cdot,\cdot\rangle_{\partial\Omega}$ remain unchanged. Thus, we can define a new dual norm $|||\cdot|||^*\colon H^{-\frac{1}{2}}(\partial\Omega) \to \mathbb{R}$ as the mapping with the property that for all $\sigma \in H^{-\frac{1}{2}}(\partial\Omega)$ it holds that

$$|||\sigma|||^* := \sup_{0\neq\psi\in H^{\frac{1}{2}}(\partial\Omega)} \frac{\langle\sigma,\psi\rangle_{\partial\Omega}}{|||\psi|||},$$

and we observe that the new $|||\cdot|||^*$ dual norm on $H^{-\frac{1}{2}}(\partial\Omega)$ is equivalent to the canonical dual norm $\|\cdot\|_{H^{-\frac{1}{2}}(\partial\Omega)}$ with equivalence constant that is once again independent of N.

Remark 3.7. It is a simple exercise to prove that the Dirichlet-to-Neumann map $\mathrm{DtN}\colon \breve{H}^{\frac{1}{2}}(\partial\Omega) \to \breve{H}^{-\frac{1}{2}}(\partial\Omega)$ is invertible and satisfies for all $\tilde{\lambda} \in \breve{H}^{\frac{1}{2}}(\partial\Omega)$

$$|||\mathrm{DtN}\tilde{\lambda}|||^* = |||\tilde{\lambda}|||.$$

This fact will be used often in the sequel.

Next, we define the higher regularity spaces and norms that are used in the error estimates. We remind the reader that we denote by $\mathcal{Y}_\ell^m$ the real spherical harmonic of degree ℓ and order m as defined through Definition 2.9 in Section 2.3.

Definition 3.8. Let $s \geq 0$ be a real number and let $\mathcal{O}_{\mathbf{x}_0} \subset \mathbb{R}^3$ be an open ball of radius $r > 0$ centred at the point $\mathbf{x}_0 \in \mathbb{R}^3$. Then we define constructively the fractional Sobolev space $H^s(\partial\mathcal{O}_{\mathbf{x}})$ as the set

$$H^s(\partial\mathcal{O}_{\mathbf{x}_0}) := \Big\{ u\colon \partial\mathcal{O}_{\mathbf{x}_0} \to \mathbb{R} \text{ such that } u(\mathbf{x}) = \sum_{\ell=0}^{\infty}\sum_{m=-\ell}^{m=+\ell} [u]_\ell^m \mathcal{Y}_\ell^m\left(\frac{\mathbf{x}-\mathbf{x}_0}{|\mathbf{x}-\mathbf{x}_0|}\right)$$
$$\text{where all } [u]_\ell^m \in \mathbb{R} \text{ satisfy } \sum_{\ell=1}^{\infty}\sum_{m=-\ell}^{m=+\ell}\left(\frac{l}{r}\right)^{2s}([u]_\ell^m)^2 < \infty\Big\},$$

equipped with the inner product

$$(u,v)_{H^s(\partial\mathcal{O}_{\mathbf{x}_0})} := r^2[u]_0^0\,[v]_0^0 + r^2\sum_{\ell=1}^{\infty}\sum_{m=-\ell}^{m=+\ell}\left(\frac{\ell}{r}\right)^{2s}[u]_\ell^m[v]_\ell^m \qquad \forall u,v\in H^s(\partial\mathcal{O}_{\mathbf{x}_0}). \quad (3.3)$$

Additionally, we write $|||\cdot|||_{H^s(\partial\mathcal{O}_{\mathbf{x}_0})}$ to denote the norm induced by the inner product $(\cdot,\cdot)_{H^s(\partial\mathcal{O}_{\mathbf{x}_0})}$.

Remark 3.9. Definition 3.8 is an intrinsic definition of the fractional Sobolev space $H^s(\partial\mathcal{O}_{\mathbf{x}_0})$, which coincides with the definition of these fractional Sobolev spaces involving the Sobolev-Slobodeckij inner product (see, e.g., [50]). The equivalence follows from the fact that the spherical harmonics are eigenvectors of the self-adjoint Laplace-Beltrami operator $\Delta_{\partial\mathcal{O}_{\mathbf{x}_0}}$ as discussed in, for example, [131, Chapter 1, Section 7].

Definition 3.8 suggests a natural intrinsic definition of the fractional Sobolev spaces on $\partial\Omega$.

Definition 3.10. Let $s\geq 0$ be a real number. Then we define the Hilbert space $H^s(\partial\Omega)$ as the set

$$H^s(\partial\Omega) := \left\{u\colon \partial\Omega\to\mathbb{R} \text{ such that } \forall i\in 1,\dots,N\colon u|_{\partial\Omega_i}\in H^s(\partial\Omega_i)\right\},$$

equipped with the inner product

$$(u,v)_{H^s(\partial\Omega)} := \sum_{i=1}^{N}(u,v)_{H^s(\partial\Omega_i)} \qquad \forall u,v\in H^s(\partial\Omega). \quad (3.4)$$

Additionally, we write $|||\cdot|||_{H^s(\partial\Omega)}$ to denote the norm induced by the inner product $(\cdot,\cdot)_{H^s(\partial\Omega)}$.

Remark 3.11. A direct calculation shows that the norm $|||\cdot|||_{H^{\frac{1}{2}}(\partial\Omega)}$ coincides with the $|||\cdot|||$ norm defined through Definition 3.4. Moreover, the $|||\cdot|||_{H^{\frac{1}{2}}(\partial\Omega)}$ norm coincides with the $\|\cdot\|_{W^{\ell_{\max}}}$ norm on the space $W^{\ell_{\max}}$.

We are now ready to state our main results.

Theorem 3.12 (Error Estimates)**.**

Let $\ell_{\max}\in\mathbb{N}$, let $\sigma_f\in H^s(\partial\Omega)$ for some $s\geq 0$, let $\mathcal{E}_{\sigma_f}\colon H^{-\frac{1}{2}}(\partial\Omega)\to\mathbb{R}$ be the electrostatic energy functional defined through Definition 3.1, let $\nu\in H^{-\frac{1}{2}}(\partial\Omega)$ be the unique solution to the weak formulation (2.5) with right hand side given by σ_f, let $\nu_{\ell_{\max}}\in W^{\ell_{\max}}$ be the unique solution to the Galerkin discretisation defined through Equation (2.8), and let $\mathbb{Q}_0^\perp\colon H^{-\frac{1}{2}}(\partial\Omega)\to\breve{H}^{-\frac{1}{2}}(\partial\Omega)$ denote the projection operator defined through Lemma 3.2. Then there exist constants $C_{\text{charge}}, C_{\text{energy}}>0$ that depend on the radii of the open balls, the dielectric constants and the minimal inter-sphere separation distance but are independent of both s and the number of open balls N such that

$$|||\nu-\nu_{\ell_{\max}}|||^* \leq C_{\text{charge}}\left(\frac{\max r_j}{\ell_{\max}+1}\right)^{s+\frac{1}{2}}\left(|||\mathbb{Q}_0^\perp\nu|||_{H^s(\partial\Omega)} + \frac{2}{\kappa_0}|||\mathbb{Q}_0^\perp\sigma_f|||_{H^s(\partial\Omega)}\right),$$

$$\left|\mathcal{E}_{\sigma_f}(\nu) - \mathcal{E}_{\sigma_f}(\nu_{\ell_{\max}})\right| \leq C_{\text{energy}} \left(\frac{\max r_i}{\ell_{\max}+1}\right)^{2s+1} \left(|||\mathbb{Q}_0^{\perp}\nu|||^2_{H^s(\partial\Omega)} + \frac{2}{\kappa_0}|||\mathbb{Q}_0^{\perp}\sigma_f|||^2_{H^s(\partial\Omega)}\right).$$

Theorem 3.12 is a standard a priori error estimate for the approximate induced surface charge and approximate electrostatic energy obtained by solving the Galerkin discretisation (2.8). We emphasise that the most important aspect of this error estimate is that the convergence rate pre-factors C_{charge} and C_{energy} are *explicitly independent of the number of objects* N. Consequently, for any geometry in the family of geometries $\{\Omega_{\mathcal{F}}\}_{\mathcal{F}\in\mathcal{J}}$ satisfying assumptions **GA1)-GA3)**, the following holds: Given a fixed number of degrees of freedom $\ell_{\max}$ per sphere, the relative error in the induced surface charge and in the total electrostatic energy *does not increase* as N increases. This implies in particular that for any configuration in the family of geometries $\{\Omega_{\mathcal{F}}\}_{\mathcal{F}\in\mathcal{J}}$, in order to guarantee the same relative accuracy in the induced surface charge and electrostatic energy, one does not need to increase the number of degrees of freedom per sphere as $N_{\mathcal{F}}$ increases.

Theorem 3.13 (Exponential Convergence)**.** *Let $\ell_{\max} \in \mathbb{N}$, let C_{charge} and C_{energy} denote the convergence rate pre-factors from Theorem 3.12, let $\sigma_f \in C^{\infty}(\partial\Omega)$ be analytic on $\partial\Omega$ in the sense that the local spherical harmonics coefficients of σ_f on each sphere decay exponentially fast, let $\mathcal{E}_{\sigma_f}\colon H^{-\frac{1}{2}}(\partial\Omega) \to \mathbb{R}$ be the electrostatic energy functional defined through Definition 5.1, and let $\nu \in H^{-\frac{1}{2}}(\partial\Omega)$ and $\nu_{\ell_{\max}} \in W^{\ell_{\max}}$ be the unique solutions to the weak formulation (2.5) and Galerkin discretisation (2.8) with right hand sides given by σ_f respectively. For $\ell_{\max}$ sufficiently large, if ν is analytic on $\partial\Omega$ then there exist constants $C_{\nu,\sigma_f} > 0$ depending on the exact solution ν and the free charge σ_f, and $C_r > 0$ depending only on the maximum radius of the open balls such such that*

$$\frac{1}{\sqrt{N}}|||\nu - \nu_{\ell_{\max}}|||^* \leq \sqrt{C_r} C_{\nu,\sigma_f} C_{\text{charge}} \exp\left(-\frac{1}{4C_{\nu,\sigma_f}}\frac{\ell_{\max}+1}{\max r_j}\right),$$

$$\frac{1}{N}\left|\mathcal{E}_{\sigma_f}(\nu) - \mathcal{E}_{\sigma_f}(\nu_{\ell_{\max}})\right| \leq C_r C^2_{\nu,\sigma_f} C_{\text{energy}} \exp\left(-\frac{1}{2C_{\nu,\sigma_f}}\frac{\ell_{\max}+1}{\max r_j}\right).$$

Definition 2.11 of the approximation space implies that the numerical method defined by Equation (2.8) is essentially a spectral Galerkin method, which are well-known to demonstrate exponential convergence for sufficiently smooth solution functions. Theorem 3.13 provides a proof of this intuitive result. We emphasise that the hypotheses of Theorem 3.13 are analogous to the hypotheses typically assumed by the discontinuous Galerkin finite element community for *hp* finite elements (see, e.g., [102, 103, 104]).

Remark 3.14. Consider Theorems 3.12 and 3.13. In both of these theorems, the approximate electrostatic energy is assumed to be $\mathcal{E}_{\sigma_f}(\nu_{\ell_{\max}})$ where $\nu_{\ell_{\max}} \in W^{\ell_{\max}}$ is the unique solution to the Galerkin discretisation (2.8). In practice however, if the free charge $\sigma_f \in H^{-\frac{1}{2}}(\partial\Omega)$ is an infinite-dimensional function, one typically computes instead the quantity $\mathcal{E}_{\mathbb{Q}_{\ell_{\max}}\sigma_f}(\nu_{\ell_{\max}})$ where $\mathbb{Q}_{\ell_{\max}}\sigma_f \in W^{\ell_{\max}}$ denotes the projection (in a precise sense that is clarified in Definition 3.30) of the free charge σ_f onto the approximation space $W^{\ell_{\max}}$. Using the subsequent analysis we present in this chapter, it is a simple exercise to obtain corresponding convergence rates for the quantity $\mathcal{E}_{\mathbb{Q}_{\ell_{\max}}\sigma_f}(\nu_{\ell_{\max}})$ that are essentially identical to those of Theorems 3.12 and 3.13. Note, however, that computing $\mathcal{E}_{\mathbb{Q}_{\ell_{\max}}\sigma_f}(\nu_{\ell_{\max}})$ in practical terms likely introduces an additional error due to the

use of numerical quadrature on a sphere when computing $\mathbb{Q}_{\ell_{\max}}\sigma_f$, which we do not precisely quantify.

Remark 3.15. Consider Theorems 3.12 and 3.13. It is a useful exercise to state explicitly the scaling in terms of N of the different constants and quantities of interest appearing in these results for a simple family of geometries $\{\Omega_{\mathcal{F}}^-\}_{\mathcal{F}\in\mathcal{J}}$. To this end, we consider the following geometrical setting: For each natural number $L > 1$, we define the geometry $\Omega_L^- := \cup_{i=1}^{(L+1)^3}\Omega_i$ as a collection of $N = (L+1)^3$ open balls, each of radius r located at the vertices of a simple cubic lattice of edge length $\rho > 2r$ as shown in Figure 3.1.

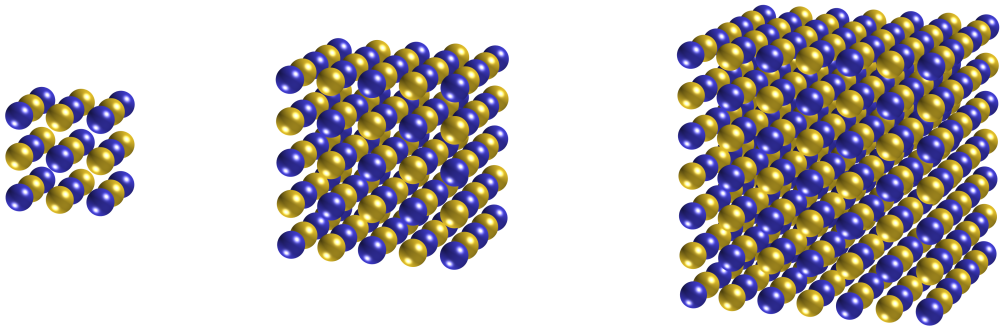

Figure 3.1: From left to right: the geometry Ω_2^- with 27 particles, the geometry Ω_4^- with 125 particles, and the geometry Ω_6^- with 343 particles.

Next, let us assume that

$$||\sigma_{f,j}||^2_{H^{-\frac{1}{2}}(\partial\Omega_j)} = \mathcal{O}(1) \quad \forall j \in \{1,\dots,N\}, \text{ and}$$
$$||\nu_j||^2_{H^{-\frac{1}{2}}(\partial\Omega_j)} = \mathcal{O}(N^\alpha) \quad \text{for some } \alpha \geq 0 \text{ and } \forall j \in \{1,\dots,N\},$$

where $\sigma_{f,j} := \sigma_f|_{\partial\Omega_j}$ and $\nu_j := \nu|_{\partial\Omega_j}$. We emphasise here that the precise scaling of the solution ν is a priori unknown since it depends not only on the scaling of σ_f, which—as input data— can be assumed to be known but also on the scaling of the inf-sup constant of the operator $\mathcal{A}^*$, which is not precisely quantified in this chapter. Under these assumptions however, a careful study of the proofs of Theorems 3.12 and 3.13 reveals the following scaling in terms of N of key constants and quantities of interest in our error estimates.

We conclude this section by emphasising that, taken together, Theorems 3.12 and 3.13 establish that the accuracy of our numerical algorithm is robust with respect to the number of open balls N for any family of geometries satisfying the assumptions **GA1)-GA3)**. In particular, Theorem 3.12 implies that our numerical method is N-error stable in the computation of the *induced surface charge* and *total electrostatic energy*. Of course, in order to prove that the numerical method is *linear scaling in accuracy*, we would have to prove, in addition, that for a fixed number of degrees of freedom per sphere, the computational cost of solving the linear system obtained from the Galerkin discretisation (2.8) scales as $\mathcal{O}(N)$. Numerical evidence (see [127]) suggests that this is indeed the case,

Constant or Quantity of Interest	Scaling in terms of N
$\|\|\|\sigma_f\|\|\|_{H^s(\partial\Omega)}$	$\mathcal{O}(\sqrt{N})$
$\|\|\|\nu\|\|\|_{H^s(\partial\Omega)}$	$\mathcal{O}(\sqrt{N^{\alpha+1}})$
C_{charge}	$\mathcal{O}(1)$
C_{energy}	$\mathcal{O}(1)$
C_{ν,σ_f}	$\mathcal{O}(\sqrt{N^{\alpha}})$
$\|\|\|\nu - \nu_{\ell_{\max}}\|\|\|^*$	$\mathcal{O}(\sqrt{N^{\alpha+1}})$
$\mathcal{E}_{\sigma_f}(\nu) - \mathcal{E}_{\sigma_f}(\nu_{\ell_{\max}})$	$\mathcal{O}(N^{\alpha+1})$

Table 3.1: Scaling of various quantities appearing in Theorems 3.12 and 3.13.

and a detailed complexity analysis which provides a theoretical justification is the subject of Chapter 4.

3.2 Supporting Numerical Evidence

The goal of this section is to briefly provide numerical evidence in support of our main results Theorems 3.12 and 3.13. Our numerical experiments will therefore show that

- For a fixed number of degrees of freedom per sphere and geometries satisfying the assumptions **GA1)-GA3)**, the average error in the induced surface charge remains bounded as the number of open balls N in the system is increased.
- For a fixed number of open balls N in the system, the average error in the induced surface charge converges exponentially as the number of degrees of freedom per sphere is increased.

We consider the following geometric setting: The external medium is assumed to be vacuum which has a dielectric constant $\kappa_0 = 1$. Two types of dielectric spheres are considered, one with radius 1, dielectric constant 10, and net negative free charge, and the other with radius 2, dielectric constant 5 and net positive free charge. Moreover, in order to include the effect of the minimal inter-sphere separation distance, we consider two sets of numerical experiments. The first involves the dielectric spheres arranged on a three dimensional, regular cubic lattice with edge length 10 and the other involves a similar lattice with a smaller edge length of 5 as displayed in Figures 3.2a and 3.2b respectively. All numerical simulations were run using a relative tolerance of 10^{-14}.

Figures 3.3a and 3.3b display the average error in the induced surface charge as the number of dielectric spheres N is increased for the two types of lattices. The reference solution in both cases was constructed by setting the maximum degree of spherical harmonics in the approximation space on each sphere as $\ell_{\max} = 20$. The approximate solutions were all constructed using $\ell_{\max} = 6$.

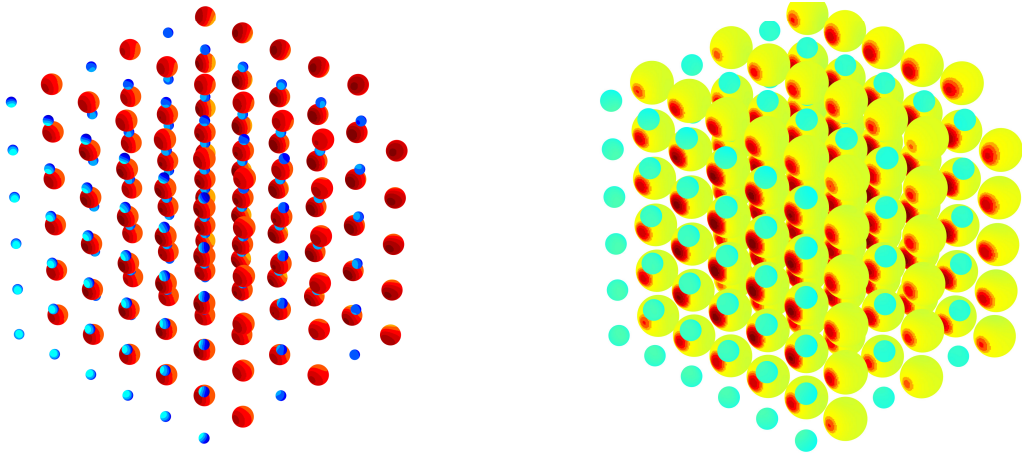

(a) Dielectric spheres arranged on a three dimensional, regular cubic lattice with edge length 10.

(b) Dielectric spheres arranged on a three dimensional, regular cubic lattice with edge length 5.

Figure 3.2: The geometric settings for both sets of numerical experiments.

Figures 3.4a and 3.4b display the average error in the induced surface charge as the maximum degree of spherical harmonics $\ell_{\max}$ in the approximation space on each sphere is increased. The number of dielectric spheres was chosen as $N = 215$. Once again, the reference solution in both cases was constructed by setting the maximum degree of spherical harmonics as $\ell_{\max} = 20$.

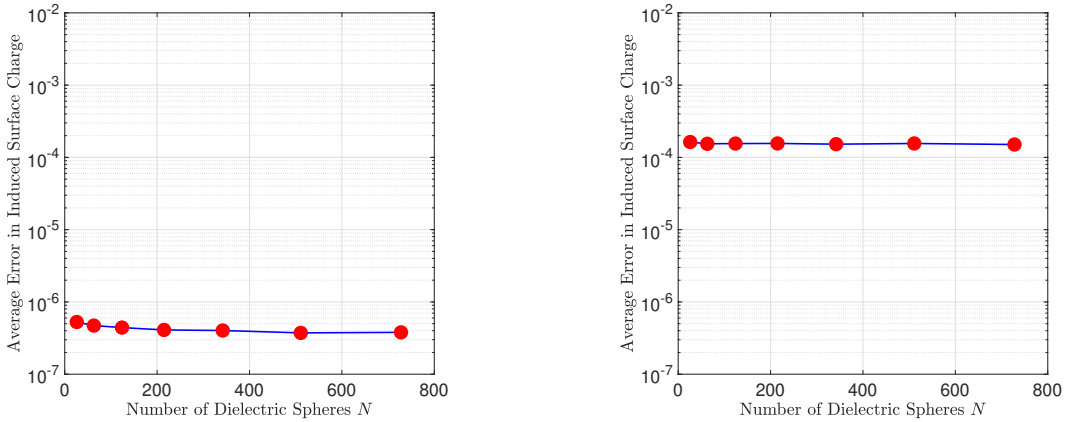

(a) Results for the cubic lattice with edge length 10.

(b) Results for the cubic lattice with edge length 5.

Figure 3.3: Log-lin plot of the average error in the induced surface charge versus the number of dielectric spheres N.

It is readily seen that both sets of numerical results are in agreement with the conclusions of our main results Theorems 3.12 and Theorem 3.13. Furthermore, we observe that the average error in the induced surface charge increases if the distance between

neighbouring dielectric particles is reduced which suggests some dependence of the approximation error on the minimal inter sphere separation distance. This dependence will be the subject of more discussion in Section 3.3.

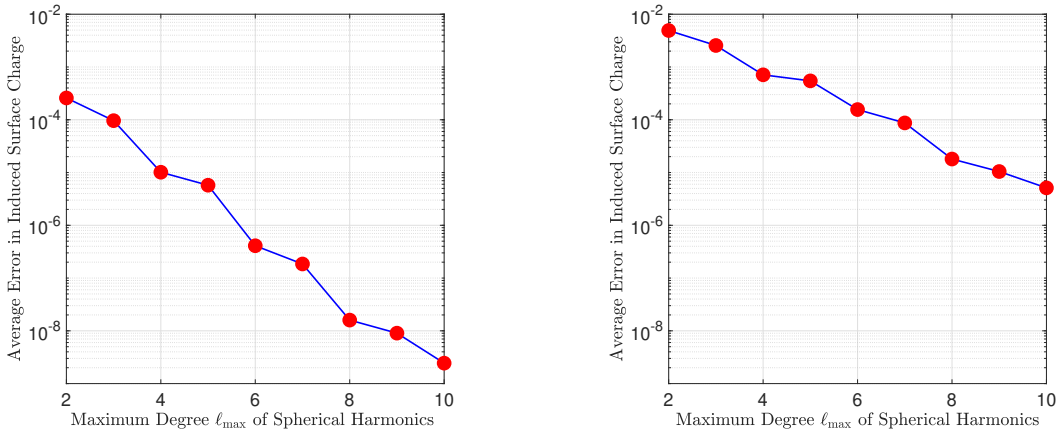

(a) Results for the cubic lattice with edge length 10.

(b) Results for the cubic lattice with edge length 5.

Figure 3.4: Log-lin plot of the average error in the induced surface charge versus the maximum degree $\ell_{\max}$ of spherical harmonics in the approximation space.

3.3 Proofs

As discussed in Section 2.4, we need to introduce a new analysis in order to prove our main results Theorems 3.12 and 3.13. To this end, we begin by observing that the single layer boundary operator $\mathcal{V}\colon H^{-\frac{1}{2}}(\partial\Omega) \to H^{\frac{1}{2}}(\partial\Omega)$ is a bijection. Therefore, the integral equation (2.3) can in fact be reformulated in terms of an unknown surface electrostatic potential $\lambda := \mathcal{V}\nu \in H^{\frac{1}{2}}(\partial\Omega)$.

Integral equation formulation for the electrostatic potential

Let $\sigma_f \in H^{-\frac{1}{2}}(\partial\Omega)$. Find $\lambda \in H^{\frac{1}{2}}(\partial\Omega)$ with the property that

$$\mathcal{A}\lambda = \lambda - \mathcal{V}\mathrm{DtN}\Big(\frac{\kappa_0 - \kappa}{\kappa_0}\lambda\Big) = \frac{1}{\kappa_0}\mathcal{V}\sigma_f. \tag{3.5}$$

Naturally, the integral equation (3.5) has a straightforward weak formulation.

Weak formulation of the Integral Equation (3.5)

Let $\sigma_f \in H^{-\frac{1}{2}}(\partial\Omega)$ and let $\mathcal{A}\colon H^{\frac{1}{2}}(\partial\Omega) \to H^{\frac{1}{2}}(\partial\Omega)$ be the operator defined through Definition 2.8. Find $\lambda \in H^{\frac{1}{2}}(\partial\Omega)$ such that for all $\sigma \in H^{-\frac{1}{2}}(\partial\Omega)$ it holds that

$$\langle \sigma, \mathcal{A}\lambda\rangle_{\partial\Omega} = \frac{1}{\kappa_0}\langle \sigma, \mathcal{V}\sigma_f\rangle_{\partial\Omega}\,. \tag{3.6}$$

3. ERROR ANALYSIS OF THE INTEGRAL EQUATION FORMULATION OF THE N-BODY DIELECTRIC SPHERES PROBLEM

The integral equation formulation (3.5) now leads to a corresponding Galerkin discretisation for an unknown approximate surface electrostatic potential $\lambda_{\ell_{\max}} \in W^{\ell_{\max}}$.

Galerkin discretisation of the Integral Equation (3.5) Let $\sigma_f \in H^{-\frac{1}{2}}(\partial\Omega)$ and let $\ell_{\max} \in \mathbb{N}$. Find $\widehat{\lambda}_{\ell_{\max}} \in W^{\ell_{\max}}$ such that for all $\widehat{\psi}_{\ell_{\max}} \in W^{\ell_{\max}}$ it holds that

$$\left(\widehat{\psi}_{\ell_{\max}}, \mathcal{A}\widehat{\lambda}_{\ell_{\max}}\right)_{L^2(\partial\Omega)} = \frac{1}{\kappa_0}\left(\widehat{\psi}_{\ell_{\max}}, \mathcal{V}\sigma_f\right)_{L^2(\partial\Omega)}. \tag{3.7}$$

We emphasise that for the purpose of applications, one is typically interested in calculating either the induced surface charge $\nu \in H^{-\frac{1}{2}}(\partial\Omega)$ or the total electrostatic energy $\mathcal{E}_{\sigma_f}(\nu)$, which itself can be obtained directly from the induced surface charge ν, and this is precisely why our main results Theorems 3.12 and 3.13 have been formulated in terms of the induced surface charge ν rather than the surface electrostatic potential $\lambda \in H^{\frac{1}{2}}(\partial\Omega)$. One may therefore wonder why we need introduce the weak formulation (3.6) for the surface electrostatic potential λ and its Galerkin discretisation (3.7) at all.

The key difficulty in our analysis is that the continuity constant of the relevant boundary integral operator and the discrete inf-sup constant both appear as pre-factors in the quasi-optimality bound and hence also the error estimates appearing in Theorems 3.12 and 3.13. It therefore becomes essential to obtain both a continuity constant and an inf-sup constant that is independent of the number of balls N in the N-body problem. Unfortunately, we have been unable to obtain such N-independent continuity and stability constants if we adopt a direct analysis of the weak formulation (2.5) for the induced surface ν and its Galerkin discretisation (2.8).

The weak formulation (3.6) and the Galerkin discretisation (3.7) have thus been introduced as *analytical* tools that will aid our numerical analysis. As we will later show, the difficulties highlighted above can be avoided if we analyse first the weak formulation (3.6) and its Galerkin discretisation (3.7) involving the exact and approximate surface electrostatic potential and then obtain as a corollary, analogous results for the weak formulation (2.5) and the Galerkin discretisation (2.8) and also proofs for Theorems 3.12 and 3.13.

We divide the remainder of this section into three parts. We first prove that the weak formulation (3.6) and the Galerkin discretisation (3.7) are well-posed, and obtain a *partial* quasi-optimality result for the approximate surface electrostatic potential. Next, we prove that the weak formulation (2.5) and the Galerkin discretisation (2.8) are also well-posed, and obtain an approximation result for the induced surface charge. Finally, we provide proofs for Theorems 3.12 and 3.13.

3.3.1 Well-posedness analysis for the surface electrostatic potential

3.3.1.1 Limitations of the classical analysis of the infinite-dimensional problem

The first step in the well-posedness analysis of the weak formulation (3.6) of the boundary integral equation (3.5) is to prove the continuity of the underlying linear boundary integral operator $\mathcal{A}\colon H^{\frac{1}{2}}(\partial\Omega) \to H^{\frac{1}{2}}(\partial\Omega)$ defined through Definition 2.8. To this end, let us first note that since the set Ω^- is, in particular, a C^1 domain, the double layer boundary integral operator $\mathcal{K}\colon H^{\frac{1}{2}}(\partial\Omega) \to H^{\frac{1}{2}}(\partial\Omega)$ can be shown to continuously map $L^2(\partial\Omega)$ into $L^2(\partial\Omega)$ (see [65, Theorem 2.1]), and therefore, the L^2 operator norm $\|\mathcal{K}\|_{L^2(\partial\Omega)}$ of $\mathcal{K}$ is well defined.

Lemma 3.16. *Let the constants $c_{\mathcal{V}}$ and $c_{\mathcal{K}}$ be defined as in Theorem 1.27 and Theorem 1.28 respectively from Section 1.4, let $\|\mathcal{K}\|_{L^2(\partial\Omega)}$ denote the L^2 operator norm of the double layer boundary operator $\mathcal{K}\colon H^{\frac{1}{2}}(\partial\Omega) \to H^{\frac{1}{2}}(\partial\Omega)$, and let the constant $C_{\mathcal{A}}$ be defined as*

$$C_{\mathcal{A}} := 1 + \max\left|\frac{\kappa - \kappa_0}{\kappa_0}\right| \sqrt{\left(\frac{1}{2} + \|\mathcal{K}\|_{L^2(\partial\Omega)}\right)^2 (1 + \max r_i) + \frac{c_{\text{equiv}}^2 c_{\mathcal{K}}^3}{c_{\mathcal{V}}}}.$$

Then the linear operator $\mathcal{A}\colon H^{\frac{1}{2}}(\partial\Omega) \to H^{\frac{1}{2}}(\partial\Omega)$ defined in Definition 2.8 satisfies

$$\|\mathcal{A}\|_{OP} := \sup_{0 \neq \lambda \in H^{\frac{1}{2}}(\partial\Omega)} \frac{|||\mathcal{A}\lambda|||}{|||\lambda|||} \leq C_{\mathcal{A}}.$$

Proof. Let $\lambda \in H^{\frac{1}{2}}(\partial\Omega)$. Then it holds that

$$|||\mathcal{A}\lambda||| = \left|\left|\left|\lambda - \mathcal{V}\mathrm{DtN}\left(\frac{\kappa_0 - \kappa}{\kappa_0}\lambda\right)\right|\right|\right| \leq |||\lambda||| + \left|\left|\left|\mathcal{V}\mathrm{DtN}\left(\frac{\kappa_0 - \kappa}{\kappa_0}\lambda\right)\right|\right|\right|.$$

Let $\lambda_\kappa := \frac{\kappa_0 - \kappa}{\kappa_0}\lambda$. Using Definition 3.4 of the $|||\cdot|||$ norm we obtain

$$|||\mathcal{V}\mathrm{DtN}\lambda_\kappa|||^2 = \|\mathbb{P}_0 \mathcal{V}\mathrm{DtN}\lambda_\kappa\|_{L^2(\partial\Omega)}^2 + \langle \mathrm{DtN}\mathcal{V}\mathrm{DtN}\lambda_\kappa, \mathcal{V}\mathrm{DtN}\lambda_\kappa\rangle_{\partial\Omega}.$$

Let us first focus on the second term. Using the boundedness result Lemma 1.32 from Section 1.4, we obtain

$$\begin{aligned}
\langle \mathrm{DtN}\mathcal{V}\mathrm{DtN}\lambda_\kappa, \mathcal{V}\mathrm{DtN}\lambda_\kappa\rangle_{\partial\Omega} &= \left\langle \mathcal{V}^{-1}\mathcal{V}\mathrm{DtN}\mathcal{V}\mathrm{DtN}\lambda_\kappa, \mathcal{V}\mathrm{DtN}\lambda_\kappa\right\rangle_{\partial\Omega} \\
&= \left((\mathcal{V}\mathrm{DtN})^2\lambda_\kappa, \mathcal{V}\mathrm{DtN}\lambda_\kappa\right)_{\mathcal{V}^{-1}} \\
&\leq \left\|(\mathcal{V}\mathrm{DtN})^2\lambda_\kappa\right\|_{\mathcal{V}^{-1}} \left\|\mathcal{V}\mathrm{DtN}\lambda_\kappa\right\|_{\mathcal{V}^{-1}} \\
&\leq c_{\mathcal{K}}^2 \|\lambda_\kappa\|_{\mathcal{V}^{-1}} \; c_{\mathcal{K}} \|\lambda_\kappa\|_{\mathcal{V}^{-1}} \\
&\leq \frac{c_{\mathcal{K}}^3 c_{\text{equiv}}^2}{c_{\mathcal{V}}} |||\lambda_\kappa|||^2 \leq \frac{c_{\mathcal{K}}^3 c_{\text{equiv}}^2}{c_{\mathcal{V}}} \max\left|\frac{\kappa - \kappa_0}{\kappa_0}\right|^2 |||\lambda|||^2.
\end{aligned}$$

Next, we consider the first term. The Calderón identities (see Lemma 1.31) yield

$$\begin{aligned}\|\mathbb{P}_0\mathcal{V}\mathrm{DtN}\lambda_\kappa\|^2_{L^2(\partial\Omega)} &= \left\|\mathbb{P}_0\Big(\frac{1}{2}I+\mathcal{K}\Big)\lambda_\kappa\right\|^2_{L^2(\partial\Omega)} \leq \Big(\frac{1}{2}+\|\mathcal{K}\|_{L^2(\partial\Omega)}\Big)^2\|\lambda_\kappa\|^2_{L^2(\partial\Omega)}\\ &\leq\Big(\frac{1}{2}+\|\mathcal{K}\|_{L^2(\partial\Omega)}\Big)^2\max\left|\frac{\kappa-\kappa_0}{\kappa_0}\right|^2\|\lambda\|^2_{L^2(\partial\Omega)}.\end{aligned}$$

Notice that

$$\begin{aligned}\|\lambda\|^2_{L^2(\partial\Omega)} &= \|\mathbb{P}_0\lambda\|^2_{L^2(\partial\Omega)}+\|\mathbb{P}_0^\perp\lambda\|^2_{L^2(\partial\Omega)} = |||\mathbb{P}_0\lambda|||^2+\|\mathbb{P}_0^\perp\lambda\|^2_{L^2(\partial\Omega)}\\ &\leq |||\mathbb{P}_0\lambda|||^2+\max r_i|||\mathbb{P}_0^\perp\lambda|||^2 \leq (1+\max r_i)|||\lambda|||^2.\end{aligned}$$

We can therefore conclude that

$$\left|\left|\left|\mathcal{V}\mathrm{DtN}\Big(\frac{\kappa_0-\kappa}{\kappa_0}\lambda\Big)\right|\right|\right| \leq \max\left|\frac{\kappa-\kappa_0}{\kappa_0}\right|\sqrt{\Big(\frac{1}{2}+\|\mathcal{K}\|_{L^2(\partial\Omega)}\Big)^2(1+\max r_i)+\frac{c_{\mathcal{K}}^3c_{\mathrm{equiv}}^2}{c_{\mathcal{V}}}}|||\lambda|||.$$

The proof now follows. □

Remark 3.17. Consider the setting of Lemma 3.16. The continuity constant $C_{\mathcal{A}}$ of the operator $\mathcal{A}$ as determined in Lemma 3.16 depends on the operator norm of the double layer boundary operator $\mathcal{K}$. Standard bounds for this operator norm depend on the diameter of the domain Ω^- (see, e.g., [68, Chapter 7] or [185, Chapter 3]), which implies that the continuity constant $C_{\mathcal{A}}$ could potentially increase as the number of open balls N increases.

Notice however, that the dependence of the continuity constant $C_{\mathcal{A}}$ on the operator norm $\|\mathcal{K}\|_{L^2(\partial\Omega)}$ appears only when evaluating the operator norm $\|\mathcal{V}\mathrm{DtN}\|_{L^2(\partial\Omega)}$. In principle, it is possible to refine the estimate for the operator norm $\|\mathcal{V}\mathrm{DtN}\|_{L^2(\partial\Omega)}$ using the addition theorem for spherical harmonics and the so-called Multipole-to-Local operators introduced by Greengard and Rokhlin [87]. Unfortunately, it turns out that for a completely arbitrary geometry $\Omega^- = \cup_{i=1}^N\Omega_i$, it is *not possible to entirely eliminate the dependence of the continuity constant $C_{\mathcal{A}}$ on the number of open balls N*. Indeed, an explicit counter-example can be constructed.

Obviously, this degradation of the continuity constant poses a serious problem if wish to obtain error estimates independent of N. Fortunately, as we will now show, it is possible to circumvent this issue by taking advantage of the particular structure of the BIEs (2.3) and (3.5).

3.3.1.2 The new analysis of the infinite-dimensional problem

In principle, the next step in our analysis would be to prove that the weak formulation (3.6) is well-posed. In view of Remark 3.17 however, we cannot obtain N-independent stability and continuity constants using a straightforward analysis of the boundary integral operator $\mathcal{A}$, and we must therefore adopt a smarter, indirect approach. To this

end, we will appeal to the complementary decompositions of the spaces $H^{\frac{1}{2}}(\partial\Omega)$ and $H^{-\frac{1}{2}}(\partial\Omega)$ introduced in Lemma 3.2. This complementary decomposition, together with Remark 3.3, allows us to rewrite the weak formulation (3.6) in terms of trial and test functions that belong to the spaces $\mathcal{C}(\partial\Omega)$, $\breve{H}^{\frac{1}{2}}(\partial\Omega)$, and $\breve{H}^{-\frac{1}{2}}(\partial\Omega)$.

Modified weak formulation of the Integral Equation (3.5)

Let $\sigma_f \in H^{-\frac{1}{2}}(\partial\Omega)$. Find functions $(\lambda_0, \tilde{\lambda}) \in \mathcal{C}(\partial\Omega) \times \breve{H}^{\frac{1}{2}}(\partial\Omega)$ such that for all test functions $(\sigma_0, \tilde{\sigma}) \in \mathcal{C}(\partial\Omega) \times \breve{H}^{-\frac{1}{2}}(\partial\Omega)$ it holds that

$$\langle \sigma_0, \lambda_0 \rangle_{\partial\Omega} - \left\langle \sigma_0, \mathcal{V}\mathrm{DtN}\left(\frac{\kappa_0 - \kappa}{\kappa_0}\tilde{\lambda}\right)\right\rangle_{\partial\Omega} = \frac{1}{\kappa_0}\langle \sigma_0, \mathcal{V}\sigma_f\rangle_{\partial\Omega}\,, \tag{3.8}$$

$$\left\langle \tilde{\sigma}, \tilde{\lambda}\right\rangle_{\partial\Omega} - \left\langle \tilde{\sigma}, \mathcal{V}\mathrm{DtN}\left(\frac{\kappa_0 - \kappa}{\kappa_0}\tilde{\lambda}\right)\right\rangle_{\partial\Omega} = \frac{1}{\kappa_0}\langle \tilde{\sigma}, \mathcal{V}\sigma_f\rangle_{\partial\Omega}\,. \tag{3.9}$$

It is a simple exercise to prove that the modified weak formulation (3.8)-(3.9) is indeed equivalent to the weak formulation (3.6).

Consider now Equations (3.8) and (3.9). We observe that Equation (3.9) involves only the unknown function $\tilde{\lambda} \in \breve{H}^{\frac{1}{2}}(\partial\Omega)$. It is therefore clear that if Equation (3.9) is uniquely solvable, then Equation (3.8) is also uniquely solvable, and hence the weak formulation (3.5) is well-posed. Following standard practice in functional analysis, we prove unique solvability of Equation (3.9) by establishing that the underlying reduced bilinear form is bounded and satisfies the inf-sup condition.

Remark 3.18. In principle, one could use the same complementary decomposition to split the weak formulation (2.5) for the induced surface charge ν. In this case however, we do not obtain the useful "upper-triangular" structure highlighted above, and consequently our subsequent analysis cannot be applied.

Definition 3.19. We define the "reduced" bilinear form $\tilde{a}\colon \breve{H}^{\frac{1}{2}}(\partial\Omega) \times \breve{H}^{-\frac{1}{2}}(\partial\Omega) \to \mathbb{R}$ as the mapping with the property that for all $\tilde{\lambda} \in \breve{H}^{\frac{1}{2}}(\partial\Omega)$ and all $\tilde{\sigma} \in \breve{H}^{-\frac{1}{2}}(\partial\Omega)$ it holds that

$$\tilde{a}(\tilde{\lambda}, \tilde{\sigma}) := \left\langle \tilde{\sigma}, \tilde{\lambda}\right\rangle_{\partial\Omega} - \left\langle \tilde{\sigma}, \mathcal{V}\mathrm{DtN}\left(\frac{\kappa_0 - \kappa}{\kappa_0}\tilde{\lambda}\right)\right\rangle_{\partial\Omega}.$$

We first prove that the reduced bilinear form $\tilde{a}$ is bounded.

Lemma 3.20. *Let the constant $C_{\tilde{A}}$ be defined as*

$$C_{\tilde{A}} := 1 + \max\left|\frac{\kappa - \kappa_0}{\kappa_0}\right| \cdot \left(\frac{c_{\mathcal{K}}^{\frac{3}{2}} c_{\mathrm{equiv}}}{\sqrt{c_{\mathcal{V}}}}\right), \tag{3.10}$$

and let the bilinear form $\tilde{a}\colon \breve{H}^{\frac{1}{2}}(\partial\Omega) \times \breve{H}^{-\frac{1}{2}}(\partial\Omega) \to \mathbb{R}$ be defined as in Definition 3.19. Then for all $\tilde{\lambda} \in \breve{H}^{\frac{1}{2}}(\partial\Omega)$ and all $\tilde{\sigma} \in \breve{H}^{-\frac{1}{2}}(\partial\Omega)$ it holds that

$$|\tilde{a}(\tilde{\lambda}, \tilde{\sigma})| \leq C_{\tilde{A}} |||\tilde{\lambda}||| \, |||\tilde{\sigma}|||^*.$$

Proof. Let the linear operator $\tilde{\mathcal{A}}\colon \breve{H}^{\frac{1}{2}}(\partial\Omega) \to \breve{H}^{\frac{1}{2}}(\partial\Omega)$ be defined as $\tilde{A} := \mathbb{P}_0^{\perp}\mathcal{A}\mathbb{P}_0^{\perp}$. Then $\tilde{\mathcal{A}}$ is the linear operator associated with the reduced bilinear form $\tilde{a}$. Since $|||\mathbb{P}_0^{\perp}\lambda||| \leq |||\lambda|||$ for all $\lambda \in H^{\frac{1}{2}}(\partial\Omega)$, the proof becomes identical to the first part of the proof of Lemma 3.16 with one minor modification. □

Remark 3.21. Consider the setting of Lemma 3.20 and the continuity constant $C_{\tilde{\mathcal{A}}}$ of the modified boundary integral operator $\tilde{\mathcal{A}}$. We observe that the constant $c_{\mathcal{K}}$ is bounded by one, and therefore the only non quantified constant appearing in the expression of $C_{\tilde{\mathcal{A}}}$ is the coercivity constant $c_{\mathcal{V}}$ of the single layer boundary operator. A priori, it is not clear how this coercivity constant depends on the geometrical setting of our problem including the number of open balls N in our system. The next step in our analysis therefore, is to obtain a closed form expression for this coercivity constant and to show in particular that it does not explicitly depend on N.

We first require the following lemma:

Lemma 3.22. *There exist constants $c_{\text{int}}, c_{\text{ext}} > 0$ that are independent of the number N of open balls such that for all harmonic functions $v \in H^1(\Omega^-)$ and $w \in H^1(\Omega^+)$ it holds that*

$$\|\gamma_N^- v\|_{H^{-\frac{1}{2}}(\partial\Omega)} \leq c_{\text{int}}\|\nabla v\|_{L^2(\Omega^-)}, \quad \text{and} \quad \|\gamma_N^+ w\|_{H^{-\frac{1}{2}}(\partial\Omega)} \leq c_{\text{ext}}\|\nabla w\|_{L^2(\Omega^+)}.$$

Additionally, the constant c_{int} depends only on the radii $\{r_j\}_{j=1}^N$ of the open balls while the constant c_{ext} depends on both the radii of the open balls as well as the minimum inter-sphere separation distance, i.e., $\min_{\substack{i,j\in\{1,\dots,N\}\\ i\neq j}} \left(|\mathbf{x}_i - \mathbf{x}_j| - r_i - r_j\right)$.

Proof. The first bound is straightforward to prove. Indeed, let $\mathcal{E}_{\mathcal{H}}^{\text{int}}\colon H^{\frac{1}{2}}(\partial\Omega) \to H^1(\Omega^-)$ be defined as the interior harmonic extension operator on Ω^-. A direct calculation yields

$$\begin{aligned}
\|\gamma_N^- v\|_{H^{-\frac{1}{2}}(\partial\Omega)} &= \sup_{0\neq\lambda\in H^{\frac{1}{2}}(\partial\Omega)} \frac{\langle\gamma_N^- v, \lambda\rangle_{\partial\Omega}}{\|\lambda\|_{H^{\frac{1}{2}}(\partial\Omega)}} = \sup_{0\neq\lambda\in H^{\frac{1}{2}}(\partial\Omega)} \frac{\int_{\Omega^-}\nabla v(x)\cdot\nabla\mathcal{E}_{\mathcal{H}}^{\text{int}}\lambda(x)\,dx}{\|\lambda\|_{H^{\frac{1}{2}}(\partial\Omega)}} \\
&\leq \|\nabla v\|_{L^2(\Omega^-)} \sup_{0\neq\lambda\in H^{\frac{1}{2}}(\partial\Omega)} \frac{\|\nabla\mathcal{E}_{\mathcal{H}}^{\text{int}}\lambda\|_{L^2(\Omega^-)}}{\|\lambda\|_{H^{\frac{1}{2}}(\partial\Omega)}} \\
&\leq \|\nabla v\|_{L^2(\Omega^-)} \sup_{0\neq\lambda\in H^{\frac{1}{2}}(\partial\Omega)} \frac{\|\mathcal{E}_{\mathcal{H}}^{\text{int}}\lambda\|_{H^1(\Omega^-)}}{\|\lambda\|_{H^{\frac{1}{2}}(\partial\Omega)}} \\
&\leq c_{\text{equiv}}\|\mathcal{E}_{\mathcal{H}}^{\text{int}}\|_{\text{OP}}\|\nabla v\|_{L^2(\Omega^-)},
\end{aligned}$$

where the N-independent norm equivalence constant c_{equiv} arises due to the fact that by our convention, $H^{\frac{1}{2}}(\partial\Omega)$ is equipped with the new $|||\cdot|||$ given by Definition 3.4 rather than the Sobolev-Slobodeckij norm $\|\cdot\|_{H^{\frac{1}{2}}(\partial\Omega)}$. Since Ω^- is simply the union of non-intersecting open balls, i.e., $\Omega^- = \cup_{j=1}^N\Omega_j$, it is easy to see that the operator norm

$\|\mathcal{E}^{\mathrm{int}}_{\mathcal{H}}\|_{\mathrm{OP}}$ depends only on the radii $\{r_j\}_{j=1}^N$ of the open balls $\{\Omega_j\}_{j=1}^N$ and is independent of the number N of open balls. This completes the proof for the first bound.

In order to compute the second bound, we require more work. The essential idea is to mimic the proof for the first bound but this requires us to first define an extension operator $\mathcal{E}_{\mathrm{external}}\colon H^{\frac{1}{2}}(\partial\Omega) \to H^1(\Omega^+)$ whose operator norm is also independent of N. We proceed in four steps.

Step 1) We first define a family of one-dimensional continuously differentiable cutoff functions. To this end, let $r > 0$ and $\epsilon > 0$ be real numbers. We define the cubic polynomial $p_{r,\epsilon}\colon \mathbb{R} \to \mathbb{R}$ as

$$\forall x \in \mathbb{R}\colon \quad p_{r,\epsilon}(x) = \frac{1}{\epsilon^3}\Big(2x^3 - 3(2r+\epsilon)x^2 + 6r(r+\epsilon)x - (r+\epsilon)^2(2r-\epsilon)\Big).$$

Then for any $r > 0$ and $\epsilon > 0$ we define the cutoff function $\phi_{r,\epsilon}\colon \mathbb{R} \to [0,1]$ as the mapping with the mapping with the property that for all $x \in \mathbb{R}$ it holds that

$$\phi_{r,\epsilon}(x) := \begin{cases} 1 & \text{if } x \leq r, \\ p_{r,\epsilon}(x) & \text{if } x \in (r, r+\epsilon), \\ 0 & \text{if } x \geq r+\epsilon. \end{cases}$$

Let $r > 0$ and $\epsilon > 0$ be fixed. It can readily be verified that the cutoff function $\phi_{r,\epsilon} \in C^1(\mathbb{R})$, $\|\phi_{r,\epsilon}\|_{L^\infty(\mathbb{R})} = 1$, and furthermore that $\|\phi'_{r,\epsilon}\|_{L^\infty(\mathbb{R})} = \frac{3}{2\epsilon}$.

Step 2) Let $i \in \{1, \ldots, N\}$. We define the (exterior) harmonic extension operator $\mathcal{E}^{\mathrm{ext}}_{i,\mathcal{H}}\colon H^{\frac{1}{2}}(\partial\Omega_i) \to H^1(\mathbb{R}^3 \setminus \Omega_i)$ as follows: Given any $\lambda_i \in H^{\frac{1}{2}}(\partial\Omega_i)$, there exist coefficients $[\lambda_i]_\ell^m$, $\ell \in \mathbb{N}_0$, $-\ell \leq m \leq \ell$ such that for all $\mathbf{x} \in \partial\Omega_i$ it holds that

$$\lambda_i(\mathbf{x}) = \sum_{\ell=0}^{m=\ell} \sum_{m=-\ell} [\lambda_i]_\ell^m \mathcal{Y}_\ell^m\left(\frac{\mathbf{x}-\mathbf{x}_i}{|\mathbf{x}-\mathbf{x}_i|}\right).$$

We therefore define

$$\big(\mathcal{E}^{\mathrm{ext}}_{i,\mathcal{H}}\lambda_i\big)(\mathbf{x}) := \sum_{\ell=0}^{\infty} \sum_{m=-\ell}^{m=\ell} [\lambda_i]_\ell^m \left(\frac{r_i}{|\mathbf{x}-\mathbf{x}_i|}\right)^{\ell+1} \mathcal{Y}_\ell^m\left(\frac{\mathbf{x}-\mathbf{x}_i}{|\mathbf{x}-\mathbf{x}_i|}\right), \tag{3.11}$$

for all $\mathbf{x} \in \mathbb{R}^3$ such that $|\mathbf{x}-\mathbf{x}_i| \geq r_i$. The boundedness of this operator can be deduced from the well-posedness and regularity results on the exterior Dirichlet problem for the Laplace equation.

Step 3) We now recall that we have by assumption that the minimum separation distance of the open balls $\{\Omega_i\}_{i=1}^N$ is uniformly bounded below with respect to N. Let $\widetilde{\epsilon} > 0$ be a

lower bound for this separation distance and define $\epsilon := \frac{\widetilde{\epsilon}}{4}$. Moreover, let once again $i \in \{1, \ldots, N\}$. We now define the *local* extension operator $\mathcal{E}^i_{\text{external}} \colon H^{\frac{1}{2}}(\partial\Omega_i) \to H^1(\Omega^+)$ as the mapping with the property that for all $\lambda_i \in H^{\frac{1}{2}}(\partial\Omega_i)$ and all $\mathbf{x} \in \Omega^+$ it holds that

$$\big(\mathcal{E}^i_{\text{external}}\lambda_i\big)(\mathbf{x}) := \big(\mathcal{E}^{\text{ext}}_{i,\mathcal{H}}\lambda_i\big)(\mathbf{x})\phi_{r_i,\epsilon}\big(|\mathbf{x}-\mathbf{x}_i|\big).$$

Intuitively, this local extension operator $\mathcal{E}^i_{\text{external}}$ takes as input Dirichlet data on $\partial\Omega_i$, constructs the exterior harmonic extension according to Equation (3.11), and then multiplies this extension with a smooth cut-off function. The following properties of this local extension operator can easily be deduced:

Property 1: For all $\mathbf{x} \in \Omega^+$ it holds that $\big|\big(\mathcal{E}^i_{\text{external}}\lambda_i\big)(\mathbf{x})\big| \leq \Big|\big(\mathcal{E}^{\text{ext}}_{i,\mathcal{H}}\lambda_i\big)(\mathbf{x})\Big|$.

Property 2: For all $\mathbf{x} \in \Omega^+$ such that $|\mathbf{x}-\mathbf{x}_i| \geq r_i + \epsilon$, it holds that $\big(\mathcal{E}^i_{\text{external}}\lambda_i\big)(\mathbf{x}) = 0$. In other words, the local extension operator $\mathcal{E}^i_{\text{external}}$ is zero outside a ball of radius $r_i + \epsilon$ centred at $\mathbf{x}_i$, i.e., the centre of the open ball Ω_i. This implies in particular that the local extension operator $\mathcal{E}^i_{\text{external}}$ is zero on all closed balls $\overline{\Omega_j}, j \in \{1, \ldots, N\}$ such that $j \neq i$.

Property 3: For all $\mathbf{x} \in \Omega^+$ such that $|\mathbf{x}-\mathbf{x}_i| < r_i + \epsilon$, the gradient $\nabla_{\mathbf{x}}\big(\mathcal{E}^i_{\text{external}}\lambda_i\big)(\mathbf{x})$ in cartesian coordinates satisfies:

$$\begin{aligned}
|\nabla_{\mathbf{x}}\big(\mathcal{E}^i_{\text{external}}\lambda_i\big)(\mathbf{x})| &= \Big|\phi_{r_i,\epsilon}\big(|\mathbf{x}-\mathbf{x}_i|\big)\nabla_{\mathbf{x}}\big(\mathcal{E}^{\text{ext}}_{i,\mathcal{H}}\lambda_i\big)(\mathbf{x}) + \big(\mathcal{E}^{\text{ext}}_{i,\mathcal{H}}\lambda_i\big)(\mathbf{x})\nabla_{\mathbf{x}}\phi_{r_i,\epsilon}\big(|\mathbf{x}-\mathbf{x}_i|\big)\Big| \\
&\leq \Big|\nabla_{\mathbf{x}}\big(\mathcal{E}^{\text{ext}}_{i,\mathcal{H}}\lambda_i\big)(\mathbf{x})\Big| + \Big|\big(\mathcal{E}^{\text{ext}}_{i,\mathcal{H}}\lambda_i\big)(\mathbf{x})\phi'_{r_i,\epsilon}\big(|\mathbf{x}-\mathbf{x}_i|\big)\Big| \\
&= \Big|\nabla_{\mathbf{x}}\big(\mathcal{E}^{\text{ext}}_{i,\mathcal{H}}\lambda_i\big)(\mathbf{x})\Big| + \frac{3}{2\epsilon}\Big|\big(\mathcal{E}^{\text{ext}}_{i,\mathcal{H}}\lambda_i\big)(\mathbf{x})\Big|.
\end{aligned}$$

Of course, we have not yet shown that the mapping $\mathcal{E}^i_{\text{external}} \colon H^{\frac{1}{2}}(\partial\Omega_i) \to H^1(\Omega^+)$ is bounded as claimed. In order to show this, let us denote by $B_{r_i+\epsilon}(\mathbf{x}_i)$ the open ball of radius $r_i + \epsilon$ with centre at $\mathbf{x}_i$. Combining properties 1 and 3 yields that

$$\begin{aligned}
\|\mathcal{E}^i_{\text{external}}\lambda_i\|^2_{H^1(\Omega^+)} &= \int_{\Omega^+} \frac{|\mathcal{E}^i_{\text{external}}\lambda_i(\mathbf{x})|^2}{1+|\mathbf{x}|^2}\,d\mathbf{x} + \int_{\Omega^+} |\nabla_{\mathbf{x}}\big(\mathcal{E}^i_{\text{external}}\lambda_i\big)(\mathbf{x})|^2\,d\mathbf{x} \\
&\leq \left(1 + \frac{9}{2\epsilon^2}\right)\int_{\Omega^+\cap B_{r_i+\epsilon}(\mathbf{x}_i)} |\mathcal{E}^{\text{ext}}_{i,\mathcal{H}}\lambda_i(\mathbf{x})|^2\,d\mathbf{x} \\
&\quad + 2\int_{\Omega^+\cap B_{r_i+\epsilon}(\mathbf{x}_i)} \Big|\nabla_{\mathbf{x}}\big(\mathcal{E}^{\text{ext}}_{i,\mathcal{H}}\lambda_i\big)(\mathbf{x})\Big|^2\,d\mathbf{x} \\
&\leq \max\left\{2, 1 + \frac{9}{2\epsilon^2}\right\}\|\mathcal{E}^{\text{ext}}_{i,\mathcal{H}}\lambda_i\|^2_{H^1\left(\Omega^+\cap B_{r_i+\epsilon}(\mathbf{x}_i)\right)}.
\end{aligned}$$

In order to simplify the final expression we first use Equation (3.11) to simplify the $L^2\big(\Omega^+ \cap B_{r_i+\epsilon}(\mathbf{x}_i)\big)$ norm. Recall that we have adopted the convention that the

space $H^{\frac{1}{2}}(\partial\Omega_i)$ is equipped with the norm $|||\cdot|||_{H^{\frac{1}{2}}(\partial\Omega_i)}$ defined through Definition 3.8. A direct calculation thus yields

$$\begin{aligned}\|\mathcal{E}^{\text{ext}}_{i,\mathcal{H}}\lambda_i\|^2_{L^2\left(\Omega^+\cap B_{r_i+\epsilon}(\mathbf{x}_i)\right)} &\leq \frac{1}{3}\left((r_i+\epsilon)^3 - r_i^3\right)\sum_{\ell=0}^{\infty}\sum_{m=-\ell}^{\ell}([\lambda_i]^m_\ell)^2 \\ &= \left(\epsilon r_i^2 + \epsilon^2 r_i + \frac{\epsilon^3}{3}\right)\sum_{\ell=0}^{\infty}\sum_{m=-\ell}^{\ell}([\lambda_i]^m_\ell)^2 \\ &\leq \epsilon\max\left\{\frac{1}{r_i}, \frac{1}{r_i^2}\right\}\left(r_i^2 + \epsilon r_i + \frac{\epsilon^2}{3}\right)|||\lambda_i|||^2_{H^{\frac{1}{2}}(\partial\Omega_i)}.\end{aligned}$$

Next, we use the fact that the local extension $\mathcal{E}^{\text{ext}}_{i,\mathcal{H}}\lambda_i$ is a harmonic function so that Green's identity applies in the domain $\Omega^+\cap B_{r_i+\epsilon}(\mathbf{x}_i)$. Simple calculus then yields that

$$\begin{aligned}\|\nabla\mathcal{E}^{\text{ext}}_{i,\mathcal{H}}\lambda_i\|^2_{L^2\left(\Omega^+\cap B_{r_i+\epsilon}(\mathbf{x}_i)\right)} &= r_i^2\sum_{\ell=0}^{\infty}\sum_{m=-\ell}^{\ell}\frac{\ell+1}{r_i}([\lambda_i]^m_\ell)^2 \\ &\quad - (r_i+\epsilon)^2\sum_{\ell=0}^{\infty}\sum_{m=-\ell}^{\ell}\frac{\ell+1}{r_i+\epsilon}([\lambda_i]^m_\ell)^2\left(\frac{r_i}{r_i+\epsilon}\right)^{2\ell+2} \\ &= r_i^2\sum_{\ell=0}^{\infty}\sum_{m=-\ell}^{\ell}(\ell+1)([\lambda_i]^m_\ell)^2\left(\frac{1}{r_i} - \frac{1}{r_i+\epsilon}\left(\frac{r_i}{r_i+\epsilon}\right)^{2\ell}\right) \\ &= r_i^2\sum_{\ell=0}^{\infty}\sum_{m=-\ell}^{\ell}(\ell+1)([\lambda_i]^m_\ell)^2\frac{(r_i+\epsilon)^{2\ell+1} - r_i^{2\ell+1}}{r_i(r_i+\epsilon)^{2\ell+1}}.\end{aligned}$$

This last expression can be further simplified by observing that for all $\ell \geq 0$ it holds that

$$\begin{aligned}\frac{(r_i+\epsilon)^{2\ell+1} - r_i^{2\ell+1}}{r_i(r_i+\epsilon)^{2\ell+1}} &= \frac{(1+\frac{\epsilon}{r_i})^{2\ell+1} - 1}{r_i(1+\frac{\epsilon}{r_i})^{2\ell+1}} = \frac{\frac{\epsilon}{r_i}(1+\frac{\epsilon}{r_i})^{2\ell} + (1+\frac{\epsilon}{r_i})^{2\ell} - 1}{r_i(1+\frac{\epsilon}{r_i})^{2\ell+1}} \\ &\leq \frac{\epsilon}{r_i^2}\frac{(1+\frac{\epsilon}{r_i})^{2\ell}}{(1+\frac{\epsilon}{r_i})^{2\ell+1}} \leq \frac{\epsilon}{r_i^2}.\end{aligned}$$

We conclude that

$$\begin{aligned}\|\nabla\mathcal{E}^{\text{ext}}_{i,\mathcal{H}}\lambda_i\|^2_{L^2\left(\Omega^+\cap B_{r_i+\epsilon}(\mathbf{x}_i)\right)} &\leq \epsilon\sum_{\ell=0}^{\infty}\sum_{m=-\ell}^{\ell}(\ell+1)([\lambda_i]^m_\ell)^2 \\ &\leq 2\epsilon\max\left\{\frac{1}{r_i}, \frac{1}{r_i^2}\right\}|||\lambda_i|||^2_{H^{\frac{1}{2}}(\partial\Omega_i)}.\end{aligned}$$

Consequently, we can define a constant $C_{r_i,\epsilon} > 0$ depending only on ϵ and r_i as

$$C_{r_i,\epsilon} := \epsilon \max\left\{\frac{1}{r_i}, \frac{1}{r_i^2}\right\} \max\{r_i^2 + \epsilon r_i + \frac{\epsilon^2}{3}, 2\}, \tag{3.12}$$

and we obtain that

$$\begin{aligned} \|\mathcal{E}^i_{\text{external}}\lambda_i\|^2_{H^1(\Omega^+)} &\leq \max\left\{2, 1 + \frac{9}{2\epsilon^2}\right\} \|\mathcal{E}^{\text{ext}}_{i,\mathcal{H}}\lambda_i\|^2_{H^1\left(\Omega^+ \cap B_{r_i+\epsilon}(\mathbf{x}_i)\right)} \\ &\leq \max\left\{2, 1 + \frac{9}{2\epsilon^2}\right\} C_{r_i,\epsilon} |||\lambda_i|||^2_{H^{\frac{1}{2}}(\partial\Omega_i)}. \end{aligned} \tag{3.13}$$

It follows that the local extension operator $\mathcal{E}^i_{\text{external}} \colon H^{\frac{1}{2}}(\partial\Omega_i) \to H^1(\Omega^+)$ is indeed bounded.

Step 4) We are now ready to define the extension operator $\mathcal{E}_{\text{external}} \colon H^{\frac{1}{2}}(\partial\Omega) \to H^1(\Omega^+)$. Given $\lambda \in H^{\frac{1}{2}}(\partial\Omega)$ and denoting $\lambda_i := \lambda|_{\partial\Omega_i}$ for each $i \in \{1, \ldots, N\}$, we define:

$$\mathcal{E}_{\text{external}}(\lambda) := \sum_{i=1}^{N} \mathcal{E}^i_{\text{external}}\lambda_i.$$

Property 2 of the local extension operators $\mathcal{E}^i_{\text{external}}$, $i = 1, \ldots, N$ now yields that $\gamma^+\big(\mathcal{E}_{\text{external}}(\lambda)\big) = \lambda$. Moreover, from the bound (3.13) we see that

$$\begin{aligned} \|\mathcal{E}_{\text{external}}(\lambda)\|^2_{H^1(\Omega^+)} &\leq \max\left\{2, 1 + \frac{9}{\epsilon^2}\right\} \max_{i=1,\ldots,N} C_{r_i,\epsilon} \sum_{i=1}^{N} |||\lambda_i|||^2_{H^{\frac{1}{2}}(\partial\Omega_i)} \\ &= \max\left\{2, 1 + \frac{9}{\epsilon^2}\right\} \max_{i=1,\ldots,N} C_{r_i,\epsilon} |||\lambda|||^2. \end{aligned}$$

Thus, the mapping $\mathcal{E}_{\text{external}} \colon H^{\frac{1}{2}}(\partial\Omega) \to H^1(\Omega^+)$ is indeed a bounded extension operator with operator norm

$$\|\mathcal{E}_{\text{external}}\|^2_{\text{OP}} := \max\left\{2, 1 + \frac{9}{\epsilon^2}\right\} \max_{i=1,\ldots,N} C_{r_i,\epsilon},$$

Notice that the operator norm is independent of the number N of open balls and depends only the radii of the open balls $\{\Omega_i\}_{i=1}^N$ and the minimal inter-sphere separation distance ϵ. Furthermore, it follows from Equation (3.12) that $\max_{i=1,\ldots,N} C_{r_i,\epsilon} = \mathcal{O}(\epsilon)$ as $\epsilon \to 0$. Consequently, we obtain that $\|\mathcal{E}_{\text{external}}\|^2_{\text{OP}} = \mathcal{O}\big(\frac{1}{\epsilon}\big)$ as $\epsilon \to 0$.

Using the extension operator $\mathcal{E}_{\text{external}}$ we have just defined, we can mimic the calculations performed in the beginning of this proof in order to obtain the second, required bound:

$$\|\gamma_N^+ w\|_{H^{-\frac{1}{2}}(\partial\Omega)} \leq c_{\text{equiv}} \|\mathcal{E}_{\text{external}}\|_{\text{OP}} \|\nabla w\|_{L^2(\Omega^+)}.$$

Here, the N-independent norm equivalence constant c_{equiv} arises once again due to the fact that the canonical dual norm $\|\cdot\|_{H^{-\frac{1}{2}}(\partial\Omega)}$ is defined with respect to the Sobolev-Slobodeckij norm $\|\cdot\|_{H^{\frac{1}{2}}(\partial\Omega)}$ rather than the new $|||\cdot|||$ norm given by Definition 3.4. Defining $c_{\text{int}} := c_{\text{equiv}}\|\mathcal{E}_{\mathcal{H}}^{\text{int}}\|_{\text{OP}}$ and $c_{\text{ext}} := c_{\text{equiv}}\|\mathcal{E}_{\text{external}}\|_{\text{OP}}$ completes the proof. □

We can now deduce a lower bound for the coercivity constant $c_{\mathcal{V}}$ of the single layer boundary operator.

Lemma 3.23. *Let the constants $c_{\text{int}} > 0$ and $c_{\text{ext}} > 0$ be defined as in Lemma 3.22 and let $c_{\mathcal{V}} > 0$ denote the coercivity constant of the single layer boundary operator $\mathcal{V}\colon H^{\frac{1}{2}}(\partial\Omega) \to H^{\frac{1}{2}}(\partial\Omega)$. Then it holds that*

$$c_{\mathcal{V}} \geq \frac{1}{2}\min\left\{\frac{1}{c_{\text{int}}^2}, \frac{1}{c_{\text{ext}}^2}\right\}.$$

Proof. Let $\sigma \in H^{-\frac{1}{2}}(\partial\Omega)$ and let $u = \mathcal{S}\sigma \in H^1_{\text{loc}}(\mathbb{R}^3)$. It follows from the jump properties of the single layer potential (see Theorem 1.23 in Section 1.4) that

$$\langle \sigma, \mathcal{V}\sigma\rangle_{\partial\Omega} = \int_{\Omega^-} |\nabla u(x)|^2\, dx + \int_{\Omega^+} |\nabla u(x)|^2\, dx.$$

Lemma 3.22 therefore yields that

$$\begin{aligned}
\langle \sigma, \mathcal{V}\sigma\rangle_{\partial\Omega} &\geq \frac{1}{c_{\text{int}}^2}\|\gamma_N^- u\|^2_{H^{-\frac{1}{2}}(\partial\Omega)} + \frac{1}{c_{\text{ext}}^2}\|\gamma_N^+ u\|^2_{H^{-\frac{1}{2}}(\partial\Omega)} \\
&\geq \min\left\{\frac{1}{c_{\text{int}}^2}, \frac{1}{c_{\text{ext}}^2}\right\}\left(\|\gamma_N^- u\|^2_{H^{-\frac{1}{2}}(\partial\Omega)} + \|\gamma_N^+ u\|^2_{H^{-\frac{1}{2}}(\partial\Omega)}\right) \\
&\geq \min\left\{\frac{1}{c_{\text{int}}^2}, \frac{1}{c_{\text{ext}}^2}\right\}\left(\frac{1}{2}\|\gamma_N^- u - \gamma_N^+ u\|^2_{H^{-\frac{1}{2}}(\partial\Omega)}\right) \\
&= \frac{1}{2}\min\left\{\frac{1}{c_{\text{int}}^2}, \frac{1}{c_{\text{ext}}^2}\right\}\|\sigma\|^2_{H^{-\frac{1}{2}}(\partial\Omega)}.
\end{aligned}$$

□

Remark 3.24. Consider the settings of Lemma 3.22 and Lemma 3.23. Two facts can be deduced from the proofs of these results. First, that the coercivity constant $c_{\mathcal{V}}$ of the single layer boundary operator depends only on the radii $\{r_j\}_{j=1}^N$ of the open balls $\{\Omega_j\}_{j=1}^N$ and the minimal inter-sphere separation distance. As a consequence, the continuity constant $C_{\widetilde{\mathcal{A}}}$ of the reduced bilinear form $\tilde{a}$ (see Lemma 3.20) depends only on the radii of the open balls, the minimal inter-sphere separation distance, and the dielectric constants $\{\kappa_j\}_{j=1}^N$. Second, we have also obtained significant insight into the behaviour of the coercivity constant $c_{\mathcal{V}}$ for small minimal inter-sphere separation distance. Indeed, let $\epsilon := \min_{\substack{i,j\in\{1,\dots,N\}\\ i\neq j}}\left(|\mathbf{x}_i - \mathbf{x}_j| - r_i - r_j\right)$. Then $c_{\mathcal{V}} = \mathcal{O}(\epsilon)$ for $\epsilon \to 0$. This result implies that the continuity constant $C_{\widetilde{\mathcal{A}}}$ grows with rate at most $\mathcal{O}(\frac{1}{\sqrt{\epsilon}})$ as $\epsilon \to 0$.

Now that we have analysed the continuity constant $C_{\tilde{A}}$ of the reduced bilinear form $\tilde{a}\colon \breve{H}^{\frac{1}{2}}(\partial\Omega) \times \breve{H}^{-\frac{1}{2}}(\partial\Omega) \to \mathbb{R}$ in detail, the next step in our analysis is to prove that this bilinear form satisfies the inf-sup condition.

Lemma 3.25. *Let the bilinear form $\tilde{a}\colon \breve{H}^{\frac{1}{2}}(\partial\Omega) \times \breve{H}^{-\frac{1}{2}}(\partial\Omega) \to \mathbb{R}$ be defined as in Definition 3.19. Then there exists a constant $\beta_{\tilde{A}} > 0$ that depends only on the dielectric function κ and the dielectric constant $\kappa_0 > 0$ of the external medium such that*

(i) It holds that

$$\inf_{0\neq\tilde{\lambda}\in\breve{H}^{\frac{1}{2}}(\partial\Omega)} \sup_{0\neq\tilde{\sigma}\in\breve{H}^{-\frac{1}{2}}(\partial\Omega)} \frac{|\tilde{a}(\tilde{\lambda},\tilde{\sigma})|}{|||\tilde{\lambda}||| \, |||\tilde{\sigma}|||^*} \geq \beta_{\tilde{A}} > 0; \qquad \text{(Bounded Below)}$$

(ii) For all $0 \neq \tilde{\sigma} \in \breve{H}^{-\frac{1}{2}}(\partial\Omega)$ it holds that

$$\sup_{0\neq\tilde{\lambda}\in\breve{H}^{\frac{1}{2}}(\partial\Omega)} |\tilde{a}(\tilde{\lambda},\tilde{\sigma})| > 0. \qquad \text{(Dense Range)}$$

Proof. The proof relies on the fact that the Dirichlet-to-Neumann map $\mathrm{DtN}\colon \breve{H}^{\frac{1}{2}}(\partial\Omega) \to \breve{H}^{-\frac{1}{2}}(\partial\Omega)$ is an isomorphism. We first prove Property *(i)*. To this end, let $\widehat{\lambda} \in \breve{H}^{\frac{1}{2}}(\partial\Omega)$ be arbitrary. We decompose $\widehat{\lambda}$ as the sum of two functions as follows:

$$\widehat{\lambda} = \widehat{\lambda}_+ + \widehat{\lambda}_-.$$

Here, $\widehat{\lambda}_+ \in \breve{H}^{\frac{1}{2}}(\partial\Omega)$ is a function equal to $\widehat{\lambda}$ on all spheres $\partial\Omega_i$, $i \in \{1,\dots,N\}$ such that $\kappa_i - \kappa_0 > 0$ and zero otherwise. Similarly, $\widehat{\lambda}_- \in \breve{H}^{\frac{1}{2}}(\partial\Omega)$ is a function equal to $\widehat{\lambda}$ on all spheres $\partial\Omega_i$, $i \in \{1,\dots,N\}$ such that $\kappa_i - \kappa_0 < 0$ and zero otherwise. We recall that due to the modelling assumption **MA3)** from Section 2.2, we have $\kappa \neq \kappa_0$ (see also Remark 2.5).

We now define a corresponding test function $\widehat{\sigma} \in \breve{H}^{\frac{1}{2}}(\partial\Omega)$ by setting

$$\widehat{\sigma} := \frac{\kappa-\kappa_0}{\kappa_0}\mathrm{DtN}\widehat{\lambda}_+ - \frac{\kappa-\kappa_0}{\kappa_0}\mathrm{DtN}\widehat{\lambda}_-.$$

For notational convenience, we define sets of indices $N_+, N_- \subset \mathbb{N}$ such that $i \in N_+ \iff \kappa_i - \kappa_0 > 0$ and $i \in N_- \iff \kappa_i - \kappa_0 < 0$. Moreover, for all $j = 1,\dots,N$ we define

$$\widehat{\lambda}_j := \begin{cases} \widehat{\lambda} & \text{on } \partial\Omega_j, \\ 0 & \text{otherwise,} \end{cases} \qquad \widehat{\sigma}_j := \begin{cases} \widehat{\sigma} & \text{on } \partial\Omega_j, \\ 0 & \text{otherwise,} \end{cases}$$

It follows that the reduced bilinear form $\tilde{a}$ satisfies

$$\tilde{a}(\widehat{\lambda},\widehat{\sigma}) = \sum_{j\in N_+} \frac{\kappa_j-\kappa_0}{\kappa_0}|||\widehat{\lambda}_j|||^2 + \sum_{j\in N_-} \frac{\kappa_0-\kappa_j}{\kappa_0}|||\widehat{\lambda}_j|||^2 + \underbrace{\left\langle \widehat{\sigma}, \mathcal{V}\mathrm{DtN}\left(\frac{\kappa-\kappa_0}{\kappa_0}\widehat{\lambda}\right)\right\rangle_{\partial\Omega}}_{:=J}.$$

Note that due to our choice of test function $\widehat{\sigma}$, the coefficients of all terms in the above two sums are positive. Therefore, let us focus on analysing the term J. Using the decomposition we have introduced, we obtain that

$$J = \left\langle \widehat{\sigma}, \mathcal{V}\mathrm{DtN}\left(\frac{\kappa-\kappa_0}{\kappa_0}\widehat{\lambda}\right)\right\rangle_{\partial\Omega} = \left\langle \mathrm{DtN}\left(\frac{\kappa-\kappa_0}{\kappa_0}\widehat{\lambda}_+\right), \mathcal{V}\mathrm{DtN}\left(\frac{\kappa-\kappa_0}{\kappa_0}\widehat{\lambda}_+\right)\right\rangle_{\partial\Omega} - \left\langle \mathrm{DtN}\left(\frac{\kappa-\kappa_0}{\kappa_0}\widehat{\lambda}_-\right), \mathcal{V}\mathrm{DtN}\left(\frac{\kappa-\kappa_0}{\kappa_0}\widehat{\lambda}_-\right)\right\rangle_{\partial\Omega}.$$

Using the Calderón identities (see Lemma 1.31), we further obtain that

$$-\left\langle \mathrm{DtN}\left(\frac{\kappa-\kappa_0}{\kappa_0}\widehat{\lambda}_-\right), \mathcal{V}\mathrm{DtN}\left(\frac{\kappa-\kappa_0}{\kappa_0}\widehat{\lambda}_-\right)\right\rangle_{\partial\Omega} = -\left\langle \mathrm{DtN}\left(\frac{\kappa-\kappa_0}{\kappa_0}\widehat{\lambda}_-\right), \left(\frac{\kappa-\kappa_0}{\kappa_0}\widehat{\lambda}_-\right)\right\rangle_{\partial\Omega} + \left\langle \mathcal{W}\left(\frac{\kappa-\kappa_0}{\kappa_0}\widehat{\lambda}_-\right), \left(\frac{\kappa-\kappa_0}{\kappa_0}\widehat{\lambda}_-\right)\right\rangle_{\partial\Omega}.$$

The non-negativity of the hypersingular operator $\mathcal{W}\colon H^{\frac{1}{2}}(\partial\Omega) \to H^{-\frac{1}{2}}(\partial\Omega)$ (see Theorem 1.28) thus implies that

$$J \geq -\left\langle \mathrm{DtN}\left(\frac{\kappa-\kappa_0}{\kappa_0}\widehat{\lambda}_-\right), \left(\frac{\kappa-\kappa_0}{\kappa_0}\widehat{\lambda}_-\right)\right\rangle_{\partial\Omega} = -\sum_{j\in N_-}\left(\frac{\kappa_j-\kappa_0}{\kappa_0}\right)^2 |||\widehat{\lambda}_j|||^2.$$

Consequently, we obtain that

$$\begin{aligned}
\tilde{a}(\widehat{\lambda},\widehat{\sigma}) &\geq \sum_{j\in N_+}\frac{\kappa_j-\kappa_0}{\kappa_0}|||\widehat{\lambda}_j|||^2 + \sum_{j\in N_-}\frac{\kappa_0-\kappa_j}{\kappa_0}|||\widehat{\lambda}_j|||^2 - \sum_{j\in N_-}\left(\frac{\kappa_0-\kappa_j}{\kappa_0}\right)^2|||\widehat{\lambda}_j|||^2 \\
&= \sum_{j\in N_+}\frac{\kappa_j-\kappa_0}{\kappa_0}|||\widehat{\lambda}_j|||^2 - \sum_{j\in N_-}\frac{\kappa_j}{\kappa_0}\frac{\kappa_j-\kappa_0}{\kappa_0}|||\widehat{\lambda}_j|||^2 \\
&\geq \min\left\{\min_{j\in N_+}\frac{\kappa_j-\kappa_0}{\kappa_0}, \min_{j\in N_-}\frac{\kappa_j}{\kappa_0}\frac{\kappa_0-\kappa_j}{\kappa_0}\right\}|||\widehat{\lambda}|||^2.
\end{aligned}$$

Furthermore, using Remark 3.7 we obtain that the norm of the test function $\widehat{\sigma}$ satisfies

$$\begin{aligned}
|||\widehat{\sigma}|||^* &= \left|\left|\left|\frac{\kappa-\kappa_0}{\kappa_0}\mathrm{DtN}\widehat{\lambda}_+ - \frac{\kappa-\kappa_0}{\kappa_0}\mathrm{DtN}\widehat{\lambda}_-\right|\right|\right|^* \\
&= \left|\left|\left|\frac{\kappa-\kappa_0}{\kappa_0}\widehat{\lambda}_+ - \frac{\kappa-\kappa_0}{\kappa_0}\widehat{\lambda}_-\right|\right|\right| \\
&\leq \max_{j=1,\dots,N}\left|\frac{\kappa_j-\kappa_0}{\kappa_0}\right| |||\widehat{\lambda}|||.
\end{aligned}$$

We therefore define the constant $\beta_{\tilde{A}} > 0$ as

$$\beta_{\tilde{A}} := \frac{\min\left\{\min_{j\in N_+}\frac{\kappa_j-\kappa_0}{\kappa_0}, \min_{j\in N_-}\frac{\kappa_j}{\kappa_0}\frac{\kappa_0-\kappa_j}{\kappa_0}\right\}}{\max_{j=1,\dots,N}\left|\frac{\kappa_j-\kappa_0}{\kappa_0}\right|}. \tag{3.14}$$

We then obtain that

$$\inf_{0\neq\tilde{\lambda}\in\breve{H}^{\frac{1}{2}}(\partial\Omega)} \sup_{0\neq\tilde{\sigma}\in\breve{H}^{-\frac{1}{2}}(\partial\Omega)} \frac{|\tilde{a}(\tilde{\lambda},\tilde{\sigma})|}{|||\tilde{\lambda}||| \, |||\tilde{\sigma}|||^*} \geq \beta_{\tilde{\mathcal{A}}},$$

which completes the proof of Property *(i)*.

Let us now turn to the proof of Property *(ii)*. Let $0 \neq \widehat{\sigma} \in \breve{H}^{-\frac{1}{2}}(\partial\Omega)$ be arbitrary and let $\mathrm{NtD}\colon \breve{H}^{-\frac{1}{2}}(\partial\Omega) \to \breve{H}^{\frac{1}{2}}(\partial\Omega)$ be the inverse of the Dirichlet-to-Neumann map. Using the decomposition and notation developed above, it is possible to define a corresponding function $\widehat{\lambda} \in \breve{H}^{\frac{1}{2}}(\partial\Omega)$ as

$$\widehat{\lambda} := \sum_{j\in N_+} \frac{\kappa_0}{\kappa_j - \kappa_0} \mathrm{NtD}\widehat{\sigma}_j - \sum_{j\in N_-} \frac{\kappa_0}{\kappa_j - \kappa_0} \mathrm{NtD}\widehat{\sigma}_j.$$

With this choice of $\widehat{\lambda}$, we immediately obtain that

$$\widehat{\sigma} = \sum_{j\in N_+} \frac{\kappa_j - \kappa_0}{\kappa_0} \mathrm{DtN}\widehat{\lambda}_j - \sum_{j\in N_-} \frac{\kappa_j - \kappa_0}{\kappa_0} \mathrm{DtN}\widehat{\lambda}_j.$$

Therefore, a similar calculation to the one used to prove Property *(i)* reveals that

$$\begin{aligned} |\tilde{a}(\widehat{\lambda},\widehat{\sigma})| &\geq \min\left\{ \min_{j\in N_+} \frac{\kappa_j - \kappa_0}{\kappa_0}, \min_{j\in N_-} \frac{\kappa_j}{\kappa_0}\frac{\kappa_0 - \kappa_j}{\kappa_0} \right\} |||\widehat{\lambda}|||^2 \\ &\geq \frac{\beta_{\tilde{\mathcal{A}}}}{\max_{j=1,\ldots,N} \left|\frac{\kappa_j - \kappa_0}{\kappa_0}\right|} \left(|||\widehat{\sigma}|||^*\right)^2. \end{aligned}$$

We conclude that for all $0 \neq \tilde{\sigma} \in \breve{H}^{-\frac{1}{2}}(\partial\Omega)$ it holds that

$$\sup_{0\neq\tilde{\lambda}\in\breve{H}^{\frac{1}{2}}(\partial\Omega)} |\tilde{a}(\tilde{\lambda},\tilde{\sigma})| > 0.$$

This completes the proof. □

An immediate consequence of Lemma 3.25 is that both the modified weak formulation (3.8)-(3.9) and the weak formulation (3.6) are well-posed.

3.3.1.3 The new analysis of the discrete problem

Our next goal is to prove that the Galerkin discretisation (3.7) is also well-posed with a stability constant that is independent of the number of open balls N. Similar to the infinite-dimensional case, we adopt an indirect approach, and reformulate Equation (3.7) as a modified Galerkin discretisation using the projection operators $\mathbb{P}_0$ and $\mathbb{P}_0^{\perp}$ introduced through Lemma 3.2. We first define the relevant approximation space.

Definition 3.26 (Reduced Global Approximation Space)**.** Let $\ell_{\max} \in \mathbb{N}$. We define the finite-dimensional Hilbert space $W_0^{\ell_{\max}} \subset \breve{H}^{\frac{1}{2}}(\partial\Omega)$ as the set

$$W_0^{\ell_{\max}} := \Big\{ u \in W^{\ell_{\max}}(\partial\Omega) \colon \mathbb{P}_0 u = 0 \Big\},$$

equipped with the $(\cdot,\cdot)_{W^{\ell_{\max}}}$ inner product.

Remark 3.27. Using the fact that the spherical harmonics functions are smooth, we can immediately infer that the finite-dimensional Hilbert spaces $W_0^{\ell_{\max}} \subset W^{\ell_{\max}} \subset \breve{H}^{\frac{1}{2}}(\partial\Omega)$ also satisfy

$$W_0^{\ell_{\max}} \subset W^{\ell_{\max}} \subset \breve{H}^{-\frac{1}{2}}(\partial\Omega) \quad \text{and} \quad \forall \lambda_{\ell_{\max}} \in W_0^{\ell_{\max}} \colon \ \|\lambda_{\ell_{\max}}\|^2_{W^{\ell_{\max}}} = |||\lambda_{\ell_{\max}}|||^2.$$

Note that if one wishes to view $W^{\ell_{\max}}$ and $W_0^{\ell_{\max}}$ as subspaces of $H^{-\frac{1}{2}}(\partial\Omega)$, then the definition of the equipped norms would have to be modified accordingly.

Modified Galerkin discretisation of the Integral Equation (3.5)

Let $\sigma_f \in H^{-\frac{1}{2}}(\partial\Omega)$. Find functions $(\lambda_0, \lambda_{\ell_{\max}}) \in \mathcal{C}(\partial\Omega) \times W_0^{\ell_{\max}}$ such that for all test functions $(\sigma_0, \sigma_{\ell_{\max}}) \in \mathcal{C}(\partial\Omega) \times W_0^{\ell_{\max}}$ it holds that

$$(\sigma_0, \lambda_0)_{L^2(\partial\Omega)} - \left(\sigma_0, \mathcal{V}\mathrm{DtN}\Big(\frac{\kappa_0 - \kappa}{\kappa_0} \lambda_{\ell_{\max}} \Big) \right)_{L^2(\partial\Omega)} = \frac{1}{\kappa_0} (\sigma_0, \mathcal{V}\sigma_f)_{L^2(\partial\Omega)}, \tag{3.15}$$

$$(\sigma_{\ell_{\max}}, \lambda_{\ell_{\max}})_{L^2(\partial\Omega)} - \left(\sigma_{\ell_{\max}}, \mathcal{V}\mathrm{DtN}\Big(\frac{\kappa_0 - \kappa}{\kappa_0} \lambda_{\ell_{\max}} \Big) \right)_{L^2(\partial\Omega)} = \frac{1}{\kappa_0} (\sigma_{\ell_{\max}}, \mathcal{V}\sigma_f)_{L^2(\partial\Omega)}. \tag{3.16}$$

It is a simple exercise to prove that the modified Galerkin discretisation (3.15)-(3.16) is indeed equivalent to the Galerkin discretisation (3.7).

The structure of the Galerkin discretisation (3.15)-(3.16) is very similar to the structure of the infinite-dimensional modified weak formulation (3.8)-(3.9). Indeed, we observe once again that Equation (3.16) involves only the unknown function $\lambda_{\ell_{\max}} \in W_0^{\ell_{\max}}$. It is therefore clear that if Equation (3.16) is uniquely solvable, then Equation (3.15) is also uniquely solvable, and hence the Galerkin discretisation (3.7) is well-posed. Moreover, thanks to the analysis carried out for the infinite-dimensional Equation (3.9), well-posedness of the finite-dimensional equation (3.16) follows almost immediately. Indeed, we have the following result.

Lemma 3.28. *Let the bilinear form $\tilde{a} \colon \breve{H}^{\frac{1}{2}}(\partial\Omega) \times \breve{H}^{-\frac{1}{2}}(\partial\Omega) \to \mathbb{R}$ be defined as in Definition 3.19, and let the constant $\beta_{\tilde{A}} > 0$ be defined through Equation (3.14) as in the proof of Lemma 3.25. Then it holds that*

$$\inf_{0 \neq \lambda_{\ell_{\max}} \in W_0^{\ell_{\max}}} \sup_{0 \neq \sigma_{\ell_{\max}} \in W_0^{\ell_{\max}}} \frac{|\tilde{a}(\lambda_{\ell_{\max}}, \sigma_{\ell_{\max}})|}{|||\lambda_{\ell_{\max}}||| \, |||\sigma_{\ell_{\max}}|||_*} \geq \beta_{\tilde{A}} > 0. \qquad \text{(Discrete inf-sup Condition)}$$

Proof. The proof uses the fact that the Dirichlet-to-Neumann operator DtN: $W_0^{\ell_{\max}} \to W_0^{\ell_{\max}}$ is an isomorphism. Indeed, consider $\lambda_j \in W_0^{\ell_{\max}}(\partial\Omega_j)$ given by

$$\lambda_j(\mathbf{x}) = \sum_{\ell=1}^{\ell_{\max}} \sum_{m=-\ell}^{m=+\ell} [\lambda_j]_\ell^m \mathcal{Y}_\ell^m \left(\frac{\mathbf{x}-\mathbf{x}_j}{|\mathbf{x}-\mathbf{x}_j|} \right).$$

Then the function $\mathrm{DtN}\lambda_j \in W_0^{\ell_{\max}}$ is given by

$$\mathrm{DtN}\lambda_j(\mathbf{x}) = \sum_{\ell=1}^{\ell_{\max}} \sum_{m=-\ell}^{m=+\ell} \frac{\ell}{r_j} [\lambda_j]_\ell^m \mathcal{Y}_\ell^m \left(\frac{\mathbf{x}-\mathbf{x}_j}{|\mathbf{x}-\mathbf{x}_j|} \right).$$

Consequently given any arbitrary function $\widehat{\lambda} \in W_0^{\ell_{\max}} \subset \breve{H}^{\frac{1}{2}}(\partial\Omega)$, we may pick as the test function $\widehat{\sigma} \in W_0^{\ell_{\max}} \subset \breve{H}^{-\frac{1}{2}}(\partial\Omega)$ given by

$$\widehat{\sigma} = \frac{\kappa - \kappa_0}{\kappa_0} \mathrm{DtN}\widehat{\lambda}_+ - \frac{\kappa - \kappa_0}{\kappa_0} \mathrm{DtN}\widehat{\lambda}_-,$$

where we have used the decomposition $\widehat{\lambda} = \widehat{\lambda}_+ + \widehat{\lambda}_-$ introduced in the proof of Lemma 3.25. The remainder of the proof is now identical to the proof of Lemma 3.25 and yields the discrete inf-sup constant $\beta_{\tilde{\mathcal{A}}}$ defined through Equation (3.14). □

Lemma 3.28 now has several important consequences:

1. Both the modified Galerkin discretisation (3.15)-(3.16) and the Galerkin discretisation (3.7) are well-posed.
2. For every choice of the approximation parameter $\ell_{\max} \in \mathbb{N}$, the finite-dimensional solution to the Galerkin discretisation (3.7) satisfies a standard quasi-optimality result.
3. Since the discrete inf-sup constant $\beta_{\tilde{\mathcal{A}}}$ is independent of the approximation space, we obtain stability and convergence to the exact solution of the approximate solutions as the approximation parameter $\ell_{\max} \to \infty$.

All of the above results can be proven using text-book functional analysis techniques. We state one particular quasi-optimality result concerning solutions to the finite-dimensional equation (3.16) which will be of use in the next subsection.

Lemma 3.29 (Partial Quasi-Optimality)**.** *Let $C_{\tilde{\mathcal{A}}} > 0$ be the continuity constant defined through Equation (3.10) in Lemma 3.20, let $\beta_{\tilde{\mathcal{A}}} > 0$ be the inf-sup constant defined through Equation (3.14) in Lemma 3.25, let $\sigma_f \in H^{-\frac{1}{2}}(\partial\Omega)$, let $\ell_{\max} \in \mathbb{N}$, let $\lambda_{\ell_{\max}} \in W_0^{\ell_{\max}}$ be the unique solution to the finite-dimensional Equation (3.16) with right hand side given by σ_f, and let $\tilde{\lambda} \in \breve{H}^{\frac{1}{2}}(\partial\Omega)$ be the unique solution to infinite-dimensional Equation (3.9) with right hand side given by σ_f. Then it holds that*

$$|||\tilde{\lambda} - \lambda_{\ell_{\max}}||| \leq \left(1 + \frac{C_{\tilde{\mathcal{A}}}}{\beta_{\tilde{\mathcal{A}}}}\right) \inf_{\psi \in W_0^{\ell_{\max}}} |||\tilde{\lambda} - \psi|||. \tag{3.17}$$

Proof. The proof is also text-book functional analysis. □

Notice that thus far, we have only proved well-posedness of the infinite-dimensional weak formulation (3.6) and the Galerkin discretisation (3.7) involving the *surface electrostatic potential*. However, the main results in Section 3.1 have been formulated for the *induced surface charge*. Therefore, the next step in our analysis will be to transfer our existing results to the infinite-dimensional weak formulation (2.5) and the Galerkin discretisation (2.8) involving the exact and approximate induced surface charge.

3.3.2 Well-posedness analysis for the induced surface charge

As the astute reader may already have realised, the well-posedness analysis for the infinite-dimensional weak formulation (2.5) and the Galerkin discretisation (2.8) is exceedingly simple because the underlying boundary integral operator is simply $\mathcal{A}^*$, i.e., the adjoint of the boundary integral operator $\mathcal{A}$, which has already been completely analysed in both the infinite-dimensional and finite dimensional setting. To facilitate the subsequent exposition, we introduce some additional notation.

Definition 3.30 (Finite-Dimensional Projection Operators)**.** Let $\ell_{\max} \in \mathbb{N}$. We define the projection operator $\mathbb{P}_{\ell_{\max}} \colon H^{\frac{1}{2}}(\partial\Omega) \to W^{\ell_{\max}}$ as the mapping with the property that for any $\psi \in H^{\frac{1}{2}}(\partial\Omega)$, $\mathbb{P}_{\ell_{\max}}\psi$ is the unique element of $W^{\ell_{\max}}$ satisfying

$$(\phi_{\ell_{\max}}, \mathbb{P}_{\ell_{\max}}\psi)_{L^2(\partial\Omega)} = \langle \phi_{\ell_{\max}}, \psi \rangle_{\partial\Omega} \qquad \forall \phi_{\ell_{\max}} \in W^{\ell_{\max}},$$

Moreover, we define the projection operator $\mathbb{Q}_{\ell_{\max}} \colon H^{-\frac{1}{2}}(\partial\Omega) \to W^{\ell_{\max}}$ as the mapping with the property that for any $\sigma \in H^{-\frac{1}{2}}(\partial\Omega)$, $\mathbb{Q}_{\ell_{\max}}\sigma$ is the unique element of $W^{\ell_{\max}}$ satisfying

$$(\mathbb{Q}_{\ell_{\max}}\sigma, \phi_{\ell_{\max}})_{L^2(\partial\Omega)} = \langle \sigma, \phi_{\ell_{\max}} \rangle_{\partial\Omega} \qquad \forall \phi_{\ell_{\max}} \in W^{\ell_{\max}}.$$

Remark 3.31. Consider the setting of Definition 3.30. It is possible to show that the projection operators $\mathbb{P}_{\ell_{\max}}$ and $\mathbb{Q}_{\ell_{\max}}$ are stable, i.e., for all $\psi \in H^{\frac{1}{2}}(\partial\Omega)$ and all $\sigma \in H^{-\frac{1}{2}}(\partial\Omega)$ it holds that

$$|||\mathbb{P}_{\ell_{\max}}\psi||| \leq |||\psi||| \quad \text{and} \quad |||\mathbb{Q}_{\ell_{\max}}\sigma|||^* \leq |||\sigma|||^*.$$

We now have the following simple result.

Theorem 3.32 (Infinite-Dimensional Well-Posedness)**.** *The infinite-dimensional weak formulation* (2.5) *of the boundary integral equation* (2.3) *is well-posed.*

Proof. The well-posedness of the infinite-dimensional weak formulation (3.6) implies that the boundary integral operator $\mathcal{A} \colon H^{\frac{1}{2}}(\partial\Omega) \to H^{\frac{1}{2}}(\partial\Omega)$ defined through Definition 2.8 is a continuous bijection. Consequently the adjoint operator $\mathcal{A}^* \colon H^{-\frac{1}{2}}(\partial\Omega) \to H^{-\frac{1}{2}}(\partial\Omega)$ is also a continuous bijection. □

A similar result holds for the Galerkin discretisation of the integral equation (2.3) for the induced surface charge.

Theorem 3.33 (Finite-Dimensional Well-Posedness)**.** *The finite-dimensional Galerkin discretisation* (2.8) *of the weak formulation* (2.5) *is well-posed.*

Proof. Let $\mathbb{P}_{\ell_{\max}} \colon H^{\frac{1}{2}}(\partial\Omega) \to W^{\ell_{\max}}$ and $\mathbb{Q}_{\ell_{\max}} \colon H^{-\frac{1}{2}}(\partial\Omega) \to W^{\ell_{\max}}$ denote the projection operators defined through Definition 3.30. The well-posedness of the finite-dimensional Galerkin discretisation (3.7) implies that the boundary integral operator $\mathbb{P}_{\ell_{\max}}\mathcal{A}\mathbb{P}_{\ell_{\max}} \colon W^{\ell_{\max}} \to W^{\ell_{\max}}$ is a continuous bijection. Consequently, the adjoint operator $\mathbb{Q}_{\ell_{\max}}\mathcal{A}^*\mathbb{Q}_{\ell_{\max}} \colon W^{\ell_{\max}} \to W^{\ell_{\max}}$ is also a continuous bijection. □

We conclude this subsection by stating a first approximation result for the solution $\nu_{\ell_{\max}} \in W^{\ell_{\max}}$ to the Galerkin discretisation (2.8).

Theorem 3.34 (First Approximability Result)**.** *Let $\ell_{\max} \in \mathbb{N}$, let $\mathbb{Q}_{\ell_{\max}} \colon H^{-\frac{1}{2}}(\partial\Omega) \to W^{\ell_{\max}}$ denote the projection operator defined through Definition 3.30, let $\mathbb{Q}^{\perp}_{\ell_{\max}} := I - \mathbb{Q}_{\ell_{\max}}$ where I is the identity map on $H^{-\frac{1}{2}}(\partial\Omega)$, let $C_{\tilde{A}} > 0$ be the continuity constant defined through Equation (3.10) in Lemma 3.20, let $\beta_{\tilde{A}} > 0$ be the inf-sup constant defined through Equation (3.14) in Lemma 3.25, let $\sigma_f \in H^{-\frac{1}{2}}(\partial\Omega)$, let $\nu \in H^{-\frac{1}{2}}(\partial\Omega)$ be the unique solution to infinite-dimensional weak formulation (2.5) with right hand side given by σ_f and let $\nu_{\ell_{\max}} \in W^{\ell_{\max}}$ be the unique solution to the finite-dimensional Galerkin discretisation (2.8) with right hand side given by σ_f. Then it holds that*

$$|||\nu - \nu_{\ell_{\max}}|||^* \leq \frac{\max\left|\frac{\kappa_0-\kappa}{\kappa_0}\right|}{\min\left|\frac{\kappa-\kappa_0}{\kappa_0}\right|}\left(1+\frac{C_{\tilde{A}}}{\beta_{\tilde{A}}}\right)\left(\left|\left|\left|\mathbb{Q}^{\perp}_{\ell_{\max}}\nu\right|\right|\right|^* + \frac{2}{\kappa_0}\left|\left|\left|\mathbb{Q}^{\perp}_{\ell_{\max}}\sigma_f\right|\right|\right|^*\right). \tag{3.18}$$

Proof. Let $\tilde{\lambda} \in \breve{H}^{\frac{1}{2}}(\partial\Omega)$ be the solution of Equation (3.9) of the modified weak formulation. It is straightforward to show that

$$\nu = \frac{\kappa_0 - \kappa}{\kappa_0}\mathrm{DtN}\tilde{\lambda} + \frac{\sigma_f}{\kappa_0}. \tag{3.19}$$

Next, let $\mathcal{A}$ be the integral operator defined through Definition 2.8, let $\widehat{\lambda}_{\ell_{\max}} \in W^{\ell_{\max}}$ be the solution to the Galerkin discretisation (3.7), and let $\mathbb{P}_{\ell_{\max}} \colon H^{\frac{1}{2}}(\partial\Omega) \to W^{\ell_{\max}}$ denote the projection operator defined through Definition 3.30. We then define the mappings

$$\mathcal{V}_{\ell_{\max}} := \mathbb{P}_{\ell_{\max}}\mathcal{V}\mathbb{Q}_{\ell_{\max}}, \qquad \mathcal{A}_{\ell_{\max}} := \mathbb{P}_{\ell_{\max}}\mathcal{A}\mathbb{P}_{\ell_{\max}}, \quad \text{and} \quad \mathcal{A}^*_{\ell_{\max}} := \mathbb{Q}_{\ell_{\max}}\mathcal{A}^*\mathbb{Q}_{\ell_{\max}},$$

and we define the function $\psi_{\ell_{\max}} := \mathcal{V}_{\ell_{\max}}\nu_{\ell_{\max}} \in W^{\ell_{\max}}$. We first claim that $\psi_{\ell_{\max}}$ satisfies the equation

$$\mathcal{A}_{\ell_{\max}}\psi_{\ell_{\max}} = \frac{1}{\kappa_0}\mathcal{V}_{\ell_{\max}}\sigma_f. \tag{3.20}$$

Indeed, since $\nu_{\ell_{\max}}$ satisfies the Galerkin discretisation (2.8) we obviously have

$$\mathcal{A}^*_{\ell_{\max}}\nu_{\ell_{\max}} = \frac{1}{\kappa_0}\mathbb{Q}_{\ell_{\max}}\sigma_f \qquad \text{which implies that} \qquad \mathcal{V}_{\ell_{\max}}\mathcal{A}^*_{\ell_{\max}}\nu_{\ell_{\max}} = \frac{1}{\kappa_0}\mathcal{V}_{\ell_{\max}}\sigma_f.$$

Using the fact that $\mathcal{V}_{\ell_{\max}}\mathcal{A}^*_{\ell_{\max}} = \mathcal{A}_{\ell_{\max}}\mathcal{V}_{\ell_{\max}}$ yields

$$\mathcal{A}_{\ell_{\max}}\psi_{\ell_{\max}} = \mathcal{A}_{\ell_{\max}}\mathcal{V}_{\ell_{\max}}\nu_{\ell_{\max}} = \mathcal{V}_{\ell_{\max}}\mathcal{A}^*_{\ell_{\max}}\nu_{\ell_{\max}} = \frac{1}{\kappa_0}\mathcal{V}_{\ell_{\max}}\sigma_f,$$

which gives the intermediary result.

We now consider again the Galerkin discretisation (2.8). Using the definition of $\psi_{\ell_{\max}}$ and the fact that $\mathbb{Q}_{\ell_{\max}}\mathrm{DtN} = \mathrm{DtN}\mathbb{P}_{\ell_{\max}}$ we obtain that

$$\nu_{\ell_{\max}} = \frac{\kappa_0-\kappa}{\kappa_0}\mathbb{Q}_{\ell_{\max}}\mathrm{DtN}\mathcal{V}\nu_{\ell_{\max}} + \frac{1}{\kappa_0}\mathbb{Q}_{\ell_{\max}}\sigma_f = \frac{\kappa_0-\kappa}{\kappa_0}\mathrm{DtN}\psi_{\ell_{\max}} + \frac{1}{\kappa_0}\mathbb{Q}_{\ell_{\max}}\sigma_f. \quad (3.21)$$

Let $\mathbb{P}_0^\perp\colon H^{\frac{1}{2}}(\partial\Omega) \to \breve{H}^{\frac{1}{2}}(\partial\Omega)$ be the projection operator defined through Lemma 3.2. Subtracting Equation (3.21) from Equation (3.19) then gives

$$\begin{aligned}
|||\nu - \nu_{\ell_{\max}}|||^* &= \Big|\Big|\Big|\frac{\kappa_0-\kappa}{\kappa_0}\mathrm{DtN}\tilde{\lambda} - \frac{\kappa_0-\kappa}{\kappa_0}\mathrm{DtN}\psi_{\ell_{\max}} + \frac{1}{\kappa_0}(\sigma_f - \mathbb{Q}_{\ell_{\max}}\sigma_f)\Big|\Big|\Big|^* \\
&\le \Big|\Big|\Big|\frac{\kappa_0-\kappa}{\kappa_0}\mathrm{DtN}\tilde{\lambda} - \frac{\kappa_0-\kappa}{\kappa_0}\mathrm{DtN}\psi_{\ell_{\max}}\Big|\Big|\Big|^* + \frac{1}{\kappa_0}|||\mathbb{Q}^\perp_{\ell_{\max}}\sigma_f|||^* \\
&= \Big|\Big|\Big|\frac{\kappa_0-\kappa}{\kappa_0}\Big(\tilde{\lambda} - \mathbb{P}_0^\perp\psi_{\ell_{\max}}\Big)\Big|\Big|\Big| + \frac{1}{\kappa_0}|||\mathbb{Q}^\perp_{\ell_{\max}}\sigma_f|||^* \\
&\le \max\Big|\frac{\kappa_0-\kappa}{\kappa_0}\Big|\,|||\tilde{\lambda} - \mathbb{P}_0^\perp\psi_{\ell_{\max}}||| + \frac{1}{\kappa_0}|||\mathbb{Q}^\perp_{\ell_{\max}}\sigma_f|||^*. \qquad (3.22)
\end{aligned}$$

Let $\lambda_{\ell_{\max}} \in W_0^{\ell_{\max}}$ denote the solution to Equation (3.16) of the modified Galerkin discretisation. The first term in the bound (3.22) can then be written as

$$|||\tilde{\lambda} - \mathbb{P}_0^\perp\psi_{\ell_{\max}}||| \le |||\lambda_{\ell_{\max}} - \mathbb{P}_0^\perp\psi_{\ell_{\max}}||| + |||\tilde{\lambda} - \lambda_{\ell_{\max}}|||. \quad (3.23)$$

The first term in Inequality (3.23) can be simplified as follows: We first define the mapping $\widetilde{\mathcal{A}}_{\ell_{\max}}\colon W_0^{\ell_{\max}} \to W_0^{\ell_{\max}}$ as $\widetilde{\mathcal{A}}_{\ell_{\max}} := \mathbb{P}_0^\perp\mathcal{A}_{\ell_{\max}}\mathbb{P}_0^\perp$. Thus, $\widetilde{\mathcal{A}}_{\ell_{\max}}$ is the operator associated with the Galerkin discretisation of the "reduced" bilinear form defined through Definition 3.19. We therefore obtain from Lemma 3.28 that

$$\begin{aligned}
|||\lambda_{\ell_{\max}} - \mathbb{P}_0^\perp\psi_{\ell_{\max}}||| &= \Big|\Big|\Big|\widetilde{\mathcal{A}}^{-1}_{\ell_{\max}}\widetilde{\mathcal{A}}_{\ell_{\max}}\big(\lambda_{\ell_{\max}} - \mathbb{P}_0^\perp\psi_{\ell_{\max}}\big)\Big|\Big|\Big| \\
&\le \frac{1}{\beta_{\tilde{\mathcal{A}}}}\Big|\Big|\Big|\widetilde{\mathcal{A}}_{\ell_{\max}}\big(\lambda_{\ell_{\max}} - \mathbb{P}_0^\perp\psi_{\ell_{\max}}\big)\Big|\Big|\Big|.
\end{aligned}$$

In order to simplify this last bound, we first use Equation (3.20), the definitions of the operators $\widetilde{\mathcal{A}}_{\ell_{\max}}$ and $\mathcal{A}_{\ell_{\max}}$ together with a simple calculation to deduce that

$$\widetilde{\mathcal{A}}_{\ell_{\max}}\mathbb{P}_0^\perp\psi_{\ell_{\max}} = \mathbb{P}_0^\perp\mathcal{A}_{\ell_{\max}}\mathbb{P}_0^\perp\psi_{\ell_{\max}} = \frac{1}{\kappa_0}\mathbb{P}_0^\perp\mathcal{V}_{\ell_{\max}}\sigma_f = \frac{1}{\kappa_0}\mathbb{P}_0^\perp\mathbb{P}_{\ell_{\max}}\mathcal{V}\mathbb{Q}_{\ell_{\max}}\sigma_f.$$

A similar calculation using the definition of $\lambda_{\ell_{\max}}$ (see Equation (3.16)) yields

$$\widetilde{\mathcal{A}}_{\ell_{\max}}\lambda_{\ell_{\max}} = \frac{1}{\kappa_0}\mathbb{P}_0^{\perp}\mathbb{P}_{\ell_{\max}}\mathcal{V}\sigma_f.$$

We can therefore deduce that

$$|||\lambda_{\ell_{\max}} - \mathbb{P}_0^{\perp}\psi_{\ell_{\max}}||| \leq \frac{1}{\beta_{\tilde{\mathcal{A}}}}|||\widetilde{\mathcal{A}}\big(\lambda_{\ell_{\max}} - \mathbb{P}_0^{\perp}\psi_{\ell_{\max}}\big)||| \leq \frac{1}{\kappa_0\beta_{\tilde{\mathcal{A}}}}\Big|\Big|\Big|\mathbb{P}_0^{\perp}\mathbb{P}_{\ell_{\max}}\mathcal{V}\mathbb{Q}_{\ell_{\max}}^{\perp}\sigma_f\big)\Big|\Big|\Big|.$$

Since $\mathrm{DtN}\colon \breve{H}^{\frac{1}{2}}(\partial\Omega) \to \breve{H}^{-\frac{1}{2}}(\partial\Omega)$ is an isomorphism and thus invertible, we can define $\Phi_{\ell_{\max}} := \mathrm{DtN}^{-1}\mathbb{Q}_{\ell_{\max}}^{\perp}\sigma_f$. We then obtain

$$\begin{aligned}\frac{1}{\kappa_0\beta_{\tilde{\mathcal{A}}}}\Big|\Big|\Big|\mathbb{P}_0^{\perp}\mathbb{P}_{\ell_{\max}}\mathcal{V}\mathbb{Q}_{\ell_{\max}}^{\perp}\sigma_f\big)\Big|\Big|\Big| &= \frac{1}{\kappa_0\beta_{\tilde{\mathcal{A}}}}\Big|\Big|\Big|\mathbb{P}_{\ell_{\max}}\mathbb{P}_0^{\perp}\mathcal{V}\mathbb{Q}_{\ell_{\max}}^{\perp}\sigma_f\big)\Big|\Big|\Big| \leq \frac{1}{\kappa_0\beta_{\tilde{\mathcal{A}}}}\Big|\Big|\Big|\mathbb{P}_0^{\perp}\mathcal{V}\mathrm{DtN}\Phi_{\ell_{\max}}\Big|\Big|\Big| \\ &\leq \frac{1}{\kappa_0\beta_{\tilde{\mathcal{A}}}}\frac{c_{\mathcal{K}}^{\frac{3}{2}}c_{\mathrm{equiv}}}{\sqrt{c_{\mathcal{V}}}}|||\Phi_{\ell_{\max}}||| = \frac{1}{\kappa_0\beta_{\tilde{\mathcal{A}}}}\frac{c_{\mathcal{K}}^{\frac{3}{2}}c_{\mathrm{equiv}}}{\sqrt{c_{\mathcal{V}}}}|||\mathbb{Q}_{\ell_{\max}}^{\perp}\sigma_f|||^*,\end{aligned}$$

where the first step in the second line follows from the arguments used in the proof of Lemma 3.16. In order to simplify the second term in the Inequality (3.23) we use the quasi-optimality result Lemma 3.29:

$$|||\tilde{\lambda} - \lambda_{\ell_{\max}}||| \leq \Big(1 + \frac{C_{\tilde{\mathcal{A}}}}{\beta_{\tilde{\mathcal{A}}}}\Big)\inf_{\psi\in W_0^{\ell_{\max}}}|||\tilde{\lambda} - \psi|||.$$

Using again the fact that $\mathrm{DtN}\colon \breve{H}^{\frac{1}{2}}(\partial\Omega) \to \breve{H}^{-\frac{1}{2}}(\partial\Omega)$ is invertible, we deduce from Equation (3.19) that

$$\tilde{\lambda} = \frac{\kappa_0}{\kappa_0 - \kappa}\mathrm{DtN}^{-1}\mathbb{Q}_0^{\perp}\nu - \frac{\kappa_0}{\kappa_0 - \kappa}\frac{1}{\kappa_0}\mathrm{DtN}^{-1}\mathbb{Q}_0^{\perp}\sigma_f.$$

Since the Dirichlet-to-Neumann mapping is bijective on $W_0^{\ell_{\max}}$, we can write

$$\begin{aligned}\inf_{\psi\in W_0^{\ell_{\max}}}|||\tilde{\lambda} - \psi||| &= \inf_{\mathrm{DtN}^{-1}\sigma_0\in W_0^{\ell_{\max}}}\Big|\Big|\Big|\frac{\kappa_0}{\kappa_0 - \kappa}\mathrm{DtN}^{-1}\mathbb{Q}_0^{\perp}\Big(\nu - \frac{1}{\kappa_0}\sigma_f\Big) - \mathrm{DtN}^{-1}\sigma_0\Big|\Big|\Big| \\ &= \inf_{\sigma_0\in W_0^{\ell_{\max}}}\Big|\Big|\Big|\frac{\kappa_0}{\kappa_0 - \kappa}\mathrm{DtN}^{-1}\Big(\mathbb{Q}_0^{\perp}\Big(\nu - \frac{1}{\kappa_0}\sigma_f\Big) - \sigma_0\Big)\Big|\Big|\Big| \\ &\leq \frac{1}{\min\left|\frac{\kappa-\kappa_0}{\kappa_0}\right|}\inf_{\sigma_0\in W_0^{\ell_{\max}}}\Big|\Big|\Big|\mathbb{Q}_0^{\perp}\Big(\nu - \frac{1}{\kappa_0}\sigma_f\Big) - \sigma_0\Big|\Big|\Big|^*.\end{aligned}$$

In the above infimum, we may pick $\sigma_0 = \mathbb{Q}_0^{\perp}\mathbb{Q}_{\ell_{\max}}\Big(\nu - \frac{1}{\kappa_0}\sigma_f\Big)$ and use the triangle inequality to obtain

$$\inf_{\psi\in W_0^{\ell_{\max}}}|||\tilde{\lambda} - \psi||| \leq \frac{1}{\min\left|\frac{\kappa-\kappa_0}{\kappa_0}\right|}\Big|\Big|\Big|\mathbb{Q}_{\ell_{\max}}^{\perp}\nu\Big|\Big|\Big|^* + \frac{1}{\min\left|\frac{\kappa-\kappa_0}{\kappa_0}\right|}\frac{1}{\kappa_0}\Big|\Big|\Big|\mathbb{Q}_{\ell_{\max}}^{\perp}\sigma_f\Big|\Big|\Big|^*.$$

Using the above calculations, we can finally bound the original Inequality (3.22) as

$$|||\nu - \nu_{\ell_{\max}}|||^* \leq \frac{\max\left|\frac{\kappa_0-\kappa}{\kappa_0}\right|}{\min\left|\frac{\kappa-\kappa_0}{\kappa_0}\right|}\left(1+\frac{C_{\tilde{\mathcal{A}}}}{\beta_{\tilde{\mathcal{A}}}}\right)\left(\left|\left|\left|\mathbb{Q}^{\perp}_{\ell_{\max}}\nu\right|\right|\right|^* + \frac{1}{\kappa_0}\left|\left|\left|\mathbb{Q}^{\perp}_{\ell_{\max}}\sigma_f\right|\right|\right|^*\right)$$
$$+ \frac{1}{\kappa_0}\frac{1}{\beta_{\tilde{\mathcal{A}}}}\max\left|\frac{\kappa_0-\kappa}{\kappa_0}\right|\frac{c_{\mathcal{K}}^{\frac{3}{2}}c_{\text{equiv}}}{\sqrt{c_{\mathcal{V}}}}\left|\left|\left|\mathbb{Q}^{\perp}_{\ell_{\max}}\sigma_f\right|\right|\right|^* + \frac{1}{\kappa_0}\left|\left|\left|\mathbb{Q}^{\perp}_{\ell_{\max}}\sigma_f\right|\right|\right|^*.$$

Using the fact that $\max\left|\frac{\kappa_0-\kappa}{\kappa_0}\right|\frac{c_{\mathcal{K}}^{\frac{3}{2}}c_{\text{equiv}}}{\sqrt{c_{\mathcal{V}}}} \leq C_{\tilde{\mathcal{A}}}$, we therefore obtain

$$\begin{aligned}|||\nu - \nu_{\ell_{\max}}|||^* &\leq \frac{\max\left|\frac{\kappa_0-\kappa}{\kappa_0}\right|}{\min\left|\frac{\kappa-\kappa_0}{\kappa_0}\right|}\left(1+\frac{C_{\tilde{\mathcal{A}}}}{\beta_{\tilde{\mathcal{A}}}}\right)\left(\left|\left|\left|\mathbb{Q}^{\perp}_{\ell_{\max}}\nu\right|\right|\right|^* + \frac{1}{\kappa_0}\left|\left|\left|\mathbb{Q}^{\perp}_{\ell_{\max}}\sigma_f\right|\right|\right|^*\right)\\ &\quad + \left(1+\frac{C_{\tilde{\mathcal{A}}}}{\beta_{\tilde{\mathcal{A}}}}\right)\frac{1}{\kappa_0}\left|\left|\left|\mathbb{Q}^{\perp}_{\ell_{\max}}\sigma_f\right|\right|\right|^*\\ &\leq \frac{\max\left|\frac{\kappa_0-\kappa}{\kappa_0}\right|}{\min\left|\frac{\kappa-\kappa_0}{\kappa_0}\right|}\left(1+\frac{C_{\tilde{\mathcal{A}}}}{\beta_{\tilde{\mathcal{A}}}}\right)\left(\left|\left|\left|\mathbb{Q}^{\perp}_{\ell_{\max}}\nu\right|\right|\right|^* + \frac{2}{\kappa_0}\left|\left|\left|\mathbb{Q}^{\perp}_{\ell_{\max}}\sigma_f\right|\right|\right|^*\right),\end{aligned}$$

as claimed. □

3.3.3 Proofs of the main results

We begin with the proof of Theorem 3.12, which involves a priori error estimates and convergence rates.

Proof of Theorem 3.12:

Consider the setting of Theorem 3.12. We first observe that for all $s \geq 0$, due to the regularity theory for boundary integral equations (see, e.g., [4, Section 9.1.4]), $\sigma_f \in H^s(\partial\Omega)$ implies that $\nu \in H^s(\partial\Omega)$.

Next, let $j \in \{1,\dots,N\}$ and let $\nu_j,\ \sigma_{f,j} \in H^s(\partial\Omega_j)$ be defined as $\nu_j := \nu|_{\partial\Omega_j}$ and $\sigma_{f,j} := \sigma_f|_{\partial\Omega_j}$. It follows that there exist coefficients $[\nu_j]_\ell^m, [\sigma_{f,j}]_\ell^m,\ \ell \in \mathbb{N}_0,\ -\ell \leq m \leq \ell$ such that for all $\mathbf{x} \in \partial\Omega_j$ it holds that

$$\nu_j(\mathbf{x}) = \sum_{\ell=0}^{\infty}\sum_{m=-\ell}^{m=+\ell}[\nu_j]_\ell^m \mathcal{Y}_\ell^m\left(\frac{\mathbf{x}-\mathbf{x}_j}{|\mathbf{x}-\mathbf{x}_j|}\right), \quad \text{and} \quad \sigma_{f,j}(\mathbf{x}) = \sum_{\ell=0}^{\infty}\sum_{m=-\ell}^{m=+\ell}[\sigma_{f,j}]_\ell^m \mathcal{Y}_\ell^m\left(\frac{\mathbf{x}-\mathbf{x}_j}{|\mathbf{x}-\mathbf{x}_j|}\right).$$

Using Definition 3.4 of the $|||\cdot|||^*$ norm, Definition 3.30 of the projection operator $\mathbb{Q}^{\perp}_{\ell_{\max}}$ and the definition of the $|||\cdot|||_{H^s(\partial\Omega)}$ norm from Equation (3.4), a simple calculation

yields

$$\begin{aligned}\left|\!\left|\!\left|\mathbb{Q}_{\ell_{\max}}^{\perp}\nu\right|\!\right|\!\right|^{*2} &\leq \sum_{j=1}^{N} r_j^2 \sum_{\ell=\ell_{\max}+1}^{\infty} \sum_{m=-\ell}^{m=+\ell} \left(\frac{\ell}{r_j}\right)^{-1} ([\nu_j]_\ell^m)^2 \\ &\leq \left(\frac{\max r_j}{\ell_{\max}+1}\right)^{1+2s} \sum_{j=1}^{N} r_j^2 \sum_{\ell=\ell_{\max}+1}^{\infty} \sum_{m=-\ell}^{m=+\ell} \left(\frac{\ell}{r_j}\right)^{2s} ([\nu_j]_\ell^m)^2 \\ &\leq \left(\frac{\max r_j}{\ell_{\max}+1}\right)^{1+2s} \left|\!\left|\!\left|\mathbb{Q}_0^{\perp}\nu\right|\!\right|\!\right|_{H^s(\partial\Omega)}^2,\end{aligned}$$

and

$$\begin{aligned}\left|\!\left|\!\left|\mathbb{Q}_{\ell_{\max}}^{\perp}\sigma_f\right|\!\right|\!\right|^{*2} &\leq \sum_{j=1}^{N} r_j^2 \sum_{\ell=\ell_{\max}+1}^{\infty} \sum_{m=-\ell}^{m=+\ell} \left(\frac{\ell}{r_j}\right)^{-1} ([\sigma_{f,j}]_\ell^m)^2 \\ &\leq \left(\frac{\max r_j}{\ell_{\max}+1}\right)^{1+2s} \sum_{j=1}^{N} r_j^2 \sum_{\ell=\ell_{\max}+1}^{\infty} \sum_{m=-\ell}^{m=+\ell} \left(\frac{\ell}{r_j}\right)^{2s} ([\sigma_{f,j}]_\ell^m)^2 \\ &\leq \left(\frac{\max r_j}{\ell_{\max}+1}\right)^{1+2s} \left|\!\left|\!\left|\mathbb{Q}_0^{\perp}\sigma_f\right|\!\right|\!\right|_{H^s(\partial\Omega)}^2.\end{aligned}$$

Using the approximability result of Theorem 3.34 then gives

$$\begin{aligned}|||\nu - \nu_{\ell_{\max}}|||^* \leq \frac{\max\left|\frac{\kappa-\kappa_0}{\kappa_0}\right|}{\min\left|\frac{\kappa-\kappa_0}{\kappa_0}\right|} \left(1+\frac{C_{\tilde{\mathcal{A}}}}{\beta_{\tilde{\mathcal{A}}}}\right) \left(\frac{\max r_j}{\ell_{\max}+1}\right)^{s+\frac{1}{2}} \\ \left(\left|\!\left|\!\left|\mathbb{Q}_0^{\perp}\nu\right|\!\right|\!\right|_{H^s(\partial\Omega)} + \frac{2}{\kappa_0}\left|\!\left|\!\left|\mathbb{Q}_0^{\perp}\sigma_f\right|\!\right|\!\right|_{H^s(\partial\Omega)}\right).\end{aligned}$$

In order to obtain the convergence rates for the electrostatic energy, we first notice that

$$|\mathcal{E}_{\sigma_f}(\nu) - \mathcal{E}_{\sigma_f}(\nu_{\ell_{\max}})| = \frac{\kappa_0}{2}\left|\left\langle \nu - \nu_{\ell_{\max}}, \frac{1}{\kappa_0}\mathcal{V}\sigma_f\right\rangle_{\partial\Omega}\right|.$$

Next, let $\lambda \in H^{\frac{1}{2}}(\partial\Omega)$ be the unique solution to BIE (3.5) for the surface electrostatic potential with right hand side given by σ_f. It follows that $\mathcal{A}\lambda = \frac{1}{\kappa_0}\mathcal{V}\sigma_f$, where $\mathcal{A}\colon H^{\frac{1}{2}}(\partial\Omega) \to H^{\frac{1}{2}}(\partial\Omega)$ is the boundary integral operator defined through Definition 2.8. We can therefore deduce that

$$|\mathcal{E}_{\sigma_f}(\nu) - \mathcal{E}_{\sigma_f}(\nu_{\ell_{\max}})| = \frac{\kappa_0}{2}\left|\left\langle \mathcal{A}^*\left(\nu - \nu_{\ell_{\max}}\right), \lambda\right\rangle_{\partial\Omega}\right|,$$

where $\mathcal{A}^*\colon H^{-\frac{1}{2}}(\partial\Omega) \to H^{-\frac{1}{2}}(\partial\Omega)$ denotes the adjoint of $\mathcal{A}$.

Let $\lambda_{\ell_{\max}} \in W_0^{\ell_{\max}}$ be the unique solution to the modified Galerkin equation (3.16). We define the function $\psi_{\ell_{\max}} \in W^{\ell_{\max}}$ by setting

$$\mathbb{P}_0^{\perp}\psi_{\ell_{\max}} = \lambda_{\ell_{\max}} \quad \text{and} \quad \mathbb{P}_0\psi_{\ell_{\max}} = \mathbb{P}_0\lambda.$$

Galerkin orthogonality (see Equation (2.8)) then implies that

$$\begin{aligned}|\mathcal{E}_{\sigma_f}(\nu) - \mathcal{E}_{\sigma_f}(\nu_{\ell_{\max}})| &= \frac{\kappa_0}{2}\left|\left\langle \mathcal{A}^*\big(\nu - \nu_{\ell_{\max}}\big), \lambda\right\rangle_{\partial\Omega}\right| = \frac{\kappa_0}{2}\left|\left\langle \mathcal{A}^*\big(\nu - \nu_{\ell_{\max}}\big), \lambda - \psi_{\ell_{\max}}\right\rangle_{\partial\Omega}\right| \\ &= \frac{\kappa_0}{2}\left|\left\langle \nu - \nu_{\ell_{\max}}, \mathcal{A}\big(\lambda - \psi_{\ell_{\max}}\big)\right\rangle_{\partial\Omega}\right|.\end{aligned}$$

Notice that the infinite-dimensional equation (2.5) and its Galerkin discretisation (2.8) for the induced surface charge together imply that $\mathbb{Q}_0(\nu - \nu_{\ell_{\max}}) = 0$. Consequently, the Cauchy-Schwarz inequality yields

$$\begin{aligned}|\mathcal{E}_{\sigma_f}(\nu) - \mathcal{E}_{\sigma_f}(\nu_{\ell_{\max}})| &= \frac{\kappa_0}{2}\left|\left\langle \nu - \nu_{\ell_{\max}}, \mathcal{A}\big(\lambda - \psi_{\ell_{\max}}\big)\right\rangle_{\partial\Omega}\right| \\ &\leq \frac{\kappa_0}{2}|||\nu - \nu_{\ell_{\max}}|||^* |||\mathbb{P}_0^\perp \mathcal{A}\mathbb{P}_0^\perp(\lambda - \psi_{\ell_{\max}})|||.\end{aligned}$$

We now recall that $\mathbb{P}_0^\perp \mathcal{A}\mathbb{P}_0^\perp = \widetilde{\mathcal{A}}$ where $\widetilde{\mathcal{A}}\colon \breve{H}^{\frac{1}{2}}(\partial\Omega) \to \breve{H}^{\frac{1}{2}}(\partial\Omega)$ is the operator associated with the "reduced" bilinear form defined through Definition 3.19. Consequently, using the continuity constant of $\widetilde{\mathcal{A}}$ (see Lemma 3.20) we deduce that

$$|||\mathbb{P}_0^\perp \mathcal{A}\mathbb{P}_0^\perp(\lambda - \psi_{\ell_{\max}})||| \leq C_{\widetilde{\mathcal{A}}}|||\widetilde{\lambda} - \lambda_{\ell_{\max}}|||,$$

where $\tilde{\lambda} = \mathbb{P}_0^\perp \lambda \in \breve{H}^{\frac{1}{2}}(\partial\Omega)$ is the unique solution to infinite-dimensional Equation (3.9) with right hand side given by σ_f. Next, using Lemma 3.29 and employing the same arguments used in the proof of Theorem 3.34, we obtain the bound

$$C_{\widetilde{\mathcal{A}}}|||\widetilde{\lambda} - \lambda_{\ell_{\max}}||| \leq \frac{\kappa_0 C_{\widetilde{\mathcal{A}}}}{\min|\kappa - \kappa_0|}\left(1 + \frac{C_{\widetilde{\mathcal{A}}}}{\beta_{\widetilde{\mathcal{A}}}}\right)\left(|||\mathbb{Q}_{\ell_{\max}}^\perp \nu|||^* + \frac{1}{\kappa_0}|||\mathbb{Q}_{\ell_{\max}}^\perp \sigma_f|||^*\right),$$

and therefore

$$\begin{aligned}|\mathcal{E}_{\sigma_f}(\nu) - \mathcal{E}_{\sigma_f}(\nu_{\ell_{\max}})| \leq \frac{\kappa_0^2 C_{\widetilde{\mathcal{A}}}}{2\min|\kappa - \kappa_0|}&\left(1 + \frac{C_{\widetilde{\mathcal{A}}}}{\beta_{\widetilde{\mathcal{A}}}}\right)|||\nu - \nu_{\ell_{\max}}|||^* \\ &\left(|||\mathbb{Q}_{\ell_{\max}}^\perp \nu|||^* + \frac{1}{\kappa_0}|||\mathbb{Q}_{\ell_{\max}}^\perp \sigma_f|||^*\right).\end{aligned}$$

The remaining proof now follows using Theorem 3.34 together with the same arguments that were used to derive the convergence rates for the induced surface charge.

□

Proof of Theorem 3.13:

Consider the setting of Theorem 3.13. We first observe that since $\sigma_f \in C^\infty(\partial\Omega)$, the regularity theory for boundary integral equations (see, e.g., [4, Section 9.1.4]) implies that $\nu \in C^\infty(\partial\Omega)$. Next, let us focus on obtaining an expression for the norm of the induced surface charge ν. To this end, let $j \in \{1, \ldots, N\}$ and let $\nu_j \in C^\infty(\partial\Omega_j)$ be

defined as $\nu_j := \nu|_{\partial\Omega_j}$. It follows that there exist coefficients $[\nu_j]_\ell^m$, $\ell \in \mathbb{N}_0, -\ell \leq m \leq \ell$ such that for all $x \in \partial\Omega_j$ it holds that

$$\nu_j(\mathbf{x}) = \sum_{\ell=0}^{\infty} \sum_{m=-\ell}^{m=+\ell} [\nu_j]_\ell^m \mathcal{Y}_\ell^m\Big(\frac{\mathbf{x}-\mathbf{x}_j}{|\mathbf{x}-\mathbf{x}_j|}\Big).$$

Let $\mathcal{E}_{\mathcal{H}}\nu_j \in C^\infty(\overline{\Omega_j})$ be the harmonic extension of ν_j inside the ball Ω_j. Then for all $x \in \overline{\Omega_j}$ it holds that

$$\big(\mathcal{E}_{\mathcal{H}}\nu_j\big)(\mathbf{x}) = \sum_{\ell=0}^{\infty} \sum_{m=-\ell}^{m=+\ell} [\nu_j]_\ell^m \Big(\frac{|\mathbf{x}-\mathbf{x}_j|}{r_j}\Big)^\ell \mathcal{Y}_\ell^m\Big(\frac{\mathbf{x}-\mathbf{x}_j}{|\mathbf{x}-\mathbf{x}_j|}\Big). \tag{3.24}$$

Using Equation (3.24), it is easy to verify that for all integers $k \in \mathbb{N}_0$ we have

$$|||\mathbb{Q}_0^\perp \nu_j|||^2_{H^k(\partial\Omega_j)} = \int_{\partial\Omega_j} \big(\mathcal{E}_{\mathcal{H}}\nu_j\big)(\mathbf{x}) \frac{\partial^{2k}\big(\mathcal{E}_{\mathcal{H}}\nu_j\big)(\mathbf{x})}{\partial\eta^{2k}}\, d\mathbf{x}, \tag{3.25}$$

where $\mathbb{Q}_0^\perp \colon H^{-\frac{1}{2}}(\partial\Omega) \to \breve{H}^{-\frac{1}{2}}(\partial\Omega)$ is the projection operator defined through Lemma 3.2 and $\eta \colon \partial\Omega_j \to \mathbb{R}^3$ is the unit outward-pointing normal vector. On the other hand, we have by assumption that $\mathcal{E}_{\mathcal{H}}\nu_j$ is analytic on $\overline{\Omega_j}$. Therefore, there exists some constant $C_{\nu_j} > 1$ that depends on the function ν_j such that for all $k \in \mathbb{N}_0$ and $\mathbf{x} \in \partial\Omega_j$ it holds that

$$\Big|\frac{\partial^k\big(\mathcal{E}_{\mathcal{H}}\nu_j\big)(\mathbf{x})}{\partial\eta^k}\Big| \leq C_{\nu_j}^{k+1} k!.$$

Defining the constant $C_\nu := \max_j C_{\nu_j}$, we obtain from Equation (3.25) that

$$|||\mathbb{Q}_0^\perp \nu_j|||^2_{H^k(\partial\Omega_j)} \leq 4\pi r_j^2 C_{\nu_j}^{2k+2}(2k)!, \quad \text{so that} \quad \frac{1}{N}|||\mathbb{Q}_0^\perp \nu|||^2_{H^k(\partial\Omega)} \leq 4\pi \max_j r_j^2 C_\nu^{2k+2}(2k)!,$$

A similar calculation which uses the fact that the harmonic extension of σ_f is analytic on $\overline{\Omega^-}$ yields that there exist some constant C_{σ_f} depending on σ_f such that

$$\frac{1}{N}|||\mathbb{Q}_0^\perp \sigma_f|||^2_{H^k(\partial\Omega)} \leq 4\pi \max_j r_j^2 C_{\sigma_f}^{2k+2}(2k)!.$$

The remaining proof is standard: We define $C_{\nu,\sigma_f} := \max\Big\{C_\nu, \Big(\frac{2}{\kappa_0}\Big)^{\frac{1}{2k+2}} C_{\sigma_f}\Big\}$ and use the error estimate from Theorem 3.12 to obtain

$$\frac{1}{N}|||\nu - \nu_{\ell_{\max}}|||^{*2} \leq 8\pi \max_j r_j^2 \frac{\max\Big|\frac{\kappa-\kappa_0}{\kappa_0}\Big|^2}{\min\Big|\frac{\kappa-\kappa_0}{\kappa_0}\Big|^2} \Big(1 + \frac{C_{\tilde{\mathcal{A}}}}{\beta_{\tilde{\mathcal{A}}}}\Big)^2 \Big(C_\nu^{2k+2}(2k)! + \frac{2}{\kappa_0} C_{\sigma_f}^{2k+2}(2k)!\Big)$$

$$\leq 8\pi \max_j r_j^2 \frac{\max\left|\frac{\kappa-\kappa_0}{\kappa_0}\right|^2}{\min\left|\frac{\kappa-\kappa_0}{\kappa_0}\right|^2}\left(1+\frac{C_{\tilde{\mathcal{A}}}}{\beta_{\tilde{\mathcal{A}}}}\right)^2\left(\frac{\max r_j}{\ell_{\max}+1}\right)^{1+2k} C_{\nu,\sigma_f}^{2k+2}(2k)!.$$

Stirling's formula then yields that

$$\left(\frac{\max r_j}{\ell_{\max}+1}\right)^{1+2k} C_{\nu,\sigma_f}^{2k+2}(2k)! \leq \left(\frac{\max r_j}{\ell_{\max}+1}\right)^{1+2k} C_{\nu,\sigma_f}^{2k+2} e^{-2k+1}(2k)^{2k+\frac{1}{2}}.$$

In particular, for $\ell_{\max}$ sufficiently large, we can choose $\alpha \in \left[\frac{1}{4C_{\nu,\sigma_f}}, \frac{1}{2C_{\nu,\sigma_f}}\right]$ such that $k = \alpha\frac{\ell_{\max}+1}{\max r_j} \in \mathbb{N}$. We then see that

$$\begin{aligned}
\left(\frac{\max r_j}{\ell_{\max}+1}\right)^{1+2k} C_{\nu,\sigma_f}^{2k+2} e^{-2k+1}(2k)^{2k+\frac{1}{2}} &= \left(\frac{\alpha}{k}\right)^{1+2k} C_{\nu,\sigma_f}^{2k+2} e^{-2k+1}(2k)^{2k+\frac{1}{2}} \\
&= \alpha^{1+2k} C_{\nu,\sigma_f}^{2k+2} e^{-2k+1} 2^{2k+\frac{1}{2}} k^{-\frac{1}{2}} \\
&= \frac{\alpha C_{\nu,\sigma_f}^2 e\sqrt{2}}{\sqrt{k}}\left(4\alpha^2 C_{\nu,\sigma_f}^2 \frac{1}{e^2}\right)^k \\
&\leq \frac{\sqrt{\alpha}}{\sqrt{\frac{\ell_{\max}+1}{\max r_j}}} C_{\nu,\sigma_f}^2 \sqrt{2} e^{-2k+1} \\
&\leq \sqrt{2\max r_j} C_{\nu,\sigma_f}^2 \exp\left(-2\alpha\frac{\ell_{\max}+1}{\max r_j}+1\right) \\
&\leq \sqrt{2\max r_j} C_{\nu,\sigma_f}^2 \exp\left(-\frac{1}{2C_{\nu,\sigma_f}}\frac{\ell_{\max}+1}{\max r_j}+1\right).
\end{aligned}$$

We conclude that

$$\begin{aligned}
\frac{1}{\sqrt{N}}|||\nu-\nu_{\ell_{\max}}|||^* \leq \sqrt{8\pi\max r_j^2}(2\max r_j)^{\frac{1}{4}} C_{\nu,\sigma_f} \frac{\max\left|\frac{\kappa-\kappa_0}{\kappa_0}\right|}{\min\left|\frac{\kappa-\kappa_0}{\kappa_0}\right|}\left(1+\frac{C_{\tilde{\mathcal{A}}}}{\beta_{\tilde{\mathcal{A}}}}\right) \\
\exp\left(-\frac{1}{4C_{\nu,\sigma_f}}\frac{\ell_{\max}+1}{\max r_j}+\frac{1}{2}\right).
\end{aligned}$$

This essentially completes the proof for the exponential convergence of the approximate induced surface charge. The proof for the exponential convergence of the approximate total electrostatic energy is nearly identical.

□

3.4 Conclusion

In this chapter, we presented a well-posedness analysis of the second kind boundary integral equation (2.3) for the induced surface charges resulting on a large number of

dielectric spheres of varying radii and dielectric constants, embedded in a homogenous dielectric medium and undergoing mutual polarisation. As part of our analysis, we established the well-posedness of the Galerkin discretisation (2.8) of this BIE and we derived a priori error estimates and convergence rates for both the induced surface charge and total electrostatic energy of the system that *do not have any explicit dependence on the number of dielectric spheres N in the system*. In order to achieve this, we introduced a new analysis of second kind boundary integral equations posed on spherical domains. We have therefore established N-error stability of our numerical algorithm with respect to the induced surface charge and the electrostatic energy for any family of geometries satisfying the assumptions **GA1)-GA3)**.

In order to complete a scalability analysis of the numerical algorithm under consideration and in particular to determine if it is *linear scaling in cost* and therefore *linear scaling in accuracy*, it is also necessary to analyse computational aspects of the algorithm such as the conditioning of the linear system that arises from the Galerkin discretisation (2.8). This topic, as well as related computational considerations, is the subject of Chapter 4.

4

Complexity Analysis of the Integral Equation Formulation of the N-Body Dielectric Spheres Problem

Throughout this chapter, we will assume the setting of Chapters 1 and 2. Moreover, we will frequently refer to the weak formulation (2.5) and the Galerkin discretisation (2.8) of the second kind boundary integral equation (2.3) which describes the induced surface charge resulting on dielectric spherical particles undergoing mutual polarisation. Finally, we will also use the analysis and main result Theorem 9.8 of Chapter 3.

The aim of this chapter is to present a detailed complexity analysis for computing the induced surface charge and total electrostatic energy using the Galerkin discretisation (2.8) with the goal of showing that the method is linear scaling in cost. Our main result will show that– under mild assumptions– the number of linear solver iterations required to obtain an approximate solution to the Galerkin discretisation (2.8), up to a given tolerance, does not explicitly depend on N, i.e., the number of dielectric particles in the system. Consequently, the number of linear solver iterations required to compute an approximate solution is uniformly bounded for any geometry in the family of geometries $\{\Omega_{\mathcal{F}}\}_{\mathcal{F}\in\mathcal{J}}$ satisfying assumptions **GA1)-GA3)**. Since the fast multipole method (FMM) allows us to compute approximate matrix-vector products involving the solution matrix using $\mathcal{O}(N)$ operations, it will follow that an approximate solution with a given and fixed relative error can indeed be constructed by means of an iterative method using only $\mathcal{O}(N)$ operations. Combined with the analysis presented in Chapter 3 which establishes N-error stability, this result will confirm that our Galerkin method is *linear scaling in accuracy* for the computation of the induced surface charge and electrostatic energy.

4.1 Brief Recap

For ease of exposition, let us first briefly recall some key mathematical objects that were introduced in Chapter 3.

Definition 4.1. Let $\mathbb{P}_0^{\perp}\colon H^{\frac{1}{2}}(\partial\Omega) \to \breve{H}^{\frac{1}{2}}(\partial\Omega)$ denote the projection operator associated with the complementary decomposition introduced in Lemma 3.2, and let the boundary integral operator $\mathcal{A}\colon H^{\frac{1}{2}}(\partial\Omega) \to H^{\frac{1}{2}}(\partial\Omega)$ be defined as in Definition 2.8 in Section 2.3. Then we define the linear operator $\widetilde{\mathcal{A}}\colon \breve{H}^{\frac{1}{2}}(\partial\Omega) \to \breve{H}^{\frac{1}{2}}(\partial\Omega)$ as $\widetilde{\mathcal{A}} := \mathbb{P}_0^{\perp}\mathcal{A}\mathbb{P}_0^{\perp}$, and we refer to $\widetilde{\mathcal{A}}$ as the 'modified' boundary integral operator.

Remark 4.2. We recall that $\widetilde{\mathcal{A}}\colon \breve{H}^{\frac{1}{2}}(\partial\Omega) \to \breve{H}^{\frac{1}{2}}(\partial\Omega)$ is the linear operator associated with the "reduced" bilinear form $\tilde{a}\colon \breve{H}^{\frac{1}{2}}(\partial\Omega) \times \breve{H}^{-\frac{1}{2}}(\partial\Omega) \to \mathbb{R}$ defined through Definition 3.19 in Chapter 3. Moreover, this "reduced" bilinear form was the subject of extensive discussion in Chapter 3. In particular, we have precise estimates on the continuity constant $C_{\widetilde{\mathcal{A}}}$ and inf-sup constant $\beta_{\widetilde{\mathcal{A}}}$ of the operator $\widetilde{A}$ through Lemmas 3.20 and 3.25 respectively.

The 'modified' boundary integral operator $\widetilde{\mathcal{A}}$ played a key role in the so-called 'modified' Galerkin discretisation (3.15)-(3.16) of the BIE (3.5) that describes the so-called surface electrostatic potential $\lambda := \mathcal{V}\nu$ (see Chapter 3). To aid the subsequent analysis we present in this chapter however, it is necessary to introduce the so-called "reduced" Galerkin discretisation of the Integral equation (3.5) with modified right-hand side. We remind the reader that throughout this chapter, we will frequently refer to the approximation space $W^{\ell_{\max}}, \ell_{\max} \in \mathbb{N}_0$ which was defined through Definition 2.11 in Section 2.3.

"Reduced" Galerkin discretisation of Integral Equation (3.5) with modified RHS

Let $\sigma_f \in H^{-\frac{1}{2}}(\partial\Omega)$, let $\ell_{\max} \in \mathbb{N}$, and let $\mathbb{Q}_{\ell_{\max}}\colon H^{-\frac{1}{2}}(\partial\Omega) \to W^{\ell_{\max}}$ be the projection operator on the approximation space as defined in Definition 3.30. Find $\lambda_{\ell_{\max}} \in W_0^{\ell_{\max}}$ such that for all $\sigma_{\ell_{\max}} \in W_0^{\ell_{\max}}$ it holds that

$$\left(\widetilde{\mathcal{A}}\lambda_{\ell_{\max}}, \sigma_{\ell_{\max}}\right)_{L^2(\partial\Omega)} = \frac{1}{\kappa_0}\left(\mathcal{V}\mathbb{Q}_{\ell_{\max}}\sigma_f, \sigma_{\ell_{\max}}\right)_{L^2(\partial\Omega)}. \tag{4.1}$$

Notice that Equation (4.1) is slightly different from the true Galerkin discretisation (3.16) of the BIE (3.5) on the reduced approximation space $W_0^{\ell_{\max}}$. This is because, in contrast to Equation (3.16), the right-hand side of Equation (4.1) is not precisely the projection of the right-hand side of the BIE (3.5) onto $W_0^{\ell_{\max}}$ unless $\sigma_f \in W^{\ell_{\max}}$. The following remark is therefore important.

Remark 4.3. Consider the true Galerkin discretisation (3.16) of the BIE (3.5) on the reduced approximation space $W_0^{\ell_{\max}}$ and the so-called "reduced" Galerkin discretisation (4.1) with modified RHS. It is important to note that we have frequently used, in Chapter 3, the notation $\lambda_{\ell_{\max}} \in W_0^{\ell_{\max}}$ to denote the solution of Equation (3.16), and we are using, here in Chapter 4, the same notation $\lambda_{\ell_{\max}} \in W_0^{\ell_{\max}}$ to denote the solution of

Equation (4.1). However, these two solutions are not, in general, the same. We therefore encourage the reader to pay close attention to the definition of $\lambda_{\ell_{\max}}$ when it appears in the subsequent results.

The reason we have introduced this modified "reduced" Galerkin discretisation is that if we have obtained a solution to Equation (4.1), then a solution to the original Galerkin discretisation (2.8) for the induced surface charge can be computed easily. Indeed, we have the following lemma.

Lemma 4.4. *Let $\sigma_f \in H^{-\frac{1}{2}}(\partial\Omega)$, let $\ell_{\max} \in \mathbb{N}$, let $\mathbb{Q}_{\ell_{\max}} \colon H^{-\frac{1}{2}}(\partial\Omega) \to W^{\ell_{\max}}$ denote the projection operator defined through Definition 3.30, let $\lambda_{\ell_{\max}} \in W_0^{\ell_{\max}}$ be the solution of the "reduced" Galerkin discretisation (4.1) with modified right hand side given by σ_f, and let $\nu_{\ell_{\max}} \in W^{\ell_{\max}}$ be the solution of the original Galerkin discretisation (2.8) with right hand side given by σ_f. Then it holds that*

$$\nu_{\ell_{\max}} = \frac{\kappa_0 - \kappa}{\kappa_0} \mathrm{DtN} \lambda_{\ell_{\max}} + \frac{1}{\kappa_0} \mathbb{Q}_{\ell_{\max}} \sigma_f.$$

Proof. See the proof of Theorem 3.34 in Chapter 3. □

Lemma 4.4 suggests a very natural two-step procedure to obtain a solution $\nu_{\ell_{\max}}$ to the Galerkin discretisation (2.8) for the induced surface charge: We first solve the "reduced" Galerkin discretisation (4.1) with modified RHS to obtain the function $\lambda_{\ell_{\max}}$, and we then use the affine mapping stated in Lemma 4.4 to obtain $\nu_{\ell_{\max}}$. This procedure will be used when we describe our solution strategy for obtaining the approximate induced surface charge $\nu_{\ell_{\max}}$.

4.2 Convergence Analysis of the Linear Solver and Solution Strategies

We begin this section by describing in more detail the obstacles we face in performing a detailed convergence analysis. Our main goal is to prove that we can obtain a solution– up to given and fixed tolerance– to the Galerkin discretisation (2.8) for the approximate induced surface charge $\nu_{\ell_{\max}}$ *using only* $\mathcal{O}(N)$ *operations.* Naturally, computing a solution to the finite-dimensional equation (2.8) involves solving a linear system, which is typically done using a Krylov subspace solver. Consequently, in order to obtain the required $\mathcal{O}(N)$ scaling, we must show that

B1) It is possible to perform matrix vector multiplications involving the underlying solution matrix using $\mathcal{O}(N)$ operations;

B2) It is possible to obtain an upper bound independent of N on the number of iterations of the Krylov subspace solver required to obtain the solution of the linear system (up to some tolerance).

Let us first consider B1). Notice that the underlying boundary integral operators $\mathcal{A}^*$ and $\mathcal{A}$ defined through Definition 2.8 in Chapter 2 are constructed from the single layer boundary operator $\mathcal{V}$, the Dirichlet-to-Neumann map DtN, the identity map, and the dielectric function κ. Given our choice of approximation space $W^{\ell_{\max}}$, the DtN map, the identity map, and the dielectric function κ can be written as diagonal matrices. Furthermore, the fast multipole method (FMM) can be used to compute the action of $\mathcal{V}$ on an arbitrary element of $W^{\ell_{\max}}$ up to a given accuracy in $\mathcal{O}(N)$ operations. Thus, all matrix-vector products involving the solution matrix obtained from the discretisation of $\mathcal{A}^*$ (and also $\mathcal{A}$) can be performed in $\mathcal{O}(N)$ up to a given accuracy (see also [127] for further details).

Next, let us consider the statement B2), which requires us to perform a convergence analysis of the Krylov subspace solver used to solve the linear system arising from Galerkin discretisation (2.8). Here, we encounter the first obstacle: It is well known that the convergence behaviour of Krylov subspace solvers depends crucially on the spectrum of the operator that is being discretised, i.e., $\mathcal{A}^*$. The spectrum in turn depends on the continuity and coercivity/inf-sup constants of the operator, which themselves are obtained through a detailed numerical analysis. However, the analysis we presented in Chapter 3 of this dissertation derived explicit N-independent continuity and inf-sup constants only for the *'modified' boundary integral operator* $\widetilde{\mathcal{A}}$ and used an indirect approach to obtain convergence rates for the Galerkin discretisation (2.8). Unfortunately, we have little explicit information on the spectrum of $\mathcal{A}^*$ and certainly no N-independent bounds on the largest and smallest eigenvalues.

Our solution to this obstacle is to adopt once again an indirect route: Given a free charge $\sigma_f \in H^{-\frac{1}{2}}(\partial\Omega)$

Step 1) We solve the 'reduced' Galerkin discretisation (4.1) with modified RHS to obtain $\lambda_{\ell_{\max}} \in W_0^{\ell_{\max}}$ for some $\ell_{\max} \in \mathbb{N}$. This step will require the solution of a linear system using a Krylov subspace solver.

Step 2) We make use of Lemma 4.4 to compute the solution $\nu_{\ell_{\max}} \in W^{\ell_{\max}}$ to the original Galerkin discretisation (2.8) using $\lambda_{\ell_{\max}}$. This step does not require an additional linear system to be solved.

Naturally, the advantage of this strategy is that the required spectral information of the operator $\widetilde{\mathcal{A}}$ is available from our prior analysis in Chapter 3.

It therefore remains to perform a convergence analysis of the Krylov subspace solver used to solve the linear system arising from the Galerkin discretisation (4.1). We now encounter the second difficulty: Since the boundary integral operator $\widetilde{\mathcal{A}}$ is obviously *non-symmetric*, we solve the linear system associated with the Galerkin discretisation (4.1) using the GMRES solver introduced by Saad and Schultz [183]. And the convergence behaviour of GMRES is, in general, considerably more complex than that of the well-known conjugate gradient (CG) method (see, e.g., [125] for a comprehensive discussion).

Broadly speaking, the GMRES solver can be applied to four qualitatively different (real) solution matrices $\boldsymbol{A}$:

M1) Symmetric matrices, i.e., $\boldsymbol{A} = \boldsymbol{A}^{\mathrm{T}}$: In this case the convergence behaviour of GMRES depends only on the spectrum of the solution matrix. Moreover, since the spectrum of the solution matrix is purely real, estimates of the residual at each iteration can be obtained using only the largest and smallest eigenvalues (see, e.g., [67, Chapter 3]).

M2) Non-symmetric normal matrices, i.e., $\boldsymbol{A}\boldsymbol{A}^{\mathrm{T}} = \boldsymbol{A}^{\mathrm{T}}\boldsymbol{A}$: In principle, the convergence behaviour of GMRES in this case also depends only the spectrum of the solution matrix. However, since the spectrum of the solution matrix need not be real, useful bounds on the residual at each iteration cannot be obtained using only the eigenvalues with largest and smallest real parts. Instead one typically requires information on the distribution of the full spectrum in the complex plane (see, e.g., [181, Section 4]).

M3) Non-normal diagonalisable matrices, i.e., $\boldsymbol{A} = \boldsymbol{X}^{-1}\boldsymbol{D}\boldsymbol{X}$ for some diagonal matrix $\boldsymbol{D}$ and non-unitary matrix $\boldsymbol{X}$: In this case, the convergence behaviour of GMRES is typically less known since the estimates on the residual at each iteration depend not only on the spectrum of solution matrix but also on the conditioning of the matrix $\boldsymbol{X}$ appearing in its diagonalisation, which, in general, is unknown (see, e.g., [182, Chapter 6]).

M4) Non-diagonalisable matrices: In this case, the convergence behaviour of GMRES is significantly more difficult to analyse and there are only partial theoretical results (see, e.g., [156] for an approach based on the pseudospectrum and [58, 59, 61] for approaches based on the so-called *field of values*).

Consequently, in order to have a reasonable hope of analysing the convergence behaviour of GMRES applied to the linear system arising from the Galerkin discretisation (4.1), we must show that the matrix discretisation of $\widetilde{\mathcal{A}}$ is either normal or diagonalisable. Unfortunately, the matrix discretisation of $\widetilde{\mathcal{A}}$ is not normal since the operators $\mathcal{V}$ and DtN do not commute in general. Consequently, we must prove that the matrix discretisation of $\widetilde{\mathcal{A}}$ is diagonalisable. Notice that since the convergence behaviour of GMRES depends on the conditioning of the matrix appearing in the diagonalisation, the exact choice of diagonalisation is vital.

4.2.1 The diagonalization of the operator $\widetilde{\mathcal{A}}$

We will assume throughout this subsection that the discretisation parameter $\ell_{\max} \in \mathbb{N}$ is fixed. Additionally, in order to obtain a useful diagonalisation, we will assume in the sequel that the dielectric function κ satisfies one of two conditions:

1. Either $\kappa_j > \kappa_0$ for all $j = 1, \ldots, N$;
2. Or $\kappa_j < \kappa_0$ for all $j = 1, \ldots, N$.

From a practical point of view, this additional constraint is not too restrictive since it covers the two cases which typically arise in physical applications: The case of weakly polarisable particles embedded in a highly polarisable solvent and the case of highly polarisable particles embedded in a weakly polarisable medium. Examples of the former include teflon, Poly(methyl methacrylate) (PMMA), polyethylene or polypropylene particles in water [128]. Examples of the later include a wide range of Titanium-based oxides or certain highly polarisable polymer particles in air [165].

Definition 4.5 (Finite Dimensional Operators)**.** Let $\widetilde{\mathcal{A}}\colon \breve{H}^{\frac{1}{2}}(\partial\Omega) \to \breve{H}^{\frac{1}{2}}(\partial\Omega)$ be the 'modified' boundary integral operator defined through Definition 4.1, let $\mathcal{V}\colon H^{-\frac{1}{2}}(\partial\Omega) \to H^{\frac{1}{2}}(\partial\Omega)$ be the single layer boundary integral operator and let $\mathrm{DtN}\colon H^{\frac{1}{2}}(\partial\Omega) \to H^{-\frac{1}{2}}(\partial\Omega)$ be the Dirichlet-to-Neumann map. Then we define the finite dimensional operators $\widetilde{\mathcal{A}}_{\ell_{\max}}\colon W_0^{\ell_{\max}} \to W_0^{\ell_{\max}}$, $\mathcal{V}_{\ell_{\max}}\colon W_0^{\ell_{\max}} \to W_0^{\ell_{\max}}$ and $\mathrm{DtN}_{\ell_{\max}}\colon W_0^{\ell_{\max}} \to W_0^{\ell_{\max}}$ as

$$\begin{aligned}\widetilde{\mathcal{A}}_{\ell_{\max}} &:= \mathbb{P}_{\ell_{\max}}\mathbb{P}_0^{\perp}\widetilde{\mathcal{A}},\\ \mathcal{V}_{\ell_{\max}} &:= \mathbb{P}_{\ell_{\max}}\mathbb{P}_0^{\perp}\mathcal{V},\\ \mathrm{DtN}_{\ell_{\max}} &:= \mathbb{P}_{\ell_{\max}}\mathrm{DtN}.\end{aligned}$$

Here, $\mathbb{P}_0^{\perp}\colon H^{\frac{1}{2}}(\partial\Omega) \to \breve{H}^{\frac{1}{2}}(\partial\Omega)$ is the projection operator associated with the complementary decomposition introduced through Lemma 3.2 in Chapter 3, and $\mathbb{P}_{\ell_{\max}}\colon H^{\frac{1}{2}}(\partial\Omega) \to W_0^{\ell_{\max}}$ is the projection operator on the approximation space as defined through Definition 3.30.

Remark 4.6. Consider the setting of Definition 4.5. We emphasise that the operators $\mathcal{V}_{\ell_{\max}}$ and $\mathrm{DtN}_{\ell_{\max}}$ are L^2-symmetric, i.e., for all $\psi_{\ell_{\max}}, \sigma_{\ell_{\max}} \in W_0^{\ell_{\max}}$ it holds that

$$\begin{aligned}(\psi_{\ell_{\max}}, \mathcal{V}_{\ell_{\max}}\sigma_{\ell_{\max}})_{L^2(\partial\Omega)} &= (\mathcal{V}_{\ell_{\max}}\psi_{\ell_{\max}}, \sigma_{\ell_{\max}})_{L^2(\partial\Omega)}\,,\\ (\psi_{\ell_{\max}}, \mathrm{DtN}_{\ell_{\max}}\sigma_{\ell_{\max}})_{L^2(\partial\Omega)} &= (\mathrm{DtN}_{\ell_{\max}}\psi_{\ell_{\max}}, \sigma_{\ell_{\max}})_{L^2(\partial\Omega)}\,.\end{aligned}$$

This is a subtle but important detail since the space $W_0^{\ell_{\max}}$ is a priori equipped with the $W^{\ell_{\max}}$ inner product (see Definition 2.11), and $\mathcal{V}_{\ell_{\max}}$ is *not* symmetric with respect to the $W^{\ell_{\max}}$ inner product.

Definition 4.7. We define the L^2-symmetric, positive definite, finite-dimensional operator $\mathrm{DtN}^{\kappa}_{\ell_{\max}}\colon W_0^{\ell_{\max}} \to W_0^{\ell_{\max}}$ as the mapping with the property that for all $\psi_{\ell_{\max}} \in W_0^{\ell_{\max}}$ it holds that

$$\mathrm{DtN}^{\kappa}_{\ell_{\max}}\psi_{\ell_{\max}} := \left|\frac{\kappa - \kappa_0}{\kappa_0}\right| \mathrm{DtN}_{\ell_{\max}}\psi_{\ell_{\max}}.$$

Consider Definitions 4.5 and 4.7, and let $I_{\ell_{\max}}\colon W_0^{\ell_{\max}} \to W_0^{\ell_{\max}}$ denote the identity mapping. It follows that

$$\widetilde{\mathcal{A}}_{\ell_{\max}} = \begin{cases} I_{\ell_{\max}} + \mathcal{V}_{\ell_{\max}}\mathrm{DtN}^{\kappa}_{\ell_{\max}} & \text{if } \kappa > \kappa_0,\\ I_{\ell_{\max}} - \mathcal{V}_{\ell_{\max}}\mathrm{DtN}^{\kappa}_{\ell_{\max}} & \text{if } \kappa < \kappa_0.\end{cases} \tag{4.2}$$

Equation (4.2) suggests a natural diagonalisation strategy: Since $\mathrm{DtN}^{\kappa}_{\ell_{\max}}$ is symmetric positive definite, the associated square root operator $(\mathrm{DtN}^{\kappa}_{\ell_{\max}})^{\frac{1}{2}} : W_0^{\ell_{\max}} \to W_0^{\ell_{\max}}$ can be defined and used to diagonalise $\widetilde{\mathcal{A}}$.

Definition
4.8. We define the L^2-symmetric, finite-dimensional operator $\widetilde{\mathcal{A}}^{\mathrm{sym}}_{\ell_{\max}} : W_0^{\ell_{\max}} \to W_0^{\ell_{\max}}$ as

$$\widetilde{\mathcal{A}}^{\mathrm{sym}}_{\ell_{\max}} := \begin{cases} I_{\ell_{\max}} + (\mathrm{DtN}^{\kappa}_{\ell_{\max}})^{\frac{1}{2}} \mathcal{V}_{\ell_{\max}} (\mathrm{DtN}^{\kappa}_{\ell_{\max}})^{\frac{1}{2}} & \text{if } \kappa > \kappa_0, \\ I_{\ell_{\max}} - (\mathrm{DtN}^{\kappa}_{\ell_{\max}})^{\frac{1}{2}} \mathcal{V}_{\ell_{\max}} (\mathrm{DtN}^{\kappa}_{\ell_{\max}})^{\frac{1}{2}} & \text{if } \kappa < \kappa_0. \end{cases}$$

Remark 4.9. Consider Definition 4.8. We observe immediately that the finite-dimensional operators $\widetilde{\mathcal{A}}_{\ell_{\max}}$ and $\widetilde{\mathcal{A}}^{\mathrm{sym}}_{\ell_{\max}}$ are *similar*, i.e., it holds that

$$\widetilde{\mathcal{A}}_{\ell_{\max}} = (\mathrm{DtN}^{\kappa}_{\ell_{\max}})^{-\frac{1}{2}} \widetilde{\mathcal{A}}^{\mathrm{sym}}_{\ell_{\max}} (\mathrm{DtN}^{\kappa}_{\ell_{\max}})^{\frac{1}{2}}. \tag{4.3}$$

Although we have not obtained an explicit diagonalisation of $\widetilde{\mathcal{A}}_{\ell_{\max}}$, we have shown that it is similar to the L^2-symmetric operator $\widetilde{\mathcal{A}}^{\mathrm{sym}}_{\ell_{\max}}$. In fact our subsequent convergence analysis does not require an explicit diagonalisation and the relation (4.3) will be sufficient.

Since the finite-dimensional operator $\widetilde{\mathcal{A}}^{\mathrm{sym}}_{\ell_{\max}}$ will feature prominently in our convergence analysis, we must obtain bounds on the spectrum of this operator. Notice that $\widetilde{\mathcal{A}}^{\mathrm{sym}}_{\ell_{\max}}$ is L^2-symmetric, and thus has purely real eigenvalues. The next lemma gives bounds on the smallest and largest eigenvalues of this operator.

Lemma 4.10. *Let the symmetric, finite-dimensional operator $\widetilde{\mathcal{A}}^{\mathrm{sym}}_{\ell_{\max}} : W_0^{\ell_{\max}} \to W_0^{\ell_{\max}}$ be defined as in Definition 4.8, let the continuity constant $C_{\widetilde{\mathcal{A}}}$ of the operator $\widetilde{\mathcal{A}}$ be defined as in Lemma 3.20, let the constant $\alpha_0 \in \mathbb{R}$ be defined as*

$$\alpha_0 := \begin{cases} 1 & \text{if } \kappa > \kappa_0, \\ \min \frac{\kappa}{\kappa_0} & \text{if } \kappa < \kappa_0, \end{cases}$$

and let $\mu_0 \in \mathbb{R}$ and $\mu_{\max} \in \mathbb{R}$ denote the smallest and largest eigenvalue respectively of $\widetilde{\mathcal{A}}^{\mathrm{sym}}_{\ell_{\max}}$. Then it holds that

$$\mu_0 \geq \alpha_0 \qquad \text{and} \qquad \mu_{\max} \leq C_{\widetilde{\mathcal{A}}}.$$

Proof. We first prove the bound for the largest eigenvalue $\mu_{\max} \in \mathbb{R}$. Let $\psi^{\ell_{\max}}_{\max} \in W_0^{\ell_{\max}}$ denote the eigenfunction corresponding to $\mu_{\max}$. We then have by the similarity of the operators $\widetilde{\mathcal{A}}_{\ell_{\max}}$ and $\widetilde{\mathcal{A}}^{\mathrm{sym}}_{\ell_{\max}}$ (see Remark 4.9) that

$$\mu_{\max} \psi^{\ell_{\max}}_{\max} = \widetilde{\mathcal{A}}^{\mathrm{sym}}_{\ell_{\max}} \psi^{\ell_{\max}}_{\max} = (\mathrm{DtN}^{\kappa}_{\ell_{\max}})^{\frac{1}{2}} \widetilde{\mathcal{A}}_{\ell_{\max}} (\mathrm{DtN}^{\kappa}_{\ell_{\max}})^{-\frac{1}{2}} \psi^{\ell_{\max}}_{\max}.$$

Define the function $\phi_{\max}^{\ell_{\max}} := (\mathrm{DtN}^{\kappa})^{-\frac{1}{2}}\psi_{\max}^{\ell_{\max}}$. A straightforward calculation yields

$$\mu_{\max}\phi_{\max}^{\ell_{\max}} = \widetilde{\mathcal{A}}_{\ell_{\max}}\phi_{\max}^{\ell_{\max}},$$

which implies that

$$\mu_{\max}^2 |||\phi_{\max}^{\ell_{\max}}|||^2 = |||\widetilde{\mathcal{A}}_{\ell_{\max}}\phi_{\max}^{\ell_{\max}}|||^2.$$

Consequently, we obtain from Lemma 3.20 that $\mu_{\max} \leq C_{\widetilde{\mathcal{A}}}$. Next, we prove the estimate for the smallest eigenvalue $\mu_0 \in \mathbb{R}$. Let $\psi_0^{\ell_{\max}} \in W_0^{\ell_{\max}}$ denote the eigenfunction corresponding to μ_0 and define $\phi_0^{\ell_{\max}} := (\mathrm{DtN}^{\kappa})^{-\frac{1}{2}}\psi_0^{\ell_{\max}}$. A similar calculation as above yields that

$$\mu_0\phi_0^{\ell_{\max}} = \widetilde{\mathcal{A}}_{\ell_{\max}}\phi_0^{\ell_{\max}}. \tag{4.4}$$

Consider first the case $\kappa > \kappa_0$. From Equation (4.4) and the definition of $\widetilde{\mathcal{A}}_{\ell_{\max}}$ we have

$$\begin{aligned}\mu_0 \left(\phi_0^{\ell_{\max}}, \mathrm{DtN}_{\ell_{\max}}^{\kappa}\phi_0^{\ell_{\max}}\right)_{L^2(\partial\Omega)} &= \left(\phi_0^{\ell_{\max}}, \mathrm{DtN}_{\ell_{\max}}^{\kappa}\phi_0^{\ell_{\max}}\right)_{L^2(\partial\Omega)} \\ &\quad + \left(\mathcal{V}\mathrm{DtN}_{\ell_{\max}}^{\kappa}\phi_0^{\ell_{\max}}, \mathrm{DtN}_{\ell_{\max}}^{\kappa}\phi_0^{\ell_{\max}}\right)_{L^2(\partial\Omega)} \\ &\geq \left(\phi_0^{\ell_{\max}}, \mathrm{DtN}_{\ell_{\max}}^{\kappa}\phi_0^{\ell_{\max}}\right)_{L^2(\partial\Omega)},\end{aligned}$$

where the second step uses the coercivity of $\mathcal{V}$ (see Theorem 1.27 in Section 1.4). This yields $\mu_0 \geq 1$.

Next, we consider the case $\kappa < \kappa_0$. We obtain from Equation (4.4) and the definition of $\widetilde{\mathcal{A}}_{\ell_{\max}}$ that

$$(\mu_0 - 1)\left(\phi_0^{\ell_{\max}}, \mathrm{DtN}_{\ell_{\max}}^{\kappa}\phi_0^{\ell_{\max}}\right)_{L^2(\partial\Omega)} = -\left(\mathcal{V}\mathrm{DtN}_{\ell_{\max}}^{\kappa}\phi_0^{\ell_{\max}}, \mathrm{DtN}_{\ell_{\max}}^{\kappa}\phi_0^{\ell_{\max}}\right)_{L^2(\partial\Omega)}. \tag{4.5}$$

We define the function $\phi_0^{\kappa,\ell_{\max}} := \left|\frac{\kappa-\kappa_0}{\kappa_0}\right| \phi_0^{\ell_{\max}}$. Using the Calderón identities (see Lemma 1.31 in Section 1.4), we see that

$$\begin{aligned}\left(\mathcal{V}\mathrm{DtN}_{\ell_{\max}}^{\kappa}\phi_0^{\ell_{\max}}, \mathrm{DtN}_{\ell_{\max}}^{\kappa}\phi_0^{\ell_{\max}}\right)_{L^2(\partial\Omega)} &= \left(\mathrm{DtN}_{\ell_{\max}}\phi_0^{\kappa,\ell_{\max}}, \phi_0^{\kappa,\ell_{\max}}\right)_{L^2(\partial\Omega)} - \left(\mathcal{W}\phi_0^{\kappa,\ell_{\max}}, \phi_0^{\kappa,\ell_{\max}}\right)_{L^2(\partial\Omega)} \\ &\leq \left(\mathrm{DtN}_{\ell_{\max}}\phi_0^{\kappa,\ell_{\max}}, \phi_0^{\kappa,\ell_{\max}}\right)_{L^2(\partial\Omega)},\end{aligned}$$

where the inequality follows from the non-negativity of the hypersingular operator $\mathcal{W}$ (see Theorem 1.28 in Section 1.4). Using this bound in Equation (4.5) then yields

$$(\mu_0 - 1)\sum_{j=1}^{N}\left|\frac{\kappa_j - \kappa_0}{\kappa_0}\right|\left(\mathrm{DtN}_{\ell_{\max}}\phi_0^{\ell_{\max}}, \phi_0^{\ell_{\max}}\right)_{L^2(\partial\Omega_j)}$$

$$\geq -\sum_{j=1}^{N} \left| \frac{\kappa_j - \kappa_0}{\kappa_0} \right|^2 \left(\mathrm{DtN}_{\ell_{\max}} \phi_0^{\ell_{\max}}, \phi_0^{\ell_{\max}} \right)_{L^2(\partial\Omega_j)}.$$

Simple calculus and the fact that $\kappa < \kappa_0$ by assumption, allows us to conclude that $\mu_0 \geq \min_{j=1,\dots,N} \frac{\kappa_j}{\kappa_0}$. □

We now have all the ingredients necessary to analyse the convergence behaviour of GMRES applied to the linear system arising from the "reduced" Galerkin discretisation (4.1) with modified RHS.

4.2.2 GMRES convergence analysis and solution strategy

We begin this subsection by fixing some additional notation. As a first step we would like to write explicitly the linear system arising from the Galerkin discretisation (4.1). In view of Definition 3.26 of our approximation space $W_0^{\ell_{\max}}$, the natural choice of basis functions are the local spherical harmonics on each sphere.

Definition 4.11 (Choice of Basis)**.** Let $\ell_{\max} \in \mathbb{N}$. We denote for each $j \in \{1, \dots, N\}$ and all $\ell \in \{1, \dots, \ell_{\max}\}$, $-\ell \leq m \leq \ell$ the function $\mathcal{Y}_{\ell m}^j \colon \partial\Omega \to \mathbb{R}$ defined as

$$\mathcal{Y}_{\ell m}^j(\mathbf{x}) := \begin{cases} \mathcal{Y}_\ell^m \left(\frac{\mathbf{x}-\mathbf{x}_j}{|\mathbf{x}-\mathbf{x}_j|} \right) & \text{for all } \mathbf{x} \in \partial\Omega_j, \\ 0 & \text{otherwise,} \end{cases}$$

and we equip the approximation space $W_0^{\ell_{\max}}$ with the basis $\{\mathcal{Y}_{\ell m}^j\}$. Here, $\mathcal{Y}_\ell^m$ denotes the spherical harmonic of degree ℓ and order m as defined in Definition 2.9 in Section 2.3.

Notation: Let $\ell_{\max} \in \mathbb{N}$. We will henceforth denote by $M := N \cdot (\ell_{\max} + 1)^2 - N$, the dimension of the approximation space $W_0^{\ell_{\max}}$. Notice that the dimension of the space $W^{\ell_{\max}}$ is then given by $M + N$.

Remark 4.12. Consider Definition 4.11 of the basis functions on $W_0^{\ell_{\max}}$. These functions establish an isomorphism between $W_0^{\ell_{\max}}$ and $\mathbb{R}^M$. Indeed, we associate an arbitrary $\psi \in W_0^{\ell_{\max}}$ with $\boldsymbol{\psi} \in \mathbb{R}^M$ defined as

$$[\boldsymbol{\psi}_i]_\ell^m := \left(\psi, \mathcal{Y}_{\ell m}^j \right)_{L^2(\partial\Omega_i)}, \qquad \text{for } i \in \{1, \dots, N\}, \quad \ell \in \{1, \dots, \ell_{\max}\} \quad \text{and} \quad -\ell \leq m \leq \ell.$$

Consequently, given functions in the space $W_0^{\ell_{\max}}$, we will often refer to their vector representations in $\mathbb{R}^M$ and vice versa. Moreover, to facilitate identification we will frequently use bold symbols for the vector representations.

Definition 4.13. Let $\ell_{\max} \in \mathbb{N}$, let $\mathbb{Q}_{\ell_{\max}} \colon H^{-\frac{1}{2}}(\partial\Omega) \to W^{\ell_{\max}}$ denote the projection operator on the approximation space as defined through Definition 3.30, and let $\sigma_f \in H^{-\frac{1}{2}}(\partial\Omega)$. Then

- We define the right-hand side vector $\boldsymbol{\sigma_f} \in \mathbb{R}^M$ as

$$[\boldsymbol{\sigma_f}_i]_\ell^m := \frac{1}{\kappa_0} \left(\mathcal{V}\mathbb{Q}_{\ell_{\max}} \sigma_f, \mathcal{Y}_{\ell m}^i\right)_{L^2(\partial\Omega_i)}$$

  for $i \in \{1, \ldots, N\}$, $\ell \in \{1, \ldots, \ell_{\max}\}$, and $-\ell \leq m \leq \ell$.

- We define the diagonal positive definite matrix $\mathbf{DtN}^\kappa \in \mathbb{R}^{M \times M}$ as

$$[\mathbf{DtN}_{ij}^\kappa]_{\ell\ell'}^{mm'} := \left((\mathrm{DtN}_{\ell_{\max}}^\kappa)^{\frac{1}{2}} \mathcal{Y}_{\ell' m'}^j, \mathcal{Y}_{\ell m}^i\right)_{L^2(\partial\Omega_i)}$$

  for $i, j \in \{1, \ldots, N\}$, $\ell, \ell' \in \{1, \ldots, \ell_{\max}\}$, and $-\ell \leq m, m' \leq \ell$.

- We define the solution matrix $\boldsymbol{A} \in \mathbb{R}^{M \times M}$ as

$$[\boldsymbol{A}_{ij}]_{\ell\ell'}^{mm'} := \left(\widetilde{\mathcal{A}}_{\ell_{\max}} \mathcal{Y}_{\ell' m'}^j, \mathcal{Y}_{\ell m}^i\right)_{L^2(\partial\Omega_i)}$$

  for $i, j \in \{1, \ldots, N\}$, $\ell, \ell' \in \{1, \ldots, \ell_{\max}\}$, and $-\ell \leq m, m' \leq \ell$.

- We define the symmetrised solution matrix $\boldsymbol{A}^{\mathrm{sym}} \in \mathbb{R}^{M \times M}$ as

$$[\boldsymbol{A}_{ij}^{\mathrm{sym}}]_{\ell\ell'}^{mm'} := \left(\widetilde{\mathcal{A}}_{\ell_{\max}}^{\mathrm{sym}} \mathcal{Y}_{\ell' m'}^j, \mathcal{Y}_{\ell m}^i\right)_{L^2(\partial\Omega_i)}$$

  for $i, j \in \{1, \ldots, N\}$, $\ell, \ell' \in \{1, \ldots, \ell_{\max}\}$, and $-\ell \leq m, m' \leq \ell$.

Two remarks are now in order.

Remark 4.14. Consider Definition 4.13. A direct calculation shows that the matrices $\boldsymbol{A}$ and $\boldsymbol{A}^{\mathrm{sym}}$ are similar and we have

$$\boldsymbol{A} = (\mathbf{DtN}^\kappa)^{-1} \boldsymbol{A}^{\mathrm{sym}} \mathbf{DtN}^\kappa.$$

Remark 4.15. Consider Definition 4.13. We emphasise that the solution matrix $\boldsymbol{A}$ and the symmetrised solution matrix $\boldsymbol{A}^{\mathrm{sym}}$ are nothing else than the representation in the basis of local spherical harmonics functions of the finite-dimensional operators $\widetilde{\mathcal{A}}_{\ell_{\max}}$ and $\widetilde{\mathcal{A}}_{\ell_{\max}}^{\mathrm{sym}}$ defined through Definitions 4.1 and 4.8 respectively. We can therefore write the "reduced" Galerkin discretisation (4.1) with modified RHS as expected in matrix form.

Matrix formulation of the "reduced" Galerkin discretisation (4.1)

Let $\ell_{\max} \in \mathbb{N}$, let $\sigma_f \in H^{-\frac{1}{2}}(\partial\Omega)$, and let the vector $\boldsymbol{\sigma_f} \in \mathbb{R}^M$ and the matrix $\boldsymbol{A} \in \mathbb{R}^{M \times M}$ be defined as in Definition 4.13. Find a vector $\boldsymbol{\lambda} \in \mathbb{R}^M$ such that

$$\boldsymbol{A}\boldsymbol{\lambda} = \boldsymbol{\sigma_f}. \tag{4.6}$$

We are now ready to state our main convergence result.

Theorem 4.16 (Convergence Analysis for GMRES-based Strategy)**.**
Let $\ell_{\max} \in \mathbb{N}$, let $\sigma_f \in H^{-\frac{1}{2}}(\partial\Omega)$, let $\nu_{\ell_{\max}} \in W^{\ell_{\max}}$ be the unique solution to the Galerkin discretisation (2.8) for the induced surface charge with right hand side given by σ_f, and let $\mathbb{P}_0^{\perp}\colon H^{\frac{1}{2}}(\partial\Omega) \to \breve{H}^{\frac{1}{2}}(\partial\Omega)$ and $\mathbb{Q}_{\ell_{\max}}\colon H^{\frac{1}{2}}(\partial\Omega) \to W^{\ell_{\max}}$ be the projection operators defined through Lemma 3.2 and Definition 3.30 respectively. Then for every $\epsilon > 0$ there exists a function $\nu_{\ell_{\max}}^{\text{approx}} \in W^{\ell_{\max}}$ and a natural number $R_\epsilon > 0$ that depends on ϵ, the radii of the open balls, the dielectric constants and the minimal inter-sphere separation distance but is independent of the number of open balls N such that $\nu_{\ell_{\max}}^{\text{approx}}$ can be computed using at most R_ϵ iterations of GMRES and such that the following error estimate holds

$$\frac{|||\nu_{\ell_{\max}}^{\text{approx}} - \nu_{\ell_{\max}}|||^*}{|||\mathbb{P}_0^{\perp}\nu_{\ell_{\max}}|||^* + \frac{1}{\kappa_0}|||\mathbb{P}_0^{\perp}\mathbb{Q}_{\ell_{\max}}\sigma_f|||^*} < \epsilon.$$

Proof. We begin by defining the affine transformation $\mathcal{B}\colon W_0^{\ell_{\max}} \to W^{\ell_{\max}}$ as the mapping with the property that for all $\psi_{\ell_{\max}} \in W_0^{\ell_{\max}}$ it holds that

$$\mathcal{B}\psi_{\ell_{\max}} = \frac{\kappa_0 - \kappa}{\kappa_0}\text{DtN}\psi_{\ell_{\max}} + \frac{1}{\kappa_0}\mathbb{Q}_{\ell_{\max}}\sigma_f. \tag{4.7}$$

Let $\lambda_{\ell_{\max}} \in W_0^{\ell_{\max}}$ denote the solution to the "reduced' Galerkin discretisation with modified RHS (4.1). It follows from Lemma 4.4 that $\mathcal{B}\lambda_{\ell_{\max}} = \nu_{\ell_{\max}}$. Thus for any function $\psi_{\ell_{\max}} \in W_0^{\ell_{\max}}$ it holds that

$$\begin{aligned}|||\nu_{\ell_{\max}} - \mathcal{B}\psi_{\ell_{\max}}|||^* &= \left|\left|\left|\frac{\kappa_0 - \kappa}{\kappa_0}\text{DtN}\Big(\lambda_{\ell_{\max}} - \psi_{\ell_{\max}}\Big)\right|\right|\right|^* \\ &\leq \max\left|\frac{\kappa_0 - \kappa}{\kappa_0}\right||||\lambda_{\ell_{\max}} - \psi_{\ell_{\max}}|||.\end{aligned}$$

Let $\epsilon > 0$ be fixed and let $\widetilde{\epsilon} := \frac{\epsilon}{\max\left|\frac{\kappa_0 - \kappa}{\kappa_0}\right|}$. It follows that

$$||||\lambda_{\ell_{\max}} - \psi_{\ell_{\max}}||| < \widetilde{\epsilon} \implies |||\nu_{\ell_{\max}} - \mathcal{B}\psi_{\ell_{\max}}|||^* < \epsilon. \tag{4.8}$$

We will therefore show that there exists a natural number R_ϵ that depends on ϵ, the radii of the open balls, the dielectric constants and the minimal inter-sphere separation distance but is independent of the number of open balls N such that one can compute a function $\psi_{\ell_{\max}} \in W_0^{\ell_{\max}}$ using at most R_ϵ iterations of GMRES and such that

$$|||\lambda_{\ell_{\max}} - \psi_{\ell_{\max}}||| < \widetilde{\epsilon}. \tag{4.9}$$

This will allow us to define $\nu_{\ell_{\max}}^{\text{approx}} := \mathcal{B}\psi_{\ell_{\max}}$ and hence complete the proof.

Consider the matrix Equation (4.6). Let $\boldsymbol{\lambda}_0 \in \mathbb{R}^M$ be some initialisation and let $\boldsymbol{\lambda}_k \in \mathbb{R}^M$, $k \in \mathbb{N}$ denote the k^{th} iterate generated by GMRES applied to this linear

system. Next, let $\boldsymbol{r}_k := \boldsymbol{\sigma_f} - \boldsymbol{A}\boldsymbol{\lambda}_k$, $k \in \mathbb{N}_0$ denote the k^{th} residual. It is well known (see, e.g., [84] or [125]) that for all natural numbers $k \in \mathbb{N}$ the GMRES residual $\boldsymbol{r}_k$ satisfies

$$|\boldsymbol{r}_k| = \min_{p\in\pi_k} |p(\boldsymbol{A})\,\boldsymbol{r}_0| \leq \min_{p\in\pi_k} \|p(\boldsymbol{A})\|_2 |\boldsymbol{r}_0|, \tag{4.10}$$

where π_k denotes the set of all polynomials $p\colon \mathbb{R} \to \mathbb{R}$ of degree at most k such that $p(0) = 1$, $|\cdot|$ denotes the standard Euclidean norm in $\mathbb{R}^M$ and $\|\cdot\|_2$ denotes the matrix norm induced by the standard Euclidean norm in $\mathbb{R}^M$.

Using Remark 4.14 and the fact that the matrix $\boldsymbol{A}^{\text{sym}}$ is symmetric, the bound (4.10) can be simplified (see, e.g., [125]) to obtain

$$\begin{aligned} |\boldsymbol{r}_k| &\leq \min_{p\in\pi_k} \|p(\boldsymbol{A}^{\text{sym}})\|_2 \|(\mathbf{DtN}^\kappa)^{-1}\|_2 \|\mathbf{DtN}^\kappa\|_2 |\boldsymbol{r}_0|, \\ &\leq \min_{p\in\pi_k} \max_n |p(\mu_n)| \|(\mathbf{DtN}^\kappa)^{-1}\|_2 \|\mathbf{DtN}^\kappa\|_2 |\boldsymbol{r}_0|, \end{aligned}$$

where μ_n, $n = 0, \ldots, M-1$ denote the (ascendingly ordered) eigenvalues of the matrix $\boldsymbol{A}^{\text{sym}}$. We now simplify each term in this estimate.

Due to Lemma 4.10 we know that all eigenvalues of $\boldsymbol{A}^{\text{sym}}$ are positive and we have explicit bounds on the smallest eigenvalue μ_0 and the largest eigenvalue μ_{M-1} of this matrix. Consequently, we can employ the standard approach of using Chebyshev polynomials of the first kind to estimate the min-max problem (see, e.g., [67, Chapter 3]). We thus obtain

$$\min_{p\in\pi_k} \max_n |p(\mu_n)| \leq 2 \left(\frac{\sqrt{\frac{C_{\tilde{\mathcal{A}}}}{\alpha_0}} - 1}{\sqrt{\frac{C_{\tilde{\mathcal{A}}}}{\alpha_0}} + 1} \right)^k,$$

where $\alpha_0, C_{\tilde{\mathcal{A}}}$ are bounds on the smallest and largest eigenvalues of $\boldsymbol{A}^{\text{sym}}$ respectively, as computed in Lemma 4.10.

Next, we note that by definition, each non-zero entry of the diagonal positive definite matrix $\mathbf{DtN}^\kappa$ is given by

$$\begin{aligned} [\mathbf{DtN}^\kappa_{jj}]^{mm}_{\ell\ell} &= \left|\frac{\kappa_j - \kappa_0}{\kappa_0}\right|^{\frac{1}{2}} \left((\mathrm{DtN}_{\ell_{\max}})^{\frac{1}{2}} \mathcal{Y}^j_{\ell m}, \mathcal{Y}^j_{\ell m} \right)_{L^2(\partial\Omega_j)} \\ &= \left|\frac{\kappa_j - \kappa_0}{\kappa_0}\right|^{\frac{1}{2}} r_j^2 \sqrt{\frac{\ell}{r_j}} \quad \text{for } j \in \{1, \ldots, N\},\ \ell \in \{1, \ldots, \ell_{\max}\},\ \text{and}\ \ -\ell \leq m \leq \ell. \end{aligned}$$

If we denote by $\chi_0 \in \mathbb{R}$ and $\chi_{\max} \in \mathbb{R}$ the smallest and largest entry respectively of the matrix $\mathbf{DtN}^\kappa$, we have

$$\chi_0 = \min \left|\frac{\kappa - \kappa_0}{\kappa_0}\right|^{\frac{1}{2}} \min_{j=1\ldots,N} r_j^{\frac{3}{2}}, \qquad \text{and} \qquad \chi_{\max} = \max \left|\frac{\kappa - \kappa_0}{\kappa_0}\right|^{\frac{1}{2}} \max_{j=1\ldots,N} r_j^{\frac{3}{2}} \sqrt{\ell_{\max}}.$$

We thus obtain that

$$\|(\mathbf{DtN}^\kappa)^{-1}\|_2 = \frac{1}{\chi_0} = \frac{1}{\min \left|\frac{\kappa-\kappa_0}{\kappa_0}\right|^{\frac{1}{2}} \min_{j=1\ldots,N} r_j^{\frac{3}{2}}}$$

and

$$\left\|\mathbf{DtN}^{\kappa}\right\|_2 = \chi_{\max} = \max\left|\frac{\kappa-\kappa_0}{\kappa_0}\right|^{\frac{1}{2}} \max_{j=1\ldots,N} r_j^{\frac{3}{2}}\sqrt{\ell_{\max}}.$$

The estimate (4.10) can therefore be bounded as

$$|\boldsymbol{r}_k| \leq 2\sqrt{\ell_{\max}}\left(\frac{\sqrt{\frac{C_{\widetilde{\mathcal{A}}}}{\alpha_0}}-1}{\sqrt{\frac{C_{\widetilde{\mathcal{A}}}}{\alpha_0}}+1}\right)^k \left(\frac{\max|\kappa-\kappa_0|\max_{j=1\ldots,N} r_j^3}{\min|\kappa-\kappa_0|\min_{j=1\ldots,N} r_j^3}\right)^{\frac{1}{2}} |\boldsymbol{r}_0|.$$

Next, for each $k \in \mathbb{N}_0$ we denote by $\lambda_k^{\ell_{\max}} \in W_0^{\ell_{\max}}$ the function associated with the vector $\boldsymbol{\lambda}_k \in \mathbb{R}^m$. Using the fact that $\boldsymbol{\sigma_f} = \boldsymbol{A\lambda}$ and Definition 4.13, we obtain by a direct calculation that

$$\begin{aligned}
|\boldsymbol{r}_k| = |\boldsymbol{A\lambda} - \boldsymbol{A\lambda}_k| &\geq \min_{j=1,\ldots,N} r_j \left\|\widetilde{\mathcal{A}}_{\ell_{\max}}\lambda_{\ell_{\max}} - \widetilde{\mathcal{A}}_{\ell_{\max}}\lambda_k^{\ell_{\max}}\right\|_{L^2(\partial\Omega)} \\
&\geq \left(\frac{\min_{j=1,\ldots,N} r_j^3}{\ell_{\max}}\right)^{\frac{1}{2}} \left|\left|\left|\widetilde{\mathcal{A}}_{\ell_{\max}}\lambda_{\ell_{\max}} - \widetilde{\mathcal{A}}_{\ell_{\max}}\lambda_k^{\ell_{\max}}\right|\right|\right| \\
&\geq \beta_{\widetilde{\mathcal{A}}}\left(\frac{\min_{j=1,\ldots,N} r_j^3}{\ell_{\max}}\right)^{\frac{1}{2}} \left|\left|\left|\lambda_{\ell_{\max}} - \lambda_k^{\ell_{\max}}\right|\right|\right|,
\end{aligned}$$

where the last step follows from Lemma 3.28 in Chapter 3, which establishes the existence of the discrete inf-sup constant $\beta_{\widetilde{\mathcal{A}}} > 0$ for the modified boundary integral operator $\widetilde{\mathcal{A}}$. In a similar fashion if we pick the initialisation $\boldsymbol{\lambda}_0 \equiv 0$ we have

$$|\boldsymbol{r}_0| \leq C_{\widetilde{\mathcal{A}}} \max_{j=1\ldots,N} r_j^{\frac{3}{2}} |||\lambda_{\ell_{\max}}|||.$$

It therefore follows that

$$\left|\left|\left|\lambda_{\ell_{\max}} - \lambda_k^{\ell_{\max}}\right|\right|\right| \leq \frac{2C_{\widetilde{\mathcal{A}}}\ell_{\max}}{\beta_{\widetilde{\mathcal{A}}}} \frac{\max_{j=1\ldots,N} r_j^3}{\min_{j=1,\ldots,N} r_j^3} \left(\frac{\sqrt{\frac{C_{\widetilde{\mathcal{A}}}}{\alpha_0}}-1}{\sqrt{\frac{C_{\widetilde{\mathcal{A}}}}{\alpha_0}}+1}\right)^k \left(\frac{\max|\kappa-\kappa_0|}{\min|\kappa-\kappa_0|}\right)^{\frac{1}{2}} |||\lambda_{\ell_{\max}}|||. \tag{4.11}$$

Finally, in view of Equation (4.7) we observe that

$$\begin{aligned}
|||\lambda_{\ell_{\max}}||| &= \left|\left|\left|\frac{\kappa_0}{\kappa_0-\kappa}\mathrm{DtN}^{-1}\mathbb{P}_0^{\perp}\left(\nu_{\ell_{\max}} - \frac{1}{\kappa_0}\mathbb{Q}_{\ell_{\max}}\sigma_f\right)\right|\right|\right| \\
&= \left|\left|\left|\frac{\kappa_0}{\kappa_0-\kappa}\mathbb{P}_0^{\perp}\left(\nu_{\ell_{\max}} - \frac{1}{\kappa_0}\mathbb{Q}_{\ell_{\max}}\sigma_f\right)\right|\right|\right|^* \\
&\leq \max\left|\frac{\kappa_0}{\kappa-\kappa_0}\right|\left(|||\mathbb{P}_0^{\perp}\nu_{\ell_{\max}}|||^* + \frac{1}{\kappa_0}|||\mathbb{P}_0^{\perp}\mathbb{Q}_{\ell_{\max}}\sigma_f|||^*\right).
\end{aligned}$$

Therefore, we define the constant

$$\Upsilon_{\text{GMRES}} := \frac{2C_{\widetilde{\mathcal{A}}}}{\beta_{\widetilde{\mathcal{A}}}} \frac{\max_{j=1\ldots,N} r_j^3}{\min_{j=1,\ldots,N} r_j^3} \left(\frac{\max|\kappa - \kappa_0|}{\min|\kappa - \kappa_0|} \right)^{\frac{1}{2}} \max\left| \frac{\kappa_0}{\kappa - \kappa_0} \right|,$$

and we write the bound (4.11) in a more succinct form as

$$\left|\left|\left| \lambda_{\ell_{\max}} - \lambda_k^{\ell_{\max}} \right|\right|\right| \leq \Upsilon_{\text{GMRES}} \ell_{\max} \left(\frac{\sqrt{\frac{C_{\widetilde{\mathcal{A}}}}{\alpha_0}} - 1}{\sqrt{\frac{C_{\widetilde{\mathcal{A}}}}{\alpha_0}} + 1} \right)^k \left(|||\mathbb{P}_0^{\perp} \nu_{\ell_{\max}}|||^* + \frac{1}{\kappa_0} |||\mathbb{P}_0^{\perp} \mathbb{Q}_{\ell_{\max}} \sigma_f|||^* \right).$$

Consequently, we can define the natural number R_ϵ as

$$R_\epsilon := \left\lceil \frac{\log\left(\frac{\widetilde{\epsilon}}{\ell_{\max} \Upsilon_{\text{GMRES}}} \right)}{\log\left(\frac{\sqrt{\frac{C_{\widetilde{\mathcal{A}}}}{\alpha_0}} - 1}{\sqrt{\frac{C_{\widetilde{\mathcal{A}}}}{\alpha_0}} + 1} \right)} \right\rceil. \tag{4.12}$$

We then obtain

$$\left|\left|\left| \lambda_{\ell_{\max}} - \lambda_{R_\epsilon}^{\ell_{\max}} \right|\right|\right| < \widetilde{\epsilon} \left(|||\mathbb{P}_0^{\perp} \nu_{\ell_{\max}}|||^* + \frac{1}{\kappa_0} |||\mathbb{P}_0^{\perp} \mathbb{Q}_{\ell_{\max}} \sigma_f|||^* \right),$$

which yields, using Inequality (4.8),

$$\frac{|||\nu_{\ell_{\max}} - \mathcal{B}\lambda_{R_\epsilon}^{\ell_{\max}}|||^*}{|||\mathbb{P}_0^{\perp} \nu_{\ell_{\max}}|||^* + \frac{1}{\kappa_0} |||\mathbb{P}_0^{\perp} \mathbb{Q}_{\ell_{\max}} \sigma_f|||^*} < \epsilon.$$

Defining $\nu_{\ell_{\max}}^{\text{approx}} := \mathcal{B}\lambda_{R_\epsilon}^{\ell_{\max}}$ therefore completes the proof. □

Some explanatory remarks are now in order.

Remark 4.17. Consider the setting and proof of Theorem 4.16. In practice, the function $\nu_{\ell_{\max}}^{\text{approx}} := \mathcal{B}\lambda_{R_\epsilon}^{\ell_{\max}} \in W^{\ell_{\max}}$ is represented as a vector $\boldsymbol{\nu}^{\text{approx}} \in \mathbb{R}^{M+N}$. This can be done as follows:

First, let $\boldsymbol{\lambda}_{R_\epsilon} \in \mathbb{R}^M$, i.e., the R_ϵ^{th} GMRES iterate, be the vector representation of $\lambda_{R_\epsilon}^{\ell_{\max}} \in W^{\ell_{\max}}$. Next, inspired by Definition 4.11, we equip the space $W^{\ell_{\max}}$ with a basis of local spherical harmonics functions $\left\{ \mathcal{Y}_{\ell m}^i \right\}$, $i \in \{1, \ldots, N\}$ and $\ell \in \{0, \ldots, \ell_{\max}\}$, $-\ell \leq m \leq \ell$. Using the notation $[\boldsymbol{\lambda}_{R_\epsilon}^i]_\ell^m$, $i \in \{1, \ldots, N\}$ and $\ell \in \{1, \ldots, \ell_{\max}\}$, $-\ell \leq m \leq \ell$ to denote the entries of $\boldsymbol{\lambda}_{R_\epsilon}$:

- We define the vector $\boldsymbol{\Psi} \in \mathbb{R}^{M+N}$ as

$$[\boldsymbol{\Psi}_i]_\ell^m := \begin{cases} 0 & \text{for } i \in \{1,\dots,N\},\ \ell, m = 0, \\ \frac{\kappa_0-\kappa_i}{\kappa_0}[\boldsymbol{\lambda}^i_{R_\epsilon}]_\ell^m\big(\mathrm{DtN}\mathcal{Y}^i_{\ell m}, \mathcal{Y}^i_{\ell m}\big) & \text{for } i \in \{1,\dots,N\},\ \ell \in \{1,\dots,\ell_{\max}\},\ m \in [-\ell,\ell]. \end{cases}$$

- We define the vector $\boldsymbol{\sigma}^{\boldsymbol{Q}}_{\boldsymbol{f}} \in \mathbb{R}^{M+N}$ as

$$[\boldsymbol{\sigma}^{\boldsymbol{Q}}_{\boldsymbol{f}\ i}]_\ell^m := \frac{1}{\kappa_0}\left(\sigma_f, \mathcal{Y}^i_{\ell m}\right)_{L^2(\partial\Omega_i)}$$

  for $i \in \{1,\dots,N\}$, $\ell \in \{0,\dots,\ell_{\max}\}$, and $-\ell \le m \le \ell$.

It then follows from Definition (4.7) of the affine map $\mathcal{B}$ that the vector representation $\boldsymbol{\nu}^{\text{approx}} \in \mathbb{R}^{M+N}$ of $\nu^{\text{approx}}_{\ell_{\max}}$ is simply given by

$$\boldsymbol{\nu}^{\text{approx}} := \boldsymbol{\Psi} + \boldsymbol{\sigma}^{\boldsymbol{Q}}_{\boldsymbol{f}}. \tag{4.13}$$

Remark 4.18. Consider the proof of Theorem 4.16. Equation (4.12) describes the behaviour of our bound R_ϵ on the number of GMRES iterations required to obtain an approximate solution with relative error smaller than ϵ. In particular, we observe that

- R_ϵ grows moderately as $\log(\ell_{\max})$ for increasing $\ell_{\max}$. Here, $\ell_{\max}$ is the discretisation parameter for the approximation space. As we discuss in Section 4.3 on numerical results, we typically pick $\ell_{\max} \in \{5,\dots,20\}$ so we do not observe growth in the number of linear solver iterations for increasing $\ell_{\max}$ in practical numerical simulations.
- R_ϵ grows as moderately $\log(\Upsilon_{\text{GMRES}})$ for increasing Υ_{GMRES}. Here, Υ_{GMRES} is the constant defined in the proof of Theorem 4.16 and depends on geometrical parameters such as the radii of the spheres and the dielectric constants, and the continuity and inf-sup constant of the operator $\widetilde{\mathcal{A}}$.
- R_ϵ grows as $\sqrt{\frac{C_{\widetilde{\mathcal{A}}}}{\alpha_0}}$. Here, $C_{\widetilde{\mathcal{A}}}$ and α_0 are bounds on the largest and smallest eigenvalues respectively of the symmetric, finite-dimensional operator $\widetilde{\mathcal{A}}^{\text{sym}}_{\ell_{\max}}$ (see Lemma 4.10) and are given by

$$\alpha_0 = \begin{cases} 1 & \text{if } \kappa > \kappa_0, \\ \min \frac{\kappa}{\kappa_0} & \text{if } \kappa < \kappa_0, \end{cases} \qquad C_{\widetilde{\mathcal{A}}} = 1 + \max\left|\frac{\kappa-\kappa_0}{\kappa_0}\right| \frac{c_{\text{equiv}}}{\sqrt{c_{\mathcal{V}}}}.$$

Consequently, we would expect R_ϵ to be large if

- $\kappa < \kappa_0$ and $\min \frac{\kappa}{\kappa_0}$ is very small;
- $\kappa > \kappa_0$ and $\max \frac{\kappa}{\kappa_0}$ is very large;
- The coercivity constant $c_{\mathcal{V}}$ is very small. We have shown in Chapter 2 (see Lemmas 3.22 and 3.23) that $c_{\mathcal{V}} = \mathcal{O}(\delta)$ for small δ, where δ is the minimum inter-sphere separation distance.

Remark 4.19. Theorem 4.16 show that one can obtain an approximation to the solution $\nu_{\ell_{\max}}$ of the Galerkin discretisation (2.8) for the induced surface charge– up to a given relative error tolerance ϵ– by solving the linear system (4.6) using GMRES, and the number of iterations required does no explicitly depend on N. In particular the number of linear solver iterations is *uniformly bounded* for any family of geometries $\{\Omega_{\mathcal{F}}\}_{\mathcal{F}\in\mathcal{I}}$ satisfying assumptions **GA1)-GA3)**.

Of course, in practice, the error of each GMRES iterate is unknown and the solver is typically run until some relative residual tolerance is reached. Numerical experiments we have performed (see Section 4.3 for specific geometric settings) indicate that the relative residual is typically one order of magnitude larger than the relative error so a very conservative strategy would be to set the GMRES tolerance two orders of magnitude lower than the desired relative error tolerance.

GMRES-based solution strategy for obtaining the induced surface charge and the electrostatic energy

Given a free charge $\sigma_f \in H^{-\frac{1}{2}}(\partial\Omega)$, the goal is to obtain– up to some given tolerance– the solution $\nu_{\ell_{\max}} \in W^{\ell_{\max}}$ to the Galerkin discretisation (2.8) for the induced surface charge. Additionally, it might be necessary to compute the approximate electrostatic energy of the system $\mathcal{E}_{\mathbb{Q}_{\ell_{\max}}\sigma_f}(\nu_{\ell_{\max}})$.

1. Fix $\ell_{\max} \in \mathbb{N}$ and use Definition 4.13 to compute the right-hand side vector $\boldsymbol{\sigma_f} \in \mathbb{R}^M$. Due to the use of the FMM, the total computational cost of this step is $\mathcal{O}(N)$.

2. Use GMRES to solve– up to some tolerance– the linear system (4.6) involving $\boldsymbol{A}$ and $\boldsymbol{\sigma_f}$. This yields a solution vector $\boldsymbol{\lambda}^{\text{approx}} \in \mathbb{R}^M$. Notice that $\boldsymbol{\lambda}^{\text{approx}}$ is the vector representation of the function $\lambda^{\text{approx}}_{\ell_{\max}} \in W_0^{\ell_{\max}}$ which is an approximation to the true solution $\lambda_{\ell_{\max}}$ of the "reduced" Galerkin discretisation (4.1) with modified RHS. Thanks to the FMM, the cost of a single matrix vector product involving $\boldsymbol{A}$ is $\mathcal{O}(N)$. Moreover, due to Theorem 4.16, the total number of iterations of GMRES required in this step is independent of N. Consequently, the total computational cost of this step is also $\mathcal{O}(N)$.

3. Following the procedure outlined in Remark 4.17, use the solution vector $\boldsymbol{\lambda}^{\text{approx}} \in \mathbb{R}^M$ to compute the vector $\boldsymbol{\nu}^{\text{approx}} \in \mathbb{R}^{M+N}$. Clearly, the computational cost of this step is $\mathcal{O}(N)$.

4. $\boldsymbol{\nu}^{\text{approx}}$ is now the vector representation of some function $\nu^{\text{approx}}_{\ell_{\max}} \in W^{\ell_{\max}}$ that is the required approximation of the true solution $\nu_{\ell_{\max}}$ to the Galerkin discretisation (2.8).

5. If required, the approximate electrostatic energy $\mathcal{E}_{\mathbb{Q}_{\ell_{\max}}\sigma_f}(\nu_{\ell_{\max}})$ can be computed using Definition 3.1. Since this requires a single FMM call, the computational cost of this step is also $\mathcal{O}(N)$.

We conclude this subsection by emphasising once again the key implication of Theorem 4.16 and the solution strategy highlighted above: For any geometry in the family of geometries $\{\Omega_{\mathcal{F}}\}_{\mathcal{F}\in\mathcal{J}}$ satisfying assumptions **GA1)-GA3)**, we can compute- up to any given error tolerance– the solution to the Galerkin discretisation (2.8) using $\mathcal{O}(N_{\mathcal{F}})$ operations, where $N_{\mathcal{F}}$ denotes the number of particles in the geometry $\Omega_{\mathcal{F}}$. We have thus demonstrated that our numerical method is linear scaling in cost. Combined with the error analysis presented in Chapter 3 (see, e.g., Theorem 3.12) we can conclude that our numerical method is also *linear scaling in accuracy*, i.e., for any geometry in the family of geometries $\{\Omega_{\mathcal{F}}\}_{\mathcal{F}\in\mathcal{J}}$ satisfying assumptions **GA1)-GA3)**, the computational cost of obtaining the approximate induced surface charge or electrostatic energy up to a fixed average or relative error scales linearly in $N_{\mathcal{F}}$.

4.2.3 An approach based on the conjugate gradient method

Notice that the convergence analysis we presented in Section 4.2.2 relied crucially on the similarity of the finite dimensional operators $\widetilde{\mathcal{A}}$ defined through Definition 4.1 and $\widetilde{\mathcal{A}}^{\mathrm{sym}}$ defined though Definition 4.8. The goal of this section is to further exploit this similarity and outline a solution strategy based on the use of the conjugate gradient (CG) method rather than GMRES. Throughout this subsection, we assume the setting of Section 4.2.2.

Definition 4.20. Let $\ell_{\max}\in\mathbb{N}$, let $\sigma_f\in H^{-\frac{1}{2}}(\partial\Omega)$, and let the vector $\boldsymbol{\sigma_f}\in\mathbb{R}^M$ and the diagonal positive definite matrix $\mathbf{DtN}^{\kappa}\in\mathbb{R}^{M\times M}$ be defined as in Definition 4.13. Then we define the vector $\widetilde{\boldsymbol{\sigma_f}}\in\mathbb{R}^M$ as

$$\widetilde{\boldsymbol{\sigma_f}} := \mathbf{DtN}^{\kappa}\boldsymbol{\sigma_f}.$$

Using Definition 4.20, we can formulate a matrix equation associated with the symmetric finite-dimensional operator $\widetilde{\mathcal{A}}^{\mathrm{sym}}$.

Symmetric matrix equation for $\widetilde{\mathcal{A}}^{\mathrm{sym}}$:

Let $\ell_{\max}\in\mathbb{N}$, let $\sigma_f\in H^{-\frac{1}{2}}(\partial\Omega)$, let the symmetric matrix $\boldsymbol{A}^{\mathrm{sym}}\in\mathbb{R}^{M\times M}$ be defined as in Definition 4.13, and let the vector $\widetilde{\boldsymbol{\sigma_f}}\in\mathbb{R}^M$ be defined as in Definition 4.20. Find a vector $\boldsymbol{\lambda}^{\mathrm{sym}}\in\mathbb{R}^M$ such that

$$\boldsymbol{A}^{\mathrm{sym}}\boldsymbol{\lambda}^{\mathrm{sym}} = \widetilde{\boldsymbol{\sigma_f}}. \tag{4.14}$$

Notice that Equation (4.14) is well-posed since $\boldsymbol{A}^{\mathrm{sym}}$ is symmetric positive definite (see Lemma 4.10). Furthermore, if we denote by $\boldsymbol{\lambda}\in\mathbb{R}^M$ and $\boldsymbol{\lambda}^{\mathrm{sym}}\in\mathbb{R}^M$ the solutions to the matrix equations (4.6) and (4.14) respectively, then it is easy to see that

$$\boldsymbol{\lambda} = (\mathbf{DtN}^{\kappa})^{-1}\boldsymbol{\lambda}^{\mathrm{sym}}. \tag{4.15}$$

Equation (4.15) suggests that we can avoid the use of GMRES for solving the non-symmetric matrix Equation (4.6) and instead solve the symmetric matrix Equation (4.14)

using the CG method. Our next result presents the convergence analysis of this alternative approach.

Theorem 4.21 (Convergence Analysis for CG-based Strategy)**.** *Let $\ell_{\max} \in \mathbb{N}$, let $\sigma_f \in H^{-\frac{1}{2}}(\partial\Omega)$, let $\nu_{\ell_{\max}} \in W^{\ell_{\max}}$ be the unique solution to the Galerkin discretisation (2.8) for the induced surface charge with right hand side given by σ_f, and let $\mathbb{P}_0^{\perp}\colon H^{\frac{1}{2}}(\partial\Omega) \to \breve{H}^{\frac{1}{2}}(\partial\Omega)$ and $\mathbb{Q}_{\ell_{\max}}\colon H^{\frac{1}{2}}(\partial\Omega) \to W^{\ell_{\max}}$ be the projection operators defined through Lemma 3.2 and Definition 3.30 respectively. Then for every $\epsilon > 0$ there exists a function $\nu_{\ell_{\max}}^{\text{approx}} \in W^{\ell_{\max}}$ and a natural number $S_\epsilon > 0$ that depends on ϵ, the radii of the open balls, the dielectric constants and the minimal inter-sphere separation distance but is independent of the number of open balls N such that $\nu_{\ell_{\max}}^{\text{approx}}$ can be computed using at most S_ϵ iterations of the conjugate gradient method and such that the following error estimate holds*

$$\frac{|||\nu_{\ell_{\max}}^{\text{approx}} - \nu_{\ell_{\max}}|||^*}{|||\mathbb{P}_0^{\perp}\nu_{\ell_{\max}}|||^* + \frac{1}{\kappa_0}|||\mathbb{P}_0^{\perp}\mathbb{Q}_{\ell_{\max}}\sigma_f|||^*} < \epsilon.$$

Proof. The proof of Theorem 4.21 is very similar to the proof of Theorem 4.16. For the sake of brevity therefore, we do not present all details.

Let $\epsilon > 0$ be fixed, let $\widetilde{\epsilon} := \frac{\epsilon}{\max\left|\frac{\kappa-\kappa_0}{\kappa_0}\right|}$, and let $\lambda_{\ell_{\max}} \in W_0^{\ell_{\max}}$ denote the solution to the Galerkin discretisation (4.1). Following the steps of the proof of Theorem 4.16, it is clear that we must show the existence of a natural number S_ϵ that depends on ϵ, the radii of the open balls, the dielectric constants and the minimal inter-sphere separation distance but is independent of the number of open balls N such that we can compute a function $\psi_{\ell_{\max}} \in W_0^{\ell_{\max}}$ using at most S_ϵ iterations of the CG method and such that

$$|||\lambda_{\ell_{\max}} - \psi_{\ell_{\max}}||| < \widetilde{\epsilon}.$$

Consider the symmetric matrix Equation (4.14). Let the initialisation $\boldsymbol{\lambda}_0^{\text{sym}} \in \mathbb{R}^M$ be zero, let $\boldsymbol{\lambda}_k^{\text{sym}} \in \mathbb{R}^M$, $k \in \mathbb{N}$ denote the k^{th} iterate generated by CG applied to this linear system. Next, let $\boldsymbol{r}_k := \widetilde{\boldsymbol{\sigma_f}} - \boldsymbol{A}^{\text{sym}}\boldsymbol{\lambda}_k^{\text{sym}}$, $k \in \mathbb{N}_0$ denote the k^{th} residual. The standard convergence analysis for the CG method (see, e.g., [125]) then yields

$$\|\boldsymbol{r}_k\|_{\boldsymbol{A}^{\text{sym}}} \leq 2\left(\frac{\sqrt{\frac{C_{\widetilde{\mathcal{A}}}}{\alpha_0}} - 1}{\sqrt{\frac{C_{\widetilde{\mathcal{A}}}}{\alpha_0}} + 1}\right)^k \|\widetilde{\boldsymbol{\sigma_f}}\|_{\boldsymbol{A}^{\text{sym}}}, \tag{4.16}$$

where the constants $C_{\widetilde{\mathcal{A}}}, \alpha_0$ are bounds on the smallest and largest eigenvalues of $\boldsymbol{A}^{\text{sym}}$ as obtained in Lemma 4.10, and $\|\cdot\|_{\boldsymbol{A}^{\text{sym}}}$ is the norm on $\mathbb{R}^M$ induced by the symmetric positive definite matrix $\boldsymbol{A}^{\text{sym}}$.

Next, using simple algebra and Equation 4.15 we obtain that

$$\begin{aligned}\|\widetilde{\boldsymbol{\sigma_f}}\|_{\boldsymbol{A}^{\text{sym}}} &\leq \sqrt{C_{\widetilde{\mathcal{A}}}}|\widetilde{\boldsymbol{\sigma_f}}| = \sqrt{C_{\widetilde{\mathcal{A}}}}|\boldsymbol{A}^{\text{sym}}\boldsymbol{\lambda}^{\text{sym}}| \leq \sqrt{C_{\widetilde{\mathcal{A}}}^3}|\boldsymbol{\lambda}^{\text{sym}}| = \sqrt{C_{\widetilde{\mathcal{A}}}^3}|\mathbf{D}\mathbf{t}\mathbf{N}^{\kappa}\boldsymbol{\lambda}| \\ &\leq \sqrt{C_{\widetilde{\mathcal{A}}}^3}\chi_{\max}|\boldsymbol{\lambda}| \leq \sqrt{C_{\widetilde{\mathcal{A}}}^3 \max_{j=1,\ldots,N} r_j^3}\chi_{\max}|||\lambda_{\ell_{\max}}|||,\end{aligned} \tag{4.17}$$

where $\chi_{\max}$ is the largest eigenvalue of the matrix $\mathbf{DtN}^{\kappa}$ and is defined as in the proof of Theorem 4.16.

Let $\lambda_k^{\ell_{\max}} \in W_0^{\ell_{\max}}$ be the function associated with the vector $\boldsymbol{\lambda}_k^{\text{sym}}$. A similar calculation, together with Equation 4.15 yields

$$\begin{aligned}\|\boldsymbol{r}_k\|_{\boldsymbol{A}^{\text{sym}}} &\geq \sqrt{\alpha_0}\left|\widetilde{\boldsymbol{\sigma_f}} - \boldsymbol{A}^{\text{sym}}\boldsymbol{\lambda}_k^{\text{sym}}\right| \geq \sqrt{\alpha_0^3}\left|\boldsymbol{\lambda}^{\text{sym}} - \boldsymbol{\lambda}_k^{\text{sym}}\right| \geq \sqrt{\alpha_0^3\chi_0}\left|\boldsymbol{\lambda} - (\mathbf{DtN}^{\kappa})^{-1}\boldsymbol{\lambda}_k^{\text{sym}}\right| \\ &\geq \sqrt{\frac{\alpha_0^3 \min_{j=1,\dots,N} r_j^3}{\ell_{\max}}\chi_0}\left|\left|\left|\lambda_{\ell_{\max}} - (\mathrm{DtN}^{\kappa})^{-\frac{1}{2}}\lambda_k^{\ell_{\max}}\right|\right|\right|, \end{aligned} \tag{4.18}$$

where χ_0 is the smallest eigenvalue of the matrix $\mathbf{DtN}^{\kappa}$ and is also defined as in the proof of Theorem 4.16.

Combining the estimates (4.16), (4.17), and (4.18) and plugging in the definitions of the eigenvalues χ_0 and $\chi_{\max}$ we obtain that

$$\begin{aligned}\left|\left|\left|\lambda_{\ell_{\max}} - (\mathrm{DtN}^{\kappa})^{-\frac{1}{2}}\lambda_k^{\ell_{\max}}\right|\right|\right| \leq 2\ell_{\max}\sqrt{\frac{C_{\widetilde{\mathcal{A}}}^3}{\alpha_0^3}\frac{\max_{j=1,\dots,N} r_j^3}{\min_{j=1,\dots,N} r_j^3}}\left(\frac{\sqrt{\frac{\alpha_{\max}}{\alpha_0}}-1}{\sqrt{\frac{C_{\widetilde{\mathcal{A}}}}{\alpha_0}}+1}\right)^k \\ \left(\frac{\max|\kappa-\kappa_0|}{\min|\kappa-\kappa_0|}\right)^{\frac{1}{2}}\left|\left|\left|\lambda_{\ell_{\max}}\right|\right|\right|.\end{aligned}$$

The remainder of the proof is now essentially identical to the proof of Theorem 4.16. Indeed, we define the constant $\Upsilon_{\text{CG}} > 0$ and the natural number S_ϵ as

$$\Upsilon_{\text{CG}} := 2\sqrt{\frac{C_{\widetilde{\mathcal{A}}}^3}{\alpha_0^3}\frac{\max_{j=1\dots,N} r_j^3}{\min_{j=1,\dots,N} r_j^3}}\left(\frac{\max|\kappa-\kappa_0|}{\min|\kappa-\kappa_0|}\right)^{\frac{1}{2}}\max\left|\frac{\kappa_0}{\kappa-\kappa_0}\right|,$$

and

$$S_\epsilon := \left\lceil \frac{\log\left(\frac{\widetilde{\epsilon}}{\ell_{\max}\Upsilon_{\text{CG}}}\right)}{\log\left(\frac{\sqrt{\frac{C_{\widetilde{\mathcal{A}}}}{\alpha_0}}-1}{\sqrt{\frac{C_{\widetilde{\mathcal{A}}}}{\alpha_0}}+1}\right)} \right\rceil. \tag{4.19}$$

We then obtain using Inequality (4.8) that

$$\frac{\left|\left|\left|\nu_{\ell_{\max}} - \mathcal{B}(\mathrm{DtN}^{\kappa})^{-\frac{1}{2}}\lambda_{s_\epsilon}^{\ell_{\max}}\right|\right|\right|^*}{\left|\left|\left|\mathbb{P}_0^{\perp}\nu_{\ell_{\max}}\right|\right|\right|^* + \frac{1}{\kappa_0}\left|\left|\left|\mathbb{P}_0^{\perp}\mathbb{Q}_{\ell_{\max}}\sigma_f\right|\right|\right|^*} < \epsilon.$$

Defining $\nu_{\ell_{\max}}^{\text{approx}} := \mathcal{B}(\mathrm{DtN}^{\kappa})^{-\frac{1}{2}}\lambda_{s_\epsilon}^{\ell_{\max}}$ completes the proof. □

Two further remarks are in order.

Remark 4.22. Consider the setting and proof of Theorem 4.21. We emphasise again that in practice, the function $\nu_{\ell_{\max}}^{\text{approx}} := \mathcal{B}(\text{DtN}^{\kappa})^{-\frac{1}{2}}\lambda_{S_\epsilon}^{\ell_{\max}} \in W^{\ell_{\max}}$ is represented as a vector $\boldsymbol{\nu}^{\text{approx}} \in \mathbb{R}^{M+N}$. This can be done by following the procedure described in Remark 4.17. Notice that although this construction involves computing the action of the inverse matrix $(\mathbf{DtN}^{\kappa})^{-1}$, this is not a problem since $\mathbf{DtN}^{\kappa}$ is diagonal.

Remark 4.23. Consider the proofs of Theorems 4.16 and 4.21. It is natural to ask how the bound R_ϵ on the number of GMRES iterations and the bound S_ϵ on the number of CG iterations compare for a given error tolerance $\epsilon > 0$. Using Equations (4.12) and (4.19) and the definitions of the constants Υ_{CG} and Υ_{GMRES}, we see that

$$R_\epsilon < S_\epsilon \quad \iff \quad \frac{C_{\widetilde{\mathcal{A}}}}{\beta_{\widetilde{\mathcal{A}}}} < \sqrt{\frac{C_{\widetilde{\mathcal{A}}}^3}{\alpha_0^3}} \iff \sqrt{\frac{\alpha_0^3}{C_{\widetilde{\mathcal{A}}}}} < \beta_{\widetilde{\mathcal{A}}}.$$

Since explicit expressions for all the above variables are available, one could– in principle– determine whether $R_\epsilon < S_\epsilon$ or vice versa for a given geometric configuration. We emphasise however that since R_ϵ and S_ϵ grow only as $\log(\Upsilon_{\text{GMRES}})$ and $\log(\Upsilon_{\text{CG}})$ respectively, we expect so see only minor differences between the number of GMRES and CG iterations in practice– unless the physical or geometric constants are abnormally large or small (see the numerical results in Section 4.3).

Notice that the above estimates do not consider the computational cost of each linear solver iteration. Thus, if one uses GMRES without restart, then the computational cost of each GMRES iteration can grow substantially large for $R_\epsilon \gg 1$. In such a situation, it might be advantageous to use the CG method instead even if $R_\epsilon < S_\epsilon$.

CG-based solution strategy for obtaining the induced surface charge and the electrostatic energy

Given a free charge $\sigma_f \in H^{-\frac{1}{2}}(\partial\Omega)$, the goal is to obtain– up to some given tolerance– the solution $\nu_{\ell_{\max}} \in W^{\ell_{\max}}$ to the Galerkin discretisation (2.8) for the induced surface charge. Additionally, it might be necessary to compute the approximate electrostatic energy of the system $\mathcal{E}_{\mathbb{Q}_{\ell_{\max}}\sigma_f}(\nu_{\ell_{\max}})$.

1. Fix $\ell_{\max} \in \mathbb{N}$ and use Definitions 4.13 and 4.20 to compute the right-hand side vector $\widetilde{\boldsymbol{\sigma_f}} \in \mathbb{R}^M$. Due to the use of the FMM and the fact that $\mathbf{DtN}^{\kappa}$ is a diagonal matrix, the total computational cost of this step is $\mathcal{O}(N)$.

2. Use the CG method to solve– up to some tolerance– the linear system (4.14) involving $\boldsymbol{A}^{\text{sym}}$ and $\widetilde{\boldsymbol{\sigma_f}}$. This yields a solution vector $\boldsymbol{\lambda}_{\text{approx}}^{\text{sym}} \in \mathbb{R}^M$. Once again, the cost of a single matrix vector product involving $\boldsymbol{A}^{\text{sym}}$ is $\mathcal{O}(N)$ thanks to the FMM. Due to Theorem 4.21, the total number of CG iterations required in this step is independent of N, and therefore the total computational cost of this step is also $\mathcal{O}(N)$.

3. Use the solution vector $\boldsymbol{\lambda}_{\text{approx}}^{\text{sym}} \in \mathbb{R}^M$ to compute the vector $\boldsymbol{\nu}^{\text{approx}} \in \mathbb{R}^{M+N}$. As mentioned in Remark 4.22, this can be done following the procedure outlined in

Remark 4.17 with a few obvious modifications. The computational cost of this step is $\mathcal{O}(N)$.

4. $\boldsymbol{\nu}^{\text{approx}}$ is now the vector representation of some function $\nu_{\ell_{\max}}^{\text{approx}} \in W^{\ell_{\max}}$ that is the required approximation of the true solution $\nu_{\ell_{\max}}$ to the Galerkin discretisation (2.8).

5. If required, the approximate electrostatic energy $\mathcal{E}_{\mathbb{Q}_{\ell_{\max}}\sigma_f}(\nu_{\ell_{\max}})$ can be computed using Definition 3.1. Since this requires a single FMM call, the computational cost of this step is also $\mathcal{O}(N)$.

4.3 Numerical Experiments

The goal of this section is two-fold. First, we wish to present numerical results supporting the conclusions of Theorem 4.16 and 4.21 which concern the number of linear solver iterations required to obtain an approximate solution to the underlying linear system, up to a given and fixed relative error. Second, we would like to provide numerical evidence that the solution strategies presented in Section 4.2 are indeed linear scaling in accuracy. Demonstrating this linear scaling behaviour is rather subtle as we explain below.

The key complication is that the FMM, which is used to compute matrix-vector products involving the solution matrix, is not exact (see, e.g., [87]) and introduces an approximation error as soon as one increases the depth of the octree structure of the bounding box containing all multipole sources. This is because the FMM uses an approximate so-called 'far field' to compute interactions between multipole sources that belong to well-separated leaves of the octree. Note that increasing the depth of the octree is required to maintain linear scaling complexity for larger matrices, i.e., for matrices corresponding to systems with an increasing number N of dielectric particles. In principle, the error introduced by the far-field computations can be made arbitrarily small by increasing the maximal degree of spherical harmonics that are used in the multipole expansions of the underlying kernel but increasing the expansion degree also increases the computational cost of each matrix-vector product. There is thus a tradeoff between the computational cost and accuracy of the FMM.

Consequently, in Section 4.3.2, we will first explore the interplay between the FMM error and discretisation error for different values of the system parameters. Based on these results, we will pick FMM system parameters that result in a linear scaling in accuracy solution strategy such that the FMM error does not dominate the discretisation error. We remark that we will restrict our attention to the computation of the induced surface charge but similar numerical results are obtained in the case of the electrostatic energy.

4.3.1 Validation of theoretical results

Since standard FMM libraries typically consider point charges as input, we have used instead a modification of the ScalFMM library (see [127] for an explanation of the modifications and [1, 14, 153] for details on ScalFMM). The subsequent numerical simulations were performed with a single level FMM octree so as to avoid using the approximate 'far-field' and to perform all computations using the exact FMM 'near-field' instead. Unless stated otherwise, the discretisation parameter was fixed as $\ell_{\max} = 5$.

N-independence Our first set of numerical experiments is designed to demonstrate that the number of linear solver iterations required to obtain an approximation of $\nu_{\ell_{\max}}$, i.e., the solution to the Galerkin discretisation (2.8) for the induced surface charge, up to a given relative error is independent of the number N of dielectric particles.

We adopt the following geometric setting: We consider dielectric spheres of radius 1 and dielectric constant $\kappa = 10$ arranged on a regular cubic lattice of edge length 2.5. The spheres carry alternating unit positive and negative charges, and the background medium is assumed to be vacuum so that $\kappa_0 = 1$. An example of the problem geometry is displayed in Figure 4.1a. The number of spheres is increased simply by increasing the size of the lattice.

Figure 4.1b displays the number of GMRES and CG iterations required to produce an approximation $\nu_{\ell_{\max}}^{\text{approx}}$ of the true solution $\nu_{\ell_{\max}}$ with a given relative error tolerance. The true solution $\nu_{\ell_{\max}}$ was calculated by solving the linear system with tolerance 10^{-13} and the relative error was calculated exactly as in Theorems 4.16 and 4.21. Clearly, the numerical results agree with Theorems 4.16 and 4.21. Interestingly, for lower error tolerances, the number of CG iterations is smaller than the number of GMRES iterations and the situation is reversed for higher tolerances.

Dependence on the dielectric constant ratio Next, we explore the effects of different dielectric constant ratios on the number of linear solver iterations required to obtain an approximate solution satisfying a given error tolerance. The bounds obtained in Theorems 4.16 and 4.21 and Remark 4.18 indicate that

- If $\kappa > \kappa_0$, then the number of iterations should grow at most as $\sqrt{\frac{\max \kappa}{\kappa_0}}$ for increasing $\frac{\max \kappa}{\kappa_0}$.
- If $\kappa < \kappa_0$, then the number of iterations should grow at most as $\sqrt{\frac{\kappa_0}{\min \kappa}}$ for increasing $\frac{\kappa}{\min \kappa_0}$.

The problem geometry is similar to the one from the previous test case. We consider a total of 125 identical dielectric spheres of radius 1 with alternating positive and negative charge, arranged on a regular cubic lattice of edge length 2.5. We set $\kappa_0 = 1$ and we allow the dielectric constant κ of the spheres to vary from extremely high to extremely low. In all cases, the true solution $\nu_{\ell_{\max}}$ was calculated by solving the linear system with tolerance 10^{-13}.

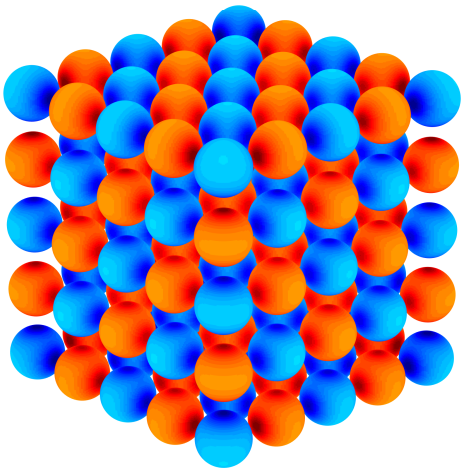

(a) The basic geometric setting of our numerical experiments. The dielectric spheres are arranged on a three dimensional, regular cubic lattice with edge length 2.5.

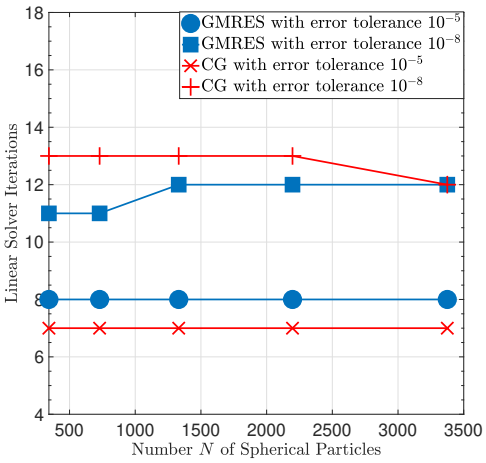

(b) Linear Solver iterations required to obtain an approximate solution with a given error tolerance as a function of the number N of dielectric particles.

Figure 4.1: Left: An example of the problem geometry. Right: The linear solver iterations as a function of the number N of spherical particles.

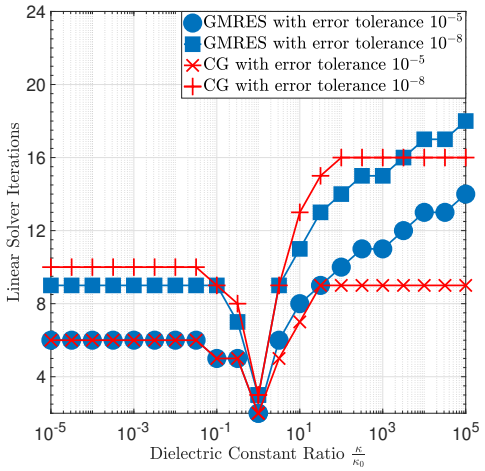

(a) Linear Solver iterations required to obtain an approximate solution with a given error tolerance as a function of the dielectric constant ratio.

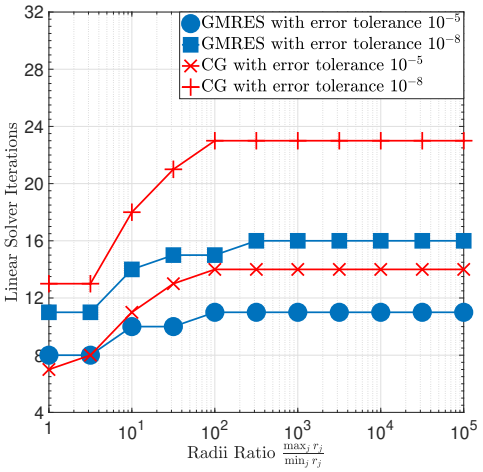

(b) Linear Solver iterations required to obtain an approximate solution with a given error tolerance as a function of the radii ratio.

Figure 4.2: Left: The linear solver iterations as a function of the dielectric constant ratio $\frac{\kappa}{\kappa_0}$. Right: The linear solver iterations as a function of the radii ratio $\frac{\max r_j}{\min r_j}$.

Figure 4.2a displays the number of GMRES and CG iterations required to produce an approximation to the true solution satisfying a given error tolerance. For very large dielectric ratio $\frac{\kappa}{\kappa_0}$, the number of GMRES iterations seems to grow logarithmically while

the number of CG iterations grows at first but soon reaches a plateau. On the other hand, for very small dielectric ratio $\frac{\kappa}{\kappa_0}$, the number of iterations in both cases quickly reach a plateau. These results suggest that the bounds we have obtained in Theorems 4.16 and 4.21 may not be sharp. Interestingly, we again observe that for low error tolerances, CG outperforms GMRES.

Dependence on the radii ratio We now consider the dependence of the number of linear solver iterations on the ratio of the maximum and minimum radius of the dielectric spherical particles. As mentioned in Remark 4.18, we expect the number of iterations to grow at most as $\log(\frac{\max_{j=1,\ldots,N} r_j}{\min_{j=1,\ldots,N} r_j})$.

The geometric setting consists of 125 dielectric spheres with dielectric constant $\kappa = 10$, carrying alternating unit positive and negative charges, arranged on a regular cubic lattice of edge length 2.5. We set $\kappa_0 = 1$ and we further set the radii of half of the dielectric spheres to one. The radii of all other dielectric spheres is set to r and we vary r from 10^{-5} to 1. As before, the true solution is calculated by setting the linear solver tolerance to 10^{-13}.

Figure 4.2b displays the numerical results. In contrast to our theoretical results, the numerical simulations suggest that the number of iterations at first grow logarithmically as the radii ratio $\frac{\max_{j=1,\ldots,N} r_j}{\min_{j=1,\ldots,N} r_j}$ increases but the growth soon stops and for sufficiently large radii ratio, the number of iterations remains constant. We observe that for large radii ratios, GMRES significantly outperforms CG.

Dependence on the separation distance Finally, we explore the dependence of the number of linear solver iterations on the minimal inter-sphere separation distance. We recall from Remark 4.18 that we expect the number of linear solver iterations to grow at most as $c_{\mathcal{V}}^{-\frac{1}{4}}$ where $c_{\mathcal{V}}$ is the coercivity constant of the single layer boundary operator. Moreover, we have shown in Chapter 3 of this dissertation (see Lemmas 3.22 and 3.23) that $c_{\mathcal{V}} = \mathcal{O}(\delta)$ for small δ where δ is the minimum inter-sphere separation distance.

We consider once again 125 identical dielectric spheres of radius 1 and dielectric constant $\kappa = 10$ with alternating positive and negative charge, arranged on a regular cubic lattice of edge length E. We assume the background medium to be vacuum so that $\kappa_0 = 1$ and we vary the edge length E from $2+10^{-4}$ to 7. Thus, the minimum separation varies from 10^{-4} to 5. In all cases, the true solution $\nu_{\ell_{\max}}$ was calculated by solving the linear system with tolerance 10^{-13}. Figure 4.3a displays the numerical results.

There are two features of interest in these numerical results. First, we observe that for very small separation distances, the number of CG iterations far exceeds the number of GMRES iterations. Second, we observe that while the number of iterations in both cases grows as the separation distance decreases, the growth stops at some point and the number of iterations plateaus. We conjecture that this is due to the fact that we use the continuity constant $C_{\widetilde{\mathcal{A}}}$ of the infinite-dimensional operator $\widetilde{\mathcal{A}}$ to bound the largest eigenvalue of the solution matrix, and functions which achieve (or approximately achieve) the upper bound $C_{\widetilde{A}}$ are not well-approximated in the approximation space $W_0^{\ell_{\max}}$ for

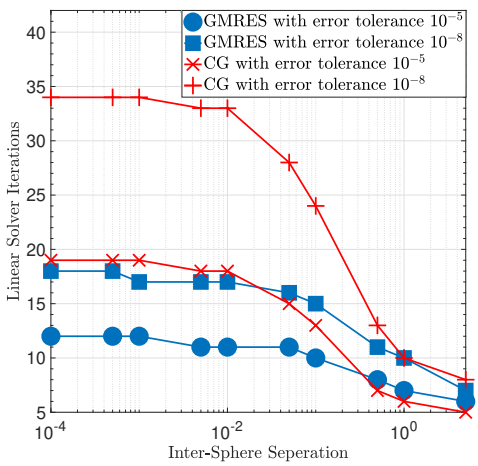

(a) Linear Solver iterations required to obtain an approximate solution with a given error tolerance as a function of the minimum inter-sphere separation distance.

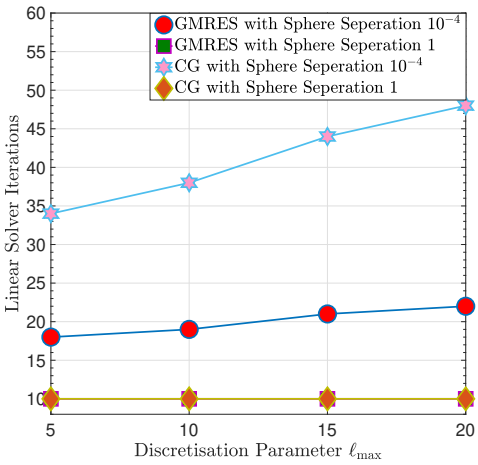

(b) Linear Solver iterations required to obtain an approximate solution with error tolerance 10^{-8} as a function of $\ell_{\max}$ for very small and moderate separation distances.

Figure 4.3: Left: The linear solver iterations as a function of the minimum sphere separation. Right: The linear solver iterations as a function of $\ell_{\max}$ for very small and moderate separations.

small $\ell_{\max}$.

To test the above hypothesis, we plot in Figure 4.3b the number of linear solver iterations for different values of $\ell_{\max}$ with edge lengths $E = 2 + 10^{-4}$ and $E = 3$. The error tolerance was set to 10^{-8}. We observe that the number of iterations remains constant in the case $E = 1$ but increases in the case $E = 10^{-4}$, which supports our conjecture.

4.3.2 FMM error and linear scaling solution strategy

We now explore the interplay between the discretisation error and the error introduced by the FMM. As mentioned at the start of this section, given a system of N interacting particles, the FMM can compute matrix-vector products using only $\mathcal{O}(N)$ operations but this comes at the cost of introducing an approximation error. The approximation error typically grows as one increases the tree depth D, i.e., the number of levels in the octree structure of the FMM bounding box because this usually results in more particle interactions being computed using the less-accurate 'far-field' computation of the FMM. Conversely, the approximation error decreases if one increases the maximal degree P of spherical harmonics used in the multipole expansion of the FMM kernel.

Consequently, the first goal of this section is to observe numerically how the FMM error compares with the discretisation error for different values of D, P and $\ell_{\max}$. Based

on these results, we propose appropriate values of D and P such that for an increasing number N of particles, an approximate solution to the Galerkin equation (2.8) can be computed in $\mathcal{O}(N)$ operations and such that the FMM approximation error does not dominate the discretisation error. Finally, we present numerical results on the computation times of our algorithm for increasing N which utilise the proposed values of P and D.

All subsequent numerical experiments involve the following geometric setting: We consider two types of dielectric spheres arranged on a regular cubic lattice of edge length 7. The first type of dielectric spheres have radius 3, dielectric constant 10 and carry unit negative charge, and the second type of dielectric spheres have radius 2, dielectric constant 5 and carry unit positive charge. The background medium is assumed to be vacuum so that $\kappa_0 = 1$, and the number of spheres is increased simply by increasing the size of the lattice.

We consider two choices of the discretisation parameter, namely, $\ell_{\max} = 5$ and $\ell_{\max} = 10$. We compute so-called 'pure discrete' solutions to the Galerkin discretisation (2.8) in each of the two cases for a different number N of spherical particles. These solutions are all computed using a one-level FMM tree, which results in the use of the exact 'near-field' computation of the FMM. Additionally, the linear solver tolerance in each case is set to 10^{-10}. Consequently, these pure discrete solutions can be assumed to have negligible FMM and linear solver errors. Unfortunately, since we wish to use the exact 'near-field' computations of the FMM, the computational cost of obtaining each pure discrete solution grows as $\mathcal{O}(N^2)$. This limits the total number of spheres we consider to 1728.

Next, we compute 'approximate' solutions for both values of $\ell_{\max}$ by repeating the above computations for different values of the FMM parameters D and P whilst keeping all other parameters identical. In addition, we compute the 'reference' solution ν to the BIE (2.3) by setting $\ell_{\max} = 20$ and using a linear solver tolerance of 10^{-13}. Our goal now is to

- Compute the *approximation error due to the FMM* by comparing the pure discrete solutions and the approximate solutions computed above;
- Compute the *discretisation error* by comparing the pure discrete solutions and the reference solution computed above.

Figures 4.4a and 4.4b display the relative FMM and discretisation errors (relative errors are calculated using the $|||\cdot|||^*$ norm) in all cases. Although, it is difficult to form a definitive conclusion based on a limited data set, we observe two broad trends:

- The FMM error far exceeds the discretisation error if N is small and D is high. We deduce from this that D should only be increased in proportion with N. Based on these results, the FMM error is minimised if a 2 level tree is used for 512 particles, which translates to exactly 8 particles per leaf. One possible strategy for attaining

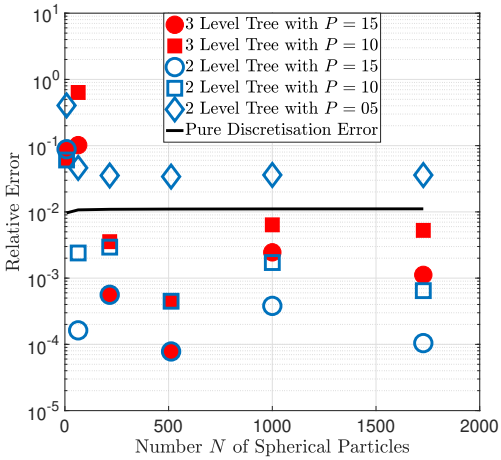

(a) Relative FMM and discretisation errors as a function of the number N of spherical particles in the case $\ell_{\max} = 5$.

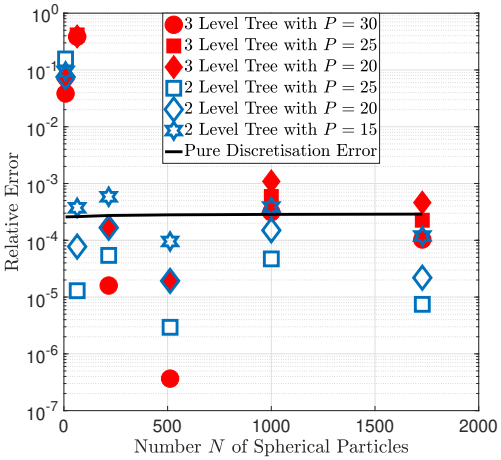

(b) Relative FMM and discretisation errors as a function of the number N of spherical particles in the case $\ell_{\max} = 10$.

Figure 4.4: FMM errors vs. discretisation errors for different choices of FMM parameters.

this optimal particle per leaf ratio is to to start with a 1 level tree and increase D until there are no more than 32 particles in each leaf. Notice that the choice of D is independent of $\ell_{\max}$ and depends only on the number of particles N.

- As expected, the FMM error decreases as the expansion degree P is increased. Unfortunately, the computational cost of the FMM grows as $\mathcal{O}(P^3)$ so the optimal strategy is to find the minimum P such that the FMM error is strictly smaller than the discretisation error. Based on the results presented here, one possible choice could be $P = 2\ell_{\max}$. We remark that the choice of P is independent of the number of particles N and depends only on the discretisation parameter $\ell_{\max}$.

Equipped with this methodology for picking the FMM parameters P and D, we can now compute approximate solutions to the Galerkin discretisation (2.8) for the two cases $\ell_{\max} = 5$ and $\ell_{\max} = 10$, and an increasing number N of spherical particles. Our goal is to demonstrate numerically that both the GMRES-based and CG-based solution strategies are linear scaling in cost whilst having some reassurance that the FMM error does not dominate the discretisation error for this specific geometric setting.

All numerical simulations were performed on a 2016 MacBook laptop with a 2.6 GHz Intel Core i7 processor and 16GB of 2133 MHz LPDDR3 memory. Additionally, we set the linear solver tolerance to 10^{-6} and 10^{-9} in the case $\ell_{\max} = 5$ and $\ell_{\max} = 10$ respectively. Our results are displayed in Figures 4.5a and 4.5b and indicate excellent agreement with linear scaling behaviour. We see furthermore that the computation times for the CG and GMRES-based approaches are almost identical. Of course, if the geometric setting of the numerical simulations were to be changed, then one linear solver could potentially outperform the other in accordance with the numerical study presented in Section 4.3.1.

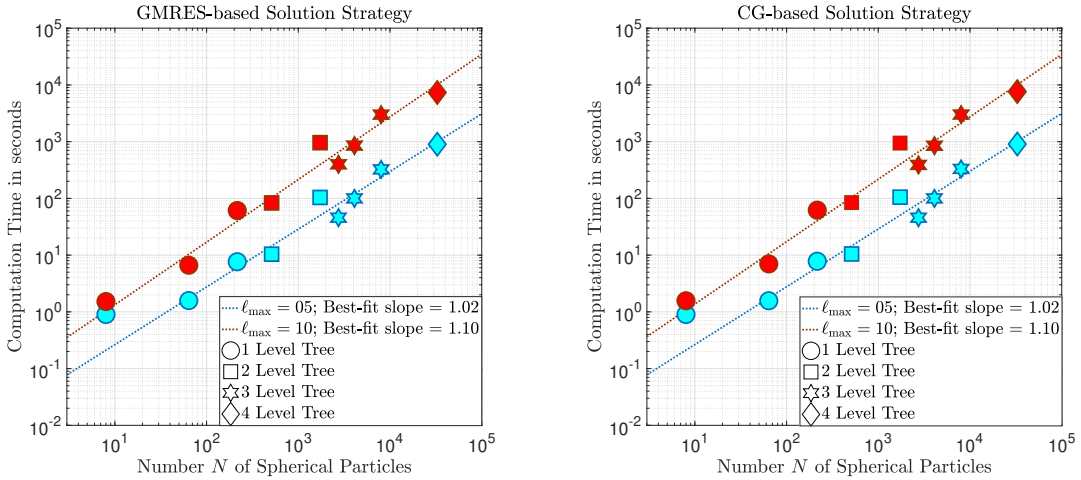

(a) Computation times for the GMRES-based solution strategy as a function of the number N of spherical particles.

(b) Computation times for the CG-based solution strategy as a function of the number N of spherical particles.

Figure 4.5: Computation times for our solution strategies

4.4 Conclusion

In Chapters 3 and 4, we have presented a detailed analysis of the second kind boundary integral equation (2.3) that describes the interaction of N charged, dielectric spherical particles undergoing mutual polarisation. Our goal has been to perform a full scalability analysis of the Galerkin method used to solve this BIE and to establish that the method is *linear scaling in accuracy* for the computation of the induced surface charge and total electrostatic energy of the system. In other words, we wished to demonstrate that in order to obtain approximations to these physical quantities of interest with a fixed average or relative error, the computational cost of the algorithm scales as $\mathcal{O}(N)$. In order to show that an N-body numerical method is linear scaling in accuracy, it is sufficient to show that it is (a) *N-error stable*, i.e., for a fixed number of degrees of freedom per object the relative or average error does not increase with N and (b) linear scaling in cost, i.e., for a fixed number of degrees of freedom per object, only $\mathcal{O}(N)$ operations are needed to compute an approximate solution. Accordingly, we presented in Chapter 3, the numerical analysis of the Galerkin method and derived convergence rates for the induced surface charges and total electrostatic energy that did not explicitly depend on N. This allowed us to deduce N-error stability of our algorithm for any family of geometries satisfying the assumptions **GA1)-GA3)**.

The goal of Chapter 4 was to establish that the Galerkin method is also linear scaling in cost. To this end, we presented a convergence analysis of GMRES for the linear system arising from the Galerkin discretisation of the BIE and proved that under mild assumptions, there exists an upper bound– explicitly independent of N– for the number of GMRES iterations required to obtain an approximate solution of the underlying linear system up to a given relative error tolerance. Combined with the use of the FMM to com-

pute matrix-vector products in $\mathcal{O}(N)$, this result establishes that the numerical method is linear scaling in cost for any family of geometries satisfying the assumptions **GA1)-GA3)**. In view of the results of Chapter 2, we can conclude that our numerical method is indeed linear scaling in accuracy in the computation of the induced surface charges and total electrostatic energy for any family of geometries satisfying the assumptions **GA1)-GA3)**.

In addition to the main result of Chapter 4, we also demonstrated how to 'symmetrise' the underlying linear system and subsequently proposed an equivalent, symmetric linear system that can be solved using the conjugate gradient method (CG) rather than GMRES. A convergence analysis of this alternative approach showed that there exists an upper bound– also independent of N and qualitatively similar to the GMRES bound– for the number of CG iterations required to obtain an approximate solution of the underlying linear system up to a given relative tolerance. Finally, we presented a detailed numerical study with the goal of both supporting our theoretical results and exploring the dependence of the error on various system parameters.

4. COMPLEXITY ANALYSIS OF THE INTEGRAL EQUATION FORMULATION OF THE N-BODY DIELECTRIC SPHERES PROBLEM

5

A Linear Scaling in Accuracy Numerical Method for Computing the Electrostatic Forces in the N-Body Dielectric Spheres Problem

Throughout this chapter, we will assume the setting of Chapters 1 and 2. Moreover, we will frequently refer to the weak formulation (2.5) and the Galerkin discretisation (2.8) of the second kind boundary integral equation (2.3) which describes the induced surface charge resulting on dielectric spherical particles undergoing mutual polarisation. Finally, we will also use the analysis and main results of Chapters 3 and 4.

The numerical and computational analysis we have presented thus far in Chapters 3 and 4 involves the *induced surface charge* and the *total electrostatic energy* arising from the interaction of these dielectric particles. A third important quantity of physical interest is the electrostatic force between these charged particles. An efficient and accurate computation of the forces is particularly important if one wishes to run dynamics simulations (see, e.g., [128]). The goal of this chapter is to outline strategies to obtain these electrostatic forces and perform an error and complexity analysis of such strategies.

5.1 Definition of the Exact and Approximate Electrostatic Forces

There are at least two approaches to defining the electrostatic forces in non-relativistic settings, one popular in the computational chemistry community and the other originating in the physics literature: Chemists tend to view the total electrostatic energy as the fundamental quantity of interest and define the electrostatic forces as functions of this

energy (see, for instance, [80, 83, 137, 140, 184]). Physicists on the other hand usually view Maxwell's equations for the electric and magnetic fields as the starting point of any study of electromagnetic phenomena (see, e.g., [66, 88, 162, 167]). In this formalism, the electromagnetic force is given by the so-called Lorentz force law (see, e.g., [66, Chapter 27] or [162, Chapter 10]) which defines the force in terms of the *electric and magnetic fields*. Naturally, in the absence of electrodynamic effects and magnetic fields, the electrostatic force is defined purely in terms of the electric field.

Although the two definitions seemingly arise from different physical considerations and have a priori different physical interpretations, they are in fact completely equivalent, both in the exact case, i.e., when the input is the exact solution $\nu \in H^{\frac{1}{2}}(\partial\Omega)$ to the BIE (2.3) as well as the approximate case, i.e., when the input is the solution $\nu_{\ell_{\max}} \in W^{\ell_{\max}}$ to the Galerkin discretisation (2.8). For the sake of completeness, we present both definitions of the electrostatic forces and then show in Chapter 5.1.3 that these definitions are equivalent. We remind the reader that we have assumed throughout Chapters 3-5 that the modelling assumptions **MA1)-MA5)** and geometrical assumptions **GA1)-GA3)** from Section 2.2 hold.

5.1.1 Electrostatic energy-based approach

To facilitate the readability of the subsequent exposition, let us begin by recalling the formal definition of the energy function and the exact electrostatic energy from Chapter 3.

Definition 5.1 (Energy Function and Exact Electrostatic Energy)**.**
Let $\mathcal{V}\colon H^{-\frac{1}{2}}(\partial\Omega) \to H^{\frac{1}{2}}(\partial\Omega)$ be the single layer boundary operator as defined through Definition 1.25 in Section 1.4. We define the energy function $\mathcal{E}\colon H^{-\frac{1}{2}}(\partial\Omega) \times H^{-\frac{1}{2}}(\partial\Omega) \to \mathbb{R}$ as the mapping with the property that for all $\sigma_1, \sigma_2 \in H^{-\frac{1}{2}}(\partial\Omega)$ it holds that

$$\mathcal{E}(\sigma_1, \sigma_2) := \frac{1}{2}\langle \sigma_1, \mathcal{V}\sigma_2 \rangle_{H^{-\frac{1}{2}}(\partial\Omega)\times H^{\frac{1}{2}}(\partial\Omega)} = \frac{1}{2}\langle \sigma_2, \mathcal{V}\sigma_1 \rangle_{H^{-\frac{1}{2}}(\partial\Omega)\times H^{\frac{1}{2}}(\partial\Omega)}.$$

Furthermore, if $\sigma_f \in H^{-\frac{1}{2}}(\partial\Omega)$ is a given free charge, and $\nu \in H^{-\frac{1}{2}}(\partial\Omega)$ denotes the solution to the boundary integral equation (2.3) for the induced surface charge with right-hand side generated by σ_f, then we define the exact electrostatic energy of the system as

$$\mathcal{E}^{\text{exact}}_{\sigma_f} := \mathcal{E}(\sigma_f, \nu).$$

The exact electrostatic forces are now defined as follows.

Definition 5.2 (First Definition of the Forces)**.**
Let $\sigma_f \in H^{-\frac{1}{2}}(\partial\Omega)$ be a given free charge, let $\nu \in H^{-\frac{1}{2}}(\partial\Omega)$ denote the unique solution to the BIE (2.3) for the induced surface charge with right-hand side generated by σ_f, and let $\mathcal{E}^{\text{exact}}_{\sigma_f}$ denote the total electrostatic energy of this system as defined by Definition 5.1.

Then for each $i = 1, \ldots, N$ we define the net force acting on the dielectric particle represented by Ω_i as the vector $\widetilde{\boldsymbol{F}}_i \in \mathbb{R}^3$ given by

$$\widetilde{\boldsymbol{F}}_i := -\nabla_{\mathbf{x}_i} \mathcal{E}_{\sigma_f}^{\text{exact}},$$

where the gradient is taken with respect to the location $\mathbf{x}_i \in \mathbb{R}^3$ of the centre of the open ball Ω_i.

Some remarks are now in order.

Remark 5.3. Consider Definitions 5.1 and 5.2. We observe that the total electrostatic energy $\mathcal{E}_{\sigma_f}^{\text{exact}}$ is, in particular, a function of the induced surface charge ν, and since ν is the solution to the BIE (2.3), it will implicitly depend on the locations $\{\mathbf{x}_i\}_{i=1}^N$ of the centres of the open balls $\{\Omega_i\}_{i=1}^N$. Thus, the exact electrostatic energy also implicitly depends on $\{\mathbf{x}_i\}_{i=1}^N$.

Remark 5.4. It is possible to give an intuitive interpretation of Definition 5.2 of the electrostatic forces. Indeed, assume that the free charge σ_f and other physical parameters such as the dielectric constants and the radii $\{r_i\}_{i=1}^N$ of the open balls $\{\Omega_i\}_{i=1}^N$ are fixed. Then the resulting induced surface charge ν is uniquely determined by the locations $\{\mathbf{x}_i\}_{i=1}^N$ of the centres of the open balls $\{\Omega_i\}_{i=1}^N$. Thus the electrostatic energy $\mathcal{E}(\sigma_f, \cdot)$ can be viewed as a function of $\{\mathbf{x}_i\}_{i=1}^N$. The set of values of $\mathcal{E}(\sigma_f, \cdot)$ for all admissible sphere centres $\{\mathbf{x}_i\}_{i=1}^N$ defines a so-called potential energy surface (PES), and the graph of this PES is a $3N$-dimensional manifold. Consequently, given a fixed choice of sphere centres $\{\mathbf{x}_i\}_{i=1}^N$, the force acting on each dielectric particle (up to a scaling factor) is given by the negative gradient of the PES at the point $\{\mathbf{x}_i\}_{i=1}^N$.

Definition 5.2 of the electrostatic forces requires us to first compute the exact electrostatic energy $\mathcal{E}_{\sigma_f}^{\text{exact}} = \mathcal{E}(\sigma_f, \nu)$. Of course in practice, $\mathcal{E}_{\sigma_f}^{\text{exact}}$ is not known since $\sigma_f \in H^{-\frac{1}{2}}(\partial\Omega)$ may be infinite-dimensional and the exact induced surface charge $\nu \in H^{-\frac{1}{2}}(\partial\Omega)$ that solves the BIE (2.3) is not known. It is therefore necessary to define *approximate* electrostatic forces in terms of a *discrete* electrostatic energy. We remind the reader that throughout this chapter, we will frequently refer to the approximation space $W^{\ell_{\max}}, \ell_{\max} \in \mathbb{N}_0$ which was defined through Definition 2.11 in Section 2.3.

Definition 5.5 (Discrete Electrostatic Energy)**.**
Let $\sigma_f \in H^{-\frac{1}{2}}(\partial\Omega)$ be a given free charge, let $\ell_{\max} \in \mathbb{N}$, and let $\nu_{\ell_{\max}} \in W^{\ell_{\max}}$ be the unique solution to the Galerkin discretisation (2.8) for the approximate induced surface charge with right-hand side generated by σ_f. We define the discrete electrostatic energy of the system of N dielectric particles carrying free charge σ_f as

$$\mathcal{E}_{\sigma_f}^{\ell_{\max}} := \mathcal{E}(\mathbb{Q}_{\ell_{\max}} \sigma_f, \nu_{\ell_{\max}}).$$

The approximate forces are then defined as follows.

Definition 5.6 (First Definition of the Approximate Forces)**.** Let $\sigma_f \in H^{-\frac{1}{2}}(\partial\Omega)$ be a given free charge, let $\ell_{\max} \in \mathbb{N}$, let $\nu_{\ell_{\max}} \in W^{\ell_{\max}}$ be the unique solution to the

Galerkin discretisation (2.8) for the approximate induced surface charge with right-hand side generated by σ_f, and let $\mathcal{E}_{\sigma_f}^{\ell_{\max}}$ denote the discrete electrostatic energy of this system as defined by Definition 5.5. Then for each $i = 1, \ldots, N$ we define the approximate net force acting on the dielectric particle represented by Ω_i as the vector $\widetilde{\boldsymbol{F}}_i^{\ell_{\max}} \in \mathbb{R}^3$ given by

$$\widetilde{\boldsymbol{F}}_i^{\ell_{\max}} := -\nabla_{\mathbf{x}_i} \mathcal{E}_{\sigma_f}^{\ell_{\max}},$$

where the gradient is taken with respect to the location $\mathbf{x}_i \in \mathbb{R}^3$ of the centre of the open ball Ω_i.

Remark 5.7. Consider Definition 5.5 of the discrete electrostatic energy. In analogy with the exact electrostatic energy case, we observe that the discrete electrostatic energy $\mathcal{E}(\mathbb{Q}_{\ell_{\max}}\sigma_f, \cdot)$ defines a discrete potential energy surface (dPES) for different locations of the sphere renters $\{\mathbf{x}_i\}_{i=1}^N$. Moreover, considering Definition 5.6, we see that the approximate electrostatic force is defined precisely in terms of the negative gradient of the dPES at the point $\{\mathbf{x}_i\}_{i=1}^N$.

It can now be seen why the computational chemistry community finds Definition 5.2 of the electrostatic forces appealing. Indeed, suppose that we wish to numerically simulate the movement of charged dielectric particles due to the electrostatic forces. Then at each given time step, we have by construction that the approximate electrostatic forces are consistent with the dPES. Consequently, if one uses a symplectic method to perform time-integration, then the total (discrete) energy of the system can be maintained as a conserved quantity (up to a perturbation).

5.1.2 Electric field-based approach

In order to define the electrostatic forces arising due to the interaction of charged spherical dielectric particles using the electric field, we must first define some auxiliary quantities.

Definition 5.8 (Electric Potential)**.** Let $\sigma \in H^{-\frac{1}{2}}(\partial\Omega)$ be a charge distribution supported on the boundary $\partial\Omega$ of the collection of open balls $\{\Omega_i\}_{i=1}^N$ and let $\mathcal{S}\colon H^{-\frac{1}{2}}(\partial\Omega) \to H^1_{\mathrm{loc}}(\mathbb{R}^3)$ be the single layer potential as defined through Definition 1.23 in Section 1.4. Then we define the function $\phi \in H^1_{\mathrm{loc}}(\mathbb{R}^3)$ as

$$\phi := \mathcal{S}\sigma,$$

and we say that ϕ is the electric potential produced by the charge distribution σ.

Let us recall that the electric potential ϕ is the quantity of interest in the PDE-based formulation N-body dielectric spheres electrostatic interaction problem (see the BVP (2.2) in Section 2.2). Furthermore, recalling Definition 1.25 in Section 1.4 of the single layer boundary operator $\mathcal{V}$, we see that the interior and exterior Dirichlet traces $\gamma^{\pm}\mathcal{S}\sigma := \mathcal{V}\sigma$ are well-defined.

Definition 5.9 (Electric Field)**.**

Let $\sigma \in H^{-\frac{1}{2}}(\partial\Omega)$ be a charge distribution supported on the boundary $\partial\Omega$ of the collection of open balls $\{\Omega_i\}_{i=1}^N$, and let $\phi \in H^1_{\text{loc}}(\mathbb{R}^3)$ be the electric potential produced by the charge distribution σ. Then we define the vector field $\boldsymbol{E} \in L^2_{\text{loc}}(\mathbb{R}^3;\mathbb{R}^3)$ as

$$\boldsymbol{E} := -\nabla\phi,$$

and we say that $\boldsymbol{E}$ is the electric field produced by the charge distribution σ. Here, ∇ denotes the usual gradient in Cartesian coordinates.

Remark 5.10. Consider the setting of Definition 5.9. Since the electric potential ϕ is harmonic on the complement of the boundary $\partial\Omega$, it is in fact smooth on $\mathbb{R}^3 \setminus \partial\Omega$. Consequently, the electric field $\boldsymbol{E}$ is point-wise infinitely differentiable at any $\mathbf{x} \in \mathbb{R}^3 \setminus \partial\Omega$.

Let now $i \in \{1,\dots,N\}$. It will be important to consider also the electric field generated by a charge distribution supported only on the collection of spheres $\{\partial\Omega_j\}_{\substack{j=1,\\ j\neq i}}^N$, i.e., *excluding the sphere* $\partial\Omega_i$. To this end, we first introduce some simplifying notation.

Notation: Let $i \in \{1,\dots,N\}$. We define the set $\partial\omega_i \subset \partial\Omega$ as $\partial\omega_i := \partial\Omega \setminus \partial\Omega_i$. In other words $\partial\omega_i$ is the boundary of the collection of open balls $\{\Omega_j\}_{\substack{j=1,\\ j\neq i}}^N$, i.e., *excluding the open ball* Ω_i.

Definition 5.11 (Excluded Electric Potentials and Fields)**.**

Let $\sigma \in H^{-\frac{1}{2}}(\partial\Omega)$ be a charge distribution supported on the boundary $\partial\Omega$ of the collection of open balls $\{\Omega_i\}_{i=1}^N$. Then for each $i \in \{1,\dots,N\}$

- We define $\sigma_{i,\text{exc}} \in H^{-\frac{1}{2}}(\partial\Omega)$ as

  $$\sigma_{i,\text{exc}} := \begin{cases} \sigma & \text{on } \partial\omega_i, \\ 0 & \text{on } \partial\Omega_i, \end{cases}$$

  and we say that $\sigma_{i,\text{exc}}$ is the i excluded charge distribution;

- We define the function $\phi_{i,\text{exc}} \in H^1_{\text{loc}}(\mathbb{R}^3)$ as

  $$\phi_{i,\text{exc}} := \mathcal{S}\sigma_{i,\text{exc}},$$

  and we say that $\phi_{i,\text{exc}}$ is the i excluded electric potential generated by σ;

- We define the vector field $\boldsymbol{E}_i \in L^2_{\text{loc}}(\mathbb{R}^3;\mathbb{R}^3)$ as

  $$\boldsymbol{E}_i := -\nabla\phi_{i,\text{exc}}, \tag{5.1}$$

  and we say that $\boldsymbol{E}_i$ is the i excluded electric field generated by σ.

Two remarks are in order.

Remark 5.12. Consider the setting of Definition 5.11. The vector field $\boldsymbol{E}_i$, i.e., the i excluded electric field generated by σ has a physical interpretation. This is precisely the part of the total electric field that interacts with (i.e., exerts a net electrostatic force on) the charge distribution on the spherical dielectric particle represented by Ω_i.

Remark 5.13. Consider the setting of Definition 5.11 and let $i \in \{1, \ldots, N\}$. We observe that the i excluded potential $\phi_{i,\text{exc}}$ is harmonic and therefore smooth on the complement of $\partial\omega_i$. This implies that $\phi_{i,\text{exc}}$ is smooth on the boundary $\partial\Omega_i$, i.e., on the surface of the i^{th} spherical dielectric particle. Consequently, the i excluded electric field $\boldsymbol{E}_i$ is also smooth on the boundary $\partial\Omega_i$.

We are now ready to define the electrostatic force acting on each spherical dielectric particle. As mentioned previously, the force is now defined using the well-known Lorentz force law.

Definition 5.14 (Second Definition of the Forces)**.**

Let $\sigma_f \in H^{-\frac{1}{2}}(\partial\Omega)$ be a given free charge, let $\nu \in H^{-\frac{1}{2}}(\partial\Omega)$ denote the unique solution to the BIE (2.3) for the induced surface charge with right-hand side generated by σ_f, and for each $i \in \{1, \ldots, N\}$ let $\boldsymbol{E}_i \in L^2_{\text{loc}}(\mathbb{R}^3; \mathbb{R}^3)$ denote the i excluded electric field generated by ν as defined through Definition 5.11. Then for each $i = 1, \ldots, N$ we define the net force acting on the dielectric particle represented by Ω_i as the vector $\boldsymbol{F}_i \in \mathbb{R}^3$ given by

$$\boldsymbol{F}_i := \kappa_0 \int_{\partial\Omega_i} \nu(\mathbf{x}) \boldsymbol{E}_i(\mathbf{x})\, d\mathbf{x}.$$

Remark 5.15. Consider Definition 5.14 of the electrostatic forces. We remark that since $\nu \in H^{-\frac{1}{2}}(\partial\Omega)$, the integral should be understood as a $\langle \cdot, \cdot \rangle_{H^{-\frac{1}{2}}(\partial\Omega_i) \times H^{\frac{1}{2}}(\partial\Omega_i)}$ duality pairing. In view of Remark 5.13, the i excluded electric field $\boldsymbol{E}_i$ is smooth on $\partial\Omega_i$ so the duality pairing is well-defined.

Remark 5.16. It is possible once again to give a physical interpretation of Definition 5.14 of the electrostatic forces. Indeed, given a free charge σ_f, we know that the solution ν to the BIE (2.3) yields the surface charge distribution resulting from the interaction of these polarisable spherical dielectric particles. Therefore, in order to find the net force acting on dielectric particle i, we compute the electric field generated by the induced surface charges on all other dielectric particles. This is precisely the i excluded electric field $\boldsymbol{E}_i$. Next, by a simple extension of Coulomb's law to charge distributions we obtain that the force acting on particle i is the integral of the charge distribution on particle i, i.e., $\nu|_{\partial\Omega_i}$ against the i excluded electric field scaled by the dielectric constant κ_0 of the external medium.

Clearly, Definition 5.14 of the electrostatic forces cannot be used for practical computations since it relies on knowledge of exact quantities of interest. Therefore, in analogy to Definition 5.6, we define *approximate* electrostatic forces using approximate i excluded electric potentials and electric fields for all $i = 1, \ldots, N$. More precisely, we have the following definition.

Definition 5.17 (Second Definition of the Approximate Forces)**.**
Let $\sigma_f \in H^{-\frac{1}{2}}(\partial\Omega)$ be a given free charge, let $\ell_{\max} \in \mathbb{N}$, let $\nu_{\ell_{\max}} \in W^{\ell_{\max}}$ be the unique solution to the Galerkin discretisation (2.8) for the approximate induced surface charge with right-hand side generated by σ_f, and for each $i \in \{1, \dots, N\}$ let $\boldsymbol{E}_i^{\ell_{\max}} \in L^2_{\text{loc}}(\mathbb{R}^3; \mathbb{R}^3)$ denote the i excluded electric field generated by $\nu_{\ell_{\max}}$ as defined through Definition 5.11. Then for each $i = 1, \dots, N$ we define the approximate net force acting on the dielectric particle represented by $\partial\Omega_i$ as the vector $\boldsymbol{F}_i^{\ell_{\max}} \in \mathbb{R}^3$ given by

$$\boldsymbol{F}_i^{\ell_{\max}} := \kappa_0 \int_{\partial\Omega_i} \nu_{\ell_{\max}}(\mathbf{x}) \boldsymbol{E}_i^{\ell_{\max}}(\mathbf{x})\, d\mathbf{x}. \tag{5.2}$$

Although Definitions 5.2 and 5.14 of the exact electrostatic forces and Definitions 5.6 and 5.17 of the approximate electrostatic forces might seem a priori different, we claim that the electrostatic energy-based approach and electric field-based approach are mathematically equivalent. This is the subject of the next subsection.

5.1.3 Equivalence of the energy and electric field-based approaches

The goal of this section is to establish the following result.

Theorem 5.18. *Let $\sigma_f \in H^{-\frac{1}{2}}(\partial\Omega)$ be a given free charge, let $\ell_{\max} \in \mathbb{N}$, let $\nu \in H^{-\frac{1}{2}}(\partial\Omega)$ and $\nu_{\ell_{\max}} \in W^{\ell_{\max}}$ denote the solutions to the BIE (2.3) and Galerkin discretisation (2.8) respectively with right-hand sides generated by σ_f, and for each $i \in \{1, \dots, N\}$ let $\widetilde{\boldsymbol{F}}_i, \boldsymbol{F}_i \in \mathbb{R}^3$ denote the exact electrostatic forces as defined by Definitions 5.2 and 5.14 respectively and let $\widetilde{\boldsymbol{F}}_i^{\ell_{\max}}, \boldsymbol{F}_i^{\ell_{\max}} \in \mathbb{R}^3$ denote the approximate electrostatic forces as defined by Definitions 5.6 and 5.17 respectively. Then for all $i \in \{1, \dots, N\}$ it holds that*

$$\widetilde{\boldsymbol{F}}_i = \boldsymbol{F}_i, \qquad \text{and} \qquad \widetilde{\boldsymbol{F}}_i^{\ell_{\max}} = \boldsymbol{F}_i^{\ell_{\max}}.$$

We will prove Theorem 5.18 for the approximate forces. The proof for the exact forces is similar in spirit with an additional complication due to the fact that the exact induced surface charge $\nu \in H^{-\frac{1}{2}}(\partial\Omega)$ is a distribution. Consequently, extra care must be taken when performing direct calculations involving the explicit, integral representation of the single layer boundary operator $\mathcal{V}\colon H^{-\frac{1}{2}}(\partial\Omega) \to H^{\frac{1}{2}}(\partial\Omega)$ (see Theorem 1.27 in Section 1.4).

To facilitate the proof of Theorem 5.18 in the case of the approximate forces, it is advantageous to represent elements of the approximation space $W^{\ell_{\max}}$ as vectors in Euclidean space. This requires the introduction of a basis on $W^{\ell_{\max}}$, and in view of Definition 2.11, the natural choice of basis functions are the local spherical harmonics on each sphere. In fact, we have already introduced such a basis in Chapter 4 but in an effort to avoid disrupting the flow of this chapter, we will recall this construction.

Definition 5.19 (Choice of Basis)**.** Let $\ell_{\max} \in \mathbb{N}$. For each $j \in \{1, \dots, N\}$ and all $\ell \in \{0, \dots, \ell_{\max}\}$, $-\ell \leq m \leq \ell$ we define the function $\mathcal{Y}^j_{\ell m} \colon \partial\Omega \to \mathbb{R}$ as

$$\mathcal{Y}^j_{\ell m}(\mathbf{x}) := \begin{cases} \mathcal{Y}^m_\ell \left(\frac{\mathbf{x}-\mathbf{x}_j}{|\mathbf{x}-\mathbf{x}_j|} \right) & \text{for all } \mathbf{x} \in \partial\Omega_j, \\ 0 & \text{otherwise,} \end{cases}$$

and we equip the approximation space $W_{\ell_{\max}}$ with the basis $\{\mathcal{Y}^j_{\ell m}\}$. Here, $\mathcal{Y}^m_\ell$ denotes the spherical harmonic of degree ℓ and order m as defined in Definition 2.9 in Section 2.3.

Notation: Let $\ell_{\max} \in \mathbb{N}$. We will henceforth denote by $M := N \cdot (\ell_{\max} + 1)^2$, the dimension of the approximation space $W^{\ell_{\max}}$.

Remark 5.20. Consider Definition 5.19 of the basis functions on $W^{\ell_{\max}}$. These functions establish an isomorphism between $W^{\ell_{\max}}$ and $\mathbb{R}^M$. Indeed, we associate an arbitrary function $\psi \in W^{\ell_{\max}}$ with the vector $\boldsymbol{\psi} \in \mathbb{R}^M$ defined as

$$[\boldsymbol{\psi}_i]^m_\ell := \left(\psi, \mathcal{Y}^i_{\ell m}\right)_{L^2(\partial\Omega_i)}, \text{ for } i \in \{1, \dots, N\},\ \ell \in \{0, \dots, \ell_{\max}\} \text{ and } -\ell \leq m \leq \ell.$$

Consequently, given functions in the space $W^{\ell_{\max}}$, we will often refer to their vector representations in $\mathbb{R}^M$ and vice versa. Moreover, to facilitate identification we will frequently use bold symbols for the vector representations.

Definition 5.21. Let $\ell_{\max} \in \mathbb{N}_0$, let $\sigma_f \in H^{-\frac{1}{2}}(\partial\Omega)$ be a given free charge, let $\mathcal{V} \colon H^{-\frac{1}{2}}(\partial\Omega) \to H^{\frac{1}{2}}(\partial\Omega)$ and $\mathrm{DtN} \colon H^{\frac{1}{2}}(\partial\Omega) \to H^{-\frac{1}{2}}(\partial\Omega)$ denote the single layer boundary operator and Dirichlet-to-Neumann map respectively (see Definitions 1.25 and 1.13), let $\mathcal{A} \colon H^{\frac{1}{2}}(\partial\Omega) \to H^{\frac{1}{2}}(\partial\Omega)$ denote the boundary integral operator defined through Definition 2.8 in Section 2.3, and let $\mathbb{Q}_{\ell_{\max}} \colon H^{-\frac{1}{2}}(\partial\Omega) \to W^{\ell_{\max}}$ and $\mathbb{P}_{\ell_{\max}} \colon H^{\frac{1}{2}}(\partial\Omega) \to W^{\ell_{\max}}$ denote the projection operators on the approximation space defined through Definition 3.30. Then

- We define the vector $\boldsymbol{\sigma_f} \in \mathbb{R}^M$ as

  $$[\boldsymbol{\sigma_f}_i]^m_\ell := \left(\mathbb{Q}_{\ell_{\max}}\sigma_f, \mathcal{Y}^i_{\ell m}\right)_{L^2(\partial\Omega_i)},$$

  where $i \in \{1, \dots, N\},\ \ell \in \{0, \dots, \ell_{\max}\}$ and $|m| \leq \ell$.

- We define the diagonal matrix $\mathbf{DtN}^\kappa \in \mathbb{R}^{M \times M}$ as

  $$[\mathbf{DtN}^\kappa_{ij}]^{mm'}_{\ell\ell'} := \delta_{ij} \left(\frac{\kappa_j - \kappa_0}{\kappa_0} \mathrm{DtN} \mathcal{Y}^j_{\ell' m'}, \mathcal{Y}^i_{\ell m} \right)_{L^2(\partial\Omega_i)},$$

  where $i, j \in \{1, \dots, N\},\ \ell, \ell' \in \{0, \dots, \ell_{\max}\}$ and $|m| \leq \ell,\ |m'| \leq \ell'$.

- We define the symmetric, positive definite matrix $\boldsymbol{V} \in \mathbb{R}^{M \times M}$ as

  $$[\boldsymbol{V}_{ij}]^{mm'}_{\ell\ell'} := \left(\mathcal{V}\mathcal{Y}^j_{\ell' m'}, \mathcal{Y}^i_{\ell m} \right)_{L^2(\partial\Omega_i)},$$

  where $i, j \in \{1, \dots, N\},\ \ell, \ell' \in \{0, \dots, \ell_{\max}\}$ and $|m| \leq \ell,\ |m'| \leq \ell'$.

- We define the solution matrix $\boldsymbol{A} \in \mathbb{R}^{M\times M}$ as

$$[\boldsymbol{A}_{ij}]_{\ell\ell'}^{mm'} := \left(\mathcal{A}\mathcal{Y}_{\ell' m'}^{j}, \mathcal{Y}_{\ell m}^{i}\right)_{L^2(\partial\Omega_i)},$$

  where $i,j \in \{1,\dots,N\}$, $\ell,\ell' \in \{0,\dots,\ell_{\max}\}$ and $|m| \leq \ell$, $|m'| \leq \ell'$.

Equipped with the matrix representations of the relevant boundary integrals, we are now ready to state the proof of Theorem 5.18 for the approximate forces.

Proof of Theorem 5.18. We assume the setting of Remark 5.20 and Definition 5.21 and we denote by $\boldsymbol{\nu}_{\boldsymbol{\ell_{\max}}} \in \mathbb{R}^M$ the vector representation of the solution $\nu_{\ell_{\max}} \in W^{\ell_{\max}}$ to the Galerkin discretisation (2.8). We divide the proof into two steps:

- We first show that for each $i \in \{1,\dots,N\}$ and $\alpha = 1,2,3$ it holds that

$$\left(\widetilde{\boldsymbol{F}}_i^{\ell_{\max}}\right)_\alpha = -\frac{1}{2}\kappa_0\, \boldsymbol{\nu}_{\boldsymbol{\ell_{\max}}} \cdot \left(\partial_{\mathbf{x}_i^\alpha} \boldsymbol{V}\right) \boldsymbol{\nu}_{\boldsymbol{\ell_{\max}}},$$

  where $\left(\widetilde{\boldsymbol{F}}_i^{\ell_{\max}}\right)_\alpha$ denotes the α^{th} component of the approximate force $\widetilde{\boldsymbol{F}}_i^{\ell_{\max}}$ and $\partial_{\mathbf{x}_i^\alpha}$ denotes the α^{th} component of the sphere-centred gradient $\nabla_{\mathbf{x}_i}$.

- In the second step we use this expression to show that $\widetilde{\boldsymbol{F}}_i^{\ell_{\max}} = \boldsymbol{F}_i^{\ell_{\max}}$.

Step 1: Consider Definition 5.5 of the discrete electrostatic energy. A direct calculation shows that

$$\mathcal{E}_{\sigma_f}^{\ell_{\max}} = \frac{1}{2}\boldsymbol{\sigma_f} \cdot \boldsymbol{V}\boldsymbol{\nu}_{\boldsymbol{\ell_{\max}}}.$$

Let $i \in \{1,\dots,N\}$ and $\alpha \in \{1,2,3\}$ be fixed. Using Definition 5.6 of the approximate force and the fact that the vector $\boldsymbol{\sigma_f}$ is independent of the sphere centre locations $\{\mathbf{x}_i\}_{i=1}^N$ (see Definition 5.21), we see that

$$\left(\widetilde{\boldsymbol{F}}_i^{\ell_{\max}}\right)_\alpha = -\frac{1}{2}\boldsymbol{\sigma_f} \cdot \partial_{\mathbf{x}_i^\alpha}\boldsymbol{V}\boldsymbol{\nu}_{\boldsymbol{\ell_{\max}}} = -\frac{1}{2}\boldsymbol{\sigma_f} \cdot \partial_{\mathbf{x}_i^\alpha}\boldsymbol{\lambda}_{\boldsymbol{\ell_{\max}}}, \tag{5.3}$$

where $\boldsymbol{\lambda}_{\boldsymbol{\ell_{\max}}} := \boldsymbol{V}\boldsymbol{\nu}_{\boldsymbol{\ell_{\max}}} \in \mathbb{R}^M$ is the vector representation of $\lambda_{\ell_{\max}} := \mathbb{P}_{\ell_{\max}}\mathcal{V}\nu_{\ell_{\max}} \in W^{\ell_{\max}}$. Consequently, it suffices to compute the sphere-centred partial derivatives of $\boldsymbol{\lambda}_{\boldsymbol{\ell_{\max}}}$. Using the Galerkin discretisation (2.8) for the approximate induced surface charge, it is an easy exercise to show that the vector $\boldsymbol{\lambda}_{\boldsymbol{\ell_{\max}}}$ solves the finite-dimensional BIE

$$\boldsymbol{A}\boldsymbol{\lambda}_{\boldsymbol{\ell_{\max}}} = \frac{1}{\kappa_0}\boldsymbol{V}\boldsymbol{\sigma_f}. \tag{5.4}$$

Consequently, taking the derivative on both sides of Equation (5.4) and using the chain rule yields

$$\boldsymbol{A}\left(\partial_{\mathbf{x}_i^\alpha}\boldsymbol{\lambda}_{\boldsymbol{\ell_{\max}}}\right) = \frac{1}{\kappa_0}\left(\partial_{\mathbf{x}_i^\alpha}\boldsymbol{V}\right)\boldsymbol{\sigma_f} - \left(\partial_{\mathbf{x}_i^\alpha}\boldsymbol{A}\right)\boldsymbol{\lambda}_{\boldsymbol{\ell_{\max}}}.$$

Next, using Definition 2.8 from Section 2.3 of the boundary integral operator $\mathcal{A}\colon H^{\frac{1}{2}}(\partial\Omega) \to H^{\frac{1}{2}}(\partial\Omega)$ we write the solution matrix $\boldsymbol{A}$ as

$$\boldsymbol{A} = \boldsymbol{I}_{\boldsymbol{\ell}_{\mathbf{max}}} + \boldsymbol{V}\mathbf{DtN}^{\kappa},$$

where $\boldsymbol{I}_{\boldsymbol{\ell}_{\mathbf{max}}} \in \mathbb{R}^{M\times M}$ is the identity matrix. We now observe that both $\boldsymbol{I}_{\boldsymbol{\ell}_{\mathbf{max}}}$ and the matrix $\mathbf{DtN}^{\kappa}$ (see Definition 5.21) are independent of the sphere centre locations $\{\mathbf{x}_i\}_{i=1}^N$. Consequently, it holds that

$$-\partial_{\mathbf{x}_i^\alpha}\boldsymbol{A} = -\big(\partial_{\mathbf{x}_i^\alpha}\boldsymbol{V}\big)\mathbf{DtN}^{\kappa}.$$

A simple calculation then yields

$$\boldsymbol{A}\big(\partial_{\mathbf{x}_i^\alpha}\boldsymbol{\lambda}_{\boldsymbol{\ell}_{\mathbf{max}}}\big) = \big(\partial_{\mathbf{x}_i^\alpha}\boldsymbol{V}\big)\frac{1}{\kappa_0}\boldsymbol{\sigma}_{\boldsymbol{f}} - \big(\partial_{\mathbf{x}_i^\alpha}\boldsymbol{V}\big)\mathbf{DtN}^{\kappa}\boldsymbol{\lambda}_{\boldsymbol{\ell}_{\mathbf{max}}} = \big(\partial_{\mathbf{x}_i^\alpha}\boldsymbol{V}\big)\boldsymbol{\nu}_{\boldsymbol{\ell}_{\mathbf{max}}}, \tag{5.5}$$

where the last equality follows from the fact that $\boldsymbol{\nu}_{\boldsymbol{\ell}_{\mathbf{max}}} = \frac{1}{\kappa_0}\boldsymbol{\sigma}_{\boldsymbol{f}} - \mathbf{DtN}^{\kappa}\boldsymbol{\lambda}_{\boldsymbol{\ell}_{\mathbf{max}}}$, which is a result that has been used (in a slightly different form) many times in Chapters 3 and 4 (see, e.g., Lemma 4.4), and can be deduced directly from the Galerkin discretisation (2.8).

Next, let $\boldsymbol{A}^{\mathrm{T}} \in \mathbb{R}^{M\times M}$ denote the transpose of $\boldsymbol{A}$. Clearly, $\boldsymbol{A}^{\mathrm{T}}$ is the matrix representation (with respect to the basis 5.19) of the finite-dimensional operator $\mathbb{Q}_{\ell_{\max}}\mathcal{A}^*\mathbb{Q}_{\ell_{\max}}\colon W^{\ell_{\max}} \to W^{\ell_{\max}}$, i.e., the operator associated with the Galerkin discretisation (2.8) for the approximate induced surface charge. Since the Galerkin discretisation (2.8) is well-posed, the matrices $\boldsymbol{A}^{\mathrm{T}}$ and $\boldsymbol{A}$ are both invertible. Consequently, we can use Equations (5.3) and (5.5) to write the approximate electrostatic force $\widetilde{\boldsymbol{F}}_i^{\ell_{\max}}$ as

$$\begin{aligned}\Big(\widetilde{\boldsymbol{F}}_i^{\ell_{\max}}\Big)_\alpha &= -\frac{1}{2}\,\boldsymbol{\sigma}_{\boldsymbol{f}}\cdot\partial_{\mathbf{x}_i^\alpha}\boldsymbol{\lambda}_{\boldsymbol{\ell}_{\mathbf{max}}} = -\frac{1}{2}\,\boldsymbol{\sigma}_{\boldsymbol{f}}\cdot\big(\boldsymbol{A}^{-1}\big(\partial_{\mathbf{x}_i^\alpha}\boldsymbol{V}\big)\boldsymbol{\nu}_{\boldsymbol{\ell}_{\mathbf{max}}}\big)\\ &= -\frac{1}{2}\,\big(\boldsymbol{A}^{\mathrm{T}}\big)^{-1}\boldsymbol{\sigma}_{\boldsymbol{f}}\cdot\big(\partial_{\mathbf{x}_i^\alpha}\boldsymbol{V}\big)\boldsymbol{\nu}_{\boldsymbol{\ell}_{\mathbf{max}}}.\end{aligned}$$

Finally, in view of the Galerkin discretisation (2.8) we have $\big(\boldsymbol{A}^{\mathrm{T}}\big)^{-1}\boldsymbol{\sigma}_{\boldsymbol{f}} = \kappa_0\boldsymbol{\nu}_{\boldsymbol{\ell}_{\mathbf{max}}}$ so that

$$\Big(\widetilde{\boldsymbol{F}}_i^{\ell_{\max}}\Big)_\alpha = -\frac{1}{2}\kappa_0\,\boldsymbol{\nu}_{\boldsymbol{\ell}_{\mathbf{max}}}\cdot\big(\partial_{\mathbf{x}_i^\alpha}\boldsymbol{V}\big)\boldsymbol{\nu}_{\boldsymbol{\ell}_{\mathbf{max}}}. \tag{5.6}$$

Step 2: We will now attempt to simplify the expression (5.6) for the approximate electrostatic forces. To this end, let $\mathbb{S}^2 \subset \mathbb{R}^3$ denote the unit sphere and for each $i \in \{1,\ldots,N\}$ let $\nu_i^{\ell_{\max}} := \nu_{\ell_{\max}}|_{\partial\Omega_i}$. Using Definition 5.21 of the matrix $\boldsymbol{V}$ and a simple change of variables, Equation (5.6) can be written in the form

$$\begin{aligned}\widetilde{\boldsymbol{F}}_i^{\ell_{\max}} = -\frac{1}{2}\kappa_0\sum_{k=1}^{N}\sum_{j=1}^{N} r_k^2 r_j^2 \int_{\mathbb{S}^2}\int_{\mathbb{S}^2} \nu_k^{\ell_{\max}}\big(\mathbf{x}_k + r_k\mathbf{t}\big)\nu_j^{\ell_{\max}}\big(\mathbf{x}_j + r_j\mathbf{s}\big)\\ \cdot\left(\nabla_{\mathbf{x}_i}\frac{1}{|\mathbf{x}_j + r_j\mathbf{s} - (\mathbf{x}_k + r_k\mathbf{t})|}\right)d\mathbf{s}d\mathbf{t}.\end{aligned}$$

A straightforward calculation shows that the only non-zero terms in this double sum involve indices $j, k \in \{1, \dots, N\}$ such that $j \neq i, k = i$ and $j = i, k \neq i$. As a consequence, it holds that

$$\begin{aligned}\widetilde{\boldsymbol{F}}_i^{\ell_{\max}} = &-\frac{1}{2}\kappa_0 r_i^2 \sum_{\substack{k=1\\k\neq i}}^{N} r_k^2 \int_{\mathbb{S}^2}\int_{\mathbb{S}^2} \nu_k^{\ell_{\max}}\big(\mathbf{x}_k + r_k\mathbf{t}\big)\nu_i^{\ell_{\max}}\big(\mathbf{x}_i + r_i\mathbf{s}\big) \\ &\qquad\qquad \cdot \left(\nabla_{\mathbf{x}_i} \frac{1}{|\mathbf{x}_i + r_i\mathbf{s} - (\mathbf{x}_k + r_k\mathbf{t})|}\right) d\mathbf{s}d\mathbf{t} \\ &-\frac{1}{2}\kappa_0 r_i^2 \sum_{\substack{j=1\\j\neq i}}^{N} r_j^2 \int_{\mathbb{S}^2}\int_{\mathbb{S}^2} \nu_i^{\ell_{\max}}\big(\mathbf{x}_i + r_i\mathbf{t}\big)\nu_j^{\ell_{\max}}\big(\mathbf{x}_j + r_j\mathbf{s}\big) \\ &\qquad\qquad \cdot \left(\nabla_{\mathbf{x}_i} \frac{1}{|\mathbf{x}_j + r_j\mathbf{s} - (\mathbf{x}_i + r_i\mathbf{t})|}\right) d\mathbf{s}d\mathbf{t}.\end{aligned}$$

We can now use simple calculus and the symmetries in the above sum to obtain

$$\begin{aligned}\widetilde{\boldsymbol{F}}_i^{\ell_{\max}} = &-\kappa_0 r_i^2 \int_{\mathbb{S}^2} \nu_i^{\ell_{\max}}\big(\mathbf{x}_i + r_i\mathbf{t}\big) \sum_{\substack{j=1\\j\neq i}}^{N} r_j^2 \int_{\mathbb{S}^2} \nu_j^{\ell_{\max}}\big(\mathbf{x}_j + r_j\mathbf{s}\big) \\ &\qquad\qquad \cdot \left(\frac{\mathbf{x}_i + r_i\mathbf{s} - (\mathbf{x}_j + r_j\mathbf{t})}{|\mathbf{x}_j + r_j\mathbf{s} - (\mathbf{x}_j + r_i\mathbf{t})|^3}\right) d\mathbf{s}d\mathbf{t},\end{aligned}$$

and therefore,

$$\begin{aligned}\widetilde{\boldsymbol{F}}_i^{\ell_{\max}} &= -\kappa_0 \int_{\partial\Omega_i} \nu_i^{\ell_{\max}}(\mathbf{y}) \sum_{\substack{j=1\\j\neq i}}^{N} \int_{\partial\Omega_j} \nu_j^{\ell_{\max}}(\mathbf{x}) \frac{\mathbf{y}-\mathbf{x}}{|\mathbf{y}-\mathbf{x}|^3}\, d\mathbf{x}d\mathbf{y} \\ &= \kappa_0 \int_{\partial\Omega_i} \nu_i^{\ell_{\max}}(\mathbf{y})\boldsymbol{E}_i(\mathbf{y})\, d\mathbf{y} = \boldsymbol{F}_i^{\ell_{\max}}.\end{aligned}$$

□

We conclude this section by observing that due to Theorem 5.18, all remarks concerning the electrostatic energy-based definition of the forces are applicable to the electric field-based definition of the forces. In particular, we can view the approximate forces $\{\boldsymbol{F}_i^{\ell_{\max}}\}_{i=1}^N$ as the gradient of the discrete potential energy surface (dPES) at the point $\{\mathbf{x}_i\}_{i=1}^N$.

5.2 Error Analysis for the Electrostatic Forces

Throughout this section we will assume the setting of Section 5.1.2. In particular, we define the net electrostatic forces acting on each dielectric particles in terms of the electric

field as in Definition 5.14 and we define the *approximate* net electrostatic force acting on each dielectric particles in terms of the electric field as in Definition 5.17. In view of Theorem 5.18 in Section 5.1.3, this choice results in no loss of generality.

In order to present a clear and concise exposition, we organise the remainder of this section as follows. In Section 5.2.1, we state our main results on the approximability and rate of convergence of the approximate electrostatic forces, and we discuss the hypothesis and conclusions of these theorems. In Section 5.2.2, we state and prove intermediary lemmas which we require for our analysis. These lemmas are then used to prove the main results of Section 5.2.1.

5.2.1 Main result and discussion

Notation: Given a vector $\mathbb{X} \in \mathbb{R}^3$, we will write $(\mathbb{X})_\alpha,\ \alpha = 1,2,3$ to denote the components of $\mathbb{X}$. In the same spirit, we will write $\partial_\alpha(\cdot),\ \alpha = 1,2,3$ for the α^{th} component of the gradient of some scalar field in the Cartesian coordinate system.

Theorem 5.22 (Approximability of the Electrostatic Forces)**.**

Let $\sigma_f \in H^s(\partial\Omega)$ for some $s > -\frac{1}{2}$, let $\ell_{\max} \in \mathbb{N}$, let $\nu \in H^s(\partial\Omega)$ and $\nu_{\ell_{\max}} \in W^{\ell_{\max}}$ denote the unique solutions to the BIE (2.3) and Galerkin discretisation (2.8) with right-hand sides generated by σ_f, and for each $i \in \{1,\dots,N\}$ let $\boldsymbol{F}_i, \boldsymbol{F}_i^{\ell_{\max}} \in \mathbb{R}^3$ denote the exact and approximate force acting on the dielectric particle represented by Ω_i as defined through Definitions 5.14 and 5.17 respectively. Then it holds that

$$\lim_{\ell_{\max}\to\infty} \sum_{i=1}^{N} \sum_{\alpha=1}^{3} \left| (\boldsymbol{F}_i)_\alpha - \left(\boldsymbol{F}_i^{\ell_{\max}}\right)_\alpha \right| = 0.$$

Remark 5.23. Consider Theorem 5.22. Notice that we require that the free charge $\sigma_f \in H^s(\Omega)$ for some $s > -\frac{1}{2}$. This regularity requirement agrees with the convergence rates for the induced surface charge given by Theorem 3.12 and therefore cannot be improved. Unfortunately, as we will show in Section 5.2.2, the techniques used to prove this theorem lead to convergence rates with a pre-factor that depends on N.

The next theorem establishes N-independent convergence rates for the electrostatic forces under the assumption of increased regularity for the free charge σ_f.

Theorem 5.24 (N-independent Convergence Rates for the Electrostatic Forces)**.** *Let $s \geq \frac{1}{2}$, let $\sigma_f \in H^s(\partial\Omega)$ be a given free charge, let $\ell_{\max} \in \mathbb{N}$, let $\nu \in H^s(\partial\Omega)$ and $\nu_{\ell_{\max}} \in W^{\ell_{\max}}$ be the unique solutions to the BIE (2.3) and Galerkin discretisation (2.8) with right-hand sides generated by σ_f, and for each $i \in \{1,\dots,N\}$ let $\boldsymbol{F}_i$ and $\boldsymbol{F}_i^{\ell_{\max}}$ denote the net force and approximate net force as defined through Definitions 5.14 and 5.17 respectively. Then there exists a constant $C_{\text{Force}} > 0$ that depends on s, the dielectric constants, the radii of the open balls, and the minimum inter-sphere separation distance but is independent of the number N of dielectric particles such that for $\ell_{\max}$ sufficiently large it holds that*

$$\sum_{i=1}^{N}\sum_{\alpha=1}^{3}\left|(\boldsymbol{F}_i)_\alpha-\left(\boldsymbol{F}_i^{\ell_{\max}}\right)_\alpha\right| \leq C_{\text{force}}\left(\frac{\max r_j}{\ell_{\max}+1}\right)^{-\frac{1}{2}+s}\left(|||\nu|||^2_{H^s(\partial\Omega)}+|||\mathbb{Q}_0^{\perp}\sigma_f|||^2_{H^s(\partial\Omega)}\right). \tag{5.7}$$

Remark 5.25. Consider the setting of Theorem 5.24. The dependence of the pre-factor C_{Force} on the regularity index $s \geq \frac{1}{2}$ is an artefact which arises due to our attempt to write the final convergence rates (5.7) in a concise and aesthetically appealing form. The proof of Theorem 5.24 will show that this dependence on s can be removed at the cost of obtaining a more tedious final expression.

Theorem 5.24 has the following important (but unsurprising) corollary.

Corollary 5.26 (Exponential Convergence of the Electrostatic Forces)**.**
Let C_{force} denote the convergence rate pre-factor in Theorem 5.24, let $\sigma_f \in C^\infty(\partial\Omega)$ be analytic on $\partial\Omega$ in the sense that the local spherical harmonics coefficients of σ_f on each sphere decay exponentially fast, let $\ell_{\max} \in \mathbb{N}$, let $\nu \in H^{-\frac{1}{2}}(\partial\Omega)$ and $\nu_{\ell_{\max}} \in W^{\ell_{\max}}$ be the unique solutions to the BIE (2.3) and Galerkin discretisation (2.8) with right-hand sides generated by σ_f, and for each $i \in \{1,\ldots,N\}$ let $\boldsymbol{F}_i$ and $\boldsymbol{F}_i^{\ell_{\max}}$ denote the exact and approximate electrostatic forces acting on the particle represented by Ω_i as given by Definitions 5.14 and 5.17 respectively. For $\ell_{\max}$ sufficiently large, if ν is analytic on $\partial\Omega$ then there exist constants $C^\alpha_{\nu,\sigma_f}, C^\beta_{\nu,\sigma_f} > 0$ depending on geometric parameters, the exact solution ν, and the free charge σ_f such that

$$\frac{1}{N}\sum_{i=1}^{N}\sum_{\alpha=1}^{3}\left|(\boldsymbol{F}_i)_\alpha-\left(\boldsymbol{F}_i^{\ell_{\max}}\right)_\alpha\right| \leq C_{\text{force}}C^\alpha_{\nu,\sigma_f}\exp\left(-C^\beta_{\nu,\sigma_f}\sqrt{\frac{\ell_{\max}+1}{\max r_j}}\right).$$

Proof. The proof of Corollary 5.26 uses the convergence rates obtained from Theorem 5.24 and is a standard exercise in the analysis of spectral Galerkin methods (see, e.g., the arguments in [102, 103]). For more details, we refer the interested reader to the proof of Theorem 3.13 in Chapter 3 which establishes the exponential convergence of the approximate induced surface charge and can be copied nearly word for word to prove Corollary 5.26. □

Next, we would like to discuss in more detail the hypothesis and conclusions of Theorem 5.24. We frame this discussion in the form of two remarks.

Remark 5.27 (*Scaling of the Error Estimates in Theorem 5.24*).

As mentioned in the introduction, the goal of this chapter is to show that, under suitable geometric assumptions, the Galerkin method proposed through the BIE (2.3) and the discretisation (2.8) can be used to obtain the electrostatic forces with *linear scaling accuracy*. A necessary condition to achieve this is to show that the approximate forces we compute are N-error stable, i.e., for a fixed number of degrees of freedom per sphere, the relative or average error in the approximate approximate forces for different geometrical configurations does not increase with the number N of dielectric particles. In Chapter 3, we showed precisely this result for the approximate induced surface charges induced on

any family of geometries $\{\Omega_{\mathcal{F}}\}_{\mathcal{F}\in\mathcal{I}}$ satisfying the assumptions **GA1)-GA3)** introduced in Section 2.2.

Consider Theorem 5.24. Since the constant $C_{\text{force}} > 0$ does not explicitly depend on N, we can deduce two conclusions from the convergence rate (5.7):

C1) It holds that

$$\frac{\sum_{i=1}^{N}\sum_{\alpha=1}^{3}\left|(\boldsymbol{F}_i)_\alpha - \left(\boldsymbol{F}_i^{\ell_{\max}}\right)_\alpha\right|}{\|\nu\|^2_{H^s(\partial\Omega)} + \|\mathbb{Q}_0^{\perp}\sigma_f\|^2_{H^s(\partial\Omega)}} \leq \left(\frac{\max r_j}{\ell_{\max}+1}\right)^{-\frac{1}{2}+s} C_{\text{force}},$$

with right-hand side that is independent of N. Consequently, for any family of geometries $\{\Omega_{\mathcal{F}}\}_{\mathcal{F}\in\mathcal{I}}$ satisfying assumptions **GA1)-GA3)**, the approximate forces–relative to the sum squared of the exact induced surface charge ν and free charge σ_f– are indeed independent of $N_{\mathcal{F}}$. Here, $N_{\mathcal{F}}$ denotes the number of particles in an arbitrary geometry $\Omega_{\mathcal{F}}$ and takes the role of N above. We emphasise that this result is nearly identical to the one obtained for the error in the total electrostatic energy (see Theorem 3.12 in Chapter 3).

C2) Let $i \in \{1,\dots,N\}$ and let $\nu_i := \nu|_{\partial\Omega_i}$ and $\sigma_{f,i} := \sigma_f|_{\partial\Omega_i}$. If the induced surface charge ν and free charge σ_f are both of order 1 on each sphere, i.e., if $|||\nu_i|||_{H^s(\partial\Omega_i)}$, $|||\sigma_{f,i}|||_{H^s(\partial\Omega_i)} = \mathcal{O}(1)$ then it holds that

$$\left|||\nu|||^2_{H^s(\partial\Omega)} + \left|||\mathbb{Q}_0^{\perp}\sigma_f|||^2_{H^s(\partial\Omega)} = \mathcal{O}(N),\right.\right.$$

and it therefore holds that

$$\frac{1}{N}\sum_{i=1}^{N}\sum_{\alpha=1}^{3}\left|(\boldsymbol{F}_i)_\alpha - \left(\boldsymbol{F}_i^{\ell_{\max}}\right)_\alpha\right| = \mathcal{O}(1).$$

In other words, for any family of geometries $\{\Omega_{\mathcal{F}}\}_{\mathcal{F}\in\mathcal{I}}$ satisfying assumptions **GA1)-GA3)**, if the discretisation parameter $\ell_{\max}$ is fixed and the induced surface charge ν and free charge σ_f are both $\mathcal{O}(1)$ on each sphere, then the average error in the approximate forces does not increase for increasing $N_{\mathcal{F}}$.

Remark 5.28 (*Assumptions of Theorem* 5.24). Consider once again Theorem 5.24. Notice that we require that the free charge $\sigma_f \in H^s(\partial\Omega)$ for $s > \frac{1}{2}$. This is in contrast to Theorem 5.22, which establishes approximability of the forces even if $-\frac{1}{2} < s < \frac{1}{2}$. Although suboptimal from a mathematical perspective, this additional regularity assumption does not preclude us from using these error estimates in most practical situations. This is due to the fact that in many physical applications, the open balls $\{\Omega_i\}_{i=1}^N$ represent *homogenous* dielectric particles, and for homogenous particles, physical arguments imply that the free charge σ_f must be distributed uniformly on each sphere $\partial\Omega_i$. In other words, for a variety of physical applications (see, e.g., [126, 127, 128, 129]), we have $\sigma_f \in C^\infty(\partial\Omega)$, which in turn means that the convergence rates (5.7) for the electrostatic forces are valid for all $s > \frac{1}{2}$.

5.2.2 Auxiliary lemmas and proofs of the main results

To aid the analysis of this section, we first introduce some additional notation. Essentially, we wish to introduce local versions of the projection operators on the approximation space (see Definition 3.30 in Chapter 3), norms (see Definition 3.4 in Chapter 3), and the Dirichlet trace operator on each sphere.

Notation:

- Let $i \in \{1, \dots, N\}$ and $\ell \in \mathbb{N}_0$. We define the projection operator $\mathbb{P}_{i,\ell}\colon\ H^{\frac{1}{2}}(\partial\Omega_i) \to W^{\ell}(\partial\Omega_i)$ as the mapping with the property that for any $\psi \in H^{\frac{1}{2}}(\partial\Omega)$, $\mathbb{P}_{i,\ell}\psi$ is the unique element of $W^{\ell}(\partial\Omega_i)$ satisfying

$$(\phi_{\ell_{\max}}, \mathbb{P}_{i,\ell}\psi)_{L^2(\partial\Omega)} = \langle \phi_{\ell_{\max}}, \psi \rangle_{H^{-\frac{1}{2}}(\partial\Omega_i)\times H^{\frac{1}{2}}(\partial\Omega_i)} \qquad \forall \phi_{\ell_{\max}} \in W^{\ell}(\partial\Omega_i),$$

  Similarly, we define the projection operator $\mathbb{Q}_{i,\ell}\colon H^{-\frac{1}{2}}(\partial\Omega_i) \to W^{\ell}(\partial\Omega_i)$ as the mapping with the property that for any $\sigma \in H^{-\frac{1}{2}}(\partial\Omega_i)$, $\mathbb{Q}_{i,\ell}\sigma$ is the unique element of $W^{\ell_{\max}}(\partial\Omega)$ satisfying

$$(\mathbb{Q}_{i,\ell}\sigma, \phi_{\ell_{\max}})_{L^2(\partial\Omega)} = \langle \sigma, \phi_{\ell_{\max}} \rangle_{H^{-\frac{1}{2}}(\partial\Omega_i)\times H^{\frac{1}{2}}(\partial\Omega_i)} \qquad \forall \phi_{\ell_{\max}} \in W^{\ell}(\partial\Omega_i).$$

- Let $i \in \{1, \dots, N\}$ and $\ell \in \mathbb{N}_0$. We define the projection operators $\mathbb{P}^{\perp}_{i,\ell}\colon H^{\frac{1}{2}}(\partial\Omega_i) \to \big(W^{\ell_{\max}}(\partial\Omega_i)\big)^{\perp}$ and $\mathbb{Q}^{\perp}_{i,\ell}\colon H^{-\frac{1}{2}}(\partial\Omega_i) \to \big(W^{\ell_{\max}}(\partial\Omega_i)\big)^{\perp}$ as $\mathbb{P}^{\perp}_{i,\ell} := I - \mathbb{P}_{i,\ell}$ and $\mathbb{Q}^{\perp}_{i,\ell} := I - \mathbb{Q}_{i,\ell}$ where I denotes the identity operator on the relevant trace space.

- Furthermore, for all $i \in \{1, \dots, N\}$ and $\lambda_i \in H^{\frac{1}{2}}(\partial\Omega_i)$ we define

$$|||\lambda_i|||_i^2 := \|\mathbb{P}_{i,0}\lambda_i\|^2_{L^2(\partial\Omega_i)} + \langle \mathrm{DtN}\lambda_i, \lambda_i \rangle_{H^{-\frac{1}{2}}(\partial\Omega_i)\times H^{\frac{1}{2}}(\partial\Omega_i)}.$$

- In addition, for all $i \in \{1, \dots, N\}$ and $\sigma_i \in \breve{H}^{-\frac{1}{2}}(\partial\Omega_i)$ we define

$$|||\sigma_i|||_i^* := |||\mathrm{DtN}_i^{-1}\sigma_i|||_i,$$

  where the mapping $\mathrm{DtN}_i^{-1}\colon \breve{H}^{-\frac{1}{2}}(\partial\Omega_i) \to \breve{H}^{\frac{1}{2}}(\partial\Omega_i)$ is the inverse of the Dirichlet-to-Neumann map on $\partial\Omega_i$.

- Moreover, for all $i \in \{1, \dots, N\}$ we denote by $\gamma_i^- : H^1(\Omega_i) \to H^{\frac{1}{2}}(\partial\Omega_i)$ the interior Dirichlet trace operator on the open ball Ω_i.

Lemma 5.29 (Estimate for the Exact Excluded Electric Field)**.**
Let $\sigma \in H^{-\frac{1}{2}}(\partial\Omega)$ be a given charge distribution and for each $i \in \{1, \dots, N\}$ let $\phi_{i,\mathrm{exc}} \in H^1_{\mathrm{loc}}(\mathbb{R}^3)$ and $\boldsymbol{E}_i \in L^2_{\mathrm{loc}}(\mathbb{R}^3;\mathbb{R}^3)$ denote, respectively, the i excluded electric potential and electric field generated by σ as defined through Definition 5.11. Then for all $i \in \{1, \dots, N\}$

there exists a constant $\widetilde{C_{r_i}} > 0$ *that depends only on the radius* r_i *of the open ball* Ω_i *such that for each* $\alpha = 1, 2, 3$ *it holds that*

$$|||\gamma_i^-\left(\boldsymbol{E}_i\right)_\alpha|||_i^2 \leq \widetilde{C_{r_i}}\left|\left|\left|\mathbb{P}_{0,i}^{\perp}\gamma_i^-\phi_{i,\mathrm{exc}}\right|\right|\right|_{H^{\frac{3}{2}}(\partial\Omega_i)}^2.$$

Remark 5.30. Consider Lemma 5.29. We recall from Remark 5.13 that the i excluded electric potential $\phi_{i,\mathrm{exc}}$ and electric field $\boldsymbol{E}_i$ are both smooth on $\overline{\Omega_i}$ for each $i \in \{1, \ldots, N\}$. Consequently, the norms appearing in the estimate are well-defined. Furthermore, although the conclusion of Lemma 5.29 might seem obvious, the key novelty of this result is that the constant $\widetilde{C_{r_i}}$ appearing in the bound depends only on the radius r_i of the sphere Ω_i and is, in particular, independent of the number N of dielectric spherical particles.

Proof of Lemma 5.29. Let $\{i \in 1 \ldots, N\}$ be fixed. As emphasised previously, Remark 5.13 implies that $\phi_{i,\mathrm{exc}} \in C^\infty(\overline{\Omega_i})$. In view of Definition 3.10 from Chapter 3 therefore, there exist coefficients $[\phi_i]_\ell^m$, $\ell \in \mathbb{N}_0$, $-\ell \leq m \leq \ell$ satisfying suitable decay properties such that for all $\mathbf{x} \in \partial\Omega_i$ it holds that

$$\phi_{i,\mathrm{exc}}(\mathbf{x}) = \sum_{\ell=0}^{\infty}\sum_{m=-\ell}^{m=\ell}[\phi_i]_\ell^m \mathcal{Y}_\ell^m\left(\frac{\mathbf{x}-\mathbf{x}_i}{|\mathbf{x}-\mathbf{x}_i|}\right).$$

Since the electric potential $\phi_{i,\mathrm{exc}}$ is harmonic on Ω_i, standard results (see, e.g., [68, Chapter 2(H)]) yield that we have the following representation of $\phi_{i,\mathrm{exc}}$ in $\overline{\Omega_i}$:

$$\phi_{i,\mathrm{exc}} = \sum_{\ell=0}^{\infty}\sum_{m=-\ell}^{m=\ell}[\phi_i]_\ell^m \frac{|\mathbf{x}-\mathbf{x}_i|^\ell}{r_i^\ell}\mathcal{Y}_\ell^m\left(\frac{\mathbf{x}-\mathbf{x}_i}{|\mathbf{x}-\mathbf{x}_i|}\right) \quad \forall \mathbf{x} \in \overline{\Omega_i}. \tag{5.8}$$

We recall from Definition 5.11 of $\boldsymbol{E}_i$ that $\gamma_i^-\left(\boldsymbol{E}_i\right)_\alpha = \gamma_i^-\partial_\alpha\phi_{i,\mathrm{exc}}$ for each $\alpha = 1, 2, 3$. Since $\phi_{i,\mathrm{exc}}$ is smooth in a neighbourhood of the sphere Ω_i (see Remark 5.13), we can use Equation (5.8) to obtain an expression for the derivative in $\overline{\Omega_i}$ and then simply take the restriction of this derivative on the boundary $\partial\Omega_i$. To this end, we first observe that for all $\mathbf{x} \in \overline{\Omega_i}$ it holds that

$$\left(\partial_\alpha\phi_{i,\mathrm{exc}}\right)(\mathbf{x}) = \sum_{\ell=0}^{\infty}\sum_{m=-\ell}^{m=\ell}\frac{1}{r_i^\ell}[\phi_i]_\ell^m\,\partial_\alpha\left(|\mathbf{x}-\mathbf{x}_i|^\ell\mathcal{Y}_\ell^m\left(\frac{\mathbf{x}-\mathbf{x}_i}{|\mathbf{x}-\mathbf{x}_i|}\right)\right). \tag{5.9}$$

Clearly, the next step would be to bound the quantity $|||\gamma_i^-\left(\partial_\alpha\phi_{i,\mathrm{exc}}\right)|||_i$ using the expression given by Equation (5.9). However, in order to evaluate the $|||\cdot|||_i$ norm, we require the projection of the trace onto the space of constant functions $\mathcal{C}(\partial\Omega_i)$. Therefore, our next step is to simplify the series expansion above. Observe that the $\ell = 0$ term in the series expansion (5.9) is zero. Furthermore, the $\ell = 1$ terms are easy to simplify. Indeed, using the definition of the spherical harmonics in Cartesian coordinates, we have

$$\partial_\alpha|\mathbf{x}-\mathbf{x}_i|\mathcal{Y}_1^m\left(\frac{\mathbf{x}-\mathbf{x}_i}{|\mathbf{x}-\mathbf{x}_i|}\right) = \begin{cases}\sqrt{\frac{3}{4\pi}} & \text{if } (m,\alpha) \in \{(-1,2),(0,3),(1,1)\},\\ 0 & \text{otherwise.}\end{cases}$$

Therefore, with the introduction of an appropriate binary-valued map $k(m,\alpha) \in \{0,1\}$ we can write

$$\begin{aligned}\big(\partial_\alpha \phi_{i,\mathrm{exc}}\big)(\mathbf{x}) = \sum_{\ell=2}^{\infty}\sum_{m=-\ell}^{m=\ell} \frac{1}{r_i^\ell}[\phi_i]_\ell^m\, \partial_\alpha\left(|\mathbf{x}-\mathbf{x}_i|^\ell \mathcal{Y}_\ell^m\left(\frac{\mathbf{x}-\mathbf{x}_i}{|\mathbf{x}-\mathbf{x}_i|}\right)\right) \\ + \underbrace{\sum_{m=-1}^{m=1}\sqrt{\frac{3}{4\pi r_i^2}}[\phi_i]_1^m\, k(m,\alpha)}_{:=C_{\mathrm{const}}.} \quad \forall \mathbf{x}\in\overline{\Omega_i}.\end{aligned}$$

We have thus decomposed $\partial_\alpha\phi_{i,\mathrm{exc}}$ on the ball $\overline{\Omega_i}$ as the sum of two terms, one of which is a constant C_{const}. We claim that in fact $\mathbb{P}_{0,i}\left(\gamma_i^-\left(\partial_\alpha\phi_{i,\mathrm{exc}}\right)\right) = C_{\mathrm{const}}$. To justify the claim, it suffices to consider the function $\psi_i^\alpha := \partial_\alpha\phi_{i,\mathrm{exc}} - C_{\mathrm{const}}$ and show that $\psi_i^\alpha \in \breve{H}^{\frac{1}{2}}(\partial\Omega_i)$. By definition we have that

$$\psi_i^\alpha(\mathbf{x}) = \sum_{\ell=2}^{\infty}\sum_{m=-\ell}^{m=\ell} \frac{1}{r_i^\ell}[\phi_i]_\ell^m\, \partial_\alpha\left(|\mathbf{x}-\mathbf{x}_i|^\ell \mathcal{Y}_\ell^m\left(\frac{\mathbf{x}-\mathbf{x}_i}{|\mathbf{x}-\mathbf{x}_i|}\right)\right) \quad \forall \mathbf{x}\in\overline{\Omega_i}.$$

It is well known (see, e.g., [8, Chapter 5] or [147, Chapter 8]) that the function $|\mathbf{x}-\mathbf{x}_i|^\ell \mathcal{Y}_\ell^m\left(\frac{\mathbf{x}-\mathbf{x}_i}{|\mathbf{x}-\mathbf{x}_i|}\right)$ is a homogenous, harmonic polynomial of degree ℓ in the variables $(\mathbf{x}-\mathbf{x}_i)_\alpha,\ \alpha=1,2,3$. Consequently, the partial derivative $\partial_\alpha\left(|\mathbf{x}-\mathbf{x}_i|^\ell \mathcal{Y}_\ell^m\left(\frac{\mathbf{x}-\mathbf{x}_i}{|\mathbf{x}-\mathbf{x}_i|}\right)\right)$ must be a homogenous, harmonic polynomial of degree $\ell-1$ in $(\mathbf{x}-\mathbf{x}_i)_\alpha,\ \alpha=1,2,3$. It follows that there exist coefficients $[d]_\ell^m,\ \ell\geq 1,\ -\ell\leq m\leq \ell$ such that the function ψ_i^α can be written as

$$\psi_i^\alpha(\mathbf{x}) = \sum_{\ell=1}^{\infty}\sum_{m=-\ell}^{m=\ell} \frac{1}{r_i^\ell}[d]_\ell^m |\mathbf{x}-\mathbf{x}_i|^\ell \mathcal{Y}_\ell^m\left(\frac{\mathbf{x}-\mathbf{x}_i}{|\mathbf{x}-\mathbf{x}_i|}\right) \quad \forall \mathbf{x}\in\overline{\Omega_i},$$

and therefore $\gamma_i^-\psi \in \breve{H}^{\frac{1}{2}}(\partial\Omega_i)$ as claimed. Recalling now the definition of the local $|||\cdot|||_i$ norm, we see that

$$\begin{aligned}|||\gamma_i^-\partial_\alpha\phi_{i,\mathrm{exc}}|||_i^2 &= \|\mathbb{P}_{0,i}\gamma_i^-\partial_\alpha\phi_{i,\mathrm{exc}}\|_{L^2(\partial\Omega_i)}^2 + \left\langle \mathrm{DtN}\gamma_i^-\psi_i^\alpha, \gamma_i^-\psi_i^\alpha\right\rangle_{H^{-\frac{1}{2}}(\partial\Omega_i)\times H^{\frac{1}{2}}(\partial\Omega_i)} \\ &= 4\pi r_i^2 C_{\mathrm{const}}^2 + \left\langle \mathrm{DtN}\gamma_i^-\psi_i^\alpha, \gamma_i^-\psi_i^\alpha\right\rangle_{H^{-\frac{1}{2}}(\partial\Omega_i)\times H^{\frac{1}{2}}(\partial\Omega_i)}. \end{aligned} \tag{5.10}$$

Our next task is to obtain a simple bound for the above duality pairing. Recall that by definition $\phi_{i,\mathrm{exc}}$ is harmonic on Ω_i and it therefore follows that any partial derivative $\partial_\alpha\phi_{i,\mathrm{exc}},\ \alpha=1,2,3$ is also harmonic in Ω_i. Consequently, Green's identity yields that

$$|\psi_i^\alpha|_{H^1(\Omega_i)}^2 := \int_{\Omega_i} |\nabla\psi_i^\alpha(\mathbf{x})|^2\, d\mathbf{x} = \left\langle \mathrm{DtN}\gamma_i^-\psi_i^\alpha, \gamma_i^-\psi_i^\alpha\right\rangle_{H^{-\frac{1}{2}}(\partial\Omega_i)\times H^{\frac{1}{2}}(\partial\Omega_i)},$$

where $|\cdot|_{H^1(\Omega_i)}$ denotes the usual H^1 semi-norm on Ω_i. Let $|\cdot|_{H^2(\Omega_i)}$ denote the usual H^2 semi-norm on Ω_i. It is then clear that $|\partial_\alpha\phi_{i,\mathrm{exc}}|_{H^1(\Omega_i)}^2 \leq |\phi_{i,\mathrm{exc}}|_{H^2(\Omega_i)}^2$. Furthermore, it is

straightforward to show that there exists a constant C_{r_i} depending only on the radius r_i such that

$$\left\langle \mathrm{DtN}\gamma_i^- \partial_\alpha \phi_{i,\mathrm{exc}}, \gamma_i^- \partial_\alpha \phi_{i,\mathrm{exc}} \right\rangle_{H^{-\frac{1}{2}}(\partial\Omega_i)\times H^{\frac{1}{2}}(\partial\Omega_i)} \leq |\phi_{i,\mathrm{exc}}|^2_{H^2(\Omega_i)} \leq C_{r_i} \left|\left|\left| \mathbb{P}^\perp_{0,i} \gamma_i^- \phi_{i,\mathrm{exc}} \right|\right|\right|^2_{H^{\frac{3}{2}}(\partial\Omega_i)}.$$

Using this bound in Equation (5.10), we obtain that

$$\left|\left|\left| \gamma_i^- \partial_\alpha \phi_{i,\mathrm{exc}} \right|\right|\right|_i^2 \leq 4\pi r_i^2 C^2_{\mathrm{const}} + C_{r_i} \left|\left|\left| \mathbb{P}^\perp_{0,i} \gamma_i^- \phi_{i,\mathrm{exc}} \right|\right|\right|^2_{H^{\frac{3}{2}}(\partial\Omega_i)}.$$

Moreover, since C_{const} depends on the radius r_i and the coefficients $[\phi_i]_1^m$, $m \in \{-1,0,1\}$, we can deduce the existence of yet another constant $\widetilde{C_{r_i}} > 0$ also depending only r_i such that

$$\left|\left|\left| \gamma_i^- \left(\boldsymbol{E}_i\right)_\alpha \right|\right|\right|_i^2 \leq \widetilde{C_{r_i}} \left|\left|\left| \mathbb{P}^\perp_{0,i} \gamma_i^- \phi_{i,\mathrm{exc}} \right|\right|\right|^2_{H^{\frac{3}{2}}(\partial\Omega_i)}.$$

□

Next, we present a similar estimate on the so-called "lower order" modes of the excluded electric fields. The importance of this result can be seen by examining Definition 5.17 of the approximate electrostatic forces and observing that these are defined using *only the lower order modes* of the excluded electric fields.

Lemma 5.31 (Estimate for the Lower Modes of the Excluded Electric Field)**.** *Let $\sigma \in H^{-\frac{1}{2}}(\partial\Omega)$ be a given charge distribution and for each $i \in \{1,\ldots,N\}$ let $\phi_{i,\mathrm{exc}} \in H^1_{\mathrm{loc}}(\mathbb{R}^3)$ and $\boldsymbol{E}_i \in L^2_{\mathrm{loc}}(\mathbb{R}^3;\mathbb{R}^3)$ denote, respectively, the i excluded electric potential and electric field generated by σ as defined through Definition 5.11. Then for all $i \in \{1,\ldots,N\}$ there exists a constant $\widetilde{C_{r_i}} > 0$ that depends only on the radius r_i of the open ball Ω_i such that for each $\alpha = 1,2,3$ it holds that*

$$\left|\left|\left| \mathbb{P}_{\ell_{\max},i} \gamma_i^- \left(\boldsymbol{E}_i\right)_\alpha \right|\right|\right|_i^2 \leq \widetilde{C_{r_i}} \left|\left|\left| \mathbb{P}_{\ell_{\max}+1,i} \mathbb{P}^\perp_0 \gamma_i^- \phi_{i,\mathrm{exc}} \right|\right|\right|^2_{H^{\frac{3}{2}}(\partial\Omega_i)}.$$

Proof. The proof is essentially identical to the proof of Lemma 5.29 with one modification. For the sake of brevity therefore, we present only the main steps. Indeed, repeating the steps of the proof of Lemma 5.29 we arrive at Equation (5.9) which states that for all $\mathbf{x} \in \overline{\Omega_i}$ it holds that

$$\left(\partial_\alpha \phi_{i,\mathrm{exc}}\right)(\mathbf{x}) = \sum_{\ell=0}^{\infty} \sum_{m=-\ell}^{m=\ell} \frac{1}{r_i^\ell} [\phi_i]_\ell^m \, \partial_\alpha \left(|\mathbf{x}-\mathbf{x}_i|^\ell \mathcal{Y}_\ell^m \left(\frac{\mathbf{x}-\mathbf{x}_i}{|\mathbf{x}-\mathbf{x}_i|} \right) \right).$$

Notice that this series expansion can be written as the sum of two terms. Indeed, we define $\xi \in C^\infty(\overline{\Omega_i})$ as

$$\xi(\mathbf{x}) := \sum_{\ell=\ell_{\max}+2}^{\infty} \sum_{m=-\ell}^{m=\ell} \frac{1}{r_i^\ell} [\phi_i]_\ell^m \, \partial_\alpha \left(|\mathbf{x}-\mathbf{x}_i|^\ell \mathcal{Y}_\ell^m \left(\frac{\mathbf{x}-\mathbf{x}_i}{|\mathbf{x}-\mathbf{x}_i|} \right) \right).$$

so that for all $\mathbf{x} \in \overline{\Omega_i}$ it holds that

$$\big(\partial_\alpha \phi_{i,\mathrm{exc}}\big)(\mathbf{x}) = \sum_{\ell=0}^{\ell_{\max}+1} \sum_{m=-\ell}^{m=\ell} \frac{1}{r_i^\ell} [\phi_i]_\ell^m \, \partial_\alpha \left(|\mathbf{x}-\mathbf{x}_i|^\ell \mathcal{Y}_\ell^m \left(\frac{\mathbf{x}-\mathbf{x}_i}{|\mathbf{x}-\mathbf{x}_i|} \right) \right) + \xi(\mathbf{x}).$$

We now claim that $\mathbb{P}_{\ell_{\max},i} \gamma_i^- \xi = 0$. Indeed, as argued in the proof of Lemma 5.29, the function $|\mathbf{x}-\mathbf{x}_i|^\ell \mathcal{Y}_\ell^m \left(\frac{\mathbf{x}-\mathbf{x}_i}{|\mathbf{x}-\mathbf{x}_i|} \right)$ is a homogenous, harmonic polynomial of degree ℓ in the variables $(\mathbf{x}-\mathbf{x}_i)_\alpha$, $\alpha = 1,2,3$. This implies that for $\ell \geq 1$ the partial derivative $\partial_\alpha \left(|\mathbf{x}-\mathbf{x}_i|^\ell \mathcal{Y}_\ell^m \left(\frac{\mathbf{x}-\mathbf{x}_i}{|\mathbf{x}-\mathbf{x}_i|} \right) \right)$ is a homogenous, harmonic polynomial of degree $\ell - 1$ in $(\mathbf{x} - \mathbf{x}_i)_\alpha$, $\alpha = 1,2,3$. Consequently, we obtain the existence of coefficients $[d]_\ell^m$, $\ell \geq 1$, $-\ell \leq m \leq \ell$ such that the function ξ can be written as

$$\xi(\mathbf{x}) = \sum_{\ell=\ell_{\max}+1}^{\infty} \sum_{m=-\ell}^{m=\ell} \frac{1}{r_i^\ell} [d]_\ell^m |\mathbf{x}-\mathbf{x}_i|^\ell \mathcal{Y}_\ell^m \left(\frac{\mathbf{x}-\mathbf{x}_i}{|\mathbf{x}-\mathbf{x}_i|} \right) \quad \forall \mathbf{x} \in \overline{\Omega_i},$$

and therefore $\mathbb{P}_{\ell_{\max},i} \gamma_i^- \xi = 0$ as claimed.

The remainder of the proof is now essentially identical to the proof of Lemma 5.29 with obvious changes. Indeed, repeating the arguments we presented previously, we arrive at the inequality:

$$\left|\left|\left| \mathbb{P}_{\ell_{\max},i} \gamma_i^- \big(\boldsymbol{E}_i\big)_\alpha \right|\right|\right|_i^2 \leq \widetilde{C_{r_i}} \left|\left|\left| \mathbb{P}_{\ell_{\max}+1,i} \mathbb{P}_{0,i}^\perp \gamma_i^- \phi_{i,\mathrm{exc}} \right|\right|\right|_{H^{\frac{3}{2}}(\partial\Omega_i)}^2,$$

where the constant $\widetilde{C_{r_i}}$ is defined as in the proof of Lemma 5.29. □

In fact, Lemmas 5.29 and 5.31 are the only tools required to prove Theorem 5.22 on the approximability of the electrostatic forces. In order to prove Theorem 5.24 however, we require an additional result, which follows as a straightforward corollary of Lemmas 5.29 and 5.31 in the special case when the charge distribution σ satisfies $\sigma \in H^s(\partial\Omega)$ for some $s \geq \frac{1}{2}$.

Corollary 5.32 (Estimates in terms of Induced Surface Charges)**.**
Let $s \geq \frac{1}{2}$. Let $\sigma \in H^s(\partial\Omega)$ be a given charge distribution and for each $i \in \{1,\ldots,N\}$ let $\boldsymbol{E}_i \in L^2_{\mathrm{loc}}(\mathbb{R}^3;\mathbb{R}^3)$ denote the i excluded electric field generated by σ as defined through Definition 5.11. Then there exists a constant $C_{field} > 0$ that depends only on the radii $\{r_j\}_{i=1}^N$ of the open balls $\{\Omega_j\}_{i=1}^N$ such that for each $\alpha = 1,2,3$ the following hold:

$$\sum_{i=1}^N \left|\left|\left| \gamma_i^- \big(\boldsymbol{E}_i\big)_\alpha \right|\right|\right|_i^2 \leq C_{\mathrm{field}} \left(\left|\left|\left| \mathbb{P}_0^\perp \mathcal{V}\sigma \right|\right|\right|_{H^{\frac{3}{2}}(\partial\Omega)}^2 + \left|\left|\left| \mathbb{Q}_0^\perp \sigma \right|\right|\right|^2 \right), \tag{5.11}$$

$$\begin{aligned}\sum_{i=1}^N \left|\left|\left| \mathbb{P}_{\ell_{\max},i} \gamma_i^- \big(\boldsymbol{E}_i\big)_\alpha \right|\right|\right|_i^2 \leq C_{\mathrm{field}} &\left(\frac{\ell_{\max}+1}{\min r_i} \right)^2 \\ &\cdot \left(\left|\left|\left| \mathbb{P}_{\ell_{\max}+1} \mathbb{P}_0^\perp \mathcal{V}\sigma \right|\right|\right|^2 + \left(\left|\left|\left| \mathbb{Q}_{\ell_{\max}+1} \mathbb{Q}_0^\perp \sigma \right|\right|\right|^* \right)^2 \right).\end{aligned} \tag{5.12}$$

Proof. We first prove the estimate (5.11). Let $\lambda := \mathcal{V}\sigma \in H^{\frac{1}{2}}(\partial\Omega)$, let $i \in \{1, \dots, N\}$ be fixed, let $\phi_{i,\mathrm{exc}} \in H^1_{\mathrm{loc}}(\mathbb{R}^3)$ be the i excluded electric potential, let $\sigma_i := \sigma|_{\partial\Omega_i}$, and let $\widetilde{\sigma_i} \in H^{-\frac{1}{2}}(\partial\Omega)$ be defined as

$$\widetilde{\sigma_i} = \begin{cases} \sigma_i & \text{on } \partial\Omega_i, \\ 0 & \text{otherwise.} \end{cases}$$

By definition of the i excluded electric potential $\phi_{i,\mathrm{exc}}$, we have that

$$\gamma_i^- \phi_{i,\mathrm{exc}} = \mathcal{V}\big(\sigma - \widetilde{\sigma_i}\big).$$

Thus, Lemma 5.29 together with the triangle inequality yields that

$$\begin{aligned} \left|\left|\left|\gamma_i^-\left(\boldsymbol{E}_i\right)_\alpha\right|\right|\right|_i^2 &\leq \widetilde{C_{r_i}} \left|\left|\left|\mathbb{P}_{0,i}^\perp \gamma_i^- \phi_{i,\mathrm{exc}}\right|\right|\right|^2_{H^{\frac{3}{2}}(\partial\Omega_i)} \\ &\leq 2\widetilde{C_{r_i}} \left(\left|\left|\left|\mathbb{P}_{0,i}^\perp \mathcal{V}\sigma\right|\right|\right|^2_{H^{\frac{3}{2}}(\partial\Omega_i)} + \left|\left|\left|\mathbb{P}_{0,i}^\perp \mathcal{V}\widetilde{\sigma_i}\right|\right|\right|^2_{H^{\frac{3}{2}}(\partial\Omega_i)} \right). \end{aligned}$$

Notice that this step is valid only because we have assumed that $\sigma \in H^s(\partial\Omega)$ for some $s \geq \frac{1}{2}$ which implies that $\mathcal{V}\sigma \in H^{\frac{3}{2}}(\partial\Omega)$ (see, e.g., Remark 1.26 in Section 1.4 for a justification of this increased regularity).

It remains to simplify the second term in the above estimate. To this end, we observe that in view of Definition 3.10, there exist coefficients $[\sigma_i]_\ell^m$, $\ell \in \mathbb{N}_0$, $-\ell \leq m \leq \ell$ satisfying suitable decay properties such that for all $\mathbf{x} \in \partial\Omega_i$ it holds that

$$\widetilde{\sigma_i}(\mathbf{x}) = \sigma_i(\mathbf{x}) = \sum_{\ell=0}^{\infty} \sum_{m=-\ell}^{m=\ell} [\sigma_i]_\ell^m \mathcal{Y}_\ell^m \left(\frac{\mathbf{x} - \mathbf{x}_i}{|\mathbf{x} - \mathbf{x}_i|} \right).$$

Using the fact that $\widetilde{\sigma_i}$ is supported only on the sphere $\partial\Omega_i$ and the spherical harmonics are eigenfunctions of the single layer boundary operator on the sphere (see, e.g., [42, 205]) we obtain that

$$\big(\mathcal{V}\widetilde{\sigma_i}\big)(\mathbf{x}) = \sum_{\ell=0}^{\infty} \sum_{m=-\ell}^{m=\ell} \frac{r_i}{2\ell+1} [\sigma_i]_\ell^m \mathcal{Y}_\ell^m \left(\frac{\mathbf{x} - \mathbf{x}_i}{|\mathbf{x} - \mathbf{x}_i|} \right).$$

A direct calculation now shows that $\left|\left|\left|\mathbb{P}_{0,i}^\perp \gamma_i^- \mathcal{V}\widetilde{\sigma_i}\right|\right|\right|^2_{H^{\frac{3}{2}}(\partial\Omega_i)} \leq \left|\left|\left|\mathbb{Q}_{0,i}^\perp \sigma_i\right|\right|\right|_i^2$. Consequently, we obtain that

$$\left|\left|\left|\gamma_i^-\left(\boldsymbol{E}_i\right)_\alpha\right|\right|\right|_i^2 \leq 2\widetilde{C_{r_i}} \left(\left|\left|\left|\mathbb{P}_{0,i}^\perp \mathcal{V}\sigma\right|\right|\right|^2_{H^{\frac{3}{2}}(\partial\Omega_i)} + \left|\left|\left|\mathbb{Q}_{0,i}^\perp \sigma_i\right|\right|\right|_i^2 \right).$$

Defining the constant $C_{\mathrm{field}} := 2 \max_{i=1,\dots,N} \widetilde{C_{r_i}}$ and taking the sum over all $i \in \{1, \dots, N\}$ yields the estimate (5.11). The estimate (5.12) can be deduced by repeating the above arguments and using the equivalence of norms on the space $W^{\ell_{\max}}$. □

We are now ready to state the proofs of Theorem 5.22 and Theorem 5.24.

***Proof of Theorem** 5.22.* Let $i \in \{1, \dots, N\}$ be fixed. Let $\boldsymbol{E}_i \in L^2_{\mathrm{loc}}(\mathbb{R}^3;\mathbb{R}^3)$ and $\boldsymbol{E}_i^{\ell_{\max}} \in L^2_{\mathrm{loc}}(\mathbb{R}^3;\mathbb{R}^3)$ denote the i excluded electric fields generated by the charge distributions ν and $\nu_{\ell_{\max}}$ respectively as defined through Definition 5.11. Furthermore, let $\phi_{i,\mathrm{exc}}$ and $\phi_{i,\mathrm{exc}}^{\ell_{\max}} \in H^1_{\mathrm{loc}}(\mathbb{R}^3)$ denote the i excluded exact and approximate electric potentials generated by the charge distributions ν and $\nu_{\ell_{\max}}$ respectively as defined through Definition 5.11. Finally, let $\nu_i := \nu|_{\partial\Omega_i}$ and $\nu_i^{\ell_{\max}} := \nu_{\ell_{\max}}|_{\partial\Omega_i}$.

Definitions 5.14 and 5.17 of the exact and approximate net forces then yield that for each $\alpha = 1, 2, 3$ it holds

$$\begin{aligned}
\left|(\boldsymbol{F}_i)_\alpha - \left(\boldsymbol{F}_i^{\ell_{\max}}\right)_\alpha\right| &= \left| \left\langle \nu_i, \gamma_i^-\left(\boldsymbol{E}_i\right)_\alpha \right\rangle_{H^{-\frac{1}{2}}(\partial\Omega_i)\times H^{\frac{1}{2}}(\partial\Omega_i)} \right. \\
&\quad \left. - \left\langle \nu_i^{\ell_{\max}}, \gamma_i^-\left(\boldsymbol{E}_i^{\ell_{\max}}\right)_\alpha \right\rangle_{H^{-\frac{1}{2}}(\partial\Omega_i)\times H^{\frac{1}{2}}(\partial\Omega_i)} \right| \\
&\leq \underbrace{\left| \left\langle \nu_i - \nu_i^{\ell_{\max}}, \gamma_i^-\left(\boldsymbol{E}_i\right)_\alpha \right\rangle_{H^{-\frac{1}{2}}(\partial\Omega_i)\times H^{\frac{1}{2}}(\partial\Omega_i)} \right|}_{:=(\mathrm{I})} \\
&\quad + \underbrace{\left| \left\langle \nu_i^{\ell_{\max}}, \gamma_i^-\left(\boldsymbol{E}_i - \boldsymbol{E}_i^{\ell_{\max}}\right)_\alpha \right\rangle_{H^{-\frac{1}{2}}(\partial\Omega_i)\times H^{\frac{1}{2}}(\partial\Omega_i)} \right|}_{:=(\mathrm{II})}.
\end{aligned}$$

Let us first consider the term (I). The Cauchy-Schwarz inequality yields that

$$(\mathrm{I}) \leq |||\nu_i - \nu_i^{\ell_{\max}}|||_i^* \; |||\gamma_i^-\left(\boldsymbol{E}_i\right)_\alpha|||_i.$$

Using Lemma 5.29 we further obtain

$$(\mathrm{I}) \leq \sqrt{\widetilde{C_{r_i}}}|||\nu_i - \nu_i^{\ell_{\max}}|||_i^* \; |||\mathbb{P}_{0,i}^\perp \gamma_i^- \phi_{i,\mathrm{exc}}|||_{H^{\frac{3}{2}}(\partial\Omega_i)}.$$

It is well known that the trace operator $\gamma_i^- \colon H^2(\Omega_i) \to H^{\frac{3}{2}}(\partial\Omega)$ is continuous (see Remark 1.7 in Section 1.3 or, e.g., [147, Chapter 3]). Denoting by $C_{\mathrm{trace,i}}$ the continuity constant, we obtain

$$(\mathrm{I}) \leq \sqrt{C_{\mathrm{trace,i}}^2 \widetilde{C_{r_i}}} \; |||\nu_i - \nu_i^{\ell_{\max}}|||_i^* \; \|\phi_{i,\mathrm{exc}}\|_{H^2(\Omega_i)}.$$

Let us now focus on the term (II). Notice that $\nu_i^{\ell_{\max}} \in W^{\ell_{\max}}(\partial\Omega_i)$. Consequently, it holds that

$$\begin{aligned}
(\mathrm{II}) &= \left| \left\langle \nu_i^{\ell_{\max}}, \mathbb{P}_{\ell_{\max},i}\gamma_i^-\left(\boldsymbol{E}_i - \boldsymbol{E}_i^{\ell_{\max}}\right)_\alpha \right\rangle_{H^{-\frac{1}{2}}(\partial\Omega_i)\times H^{\frac{1}{2}}(\partial\Omega_i)} \right| \\
&\leq |||\nu_i^{\ell_{\max}}|||_i^* \; |||\mathbb{P}_{\ell_{\max},i}\gamma_i^-\left(\boldsymbol{E}_i - \boldsymbol{E}_i^{\ell_{\max}}\right)_\alpha|||_i
\end{aligned}$$

Due to the linearity of the underlying operators, we can use Lemma 5.31 to obtain

$$\begin{aligned}\text{(II)} &\leq \sqrt{\widetilde{C_{r_i}}}\,|||\nu_i^{\ell_{\max}}|||_i^* \,\big|\big|\big|\mathbb{P}_{0,i}^{\perp}\gamma_i^-\big(\phi_{i,\mathrm{exc}}-\phi_{i,\mathrm{exc}}^{\ell_{\max}}\big)\big|\big|\big|_{H^{\frac{3}{2}}(\partial\Omega_i)}\\ &\leq \sqrt{C_{\mathrm{trace,i}}^2\widetilde{C_{r_i}}}\,|||\nu_i^{\ell_{\max}}|||_i^* \,\big\|\phi_{i,\mathrm{exc}}-\phi_{i,\mathrm{exc}}^{\ell_{\max}}\big\|_{H^2(\Omega_i)}.\end{aligned}$$

Next, we consider the function $\phi_{i,\mathrm{exc}}$. Let $\mathbf{y}\in\Omega_i$ be fixed. Simple calculus reveals that for any $\alpha,\beta\in\{1,2,3\}$ we have

$$\phi_{i,\mathrm{exc}}(\mathbf{y})=\sum_{\substack{j=1\\ j\neq i}}^{N}\int_{\partial\Omega_j}\frac{\nu_j(\mathbf{x})}{|\mathbf{x}-\mathbf{y}|}\,d\mathbf{x},\quad \big(\partial_\alpha\phi_{i,\mathrm{exc}}\big)(\mathbf{y})=\sum_{\substack{j=1\\ j\neq i}}^{N}\int_{\partial\Omega_j}\frac{\nu_j(\mathbf{x})\big(\mathbf{x}-\mathbf{y}\big)_\alpha}{|\mathbf{x}-\mathbf{y}|^3}\,d\mathbf{x},$$
$$\big(\partial_\beta\partial_\alpha\phi_{i,\mathrm{exc}}\big)(\mathbf{y})=\sum_{\substack{j=1\\ j\neq i}}^{N}\int_{\partial\Omega_j}\frac{3\nu_j(\mathbf{x})\big(\mathbf{x}-\mathbf{y}\big)_\alpha\big(\mathbf{x}-\mathbf{y}\big)_\beta}{|\mathbf{x}-\mathbf{y}|^5}-\frac{\delta_{\alpha\beta}\,\nu_j(\mathbf{x})}{|\mathbf{x}-\mathbf{y}|^3}\,d\mathbf{x}.$$

Notice that the sum in each case is over all spheres $\partial\Omega_j$, $j=1,\ldots,N$ with $j\neq i$ whereas $\mathbf{y}\in\partial\Omega_i$. Consequently, the kernel in each integral is infinitely smooth and we can, for instance, write

$$|\phi_{i,\mathrm{exc}}(\mathbf{y})|^2\leq\sum_{\substack{j=1\\ j\neq i}}^{N}\Big|\int_{\partial\Omega_j}\frac{\nu_j(\mathbf{x})}{|\mathbf{x}-\mathbf{y}|}\,d\mathbf{x}\Big|^2\leq\sum_{\substack{j=1\\ j\neq i}}^{N}|||\nu_j|||_j^{*2}\Big|\Big|\Big|\frac{1}{|\cdot-\mathbf{y}|}\Big|\Big|\Big|_j^2,$$

where the norm $\Big|\Big|\Big|\frac{1}{|\cdot-\mathbf{y}|}\Big|\Big|\Big|_j^2$ is finite for each $j=1,\ldots,N$ with $j\neq i$, and depends only on the radii of the open balls and the minimum separation of the sphere $\partial\Omega_i$ from all other spheres. With this observation, it is easy to conclude that there exists a constant $K_{i,\mathrm{geom}}$ depending on the radii of the open balls and the minimum inter-sphere separation distance but independent of N such that

$$|\phi_{i,\mathrm{exc}}(\mathbf{y})|^2\leq K_{i,\mathrm{geom}}\sum_{\substack{j=1\\ j\neq i}}^{N}|||\nu_j|||_j^{*2}\leq K_{i,\mathrm{geom}}|||\nu|||^{*2}.$$

Similar considerations also apply to the derivatives of $\phi_{i,\mathrm{exc}}$. We can therefore conclude that there exists a constant $G_i>0$ depending on the radii of the open balls and the minimum inter-sphere separation distance but independent of N such that

$$\|\phi_{i,\mathrm{exc}}\|_{H^2(\Omega_i)}\leq G_i|||\nu|||^*.$$

Moreover, using linearity we similarly obtain that

$$\big\|\phi_{i,\mathrm{exc}}-\phi_{i,\mathrm{exc}}^{\ell_{\max}}\big\|_{H^2(\Omega_i)}\leq G_i|||\nu-\nu_{\ell_{\max}}|||^*.$$

Consequently, recalling the terms (I) and (II) we obtain that for each $\alpha = 1, 2, 3$ it holds that

$$\left|(\boldsymbol{F}_i)_\alpha - \left(\boldsymbol{F}_i^{\ell_{\max}}\right)_\alpha\right| \leq \text{(I)} + \text{(II)} \leq \sqrt{G_i^2 C_{\text{trace,i}}^2 \widetilde{C_{r_i}}} |||\nu_i - \nu_i^{\ell_{\max}}|||_i^* |||\nu|||^* + \sqrt{G_i^2 C_{\text{trace,i}}^2 \widetilde{C_{r_i}}} |||\nu_i^{\ell_{\max}}|||_i^* |||\nu - \nu_{\ell_{\max}}|||^*.$$

Simple calculus then yields

$$\begin{aligned}\sum_{i=1}^N \left|(\boldsymbol{F}_i)_\alpha - \left(\boldsymbol{F}_i^{\ell_{\max}}\right)_\alpha\right| &\leq \sqrt{\max_i G_i^2 C_{\text{trace,i}}^2 \widetilde{C_{r_i}}} |||\nu|||^* \sum_{i=1}^N |||\nu_i - \nu_i^{\ell_{\max}}|||_i^* \\ &\quad + \sqrt{\max_i G_i^2 C_{\text{trace,i}}^2 \widetilde{C_{r_i}}} |||\nu - \nu_{\ell_{\max}}|||^* \sum_{i=1}^N |||\nu_i^{\ell_{\max}}|||_i^* \\ &\leq \sqrt{N \max_i G_i^2 C_{\text{trace,i}}^2 \widetilde{C_{r_i}}} |||\nu - \nu_{\ell_{\max}}|||^* \left(|||\nu|||^* + |||\nu_{\ell_{\max}}|||^*\right). \end{aligned} \tag{5.13}$$

The conclusion now follows by applying the error estimates for the induced surface charge given by Theorem 3.12 in Chapter 3. □

Remark 5.33. Consider the proof of Theorem 5.22. Although Inequality (5.13) can be used in conjunction with the error estimates for the induced surface charge given by Theorem 3.12 in Chapter 3 in order to derive error estimates for the electrostatic forces, the pre-factor appearing in the convergence rates will contain the term $\sqrt{N}$. An immediate consequence of this dependence is that if N increases, one must increase the number of degrees of freedom per sphere (represented by $\ell_{\max}$) in order to theoretically guarantee the same relative or average error in the electrostatic forces based on this upper bound. This would imply that the numerical method we use to obtain the forces is not linear scaling in accuracy. Fortunately, Theorem 5.24 shows that it is possible to eliminate the dependence of the convergence rates pre-factor on N if the free charge σ_f is sufficiently regular.

***Proof of Theorem** 5.24.* The proof of Theorem 5.24 is similar in spirit to the proof of Theorem 5.22. We first fix our notation.

Let $i \in \{1, \ldots, N\}$ be fixed. Let $\boldsymbol{E}_i, \boldsymbol{E}_i^{\ell_{\max}} \in L^2_{\text{loc}}(\mathbb{R}^3; \mathbb{R}^3)$ denote the i excluded electric fields generated by the charge distributions ν and $\nu_{\ell_{\max}}$ respectively as defined through Definition 5.11, and let $\nu_i := \nu|_{\partial\Omega_i}$ and $\nu_i^{\ell_{\max}} := \nu_{\ell_{\max}}|_{\partial\Omega_i}$. Arguing exactly as in the proof of Theorem 5.22, we see that for each $\alpha = 1, 2, 3$ it holds that

$$\left|(\boldsymbol{F}_i)_\alpha - \left(\boldsymbol{F}_i^{\ell_{\max}}\right)_\alpha\right| \leq |||\nu_i - \nu_i^{\ell_{\max}}|||_i^* |||\gamma_i^-\left(\boldsymbol{E}_i\right)_\alpha|||_i + |||\nu_i^{\ell_{\max}}|||_i^* |||\mathbb{P}_{\ell_{\max},i}\gamma_i^-\left(\boldsymbol{E}_i - \boldsymbol{E}_i^{\ell_{\max}}\right)_\alpha|||_i.$$

Consequently, using the Cauchy-Schwarz inequality we have

$$\sum_{i=1}^N \left|(\boldsymbol{F}_i)_\alpha - \left(\boldsymbol{F}_i^{\ell_{\max}}\right)_\alpha\right| \leq |||\nu - \nu_{\ell_{\max}}|||^* \left(\sum_{i=1}^N |||\gamma_i^-\left(\boldsymbol{E}_i\right)_\alpha|||_i^2\right)^{\frac{1}{2}}$$

$$+ |||\nu_{\ell_{\max}}|||^* \left(\sum_{i=1}^{N} |||\mathbb{P}_{\ell_{\max},i}\gamma_i^-\left(\boldsymbol{E}_i - \boldsymbol{E}_i^{\ell_{\max}}\right)_\alpha|||_i^2 \right)^{\frac{1}{2}}.$$

Next, using the linearity of the underlying operators and applying Corollary 5.32, which is now applicable since $s \geq \frac{1}{2}$ we obtain that

$$\begin{aligned}\sum_{i=1}^{N} \left|(\boldsymbol{F}_i)_\alpha - \left(\boldsymbol{F}_i^{\ell_{\max}}\right)_\alpha\right| \leq C_{\text{field}}^{\frac{1}{2}} |||\nu - \nu_{\ell_{\max}}|||^* \left(|||\mathbb{P}_0^\perp \mathcal{V}\nu|||^2_{H^{\frac{3}{2}}(\partial\Omega)} + |||\mathbb{Q}_0^\perp \nu|||^2 \right)^{\frac{1}{2}} \\ + C_{\text{field}}^{\frac{1}{2}} |||\nu_{\ell_{\max}}|||^* \left(\frac{\ell_{\max}+1}{\min r_i}\right) \Big(|||\mathbb{P}_{\ell_{\max}+1}\mathbb{P}_0^\perp \mathcal{V}(\nu - \nu_{\ell_{\max}})|||^2 \\ + |||\mathbb{Q}_{\ell_{\max}+1}\mathbb{Q}_0^\perp\left(\nu - \nu_{\ell_{\max}}\right)|||^{*2} \Big)^{\frac{1}{2}}. \quad (5.14)\end{aligned}$$

In order to simplify Inequality (5.14), we first use the triangle inequality to obtain

$$|||\nu_{\ell_{\max}}|||^* \leq |||\nu|||^* + |||\nu - \nu_{\ell_{\max}}|||^*. \quad (5.15)$$

Next, for ease of exposition, let us define the terms

$$\begin{aligned}\text{(III)} &:= |||\mathbb{P}_0^\perp \mathcal{V}\nu|||^2_{H^{\frac{3}{2}}(\partial\Omega)} + |||\mathbb{Q}_0^\perp \nu|||^2, \\ \text{(IV)} &:= |||\mathbb{P}_{\ell_{\max}+1}\mathbb{P}_0^\perp \mathcal{V}(\nu - \nu_{\ell_{\max}})|||^2 + |||\mathbb{Q}_{\ell_{\max}+1}\mathbb{Q}_0^\perp\left(\nu - \nu_{\ell_{\max}}\right)|||^{*2}.\end{aligned}$$

The term (III) can be simplified by observing that the BIE (2.3) for the induced surface charge implies that

$$\mathbb{P}_0^\perp \mathcal{V}\nu = \frac{\kappa_0}{\kappa_0 - \kappa} \mathrm{DtN}^{-1}\left(\mathbb{Q}_0^\perp \nu - \frac{1}{\kappa_0}\mathbb{Q}_0^\perp \sigma_f\right).$$

Thus, using the fact that $|||\mathrm{DtN}^{-1}\mathbb{Q}_0^\perp\sigma|||^2_{H^{\frac{3}{2}}(\partial\Omega)} = |||\mathbb{Q}_0^\perp\sigma|||^2$ for any $\sigma \in H^{-\frac{1}{2}}(\partial\Omega)$ (c.f., Definition 3.10 of the higher order norms in Chapter 3), we can conclude that there exists a constant C_{diel} depending only on the dielectric constants such that

$$\text{(III)} \leq C_{\text{diel}}^2 \left(|||\mathbb{Q}_0^\perp \nu|||^2 + |||\mathbb{Q}_0^\perp \sigma_f|||^2 \right). \quad (5.16)$$

In order to simplify (IV), we observe that the BIE (2.3) and the Galerkin discretisation (2.8) together imply that $\mathbb{Q}_0(\nu - \nu_{\ell_{\max}}) = 0$. Consequently, there exists a function $\zeta \in \breve{H}^{\frac{1}{2}}(\partial\Omega)$ such that $\zeta := \mathrm{DtN}^{-1}\nu - \nu_{\ell_{\max}}$. We therefore have

$$|||\mathbb{P}_{\ell_{\max}+1}\mathbb{P}_0^\perp \mathcal{V}(\nu - \nu_{\ell_{\max}})|||^2 \leq |||\mathbb{P}_0^\perp \mathcal{V}\mathrm{DtN}\zeta|||^2 \leq \frac{c_{\text{equiv}}^2}{c_{\mathcal{V}}} |||\zeta|||^2 = \frac{c_{\text{equiv}}^2}{c_{\mathcal{V}}} |||\mathrm{DtN}\zeta|||^{*2},$$

where the second inequality can be deduced using Lemma 1.32 in Section 1.4 following, e.g., the arguments presented in the proof of Lemma 3.16 in Chapter 3. Thus,

$$\text{(IV)} \leq \left(1 + \frac{c_{\text{equiv}}^2}{c_{\mathcal{V}}}\right) |||\nu - \nu_{\ell_{\max}}|||^{*2} \quad (5.17)$$

Using the bounds (5.15)-(5.17), we can simplify the estimate (5.14) to obtain

$$\begin{aligned}\sum_{i=1}^{N}\left|(\boldsymbol{F}_i)_\alpha-\left(\boldsymbol{F}_i^{\ell_{\max}}\right)_\alpha\right| \leq\ & C_{\text{field}}^{\frac{1}{2}}C_{\text{diel}}|||\nu-\nu_{\ell_{\max}}|||^*\Big(|||\mathbb{Q}_0^{\perp}\nu|||+|||\mathbb{Q}_0^{\perp}\sigma_f|||\Big)\\ &+C_{\text{field}}^{\frac{1}{2}}|||\nu|||^*\left(\frac{\ell_{\max}+1}{\min r_i}\right)\left(1+\frac{c_{\text{equiv}}}{\sqrt{c_{\mathcal{V}}}}\right)|||\nu-\nu_{\ell_{\max}}|||^* \qquad (5.18)\\ &+C_{\text{field}}^{\frac{1}{2}}\left(\frac{\ell_{\max}+1}{\min r_i}\right)\left(1+\frac{c_{\text{equiv}}}{\sqrt{c_{\mathcal{V}}}}\right)|||\nu-\nu_{\ell_{\max}}|||^{*2}.\end{aligned}$$

In principle, the next step is to simplify further the bound (5.18) by using the convergence rates for the induced surface charge from Theorem 3.12. However, in order to obtain a succinct final result, let us first rewrite some terms in the estimate (5.18). More precisely, using simple calculus and Definition 3.10 of the higher order norms we write for any $s \geq \frac{1}{2}$:

$$\begin{aligned}|||\mathbb{Q}_0^{\perp}\nu|||+|||\mathbb{Q}_0^{\perp}\sigma_f||| &\leq (\max r_i)^{s-\frac{1}{2}}\left(|||\nu|||_{H^s(\partial\Omega)}+|||\sigma_f|||_{H^s(\partial\Omega)}\right), \quad \text{and}\\ |||\nu|||^*\leq |||\nu|||^*+|||\sigma_f|||^* &\leq \left(1+(\max r_i)^{s+\frac{1}{2}}\right)\left(|||\nu|||_{H^s(\partial\Omega)}+|||\sigma_f|||_{H^s(\partial\Omega)}\right).\end{aligned} \qquad (5.19)$$

Using the bounds (5.19) together with the convergence rates from Theorem 3.12, we can simplify the estimate (5.18) to obtain that

$$\begin{aligned}\sum_{i=1}^{N}\left|(\boldsymbol{F}_i)_\alpha-\left(\boldsymbol{F}_i^{\ell_{\max}}\right)_\alpha\right| \leq & 2C_{\text{field}}^{\frac{1}{2}}\left(|||\nu|||^2_{H^s(\partial\Omega)}+|||\sigma_f|||^2_{H^s(\partial\Omega)}\right)\\ &\cdot\Bigg(C_{\text{charges}}C_{\text{diel}}(\max r_i)^{s-\frac{1}{2}}\left(\frac{\max r_i}{\ell_{\max}+1}\right)^{s+\frac{1}{2}}\\ &+C_{\text{charges}}\frac{\max r_i+(\max r_i)^{s+\frac{3}{2}}}{\min r_i}\left(1+\frac{c_{\text{equiv}}}{\sqrt{c_{\mathcal{V}}}}\right)\left(\frac{\max r_i}{\ell_{\max}+1}\right)^{s-\frac{1}{2}}\\ &+C_{\text{charges}}^2\frac{\max r_i}{\min r_i}\left(1+\frac{c_{\text{equiv}}}{\sqrt{c_{\mathcal{V}}}}\right)\left(\frac{\max r_i}{\ell_{\max}+1}\right)^{2s}\Bigg).\end{aligned}$$

The proof now follows by defining the constant $C_{\text{force}} > 0$ as

$$\begin{aligned}C_{\text{force}} := 2C_{\text{field}}^{\frac{1}{2}}\max\Bigg\{&C_{\text{charges}}C_{\text{diel}}(\max r_i)^{s-\frac{1}{2}},\ C_{\text{charges}}^2\frac{\max r_i}{\min r_i}\left(1+\frac{c_{\text{equiv}}}{\sqrt{c_{\mathcal{V}}}}\right),\\ &C_{\text{charges}}\frac{\max r_i+(\max r_i)^{s+\frac{3}{2}}}{\min r_i}\left(1+\frac{c_{\text{equiv}}}{\sqrt{c_{\mathcal{V}}}}\right)\Bigg\},\end{aligned}$$

and using the fact that for $s \geq \frac{1}{2}$ and $\ell_{\max}+1 > \max_{j=1,\dots,N} r_j$ it holds that

$$\left(\frac{\max r_i}{\ell_{\max}+1}\right)^{2s} \leq \left(\frac{\max r_i}{\ell_{\max}+1}\right)^{\frac{1}{2}+s} \leq \left(\frac{\max r_i}{\ell_{\max}+1}\right)^{-\frac{1}{2}+s}.$$

□

5.3 Solution Strategy and Numerical Results

The goal of this section is two-fold. First, we present a linear scaling in complexity solution strategy for computing the approximate electrostatic forces $\{\boldsymbol{F}_i^{\ell_{\max}}\}_{i=1}^N$ defined through Definition 5.17. Second, we provide numerical evidence that supports the conclusions of our theoretical results in Section 5.2.1 as well as our claim that the electrostatic forces can be computed with linear scaling (in N) computational cost.

5.3.1 Computing the electrostatic forces

In view of the discussion and results presented in Sections 5.1.2 and 5.2, the first step in the computation of the approximate electrostatic forces is obtaining the solution $\nu_{\ell_{\max}} \in W^{\ell_{\max}}$ to the Galerkin discretisation (2.8) for the approximate induced surface charge. Consequently, if we wish to obtain a linear scaling in complexity solution strategy for the computation of the approximate electrostatic forces, we *must* possess a linear scaling in complexity strategy for calculating the approximate induced surface charge $\nu_{\ell_{\max}}$. Obtaining such a strategy for the computation of the induced surface charge was discussed in detail in Chapter 3. Indeed, Theorem 4.16 of Chapter 4 states that one can use a GMRES-based solution strategy to obtain an approximation $\nu_{\ell_{\max}}^{\text{approx}} \in W^{\ell_{\max}-}$ up to a given and fixed tolerance– of $\nu_{\ell_{\max}}$ using only $\mathcal{O}(N)$ operations.

Consequently, in practice we typically compute– up to a required tolerance ϵ– an approximation $\nu_{\ell_{\max}}^{\text{approx}} \in W^{\ell_{\max}}$ of the solution $\nu_{\ell_{\max}} \in W^{\ell_{\max}}$ to the Galerkin discretisation (2.8), and we use $\nu_{\ell_{\max}}^{\text{approx}}$ rather than $\nu_{\ell_{\max}}$ to calculate the approximate electrostatic forces as defined through Definition 5.17. It is therefore important to obtain stability estimates for the approximate forces derived from the approximation $\nu_{\ell_{\max}}^{\text{approx}}$. To this end, we have the following result.

Lemma 5.34 (Stability of Forces with Respect to Linear Solver Tolerance)**.** *Let $\epsilon > 0$ and $\ell_{\max} \in \mathbb{N}$, let $\sigma_f \in H^{-\frac{1}{2}}(\partial\Omega)$ be a given free charge, let $\nu_{\ell_{\max}} \in W^{\ell_{\max}}$ be the unique solution to the Galerkin discretisation (2.8), let $\nu_{\ell_{\max}}^{\text{approx}} \in W^{\ell_{\max}}$ be an approximation to $\nu_{\ell_{\max}}$ with relative tolerance $\epsilon \ll 1$ as described in Theorem 4.16 in Chapter 4, and for each $i = 1, \ldots, N$, let $\boldsymbol{F}_i^{\ell_{\max}}$ and $\widehat{\boldsymbol{F}}_i^{\ell_{\max}}$ denote the approximate net force acting on the dielectric particle represented by Ω_i, generated by the charge distributions $\nu_{\ell_{\max}}$ and $\nu_{\ell_{\max}}^{\text{approx}}$ respectively as defined through Definition 5.17. Then there exists a constant $C_{\text{stability}} > 0$ that depends on $\ell_{\max}$, the dielectric constants, the radii of the open balls and the minimum inter-sphere separation distance but is independent of the number N of dielectric particles such that*

$$\frac{\sum_{i=1}^N \sum_{\alpha=1}^3 \left| (\boldsymbol{F}_i^{\ell_{\max}})_\alpha - (\widehat{\boldsymbol{F}}_i^{\ell_{\max}})_\alpha \right|}{|||\mathbb{Q}_0^\perp \nu_{\ell_{\max}}|||^* + |||\mathbb{Q}_0^\perp \nu|||^* + |||\mathbb{Q}_0^\perp \sigma_f|||^*} \leq \epsilon\, C_{\text{stability}} \left(|||\mathbb{Q}_0^\perp \nu_{\ell_{\max}}||| + |||\mathbb{Q}_0^\perp \sigma_f||| \right). \tag{5.20}$$

Proof. The proof of Lemma 5.34 is very similar to the proofs of Theorems 5.22 and 5.24 and relies primarily on the auxiliary lemmas stated in Section 5.2.2 together with one

result from Chapter 3.

Observe that by definition $\nu_{\ell_{\max}}$, $\nu_{\ell_{\max}}^{\text{approx}} \in W^{\ell_{\max}}$. Consequently, following the arguments presented in the proof of Theorem 5.24 which use the linearity of the underlying operators together with Corollary 5.32, we obtain that (c.f., Inequality (5.14))

$$\begin{aligned}\sum_{i=1}^{N} \left| \left(\boldsymbol{F}_i^{\ell_{\max}}\right)_\alpha - \left(\widehat{\boldsymbol{F}}_i^{\ell_{\max}}\right)_\alpha \right| \leq C_{\text{field}}^{\frac{1}{2}} \left(\frac{\ell_{\max}+1}{\min r_i}\right) \\ \left(|||\nu_{\ell_{\max}}^{\text{approx}} - \nu_{\ell_{\max}}|||^* \left(|||\mathbb{P}_{\ell_{\max}+1}\mathbb{P}_0^\perp \mathcal{V} \nu_{\ell_{\max}}|||^2 + |||\mathbb{Q}_{\ell_{\max}+1}\mathbb{Q}_0^\perp \nu_{\ell_{\max}}|||^{*2} \right)^{\frac{1}{2}} \right. \\ + |||\nu_{\ell_{\max}}^{\text{approx}}|||^* \left(|||\mathbb{P}_{\ell_{\max}+1}\mathbb{P}_0^\perp \mathcal{V}(\nu_{\ell_{\max}}^{\text{approx}} - \nu_{\ell_{\max}})|||^2 \right. \\ \left. \left. + |||\mathbb{Q}_{\ell_{\max}+1}\mathbb{Q}_0^\perp \left(\nu_{\ell_{\max}}^{\text{approx}} - \nu_{\ell_{\max}}\right)|||^{*2} \right)^{\frac{1}{2}} \right). \end{aligned} \tag{5.21}$$

In order to simplify the bound (5.21), we first define

$$\begin{aligned}\text{(T1)} &:= |||\mathbb{P}_{\ell_{\max}+1}\mathbb{P}_0^\perp \mathcal{V} \nu_{\ell_{\max}}|||^2, \\ \text{(S1)} &:= |||\mathbb{P}_{\ell_{\max}+1}\mathbb{P}_0^\perp \mathcal{V}(\nu_{\ell_{\max}}^{\text{approx}} - \nu_{\ell_{\max}})|||^2.\end{aligned}$$

The term (T1) can be simplified by first noting that

$$|||\mathbb{P}_{\ell_{\max}+1}\mathbb{P}_0^\perp \mathcal{V} \nu_{\ell_{\max}}|||^2 \leq \underbrace{|||\mathbb{P}_0^\perp \mathcal{V} \mathbb{Q}_0^\perp \nu_{\ell_{\max}}|||^2}_{:=\text{(T2)}} + \underbrace{|||\mathbb{P}_0^\perp \mathcal{V} \mathbb{Q}_0 \nu_{\ell_{\max}}|||^2}_{:=\text{(T3)}}.$$

The term (T2) can be simplified following the arguments presented in the proof of Theorem 5.24 which yielded the inequality (5.17). We thus obtain similarly that

$$\text{(T2)} = |||\mathbb{P}_0^\perp \mathcal{V} \mathbb{Q}_0^\perp \nu_{\ell_{\max}}|||^2 \leq \left(1 + \frac{c_{\text{equiv}}^2}{c_{\mathcal{V}}}\right) |||\mathbb{Q}_0^\perp \nu_{\ell_{\max}}|||^{*2}.$$

In order to simplify the term (T3), we recall that the Galerkin discretisation (2.8) implies that $\mathbb{Q}_0 \nu_{\ell_{\max}} = \frac{1}{\kappa_0}\mathbb{Q}_0 \sigma_f$. Simple algebra therefore yields that

$$\begin{aligned}\text{(T3)} = |||\mathbb{P}_0^\perp \mathcal{V} \mathbb{Q}_0 \nu_{\ell_{\max}}|||^2 &= \left|\left|\left| \frac{1}{\kappa_0} \mathbb{P}_0^\perp \mathcal{V} \mathbb{Q}_0 \sigma_f \right|\right|\right|^2 \\ &\leq 2 \underbrace{\left|\left|\left| \frac{1}{\kappa_0} \mathbb{P}_0^\perp \mathcal{V} \sigma_f \right|\right|\right|^2}_{:=\text{(T4)}} + 2 \underbrace{\left|\left|\left| \frac{1}{\kappa_0} \mathbb{P}_0^\perp \mathcal{V} \mathbb{Q}_0^\perp \sigma_f \right|\right|\right|^2}_{:=\text{(T5)}}.\end{aligned}$$

In order to simplify the term (T4), we consider the boundary integral equation (3.5) from Chapter 3 for the so-called surface electrostatic potential. Let $\lambda \in H^{\frac{1}{2}}(\partial\Omega)$ denote the unique solution to the BIE (3.5), and let the boundary integral operator

$\mathcal{A}\colon H^{\frac{1}{2}}(\partial\Omega) \to H^{\frac{1}{2}}(\partial\Omega)$ be defined as in Definition 2.8 in Section 2.3. Simple calculus then yields that

$$(\mathrm{T4}) = \left|\left|\left|\frac{1}{\kappa_0}\mathbb{P}_0^{\perp}\mathcal{V}\sigma_f\right|\right|\right|^2 = \left|\left|\left|\mathbb{P}_0^{\perp}\mathcal{A}\mathbb{P}_0^{\perp}\lambda\right|\right|\right|^2 \leq C_{\widetilde{\mathcal{A}}}^2 |||\mathbb{P}_0^{\perp}\lambda|||^2.$$

Here, $C_{\widetilde{\mathcal{A}}} > 0$ denotes the continuity constant of the operator $\mathbb{P}_0^{\perp}\mathcal{A}\mathbb{P}_0^{\perp}\colon \breve{H}^{\frac{1}{2}}(\partial\Omega) \to \breve{H}^{\frac{1}{2}}(\partial\Omega)$ as defined in Lemma 3.20. We recall that the analysis of Chapter 3 established that the continuity constant $C_{\widetilde{\mathcal{A}}}$ depends only on the dielectric constants, the radii of the open balls, and the minimum inter-sphere separation distance but is independent of the number of dielectric spheres N.

Next, using the fact that by definition $\lambda = \mathcal{V}\nu$ and recalling the arguments presented in the proof of Theorem 5.24 which yielded the inequality (5.16), we obtain

$$(\mathrm{T4}) \leq C_{\widetilde{\mathcal{A}}}^2 C_{\mathrm{diel}}^2 \left(|||\mathbb{Q}_0^{\perp}\nu|||^{*2} + |||\mathbb{Q}_0^{\perp}\sigma_f|||^{*2} \right).$$

The term (T5) can be simplified using the same argument used to obtain the bound for the term (T2). We therefore obtain

$$(\mathrm{T5}) \leq \frac{4\pi}{\kappa_0}\left(1 + \frac{c_{\mathrm{equiv}}^2}{c_{\mathcal{V}}}\right) |||\mathbb{Q}_0^{\perp}\sigma_f|||^{*2}.$$

In a similar fashion, using the fact that $\mathbb{Q}_0\left(\nu_{\ell_{\max}}^{\mathrm{approx}} - \nu_{\ell_{\max}}\right) = 0$ (see the GMRES-based solution strategy presented in Chapter 4) we obtain that

$$(\mathrm{S1}) \leq \left(1 + \frac{c_{\mathrm{equiv}}^2}{c_{\mathcal{V}}}\right) |||\nu_{\ell_{\max}}^{\mathrm{approx}} - \nu_{\ell_{\max}}|||^{*2}.$$

Inserting the bounds obtained for (T1)-(T5) and (S1) into Inequality (5.21), we obtain

$$\begin{aligned}
&\sum_{i=1}^{N} \left| \left(\boldsymbol{F}_i^{\ell_{\max}}\right)_{\alpha} - \left(\widehat{\boldsymbol{F}}_i^{\ell_{\max}}\right)_{\alpha} \right| \leq C_{\mathrm{field}}^{\frac{1}{2}} \left(\frac{\ell_{\max}+1}{\min r_i}\right) \\
&\left(|||\nu_{\ell_{\max}}^{\mathrm{approx}} - \nu_{\ell_{\max}}|||^{*} \left(\left(1 + \frac{c_{\mathrm{equiv}}}{\sqrt{c_{\mathcal{V}}}}\right) |||\mathbb{Q}_0^{\perp}\nu_{\ell_{\max}}|||^{*} + \frac{2\sqrt{2\pi}}{\sqrt{\kappa_0}} \left(1 + \frac{c_{\mathrm{equiv}}}{\sqrt{c_{\mathcal{V}}}}\right) |||\mathbb{Q}_0^{\perp}\sigma_f|||^{*} \right.\right. \\
&\qquad \left. + \sqrt{2} C_{\widetilde{\mathcal{A}}} C_{\mathrm{diel}} \left(|||\mathbb{Q}_0^{\perp}\nu|||^{*} + |||\mathbb{Q}_0^{\perp}\sigma_f|||^{*} \right) + |||\mathbb{Q}_0^{\perp}\nu_{\ell_{\max}}|||^{*} \right) \\
&\qquad + |||\nu_{\ell_{\max}}^{\mathrm{approx}}|||^{*} \left(\left(1 + \frac{c_{\mathrm{equiv}}}{\sqrt{c_{\mathcal{V}}}}\right) |||\nu_{\ell_{\max}}^{\mathrm{approx}} - \nu_{\ell_{\max}}|||^{*} \right. \\
&\qquad\qquad \left.\left. + |||\left(\nu_{\ell_{\max}}^{\mathrm{approx}} - \nu_{\ell_{\max}}\right)|||^{*} \right) \right).
\end{aligned}$$

Consequently, we can define an appropriate constant $\tilde{C}_{\text{stability}} > 0$ that depends only on $\ell_{\max}$ and the constants $C_{\text{field}}, c_{\text{equiv}}, c_{\mathcal{V}}$, and $C_{\widetilde{\mathcal{A}}} > 0$ such that

$$\sum_{i=1}^{N} \left| \left(\boldsymbol{F}_i^{\ell_{\max}}\right)_\alpha - \left(\widehat{\boldsymbol{F}}_i^{\ell_{\max}}\right)_\alpha \right| \leq \tilde{C}_{\text{stability}} |||\nu_{\ell_{\max}}^{\text{approx}} - \nu_{\ell_{\max}}|||^* \left(|||\mathbb{Q}_0^\perp \nu_{\ell_{\max}}|||^* + |||\mathbb{Q}_0^\perp \nu|||^* + |||\mathbb{Q}_0^\perp \sigma_f|||^* + |||\nu_{\ell_{\max}}^{\text{approx}}|||^* \right).$$

The remainder of the proof now follows from elementary algebra and by using the relative error tolerance of $|||\nu_{\ell_{\max}}^{\text{approx}} - \nu_{\ell_{\max}}|||^*$.

□

Remark 5.35. Consider Lemma 5.34. Essentially, this result states that if one uses an approximation $\nu_{\ell_{\max}}^{\text{approx}} \in W^{\ell_{\max}}$ to the true solution $\nu_{\ell_{\max}} \in W^{\ell_{\max}}$ of the Galerkin discretisation (2.8), with relative tolerance ϵ as detailed in Theorem 4.16, to compute the approximate electrostatic forces, then the relative error in these forces (with respect to the true approximate electrostatic forces) is bounded by ϵ times the constant $C_{\text{stability}}$, which does not explicitly depend on N. Since the tolerance ϵ can be controlled by modifying the linear solver tolerance used when computing $\nu_{\ell_{\max}}^{\text{approx}}$, it follows that for any geometrical configuration in the family of geometries $\{\Omega_{\mathcal{F}}\}_{\mathcal{F}\in\mathcal{J}}$ satisfying **GA1)-GA3)**, this relative error in the forces can be made arbitrarily small independent of the number of dielectric spheres $N_{\mathcal{F}}$.

We now state our solution strategy for computing the approximate electrostatic forces.

Solution strategy for obtaining the electrostatic forces

Given a known free charge $\sigma_f \in H^{-\frac{1}{2}}(\partial\Omega)$, the goal is to obtain for each $i \in \{1, \ldots, N\}$, the approximate net electrostatic force $\boldsymbol{F}_i^{\ell_{\max}} \in \mathbb{R}^3$ acting on the dielectric particle represented by Ω_i.

Step 1: Fix $\ell_{\max} \in \mathbb{N}$ and compute– up to some fixed tolerance– the approximate solution $\nu_{\ell_{\max}}^{\text{approx}} \in W^{\ell_{\max}}$ to the Galerkin discretisation (2.8), thereby obtaining the approximate local spherical harmonic expansion coefficients of $\nu_{\ell_{\max}}^{\text{approx}}$ on the spheres $\{\partial\Omega_i\}_{i=1}^N$. This computation can be done according to the GMRES-based solution strategy presented in Chapter 4. In view of Theorem 4.16, the computational cost of obtaining $\nu_{\ell_{\max}}^{\text{approx}}$ with a fixed and given error tolerance is $\mathcal{O}(N)$ for any geometrical configuration belonging to the family of geometries $\{\Omega_{\mathcal{F}}\}_{\mathcal{F}\in\mathcal{J}}$ satisfying **GA1)-GA3)**.

Step 2: Compute $\lambda_{\ell_{\max}}^{\text{approx}} := \mathbb{P}_{\ell_{\max}+1} \mathcal{V} \nu_{\ell_{\max}}^{\text{approx}}$. This gives access to the local spherical harmonic expansion coefficients of $\lambda_{\ell_{\max}}^{\text{approx}}$ up to order $\ell_{\max}+1$ on the spheres $\{\partial\Omega_i\}_{i=1}^N$. Notice that in view of Definition 5.17 of the approximate electrostatic force and proof of Lemma 5.31, we require only the expansion coefficients up to order $\ell_{\max}+1$. Due to the use of the FMM, the computational cost of this step is also $\mathcal{O}(N)$.

Step 3: Compute for each $\alpha = 1, 2, 3$ and all $1 \leq \ell \leq \ell_{\max} + 1$, $-\ell \leq m \leq \ell$ the partial derivatives

$$\partial_\alpha \left(|\mathbf{x}|^\ell \mathcal{Y}_\ell^m \left(\frac{\mathbf{x}}{|\mathbf{x}|} \right) \right), \quad \text{where } \mathbf{x} \in \mathbb{S}^2.$$

These partial derivatives can be computed analytically. The computational cost of this step is $\mathcal{O}(1)$.

Step 4: Using the expansion coefficients from Steps 1 and 2, the partial derivatives from Step 3, and the representation of $\partial_\alpha \phi_{i,\text{exc}}^{\text{approx}}$ given by Equation (5.9), compute for each $\alpha = 1, 2, 3$ and $i = 1, \ldots, N$, the trace $\mathbb{P}_{\ell_{\max},i} \gamma_i^- \left(\boldsymbol{E}_i^{\text{approx}} \right)_\alpha$ of the approximate i excluded electric field. This step requires $\mathcal{O}(N)$ operations.

Step 5: The approximate electrostatic forces $\{\widehat{\boldsymbol{F}}^{\ell_{\max}}\}_{i=1}^N$ acting on the dielectric particles represented by $\{\Omega_i\}_{i=1}^N$ can then be obtained by computing the integrals

$$\widehat{\boldsymbol{F}}_i^{\ell_{\max}} = \kappa_0 \int_{\partial\Omega_i} \nu_{\ell_{\max}}^{\text{approx}}(\mathbf{x}) \big(\mathbb{P}_{\ell_{\max},i} \gamma_i^- \boldsymbol{E}_i^{\text{approx}} \big)(\mathbf{x}) \, d\mathbf{x}, \quad i = 1, \ldots, N.$$

The computational cost of this step is also $\mathcal{O}(N)$. We have thus obtained $\{\widehat{\boldsymbol{F}}^{\ell_{\max}}\}_{i=1}^N$ which approximate, up to linear solver error, the required forces $\{\boldsymbol{F}^{\ell_{\max}}\}_{i=1}^N$.

We conclude this subsection by emphasising once again the key implication of Theorem 5.24 and the solution strategy stated above. Given a geometrical configuration belonging to the family of geometries $\{\Omega_\mathcal{F}\}_{\mathcal{F}\in\mathcal{J}}$ satisfying **GA1)-GA3)**, which consists of a system of $N_\mathcal{F}$ interacting dielectric particles, we can compute- up to any given error tolerance– the electrostatic forces acting on each spherical dielectric particle in $\mathcal{O}(N_\mathcal{F})$ operations. In other words our numerical method for computing the forces is linear scaling in cost. Since Theorem 5.24 yields N-independent error estimates for the electrostatic forces, the method is also N-error stable. We can therefore conclude that under the geometrical assumptions **GA1)-GA3)**, the numerical method for obtaining the electrostatic forces described in this contribution is indeed *linear scaling in accuracy*, i.e., in order to obtain the approximate forces up to a fixed average error, the computational cost scales linearly in N.

5.3.2 Numerical experiments

As mentioned in the solution strategy in Section 5.3.1, we use the FMM to compute matrix-vector products involving the global single layer boundary operator $\mathcal{V}$. This allows us to achieve the required linear scaling in cost albeit, at the cost of introducing a controllable FMM approximation error. As mentioned in Section 4.3, we use a modification of the ScalFMM library [14]. Additionally, we use the Krylov subspace solver GMRES (see, e.g., [182, 183]) to solve all underlying linear systems. In the sequel, the numerical tests one through three, which were designed to test the accuracy of our numerical algorithm were performed using a single level FMM octree and with the GMRES

tolerance set to 10^{-11}. This prevents the introduction of the FMM approximation error and linear solver error respectively.

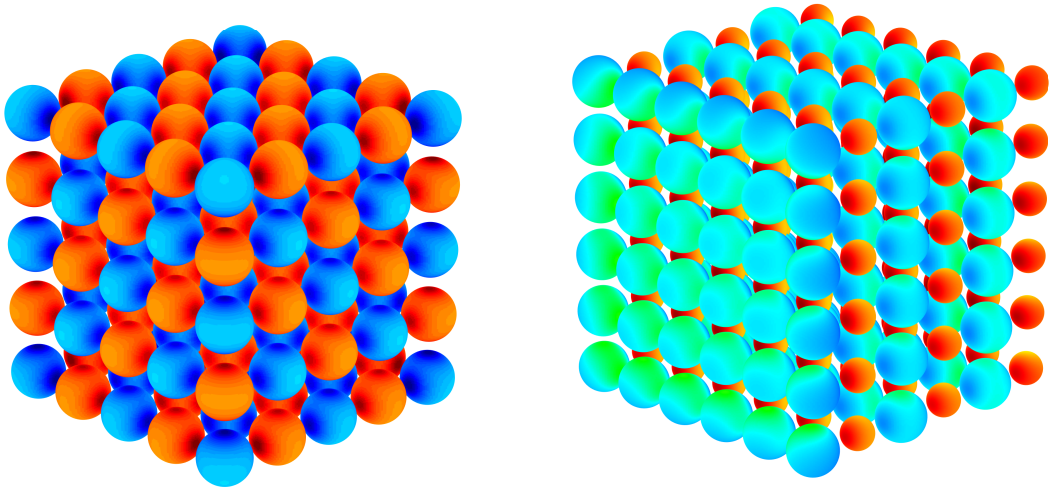

(a) Dielectric spheres with unit positive or negative charge, arranged in an alternating fashion on a three dimensional, regular cubic lattice.

(b) Dielectric spheres with unit positive or negative charge, arranged in alternating layers on a three dimensional, regular cubic lattice.

Figure 5.1: The two basic geometric settings we use for the majority of our numerical experiments. Different colours indicate the degree of polarisation with dark red indicating positive and deep blue indicating negative charge.

With one exception, the numerical experiments in this section were performed on two basic geometrical settings. Both settings consist of the same two types of dielectric spherical particles, the first with radius 3, dielectric constant 10 and carrying unit negative free charge and the second with radius 2, dielectric constant 5 and carrying unit positive free charge, arranged on a regular cubic lattice of edge length E. In the first setting however, the lattice is organised such that the positive and negatively charged particles are arranged in an alternating fashion and the edge length E is set to 6. In contrast, the lattice in the second setting is organised such that like-charged particles are arranged in layers, and we set $E = 7$. Figures 5.1a and 5.1b display the first and second types of lattice structures respectively. In both case, we assume the background medium to be vacuum so that $\kappa_0 = 1$. We remark that the total number of dielectric particles may vary from experiment to experiment.

Test 1: Exponential convergence Our first set of numerical experiments is designed to demonstrate the exponential convergence of the approximate electrostatic forces. We set the total number N of dielectric spherical particles to be 125 in the case of the first lattice (see Figure 5.1a) and 216 in the case of the second lattice (see Figure 5.1b) and compute the average error in the approximate forces $\{\boldsymbol{F}_i^{\ell_{\max}}\}_{i=1}^N$ for different values of $\ell_{\max}$. The results are displayed in Figures 5.2a and 5.2b for the first and second lattice

respectively. The reference forces $\{\boldsymbol{F}_i\}_{i=1}^N$ were obtained from the reference solution ν to the BIE (2.3), which was computed by setting the discretisation parameter $\ell_{\max} = 20$. For comparison, we have also plotted the average error in the approximate induced surface charge $\nu_{\ell_{\max}}$.

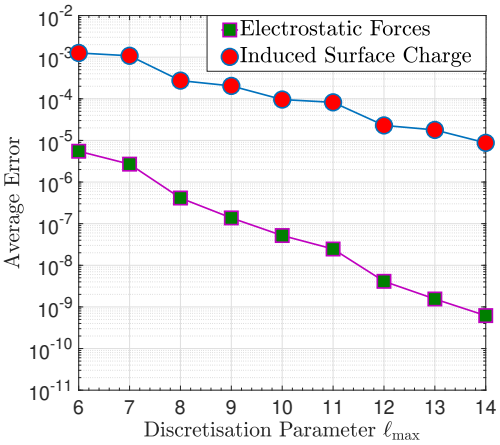

(a) Numerical results for the first type of lattice structure (Figure 5.1a).

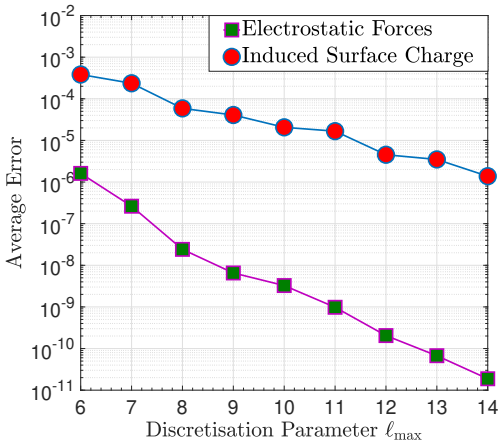

(b) Numerical results for the second type of lattice structure (Figure 5.1b).

Figure 5.2: Log-lin plots of the average error in the electrostatic forces and induced surface charge as a function of the discretisation parameter $\ell_{\max}$. For comparison, the force on each particle is $\mathcal{O}(10^{-2})$ and the charge on each sphere is $\mathcal{O}(1)$.

The numerical results displayed in Figures 5.2a and 5.2b have three key features of interest. First, we observe the exponential convergence of the approximate forces predicted by Corollary 5.26. Second, we see that the rate of convergence is slower in the case of the first lattice which has a smaller edge length E. This is in agreement with our theoretical results as we explain in the next set of numerical experiments. Finally, we observe that the convergence rates for the forces are nearly twice those (in exponential terms) of the induced surface charge. This agrees with the well-known phenomenon of the doubling of the convergence rates for linear functionals, which can be demonstrated through the so-called Aubin-Nitsche duality technique. Unfortunately, using such a duality trick leads to convergence rates for the electrostatic forces that cannot be shown to be independent of N, and we have therefore not pursued this approach.

Test 2: Dependence on the separation distance We now wish to explore in more detail, the dependence of the error in the approximate forces on the minimal inter-sphere separation distance. We recall that the pre-factor C_{force} appearing in the error estimate (5.7) for the approximate forces (see Theorem 5.24) depends both on the coercivity constant $c_{\mathcal{V}}$ of the single layer boundary operator as well as on the pre-factor C_{charges} appearing in the error estimate for the induced surface charge (see Theorem 3.12). It was shown in Chapter 3 (see Lemmas 3.22 and 3.23) that the constants $c_{\mathcal{V}}$ and C_{charges} grow *at most* as $\mathcal{O}\big(\frac{1}{\delta}\big)$ and $\mathcal{O}\big(\frac{1}{\sqrt{\delta}}\big)$ respectively for small δ where δ is the minimum inter-sphere separation distance. Consequently, we would expect the error in the approximate forces

to also grow as the inter-sphere separation decreases.

We consider two dielectric spheres placed on the z-axis at a separation of s with identical dielectric constants $\kappa_1 = \kappa_2 = 100$, fixed radius $r_1 = 1$ and varying radius r_2, and carrying unit negative and positive charge respectively. In order to obtain the true forces $\{\boldsymbol{F}_i\}_{i=1}^2$ for very small separations s, it is necessary to compute the reference solution ν to the BIE (2.3) using an extremely high value of the discretisation parameter $\ell_{\max}$. Indeed, our numerical tests indicate that an accurate approximation of the reference solution ν requires that $\ell_{\max} \approx \mathcal{O}(100)$. Our choice of geometry is thus deliberate since the axisymmetry allows us to consider an approximation space $\widetilde{W}^{\ell_{\max}} \subset W^{\ell_{\max}}$ consisting of only axisymmetric local spherical harmonics expansions.

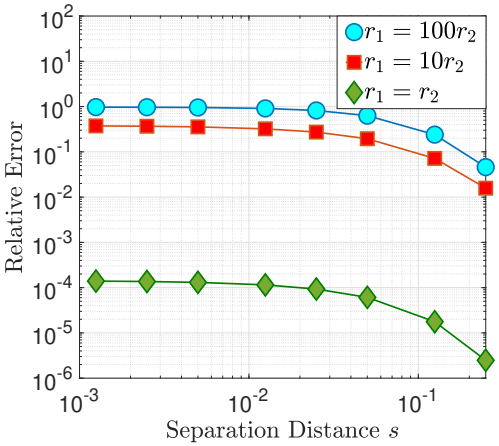

(a) Relative Error in the electrostatic forces as a function of the separation distance s.

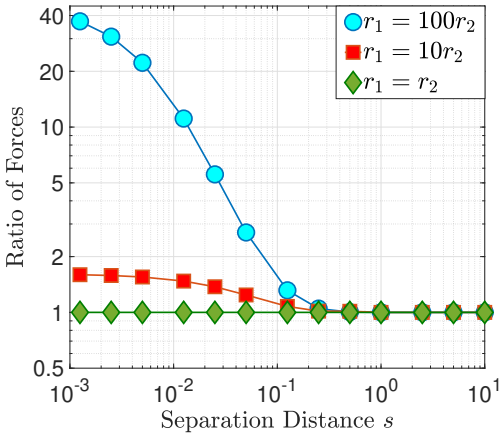

(b) Ratio of the exact and approximate forces on the first sphere as a function of the separation distance s.

Figure 5.3: The effects of the separation distance s on the approximation errors of the electrostatic forces for fixed discretisation parameter $\ell_{\max} = 10$.

Figure 5.3a displays the relative error in the approximate electrostatic forces $\{\boldsymbol{F}_i^{\ell_{\max}}\}_{i=1}^2$ for $\ell_{\max} = 10$. We immediately observe that if the radii of the two spheres are comparable, then the relative errors increase for decreasing s but quickly reach a plateau that is much smaller than one. This indicates that while the relative error in the electrostatic forces does indeed grow for decreasing separation and a fixed $\ell_{\max}$, the forces are still being approximated with a certain degree of accuracy. In contrast, we see that if $r_2 \ll 1$, then the relative errors quickly approach one for small values of s, which indicates that the approximations of the forces for this setting essentially become worthless. This conclusion is supported by Figure 5.3b where we plot the ratio of the exact and approximate force on the first sphere. We observe that the ratio remains close to one if $r_2 = r_1 = 1$ but explodes if $r_2 = 0.01$. This behaviour is explained by the fact that if $r_2 \ll 1$ and $s \to 0$, then the induced surface charge ν on the first sphere approaches a singularity at the point of contact, which is poorly represented in the approximation space $W^{\ell_{\max}}$.

Test 3: N-independence of the errors Next, we demonstrate that the average error in the approximate forces $\{\boldsymbol{F}_i^{\ell_{\max}}\}_{i=1}^N$ is independent of the number N of dielectric particles. We again consider the two types of lattices displayed in Figures 5.1a and 5.1b, and we increase N simply by increasing the size of each lattice.

Figures 5.4a and 5.4b display the average errors in the approximate electrostatic forces $\{\boldsymbol{F}_i^{\ell_{\max}}\}_{i=1^N}$ as a function of N for three choices of the discretisation parameter, namely, $\ell_{\max} = 6$, $\ell_{\max} = 9$ and $\ell_{\max} = 12$. As before, the true forces $\{\boldsymbol{F}_i\}_{i=1}^N$ were obtained from the reference solution ν to the BIE (2.3), which was calculated by setting $\ell_{\max} = 20$. Clearly the numerical results agree with the N-independent error estimate established by Theorem 5.24. We remark that since we are using the FMM with a single level octree, the computational cost of obtaining reference solutions scales as $\mathcal{O}(N^2)$ which limits the total number of spheres we consider to $N = 2197$.

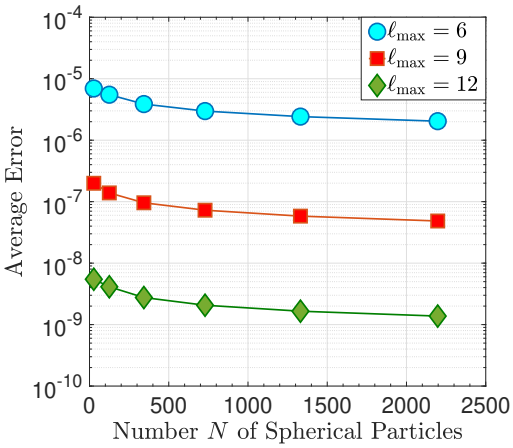

(a) Numerical results for the first type of lattice structure (Figure 5.1a).

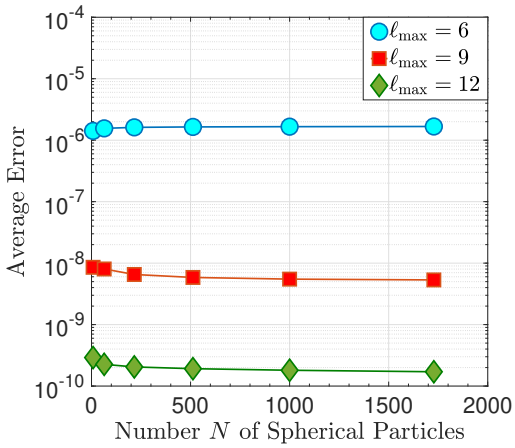

(b) Numerical results for the second type of lattice structure (Figure 5.1b).

Figure 5.4: The average errors in the electrostatic forces as a function of the number N of spherical dielectric particles. For comparison, the force on each particle is $\mathcal{O}(10^{-2})$.

Test 4: Linear scaling computation of the forces The goal of this final set of numerical experiments is to demonstrate that the approximate electrostatic forces $\{\boldsymbol{F}_i^{\ell_{\max}}\}$ can indeed be computed in $\mathcal{O}(N)$ operations for an increasing number N of dielectric spherical particles. In order to achieve this linear scaling behaviour for a given $\ell_{\max}$ and increasing N, it is necessary to carefully adjust the two main FMM parameters, i.e., the number of levels D in the octree structure of the bounding box containing all multipole sources, and the maximal degree P of spherical harmonics used in the multipole expansion of the FMM kernel.

In Section 4.3.2, we performed a detailed numerical study to obtain appropriate values of D and P for dielectric particles arranged in lattice-like configurations. As a rough guide, we proposed that

- D should be picked so that there are between 4 and 32 particles in each leaf of the FMM octree with a preferred average of 8. Note that for an increasing number N of particles, one must increase D in order to achieve the linear complexity of the FMM. On the other hand, if D is too large, then the FMM error could dominate the discretisation error leading to erroneous results.
- P should be fixed so that $P \geq 2\ell_{\max}$. Since the computational cost of each FMM call grows as $\mathcal{O}(P^3)$, it is preferable to pick P as small as possible.

Equipped with this methodology for picking the FMM parameters P and D, we compute the approximate electrostatic forces $\{\boldsymbol{F}_i^{\ell_{\max}}\}_{i=1}^N$ for the two types of lattice structures 5.1a and 5.1b and the three cases $\ell_{\max} = 6, 9$ and 12. All numerical simulations were performed on a 2016 MacBook laptop with a 2.6 GHz Intel Core i7 processor and 16GB of 2133 MHz LPDDR3 memory. Additionally, we set the linear solver tolerance to 10^{-6}, 10^{-8} and 10^{-10} and the FMM parameter P to 15, 20 and 25 in the cases $\ell_{\max} = 6$, $\ell_{\max} = 9$ and $\ell_{\max} = 12$ respectively. Our results are displayed in Figures 5.5a and 5.5b and indicate excellent agreement with linear scaling behaviour.

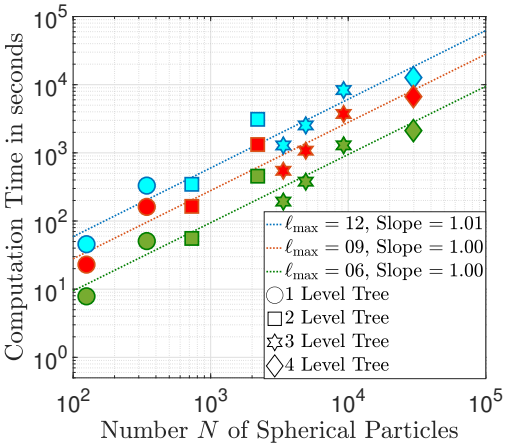

(a) Computation times for the first type of lattice structure (Figure 5.1a).

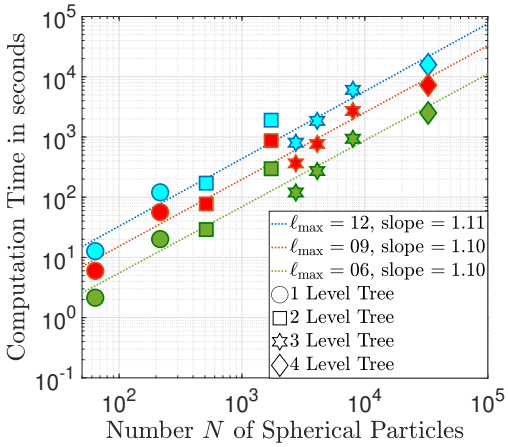

(b) Computation times for the second type of lattice structure (Figure 5.1b).

Figure 5.5: Computation times of the electrostatic forces as a function of the number N of spherical dielectric particles.

5.4 Conclusion

In this chapter, we have proposed and analysed an efficient numerical method for the computation of the electrostatic forces acting on an arbitrary number of charged, dielectric spherical particles of varying dielectric constants and radii, embedded in a homogenous polarisable medium and undergoing mutual polarisation. Our method is based on first obtaining a solution to the Galerkin discretisation (2.8) for the approximate induced surface charge resulting on these dielectric particles and using the fast multipole method

to compute matrix vector products involving the underlying solution matrix with linear scaling (in the number of particles) complexity.

Our main result is to prove that for any family of geometries $\{\Omega_{\mathcal{F}}\}_{\mathcal{F}\in\mathcal{J}}$ satisfying the assumptions **GA1)-GA3)** described in Section 2.2, the numerical method we have proposed achieves linear scaling in accuracy for the computation of the electrostatic forces, i.e., given a geometrical configuration composed of $N_{\mathcal{F}}$ dielectric spherical particles, it requires only $\mathcal{O}(N_{\mathcal{F}})$ operations to calculate the approximate forces with a given average or relative error. In order to establish this result, we derived convergence rates for the approximate forces that did not explicitly depend on the number of particles in the system. We also obtained, as a corollary of these error estimates, the exponential convergence of the approximate forces under suitable regularity assumptions. Additionally, we have provided numerical evidence that supports our theoretical results.

Part II

Domain Decomposition in Implicit Solvation Models

6

Introduction

6.1 General Context

Computational quantum chemistry is the study of the properties of matter through modelling at the molecular scale where matter is described as a collection of positively charged nuclei and negatively charged electrons. Quantum theory was first proposed and developed by the physicists Erwin Schrödinger, Werner Heisenberg, Max Born and others in the 1920s [17, 18, 99, 117, 187] but the modern mathematical formulation is due to Paul Dirac and John von Neumann [51, 158]. In quantum mechanics, the precise behaviour of matter, i.e., the behaviour of a given collection of nuclei and electrons, is described by a so-called wave function ψ that is an element of an infinite-dimensional Hilbert space $\mathbb{H}$ and that satisfies the Schrödinger equation

$$\mathcal{H}\psi = E\psi \qquad \text{(Time-independent form)}. \tag{6.1}$$

Here, $\mathcal{H}\colon D(\mathcal{H}) \to \mathbb{H}$ is the (possibly unbounded) so-called Hamiltonian operator and $E \in \mathbb{R}$ is the physical energy of the stationary system under study. The key difficulty in solving Equation (6.1) is the very high-dimensionality of the wave function ψ. Indeed, for a system composed of M nuclei and N electrons, ψ is a function of $3(N+M)$ variables in the spin-free, time-independent setting. The need to reduce the Schrödinger equation to a computationally tractable problem has led to the development of a vast literature in the past 90 years (see, e.g., [13, 56, 141, 198] for Hartree-Fock and post Hartree-Fock methods, [114, 115, 119, 163] for methods based on density functional theory, and [69, 92] for so-called quantum Monte Carlo methods). Here, we focus on one particular aspect of Equation (6.1), namely, the structure of the Hamiltonian $\mathcal{H}$, which is meant to encode the different contributions to the total energy of the system. The expression for $\mathcal{H}$ includes obvious terms such as the electrostatic interaction energy due to electron-nuclei interactions and the kinetic energy of the electrons but, depending on the physics, it may be necessary to also consider subtle secondary contributions as we discuss below.

Many physical phenomena involve the study of solute molecules embedded in a solvent, and it has been observed that certain properties of the solute molecule can change

drastically with the choice of solvent (a particularly striking example of this is the phenomenon of *solvatochromism*, see, e.g., [160, 208]). An important source of such solvation effects is the electrostatic interaction between a solute molecule and the polarisable, dielectric solvent that surrounds it. Indeed, the charge distribution on the solute molecule can produce a polarisation field inside the solvent, which in turn creates a reaction potential on the solute molecule leading to mutual polarisation. As a consequence, in order to correctly model solvation effects, one must include this so-called 'electrostatic contribution to the solvation energy' in the expression for the Hamiltonian. Attempts to correctly model the solvation energy has led to the development of an extensive literature on 'solvation models' (see. e.g., [46, 148] and the references therein) including so-called implicit solvation models which will be the chief topic of consideration in the sequel (for a brief but comprehensive overview, see e.g., [200]).

Implicit solvation models are based on the observation that practitioners are primarily interested in the properties of a given solute molecule rather than the precise state of the solvent and are therefore concerned only with properties of the solvent molecules in so far as they pertain to the solute molecule. Consequently, rather than attempting to model each individual solvent molecule in the system explicitly, one can view the solvent as a continuous medium with certain macroscopic physical properties. This assumption greatly reduces the computational complexity of the solvation model since there is now no need to prescribe explicit degree of freedom for individual solvent molecules.

Relevant implicit solvation models for this dissertation are constructed from two basic building blocks:

- The definition of the molecular cavity: In implicit solvation models, the solute molecule is typically represented as a so-called molecular cavity embedded in a continuum solvent. In mathematical terms, the molecular cavity is simply a set $\Omega \in \mathbb{R}^3$ with surface $\partial\Omega$ which results in the solvent begin described by the complement $\mathbb{R}^3 \setminus \overline{\Omega}$. Unfortunately, there is no universal consensus about how exactly the set Ω and the boundary $\partial\Omega$ should be constructed. Many definitions have been proposed in the literature including the most basic van der Waals cavity (VdW) in which each atom is represented by an open ball with an experimentally fitted radius that is obtained, for instance, from the Universal Force Field (UFF) [176]. More elaborate definitions of the solute cavity include the so-called solvent accessible surface (SAS) and the solvent excluded surface (SES). Examples of a VdW and SES cavity are displayed in Figure 6.1.

- The macroscopic properties of the continuum solvent: Depending on the physical laws that are used to describe the solute-solvent electrostatic interactions, it is possible to construct different types of implicit solvation models. In the polarisable continuum model (PCM) for instance, the solvent is modelled as a dielectric continuum (see, e.g., [22, 150, 154]) while in the COSMO model [112], the solvent is taken to be conductor-like, i.e., a medium with infinite dielectric constant. Another popular choice is the Poisson-Boltzman solvation model in which the solvent is treated as a dielectric continuum permeated by ionic charges (see, e.g., [174]).

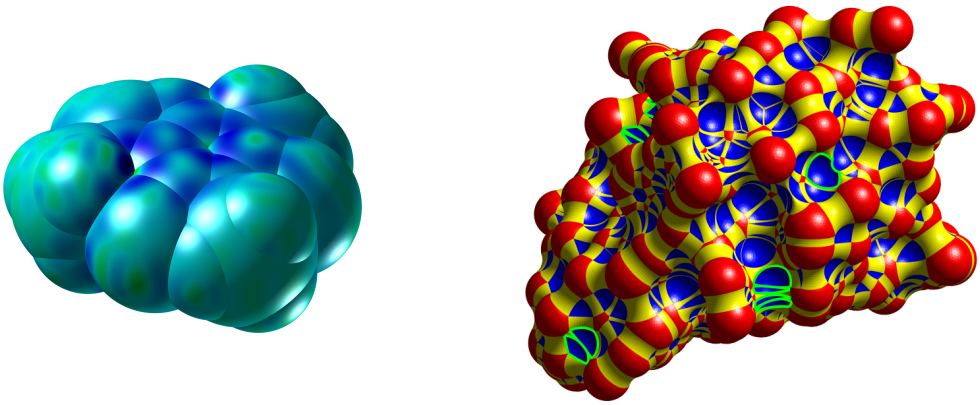

(a) The van der Waals molecular cavity of a caffeine molecule. The cavity is the union of intersecting spherical atomic cavities with each sphere corresponding to a single atom. The atomic cavities are constructed using 1.1 times the radii obtained from the Universal Force Field (UFF) [176].

(b) The SES molecular cavity of the biological molecule 1B17. Different colours indicate patches of the SES surface with different topological properties: red indicates a spherical patch, yellow indicates a toroidal patch, and blue indicates a concave patch. Reproduced with permission [172].

Figure 6.1: Examples of VdW and SES molecular cavities.

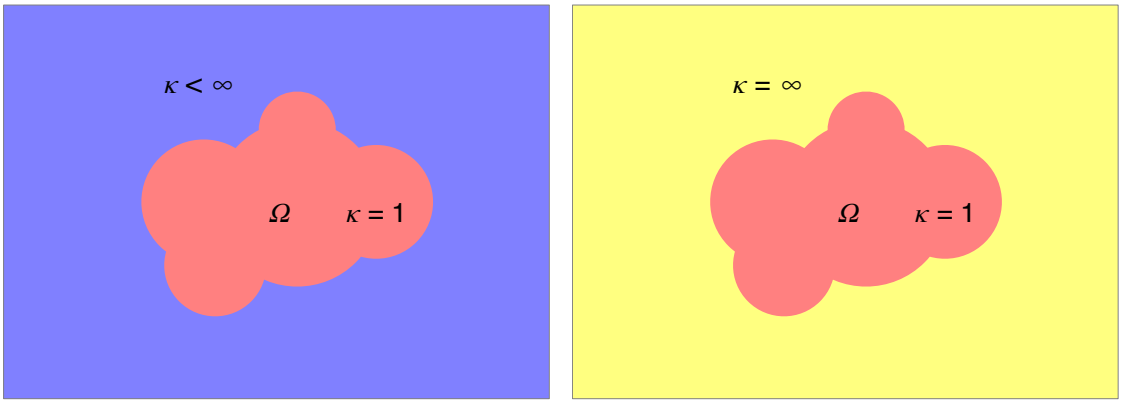

(a) The setting of the PCM Model. The solvent is modelled as a dielectric continuum with finite dielectric constant κ.

(b) The setting of the COSMO model. The solvent in this case is modelled as a conductor, i.e., a medium with infinite dielectric constant.

Figure 6.2: The PCM and COSMO models compared. The molecular cavity in both cases has been constructed using the van der Waals convention.

In this dissertation, we are primarily interested in the COSMO model, which assumes a van der Waals-type molecular cavity. In the next section, we will briefly discuss how the COSMO equations are derived in the context of so-called apparent surface charge implicit solvation models.

6.2 The COSMO Implicit Solvation Model

The following exposition is based on a contribution by Eric Cancès [200]. Throughout this section, we will assume the setting and notation of Chapter 1. To begin with, let $\Omega^- \subset \mathbb{R}^3$ be an open, bounded set with Lipschitz boundary $\partial\Omega$ and let $\Omega^+ := \mathbb{R}^3 \setminus \overline{\Omega^-}$. The set Ω^- is meant to represent the van der Waals molecular cavity of a given solute molecule. Thus, Ω^- has the following special structure: There exist $N \in \mathbb{N}$ open balls of radii $\{r_i\}_{i=1}^N$, denoted Ω_i, such that $\Omega^- = \cup_{i=1}^N \Omega_i$. An example of a typical domain Ω^- is shown in Figure 6.3. Notice that the open balls Ω_i are not disjoint.

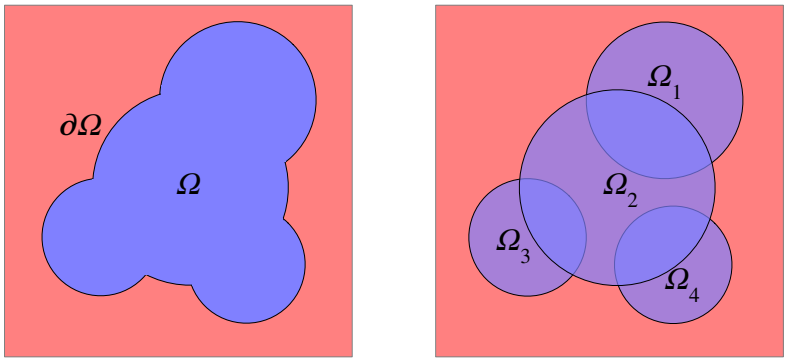

Figure 6.3: A simple example of a van der Waals molecular cavity of the type that we study in this section.

We denote by $\rho \in H^{-1}(\Omega^-)$ the charge density inside the molecular cavity. In the sequel, we always assume that the support of ρ is a proper subset of Ω^-. In particular, we assume that there is no charge distribution on the surface $\partial\Omega$ and no charge density in the solvent, i.e., in Ω^+. We further assume that the molecular cavity encloses vacuum with dielectric constant one, and that the continuum solvent is a dielectric medium with dielectric constant κ. Under these assumptions, in view of the discussion of electrostatics in dielectric media that was presented in Section 1.2, it is easy to deduce that the electric potential $\left(V^-, V^+\right) \in H^1(\Omega^-) \times H^1(\Delta; \Omega^+)$ satisfies the BVP (c.f., Equation (2.2) from Section 2.2):

$$\begin{aligned} -\Delta V^- &= \frac{\rho}{\epsilon} && \text{in } \Omega^-, \\ -\Delta V^+ &= 0 && \text{in } \Omega^+, \\ \gamma^- V^- &= \gamma^+ V^+ && \text{in } H^{\frac{1}{2}}(\partial\Omega), \\ \gamma_N^- V^- &= \kappa \gamma_N^+ V^+ && \text{in } H^{-\frac{1}{2}}(\partial\Omega). \end{aligned} \tag{6.2}$$

Since the boundary value problem (6.2) is posed on the full space $\mathbb{R}^3$, we follow the same strategy as in Part I of this dissertation, and attempt to reformulate the BVP (6.2) as an equivalent *boundary integral equation*. To this end, we first define the function $\Phi := \mathcal{N}\rho \in H^1_{\text{loc}}(\mathbb{R}^3)$ where $\mathcal{N}\colon H^{-1}_{\text{comp}}(\mathbb{R}^3) \to H^1_{\text{loc}}(\mathbb{R}^3)$ is the Newton potential as defined through Definition 1.18. Next, we define the function

$(W^-, W^+) := (V^-, V^+) - (\Phi|_{\Omega^-}, \Phi|_{\Omega^+})$. Using the properties of the Newton potential (see Lemma 1.17 and Theorem 1.23) together with the fact that ρ has compact support in Ω^-, one can conclude that the function $(W^-, W^+) \in H^1(\Omega^-) \times H^1(\Delta; \Omega^+)$ satisfies the BVP

$$\begin{aligned} -\Delta W^- &= 0 && \text{in } \Omega^-, \\ -\Delta W^+ &= 0 && \text{in } \Omega^+, \\ \gamma^- W^- &= \gamma^+ W^+ && \text{in } H^{\frac{1}{2}}(\partial\Omega), \\ \gamma_N^- W^- - \kappa \gamma_N^+ W^+ &= (\kappa - 1)\gamma_N^- \Phi && \text{in } H^{-\frac{1}{2}}(\partial\Omega). \end{aligned} \tag{6.3}$$

Using now a single layer potential ansatz (see, for instance, the proof of Lemma 2.6 in Section 1.4) yields the following boundary integral equation: Find a so-called *apparent surface charge* $\sigma \in H^{-\frac{1}{2}}(\partial\Omega)$ such that

$$\sigma - \frac{\kappa - 1}{\kappa} \mathcal{V}\mathrm{DtN}\sigma = \frac{\kappa - 1}{\kappa} \gamma_N^- \Phi \qquad \text{in } H^{-\frac{1}{2}}(\partial\Omega). \tag{6.4}$$

Here, the apparent surface charge σ is a purely mathematical construction and is related to the function (W^-, W^+) through the single layer potential $\mathcal{S}\colon H^{-\frac{1}{2}}(\partial\Omega) \to H^1_{\mathrm{loc}}(\mathbb{R}^3)$ as $(W^-, W^+) = (\mathcal{S}\sigma|_{\Omega^-}, \mathcal{S}\sigma|_{\Omega^+})$. Using now the Calderón identities (see, for instance, Lemma 1.31 in Section 2.2), Equation (6.4) can equivalently be written as

$$\frac{\kappa + 1}{2(\kappa - 1)} \sigma - \mathcal{K}^* \sigma = \gamma_N^- \Phi \qquad \text{in } H^{-\frac{1}{2}}(\partial\Omega). \tag{6.5}$$

Equation (6.5) is the DPCM equation first derived by Miertuš et al. (see [154, 199]). In a similar fashion, with Equation (6.4) or (6.5) as the starting point, one can use additional Calderón identities and jump properties of the single and double layer potentials (see, e.g., Theorem 1.23) to derive several so-called apparent surface charge methods that are used in implicit solvation modelling. This includes the original integral equation formulation (IEF) due to Cancès, Mennucci, and Tomasi [22, 149], and the IEFPCM equation (also termed SS(V)PE) derived by Mennucci, Cammi, and Tomasi (see, e.g., [150]) and independently by Daniel Chipmann [27].

The so-called COnductor-like Screening MOdel (COSMO) proposed by Klamt and Schüürmann [112] is another example of an apparent surface charge method. Under the COSMO model, the dielectric continuum solvent surrounding the molecular cavity is approximated as a conductor, i.e., one considers the limiting case $\kappa \to \infty$ of the dielectric constant. This approximation leads to a considerable simplification of the boundary integral equation (6.4). Indeed, in the COSMO framework one solves first the boundary integral equation

$$\mathcal{V}\tilde{\sigma} = -\gamma^- \Phi \qquad \text{in } H^{\frac{1}{2}}(\partial\Omega), \qquad \text{(COSMO Equation)} \tag{6.6}$$

and then approximates the true solution to Equation (6.4) as $\sigma \approx \frac{\kappa - 1}{\kappa + c}\tilde{\sigma}$, where c is an empirical scaling factor. Using the (exterior) Calderón identities (see, e.g., [185, Chapter 3.6]), it is possible to show that this approximation of the apparent surface

charge $\sigma \in H^{-\frac{1}{2}}(\partial\Omega)$ is exact in the limiting case $\kappa \to \infty$. Naturally, the key advantage of COSMO over PCM is that the BIE (6.6) is considerably simpler to solve than Equation (6.4) since it involves the coercive single layer boundary $\mathcal{V}\colon H^{-\frac{1}{2}}(\partial\Omega) \to H^{\frac{1}{2}}(\partial\Omega)$, which, in many cases, is easier and more efficient to discretise.

In the original articles that introduced them, the IEF, IEFPCM, and COSMO equations were all solved using the same basic procedure, namely, to first compute the Newton potential $\Phi := \mathcal{N}\rho$ of a given charge density ρ that is supported inside the molecular cavity Ω^-, use this to deduce the relevant boundary data on $\partial\Omega$, and then use, what essentially amounts to, a boundary element method (BEM) with a piecewise constant approximation space to solve the respective boundary integral equation (see [22, 112, 150]). This procedure, while perfectly satisfactory from a theoretical point of view, does suffer from a few computational drawbacks: First, the tessellation of the curved and usually quite complicated surface $\partial\Omega$ is a non-trivial and computationally expensive procedure and second, the linear systems that arise from the discretisation of the boundary integral equations are *dense* and not well-conditioned which increases the computational cost of computing approximate solutions. Although improvements to this BEM-based approach have subsequently been suggested including, in particular, the continuous surface charge (CSC) formalism which makes use of spherical Gaussian basis functions located at each surface element in which the cavity surface is discretised (see, e.g., [186, 211]), there was still great scope for computational improvements in apparent surface charge models. In an effort to improve the state-of-the-art, a very different approach was suggested by Cancès, Maday, and Stamm for the COSMO equation (see, e.g., [23, 135]) and later, together with Quan, for the PCM with SES and VdW molecular cavities and the linearised Poisson-Boltzmann model with a VdW molecular cavity (see [173, 174, 193]). This new approach is based on the framework of domain decomposition methods which are the topic of the next section.

6.3 Schwarz Domain Decomposition Methods

Informally, the term 'domain decomposition' refers to a general solution strategy based on splitting a partial differential equation (or its discretisation) into a collection of coupled local problems posed on subdomains that constitute a partition of the global domain. The basic motivation behind the domain decomposition strategy is rather straightforward: instead of solving a partial differential equation on a huge, possibly complex global domain, it might be computationally advantageous to solve instead the same PDE on several smaller, simpler subdomains [201, Preface]. Often these local problems can be solved in parallel which, perhaps, explains the strong correlation between the recent growth in interest in domain decomposition methods and the advent of modern high speed computing (presciently remarked by P. L. Lions in [132] and noted by M. J. Gander in [72]). It is slightly ironic therefore that the first domain decomposition method was developed purely as an *analytical tool* for proving certain results in the theory of conformal mappings.

The genesis of the domain decomposition methodology can be traced to a seminal

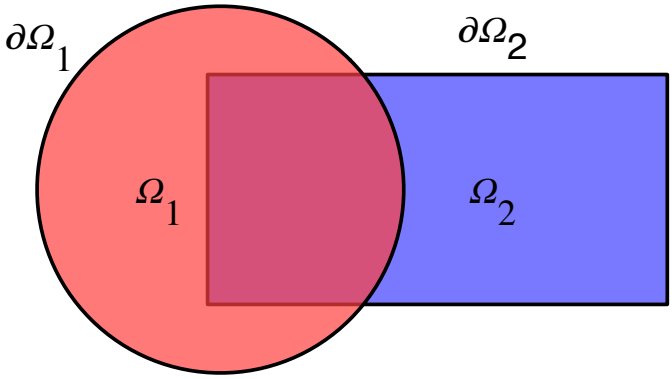

Figure 6.4: The geometry considered by Schwarz (in his original paper [189], the rectangle was in fact a square).

paper of H. A. Schwarz from 1870 [189]. Schwarz was interested in proving the existence of a minimiser in the so-called Dirichlet principle. The Dirichlet principle states that if a function u is harmonic on a bounded domain Ω with Dirichlet boundary conditions $u = g$ on $\partial\Omega$ for some $g \in C^0(\partial\Omega)$, then u attains the infimum of the Dirichlet energy functional defined as

$$\mathbb{E}(v) := \int_\Omega |\nabla v(x)|^2 \, dx \tag{6.7}$$

on the set of all functions $v \in C^1(\Omega) \cap C^0(\overline{\Omega})$ that satisfy $v = g$ on $\partial\Omega$.

The existence of a function that attains the infimum of the Dirichlet energy (6.7) for an arbitrary domain Ω and given boundary data g was taken for granted by Riemann but a counter example of a functional that does *not* attain its infimum was given by Weierstrass (this episode is discussed in [108, Chapter 8.6]). Consequently, there were attempts to derive rigorous proofs of existence for minimisers of the Dirichlet energy. Unfortunately, such proofs were initially limited to simple domains such as rectangles or disks where tools from Fourier analysis were available. It was in this context that Schwarz developed the domain decomposition methodology and used it to provide a proof of existence for more complex geometries.

In the original article [189], Schwarz considered the following problem setting: Let $\Omega_1 \subset \mathbb{R}^2$ be an an open disk, let $\Omega_2 \subset \mathbb{R}^2$ be an open rectangle such that $\Omega_1 \cap \Omega_2$ is a non-empty open set, and define $\Omega := \Omega_1 \cup \Omega_2$ as displayed in Figure 6.4. Now, given a continuous function $g \in C^0(\partial\Omega)$, the goal is to find a continuous function $u \in C^2(\Omega) \cap C^0(\overline{\Omega})$ such that

$$\begin{aligned} -\Delta u(x) &= 0 \qquad && \text{for } x \in \Omega, \\ u(x) &= g(x) && \text{for } x \in \partial\Omega. \end{aligned} \tag{6.8}$$

Schwarz's inspiration was to define an iterative procedure consisting of solving, in a successive manner, local problems on each subdomain Ω_1 and Ω_2. More precisely, starting with some initialisation $u_2^0 \in C^2(\Omega_1) \cap C^0(\overline{\Omega_1})$, Schwarz defined two sequences

of functions $\{u_1^n\}_{n\in\mathbb{N}} \subset C^2(\Omega_1)$ and $\{u_2^n\}_{n\in\mathbb{N}} \subset C^2(\Omega_2)$ such that

$$\begin{aligned}
-\Delta u_1^{n+1}(x) &= 0 && \text{for } x \in \Omega_1, & -\Delta u_2^{n+1}(x) &= 0 && \text{for } x \in \Omega_2,\\
u_1^{n+1}(x) &= g(x) && \text{for } x \in \partial\Omega_1 \cap \partial\Omega, & u_2^{n+1}(x) &= g(x) && \text{for } x \in \partial\Omega_2 \cap \partial\Omega_1,\\
u_1^{n+1}(x) &= u_2^n(x) && \text{for } x \in \partial\Omega_1 \cap \Omega_2, & u_2^{n+1}(x) &= u_1^{n+1}(x) && \text{for } x \in \partial\Omega_2 \cap \Omega_1.
\end{aligned} \tag{6.9}$$

In other words, given an initialisation u_2^0 on the subdomain Ω_2, a solution u_1^1 is constructed on Ω_1 which uses the global boundary data g on $\partial\Omega_1 \cap \partial\Omega$ and boundary data from u_2^0 on $\partial\Omega_1 \cap \Omega_2$. In the next iteration, the new solution u_2^1 on Ω_2 is constructed using the global boundary data g on $\partial\Omega_2 \cap \partial\Omega$ and boundary data from the previous iterate u_1^1 on $\partial\Omega_2 \cap \Omega_1$, and so on. Using the fact that each one of the local problems in Equation (6.9) was posed on a simple domain for which existence theory was already established and the well-known maximum principle was available, Schwarz was able to argue (not completely rigorously however) that the two sequences of functions $\{u_1^n\}_{n\in\mathbb{N}}$ and $\{u_2^n\}_{n\in\mathbb{N}}$ would converge, in the limit, to the restriction on Ω_1 and Ω_2 respectively, of the solution $u \in C^2(\Omega) \cap C^0(\overline{\Omega})$ of the global problem (6.8).

The iterative procedure defined through Equation (6.9) is known as the *alternating* Schwarz method (ASM) and is the first, most basic example of a domain decomposition method. Since its introduction by Schwarz, the ASM has been the subject of studies by numerous mathematicians and this has led to the development of a vast and quite mature literature on the theory and implementation of a variety of different domain decomposition methods (see, for instance, the excellent textbooks [54, 175, 201], the monographs [24, 72], and the references therein). A detailed discussion of the modern state of domain decomposition methods is beyond the scope our work but we wish to mention a few important developments:

- First, Schwarz domain decomposition methods have been extended to more general partial differential equations. This includes the relatively straightforward extension to any elliptic operator $\mathcal{L}$ that satisfies a maximum principle (see, e.g., [201]), as well extensions to time-dependent problems problems through so-called Schwarz waveform relaxation (see, e.g., [74]). Domain decomposition methods have also been proposed for the indefinite Helmholtz equation (see, e.g., the PhD thesis of Després [49]), and will be the subject of further discussion in Section 9.

- Second, domain decomposition methods based on *non-overlapping* subdomains have also been proposed and analysed. Indeed, Lions had already considered the case of non-overlapping subdomains in [134] and was able to show that if one replaces the Dirichlet boundary conditions on the overlap interface as in Equation (6.9), with more general *Robin*-type boundary conditions, then the resulting iterative procedure can be shown to converge using energy estimates. This idea, i.e., to replace Dirichlet interface conditions with suitable Robin-type boundary conditions has lead to the development of so-called optimised Schwarz methods (see, e.g., [71, 72, 75, 76]).

- Third, although our exposition in this section was stated in terms of classical, continuous functions, an abstract Hilbert space theory for Schwarz domain decomposition methods has also been developed. The ASM, in particular, was the subject of a series of three papers by P. L. Lions [132, 133, 134] who obtained a famous proof of convergence of the ASM using variational techniques (see also [30]). Lions, in addition, proposed a *parallel* variant of the ASM– known as the parallel Schwarz method (PSM)– which reads, for the current geometric setting as:

$$\begin{aligned} -\Delta u_1^{n+1}(x) &= 0 && \text{for } x \in \Omega_1, \\ u_1^{n+1}(x) &= g(x) && \text{for } x \in \partial\Omega_1 \cap \partial\Omega, \\ u_1^{n+1}(x) &= u_2^n(x) && \text{for } x \in \partial\Omega_1 \cap \Omega_2, \end{aligned} \qquad \begin{aligned} -\Delta u_2^{n+1}(x) &= 0 && \text{for } x \in \Omega_2, \\ u_2^{n+1}(x) &= g(x) && \text{for } x \in \partial\Omega_2 \cap \partial\Omega_1, \\ u_2^{n+1}(x) &= u_1^n(x) && \text{for } x \in \partial\Omega_2 \cap \Omega_1. \end{aligned} \tag{6.10}$$

Details on other aspects of domain decomposition methods including parallel implementation and additional computational concerns can be found in the textbooks cited above. In view of the subject of Part II of this dissertation however, we wish to highlight one particular aspect of the PSM and ASM, namely the scaling of these methods with respect to the number of subdomains in the domain decomposition. To this end, let us first state a definition due to Toselli and Widlund.

Definition 6.1 ([201, Definition 1.3])**.** Let $n \in \mathbb{N}$ and let $\Omega \subset \mathbb{R}^n$ be a fixed open and bounded set. A domain decomposition method for the solution of a partial differential equation posed on Ω is said to be *scalable*, if its rate of convergence, i.e., the number of iterations required to obtain an approximate solution with a certain residual, does not deteriorate when the number of subdomains grows.

Toselli and Widlund [201, Chapter 1.3] point out the well-established fact that, in the absence of preconditioners, classical Schwarz methods including the ASM and PSM are not scalable in the sense of Definition 6.1 (see also the discussion in [25]). Notice however, that this notion of scalability is limited to *fixed* domains Ω. The scalability properties of the PSM when the computational domain Ω is *not fixed*, i.e., when both the global domain and the number of subdomains in the decomposition are increasing, will be the key subject of our analysis in Chapter 8. First however, we will return to the setting of implicit solvation models and discuss how the PSM can be used to efficiently obtain a solution to the COSMO equation (6.6) on a molecular cavity.

6.4 ddCOSMO: A Domain Decomposition Strategy for Solving COSMO

Let us now assume the setting of Section 6.2. To simplify the subsequent exposition, we assume that the bounded open set $\Omega^- \subset \mathbb{R}^3$, which is meant to represent a van der Waals molecular cavity, is composed of precisely two intersecting spherical atomic cavities, i.e., there exist two open balls Ω_1, Ω_2 of radii $r_1, r_2 > 0$ and centres $\mathbf{x}_1, \mathbf{x}_2 \in \mathbb{R}^3$ respectively

such that $\Omega^- := \Omega_1 \cup \Omega_2$. We further assume that the molecular cavity carries a smooth charge distribution $\rho \in C_0^\infty(\Omega^-)$. The COSMO equation then reads: Find an apparent surface charge $\tilde{\sigma} \in C^\infty(\partial\Omega)$ such that

$$\mathcal{V}\tilde{\sigma}(\mathbf{x}) = -\Phi(\mathbf{x}) \qquad \text{for all } \mathbf{x} \in \partial\Omega, \tag{6.11}$$

where $\Phi := \mathcal{N}\rho \in C^\infty(\mathbb{R}^3)$ is the Newton potential (also known in this context as the Coulomb potential) generated by ρ as defined through Definition 1.18.

The key insight, which allows for a very efficient application of the parallel Schwarz method is to realise that Equation (6.11) can be reformulated as a classical boundary value problem on the bounded set Ω^- involving the Laplace equation and prescribed Dirichlet boundary conditions. Indeed, we consider the following BVP: Find a function $W \in C^\infty(\overline{\Omega})$ such that

$$\begin{aligned} -\Delta W(\mathbf{x}) &= 0 \qquad && \text{for all } \mathbf{x} \in \Omega^-, \\ W(\mathbf{x}) &= -\Phi(\mathbf{x}) && \text{for all } \mathbf{x} \in \partial\Omega. \end{aligned} \tag{6.12}$$

A straightforward calculation then shows that W is precisely the electrostatic potential generated by the apparent surface charge $\tilde{\sigma}$, i.e., $W = \mathcal{S}\tilde{\sigma}|_{\Omega^-}$. In other words, in contrast to the methodology adopted in Part I of this dissertation, we have now chosen to replace a boundary integral equation with a partial differential equation. Crucially however, the BVP (6.12) is posed on the bounded domain Ω^- which makes it much simpler to solve than the BIE (6.11). Indeed, since $\Omega^- = \Omega_1 \cup \Omega_2$, we can immediately appeal to the parallel Schwarz method described by Equation (6.10) and write the following iterative procedure for solving the BVP (6.12):

Denoting $\Gamma_1^{int} := \partial\Omega_1 \cap \Omega_2$ and $\Gamma_2^{int} := \partial\Omega_2 \cap \Omega_1$ and starting with some initialisation $(W_1^0, W_2^0) \in C^2(\Omega_1) \cap C^0(\overline{\Omega_1}) \times C^2(\Omega_2) \cap C^0(\overline{\Omega_2})$, we define two sequences of functions $\{W_1^n\}_{n\in\mathbb{N}} \subset C^2(\Omega_1)$ and $\{W_2^n\}_{n\in\mathbb{N}} \subset C^2(\Omega_2)$ such that

$$\begin{aligned} -\Delta W_1^{n+1}(\mathbf{x}) &= 0 && \text{for } \mathbf{x} \in \Omega_1, & \qquad -\Delta W_2^{n+1}(\mathbf{x}) &= 0 && \text{for } \mathbf{x} \in \Omega_2, \\ W_1^{n+1}(\mathbf{x}) &= -\Phi(\mathbf{x}) && \text{for } \mathbf{x} \in \partial\Omega_1 \cap \partial\Omega, & \qquad W_2^{n+1}(\mathbf{x}) &= -\Phi(\mathbf{x}) && \text{for } \mathbf{x} \in \partial\Omega_2 \cap \partial\Omega_1, \\ W_1^{n+1}(\mathbf{x}) &= W_2^n(\mathbf{x}) && \text{for } \mathbf{x} \in \Gamma_1^{int}, & \qquad W_2^{n+1}(\mathbf{x}) &= W_1^n(\mathbf{x}) && \text{for } \mathbf{x} \in \Gamma_2^{int}. \end{aligned} \tag{6.13}$$

The advantage of introducing this domain decomposition procedure is that each local problem in Equation (6.13) consists of solving the Laplace equation on an open ball with prescribed Dirichlet boundary data. It is well known (see, e.g., [68, Chapter 2(H)] as well as prior calculations in Section 5.2) that solutions to the Laplace equation on open balls can be written in terms of linear combinations of spherical harmonics functions multiplied with radial monomials. As a consequence, the local BVP on $\Omega_i, i \in \{1, 2\}$ given through Equation (6.13) can be approximately solved using a Galerkin method employing a basis of the form (c.f., Definition 2.10 in Section 2.3):

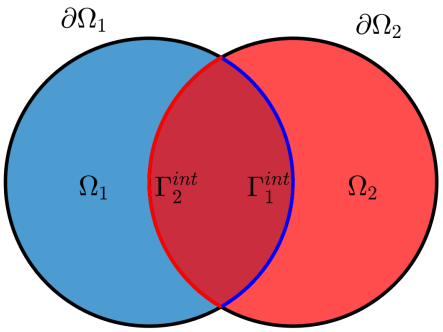

Figure 6.5: The geometrical setting for Equation (6.13). We observe that the molecular cavity Ω^- is composed of two intersecting atomic cavities Ω_1 and Ω_2.

$$\mathbb{V}_{\ell_{\max}}(\Omega_i) := \Big\{ v \colon \Omega_i \to \mathbb{R} \text{ such that } v(\mathbf{x}) = \sum_{\ell=0}^{\ell_{\max}} \sum_{m=-\ell}^{m=+\ell} [v_i]_\ell^m \left(\frac{|\mathbf{x}-\mathbf{x}_i|}{r_i} \right)^\ell \mathcal{Y}_\ell^m \left(\frac{\mathbf{x}-\mathbf{x}_i}{|\mathbf{x}-\mathbf{x}_i|} \right) \\ \text{where all } [v_i]_\ell^m \in \mathbb{R},\ \ell_{\max} \in \mathbb{N} \Big\}, \tag{6.14}$$

The parallel Schwarz method defined through Equation (6.13) which employs an approximation space of the form (6.14) and is used to solve the differential form of the COSMO equations is known as ddCOSMO.

The ddCOSMO algorithm is the subject of several articles in the literature including details on how to implement the algorithm in the context of quantum mechanics or molecular dynamics based simulations of solute molecules (see, e.g., [23, 80, 135, 137]). Numerical results in these articles indicate that the current implementation of ddCOSMO is nearly two orders of magnitude faster than state-of-the-art BEM codes thus establishing the domain decomposition paradigm as a significant advance in the state-of-the-art for solvation modelling. Some additional aspects of the ddCOSMO algorithm are discussed below:

a) ***Extension to multiple subdomains.*** The ddCOSMO algorithm defined through Equation (6.13) can be extended to molecular cavities composed of multiple overlapping spherical atomic cavities. This requires the introduction of suitable partition of unity functions on the boundary of each subdomain as discussed in detail in Chapter 8.

b) ***Implementation of ddCOSMO.*** It is pertinent to mention here that the current implementation of ddCOSMO does not actually use the iterative procedure

defined through Equation (6.13). Instead, a linear system is first constructed using a classical Galerkin procedure with local approximation spaces of the form (6.14). The solution to this linear system is then approximated using the DIIS algorithm introduced by Peter Pulay in quantum computational chemistry [169] or, alternatively, using GMRES [183]. From this perspective, the parallel Schwarz method given by Equation (6.13) can be viewed as a block-Jacobi algorithm applied to the underlying linear system.

c) ***Variational formulation and numerical analysis.*** The ddCOSMO algorithm described here has been stated in terms of classical, continuous functions for which a basic well-posedness theory (in the exact case, i.e., without introducing a discretisation) is available in the literature (see, e.g., Lions [133]). However, in order to obtain a more comprehensive well-posedness theory, it is desirable to reframe the ddCOSMO equations as a variational problem on abstract Hilbert spaces. Such a weak formulation is obviously necessary if one wishes to derive a priori error estimates for the Galerkin discretisation of ddCOSMO. Unfortunately, as of the writing of this dissertation, no satisfactory variational framework for ddCOSMO has been proposed in the literature (for technical reasons, the iterated projection framework of Lions [132] does not work in this situation). In particular, the well-posedness of the Galerkin discretisation of the ddCOSMO equations is still an open problem. The author of this dissertation has obtained some partial, unpublished results in this direction but these are far from satisfactory.

A question that becomes very relevant when one considers the context of the ddCOSMO algorithm, namely, implicit solvation modelling, is how the convergence rate of ddCOSMO is affected by the geometry of the solute molecule. In particular, how does the convergence rate of ddCOSMO behave when the number N of subdomains, i.e., spherical atomic cavities, composing the molecular cavity increases? In contrast to the consensus in the domain decomposition community (see the scalability discussion in Section 6.3), numerical results in [23] indicated that the convergence rate of ddCOSMO for many solute molecules did *not* deteriorate with increasing N. It is important to note that in this situation, the global domain Ω which describes the molecular cavity is *not fixed*. Instead both the size of Ω as well as the number of subdomains N is increasing, and the problem setting is therefore different from the one typically considered by the domain decomposition community and used to define the classical notion of scalability (see Definition 6.1).

The goal of Part II of this dissertation is to present some results on the convergence behaviour and scalability properties of the parallel Schwarz method for domain decomposition problems on domains composed of the union of many intersecting spherical subdomains. In order to highlight the novelty of our subsequent work, we present in the next Section 6.5 a brief overview of the existing literature on the scalability of Schwarz methods and discuss how our results improve the existing state-of-the-art.

6.5 Existing Literature on the Scalability of Domain Decomposition Methods

We begin this section by introducing a notion from the theory of parallel computing that is particularly relevant to discussions of scalability in the context of ddCOSMO.

Definition 6.2 (Weak scalability [161, Chapter 3.6])**.** A parallel computing algorithm is said to be weakly scalable if it can solve progressively larger problems using an increasing number of processors in a fixed amount of time.

We immediately observe that the notion of weak scalability can be readily adapted to the framework of the parallel Schwarz method. Indeed, since Schwarz iterates on different subdomains can be computed in parallel, it is possible to assign each local problem to a different processor and then determine the number of iterations necessary to produce an approximation to the global solution with a given error tolerance. In this setting, sufficient conditions for weak scalability of the PSM would be

(1) The cost of solving *one* local problem on a given subdomain is independent of the number of subdomains N in the domain decomposition.

(2) The number of iterations in the PSM procedure required to obtain a global solution with a given error tolerance is also independent of the number of subdomains N in the domain decomposition.

Since the cost of solving a local problem depends on the local degrees of freedom on the subdomain which can be explicitly controlled, Condition (1) is typically met for domain decomposition methods. Consequently, the scalability analysis of Schwarz methods mostly focuses on studying the validity of Condition (2) and this will be the goal of our analysis in Chapter 8. It turns out that the validity of Condition (2) is a complex question that depends strongly on the geometrical structure of the molecular cavity.

As briefly mentioned in Section 6.4, in contrast to classical Schwarz theory, the authors in [23] observed numerically that the ddCOSMO algorithm, i.e., the PSM applied to domains that represent molecular cavities, converges to a given tolerance within the same number of iterations independently of the number N of subdomains. This behaviour was observed if fixed-sized subdomains formed a "chain-like" domain such that the intersection of the boundary of each subdomain with the boundary of the global domain was non-empty. This intriguing numerical behaviour was noticed with interest by the domain decomposition community, and in a series of articles [28, 29, 30], Ciaramella and Gander were able to rigorously prove weak scalability of the PSM for "chain-like" domains of the form displayed in Figure 6.6. This result was subsequently extended in [25] to other one-level domain decomposition methods. It is crucial to note however, that all these results are valid *only* for chain-like geometries where at most, only two subdomains can have a common overlap.

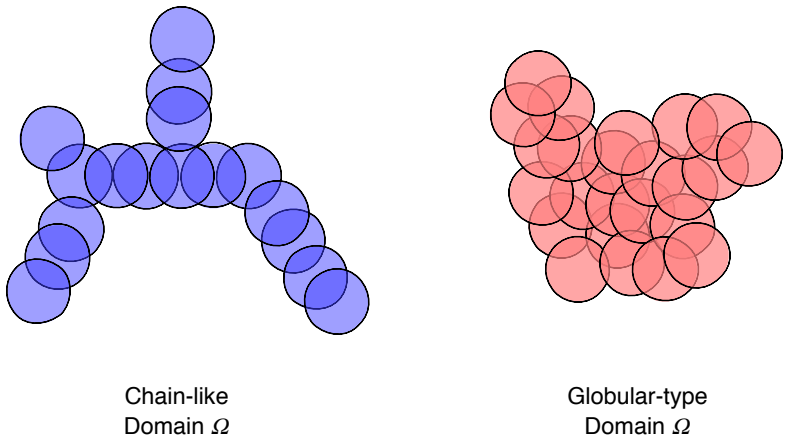

Figure 6.6: An examples of a typical "chain-like" domain (left) and a "globular" domain (right). The disks represent individual subdomains.

On the other hand, it was also observed numerically by the authors of [23] that the weak scalability of the PSM was lost if the fixed-sized subdomains formed a 'globular-type' domain Ω such that the boundaries of many subdomains lay in the interior of Ω. The following question therefore arises: is it possible to quantify the lack of scalability of the PSM for cases where several individual subdomains are entirely embedded inside the global domain? A typical example is to consider, for instance, the PSM for the solution of a one-dimensional Laplace problem and in [25], a heuristic argument is used to explain why for an unfortunate initialization, a contraction in the infinity norm of the Schwarz iterates is observed only after a number of iterations proportional to the number of N of subdomains. However, a rigorous proof is of this intuitive observation is lacking in the literature. Naturally, the problem becomes extremely technical if one considers a three-dimensional geometry involving situations where the simultaneous intersection of more than two subdomains is possible. This is not to say that this problem has not been considered at all in the literature. Indeed, some elegant results in this direction can be found in the articles [74] and [143]. Unfortunately, these existing results are not applicable for the geometric situations we are interested in.

In the article [74], the authors prove that the Schwarz waveform-relaxation method applied to the heat equation contracts at most every $m+2$ iterations, m being an integer representing the maximum distance of the subdomains from the boundary of the global domain. However, the overlapping subdomains considered in this work are constructed by 'artificially' enlarging the given non-overlapping subdomains. This construction allows the authors to avoid the case that Lions refers to as "weakly overlapping" in [133] and use the structure of the artificially constructed overlapping domain decomposition to present a convergence analysis that is based on the construction of a sequence of elliptic upper bounds. On the other hand, the PSM we consider here is always applied to molecular cavities where the subdomains are pre-determined by the atomic structure of the solute molecule and clearly weakly overlapping. Consequently, the proof given in [74] fails for the geometric settings considered in our work. It should also be remarked that the convergence analysis we will subsequently present is based on a direct study of the

PSM iteration operator which allows us to identify the 'worst initialization' and carefully track the propagation of the contraction across different subdomains comprising Ω in the course of the iterations. This is qualitatively very different from the study of the Schwarz sequence that is carried out in [74].

Another interesting convergence analysis of classical Schwarz methods for several intersecting subdomains is presented in the article [143]. This work deals with stationary advection-reaction-diffusion problems and allows one to obtain powerful scalability results. In fact, the author's analysis, which is based on the maximum principle and so-called barrier functions, even yields estimates of the contraction factor. Unfortunately, this analysis fails in the case of the Laplace equation due to the lack of advection or reaction terms, and is also not valid for domain decomposition problems in which the boundaries of many subdomains lie in the interior of the global domain.

Keeping in mind the above difficulties and lack of easily extendable results in the literature, our solution to tackling the daunting task of analysing the scalability of the PSM on molecular cavities is to proceed in a step-by-step manner:

- We first consider the PSM for the solution of a 1D Laplace problem and develop a systematic framework for this simple 'toy' problem. This first step is the subject of **Chapter 7** where we develop a basic structure for studying the lack of scalability of the PSM using the following key elements: (i) the identification of an adequate norm for studying the properties of the Schwarz operator; (ii) the maximum principle; and (iii) the idea of tracking the propagation of the contraction in the infinity norm towards the interior of the global domain Ω. Interestingly, the analysis turns out to be non-trivial even in a simple one-dimensional setting. The content of this chapter is based on the proceedings article [32].

- Subsequently, in **Chapter 8**, we analyse the convergence behaviour and scalability properties of the PSM for higher dimensional domain decomposition problems in which many subdomains may be completely embedded in the interior of the global domain and an arbitrary number of subdomains may have a common overlap. Extending the ideas of **Chapter 7**, we develop a systematic framework that allows us to bound the norm of the Schwarz iteration operator for such geometrical configurations. We provide numerical experiments that support our main results, and we consider concrete biological molecules that have been studied in solvation models in computational chemistry and understand the consequences of our analysis as it pertains to these complex bio-molecules. The content of this chapter is based on the article [33].

7

The Scalability of the Schwarz Method in One Dimension

7.1 Setting and Main Results

In this short chapter, we will study the scalability of the parallel Schwarz method (PSM) for the solution of the Laplace equation in one spatial dimension. Our goal is to identify the key ingredients in a general framework for the scalability analysis of the PSM that can be systematically extended to more realistic problems involving complicated domain decompositions in higher dimensions. The 1D Laplace problem is essentially a 'toy' model so we emphasise that most (but not all) of the results we prove here are either known or intuitively clear. The true contribution of this chapter will be the new *analysis technique* that we introduce which, as we shall see, will lead to a sharper description of the contraction behaviour of the 1D problem while simultaneously suggesting a roadmap for extensions to more general problems in higher dimensions. We remark that although our main focus in this dissertation is on the Laplace equation due to its use in the COSMO implicit model (see Section 6.4), similar analyses can be carried out for the reaction-diffusion equation. Note however, that the contraction behaviour for a reaction-diffusion equation is completely different from that of the Laplace equation, and therefore requires different arguments (see, e.g., [25] and [28]).

We first state our main results. We consider the Laplace equation in one-dimension. For $L > 0$, we must find a function $e\colon [0, L] \to \mathbb{R}$ that solves

$$(e)''(x) = 0 \quad \forall\, x \in (0, L), \qquad e(0) = 0, \qquad e(L) = 0. \tag{7.1}$$

Clearly (7.1) represents an error equation whose solution is trivially $e = 0$. In order to apply the PSM to solve (7.1), we consider a decomposition $\Omega = \cup_{j=1}^{N} \Omega_j$, where $\Omega_j := (a_j, b_j)$ with $a_1 = 0$, $b_1 = a_1 + \ell$ and $a_{j+1} = j(\ell - \delta)$, $b_{j+1} = a_{j+1} + \ell$ for $j = 1, \ldots, N-1$. Here, $\ell > 0$ is the length of each subdomain, $\delta > 0$ the overlap, and it holds that $L = N\ell - (N-1)\delta$.

Next, let $e_0\colon \Omega \to \mathbb{R}$ be some initialization. The PSM defines the sequences $\{e_j^n\}_{n\in\mathbb{N}}$

by solving for each $n \in \mathbb{N}$ the sub-problems

$$(e_j^n)''(x) = 0 \quad \forall\, x \in (a_j, b_j), \quad e_j^n(a_j) = e_{j-1}^{n-1}(a_j), \quad e_j^n(b_j) = e_{j+1}^{n-1}(b_j), \tag{7.2}$$

for each $j = 2, \ldots, N-1$ and

$$\begin{aligned} &(e_1^n)''(x) = 0 \quad \forall\, x \in (a_1, b_1), && e_1^n(a_1) = 0, && e_1^n(b_1) = e_2^{n-1}(b_1), \\ &(e_N^n)''(x) = 0 \quad \forall\, x \in (a_N, b_N), && e_N^n(a_N) = e_{N-1}^{n-1}(a_N), && e_N^n(b_N) = 0. \end{aligned}$$

Solving (7.1) and (7.2) and defining for each $n \in \mathbb{N}$ the vector $\mathbf{e}^n \in \mathbb{R}^{2N}$ as

$$\mathbf{e}^n := \begin{bmatrix} e_1^n(a_1) & e_1^n(a_2) & e_2^n(b_1) & e_2^n(a_3) & \cdots & e_j^n(b_{j-1}) & e_j^n(a_{j+1}) & \cdots & e_N^n(b_{N-1}) & e_N^n(b_N) \end{bmatrix}^\top,$$

it is possible to write the PSM iterations as $\mathbf{e}^{n+1} = T\mathbf{e}^n$. Here $T \in \mathbb{R}^{2N \times 2N}$ is a non-negative ($T_{j,k} \geq 0$), non-symmetric block tridiagonal matrix:

$$T = \begin{bmatrix} 0 & \widetilde{T_2} & 0 & \cdots & 0 & 0 & 0 \\ T_1 & 0 & T_2 & \cdots & 0 & 0 & 0 \\ \ddots & \ddots & \ddots & \ddots & \ddots & \ddots & \ddots \\ 0 & 0 & 0 & \cdots & T_1 & 0 & T_2 \\ 0 & 0 & 0 & \cdots & 0 & \widetilde{T_1} & 0 \end{bmatrix},$$

with

$$T_1 = \begin{bmatrix} 0 & 1 - \frac{\delta}{\ell} \\ 0 & \frac{\delta}{\ell} \end{bmatrix}, \qquad \widetilde{T_1} = \begin{bmatrix} 0 & 1 - \frac{\delta}{\ell} \\ 0 & 0 \end{bmatrix},$$
$$T_2 = \begin{bmatrix} \frac{\delta}{\ell} & 0 \\ 1 - \frac{\delta}{\ell} & 0 \end{bmatrix}, \qquad \widetilde{T_2} = \begin{bmatrix} 0 & 0 \\ 1 - \frac{\delta}{\ell} & 0 \end{bmatrix}.$$

Next, we denote by $\|\cdot\|$ the usual infinity norm on the relevant function space and, by an abuse of notation, also the corresponding induced matrix norm. Our goal is to analyse the convergence properties of the PSM sequence $\{e_j^n\}_{n \in \mathbb{N}}$ with respect to $\|\cdot\|$, which involves the study of the properties of the matrix T.

Our main results are summarized in the following theorem.

Theorem 7.1. *Let $N \in \mathbb{N}$ be the number of subdomains in Ω and $\mathbf{1}_N \in \mathbb{R}^{2N}$ the vector whose elements are all equal to 1. Then $\|T^n\| = \|T^n \mathbf{1}_N\| \leq 1$ for any $n \in \mathbb{N}$ and moreover,*

(a) *$\|T^{\lceil \frac{N}{2} \rceil}\| < 1$ and hence $\rho(T) < 1$, where $\rho(T)$ is the spectral radius of T.*
(b) *$\|T^{n+1}\| < \|T^n\|$ if N is even, and $\|T^{n+2}\| < \|T^n\|$ if N is odd, for $n \geq \lceil \frac{N}{2} \rceil$.*

Theorem 7.1 states clearly that the PSM converges. Moreover, it identifies $\mathbf{1}_N$ as the unit vector that maximises the infinity operator norm of the iteration matrices $T^n, n \in \mathbb{N}$. This fact is then used to prove Theorem 7.1 (b): if initialized with $\mathbf{1}_N$, after $\lceil \frac{N}{2} \rceil$ iterations

the PSM sequence contracts in the infinity norm at *every iteration* if N is even, or *every second iteration* if N is odd. Although proven for a 1-D problem, this result is much sharper than the one found in [74], which states that the PSM sequence contracts in the infinity norm at most every $\lceil \frac{N}{2} \rceil$ iterations. The proof of Theorem 7.1 (b) requires the use of two intermediate, technical Lemmas. These technical results will characterize precisely the shape of the vector $\mathbf{e}^n = T^n \mathbf{1}_N$ at every iteration n and will show how the contraction in the infinity norm propagates from the two end-points of $\partial\Omega$ towards subdomains that lie in the middle of Ω.

The proof of Theorem 7.1 is the subject of the next section. In particular, in Section 7.2.1 we demonstrate that $\|T^n\| = \|T^n \mathbf{1}_N\|$ and prove Theorem 7.1 (a), and in Section 7.2.2 we prove Theorem 7.1 (b). Notice that using Theorem 7.1, one could also estimate the spectral radius of T as

$$\rho(T) \leq \|T^{\lceil \frac{N}{2} \rceil}\|^{1/\lceil \frac{N}{2} \rceil} = \left[1 - \left(\frac{\delta}{L}\right)^{\lceil \frac{N}{2} \rceil}\right]^{1/\lceil \frac{N}{2} \rceil}.$$

This estimate can be obtained using a direct calculation involving geometric arguments. Since this bound is fairly conservative however, we do not provide a formal proof.

7.2 Proofs

7.2.1 Proof of Theorem 7.1 (a)

In what follows, we denote $P := \begin{bmatrix} 0 & 1 \\ 1 & 0 \end{bmatrix}$. Moreover, if $m \in \mathbb{N}$ and $\mathbf{v}, \mathbf{w} \in \mathbb{R}^m$, then we use the notation $\mathbf{v} < \mathbf{w}$ (resp. $\mathbf{v} > \mathbf{w}$) to mean that $v_i < w_i$ (resp. $v_i > w_i$) for each $i \in \{1, \dots, m\}$. Additionally, if $m \in \mathbb{N}$ and $\mathbf{u} \in \mathbb{R}^{2m}$, then we will frequently write $\mathbf{u} = (\mathbf{u}_1, \mathbf{u}_2, \dots, \mathbf{u}_m)$, and for each $j \in \{1, \dots, N\}$ we will denote by $(\mathbf{u}_j)_1$ and $(\mathbf{u}_j)_2$ the components of $\mathbf{u}_j \in \mathbb{R}^2$.

Lemma 7.2. *For all $n \in \mathbb{N}$ it holds that $\|T^n\| = \|T^n \mathbf{1}_N\|$.*

Proof. Let $\mathbf{w} = T^n \mathbf{1}_N$. Then for each $i \in \{1, \dots, 2N\}$ it holds that $w_i = \sum_{j=1}^{2N} (T^n)_{ij}$. Since T is non-negative, T^n is also non-negative for any $n \in \mathbb{N}$ and it holds that

$$\|T^n\| = \max_{i=1,\dots,2N} \sum_{j=1}^{2N} (T^n)_{ij} = \max_{i=1,\dots,2N} \left| \sum_{j=1}^{2N} (T^n)_{ij} \right| = \max_{i=1,\dots,2N} |w_i| = \|T^n \mathbf{1}_N\|.$$

□

Next, let $a, b, c, d \in [0, 1)$ be real numbers such that $a < b \leq c < d$. Direct calculations show that the matrices T_1 and T_2 satisfy the following relations:

$$b\,\mathbf{1}_1 < T_1 \begin{bmatrix} a \\ b \end{bmatrix} + T_2 \mathbf{1}_1 = \begin{bmatrix} (1 - \frac{\delta}{\ell})b + \frac{\delta}{\ell} \\ \frac{\delta}{\ell} b + 1 - \frac{\delta}{\ell} \end{bmatrix} < \mathbf{1}_1, \tag{7.3}$$

$$b\,\mathbf{1}_1 \le T_1 \begin{bmatrix} a \\ b \end{bmatrix} + T_2 \begin{bmatrix} c \\ d \end{bmatrix} = \begin{bmatrix} (1-\frac{\delta}{\ell})b + \frac{\delta}{\ell}c \\ \frac{\delta}{\ell}b + (1-\frac{\delta}{\ell})c \end{bmatrix} \le c\,\mathbf{1}_1, \tag{7.4}$$

$$T_1\mathbf{1}_1 + T_2\mathbf{1}_1 = \mathbf{1}_1, \qquad T_1 \begin{bmatrix} a \\ b \end{bmatrix} + T_2 \begin{bmatrix} c \\ d \end{bmatrix} = P\left(T_1 \begin{bmatrix} d \\ c \end{bmatrix} + T_2 \begin{bmatrix} b \\ a \end{bmatrix} \right), \tag{7.5}$$

where the equality in (7.4) holds if and only if $b = c$.

Definition 7.3. Let $n \in \left\{1, \dots, \lceil \frac{N}{2} \rceil\right\}$ be a natural number, we define $V^n \subset \mathbb{R}^{2N}$ as

$$V^n := \left\{ \mathbf{v} := (\mathbf{v}_1, \dots, \mathbf{v}_N) \colon \begin{cases} \mathbf{v}_j < \mathbf{1}_1 & \text{if } j \in \{1, \dots, n\} \cup \{N+1-n, \dots, N\} \\ \mathbf{v}_j = \mathbf{1}_1 & \text{otherwise} \end{cases} \right\}.$$

We now state and prove the main result that will lead directly to Theorem 7.1 (a).

Lemma 7.4. *Let $n \in \left\{1, \dots, \lceil \frac{N}{2} \rceil\right\}$ be a natural number and let $\mathbf{w} = T^n\mathbf{1}_N$. Then it holds that $T^n\mathbf{1}_N \in V^n$, and for all $j \in \{1, \dots, N\}$ it holds that $\mathbf{w}_j = P\,\mathbf{w}_{N+1-j}$.*

Proof. We proceed by induction on the iteration index n. Let $n = 1$ and $\mathbf{w} = T\mathbf{1}_N$. Then by definition of the iteration matrix T and the matrices $\widetilde{T_1}, \widetilde{T_2}$ it holds that

$$\mathbf{w}_1 = \widetilde{T_2}\mathbf{1}_1 = \begin{bmatrix} 0 \\ 1 - \frac{\delta}{\ell} \end{bmatrix} < \mathbf{1}_1, \qquad \mathbf{w}_N = \widetilde{T_1}\mathbf{1}_1 = \begin{bmatrix} 1 - \frac{\delta}{\ell} \\ 0 \end{bmatrix} < \mathbf{1}_1,$$

so that $\mathbf{w}_1 = P\,\mathbf{w}_N$. Furthermore, by (7.5) it holds that $\mathbf{w}_j = T_1\mathbf{1}_1 + T_2\mathbf{1}_1 = \mathbf{1}_1$ for all $j \in \{2, \dots, N-1\}$, and thus $\mathbf{w}_j = P\,\mathbf{w}_{N+1-j}$. Hence, Lemma 7.4 holds for $n = 1$.

Assume now that Lemma 7.4 holds for some $n \in \left\{1, \dots, \lceil \frac{N}{2} \rceil - 1\right\}$. We must show that Lemma 7.4 also holds for $n+1$. Let $\mathbf{u} = T^n\mathbf{1}_N$ and let $\mathbf{w} = T^{n+1}\mathbf{1}_N$. We proceed in three parts. First, we prove that the result holds in the case $n \ge 2$ for indices $j \in \{1, \dots, n-1\}$, then we prove it for the index $j = n$ and finally for the index $j = n+1$. Note that it is necessary to proceed in these three steps since in each of these cases $\mathbf{w}_j$ depends on $\mathbf{u}_{j-1}$ and $\mathbf{u}_{j+1}$ which take different values depending on the index j.

1. $n \ge 2$ and $j \in \{1, \dots, n-1\}$: Assume first that $j = 1$. It follows from the induction hypothesis that $\mathbf{u}_2 = P\,\mathbf{u}_{N-1} < \mathbf{1}_1$. A direct calculation similar to the one for the base case $n = 1$ reveals that $\mathbf{w}_1 = P\,\mathbf{w}_N < \mathbf{1}_1$. Now assume $j \ne 1$. It follows by the induction hypothesis that $\mathbf{u}_{j-1} = P\,\mathbf{u}_{N+2-j}$, and $P\,\mathbf{u}_{j+1} = \mathbf{u}_{N-j}$, and $\mathbf{u}_{j-1}, \mathbf{u}_{j+1} < \mathbf{1}_1$. We therefore obtain from (7.5) that

$$\mathbf{w}_j = T_1\mathbf{u}_{j-1} + T_2\mathbf{u}_{j+1} = P(T_1 P\mathbf{u}_{j+1} + T_2 P\mathbf{u}_{j-1}) = P(T_1\mathbf{u}_{N-j} + T_2\mathbf{u}_{N-j+2}) = P\mathbf{w}_{N-j+1} < \mathbf{1}_1.$$

2. $j = n$: The induction hypothesis implies that $\mathbf{u}_{n-1} = P\,\mathbf{u}_{N+2-n}$, $\mathbf{u}_{n-1} < \mathbf{1}_1$ and $\mathbf{u}_{n+1} = \mathbf{1}_1$. Hence (7.5) implies that

$$\mathbf{w}_n = T_1\mathbf{u}_{n-1} + T_2\mathbf{1}_1 = P(T_1\mathbf{1}_1 + T_2 P\mathbf{u}_{n-1}) = P(T_1\mathbf{1}_1 + T_2\mathbf{u}_{N+2-n}) = P\mathbf{w}_{N+1-n} < \mathbf{1}_1.$$

3. Let $j = n+1$: By the induction hypothesis we have that $\mathbf{u}_n = P\,\mathbf{u}_{N+1-n}$, $\mathbf{u}_{n+2} = P\,\mathbf{u}_{N-1-n}$, $\mathbf{u}_n < \mathbf{1}_1$ and $\mathbf{u}_{n+2} \leq \mathbf{1}_1$. Using (7.4) and (7.5) we get

$$\mathbf{w}_{n+1}=T_1\mathbf{u}_n+T_2\mathbf{u}_{n+2}=P(T_1P\mathbf{u}_{n+2}+T_2P\mathbf{u}_n)=P(T_1\mathbf{u}_{N-1-n}+T_2\mathbf{u}_{N+1-n})=P\mathbf{w}_{N-n}<\mathbf{1}_1.$$

It remains to show that $\mathbf{w}_k = \mathbf{1}_1$ for all $k \in \{n+2,\dots,\lceil\frac{N}{2}\rceil\}\cup\{\lceil\frac{N}{2}\rceil,\dots,N-1-n\}$. The induction hypothesis yields that $\mathbf{u} = T^n\mathbf{1}_N \in V^n$. Hence, $\mathbf{u}_k = \mathbf{1}_1$ for all $k \in \{n+1,\dots,\lceil\frac{N}{2}\rceil\} \cup \{\lceil\frac{N}{2}\rceil,\dots,N-n\}$. The result now follows by applying Equation (7.5).

□

Lemma 7.4 implies that $T^{\lceil\frac{N}{2}\rceil}\mathbf{1}_N \in V^{\lceil\frac{N}{2}\rceil}$ so that $\|T^{\lceil\frac{N}{2}\rceil}\| = \|T^{\lceil\frac{N}{2}\rceil}\mathbf{1}_N\| < 1$, which is precisely Theorem 1 (a).

7.2.2 Proof of Theorem 7.1 (b)

We first prove an intermediate lemma.

Lemma 7.5. *Let $n \in \{2,\dots,\lfloor\frac{N}{2}\rfloor - 2\}$, let $\mathbf{u} = T^n\mathbf{1}_N$ and $\mathbf{w} = T\mathbf{u}$. If for all $j \in \{1,\dots,n\}$ it holds that*

$$(\mathbf{u}_j)_1 \leq (\mathbf{u}_j)_2, \quad \textit{and} \quad \mathbf{u}_j < \mathbf{u}_{j+1}, \tag{7.6}$$

then for all $j \in \{1,\dots,n+1\}$ it holds that

$$(\mathbf{w}_j)_1 \leq (\mathbf{w}_j)_2, \quad \textit{and} \quad \mathbf{w}_j < \mathbf{w}_{j+1}. \tag{7.7}$$

Proof. We prove the result by induction over the subdomain index j. The definition of the matrices $\widetilde{T_1}$ and $\widetilde{T_2}$ implies that $0 = (\mathbf{w}_1)_1 \leq (\mathbf{w}_1)_2$, and Equation (7.4) yields that

$$\mathbf{w}_1 = \begin{bmatrix} 0 \\ (1-\frac{\delta}{L})(\mathbf{u}_2)_1 \end{bmatrix} < \begin{bmatrix} (1-\frac{\delta}{L})(\mathbf{u}_1)_2 \\ (1-\frac{\delta}{L})(\mathbf{u}_3)_1 \end{bmatrix} \leq \begin{bmatrix} (1-\frac{\delta}{L})(\mathbf{u}_1)_2 + \frac{\delta}{L}(\mathbf{u}_3)_1 \\ \frac{\delta}{L}(\mathbf{u}_1)_2 + (1-\frac{\delta}{L})(\mathbf{u}_3)_1 \end{bmatrix} = \mathbf{w}_2.$$

We now proceed to the induction step. Assume that (7.7) holds for some $j \in \{1,\dots,n\}$. We first show that $(\mathbf{w}_{j+1})_1 \leq (\mathbf{w}_{j+1})_2$. Equation (7.4) implies that it is sufficient to show that $\mathbf{u}_j \leq \mathbf{u}_{j+2}$. There are two cases: $j < n-1$ and $j \in \{n-1, n\}$. If $j < n-1$, then (7.6) yields the required result. If $j \in \{n-1, n\}$, then (7.6) and the fact that $\mathbf{u} \in V^n$ gives that $\mathbf{u}_j < \mathbf{u}_{j+2} = \mathbf{1}_1$.

Next, we show that $\mathbf{w}_{j+1} < \mathbf{w}_{j+2}$. Equation (7.4) implies that it is sufficient to show that $\mathbf{u}_j < \mathbf{u}_{j+1}$ and $\mathbf{u}_{j+2} \leq \mathbf{u}_{j+3}$. There are three cases: $j < n-1$, $j = n-1$ and $j = n$. If $j < n-1$ then (7.6) yields the required result. If $j = n-1$ then (7.6) yields that $\mathbf{u}_j < \mathbf{u}_{j+1}$ and the fact that $\mathbf{u} \in V^n$ gives that $\mathbf{u}_{j+2} = \mathbf{u}_{j+3} = \mathbf{1}_1$. If $j = n$ then (7.6) yields that $\mathbf{u}_j < \mathbf{u}_{j+1}$ and it remains to show that $\mathbf{u}_{j+2} \leq \mathbf{u}_{j+3}$. To this end, we recall that $n \leq \lfloor\frac{N}{2}\rfloor - 2$. Therefore, there are three sub-cases:

- $n < \lfloor \frac{N}{2} \rfloor - 2$ in which case $n+1 < j+2, j+3 \leq \lfloor \frac{N}{2} \rfloor$;
- $n = \lfloor \frac{N}{2} \rfloor - 2$ and N is even in which case $\mathbf{u}_{j+2} = P\mathbf{u}_{j+3}$;
- $n = \lfloor \frac{N}{2} \rfloor - 2$ and N is odd in which case $\mathbf{u}_{j+3} = P\mathbf{u}_{j+1}$.

In all three sub-cases, we obtain that $\mathbf{u}_{j+2} = \mathbf{u}_{j+3} = \mathbf{1}_1$. □

Our next lemma describes the 'shape' of the vector $T^n\mathbf{1}_N$ for natural numbers $n < \lfloor \frac{N}{2} \rfloor$.

Lemma 7.6. *Let $n \in \{1, \dots, \lfloor \frac{N}{2} \rfloor - 1\}$ be a natural number and let $\mathbf{w} = T^n\mathbf{1}_N$. Then for all $j \in \{1, \dots, n\}$ it holds that*

$$(\mathbf{w}_j)_1 \leq (\mathbf{w}_j)_2, \quad (\mathbf{w}_{N+1-j})_2 \leq (\mathbf{w}_{N+1-j})_1, \quad \textit{and} \quad \mathbf{w}_j < \mathbf{w}_{j+1}, \quad \mathbf{w}_{N+1-j} < \mathbf{w}_{N-j}.$$

Proof. By Lemma 7.4 it holds that $\mathbf{w}_j = P\,\mathbf{w}_{N+1-j}$ for each $j \in \{1, \dots, n\}$ so it suffices to show that for each $n \in \{1, \dots, \lfloor \frac{N}{2} \rfloor - 1\}$ and all $j \in \{1, \dots, n\}$ it holds that

$$(\mathbf{w}_j)_1 \leq (\mathbf{w}_j)_2 \text{ and } \mathbf{w}_j < \mathbf{w}_{j+1}. \tag{7.8}$$

We prove the result by induction over the iteration number n. Let $n = 1$. The definition of the matrix $\widetilde{T_2}$ and (7.5) yield that $\mathbf{w}_1 = \begin{bmatrix} 0 \\ 1 - \frac{\delta}{L} \end{bmatrix}$ and $\mathbf{w}_2 = \mathbf{1}_1$. Thus, (7.8) holds for $n = 1$. Next, let $n = 2$ and let $\mathbf{u} = T_N^{\mathbf{1}}$. The definition of the matrix $\widetilde{T_2}$ together with Equations (7.3) and (7.5) yields $\mathbf{w}_1 = \begin{bmatrix} 0 \\ 1 - \frac{\delta}{L} \end{bmatrix}$, $\mathbf{w}_1 < \mathbf{w}_2 < \mathbf{1}_1$ and $\mathbf{w}_3 = \mathbf{1}_1$. Thus, (7.8) holds for $n = 2$. Finally, assume that (7.8) holds for some $n \in \{2, \dots, \lfloor \frac{N}{2} \rfloor - 2\}$. It follows from Lemma 7.5 that (7.8) also holds for $n+1$. □

Next, Lemma 7.7 describes the 'shape' of the vector $T^n\mathbf{1}_N$ for natural numbers $n \geq \lfloor \frac{N}{2} \rfloor$. Together, Lemmas 7.6 and 7.7 establish that the vector $T^n\mathbf{1}_N$ is monotonically increasing as one moves from the end-points of Ω towards its centre.

Lemma 7.7. *Let $n \geq \lfloor \frac{N}{2} \rfloor$ be a natural number, and let $\mathbf{w} = T^n\mathbf{1}_N$. Then for all $j \in \{1, \dots, \lfloor \frac{N}{2} \rfloor - 1\}$ it holds that*

$$(\mathbf{w}_j)_1 \leq (\mathbf{w}_j)_2, \quad (\mathbf{w}_{N+1-j})_2 \leq (\mathbf{w}_{N+1-j})_1, \quad \textit{and} \quad \mathbf{w}_j < \mathbf{w}_{j+1}, \quad \mathbf{w}_{N+1-j} < \mathbf{w}_{N-j}.$$

In addition, if N is an odd number, then $\mathbf{w}_{\lfloor \frac{N}{2} \rfloor} \leq \mathbf{w}_{\lceil \frac{N}{2} \rceil}$ and $\mathbf{w}_{\lfloor \frac{N}{2} \rfloor + 2} < \mathbf{w}_{\lceil \frac{N}{2} \rceil}$.

Proof. Lemma 7.7 can be proven in a similar manner to Lemma 7.6 using a proof-by-induction on the iteration number n. We omit it here for brevity. □

We are now ready to prove our second main result.

Proof of Theorem 7.1 (b). Assume that $N \in \mathbb{N}$ is even. In view of Lemma 7.2, we must prove that $\|T^{n+1}\mathbf{1}_N\| < \|T^n\mathbf{1}_N\|$. Let $\mathbf{w} = T^{n+1}\mathbf{1}_N$ and $\mathbf{u} = T^n\mathbf{1}_N$. By Lemma 7.7, we know that $\|T^{n+1}\mathbf{1}_N\| = \|\mathbf{w}_{\lceil \frac{N}{2} \rceil}\|$ and $\|T^n\mathbf{1}_N\| = \|\mathbf{u}_{\lceil \frac{N}{2} \rceil}\|$.

Since $\mathbf{w} = T\mathbf{u}$, we have that $\mathbf{w}_{\lceil \frac{N}{2} \rceil} = T_1\mathbf{u}_{\lceil \frac{N}{2} \rceil - 1} + T_2\mathbf{u}_{\lceil \frac{N}{2} \rceil + 1}$. Since N is even, we obtain that $\lceil \frac{N}{2} \rceil + 1 = \frac{N}{2} + 1$ and thus, Lemma 7.4 yields that $\mathbf{u}_{\lceil \frac{N}{2} \rceil + 1} = P\mathbf{u}_{\lceil \frac{N}{2} \rceil}$. It follows that $\mathbf{w}_{\lceil \frac{N}{2} \rceil} = T_1\mathbf{u}_{\lceil \frac{N}{2} \rceil - 1} + T_2P\mathbf{u}_{\lceil \frac{N}{2} \rceil}$. From (7.4) we also obtain that

$$\mathbf{u}_{\lceil \frac{N}{2} \rceil - 1} \leq \mathbf{w}_{\lceil \frac{N}{2} \rceil} \leq P\,\mathbf{u}_{\lceil \frac{N}{2} \rceil}, \tag{7.9}$$

where the equality holds if and only if $(\mathbf{u}_{\lceil \frac{N}{2} \rceil - 1})_2 = (P\,\mathbf{u}_{\lceil \frac{N}{2} \rceil})_1 = (\mathbf{u}_{\lceil \frac{N}{2} \rceil})_2$. We know from Lemma 7.7 that $\mathbf{u}_{\lceil \frac{N}{2} \rceil - 1} < \mathbf{u}_{\lceil \frac{N}{2} \rceil}$, which yields that $(\mathbf{u}_{\lceil \frac{N}{2} \rceil - 1})_2 < (\mathbf{u}_{\lceil \frac{N}{2} \rceil})_2$. Hence the inequalities in (7.9) are strict: $\mathbf{u}_{\lceil \frac{N}{2} \rceil - 1} < \mathbf{w}_{\lceil \frac{N}{2} \rceil} < P\,\mathbf{u}_{\lceil \frac{N}{2} \rceil}$. We thus obtain that $\|T^{n+1}\mathbf{1}_N\| = \|\mathbf{w}_{\lceil \frac{N}{2} \rceil}\| < \|P\,\mathbf{u}_{\lceil \frac{N}{2} \rceil}\| = \|\mathbf{u}_{\lceil \frac{N}{2} \rceil}\| = \|T^n\mathbf{1}_N\|$. This completes the proof of the first assertion.

Assume now that $N \in \mathbb{N}$ is odd, and let $\mathbf{u} = T^n\mathbf{1}_N$, $\mathbf{w} = T^{n+1}\mathbf{1}_N$ and $\mathbf{y} = T^{n+2}\mathbf{1}_N$. Lemma 7.7 implies that

$$\|T^{n+2}\mathbf{1}_N\| = \|\mathbf{y}_{\lceil \frac{N}{2} \rceil}\|, \qquad \|T^{n+1}\mathbf{1}_N\| = \|\mathbf{w}_{\lceil \frac{N}{2} \rceil}\|, \qquad \|T^n\mathbf{1}_N\| = \|\mathbf{u}_{\lceil \frac{N}{2} \rceil}\|.$$

Since $\|T\| = 1$, we have

$$\|\mathbf{y}_{\lceil \frac{N}{2} \rceil}\| \leq \|\mathbf{w}_{\lceil \frac{N}{2} \rceil}\| \leq \|\mathbf{u}_{\lceil \frac{N}{2} \rceil}\|. \tag{7.10}$$

Clearly if $\|\mathbf{w}_{\lceil \frac{N}{2} \rceil}\| < \|\mathbf{u}_{\lceil \frac{N}{2} \rceil}\|$ then (7.10) yields that

$$\|T^{n+2}\mathbf{1}_N\| \leq \|T^{n+1}\mathbf{1}_N\| = \|\mathbf{w}_{\lceil \frac{N}{2} \rceil}\| < \|\mathbf{u}_{\lceil \frac{N}{2} \rceil}\| = \|T^n\mathbf{1}_N\|,$$

which is our claim.

Next, suppose that $\|\mathbf{w}_{\lceil \frac{N}{2} \rceil}\| = \|\mathbf{u}_{\lceil \frac{N}{2} \rceil}\|$. We show that $\|\mathbf{y}_{\lceil \frac{N}{2} \rceil}\| < \|\mathbf{w}_{\lceil \frac{N}{2} \rceil}\|$ which implies our claim. To do so, since N is odd, we use Lemma 7.4 together with the facts that $\mathbf{y} = T\mathbf{w}$ and $\mathbf{w} = T\mathbf{u}$ to obtain that $\mathbf{y}_{\lceil \frac{N}{2} \rceil} = T_1\mathbf{w}_{\lceil \frac{N}{2} \rceil - 1} + T_2P\,\mathbf{w}_{\lceil \frac{N}{2} \rceil - 1}$ and $\mathbf{w}_{\lceil \frac{N}{2} \rceil} = T_1\mathbf{u}_{\lceil \frac{N}{2} \rceil - 1} + T_2P\,\mathbf{u}_{\lceil \frac{N}{2} \rceil - 1}$ which implies

$$\mathbf{y}_{\lceil \frac{N}{2} \rceil} = (\mathbf{w}_{\lceil \frac{N}{2} \rceil - 1})_2\mathbf{1}_1, \qquad \mathbf{w}_{\lceil \frac{N}{2} \rceil} = (\mathbf{u}_{\lceil \frac{N}{2} \rceil - 1})_2\mathbf{1}_1. \tag{7.11}$$

From Lemma 7.4, we know that

$$\mathbf{u}_{\lceil \frac{N}{2} \rceil} \overset{\text{Lemma 7.4}}{=} \mathbf{w}_{\lceil \frac{N}{2} \rceil} \overset{(7.11)}{=} (\mathbf{u}_{\lceil \frac{N}{2} \rceil - 1})_2\mathbf{1}_1. \tag{7.12}$$

Using the fact that $\mathbf{w} = T\mathbf{u}$ and Equation (7.12) we have that

$$\mathbf{w}_{\lceil \frac{N}{2} \rceil - 1} \overset{(7.4)}{=} T_1\mathbf{u}_{\lceil \frac{N}{2} \rceil - 2} + T_2\,\mathbf{u}_{\lceil \frac{N}{2} \rceil} \overset{(7.12)}{=} T_1\mathbf{u}_{\lceil \frac{N}{2} \rceil - 2} + T_2(\mathbf{u}_{\lceil \frac{N}{2} \rceil - 1})_2\mathbf{1}_1.$$

Using (7.4) we obtain that

$$\mathbf{u}_{\lceil \frac{N}{2} \rceil - 2} \leq \mathbf{w}_{\lceil \frac{N}{2} \rceil - 1} \leq (\mathbf{u}_{\lceil \frac{N}{2} \rceil - 1})_2 \mathbf{1}_1. \tag{7.13}$$

where the equality holds if and only if $(\mathbf{u}_{\lceil \frac{N}{2} \rceil - 2})_2 = (\mathbf{u}_{\lceil \frac{N}{2} \rceil - 1})_2$. However, Lemma 7.7 implies that $\mathbf{u}_{\lceil \frac{N}{2} \rceil - 2} < \mathbf{u}_{\lceil \frac{N}{2} \rceil - 1}$ which immediately yields that $(\mathbf{u}_{\lceil \frac{N}{2} \rceil - 2})_2 < (\mathbf{u}_{\lceil \frac{N}{2} \rceil - 1})_2$. Hence the inequalities in (7.13) are strict and thus

$$\mathbf{w}_{\lceil \frac{N}{2} \rceil - 1} \overset{(7.13)}{<} (\mathbf{u}_{\lceil \frac{N}{2} \rceil - 1})_2 \mathbf{1}_1 \overset{(7.11)}{=} \mathbf{w}_{\lceil \frac{N}{2} \rceil}. \tag{7.14}$$

Finally, recalling (7.11) we obtain that

$$\mathbf{y}_{\lceil \frac{N}{2} \rceil} \overset{(7.11)}{=} (\mathbf{w}_{\lceil \frac{N}{2} \rceil - 1})_2 \mathbf{1}_1 \overset{(7.14)}{<} \mathbf{w}_{\lceil \frac{N}{2} \rceil},$$

which completes the proof. □

The above proof concludes Chapter 7. In the next chapter, we will attempt to extend this analysis framework to more complicated geometries in higher dimensions.

8

The Scalability of the Schwarz Method in Higher Dimensions

The goal of Chapter 8 is to extend the one-dimensional scalability analysis carried out in Chapter 7 to higher dimensions. Since we are specifically interested in the scaling properties of the ddCOSMO algorithm (see Section 6.4), the domains we consider in this chapter will represent molecular cavities and will thus be composed of the union of intersecting open balls. The reminder of Chapter 8 is organized as follows: The main ideas and results of our analysis are stated in Section 8.1. We first introduce the notation and all the mathematical objects needed for a detailed description of the domain geometry in Section 8.1.1. The PSM is formulated in Section 8.1.2 and the convergence analysis is presented in Section 8.1.3. Our main results are stated in Section 8.1.3.2 and subsequently discussed with some examples in Section 8.1.3.3. We remark that in Section 8.1 we restrict ourselves to a two-dimensional framework wherein atomic cavities are represented as disks and at most only three disks can have a common overlap. This choice is made in order to ease notation, which is otherwise very technical and complicated, and to put more focus on the techniques used to prove our results. We show in Section 8.2 how to extend our analysis to the case of arbitrary types and numbers of intersections and discuss the extension to three dimensions. Section 8.3 contains numerical experiments that support our main results. In Section 8.4, we consider biological molecules that have been studied in solvation models in computational chemistry (see, e.g., [136]) and understand the consequences of our analysis as they pertain to these complex bio-molecules. Finally, we present a short conclusion in Section 8.5.

8.1 The Schwarz Method in Two Dimensions

8.1.1 Geometric setting

We consider the Laplace equation in two dimensions. Let $\Omega \subset \mathbb{R}^2$ be an open, connected and bounded set, let $g \in C^0(\partial\Omega)$ be a given function. We are interested in finding

8. THE SCALABILITY OF THE SCHWARZ METHOD IN HIGHER DIMENSIONS

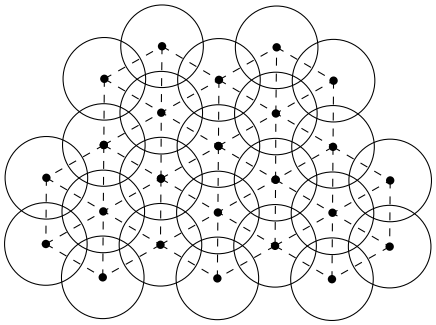

Figure 8.1: An example of a collection of disks $\{\Omega_i\}_{i=1}^N \subset \mathbb{R}^2$ on a triangular lattice composed of dots and dashed lines.

$u \in \left(C^2(\Omega) \cap C^0(\overline{\Omega})\right) \subset L^\infty(\Omega)$ with the property that

$$\begin{aligned} \Delta u &= 0 \qquad \text{in } \Omega, \\ u &= g \qquad \text{on } \partial\Omega. \end{aligned} \tag{8.1}$$

Throughout this chapter, we assume that the domain Ω has the following structure: Let $\Omega_i,\ i = 1, \ldots, N$ be a collection of N intersecting disks of radii $r_i > 0,\ i = 1, \ldots, N$. Then $\Omega = \cup_{i=1}^N \Omega_i$. An example of such a geometry is shown in Figure 8.1. In order to avoid discussing an empty theory, we assume that $N > 1$ and there exist at least two indices $i, j \in \{1, \ldots, N\}$ such that $\Omega_i \cap \Omega_j \neq \emptyset$.

We impose the following constraints on the subdomains $\Omega_i,\ i = 1, \ldots, N$:

A1) If two subdomains Ω_i and Ω_j have non-empty intersection, then there exist subsets of the boundaries $\Gamma_i \subset \partial\Omega_i \cap \Omega_j$ and $\Gamma_j \subset \partial\Omega_j \cap \Omega_i$ both of positive measure such that

$$\begin{aligned} \Gamma_i \cap \Omega_k &= \emptyset \ \forall k = 1, \ldots, N \text{ with } k \neq i, j, \\ \Gamma_j \cap \Omega_k &= \emptyset \ \forall k = 1, \ldots, N \text{ with } k \neq i, j. \end{aligned}$$

In other words, we assume that if two subdomains Ω_i and Ω_j intersect, then they must have at least a simple intersection.

A2) For any choice of distinct indices $i_1, i_2, i_3, i_4 \in \{1, \ldots, N\}$ it holds that $\Omega_{i_1} \cap \Omega_{i_2} \cap \Omega_{i_3} \cap \Omega_{i_4} = \emptyset$, i.e., at most only three distinct subdomains in the collection $\{\Omega_i\}_{i=1}^N$ have non-empty intersection. In other words, we assume that our geometry consists of at most triple intersections.

Constraint A1) is imposed purely for notational convenience, and it is readily seen that the subsequent analysis does not require such an assumption. Constraint A2) is much stronger but needs to be imposed-at least initially- in order to keep the focus on the analysis rather than the notational complexities that would otherwise be introduced. In Section 8.2, we discuss how to weaken this constraint, and show that all of our results can be extended to the case of arbitrary types of intersections.

We now develop the necessary notation.

8.1.1.1 Partition of the boundary

Let $j \in \{1, \dots, N\}$. Given the disk Ω_j we define the sets

$$\Gamma_j^{\text{ext}} := \partial\Omega_j \cap \partial\Omega, \quad \Gamma_j^{\text{int}} := \overline{\partial\Omega_j \setminus \Gamma_j^{\text{ext}}}.$$

These sets represent a decomposition of the boundary $\partial\Omega_j$ into an 'external' part Γ_j^{ext} that is common with the boundary $\partial\Omega$ of the global domain and an 'internal' part Γ_j^{int} that is contained in the global domain Ω. Notice that the sets Γ_j^{ext} and Γ_j^{int} are both closed. An example of a domain $\Omega = \cup_{j=1}^N \Omega_j$ and the decomposition of the subdomain boundaries $\partial\Omega_j$ is shown in Figure 8.2.

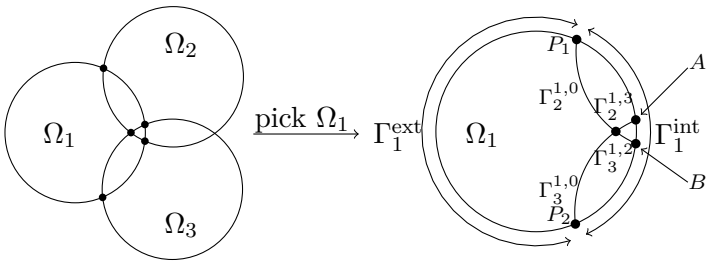

Figure 8.2: An example of three intersecting subdomains Ω_1, Ω_2 and Ω_3 (left), external and internal boundaries of Ω_1, and boundaries of Ω_2 and Ω_3 intersecting Ω_1 (right).

Next, a further decomposition of Γ_j^{int} is considered. To this end, we first define the set N_j as

$$N_j := \{i \in \mathbb{N}, i \neq j : \Omega_i \cap \Omega_j \neq \emptyset\}.$$

Thus, N_j is the set of indices of all subdomains $\{\Omega_i\}_{i=1, i\neq j}^N$ that intersect the subdomain Ω_j. Informally, we refer to N_j as the index set of neighbours of Ω_j. Furthermore, given the set N_j we define for each $k \in N_j$ the set $N_{jk} \subset \mathbb{N}_0$ as

$$N_{jk} := (N_j \cap N_k) \cup \{0\}.$$

Next, for each $j \in \{1, \dots, N\}$, each $k \in N_j$ and each $i \in N_{jk}$ we define the set $\Gamma_j^{k,i} \subset \Gamma_j^{\text{int}}$ as

$$\Gamma_j^{k,i} := \begin{cases} \text{int}\,\{x \in \partial\Omega_j : x \in \Omega_k \cap \Omega_i\} & \text{if } i \neq 0, \\ \text{int}\,\big\{x \in \partial\Omega_j : (x \in \Omega_k) \wedge \big(x \notin \Omega_\ell \ \forall \ell \in N_j \text{ such that } \ell \neq k\big)\big\} & \text{if } i = 0, \end{cases}$$

where $\text{int}(\cdot)$ denotes the interior of a set. Intuitively, for a fixed $k \in N_j$ and $0 \neq i \in N_{jk}$, the set $\Gamma_j^{k,i}$ denotes the portion of $\partial\Omega_j$ that intersects both subdomain k and subdomain i, while $\Gamma_j^{k,0}$ denotes the portion of $\partial\Omega_j$ that intersects only subdomain k. We remark that the set $\Gamma_j^{k,i}$ is open for every $j \in \{1, \dots, N\}, k \in N_j$ and $i \in N_{jk}$.

These definitions allow us to partition the 'interior' part of the boundary Γ_j^{int} in a natural manner. Indeed we obtain that

$$\Gamma_j^{\text{int}} = \overline{\cup_{k \in N_j} \cup_{i \in N_{jk}} \Gamma_j^{k,i}}.$$

Notice that by definition, for a fixed $j \in \{1, \dots, N\}$ and $i, k \neq 0$ it holds that $\Gamma_j^{k,i} = \Gamma_j^{i,k}$.

As the last step, we wish to introduce the notion of so-called *skeletons* associated with each subdomain. To this end, let $j \in \{1, \dots, N\}$ and $k \in N_j$ be fixed. Then we define the sets $\mathcal{S}_{j,k}^{\text{int}}$ and $\mathcal{S}_{j,k}$ as

$$\mathcal{S}_{j,k} := \overline{\bigcup_{i \in N_{jk}} \Gamma_k^{j,i}}, \qquad \mathcal{S}_{j,k}^{\text{int}} := \mathcal{S}_{j,k} \setminus \partial\Omega_j,$$

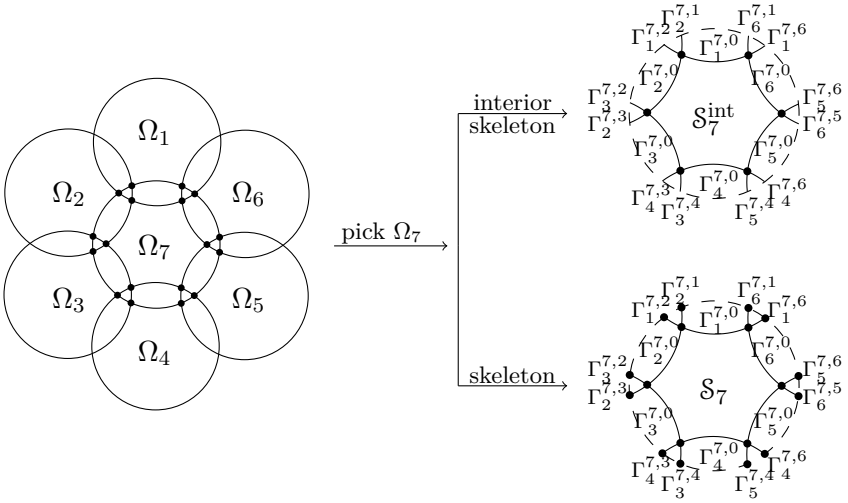

Figure 8.3: The skeleton and interior skeleton corresponding to the subdomain Ω_7 are shown. Notice that the difference between the skeleton and the interior skeleton of Ω_7 given by the points of $\mathcal{S}_7$ that intersect $\partial\Omega_7$: $\mathcal{S}_7 \setminus \mathcal{S}_7^{\text{int}} = \mathcal{S}_7 \cap \partial\Omega_7$.

Intuitively, for a fixed subdomain Ω_j and its neighbouring subdomain Ω_k, the set $\mathcal{S}_{j,k}^{\text{int}}$ consists of the closure of all the interior boundaries of the subdomain Ω_k that intersect Ω_j *excluding points on the boundary* $\partial\Omega_j$. Similarly, the set $\mathcal{S}_{j,k}$ consists of the closure of all the interior boundaries of the subdomain Ω_k that intersect $\overline{\Omega}_j$. It is now easy to see that for a fixed subdomain Ω_j it holds that

$$\bigcup_{j \in N_k} \mathcal{S}_{j,k} = \Gamma_k^{\text{int}}.$$

Finally, for a fixed $j \in \{1, \dots, N\}$ we define the sets $\mathcal{S}_j$ and $\mathcal{S}_j^{\text{int}}$ as

$$\mathcal{S}_j := \bigcup_{k \in N_j} \mathcal{S}_{j,k}, \quad \mathcal{S}_j^{\text{int}} := \bigcup_{k \in N_j} \mathcal{S}_{j,k}^{\text{int}},$$

and we say that $\mathcal{S}_j$ and $\mathcal{S}_j^{\text{int}}$ are the skeleton and the interior skeleton of the subdomain Ω_j. An example of the skeleton and interior skeleton of a subdomain Ω_j is given in Figure 8.3.

Notation: Let $u_j \in L^\infty(\mathcal{S}_j)$ be a function. Then we define the infinity norm of u_j, denoted $\|u_j\|_\infty$, as

$$\|u_j\|_\infty := \operatorname*{ess\,sup}_{\mathcal{S}_j} |u_j|.$$

Additionally, let $u_j \in L^\infty(\mathcal{S}_j)$ for each $j = 1, \ldots, N$ be a family of functions and define $\mathbf{u} := (u_1, u_2, \ldots, u_N)$. Then we define the infinity norm of $\mathbf{u}$, denoted $\|\mathbf{u}\|_\infty$ as

$$\|\mathbf{u}\|_\infty := \max_{j=1,\ldots,N} \operatorname*{ess\,sup}_{\mathcal{S}_j} |u_j|.$$

Finally, we remark that if $\mathbf{u} = (u_1, u_2, \ldots, u_N)$ is a continuous function, i.e., each $u_j,\ j = 1, \ldots, N$ is continuous on $\mathcal{S}_j$ then we write $\mathbf{u} \in \Pi_{j=1}^N C^0(\mathcal{S}_j)$. Similarly, if each $u_j,\ j = 1, \ldots, N$ is continuous on $\mathcal{S}_j^{\text{int}}$ then we write $\mathbf{u} \in \Pi_{j=1}^N C^0(\mathcal{S}_j^{\text{int}})$.

8.1.1.2 Graph and layers of a domain

Definition 8.1 (Graph of a domain $\Omega = \cup_{j=1}^N \Omega_j$)**.** Consider a domain $\Omega = \cup_{j=1}^N \Omega_j$. We define the undirected graph $\mathcal{G}$ associated with the domain Ω as the set of vertices $\mathcal{V}$ given by $\mathcal{V} := \{1, \ldots, N\}$, and the set of edges E given by $E := \{(i, j) \in \mathcal{V} \times \mathcal{V} \colon j \in N_i\}$. Furthermore, we say that the node $i \in \mathcal{V}$ is a boundary node if $\partial\Omega_i \cap \partial\Omega$ is a set of measure greater than zero.

The graph $\mathcal{G}$ associated with a domain Ω provides an easy and intuitive visualization of the connectivity of the domain. As we shall see, the convergence properties of the Schwarz method depend on the connectivity of the domain Ω.

Definition 8.2 (Layers of a graph)**.** Given a domain $\Omega = \cup_{j=1}^N \Omega_j$, consider the graph $\mathcal{G}$ associated with this domain. Then we define the layers of the graph $\mathcal{G}$ in an inductive manner as follows:

1. Layer 1 is the set of all boundary nodes of $\mathcal{G}$. This set is denoted by $\mathcal{L}_1$.
2. For any $j > 1$ we define the graph $\mathcal{G}_j$ iteratively as the set $\mathcal{W}_j := \mathcal{V} - \cup_{k=1}^{j-1} \mathcal{L}_k$ together with the associated set of edges. If $\mathcal{W}_j$ is non-empty, then Layer j is the set $\mathcal{L}_j$ of all boundary nodes of $\mathcal{G}_j$.

Moreover, $N_{\max}$ denotes the total number of layers in the graph, and we say that the domain Ω has $N_{\max}$ layers.

An example of a domain and its decomposition into layers is shown in Figure 8.4.

Definition 8.3. Let $\Omega = \cup_{j=1}^N \Omega_j$ be a domain with $N_{\max}$ layers. Then for any natural number $n \leq N_{\max}$ we define the sets $\mathcal{V}_n$ and $\mathcal{C}_n$ as follows:

$$\mathcal{V}_n := \left\{ \mathbf{v} \in \Pi_{j=1}^N C^0(\mathcal{S}_j^{\text{int}}) \colon \|\mathbf{v}\|_\infty \leq 1 \text{ and } \begin{cases} \mathbf{v}_j(x) < 1 & \forall x \in \mathcal{S}_j^{\text{int}}, \forall j \in \cup_{k=1}^n \mathcal{L}_k, \\ \mathbf{v}_j = 1 & \text{on } \mathcal{S}_j, \forall j \in \cup_{k=n+1}^{N_{\max}} \mathcal{L}_k. \end{cases} \right\},$$

$$\mathcal{C}_n := \left\{ \mathbf{v} \in \Pi_{j=1}^N C^0(\mathcal{S}_j^{\text{int}}) \colon \|\mathbf{v}\|_\infty \leq 1 \text{ and } \operatorname*{ess\,sup}_{\mathcal{S}_j} \mathbf{v}_j < 1,\ \forall j \in \cup_{k=1}^n \mathcal{L}_k \right\}.$$

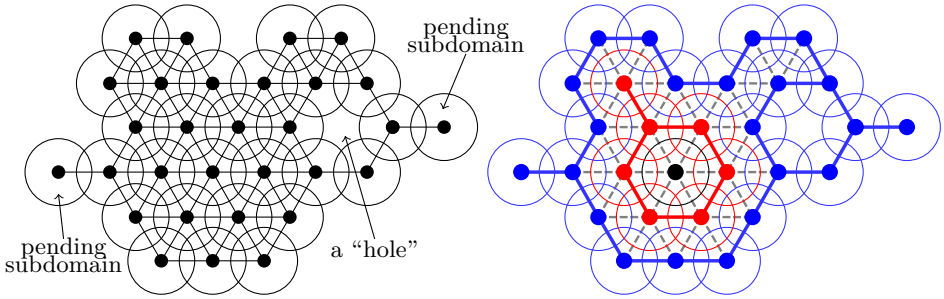

Figure 8.4: Left: An example of a domain $\Omega = \cup_{j=1}^{N} \Omega_j$ (as a collection of disks) and its corresponding graph (black nodes and edges). Notice the presence of two "pending subdomains" and a "hole". Right: Layers corresponding to the left figure. In particular, the blue nodes represent $\mathcal{L}_1$ (Layer 1), the red nodes $\mathcal{L}_2$ (Layer 2), and the black node $\mathcal{L}_3$ (Layer 3).

Intuitively, a non-negative function $\mathbf{v} \in \Pi_{j=1}^{N} C^0(\mathcal{S}_j)$ is in the set $\mathcal{V}_n$ if $\mathbf{v}_j(x) < 1$ for all points x on the *interior skeleton* of all subdomains Ω_j that belong to the first n layers of the domain. Notice that there is no constraint on the behaviour of the function $\mathbf{v}_j$ at the endpoints of the skeleton $\mathcal{S}_j$. Therefore, in some sense, the function $\mathbf{v}$ has *begun to experience a contraction* on all subdomains in the first n layers, but it cannot yet be claimed that the function $\mathbf{v}$ has infinity norm strictly smaller than one on the first n layers.

On the other hand, a non-negative function $\mathbf{w}$ in $\Pi_{j=1}^{N} C^0(\mathcal{S}_j^{\text{int}})$ is in the set $\mathcal{C}_n$ if $\operatorname{ess\,sup}_{\mathcal{S}_j} \mathbf{w}_j < 1$ on all subdomains Ω_j that belong to the first n layers of the domain. Therefore, the function $\mathbf{w}$ has *already contracted* on all subdomains in the first n layers and thus has infinity norm less than one on these subdomains.

8.1.1.3 Partition of unity, extension and restriction operators

Let $j \in \{1, \ldots, N\}$, we define for each $k \in N_j$ a function $\chi_j^k \colon \partial\Omega_j \to \mathbb{R}$, continuous on $\operatorname{int}\big(\Gamma_j^{\text{int}}\big)$, with the property that

$$\chi_j^k := \begin{cases} 1 & \text{on } \overline{\Gamma_j^{k,0}} \setminus \Gamma_j^{\text{ext}}, \\ \in [0,1] & \text{on } \overline{\Gamma_j^{k,i}} \setminus \Gamma_j^{\text{ext}} \qquad \text{for } i \in N_{j,k} \text{ with } i \neq 0, \\ 0 & \text{otherwise,} \end{cases} \tag{8.2}$$

and such that

$$\sum_{k \in N_j} \chi_j^k(x) = 1 \quad \text{for all } x \in \operatorname{int}\big(\Gamma_j^{\text{int}}\big). \tag{8.3}$$

We say that $\{\chi_j^k\}_{k \in N_j}$ are the partition of unity functions on Γ_j^{int}.

Remark 8.4. Let us consider a general domain $\Omega = \cup_{i=1}^{N} \Omega_j$. If for all $j = 1, \ldots, N$, no set Γ_j^{ext} has an isolated point, then we can readily use Equation (8.2) to define the partition of unity functions. In the pathological case where some set Γ_j^{ext} has an isolated point

(see Figure 8.5), Equation (8.2) does not provide a correct function definition. In this pathological situation, we can modify Definition (8.2) by setting at least one partition of unity function to be non-zero at this isolated point. This modification preserves the continuity requirement on the partition of unity functions.

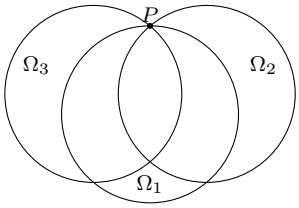

Figure 8.5: An example of a pathological geometry where the point P is an isolated point of Γ_1^{ext}. In this case, one must slightly modify the definitions of the partition of unity functions χ_1^2 and χ_1^3 at the point P in order to ensure that both functions are well-defined and continuous on $\text{int}(\Gamma_1^{\text{int}})$.

Remark 8.5. Consider a subdomain Ω_j and the partition of unity functions $\{\chi_j^k\}_{k\in N_j}$. It follows from the definition of these functions that

$$\sum_{k\in N_j} \chi_j^k(x) = 0 \quad \text{for all } x \in \Gamma_j^{\text{ext}}.$$

Consequently, there is a subset of the boundary $\partial\Omega_j$ with non-zero Lebesgue measure on which all partition of unity functions are zero if and only if $\partial\Omega_j \cap \partial\Omega$ is a set of measure greater than zero.

Remark 8.6. Consider the partition of unity functions defined through Equation (8.2). Two natural questions arise: 1) Is the assumption of continuity that we have imposed on the partition of unity functions truly necessary? 2) Does the choice of the partition of unity functions affect the iterates of the parallel Schwarz method and the asymptotic contraction factor? It can indeed be verified that the proofs of all lemmas in the subsequent Section 8.1.3.1 still hold if we drop the continuity assumption on the partition of unity functions. On the other hand, numerical experiments in Section 8.3 reveal that different choices of the partition of unity functions can lead to quantitatively slightly different Schwarz iterates.

Next, we define our harmonic extension operators. To this end, let $\Gamma_j \subseteq \partial\Omega_j$ be a non-empty open set. Then we define the mapping $\mathcal{E}_j \colon L^2(\Gamma_j) \to C^0(\Omega_j)$ as the operator with the property that given any input function $u_j \in L^2(\Gamma_j)$, the output function $w_j := \mathcal{E}_j(u_j) \in C^0(\Omega_j)$ is the unique solution to the Dirichlet problem:

$$\begin{aligned} \Delta w_j &= 0 && \text{in } \Omega_j, \\ w_j &= u_j && \text{on } \Gamma_j, \\ w_j &= 0 && \text{on } \partial\Omega_j \setminus \Gamma_j. \end{aligned}$$

Finally, we define our restriction operators. Let $C^{0,\text{pc}}(\overline{\Omega_j})$ denote the set of functions on $\overline{\Omega_j}$ that are continuous on Ω_j and *piecewise continuous* on the boundary $\partial\Omega_j$. Then,

we define the mapping $\mathcal{R}_j \colon C^{0,\mathrm{pc}}(\overline{\Omega_j}) \to C^0(\mathcal{S}_j^{\mathrm{int}}) \cap L^\infty(\mathcal{S}_j)$ as

$$\mathcal{R}_j \colon u \mapsto \mathcal{R}_j(u) = u|_{\mathcal{S}_j},$$

and we say that $\mathcal{R}_j$ is the restriction operator on Ω_j.

Intuitively, the map $\mathcal{R}_j$ takes as input a continuous function v_j defined on Ω_j with piecewise continuous values on the boundary $\partial\Omega_j$ and gives as output the restriction of this function on the skeleton $\mathcal{S}_j$. Notice that we cannot claim a priori that the output function $\mathcal{R}_j(v_j)$ is continuous on the entire skeleton $\mathcal{S}_j$ since it is possible that there is a jump discontinuity at the endpoints of the skeleton $\mathcal{S}_j$ which lie on the boundary $\partial\Omega_j$.

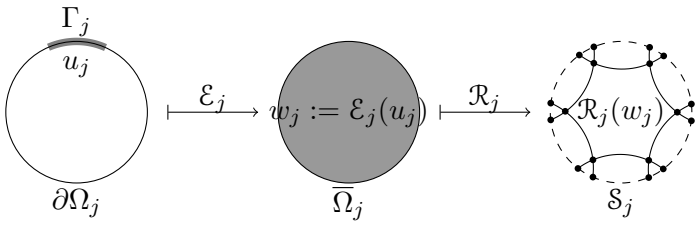

Figure 8.6: Representation of the maps $\mathcal{E}_j$ and $\mathcal{R}_j$: a function $u_j : \Gamma_j \to \mathbb{R}$ is extended harmonically in Ω_j by $\mathcal{E}_j$. The harmonic extension $w_j := \mathcal{E}_j(u_j)$ is then restricted to the skeleton $\mathcal{S}_j$ by the map $\mathcal{R}_j$.

In what follows, we will often consider the composition $\mathcal{R}_j\big(\mathcal{E}_j(\lambda)\big)$ where $\lambda \in L^2(\Gamma_j)$ and $\Gamma_j \subset \partial\Omega_j$. We remark that this composition is well defined if λ is a piecewise continuous function. A schematic representation of the mappings $\mathcal{E}_j$ and $\mathcal{R}_j$ is given in Figure 8.6.

8.1.2 The Schwarz method and the operator formulation

We wish to apply the parallel Schwarz method (PSM) in order to obtain the solution to Equation (8.1). To this end, we consider the natural decomposition of the domain Ω into the N subdomains $\{\Omega_i\}_{i=1}^N$. Then for each $j \in \{1, \dots, N\}$ we find the function $u_j \in L^\infty(\Omega_j)$ such that

$$\begin{aligned} \Delta u_j &= 0 && \text{in } \Omega_j, \\ u_j &= g && \text{on } \Gamma_j^{\mathrm{ext}}, \\ u_j &= \sum_{i \in N_j} u_i \chi_j^i && \text{in } \partial\Omega_j \setminus \Gamma_j^{\mathrm{ext}}. \end{aligned} \tag{8.4}$$

Intuitively and according to (8.4), we look for harmonic functions u_j on each subdomain Ω_j that satisfy appropriate boundary conditions. On the exterior boundary we impose the true data g, while on the interior boundary we impose Dirichlet data, which is traced from the neighbouring subdomain solutions and multiplied by our partition of unity functions.

The equivalence between the global Laplace problem (8.1) and the domain decomposition problem (8.4) will be proved later in Theorem 8.18 in Section 8.1.3.2.

Using (8.4), we obtain the following implementation of the PSM: Let $u_0 \colon \overline{\Omega} \to \mathbb{R}$ be some continuous initialization. For each $j \in \{1, \dots, N\}$ find a sequence of functions $\{u_j^n\}_{n\in\mathbb{N}} \in L^\infty(\Omega_j)$ such that $u_j^0 = u_0|_{\Omega_j}$ and for each $n \in \mathbb{N}$ it holds that

$$\begin{aligned} \Delta u_j^{n+1} &= 0 && \text{in } \Omega_j, \\ u_j^{n+1} &= g && \text{on } \Gamma_j^{\text{ext}}, \\ u_j^{n+1} &= \sum_{i\in N_j} u_i^n \chi_j^i && \text{in } \partial\Omega_j \setminus \Gamma_j^{\text{ext}}. \end{aligned} \tag{8.5}$$

In order to analyse the sequence of functions $\{u_j^n\}_{n\in\mathbb{N}}$ we consider the error equation associated with (8.5). To this end, we define for each $j \in \{1, \dots, N\}$ and each $n \in \mathbb{N}$ the error functions $e_j^n := u_j - u_j^n$. It follows that for each $j \in \{1, \dots, N\}$ the sequence of error functions $\{e_j^n\}_{n\in\mathbb{N}}$ satisfies the equation

$$\begin{aligned} \Delta e_j^{n+1} &= 0 && \text{in } \Omega_j, \\ e_j^{n+1} &= 0 && \text{on } \Gamma_j^{\text{ext}}, \\ e_j^{n+1} &= \sum_{i\in N_j} e_i^n \chi_j^i && \text{in } \partial\Omega_j \setminus \Gamma_j^{\text{ext}}. \end{aligned} \tag{8.6}$$

The key step is now to recognize that a convergence analysis of (8.6) is easier to perform using the notion of the skeleton that we introduced earlier. To do so, for each $n \in \mathbb{N}$ we define an N-dimensional vector $\mathbf{e}^n$ of error functions as

$$\mathbf{e}^n := \begin{bmatrix} \mathbf{e}_1^n \\ \mathbf{e}_2^n \\ \vdots \\ \mathbf{e}_N^n \end{bmatrix}. \tag{8.7}$$

Here, each element $\mathbf{e}_j^n$ is defined as

$$\mathbf{e}_j^n := e_j^n|_{\mathcal{S}_j}.$$

In other words, the entry $\mathbf{e}_j^n$ of the vector $\mathbf{e}^n$ is the restriction of the error function e_j^n on the skeleton $\mathcal{S}_j$ of the subdomain Ω_j.

Next, we introduce the iteration operator corresponding to the above choice of the error vector $\mathbf{e}^n$. To do so, we define the $N \times N$ matrix T by setting

$$T_{ij} := \begin{cases} P_{ij} & \text{if } j \in N_i, \\ 0 & \text{otherwise.} \end{cases} \tag{8.8}$$

The entries P_{ij} of the iteration operator T are operators defined as follows: For each fixed $i \in \{1, \dots, N\}$ and $j \in N_i$ the mapping $P_{ij} \colon C^0(\mathcal{S}_{j,i}) \to C^0(\mathcal{S}_i^{\text{int}}) \cap L^\infty(\mathcal{S}_i)$ is a linear operator such that for all $v_{j,i} \in C^0(\mathcal{S}_{j,i})$ it holds that

$$P_{ij}\mathbf{v} = \mathcal{R}_i\Big(\mathcal{E}_i\Big(v_{j,i}\chi_i^j|_{\mathcal{S}_{j,i}}\Big)\Big).$$

In other words, for a given subdomain Ω_i and a given neighbour Ω_j, the mapping P_{ij}

1. takes as input some function $v_{j,i}$ defined on the skeleton $\mathcal{S}_{j,i}$, i.e., the part of the interior boundary of subdomain Ω_i that is contained in Ω_j, and multiplies it with the partition of unity function χ_i^j,
2. extends the function $v\chi_i^j|_{\mathcal{S}_{j,i}}$ harmonically inside the domain Ω_i,
3. and then yields as output the restriction of this harmonic extension on the skeleton $\mathcal{S}_i$.

We remark that the definition of the iteration operator T implies that it is block-sparse. Indeed, the i^{th} row of T contains non-zero entries exactly at columns $j \in N_i$.

Example 8.7. *Let us consider the situation of a domain Ω consisting of seven subdomains, i.e., $\Omega = \cup_{j=1}^7 \Omega_j$ as shown in Figure 8.3. In this setting the iteration operator T is a 7×7 matrix given by*

$$T = \begin{bmatrix} 0 & P_{12} & 0 & 0 & 0 & P_{16} & P_{17} \\ P_{21} & 0 & P_{23} & 0 & 0 & 0 & P_{27} \\ 0 & P_{32} & 0 & P_{34} & 0 & 0 & P_{37} \\ 0 & 0 & P_{43} & 0 & P_{45} & 0 & P_{47} \\ 0 & 0 & 0 & P_{54} & 0 & P_{56} & P_{57} \\ P_{61} & 0 & 0 & 0 & P_{65} & 0 & P_{67} \\ P_{71} & P_{72} & P_{73} & P_{74} & P_{75} & P_{76} & 0 \end{bmatrix}.$$

The next step in our analysis is to observe that using (8.7) and (8.8), we can rewrite (8.6) as

$$\mathbf{e}^{n+1} = T\mathbf{e}^n \qquad \text{for each } n \in \mathbb{N}. \tag{8.9}$$

Lemma 8.8. *Equation (8.6) is equivalent to Equation (8.9).*

Proof. We show that (8.9) can equivalently be rewritten as (8.6). To this end, let $n \in \mathbb{N}$. Then Equation (8.9) can be written as

$$\mathbf{e}_j^n = \sum_{k=1}^{N} T_{jk}\mathbf{e}_k^{n-1} \qquad \forall j \in \{1, \dots, N\},$$

which is equivalent to

$$\mathbf{e}_j^n = \sum_{k \in N_j} P_{jk}\mathbf{e}_k^{n-1} \qquad \forall j \in \{1, \dots, N\}.$$

Using the definition of the operators P_{ik} we obtain for all $j \in \{1, \dots, N\}$

$$\mathbf{e}_j^n = \sum_{k \in N_j} \mathcal{R}_j \left(\mathcal{E}_j \left(\mathbf{e}_k^{n-1}|_{\mathcal{S}_{k,j}} \chi_j^k|_{\mathcal{S}_{k,j}} \right) \right) = \mathcal{R}_j \left(\mathcal{E}_j \Big(\sum_{k \in N_j} \mathbf{e}_k^{n-1}|_{\mathcal{S}_{k,j}} \chi_j^k|_{\mathcal{S}_{k,j}} \Big) \right). \tag{8.10}$$

A direct inspection now shows that Equation (8.10) is equivalent to Equation (8.6). □

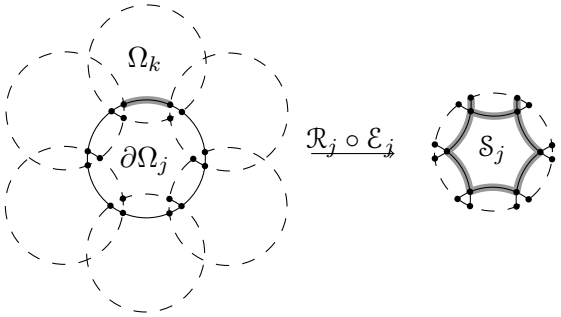

Figure 8.7: Example of the application of Lemma 8.9. A function $v : \partial\Omega_j \to \mathbb{R}$ such that $v(x) \in [0,1]$ for all $x \in \partial\Omega_j$ with $v(x) < 1$ for $x \in \Gamma_j^{k,0}$ for some k (thick gray arc in the left picture) is mapped by the operator $\mathcal{R}_j \circ \mathcal{E}_j$ on to a function $w := \mathcal{R}_j(\mathcal{E}_j(v))$ defined on $\mathcal{S}_j$ and satisfying $w(x) \in [0,1]$ for all $x \in \mathcal{S}_j$, $w(x) < 1$ for all $x \in \mathcal{S}_j^{\text{int}}$.

It therefore follows that in order to analyse the convergence of the sequence of error functions $\{e_j^n\}_{n\in\mathbb{N}}$, $j \in \{1,\dots,N\}$ defined through Equation (8.6), we must study the convergence of the error vectors $\{\mathbf{e}^n\}_{n\in\mathbb{N}}$ defined through the matrix equation (8.9). More specifically, we must analyse the structure of the Schwarz iteration operator T. This is the subject of the next Section 8.1.3.

8.1.3 Convergence analysis

8.1.3.1 Technical lemmas

The goal of this section is to introduce some technical results that we use to prove our main theorems. We begin with the following first result.

Lemma 8.9. *Let $j \in \{1,\dots,N\}$ and consider the subdomain Ω_j, let $\widetilde{u} \in L^\infty(\partial\Omega_j)$ be a non-negative, piecewise continuous function such that $\operatorname{ess\,sup}_{\partial\Omega_j} \widetilde{u} \leq 1$. Assume that there exists at least one neighbouring index $k \in N_j$ of the subdomain Ω_j such that $\widetilde{u} < 1$ in $\mathcal{S}_{k,j}^{\text{int}}$, and define the function $u^{\text{new}} \in L^\infty(\mathcal{S}_j)$ as $u^{\text{new}} := \mathcal{R}_j\left(\mathcal{E}_j(\widetilde{u})\right)$. Then it holds that*

$$0 \leq \operatorname*{ess\,sup}_{\mathcal{S}_j} u^{\text{new}} \leq 1, \quad u^{\text{new}}(x) < 1 \ \forall x \in \mathcal{S}_j^{\text{int}}.$$

An example of the application of Lemma 8.9 is given in Figure 8.7.

Proof. The proof follows from the maximum principle for harmonic functions (see, e.g., [29]) combined with the definition of the partition of unity functions introduced above. □

Next, we prove a fundamental lemma concerning the norm of the iteration operator T.

Lemma 8.10. *Let $\mathbf{1} \in \Pi_{j=1}^N C^0\left(\mathcal{S}_j\right)$ denote an N-dimensional vector with the property that every j^{th} entry of the vector is a function identically equal to 1 on the skeleton $\mathcal{S}_j$.*

Then for any natural number $n \in \mathbb{N}$ it holds that

$$\|T^n\|_{\mathrm{OP},\infty} := \sup_{\substack{\mathbf{v}\in\Pi_{j=1}^N C^0(\mathcal{S}_j^{\mathrm{int}}) \\ \|\mathbf{v}\|_\infty = 1}} \|T^n\mathbf{v}\|_\infty = \|T^n\mathbf{1}\|_\infty.$$

Proof. We first prove an intermediate result. Let $\mathbf{v}, \mathbf{u} \in \Pi_{j=1}^N C^0(\mathcal{S}_j^{\mathrm{int}})$ be two functions such that

$$\mathbf{v} \leq \mathbf{u} \quad \text{on } \cup_{j=1}^N \mathcal{S}_j.$$

We prove that

$$(T\mathbf{v}) \leq (T\mathbf{u}) \qquad \text{on } \cup_{j=1}^N \mathcal{S}_j. \tag{8.11}$$

Define $\mathbf{w} := T(\mathbf{u}-\mathbf{v})$. Then by definition of T we obtain that for each $j \in \{1,\dots,N\}$ it holds that

$$\begin{aligned}\mathbf{w}_j = \sum_{i\in N_j} P_{ji}(\mathbf{u}_i - \mathbf{v}_i) &= \sum_{i\in N_j} \mathcal{R}_j\left(\mathcal{E}_j\Big((\mathbf{u}_i - \mathbf{v}_i)|_{\mathcal{S}_{j,i}}\,\chi_j^i|_{\mathcal{S}_{j,i}}\Big)\right) \\ &= \mathcal{R}_j\left(\mathcal{E}_j\Big(\sum_{i\in N_j}(\mathbf{u}_i - \mathbf{v}_i)|_{\mathcal{S}_{j,i}}\,\chi_j^i|_{\mathcal{S}_{j,i}}\Big)\right).\end{aligned}$$

In other words, the function $\mathbf{w}_j$ is simply the restriction onto the skeleton $\mathcal{S}_j$ of the harmonic solution to a Dirichlet problem with boundary data from $\mathbf{u}-\mathbf{v}$.

Recall that we have by hypothesis that for each $j \in \{1,\dots,N\}$ it holds that $\mathbf{u}_j - \mathbf{v}_j \geq 0$ on $\mathcal{S}_j$. It follows from the maximum principle that for each $j \in \{1,\dots,N\}$ we have

$$\mathbf{w}_j \geq 0 \qquad \text{on } \mathcal{S}_j.$$

Therefore, we obtain that

$$\mathbf{w} = (T(\mathbf{u}-\mathbf{v})) \geq 0 \qquad \text{on } \cup_{j=1}^N \mathcal{S}_j.$$

This completes the proof for Equation (8.11).

We now proceed to the proof of Lemma 8.10. Note that it suffices to prove that for all natural numbers $n \in \mathbb{N}$ and all functions $\mathbf{v} \in \Pi_{j=1}^N C^0(\mathcal{S}_j^{\mathrm{int}})$ such that $\|\mathbf{v}\|_\infty = 1$ it holds that

$$(T^n\mathbf{v}) \leq (T^n\mathbf{1}) \qquad \text{on } \cup_{j=1}^N \mathcal{S}_j. \tag{8.12}$$

The proof follows easily by induction from Equation (8.11). Indeed, the base case follows immediately by picking $\mathbf{u} = \mathbf{1}$. Next, assume that (8.12) holds for some $k \in \mathbb{N}$. We define functions $\widetilde{\mathbf{v}} := T^k\mathbf{v}$ and $\widetilde{\mathbf{u}} := T^k\mathbf{1}$ and recognize that the induction hypothesis implies that

$$\widetilde{\mathbf{v}} \leq \widetilde{\mathbf{u}} \qquad \text{on } \cup_{j=1}^N \mathcal{S}_j.$$

Therefore, applying once again Equation (8.11) to the functions $\widetilde{\mathbf{v}}$ and $\widetilde{\mathbf{u}}$ yields the required result. This completes the proof. □

We are now ready to state our second fundamental result.

Lemma 8.11. *Let $\Omega = \cup_{j=1}^{N} \Omega_j$ be a domain with $N_{\max}$ layers. Then for all natural numbers $n \leq N_{\max}$ it holds that $T^n \mathbf{1} \in \mathcal{V}_n$.*

Proof. The proof proceeds by induction. We consider the base case $n = 1$ and show that $T\mathbf{1} \in \mathcal{V}_1$. To this end, let $\mathbf{v} = T\mathbf{1}$. We first consider a subdomain Ω_j such that the node j is in $\mathcal{L}_1$. Clearly, we have that $\partial\Omega_j \cap \partial\Omega \neq \emptyset$. Therefore applying Lemma 8.9 yields that $\mathbf{v}_j(x) < 1$ for all $x \in \mathcal{S}_j^{\text{int}}$. Next, consider a subdomain Ω_j such that node j is in $\mathcal{L}_2$ or higher. It follows from the definition of the layers that Ω_j does not correspond to a boundary node, and thus $\partial\Omega_j \cap \partial\Omega = \emptyset$. Using the definition of the iteration operator T, Equation (8.3), and Remark 8.5 we have that

$$\begin{aligned} \mathbf{v}_j &= \sum_{i \in N_j} P_{ji}(\mathbf{1})_i = \sum_{i \in N_j} \mathcal{R}_j \left(\mathcal{E}_j \Big((\mathbf{1})_i |_{\mathcal{S}_{j,i}} \chi_j^i |_{\mathcal{S}_{j,i}} \Big) \right) \\ &= \sum_{i \in N_j} \mathcal{R}_j \left(\mathcal{E}_j \Big(\chi_j^i |_{\mathcal{S}_{j,i}} \Big) \right) = \mathcal{R}_j \left(\mathcal{E}_j \Big(\sum_{i \in N_j} \chi_j^i |_{\mathcal{S}_{j,i}} \Big) \right) \\ &= \mathcal{R}_j \big(\mathcal{E}_j(1) \big) = (\mathbf{1})_j. \end{aligned} \tag{8.13}$$

We therefore obtain that $\mathbf{v}_j = (\mathbf{1})_j$. This completes the proof for the base case.

Assume now that the result holds for some natural number $n = k < N_{\max}$, i.e., that $T^k \mathbf{1} \in \mathcal{V}_k$. We must prove that $T^{k+1}\mathbf{1} \in \mathcal{V}_{k+1}$.

Let $\mathbf{v} := T^k \mathbf{1}$, let $\mathbf{w} := T^{k+1}\mathbf{1}$ and consider an arbitrary subdomain Ω_j. If node j is in $\mathcal{L}_1$, then Lemma 8.9 yields that $\mathbf{v}_j(x) < 1$ for all $x \in \mathcal{S}_j^{\text{int}}$. On the other hand, if node j is in $\mathcal{L}_m$ where $m \in \{2, \ldots, k+1\}$, then it follows from the definition of the layers that there must exist a neighbouring node $i' \in N_j$ such that node i' is in $\mathcal{L}_{m-1}$. The definition of the iteration operator T therefore yields

$$\begin{aligned} \mathbf{w}_j = \sum_{i \in N_j} P_{ji} \mathbf{v}_i &= \mathcal{R}_j \left(\mathcal{E}_j \Big(\mathbf{v}_{i'} |_{\mathcal{S}_{j,i'}} \chi_j^{i'} |_{\mathcal{S}_{j,i'}} \Big) \right) + \sum_{\substack{i \in N_j \\ i \neq i'}} \mathcal{R}_j \left(\mathcal{E}_j \Big(\mathbf{v}_i |_{\mathcal{S}_{j,i}} \chi_j^i |_{\mathcal{S}_{j,i}} \Big) \right) \\ &= \mathcal{R}_j \left(\mathcal{E}_j \Big(\mathbf{v}_{i'} |_{\mathcal{S}_{j,i'}} \chi_j^{i'} |_{\mathcal{S}_{j,i'}} + \sum_{\substack{i \in N_j \\ i \neq i'}} \mathbf{v}_i |_{\mathcal{S}_{j,i}} \chi_j^i |_{\mathcal{S}_{j,i}} \Big) \right). \end{aligned}$$

The induction hypothesis implies that $\mathbf{v}_{i'}(x) < 1$ for all $x \in \mathcal{S}_{i'}^{\text{int}}$. This implies in particular that $\mathbf{v}_{i'}(x) < 1$ for all $x \in \mathcal{S}_{j,i'}^{\text{int}}$. Since the function $\mathbf{w}_j$ is simply the restriction on to the skeleton $\mathcal{S}_j$ of the harmonic extension of boundary data from the function $\mathbf{v}$, we can apply Lemma 8.9 to obtain that $\mathbf{w}_j(x) < 1$ for all $x \in \mathcal{S}_j^{\text{int}}$.

If $k + 1 = N_{\max}$ then we are done. If not, then consider a subdomain Ω_j such that the node j is in $\mathcal{L}_{\widetilde{m}}$ where $\widetilde{m} \in \{k+2, \ldots, N_{\max}\}$. We must show that $\mathbf{w}_j = 1$ on $\mathcal{S}_j$.

It follows from the definition of the layers that all neighbouring nodes $\ell \in N_j$ must belong to $\mathcal{L}_{m'}$ where $m' \in \{k+1, \dots, N_{\max}\}$. Therefore, the induction hypothesis implies that for each $\ell \in N_j$ it holds that $\mathbf{v}_\ell = 1$ on $\mathcal{S}_{j,\ell}$.

Using the definition of the iteration operator T and Remark 8.5, and proceeding in the same manner as in Equation (8.13) we obtain that $\mathbf{w}_j = (\mathbf{1})_j$, and we have thus shown that $T^{k+1}\mathbf{1} = \mathbf{w} \in \mathcal{V}_{k+1}$. This completes the proof by induction. □

Our next goal is to obtain an analogous result for the set $\mathcal{C}_n$. To this end, we require the use of the following key lemma.

Lemma 8.12. *Let $\Omega = \cup_{i=1}^N \Omega_i$ be a domain with $N_{\max}$ layers, let $\mathbf{v} \in \Pi_{j=1}^N C^0\big(\mathcal{S}_j^{\text{int}}\big)$ be such that $\|\mathbf{v}_j\|_\infty \leq 1$, and let $\mathbf{w} = T\mathbf{v}$. Consider a subdomain Ω_j such that for all neighbouring indices $i \in N_j$ it holds that $\mathbf{v}_i(x) < 1$ for all $x \in \mathcal{S}_i^{\text{int}}$. Then it holds that*

$$\|\mathbf{w}_j\|_{L^\infty(\mathcal{S}_j)} := \operatorname*{ess\,sup}_{\mathcal{S}_j} \mathbf{w}_j < 1.$$

Proof. By the definition of the iteration operator we have that

$$\mathbf{w}_j = \sum_{i \in N_j} P_{ji}\mathbf{v}_i = \sum_{i \in N_j} \mathcal{R}_j\left(\mathcal{E}_j\Big(\mathbf{v}_i|_{\mathcal{S}_{j,i}}\, \chi_j^i|_{\mathcal{S}_{j,i}}\Big)\right) = \mathcal{R}_j\left(\mathcal{E}_j\Big(\sum_{i \in N_j} \mathbf{v}_i|_{\mathcal{S}_{j,i}}\, \chi_j^i|_{\mathcal{S}_{j,i}}\Big)\right).$$

Therefore, we define the function $h\colon \partial\Omega_j \to \mathbb{R}$ as

$$h(x) := \begin{cases} \sum_{i \in N_j} \mathbf{v}_i|_{\mathcal{S}_{j,i}}(x)\, \chi_j^i|_{\mathcal{S}_{j,i}}(x) & \text{if } x \in \operatorname{int}(\Gamma_j^{\text{int}}), \\ 0 & \text{otherwise.} \end{cases}$$

Next, we observe that the definition of the partition of unity functions and the assumptions of Lemma 8.12 imply two key properties of the function h.

(i) It holds that

$$h(x) = 0 \text{ for all } x \in \Gamma_j^{\text{ext}}, \qquad h(x) \leq 1 \text{ for all } x \in \Gamma_j^{\text{int}}.$$

(ii) It holds that h is a continuous function on $\operatorname{int}\big(\Gamma_j^{\text{int}}\big)$.

As a first step, we prove a third key property of the function h:

(iii) It holds that $h(x) < 1$ for all $x \in \operatorname{int}\big(\Gamma_j^{\text{int}}\big)$.

To this end, let $x \in \operatorname{int}(\Gamma_j^{\text{int}}) = \operatorname{int}\Big(\overline{\cup_{k \in N_j} \cup_{i \in N_{jk}} \Gamma_j^{k,i}}\Big)$. We distinguish two cases:

1. $x \in \overline{\Gamma_j^{k,0}}$ for some neighbouring index $k \in N_j$. We again have two cases:

- $x \in \Gamma_j^{k,0}$. Recalling the definition of the interior skeleton, we obtain also that $x \in \mathcal{S}_{k,j}^{\text{int}} \subset \mathcal{S}_k^{\text{int}}$. Thus it holds that $h(x) = \mathbf{v}_k(x)\chi_j^k(x)$. We recall that by the definition of the partition of unity functions, it holds that $\chi_j^k(x) = 1$ for $x \in \Gamma_j^{k,0}$. Furthermore, we have by assumption that $\mathbf{v}_k(x) < 1$ for $x \in \mathcal{S}_{k,j}^{\text{int}} \subset \mathcal{S}_k^{\text{int}}$. We therefore conclude that $h(x) < 1$.
- $x \notin \Gamma_j^{k,0}$, i.e., x is a boundary point of the closed set $\overline{\Gamma_j^{k,0}}$. Now, either $x \in \Gamma_j^{\text{ext}}$ or there exists some neighbouring index $\ell \in N_{jk}$ such that $x \in \overline{\Gamma_j^{k,\ell}}$. In other words, there are exactly two possibilities: either x is a boundary point of the exterior boundary of Ω_j or x is a boundary point of some triple intersection. Since $x \in \text{int}(\Gamma_j^{\text{int}})$, we have excluded the first case. The second case $x \in \overline{\Gamma_j^{k,\ell}}$ is covered below.

2. $x \in \overline{\Gamma_j^{k,\ell}}$ for some neighbouring indices $k, \ell \in N_j$. Recalling once again the definition of the skeletons, we obtain that $x \in \mathcal{S}_{k,j} \subset \mathcal{S}_k$ and $x \in \mathcal{S}_{\ell,j} \subset \mathcal{S}_\ell$. It therefore follows that

$$h(x) = \mathbf{v}_k(x)\chi_j^k(x) + \mathbf{v}_\ell(x)\chi_j^\ell(x). \tag{8.14}$$

We again have two cases:

- $x \in \mathcal{S}_k^{\text{int}}$. We have by assumption that $\mathbf{v}_k(x) < 1$ for $x \in \mathcal{S}_k^{\text{int}}$. On the other hand, we also know that $\mathbf{v}_\ell(x) \leq 1$ for $x \in \mathcal{S}_\ell$. Therefore, Equation (8.14) implies that $h(x) < 1$.
- $x \notin \mathcal{S}_k^{\text{int}}$. Since $x \in \mathcal{S}_k$, we must have that $x \in \partial\Omega_k$. It is readily seen that this in turn implies that $x \in \mathcal{S}_\ell^{\text{int}}$. Therefore, we obtain that $\mathbf{v}_\ell(x) < 1$, and $\mathbf{v}_k(x) \leq 1$. Hence, Equation (8.14) again implies that $h(x) < 1$.

We conclude that $h(x) < 1$ for all $x \in \text{int}(\Gamma_j^{\text{int}})$ and therefore Property (iii) of the function h also holds.

Consider now the skeleton $\mathcal{S}_j$ and let $\mathcal{S}_{j,k},\ k \in N_j$ be an arbitrary arc of the skeleton. We must show that $\text{ess sup}_{\mathcal{S}_{j,k}} \mathbf{w}_j < 1$. This is a slightly delicate argument since the function $\mathbf{w}_j$ need not be continuous on the closed set $\mathcal{S}_{j,k}$ due to possible jump discontinuities at the endpoints. We therefore proceed in two steps:

1. First we show that $\mathbf{w}_j(x) < 1$ for all $x \in \mathcal{S}_{j,k}^{\text{int}}$, i.e., that the function $\mathbf{w}_j$ is strictly smaller than one in the *interior* of the skeleton arc $\mathcal{S}_{j,k}$. Property (iii) of the function h yields that $h(x) < 1\ \forall x \in \Gamma_j^{\text{int}} \supset \mathcal{S}_{k,j}$. Therefore Lemma 8.9 yields that $\mathbf{w}_j(x) < 1$ for all $x \in \mathcal{S}_j^{\text{int}} \supset \mathcal{S}_{j,k}^{\text{int}}$.

2. Next we show that $\lim_{\substack{x \in \mathcal{S}_{j,k} \\ x \to \partial\Omega_j}} \mathbf{w}_j(x) < 1$. In other words we must show that the limit of the function $\mathbf{w}_j$ along the skeleton arc $\mathcal{S}_{j,k}$, as one approaches the endpoints *is strictly smaller than one*. We emphasise that this step is necessary since the

function $\mathbf{w}_j$, a priori, may contain a jump discontinuity at the endpoints of the skeleton *.

To this end, let $\hat{x} \in \partial\Omega_j$ denote any endpoint of the skeleton arc $\mathcal{S}_{j,k}$. Once again we have two cases:

- Suppose $\hat{x} \in \Gamma_j^{\text{ext}}$. Recall that $h = 0$ on Γ_j^{ext} from Property (i) and $h(x) < 1$ for all $x \in \text{int}(\Gamma_j^{\text{int}})$ from Property (iii). Thus, the Schwarz lemma (see, e.g., [111, Pages 632-635], [29] and [133, Section 3]) implies that

$$\lim_{\substack{x \in \mathcal{S}_{j,k} \\ x \to \hat{x}}} \mathbf{w}_j(x) = \alpha < 1,$$

  where α is a constant that depends on the angle at which the skeleton arc $\mathcal{S}_{j,k}$ intersects the boundary $\partial\Omega_j$ at the point $\hat{x}$.
- Suppose $\hat{x} \notin \Gamma_j^{\text{ext}}$. Then $\hat{x} \in \text{int}\big(\Gamma_j^{\text{int}}\big)$. Property (ii) of the function h implies that h is a continuous function on $\text{int}\big(\Gamma_j^{\text{int}}\big)$. This in turn implies that the harmonic extension $\mathcal{E}_j(h)$ is continuous in a neighbourhood of the point $\hat{x}$. This yields in particular that

$$\lim_{\substack{x \in \mathcal{S}_{j,k} \\ x \to \hat{x}}} \mathbf{w}_j(x) = \mathbf{w}_j(\hat{x}) = h(\hat{x}) < 1.$$

Hence, the claim holds in both cases.

It therefore follows that $\text{ess sup}_{\mathcal{S}_{j,k}} \mathbf{w}_j < 1$. Since the skeleton arc $\mathcal{S}_{j,k}$ was arbitrary, we obtain that

$$\operatorname*{ess\,sup}_{\mathcal{S}_j} \mathbf{w}_j < 1,$$

which completes the proof. □

Consider the setting of Lemma 8.12. The careful reader will observe that the proof of Lemma 8.12 required the use of all three key properties of the boundary data h. In particular, we explicitly used the fact that h is a continuous function on the interior boundary Γ_j^{int}. The continuity of the function h is itself a consequence of our earlier assumption that the partition of unity functions are continuous on the interior boundary Γ_j^{int}. One might therefore wonder if the proof of Lemma 8.12 still holds if the continuity of the partition of unity functions is not imposed. It turns out that this continuity assumption is not necessary to prove Lemma 8.12, and we may instead use the Schwarz lemma. However, as we demonstrate in Section 8.3 using some numerical examples, a choice of discontinuous partition of unity functions may lead to a quantitatively slightly worse contraction of the error at each iteration. We remark that the ddCOSMO implementation uses continuous partition of unity functions in practice.

We conclude this subsection by observing that Lemma 8.12 has the following consequence.

*This situation can arise precisely when the subdomains weakly overlap (see [133])

Lemma 8.13. *Let $\Omega = \cup_{j=1}^{N} \Omega_j$ be a domain with $N_{\max}$ layers, let $n \leq N_{\max} - 2$ be a natural number, and let $\mathbf{u} \in \mathcal{V}_n$. Then it holds that*

$$T^2\mathbf{u} \in \mathcal{C}_n. \tag{8.15}$$

Proof. Let $\mathbf{v} = T\mathbf{u}$ and let $\mathbf{w} = T^2\mathbf{u}$. Since $\mathbf{u} \in \mathcal{V}_n$ and $\|T\|_{\mathrm{OP},\infty} \leq 1$, we obtain that $\|\mathbf{w}\|_\infty \leq \|\mathbf{u}\|_\infty \leq 1$. Therefore, we need only show that $\operatorname{ess\,sup}_{\mathcal{S}_j} \mathbf{w}_j < 1$ for all $j \in \cup_{k=1}^{n} \mathcal{L}_k$.

Let $j \in \cup_{k=1}^{n} \mathcal{L}_k$ and let $\ell \in N_j$ be any neighbouring index. By the definition of the layers, we know that $\ell \in \cup_{k=1}^{n+1} \mathcal{L}_k$. On the other hand, since $\mathbf{v} \in \mathcal{V}_{n+1}$, we know that $\mathbf{v}_\ell(x) < 1$ for all $x \in \mathcal{S}_\ell^{\mathrm{int}}$. Applying Lemma 8.12 immediately yields that $\operatorname{ess\,sup}_{\mathcal{S}_j} \mathbf{w}_j < 1$. Since $j \in \cup_{k=1}^{n} \mathcal{L}_k$ was arbitrary, we conclude that $\mathbf{w} \in C_n$. □

8.1.3.2 Convergence results

We are now ready to state our main results.

Theorem 8.14. *Let $\Omega = \cup_{j=1}^{N} \Omega_j$ be a domain with $N_{\max}$ layers and let $\mathbf{u} \in \mathcal{V}_{N_{\max}}$. Then it holds that*

$$T\mathbf{u} \in \mathcal{C}_{N_{\max}}. \tag{8.16}$$

Proof. Let $\mathbf{w} = T\mathbf{u}$. We must show that for all $j \in \{1, \ldots, N\}$ it holds that $\operatorname{ess\,sup}_{\mathcal{S}_j} \mathbf{w}_j < 1$.

To this end, let $j \in \{1, \ldots, N\}$. Since $\mathbf{u} \in \mathcal{V}_{N_{\max}}$ it follows that that for all neighbouring indices $i \in N_j$ it holds that $\mathbf{u}_i(x) < 1$ for all $x \in \mathcal{S}_i^{\mathrm{int}}$. Applying Lemma 8.12 immediately yields that $\operatorname{ess\,sup}_{\mathcal{S}_j} \mathbf{w}_j < 1$. Since $j \in \{1, \ldots, N\}$ was arbitrary, this completes the proof. □

Theorem 8.14 has the following important consequence.

Corollary 8.15. *Let $\Omega = \cup_{j=1}^{N} \Omega_j$ be a domain with $N_{\max}$ layers. Then it holds that*

$$\|T^{N_{\max}+1}\|_{\mathrm{OP},\infty} < 1.$$

Proof. Lemma 8.10 implies that $\|T^{N_{\max}+1}\|_{\mathrm{OP},\infty} = \|T^{N_{\max}+1}\mathbf{1}\|_\infty$. Theorem 8.14 implies that $T^{N_{\max}+1}\mathbf{1} \in \mathcal{C}_{N_{\max}}$. By definition of the set $\mathcal{C}_{N_{\max}}$ we obtain that $\|T^{N_{\max}+1}\|_{\mathrm{OP},\infty} = \|T^{N_{\max}+1}\mathbf{1}\|_\infty < 1$. □

Remark 8.16. Consider the setting of Theorem 8.14. The relation (8.16) is sharp for $N_{\max} > 1$. See also Example 8.20 for the case $N_{\max} = 1$.

Remark 8.17. Consider the error equation (8.9). Corollary 8.15 implies that

$$\lim_{n\to\infty} \|\mathbf{e}^{n+1}\|_\infty = \lim_{n\to\infty} \|T\mathbf{e}^n\|_\infty = \lim_{n\to\infty} \|T^{n+1}\mathbf{e}^0\|_\infty \leq \lim_{n\to\infty} \|T^{n+1}\|_{\mathrm{OP},\infty} \|\mathbf{e}^0\|_\infty = 0.$$

Theorem 8.14 also allows us to prove that the global Laplace problem (8.1) and the domain decomposition problem (8.4) are indeed equivalent.

Theorem 8.18. *Equations* (8.1) *and* (8.4) *are equivalent. Therefore, the PSM converges to the solution of the global Laplace problem* (8.1).

Proof. It is well known that there exists a unique solution $u \in C^0(\overline{\Omega})$ to Equation (8.1). A direct calculation then shows that the restrictions of this function $u|_{\Omega_j}$, $j \in \{1, \dots, N\}$ on each subdomain Ω_j also satisfy Equation (8.4). Therefore, it suffices to show that Equation (8.4) must have a unique solution.

We argue by contradiction. For each $j \in \{1, \dots, N\}$, let $v_j, \widetilde{v}_j \in C^0(\Omega_j)$ be two distinct solutions to (8.4) on the subdomain Ω_j and let $w_j := v_j - \widetilde{v}_j$. It follows that

$$\begin{aligned} \Delta w_j &= 0 && \text{in } \Omega_j, \\ w_j &= 0 && \text{on } \Gamma_j^{\text{ext}}, \\ w_j &= \sum_{i \in N_j} w_i \chi_j^i && \text{on } \Gamma_j^{\text{int}}. \end{aligned} \tag{8.17}$$

Next, we define the function $\mathbf{w} \in \Pi_{j=1}^N C^0(\mathcal{S}_j^{\text{int}})$ by taking, for each $j = 1, \dots, N$, the restriction of the function w_j on the skeleton $\mathcal{S}_j$. It follows from Equation (8.17) and Lemma 8.8 that $\mathbf{w}$ satisfies the fixed-point equation $\mathbf{w} = T\mathbf{w}$. This implies in particular that

$$\mathbf{w} = T^{N_{\max}+1}\mathbf{w}, \tag{8.18}$$

where $N_{\max}$ is the number of layers in the domain Ω. Equation (8.18) now yields that $\|T^{N_{\max}+1}\|_{\text{OP},\infty} \geq 1$, which contradicts Theorem 8.14. Therefore, we must have that $\mathbf{w} \equiv 0$ which implies that $v_j = \widetilde{v}_j$ for all $j = 1, \dots, N$, and thus Equation (8.4) has a unique solution. □

8.1.3.3 Discussion on convergence results and related examples

In this section, we discuss the convergence results obtained in Section 8.1.3 and use two examples to explain the heuristic behind them and demonstrate how they can be considered an extension of existing results given in the literature [28, 29]. In particular, in Example 8.19 we show how our results are capable of precisely tracking the propagation of the contraction across the different layers comprising the domain Ω in the course of the iterations. In Example 8.20, we consider a problem defined on a linear chain of collinear subdomains and demonstrate how our results can be considered an extension of existing convergence results in the literature.

Example 8.19. *We first consider a domain Ω consisting of the union of 51 subdomains grouped in 4 layers as shown in Figure 8.8 (left). We will describe visually the results obtained in Section 8.1.3 as they apply to this particular choice of domain.*

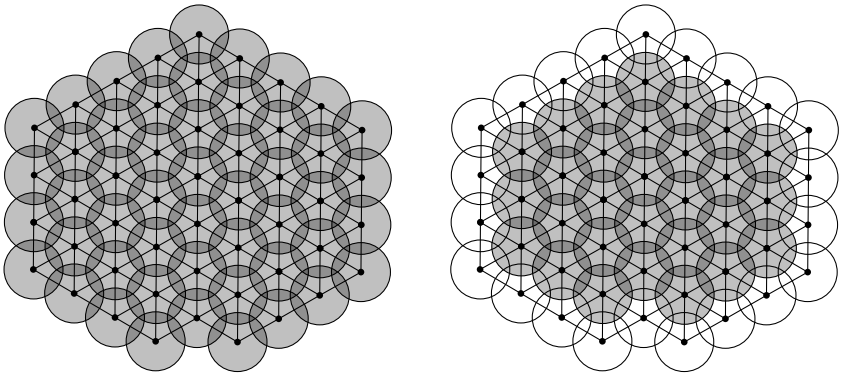

Figure 8.8: Left: Domain Ω and corresponding graph. Initial guess $\mathbf{u}^0 = 1$ (grey) on $\partial\Omega_j$ for $j = 1, \ldots, N$. Right: Result after the first iteration. The subdomains in white (layer 1) are the ones that have begun to experience a contraction, that is $\mathbf{u}^1 \in \mathcal{V}_1$.

To do so, we consider as initialization the function $\mathbf{u}^0 = \mathbf{1}$ *and follow the propagation of the contraction of the error through the course of the first five iterations of the PSM. We represent in grey the subdomains where the current approximation satisfies* $\mathbf{u}_j^n = \mathbf{1}_j$. *Moreover, we depict in white all the subdomains where the current approximation satisfies* $\mathbf{u}_j^n(x) < 1$ *for all* $x \in \mathcal{S}_j^{\text{int}}$ *and in red the subdomains such that* $\operatorname{ess\,sup}_{\mathcal{S}_j} \mathbf{u}_j^n < 1$. *Since the initialisation is* $\mathbf{u}^0 = \mathbf{1}$, *all the subdomains are grey at the iteration* 0 *(see Figure 8.8 (left)). After the first iteration, the current approximation is given by* $\mathbf{u}^1 = T\mathbf{u}^0$. *Thanks to zero external Dirichlet boundary conditions, the subdomains in the first layer* $\mathcal{L}_1$ *have begun to experience a contraction. Hence,* $\mathbf{u}^1 \in \mathcal{V}_1$ *and the first layer is white, while all the other layers are still grey (see Figure 8.8 (right)).*

After the second iteration, the current approximation is $\mathbf{u}^2 = T\mathbf{u}^1$. *The contraction propagates and thus the subdomains in layer 2 are now white while the ones in layers 3 and 4 are still grey. Hence,* $\mathbf{u}^2 \in \mathcal{V}_2$ *in agreement with Lemma 8.11 (see Figure 8.9 (left)).*

The third iteration yields $\mathbf{u}^3 = T\mathbf{u}^2$ *and reveals new behaviour. On the one hand, the contraction is still propagating towards the inner-most layer. Layer 3 has thus begun to experience a contraction and is displayed in white indicating that* $\mathbf{u}^3 \in \mathcal{V}_3$. *On the other hand, since all the subdomains in Layer 1 were surrounded by white subdomains, Layer 1 is now displayed in red in accordance with Lemma 8.12. Hence* $\mathbf{u}^3 \in \mathcal{C}_1$. *Only the three subdomains in layer 4 are still grey (see Figure 8.9 (right)).*

The fourth iteration yields $\mathbf{u}^4 = T\mathbf{u}^3$. *The contraction has propagated to Layer 4, which is displayed in white, and* $\mathbf{u}^4 \in \mathcal{V}_4$ *in accordance with Lemma 8.11. Furthermore, all the subdomains in Layer 2 which were previously surrounded by white or red subdomains at iteration 3 are now red in accordance with Lemma 8.12. Thus,* $\mathbf{u}^4 \in \mathcal{C}_2$ *(see Figure 8.10 (left)).*

Finally, we consider the fifth iteration, which yields $\mathbf{u}^5 = T\mathbf{u}^4$. *Since all the subdomains in Layers 3 and 4 were white at the previous iteration, they are now displayed in red (see Figure 8.10 (right)) indicating that* $\mathbf{u}^5 \in \mathcal{C}_5$. *In other words, we observe a*

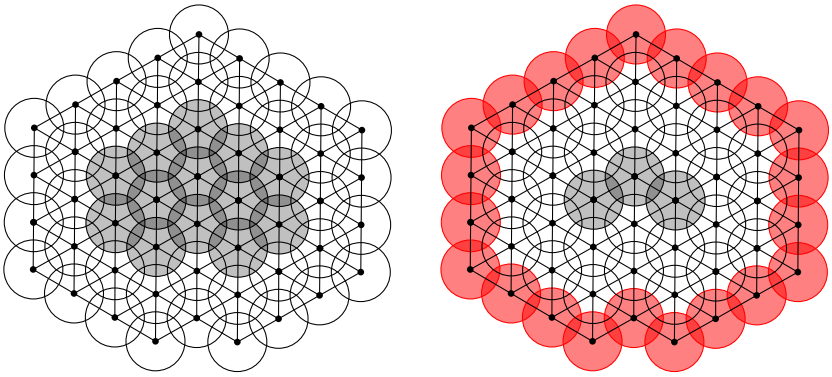

Figure 8.9: Left: Result after the second iteration. The subdomains in Layer 2 have begun to experience a contraction and hence are represented in white so that $\mathbf{u}^2 \in \mathcal{V}_2$. Right: Result after the third iteration. The contraction has now propagated to the third layer, which is displayed in white so that $\mathbf{u}^3 \in \mathcal{V}_3$. Furthermore, the subdomains in Layer 1 are represented in red since they are contracting everywhere on the skeleton, i.e., $\operatorname{ess\,sup}_{\mathcal{S}_j} \mathbf{u}_j^3 < 1$ for all $j \in \mathcal{L}_1$.

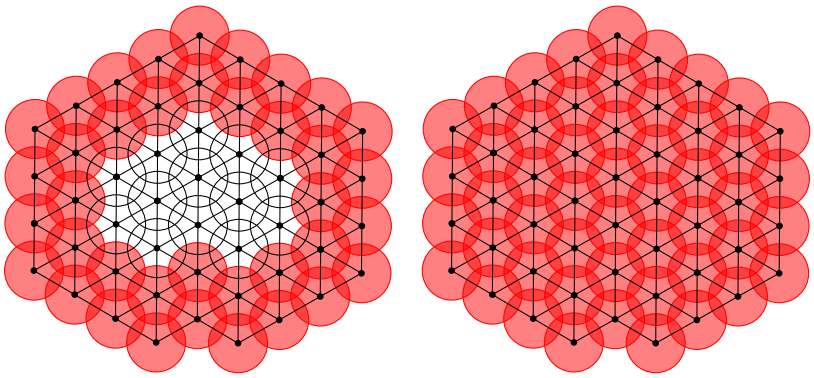

Figure 8.10: Left: Result after the fourth iteration. The contraction has propagated to the fourth layer, which is displayed in white. Since all subdomains have begun to experience a contraction, we have $\mathbf{u}^4 \in \mathcal{V}_4$. Moreover, the subdomains in Layer 1 and Layer 2 are contracting everywhere on the skeleton, i.e.,, $\operatorname{ess\,sup}_{\mathcal{S}_j} \mathbf{u}_j^4 < 1$ for all $j \in \mathcal{L}_1 \cap \mathcal{L}_2$. Thus, Layers 1 and 2 are displayed in red. Right: Result after the fifth iteration. All the subdomains are contracting everywhere in their skeletons and are therefore displayed in red. It therefore holds that $\mathbf{u}^5 \in \mathcal{C}_4$ and after $N_{\max} + 1 = 5$ iterations we finally observe a contraction in the infinity norm.

contraction in the infinity norm after precisely $N_{\max} + 1 = 4 + 1 = 5$ iterations. This is in agreement with Theorem 8.14.

Example 8.20. *Next, we consider a domain Ω consisting of a linear chain of collinear subdomains (unit disks) as shown in Figure 8.11.*

The Schwarz operator T corresponding to this geometry is the block-tridiagonal operator

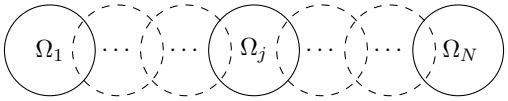

Figure 8.11: Example of a linear chain of N collinear subdomains (unit disks).

$$T = \begin{bmatrix} 0 & P_{12} & & & & & \\ P_{21} & 0 & P_{23} & & & & \\ & P_{32} & 0 & P_{34} & & & \\ & & \ddots & \ddots & \ddots & & \\ & & & P_{N-1N-2} & 0 & P_{N-1N} & \\ & & & & P_{NN-1} & 0 & \end{bmatrix}.$$

Notice how this operator resembles the Schwarz iteration operator constructed in Fourier space in the literature [25, Section 3.1] (see also [28]). In [25], the Schwarz operator is denoted by $T_{1\,\mathrm{D}}$ and it has been shown that $\|T_{1D}\|_{\mathrm{OP},\infty} = 1$, where $\|\cdot\|_{\mathrm{OP}\infty}$ is the usual infinity matrix norm. This is in agreement with Lemmas 8.10 and 8.11.

It is clear from Figure 8.20 that the considered chain is composed of a single layer since $\partial\Omega_j \cap \partial\Omega \neq \emptyset$ for all $j = 1, \ldots, N$. Lemma 8.11 implies that $T\mathbf{1} \in \mathcal{V}_1$ and Theorem 8.14 guarantees that $T^2\mathbf{1} \in \mathcal{C}_1$, which implies that one observes a contraction in the infinity norm after two iterations. This result is conservative for chains of subdomains composed of only one layer. In fact, it has been proved in [29] that the PSM for the solution of one-layer chains of subdomains contracts at each iteration (see also [30]). This result can be obtained also using our framework. Indeed, using Lemma 8.10, we can compute

$$\begin{aligned} \|T\|_{\mathrm{OP},\infty} &= \|T\mathbf{1}\|_\infty = \max_{j=1,\ldots,N} \operatorname*{ess\,sup}_{s_j} |(T\mathbf{1})_j| \\ &= \max\Big\{ \operatorname*{ess\,sup}_{s_1} |(P_{12}\mathbf{1}_2)|, \max_{j=2,\ldots,N-1} \operatorname*{ess\,sup}_{s_j} |(P_{jj-1}\mathbf{1}_{j-1} + P_{jj+1}\mathbf{1}_{j+1})|, \operatorname*{ess\,sup}_{s_N} |(P_{NN-1}\mathbf{1}_{N-1})| \Big\}. \end{aligned} \tag{8.19}$$

The definition of the operators $P_{j,k}$ implies that the functions

$$\begin{aligned} v_1 &:= (P_{12}\mathbf{1}_2), \\ v_j &:= (P_{jj-1}\mathbf{1}_{j-1} + P_{jj+1}\mathbf{1}_{j+1}),\ j = 2, \ldots, N-1, \\ v_N &:= (P_{N-1N}\mathbf{1}_N), \end{aligned}$$

solve the problems

$$\Delta v_j = 0 \text{ in } \Omega_j, \quad v_j = 1 \text{ on } \Gamma_j^{\mathrm{int}}, \quad v_j = 0 \text{ on } \Gamma_j^{\mathrm{ext}},$$

for each $j = 1, \ldots, N$. Notice that (8.19) is exactly given in [29, Theorem 7, formula (24)]. Consequently, following the same arguments as in [29], we see that

$$\operatorname*{ess\,sup}_{s_1} v_1 = \operatorname*{ess\,sup}_{s_N} v_N \leq \operatorname*{ess\,sup}_{s_j} v_j < 1,$$

for any $j = 1, \dots, N$, where the strict inequality follows by the maximum principle. The value ess $\sup_{S_j} v_j$ *can then be computed explicitly as in [29, Sections 4 and 5.1]. We therefore obtain that $\|T\|_{OP,\infty} = \rho(\alpha) < 1$, where $\rho(\alpha)$ is exactly the estimate of the contraction factor given in [29, Section 5.1].*

We also remark that it is possible in the same way to analyse other chains of fixed-sized subdomains characterized by only one layer such as the examples given in [29, 30].

8.2 Extensions to More General Settings

Recall that we began Section 8.1.1 by imposing constraints A1) and A2) on the geometry of the domain Ω. The preceding analysis confirms our claim that the constraint A1) is imposed purely to assist clarity of exposition, and can be dropped by adopting minor changes in, for instance, the definition of the index set $N_{jk},\ j = 1, \dots, N,\ k \in N_j$.

On the other hand, the constraint A2) which limits the number of simultaneously intersecting disks to three, significantly restricts the generality of our analysis. A second important limitation of our analysis is the fact that it is, a priori, restricted to disks in two dimensions and it is not yet clear if our results can be extended to domains in three dimensions consisting of the union of intersecting balls. The goal of this section is to address these shortcomings and extend the preceding analysis.

8.2.1 Extension to arbitrary number of intersections

We assume the geometric setting introduced in Section 8.1.1 and remove the constraints A1) and A2). In other words, we have assumed that the disks $\Omega_i,\ i = 1, \dots, N$ may have any type and any number of simultaneous intersections. Our goal is now to outline step-by-step the changes that must be made to the analysis of Section 8.1 so that the convergence results still hold.

8.2.1.1 Notation

Let $j \in \{1, \dots, N\}$. Given the disk Ω_j we define as before the sets

$$\Gamma_j^{\text{ext}} := \partial\Omega_j \cap \partial\Omega, \quad \Gamma_j^{\text{int}} := \overline{\partial\Omega_j \setminus \Gamma_j^{\text{ext}}}.$$

The first complication arises when we attempt to define index sets characterising the number and types of intersections. In Section 8.1.1, our task was straightforward because we assumed that the domain Ω consisted of at most triple intersecting subdomains but we have no longer imposed this constraint. In order to deal with the current more general setting, we define these index sets in an inductive manner.

Step 1) For each $j_0 = 1, \dots, N$, we define the index set of neighbours N_{j_0} as

$$N_{j_0} := \{j_1 \in \mathbb{N} \colon (j_1 \neq j_0) \wedge (\Omega_{j_1} \cap \Omega_{j_0} \neq \emptyset)\}.$$

Step 2) For each $j_0 = 1, \ldots, N$ and each $j_1 \in N_{j_0}$, we define the index set of triple intersections as

$$N_{j_0 j_1} := \Big\{ j_2 \in \{1, \ldots, N\} : \\ (j_2 \neq j_1, j_0) \wedge (\Omega_{j_2} \cap \Omega_{j_1} \cap \Omega_{j_0} \text{ is a set of non-zero measure}) \Big\}.$$

If $N_{j_0 j_1}$ is an empty set for every $j_1 \in N_{j_0}$ then we stop the procedure for this specific choice of j_0, and we set the natural number $M_{j_0} = 1$.

Step m) For each $\big(j_0, j_1, \ldots, j_{m-1}\big) \in \{1, \ldots, N\} \times N_{j_0} \times N_{j_0 j_1} \times \ldots \times N_{j_0 j_1 \ldots j_{m-2}}$ we define the index set of $m+1$-ple intersections, i.e., the set of all intersections generated by $m+1$ simultaneously intersecting subdomains as

$$N_{j_0 j_1 \ldots j_{m-1}} := \Big\{ j_m \in \{1, \ldots, N\} : \\ (j_m \neq j_{m-1}, \ldots, j_1, j_0) \wedge \Big(\bigcap_{i=0}^{i=m} \Omega_{j_i} \text{ is a set of non-zero measure} \Big) \Big\}.$$

If $N_{j_0 j_1 \ldots j_{m-1}}$ is an empty set for every $j_{m-1} \in N_{j_0 j_1 \ldots j_{m-2}}$, then we stop the procedure for this specific choice of j_0, and we set the natural number $M_{j_0} = m - 1$.

In addition, we define the constant $M = \max_{j_0} M_{j_0}$. Intuitively, the natural number $M_{j_0} + 1$ denotes the maximum number of subdomains that simultaneously intersect the boundary of subdomain Ω_{j_0}. Moreover, the natural number $M+1$ denotes the maximum number of simultaneously intersecting subdomains in the entire domain Ω. We say that our domain consists of at most $M+1$-ple intersections, i.e., the intersections in our domain are generated by at most $M+1$ simultaneously intersecting subdomains.

The next complication arises now that we attempt to define decompositions of the interior boundary $\Gamma_{j_0}^{\text{int}}$, $j_0 = 1, \ldots, N$. Let $j_0 \in \{1, \ldots, N\}$. Then we define for every natural number $n \in \{1, \ldots, M_{j_0}\}$ the set $X_{j_0}^n$ of $M-$tuples as

$$X_{j_0}^n = \Big\{ \alpha \in \mathbb{N}^M : \alpha \in \big(\Pi_{i=0}^{n-1} N_{j_0 \ldots j_i} \big) \times \{0\}^{M-n} \Big\}.$$

Intuitively, the set $X_{j_0}^1$ characterises the simple intersections of subdomain Ω_{j_0}, the set $X_{j_0}^2$ characterises the triple intersections of subdomain Ω_{j_0} and so on. In particular, the set $X_{j_0}^{M_{j_0}}$ characterises the intersections of the highest order, i.e., the $M_{j_0}+1$-ple intersections of the subdomain Ω_{j_0}. It is natural to define also for every $j_0 \in \{1, \ldots, N\}$ the set $Z_{j_0} := \bigcup_{i=1}^{M_{j_0}} X_{j_0}^i$.

Let $j \in \{1, \ldots, N\}$. For any multi-index $\alpha \in Z_j$, we define the natural number M_α as

$$M_\alpha = \operatorname{card} \{\alpha_i \neq 0\}.$$

In other words, M_α denotes the number of non-zero entries in a given multi-index $\alpha \in Z_j$. We can now define for all multi-indices $\alpha \in Z_j$ the set $\Gamma_j^\alpha \subset \partial\Omega_j$ as

$$\Gamma_j^\alpha := \operatorname{int}\Big\{x \in \partial\Omega_j \colon \big(x \in \Omega_{\alpha_j} \forall j = 1, \dots, M_\alpha\big) \wedge \big(x \notin \Omega_\ell \forall \ell \in N_j \text{ with } \ell \notin \alpha\big)\Big\},$$

where we use an abuse of notation to write $\ell \notin \alpha$, which simply means that $\ell \neq \alpha_i$ for all indices $i = 1, \dots, M$.

These definitions now imply that

$$\Gamma_j^{\text{int}} = \overline{\bigcup_{\alpha \in Z_j} \Gamma_j^\alpha}.$$

It is now straightforward to define also the skeletons associated with the subdomain Ω_j. Indeed, let $j \in \{1, \dots, N\}$ and $k \in N_j$ be fixed. Then we define the sets $\mathcal{S}_{j,k}^{\text{int}}$ and $\mathcal{S}_{j,k}$ as

$$\mathcal{S}_{j,k} := \overline{\bigcup_{\substack{\alpha \in Z_j, \\ \alpha_1 = j}} \Gamma_k^\alpha}, \qquad \mathcal{S}_{j,k}^{\text{int}} := \mathcal{S}_{j,k} \setminus \partial\Omega_j.$$

Similarly, we define the skeleton $\mathcal{S}_j$ and the interior skeleton $\mathcal{S}_j^{\text{int}}$ as

$$\mathcal{S}_j := \bigcup_{k \in N_j} \mathcal{S}_{j,k}, \qquad \mathcal{S}_j^{\text{int}} := \bigcup_{k \in N_j} \mathcal{S}_{j,k}^{\text{int}}.$$

It can be observed that with this notation

- The definition of the graph and layers of a domain remain unchanged.
- The definition of the sets $\mathcal{V}_n$ and $\mathcal{C}_n$ remains unchanged.

Of course, it becomes necessary to modify the definition of the partition of unity functions. Indeed, let $j \in \{1, \dots, N\}$. Then we define for each $k \in N_j$ a function $\chi_j^k \colon \partial\Omega_j \to \mathbb{R}$, continuous on $\operatorname{int}\big(\Gamma_j^{\text{int}}\big)$, with the property that

$$\chi_j^k := \begin{cases} 1 & \text{on } \overline{\Gamma_j^\alpha} \setminus \Gamma_j^{\text{ext}} \quad \text{for } \alpha \in Z_j \text{ such that } \alpha = (k, 0, \dots, 0), \\ \in [0,1] & \text{on } \overline{\Gamma_j^\alpha} \setminus \Gamma_j^{\text{ext}} \quad \text{for } \alpha \in Z_j \text{ such that } (\alpha_1 = k) \wedge \big(\alpha \neq (k, 0, \dots, 0)\big), \\ 0 & \text{otherwise,} \end{cases} \tag{8.20}$$

and such that

$$\sum_{k \in N_j} \chi_j^k(x) = 1 \quad \text{for all } x \in \operatorname{int}\big(\Gamma_j^{\text{int}}\big).$$

The harmonic extension operator $\mathcal{E}_j$ and the restriction operator $\mathcal{R}_j$ can now be defined analogously to Section 8.1, keeping in mind the notation we have just introduced.

8.2.1.2 Operator formulation and convergence analysis

Let us first consider the developments of Section 8.1.2. The definition of the error functions $\mathbf{e}^n,\ n \in \mathbb{N}$ in Equation 8.7 remains unchanged. Indeed, each element $\mathbf{e}_j^n,\ j = 1,\dots,N,\ n \in \mathbb{N}$ is defined as

$$\mathbf{e}_j^n := e_j^n|_{\mathcal{S}_j}.$$

Finally, we consider the lemmas and theorems we have stated in Sections 8.1.3 and 8.1.3.2. Once again, we observe that the majority of the technical lemmas still hold under the current setting. In fact only the proof of Lemma 8.12 needs to be modified but the changes are minor and occur at only one point.

Indeed, consider the setting and proof of Lemma 8.12. We must modify the proof of Property (iii) of the boundary function h: i.e., the proof that $h(x) < 1$ for all $x \in \operatorname{int}\big(\Gamma_j^{\text{int}}\big)$.

Let $x \in \operatorname{int}(\Gamma_j^{\text{int}})$. As before, we distinguish two cases.

1. Suppose $x \in \overline{\Gamma_j^\alpha}$ where $\alpha \in Z_j$ satisfies $\alpha_2 = \alpha_3, \dots, = \alpha_M = 0$ and $\alpha_1 = k$ for some $k \in N_j$. In other words, we consider the case where x belongs to the part of the boundary $\partial\Omega_j$ that is a simple intersection. We distinguish two cases.

   - $x \in \Gamma_j^\alpha$. Recalling the definition of the interior skeleton, we obtain also that $x \in \mathcal{S}_{k,j}^{\text{int}} \subset \mathcal{S}_k^{\text{int}}$. Thus it holds that $h(x) = \mathbf{v}_k(x)\chi_j^k(x)$. Using the fact that the partition of unity functions are all bounded by one, and the fact that we have by assumption $\mathbf{v}_k(x) < 1$ for $x \in \mathcal{S}_{k,j}^{\text{int}} \subset \mathcal{S}_k^{\text{int}}$, we conclude that $h(x) < 1$.
   - $x \notin \Gamma_j^\alpha$, i.e., x is a boundary point of the closed set $\overline{\Gamma_j^{\alpha^j}}$. Now, either $x \in \Gamma_j^{\text{ext}}$ or there exists some neighbouring index $\ell \in N_{jk}$ such that $x \in \overline{\Gamma_j^\beta}$ where $\beta \in Z_j$ satisfies $\beta_1 = k$ and $\beta_2 = \ell$. Since $x \in \operatorname{int}(\Gamma_j^{\text{int}})$, we have excluded the first case. The second case is covered below.

2. Suppose $x \in \overline{\Gamma_j^\alpha}$ where $\alpha \in Z_j$ satisfies $\alpha_1 = k, \alpha_2 = \ell$ for some $k \in N_j$ and some $\ell \in N_{jk}$. In other words, we consider the case where x belongs to the part of the boundary $\partial\Omega_j$ that is a triple intersection or higher. It now holds that

$$h(x) = \mathbf{v}_k\chi_j^k(x) + \mathbf{v}_\ell(x)\chi_j^\ell(x) + \sum_{i=3}^{M_\alpha} \mathbf{v}_{\alpha_i}(x)\chi_j^{\alpha_i}(x). \tag{8.21}$$

   Notice now that for all $x \in \overline{\Gamma_j^\alpha}$ the partition of unity functions satisfy $\sum_{i=1}^{M_\alpha} \chi_j^{\alpha_i}(x) = 1$, and we have by the assumptions of Lemma 8.12 that $\mathbf{v}_{\alpha_i}(x) \leq 1$ for all $i = 1,\dots,M_\alpha$. In fact, even more is true. Since $x \in \overline{\Gamma_j^{\alpha^j}} \cap \operatorname{int}\big(\Gamma_j^{\text{int}}\big)$ it is not difficult to see that either $x \in \Omega_k$ or $x \in \Omega_\ell$, i.e., x belongs to the interior of one of the two neighbouring subdomains Ω_k and Ω_ℓ. This being the case, we obtain from Lemma 8.9 that either $\mathbf{v}_k(x) < 1$ or $\mathbf{v}_\ell(x) < 1$. Equation (8.21) then implies that $h(x) < 1$. This completes the claim.

We therefore conclude that $h(x) < 1$ for all $x \in \text{int}(\Gamma_j^{\text{int}})$ and therefore Property (iii) of the function h holds also in the current more general setting. The remainder of the proof is identical.

It can now be readily checked that the proofs of the remaining lemma and theorems in Section 8.1.3 remain essentially unchanged. We conclude this subsection by remarking that the reader can now understand why we chose to begin our analysis with certain simplifying assumptions: unfortunately, in a completely general setting, the notation turns increasingly complex and it becomes easy to lose focus on the main ideas of our analysis.

8.2.2 Extensions to three dimensions

We have thus far assumed that the domain Ω is a subset of $\mathbb{R}^2$ and is decomposed into subdomains $\{\Omega_i\}_{i=1}^N$ consisting of disks. We recall from Section 6.4 however that the ddCOSMO algorithm involves solving the Laplace equation on van der Waals-type molecular cavities in three spatial dimensions. As a consequence, we now discuss the extension of the preceding analysis to computational domains that are the unions of intersecting open balls in $\mathbb{R}^3$.

To this end, let us first assume that the domain $\Omega \subset \mathbb{R}^3$ can be decomposed as the union of intersecting balls $\Omega = \cup_{i=1}^N \Omega_i$. As in Section 8.2.1, we assume that no two subdomains intersect at a single point. A careful study of Section 8.1 and 8.2.1 now reveals that this three-dimensional geometric setting does not require any change in notation. In fact, the only lemma that uses the fact that each $\Omega_i,\ i = 1, \ldots, N \subset \mathbb{R}^2$ is Lemma 8.12.

To be more concrete, assume the setting of Lemma 8.12. The final step of the proof consists of showing that

$$\lim_{\substack{x \in \mathcal{S}_{j,k} \\ x \to \partial\Omega_j}} \mathbf{w}_j(x) < 1.$$

In order to prove this result, we use the Schwarz lemma. This lemma is referenced by name in [111, Pages 632-635], and a detailed proof is provided in the case of two dimensions. Another proof of this lemma, which uses complex analysis and is therefore also valid only in two dimensions is given in [29]. Additionally, the Schwarz lemma is also referenced- this time in higher dimensions- by Lions in his classical paper on domain decomposition in [133, Section 3]. Lions claims that "... this follows easily from potential theory" but omits providing a proof. Unfortunately, apart from Lion's single comment, we have been unable to find any proof for the Schwarz lemma in three dimensions. Moreover, the fact that the proof in [29] uses tools from complex analysis prevents a straightforward extension to three dimensions.

We therefore emphasise that the only bottleneck in extending the analysis of Section 8.1 and 8.2.1 to the case of a domain $\Omega \subset \mathbb{R}^3$ composed of intersecting balls is the lack of a proof of the Schwarz lemma in three dimensions.

8.2.3 Extensions to other types of subdomains

The analysis we have presented thus far assumes that the domain Ω consists either of a union of intersecting disks in $\mathbb{R}^2$ or a union of intersecting balls in $\mathbb{R}^3$ (see Section 8.2.2). In this subsection, we briefly discuss the possibility of extending our analysis to domains composed of more general types of subdomains.

Indeed, the results we have presented in Section 8.1 and 8.2 will hold for a different choice of subdomains if

(B1) For this new choice of subdomains, it is possible to introduce definitions and notations analogous to the ones introduced in Section 8.1 such that the operator formulation of the Schwarz method as stated in Section 8.1.2 is well-posed.

(B2) For this new choice of subdomains, the *technical results* presented in Section 8.1.3 still hold.

Clearly, the well-posedness of the operator formulation of the Schwarz method as given in Section 8.1.2 requires that the boundary value problem (8.5) be well-posed on each subdomain $\Omega_j,\ j = 1, \ldots, N$. This condition is satisfied if the subdomains $\{\Omega_j\}_{j=1}^N$ are, for instance, assumed to be *Lipschitz*. Moreover, it is not difficult to see that the definitions and notations introduced in Section 8.1 involving, for instance, interior and exterior boundary sets, skeletons and partition of unity functions, can easily be extended to Lipschitz subdomains $\{\Omega_j\}_{j=1}^N$. Consequently, condition (B1) holds for the case of Lipschitz subdomains.

Unfortunately, the *analysis* we have presented in Section 8.1.3 does not hold for general Lipschitz subdomains. In order to illustrate this point, let us consider the geometry displayed in Figure 8.12.

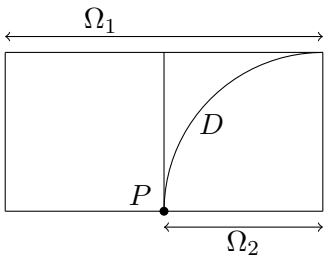

Figure 8.12: A domain Ω consisting of the union of two subdomains Ω_1 (left) and Ω_2 (right). Notice that although Ω_1 and Ω_2 are both Lipschitz, the overlap $\Omega_1 \cap \Omega_2$ is non-Lipschitz. Lemma 8.12 fails for this choice of subdomains.

We define the sets $\Omega_1 \subset \mathbb{R}^2$ and $\Omega_2 \subset \mathbb{R}^2$ as

$$\Omega_1 := (-1, 0] \times (0, 1) \cup \left\{(x, y) \in \mathbb{R}^2 \colon x \in (0, 1), y \in (\sqrt{x}, 1)\right\},$$
$$\Omega_2 := (0, 1) \times (0, 1),$$

and we define the domain $\Omega := \Omega_1 \cup \Omega_2$. Additionally, we denote by

$$D = \left\{(x, y) \in \mathbb{R}^2 \colon x \in (0, 1), y = \sqrt{x}\right\},$$

the curve that constitutes the right-side boundary of the domain Ω_1. Let us now consider Lemma 8.12 for this choice of geometry and domain decomposition. Essentially, Lemma 8.12 claims the following: Let the function $h \colon \partial\Omega_2 \to \mathbb{R}$ be defined as

$$h(x) = \begin{cases} 1 & \text{if } x \in \operatorname{int}\left(\Gamma_2^{\text{int}}\right), \\ 0 & \text{otherwise.} \end{cases}$$

Let $w_2 \in L^2(\Omega_2)$ be the harmonic extension in Ω_1 of h and let the function $w_1 \in L^2(\Omega_1)$ be the solution to the BVP

$$\begin{aligned} -\Delta w_1 &= 0 && \text{in } \Omega_1, \\ w_1 &= w_2 && \text{on int } \Gamma_1^{\text{int}}, \\ w_1 &= 0 && \text{on } \partial\Omega_1 \setminus \text{int } \Gamma_1^{\text{int}}. \end{aligned}$$

Then according to Lemma 8.12 we should have that

$$\operatorname*{ess\,sup}_{\Omega_1} w_1 < 1. \tag{8.22}$$

Consider now the proof of Lemma 8.12 and let $P \in \partial\Omega_1$ be the point $(0, 0)$, i.e., the lower endpoint of the curve D. The first case in Step (3) of the proof of Lemma 8.12 shows that

$$\lim_{\substack{x \in D \\ x \to P}} w_1(x) < 1.$$

This bound on the limit is established using the Schwarz lemma (see, e.g., [111, Pages 632-635]), which states that

$$\lim_{\substack{x \in D \\ x \to P}} w_1(x) = \alpha,$$

where $\alpha \in [0, 1]$ is a constant that depends on the angle at which the curve D intersects the boundary Γ_2^{int} at the point P. We now observe that the definition of the curve D implies that it intersects Γ_2^{int} with angle *zero* at the point P which yields $\alpha = 1$. Thus, the bound (8.22) fails, i.e., Lemma 8.12 no longer holds. We emphasise that this situation does not arise in the case of a domain $\Omega \subset \mathbb{R}^2$ that is composed of the union of intersecting disks since the boundaries of neighbouring disks do not intersect at zero angles.

Note that the geometry displayed in Figure 8.12 is known in the domain decomposition literature as an example of a domain $\Omega = \Omega_1 \cup \Omega_2$ wherein the standard proof of geometric convergence of the PSM via a contraction argument fails (see, e.g., [31]). Therefore, it is not surprising that our analysis also does not hold in this case. We remark that convergence of the PSM in this case can still be proven but requires different tools (see, e.g., [133, Section 4]).

We conclude that the analysis we have presented in Section 8.1 and 8.2 does not hold for general non-convex Lipschitz subdomains.

8.3 Numerical Experiments

The goal of this section is two-fold: First, we provide numerical evidence supporting our main convergence result Theorem 8.14, and its analogue for the case of quadruple intersecting disks. Second, we show the effect of adopting a different choice of the partition of unity functions on the convergence rates.

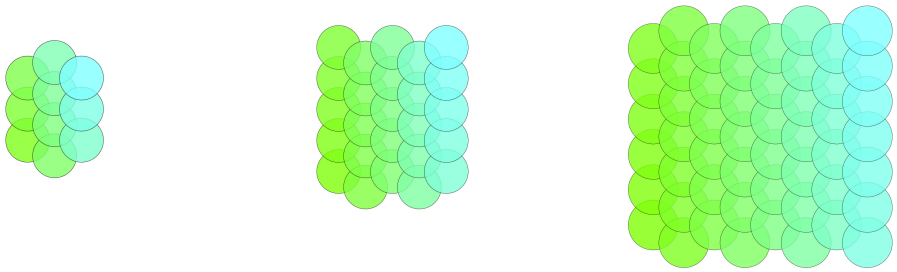

(a) $N_{\max} = 2$ Layers. **(b)** $N_{\max} = 3$ Layers. **(c)** $N_{\max} = 4$ Layers.

Figure 8.13: The different geometries used for the first set of numerical computations. The colour scheme is purely cosmetic. Note that both the radii and the distance between the centres of the subdomains in the three geometries are the same.

Figures 8.14a and 8.14b display the infinity norm of the Schwarz iterates generated through the Error Equation (8.9) using the initialisation $\mathbf{e}^0 \equiv 1$ on $\Pi_{j=1}^{j=N} \mathcal{S}_j$ for geometries with a different number of maximum layers. The different geometries are displayed in Figure 8.13. We emphasise that continuous partition of unity functions were chosen for this and all subsequent computations.

Although it is slightly difficult to see this at a glance, the numerical results displayed in Figure 8.14b follow the theoretical results exactly. Indeed, the error function always displays a first contraction at iteration number $N_{\max} + 1$. Furthermore, it is readily seen that the convergence rate of the error also depends on the total number of layers in the domain and degrades as $N_{\max}$ increases as shown in the log-lin plot displayed in Figure 8.14a. Indeed, we observe that the slope of the plots and consequently the asymptotic contraction factor degrades as $N_{\max}$ increases.

One complicated question that we did not address in the theoretical analysis of Section 8.1 is how to obtain a quantitive estimate of the contraction factor. Typically, one obtains an upper bound for the initial contraction factor, i.e., the initial decrease in the infinity norm of the Schwarz iterates (see, e.g., [28, 29, 30]), which then improves considerably in the asymptotic limit. Figures 8.15a and 8.15b display the exact infinity norm of the Schwarz iterates together with the (numerically obtained) initial and asymptotic contraction factor for geometries with $N_{\max} = 3$ and $N_{\max} = 4$ layers. We observe immediately that the first contraction in both cases is nearly two orders of magnitude smaller than the asymptotic contraction factor. The numerics therefore suggest that even if we were able to obtain an upper bound for the initial contraction factor, that is, an estimate of $\|T^{N_{\max}+1}\|_{\mathrm{OP},\infty}$, it would be extremely conservative and not useful from a practical

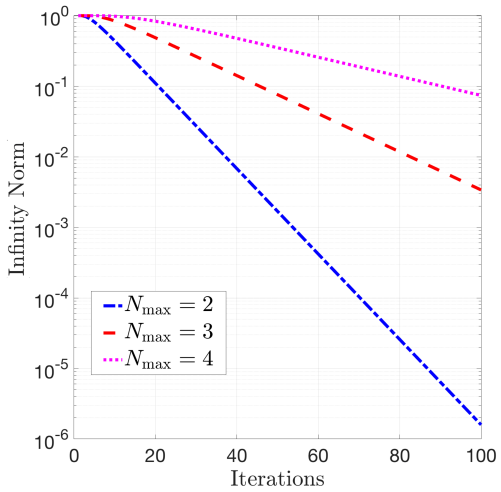

(a) Log-Lin plot of the Infinity norm of the Schwarz iterates for 100 iterations.

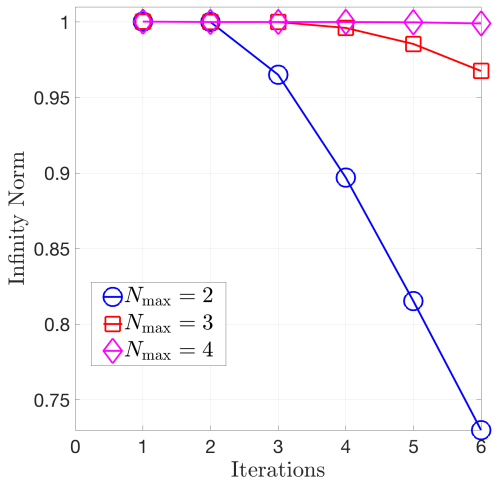

(b) Infinity norm of the Schwarz iterates for the first 6 iterations.

Figure 8.14: Numerical computations involving a computational domain with triple intersections.

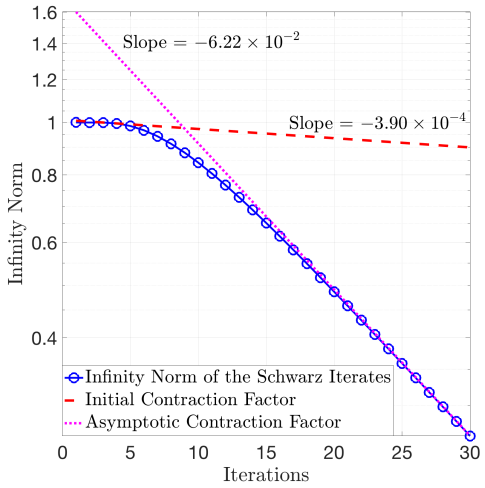

(a) Contraction Factors for $N_{\max} = 3$ layers.

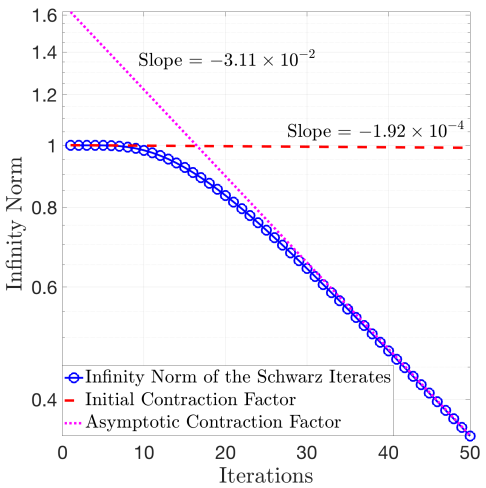

(b) Contraction Factors for $N_{\max} = 4$ layers.

Figure 8.15: Numerical computations involving a computational domain with triple intersections.

point of view.

In order to support our claim regarding the extension of Theorem 8.14 to more complicated geometries, we next repeat the above numerical computations for a computational domain consisting of quadruple intersecting subdomains. The different geometries are displayed in Figure 8.16.

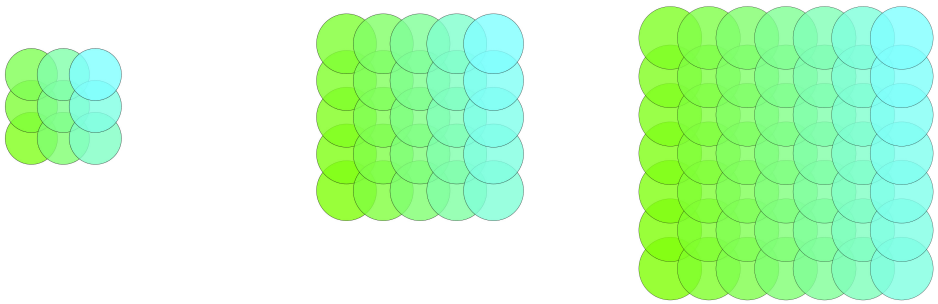

(a) $N_{\max} = 2$ Layers. **(b)** $N_{\max} = 3$ Layers. **(c)** $N_{\max} = 4$ Layers.

Figure 8.16: The different geometries used for the second set of numerical computations. The colour scheme is purely cosmetic. Note that both the radii and the distance between the centres of the subdomains in the three geometries is the same.

Figures 8.17b displays the infinity norms of the Schwarz iterates generated through the Error Equation (8.9) using the initialisation $\mathbf{e}^0 \equiv 1$ on $\Pi_{j=1}^{j=N} \mathcal{S}_j$ for quadruple intersecting geometries with a different number of maximum layers. Once again, although it might be difficult to tell at a glance, the numerical results follows the theoretical results exactly and we see a first contraction of the infinity norm at iteration number $N_{\max} + 1$.

Figure 8.17a displays the infinity norms of the Schwarz iterates as the number of iterations increases for the three geometries in a log-lin plot. Once again we observe that the asymptotic contraction factor degrades as $N_{\max}$ increases. In addition, we plot in Figures 8.18a and 8.18b the exact infinity norms of the Schwarz iterates together with the (numerically obtained) initial and asymptotic contraction factor for geometries with $N_{\max} = 3$ and $N_{\max} = 4$ layers. As before, the initial contraction factor can be seen to be at least an order of magnitude smaller than the asymptotic convergence factor.

We conclude this section by returning to a question posed in Remark 8.6: Does the choice of partition of unity functions affect the iterates of the Parallel Schwarz method and the asymptotic contraction factor? We decided to compute the infinity norm of the Schwarz iterates generated through the Error Equation (8.9) using the initialisation $\mathbf{e}^0 \equiv 1$ on $\Pi_{j=1}^{j=N} \mathcal{S}_j$ for the geometries displayed in Figure 8.13 using both the continuous partition of unity functions employed previously as well as discontinuous partition of unity functions as chosen in [72, Section 2, Page 4]. The discontinuous partition of unity functions are defined as follows: Given three intersecting subdomains $\Omega_1, \Omega_2, \Omega_3$

- We set the partition of unity functions χ_1^2, χ_1^3 on $\partial\Omega_1$ as $\chi_1^2 = 1$ on $\overline{\Gamma_1^{2,3}} \cup \overline{\Gamma_1^{2,0}}$ and $\chi_1^2 = 0$ otherwise, and $\chi_1^3 = 1$ on $\overline{\Gamma_1^{3,0}}$ and $\chi_1^3 = 0$ otherwise.

- We set the partition of unity functions χ_2^3, χ_2^1 on $\partial\Omega_2$ as $\chi_2^3 = 1$ on $\overline{\Gamma_2^{1,3}} \cup \overline{\Gamma_2^{3,0}}$ and $\chi_2^3 = 0$ otherwise, and $\chi_2^1 = 1$ on $\overline{\Gamma_2^{1,0}}$ and $\chi_2^1 = 0$ otherwise.

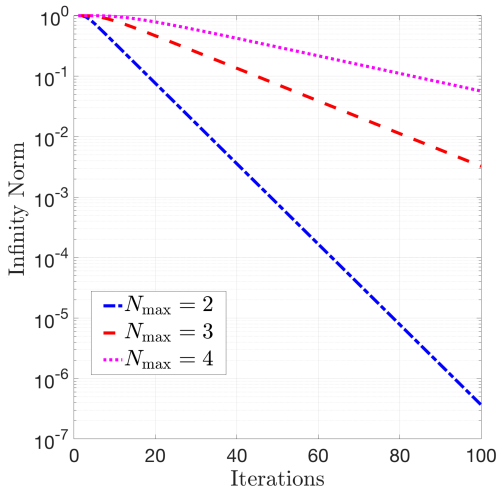

(a) Log-Lin plot of the Infinity norm of the Schwarz iterates for 100 iterations.

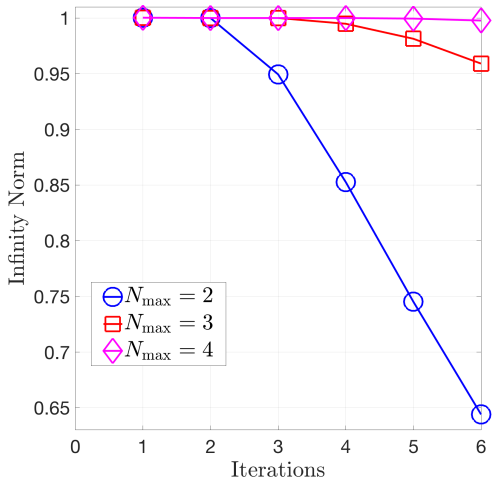

(b) Infinity norm of the Schwarz iterates for the first 6 iterations.

Figure 8.17: Numerical computations involving a computational domain with quadruple intersections.

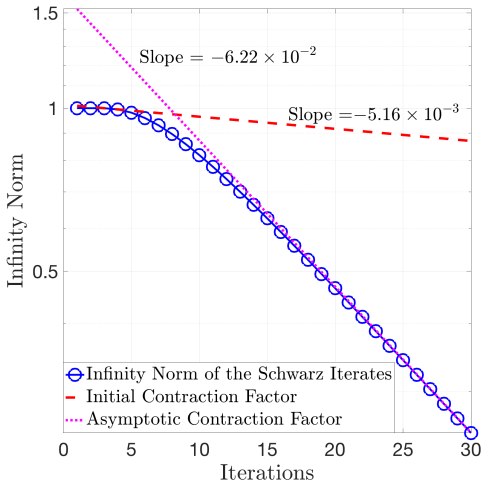

(a) Contraction Factors for $N_{\max} = 3$ layers.

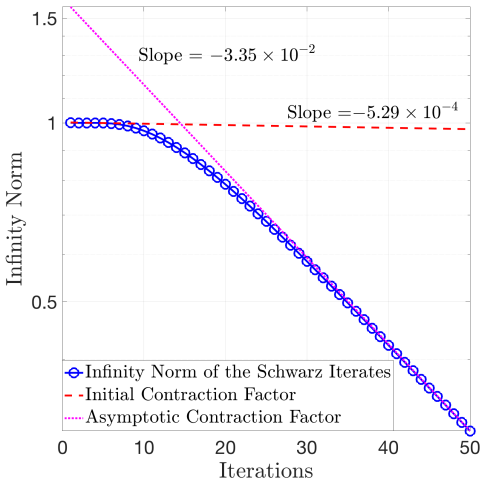

(b) Contraction Factors for $N_{\max} = 4$ layers.

Figure 8.18: Numerical computations involving a computational domain with quadruple intersections.

- We set the partition of unity functions χ_3^1, χ_3^2 on $\partial\Omega_3$ as $\chi_3^1 = 1$ on $\overline{\Gamma_3^{1,2}} \cup \overline{\Gamma_3^{1,0}}$ and $\chi_3^1 = 0$ otherwise, and $\chi_3^2 = 1$ on $\overline{\Gamma_3^{2,0}}$ and $\chi_3^2 = 0$ otherwise.

In other words given any subdomain Ω_j, on the portion of the boundary $\Gamma_j^{k,i} \subset \partial\Omega_j$ that intersects simultaneously with *two* other subdomains Ω_k and Ω_i, we take boundary data from only one neighbour. Our results are displayed in Figures 8.19, and they suggest

that

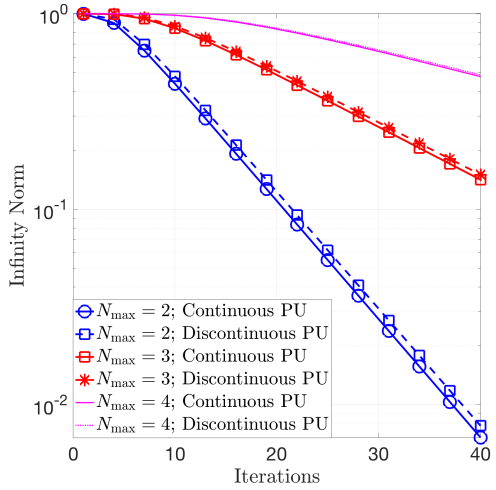

(a) Log-Lin plot of the Infinity norm of the Schwarz iterates for 40 iterations.

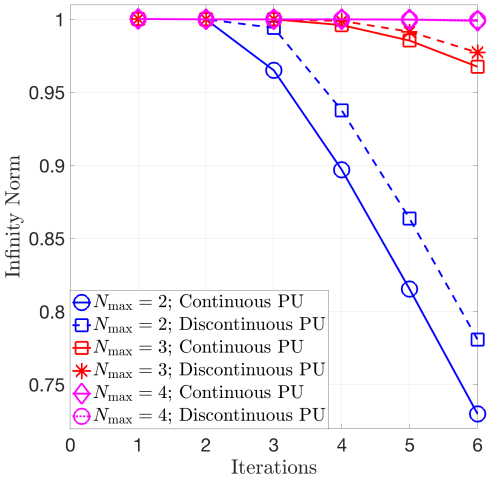

(b) Infinity norm of the Schwarz iterates for the first 6 iterations.

Figure 8.19: Numerical computations involving both continuous and discontinuous partition of unity functions. The computational domain consists of triple intersection subdomains as displayed in Figure 8.13.

- While the choice of different partition of unity functions can lead to quantitatively slightly different infinity norms of the Schwarz iterates, the asymptotic contraction factor remains unchanged;
- The first contraction in the infinity norm is always observed at iteration number $N_{\max} + 1$ regardless of the choice of the partition of unity functions.

For more information and details on the effect of the choice of partition of unity functions on the convergence of Schwarz methods, see also [73].

8.4 Application to Bio-Molecules: van der Waals and SAS Cavities

The examples considered thus far in Section 8.3 have been 'toy' problems, which are interesting from a mathematical point of view but do not have a physical origin. The goal of this section is to consider actual biological molecules that have been studied in solvation models in computational chemistry (see, e.g., [136]) and to understand the consequences of the preceding analysis as it pertains to these complex bio-molecules.

As a reference, we consider the biological molecules that were analysed in the dd-COSMO numerical study presented in [136]. The molecular are represented as van der

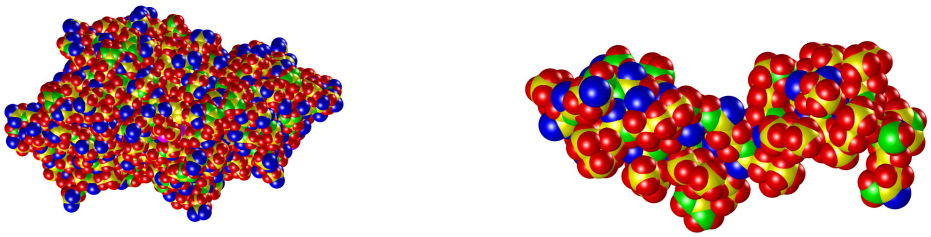

(a) Atomic Structure of Carboxylase. **(b)** Atomic Structure of Hiv-1-gp41.

Figure 8.20: Atomic Structures of 'globular' Carboxylase and 'chain-like' Hiv-1-gp41. The colour of each atomic cavity denotes the type of atom: yellow denotes Carbon, red denotes Hydrogen, green denotes Nitrogen, blue denotes Oxygen and magenta denotes Sulphur. The atomic cavities were constructed using 1.1 times the radii obtained from the Universal Force Field (UFF) [176].

Waals-type cavities, i.e., as unions of intersecting balls with each ball corresponding to one atom in the molecule. The computational domain thus consisted of a union of open balls, and the Laplace equation with a prescribed, smooth boundary condition was solved on this computational domain. The problem setting is therefore exactly of the form of Equation (8.1), except of course that the problem is posed in three dimensions. It is important to note however that we must make a choice for the value of the radius of each atomic cavity. While this is a non-trivial question in general (see, e.g., the references in [173]), the most basic convention (see, e.g., [23]) is to construct the atomic cavities using 1.1 times the radii obtained from the Universal Force Field (UFF) [176]. This is the convention we adopt as a first step.

Two representative examples of these biological molecules, Carboxylase and Hiv-1-gp41 are displayed in Figure 8.20. It is readily seen that the Carboxylase molecule is 'globular' in structure and consists of thousands of atoms, and thus thousands of subdomains in the domain decomposition setting. On the other hand, the Hiv-1-gp41 molecule is more 'chain-like' in structure and consists of less than 600 atoms. Based on these visualisations, one could expect the Carboxylase molecule to contain a large number of layers and the Hiv-1-gp41 molecule to contain fewer layers. As our preceding analysis shows, this could result in very different computational efficiencies of the parallel Schwarz method (PSM) for the two molecules as described by Equation (8.5) and implemented through the ddCOSMO numerical algorithm.

Table 8.1 displays the wall-time of the ddCOSMO algorithm as reported in [136], and we can observe the surprising result that the PSM (as a preconditioner) seems to work extremely efficiently for all the biological molecules considered here. In particular, we observe excellent scaling of the method with respect to the number of atoms in each molecule. Furthermore, our own numerical computations, which are shown in the second

Bio-Molecule	Vancomycin	UBCH5B	L-plectasin	Hiv-1-gp41	Glutaredoxin	Carboxylase
Wall-Times	1	4	1	1	2	9
Convergence Factors	0.8801	0.9287	0.8990	0.9105	0.9269	0.9324
Number of Atoms	377	2364	567	530	1277	6609

Table 8.1: Wall-times (in seconds) and asymptotic convergence rates of the ddCOSMO algorithm. Times less than 1 second have been rounded to one. The wall-times were obtained by solving the underlying linear system using the DIIS algorithm introduced by Peter Pulay in quantum computational chemistry [169]. Note that the DIIS algorithm is simply Anderson acceleration. These accelerations are applied to the PSM as a stationary method, which is essentially equivalent to GMRES preconditioned with the PSM [207]. The asymptotic convergence rates were calculated using the PSM as a stationary method.

row of Table 8.1 and displayed in Figure 8.21 indicate that there is minimal degradation of the asymptotic convergence rate of the ddCOSMO algorithm for these bio-molecules. In order to explain this observation, we decided to analyse carefully the structure of these protein molecules.

Table 8.2 contains information about geometrical aspects of each of these protein molecules that affect the convergence rate of the PSM. We indicate the total number of atoms, the number of layers which is the central component of our analysis, the average number of neighbours, the average over different subdomains of the maximum degree of intersection, and the average over different subdomains of the overlap distance between neighbouring atoms. The following two observations are now key:

- There are exactly two layers in each bio-molecule;
- The other geometrical parameters which could potentially affect the convergence rate of the PSM do not vary wildly across the different molecules.

Bio-Molecule	Vancomycin	UBCH5B	L-plectasin	Hiv-1-gp41	Glutaredoxin	Carboxylase
Number of Atoms	377	2364	567	530	1277	6609
Number of Layers	2	2	2	2	2	2
Average Number of Neighbours	15.6	19.8	16.6	16.5	18.1	20.2
Average Maximum Intersection Degree	6.16	6.27	6.11	6.12	6.50	6.24
Average Overlap	2.3	2.3	2.3	2.2	2.3	2.3

Table 8.2: Various geometrical properties of each biological molecule considered in the numerical simulations. The average overlap distance is calculated by considering a pair of neighbouring atoms, computing the difference between the sum of the two radii and the distance between the centres, and then taking the average over all pairs of neighbouring atoms.

These observations help explain our numerical results and also explain why the dd-COSMO numerical algorithm works so well in practice even for apparently globular biological molecules (see [23, 135, 137]).

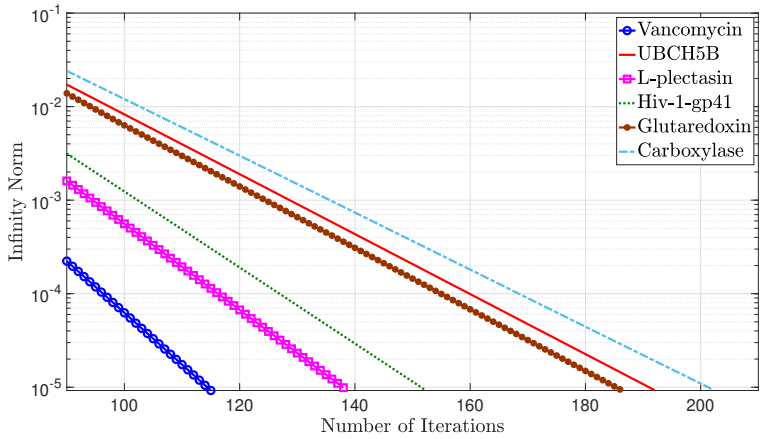

Figure 8.21: Log-Lin plot of the Infinity norm of the approximate solution after each iteration of the PSM. All simulations were initialised with a constant 'one' vector and a zero right-hand side was imposed.

In the computational chemistry community, it is often argued that using scaled van der Waals radii to construct atomic cavities leads to a sub-optimal definition of the molecular cavity that is unable to accurately capture the physical behaviour of the molecule in a polarisable medium. An alternative definition of the molecular cavity is given by the so-called Surface Accessible Surface (SAS) (see, e.g., [173]). According to this definition, each atomic cavity is constructed using the sum of two radii: the atomic van der Waals radius and a so-called 'probe radius', which can generally be taken to be 1.4 Angstrom, i.e., the approximate radius of a water molecule. As a second step therefore, we adopt the SAS convention to construct the molecular cavities. Figure 8.22 displays the SAS cavity-based atomic structure of the biological molecules Carboxylase and Hiv-1-gp41 (c.f., Figure 8.20).

We consider once again the six biological molecules analysed in [136]. Table 8.3 contains information about various geometrical aspects of each of these protein molecules using the SAS cavity definition. We observe now that the number of layers in each molecule is now greater than two while the globular molecules UBCH5B and Carboxylase have six and eight layers respectively. On the other hand, the average over different subdomains of the maximum degree of intersection and the average over different subdomains of the overlap between neighbouring atoms are both higher than before but do not differ significantly between the molecules. Thus, the main differences between these molecules are now the number of layers and the average number of neighbours. Taken together, these observations suggest that the ddCOSMO algorithm should display slower convergence behaviour for all molecules and worse behaviour for the globular molecules.

As a test case, we consider the more 'chain-like' molecules Vancomycin and Hiv-1-gp41 and the 'globular' molecule UBCH5B. Notice that both the Vancomycin and Hiv-1-gp41 molecules consist of 3 layers when using the SAS definition of the cavity. On the other hand, the molecule UBCH5B, due to it's globular structure, consists of 6

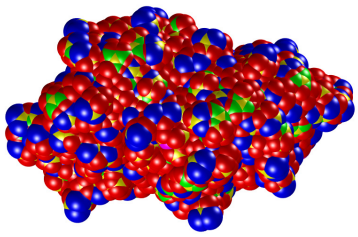

(a) Atomic Structure of Carboxylase with SAS cavities.

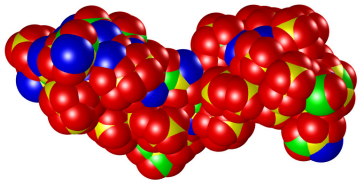

(b) Atomic Structure of Hiv-1-gp41 with SAS cavities.

Figure 8.22: Atomic Structures of 'globular' Carboxylase and 'chain-like' Hiv-1-gp41. Once again, the colour of each atomic cavity denotes the type of atom: yellow denotes Carbon, red denotes Hydrogen, green denotes Nitrogen, blue denotes Oxygen and magenta denotes Sulphur.

Bio-Molecule	Vancomycin	UBCH5B	L-plectasin	Hiv-1-gp41	Glutaredoxin	Carboxylase
Number of Atoms	377	2364	567	530	1277	6609
Number of Layers	3	6	4	3	5	8
Average Number of Neighbours	50.5	80.7	59.5	56.3	69.2	86.3
Average Maximum Intersection Degree	17.3	19.0	17.6	17.9	18.9	19.1
Average Overlap	3.6	3.7	3.8	3.6	3.7	3.8

Table 8.3: Various geometrical properties of each biological molecule with the atomic cavities constructed using the SAS definition.

layers. We solve the ddCOSMO system of equations using the PSM. Table 8.4 lists the number of iterations required to solve the linear system up to a fixed tolerance.

Bio-Molecule	Vancomycin	Hiv-1-gp41	UBCH5B
Iterations for van der Waals Cavity	115	152	192
Iterations for SAS Cavity	189	164	538

Table 8.4: The number of iterations of PSM required to solve the ddCOSMO system of equations up to a fixed tolerance for each molecule.

As expected, using the SAS definition of cavities results in a larger number of iterations being required to solve the underlying linear system. It is important to note however, that even though the Hiv-1-gp41 molecule contains about 40% more atoms than Vancomycin, the associated linear system for Hiv-1-gp41 can be solved in a fewer number of iterations than the linear system for Vancomycin. On the other hand, the linear system associated with the UBCH5B molecule, which contains 6 layers, now requires a significantly larger number of iterations to solve. These observations suggest

the following conclusions:

- The key geometrical quantities which determine fast or slow convergence of the ddCOSMO algorithm for a given molecule are the number of layers (not the number of atoms by themselves) and the number of neighbouring atoms.
- For chain-like molecules, it is possible to use the SAS definition of the cavity without affecting the number of layers too significantly, and hence the convergence properties of ddCOSMO too adversely. On the other hand, for globular molecules, using the SAS definition results in a larger number of layers and consequently worse convergence properties.

We therefore conclude that even though the SAS definition might represent a more physical representation of molecular cavities, the use of this definition for globular molecules results in a very serious deterioration in the computational efficiency of ddCOSMO.

8.5 Conclusions

In this chapter, we presented a detailed convergence and scalability analysis of the parallel Schwarz method (PSM) for the solution of the Laplace equation posed on a domain composed of the union of several intersecting spherical subdomains. The PSM in this geometric context is known as the ddCOSMO algorithm and is used to solve for the electrostatic contribution to the solvation energy of solute molecules embedded in a continuum medium (see Sections 6.2 and 6.4) so this problem is of practical relevance in computational chemistry. Our analysis, characterizing the properties of the infinite-dimensional Schwarz operator, allowed us to prove that a first contraction in the infinity norm can be achieved in at most $N_{\max} + 1$ iterations. Here $N_{\max}$ is the number of layers in the solute molecule and represents the maximal distance of the subdomains from the exterior boundary. Numerical experiments and an application to real biological molecules demonstrate the effectiveness of our analysis.

Part III

Boundary Integral Operators in Domain Decomposition

9

Continuity Estimates for Riesz Potentials on Polygonal Boundaries

9.1 Introduction

Time harmonic wave propagation phenomena are ubiquitous in a wide variety of science and engineering disciplines, two prominent examples being electromagnetic and acoustic wave scattering. Such wave phenomena are often described by Helmholtz-type equations, which have a very distinctive mathematical structure. Indeed, in contrast to standard elliptic equations such as the Laplace or screened Poisson equation, solutions to the Helmholtz equation are typically highly oscillatory which necessitates the use of very fine spatial discretisations in order to guarantee a high level of approximation accuracy. In an effort to reduce the computational cost of solving for a very high number of global degrees of freedom, a natural solution strategy is to split the global problem into a collection of coupled local problems, which immediately brings to mind the domain decomposition paradigm described in Section 6.3.

Unfortunately, it is not straightforward to devise domain decomposition methods for the Helmholtz equation. Indeed, since the Helmholtz differential operator is indefinite as opposed to coercive, solutions to the Helmholtz equation do not correspond to minima of a quadratic functional and do not satisfy a maximum principle. As a consequence, the classical parallel Schwarz method (see Section 6.3) which imposes Dirichlet-type transmission conditions on the interfaces of overlapping subdomains either *does not converge* or *converges very slowly* when applied to Helmholtz problems (see, e.g., [72, Section 4]).

Pioneering work on domain decomposition methods for the Helmholtz equation was undertaken by Bruno Després in his Phd thesis [49] and later by Gander et al. [76], Collino et al. [40] and several others (see, e.g., [20, 109]). The essential idea of such methods is to replace the classical choice of Dirichlet-type transmission conditions on subdomain interfaces with impedance-type transmission conditions.

In order to illustrate this idea, we consider the following model problem: Let $\Omega \subset \mathbb{R}^2$ be a polygonal domain with boundary denoted Γ and outward pointing unit normal vector denoted ν. Given $\omega \in \mathbb{R}$ and functions $f \in L^2(\Omega)$ and $g \in L^2(\Gamma)$, the task is to find a function $u \in H^1(\Omega)$ such that

$$\begin{aligned} -\Delta u - \omega^2 u &= f \quad \text{in } \Omega, \\ \partial_\nu u + \imath\omega u &= g \quad \text{on } \Gamma, \end{aligned} \tag{9.1}$$

where the boundary conditions are understood in an appropriate trace sense.

Equation (9.1) is an example of the non-homogeneous Helmholtz equation with impedance boundary conditions, and it is well known (see, e.g., [49]) that if $(f, g) \in L^2(\Omega) \times L^2(\Gamma)$ then there exists a unique solution $u \in H^1(\Omega)$ to the BVP (9.1) which also satisfies $\partial_\nu u \in L^2(\Gamma)$.

A domain decomposition strategy for solving the model problem (9.1) can be devised as follows. We partition Ω into two non-overlapping subdomains Ω_1 and Ω_2 with boundaries $\partial\Omega_1$ and $\partial\Omega_2$ respectively as shown in Figure 9.1. In addition, we define

$$\begin{aligned} \Sigma_{12} &= \partial\Omega_1 \cap \partial\Omega_2 \qquad \text{as a subset of } \partial\Omega_1, \\ \Sigma_{21} &= \partial\Omega_2 \cap \partial\Omega_1 \qquad \text{as a subset of } \partial\Omega_2. \end{aligned}$$

Moreover we define for each $j = 1, 2$ the set $\Sigma_{jj} = \partial\Omega_j \cap \partial\Omega$, and we denote by ν_j the outward pointing unit normal vector on the boundary $\partial\Omega_j$. With this notation, we consider the following iterative procedure: Given some initialisation $u_0 \in H^1(\Omega)$ that satisfies $\partial_{\nu_j} u_0 + \imath\omega u_0 \in L^2(\partial\Omega_j)$, find two sequences of functions $\{u_j^n\}_{n\in\mathbb{N}} \in H^1(\Omega_j)$, $j = 1, 2$ such that

$$\begin{aligned} -\Delta u_j^n - \omega^2 u_j^n &= f && \text{in } \Omega_j, \\ \partial_{\nu_j} u_j^n + \imath\omega u_j^n &= g && \text{on } \Sigma_{jj}, \\ \partial_{\nu_j} u_j^n + \imath\omega \mathscr{T}(u_j^n) &= -\partial_{\nu_k} u_k^{n-1} + \imath\omega \mathscr{T}(u_k^{n-1}) && \text{on } \Sigma_{jk}, \quad j \neq k. \end{aligned} \tag{9.2}$$

Here, $\mathscr{T}$ is an injective operator acting on functions defined on Σ_{jk}, $j \neq k$, and the boundary conditions are once again understood in an appropriate trace sense.

In the original work of Després [49], the transmission operator $\mathscr{T}$ was chosen to be the identity function, and it was shown that the two sequences of functions $\{u_1^n\}_{n\in\mathbb{N}}$ and $\{u_2^n\}_{n\in\mathbb{N}}$ converge, in a relatively weak sense, to the restriction on Ω_1 and Ω_2 respectively, of the solution $u \in H^1(\Omega)$ of the global problem (9.1). Alternative choices of $\mathscr{T}$ have, for instance, been considered by Gander et al. [76], Japhet and Nataf [109], and Boubendir et al. [20].

In addition to the lack of a general proof of convergence in a strong sense, the choices of the transmission operator $\mathscr{T}$ adopted in the references mentioned above suffer from a well-known computational deficiency, namely that the convergence rate of the iterative procedure is merely algebraic (see [40]). This is in contrast to the well-established convergence theory and geometric rate of convergence of the parallel Schwarz method applied to the Laplace problem (see [132]). In an effort to propose a better choice of $\mathscr{T}$

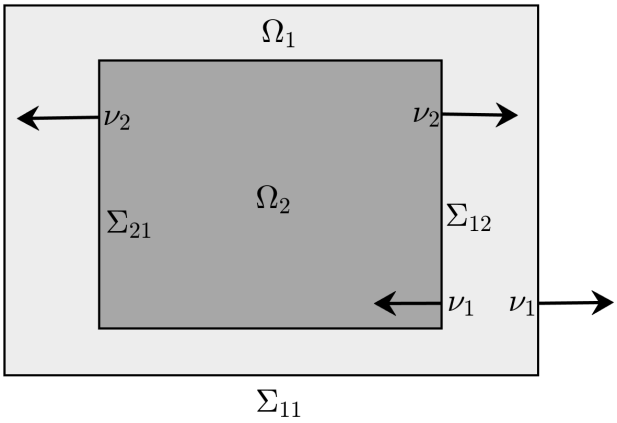

Figure 9.1: The domain decomposition $\Omega = \Omega_1 \cup \Omega_2$ used in the iterative procedure (9.2).

that could lead to a rigorous proof of geometric convergence, Collino et al. [40] proved the following result:

Theorem 9.1 ([40, Theorem 7])**.** *Consider the setting of the BVPs (9.1) and (9.2) and assume that there exists an isomorphism* $\Lambda\colon L^2(\Sigma_{12}) \to H^{-\frac{1}{2}}(\Sigma_{12})$ *such that* $\mathscr{T} = \Lambda\Lambda^*$ *where* $\Lambda^*\colon H^{\frac{1}{2}}(\Sigma_{12}) \to L^2(\Sigma_{12})$ *denotes the adjoint of* Λ*. Then there exists* $C > 0$ *and a parameter* $\tau > 0$ *such that for all* $n \in \mathbb{N}$ *it holds that*

$$\|u_1^n - u\|_{H^1(\Omega_1)} + \|u_2^n - u\|_{H^1(\Omega_2)} \leq C\tau^n.$$

Theorem 9.1 therefore suggests that an appropriate choice for the transmission operator $\mathscr{T}$ would be a pseudo-differential operator of order $\frac{1}{2}$ (see e.g., [191] for an explanation of this terminology). Such operators are straightforward to construct in the special case when the interface boundary Σ_{12} is a flat space $\mathbb{R}^d$, $d \in \mathbb{N}$. Indeed, if we consider a computational domain $\Omega \subset \mathbb{R}^3$ that is unbounded and $\Sigma_{12} = \mathbb{R}^2$ for instance, then we can define $\Lambda\colon L^2(\Sigma_{12}) \to H^{-\frac{1}{2}}(\Sigma_{12})$ as

$$\Lambda := I + \frac{1}{\sqrt{\omega}}\nabla \cdot (\mathscr{A}\nabla)\,,$$

where I denotes the identity mapping and $\mathscr{A}$ is a weakly singular integral operator belonging to the class of so-called Riesz potentials (see [194, Chapter V]). Riesz potentials on flat spaces including $\mathbb{R}^2$ have been analysed in the classical text of Stein [194, Chapter V], and using the continuity properties established therein, it is possible to prove that the transmission operator Λ satisfies the required mapping property on $\Sigma_{12} = \mathbb{R}^2$. While the definition of Λ can be extended in a natural manner to the case of more general surfaces Σ_{12}, the required mapping property, i.e., that Λ is a bounded operator from $L^2(\Sigma_{12})$ to $H^{-\frac{1}{2}}(\Sigma_{12})$ can only be established if one can first prove the corresponding continuity property of the Riesz potential on the surface Σ_{12}. Recently, such continuity

estimates on smooth surfaces Σ_{12} have been obtained by Collino et al. [41] (see also the Phd thesis of Lecouvez [120]). Unfortunately, no such result exists in the literature for an a priori non-smooth surface Σ_{12} of the form considered in our model problem. The goal of our work is therefore to establish some first continuity results for Riesz potentials in two spatial dimensions acting on polygonal boundaries. More precisely, we will prove that the Riesz potential (defined precisely in Section 9.3) acts as a bounded linear map from $L^2(\partial\Omega)$ to $H^{\frac{1}{2}}(\partial\Omega)$ on polygonal boundaries $\partial\Omega$.

The remainder of this chapter is organised as follows: In Section 9.2 we establish some notation and state precisely the definitions of weighted Sobolev spaces that we require for our analysis. Next, in Section 9.3, we define the Riesz potential on polygonal boundaries and show that the analysis of this operator on corners can be carried out using so-called Mellin transforms. Subsequently, in Section 9.4 we provide a brief recap of the Mellin transform and recall its use to characterise norms in certain Sobolev spaces. In Section 9.5 we perform a detailed study of the Mellin symbols of the Riesz potential following which we deduce, in Section 9.6, the required continuity estimates for the Riesz potential on boundaries containing corners. Finally, in Section 9.7, we present our conclusions and an outlook. The material presented in this chapter is joint work with Xavier Claeys and Benjamin Stamm, and will be submitted for publication in a peer-reviewed journal.

9.2 Basic Notions

Throughout this chapter, we will make frequent use of the classical and so-called weighted Sobolev spaces on the positive real line. Although these definitions are standard (see, e.g., [44, 185]) and we have already introduced the notion of fractional Sobolev spaces in Section 1.3, we will restate these definitions for the sake of emphasis.

Let $\Omega \subset \mathbb{R}$ be an open set. We recall from Section 1.3 that we denote by $C_0^\infty(\Omega)$ the space of infinitely differentiable functions with compact support in Ω, and we define $C_{\text{comp}}^\infty(\Omega) := \{u|_\Omega \colon u \in C_0^\infty(\mathbb{R})\}$. Next, given a function $u \in L^2(\Omega)$, we will denote by $\tilde{u} \in L^2(\mathbb{R})$, the extension of u by zero on $\mathbb{R}$, i.e.,

$$\tilde{u} = \begin{cases} u & \text{on } \Omega, \\ 0 & \text{on } \mathbb{R} \setminus \Omega. \end{cases}$$

The core of our subsequent analysis will involve Sobolev spaces on the positive real line $\mathbb{R}_+$ which we will now introduce.

Definition 9.2 (Fractional Sobolev spaces)**.** We define the Sobolev space $H^{\frac{1}{2}}(\mathbb{R}_+)$ as the completion of $C_{\text{comp}}^\infty(\mathbb{R}_+)$ with respect to the norm

$$\|u\|^2_{H^{\frac{1}{2}}(\mathbb{R}_+)} := \int_{\mathbb{R}_+} |u(x)|^2 \, dx + \underbrace{\int_{\mathbb{R}_+}\int_{\mathbb{R}_+} \frac{|u(x)-u(y)|^2}{|x-y|^2} \, dxdy}_{:=|u|^2_{H^{\frac{1}{2}}(\mathbb{R}_+)}} \quad \forall u \in L^2(\mathbb{R}_+). \tag{9.3}$$

Additionally, we define the Sobolev space $\widetilde{H}^{\frac{1}{2}}(\mathbb{R}_+)$ as the completion of $C_0^\infty(\mathbb{R}_+)$ with respect to the norm

$$\|u\|^2_{\widetilde{H}^{\frac{1}{2}}(\mathbb{R}_+)} := \int_{\mathbb{R}} |\tilde{u}(x)|^2 \, dx + \underbrace{\int_{\mathbb{R}} \int_{\mathbb{R}} \frac{|\tilde{u}(x) - \tilde{u}(y)|^2}{|x-y|^2} \, dxdy}_{:=|\tilde{u}|^2_{H^{\frac{1}{2}}(\mathbb{R})}} \quad \forall u \in L^2(\mathbb{R}_+). \tag{9.4}$$

Remark 9.3. In an analogous manner, one can define the fractional Sobolev space $H^{\frac{1}{2}}(\mathbb{R})$. For a detailed exposition on such fractional Sobolev spaces see, for instance, [90, Chapter 1].

Definition 9.4 (Dual Sobolev spaces)**.** We define the Sobolev spaces $H^{-\frac{1}{2}}(\mathbb{R}_+)$ and $\widetilde{H}^{-\frac{1}{2}}(\mathbb{R}_+)$ as the dual spaces

$$H^{-\frac{1}{2}}(\mathbb{R}_+) := \left(\widetilde{H}^{\frac{1}{2}}(\mathbb{R}_+)\right)^*, \qquad \widetilde{H}^{-\frac{1}{2}}(\mathbb{R}_+) := \left(H^{\frac{1}{2}}(\mathbb{R}_+)\right)^*,$$

equipped with the respective canonical dual norms.

Finally, we introduce the weighted Sobolev space first introduced by Kondratiev for the analysis of elliptic partial differential equations on polygonal domains. Note that we rely on the definition given by Costabel and Stephan [44], which differs slightly from the definition of Kondratiev (see [19, Section 1.7]).

Definition 9.5 (Weighted Sobolev space)**.** We define the weighted Sobolev space $W_0^{\frac{1}{2}}(\mathbb{R}_+)$ as the completion of $C_0^\infty(\mathbb{R}_+)$ with respect to the norm

$$\|u\|^2_{W_0^{\frac{1}{2}}(\mathbb{R}_+)} := \|x^{-\frac{1}{2}} u\|^2_{L^2(\mathbb{R}_+)} + |u|_{H^{\frac{1}{2}}(\mathbb{R}_+)}.$$

Given the norm defined on the weighted Sobolev space, one may suspect that there is a relation between the Sobolev space $\widetilde{H}^{\frac{1}{2}}(\mathbb{R}_+)$ and the weighted Sobolev spaces $W_0^{\frac{1}{2}}(\mathbb{R}_+)$. Indeed, we have the following Lemma due to Costabel and Stephan [44, Lemma 2.7].

Lemma 9.6. *Let $\chi \in C^\infty_{\mathrm{comp}}(\mathbb{R}_+)$. There exist constants $C_\chi, C'_\chi > 0$ such that for all $w \in W_0^{\frac{1}{2}}(\mathbb{R}_+)$ and all $u \in \widetilde{H}^{\frac{1}{2}}(\mathbb{R}_+)$ it holds that*

$$\|\chi w\|_{\widetilde{H}^{\frac{1}{2}}(\mathbb{R}_+)} \leq C_\chi \|w\|_{W_0^{\frac{1}{2}}(\mathbb{R}_+)} \quad \text{and} \quad \|\chi u\|_{W_0^{\frac{1}{2}}(\mathbb{R}_+)} \leq C'_\chi \|u\|_{\widetilde{H}^{\frac{1}{2}}(\mathbb{R}_+)}.$$

9.3 Riesz Potentials on Polygonal Boundaries

In the sequel, we denote by $\Omega \subset \mathbb{R}^2$ a bounded polygonal domain with boundary $\partial\Omega$. The Riesz potential on $\partial\Omega$ is defined as follows.

Definition 9.7 (Riesz potential on a polygonal boundary)**.** We define the operator $\mathscr{A}\colon C^\infty(\mathbb{R}^2) \to C^\infty(\mathbb{R}^2)^*$ as the mapping with the property that for all $u, v \in C^\infty(\mathbb{R}^2)$ it holds that

$$\langle \mathscr{A}(u), v\rangle_{C^\infty(\mathbb{R}^2)^* \times C^\infty(\mathbb{R}^2)} := \int_{\partial\Omega}\int_{\partial\Omega} \frac{u(\boldsymbol{y})v(\boldsymbol{x})}{\sqrt{|\boldsymbol{x}-\boldsymbol{y}|}}\, d\boldsymbol{x}d\boldsymbol{y}, \tag{9.5}$$

and we say that $\mathscr{A}$ is the Riesz potential operator on the polygonal boundary $\partial\Omega$.

As mentioned in the introduction, Riesz potential operators such as $\mathscr{A}$ have been studied in detail on flat spaces in [194, Chapter V] where it is also shown that $\mathscr{A}$ acts as a bounded operator between appropriate L^p spaces. Analyses on the continuity properties of such operators can also be found in [94, 95] for the case of smooth surfaces. But we are here specifically interested in the case of polygonal, a priori non-smooth surfaces. In particular, the goal of our analysis is to establish the following result.

Theorem 9.8 (Continuity of Riesz potentials on polygonal boundaries)**.** *Let $\mathscr{A}$ denote the Riesz potential on the polygonal boundary $\partial\Omega$ as given by Definition 9.7. Then $\mathscr{A}$ can be shown to act as a bounded linear operator from $L^2(\partial\Omega)$ into $H^{\frac{1}{2}}(\partial\Omega)$, i.e., there exists a constant $C > 0$ such that for all $u \in L^2(\partial\Omega)$ and all $v \in H^{-\frac{1}{2}}(\partial\Omega)$ it holds that*

$$\langle \mathscr{A}(u), v\rangle_{H^{\frac{1}{2}}(\partial\Omega)\times H^{-\frac{1}{2}}(\partial\Omega)} \leq C\|u\|_{L^2(\partial\Omega)}\|v\|_{H^{-\frac{1}{2}}(\partial\Omega)}.$$

In order to establish Theorem 9.8, we proceed in two main steps:

- In the first step, we consider a decomposition of the boundary $\partial\Omega$ and define an appropriate partition of unity. This allows us to study localisations of the operator $\mathscr{A}$. We demonstrate that these localisations are simple to analyse in cases where they do not contain a corner point of $\partial\Omega$.
- In the second step, we analyse localisations of $\mathscr{A}$ in the presence of corner points of $\partial\Omega$. As we will show, the appropriate tool for this analysis is the Mellin transform.

9.3.1 Localisation of the problem

We now propose a simple decomposition of the polygonal boundary $\partial\Omega$ and a partition of unity associated with this decomposition.

Notation 9.1 (Decomposition of $\partial\Omega$ and Partition of Unity)**.** We denote by $\mathscr{P}$ a finite cover of $\partial\Omega$ using open disks $\mathrm{D} \subset \mathbb{R}^2$ with centres $\boldsymbol{c}_\mathrm{D} \in \partial\Omega$ that satisfies the following conditions:

1. Each corner $\boldsymbol{c}$ of $\partial\Omega$ is the centre of a disk $\boldsymbol{c} = \boldsymbol{c}_\mathrm{D}$ for some $\mathrm{D} \in \mathscr{P}$;
2. Each such corner belongs to the closure of exactly one disk, i.e., $\boldsymbol{c} = \boldsymbol{c}_\mathrm{D} \notin \overline{\mathrm{D}}'$ for $\mathrm{D}' \in \mathscr{P}$ with $\mathrm{D}' \neq \mathrm{D}$.

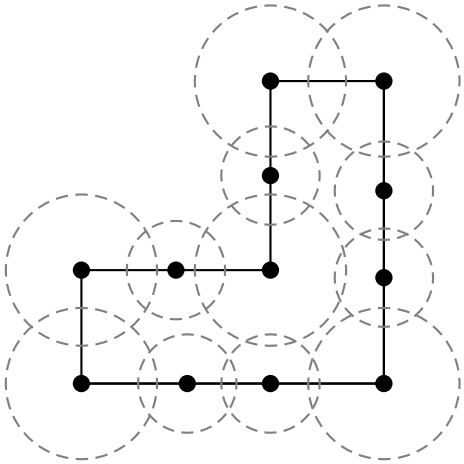

Figure 9.2: An example of the polygonal domain Ω with a decomposition of the boundary $\partial\Omega$ using a finite cover $\mathscr{P}$ of open disks.

For each $\mathrm{D} \in \mathscr{P}$, we denote $\Gamma_{\mathrm{D}} := \mathrm{D} \cap \partial\Omega$ and we note that $\partial\Omega = \cup_{\mathrm{D}\in\mathscr{P}} \Gamma_{\mathrm{D}}$. Additionally, we denote by $\{\chi_{\mathrm{D}}\}_{\mathrm{D}\in\mathscr{P}} \in C^\infty(\mathbb{R}^2)$ a *smooth* partition of unity attached to this cover, i.e., $\mathrm{supp}(\chi_{\mathrm{D}}) \subset \mathrm{D}$ for all $\mathrm{D} \in \mathscr{P}$, $\chi_{\mathrm{D}} \in C^\infty(\overline{\mathrm{D}})$ for all $\mathrm{D} \in \mathscr{P}$, and $\sum_{\mathrm{D}\in\mathscr{P}} \chi_{\mathrm{D}}(\boldsymbol{x}) = 1$ for all $\boldsymbol{x} \in \partial\Omega$.

Notice that the finite cover $\mathscr{P}$ described in Notation 9.1 is not uniquely determined. Nevertheless, by an abuse of notation we will refer, in the remainder of this chapter, to *the* finite cover $\mathscr{P}$ fixed by Notation 9.1. Equipped with this convention, the linearity of the Riesz potential yields that for all $u, v \in C^\infty(\mathbb{R}^2)$ it holds that

$$\langle \mathscr{A}(u), v\rangle_{C^\infty(\mathbb{R}^2)^*\times C^\infty(\mathbb{R}^2)} = \sum_{\mathrm{D},\mathrm{D}'\in\mathscr{P}} \int_{\partial\Omega} \mathscr{A}(\chi_{\mathrm{D}} u)(\boldsymbol{x})(\chi_{\mathrm{D}'} v)(\boldsymbol{x})\, d\boldsymbol{x}. \tag{9.6}$$

This observation suggests a natural localisation of the operator $\mathscr{A}$ corresponding to the cover $\mathscr{P}$.

Notation 9.2 (Localisations of $\mathscr{A}$)**.** Let the Riesz potential $\mathscr{A}$ be defined as in Definition 9.7, and let the finite cover $\mathscr{P}$ and partition of unity functions $\{\chi_{\mathrm{D}}\}_{\mathrm{D}\in\mathscr{P}}$ be fixed as in Notation 9.1. Then for each $\mathrm{D}, \mathrm{D}' \in \mathscr{P}$, we define the mapping $\mathscr{A}^{\chi}_{\mathrm{D},\mathrm{D}'} \colon C^\infty(\mathbb{R}^2) \to C^\infty(\mathbb{R}^2)^*$ as

$$\langle \mathscr{A}^{\chi}_{\mathrm{D},\mathrm{D}'}(u), v\rangle_{C^\infty(\mathbb{R}^2)^*\times C^\infty(\mathbb{R}^2)} := \int_{\partial\Omega} \mathscr{A}(\chi_{\mathrm{D}} u)(\boldsymbol{x})(\chi_{\mathrm{D}'} v)(\boldsymbol{x})\, d\boldsymbol{x}.$$

Remark 9.9. Consider Notation 9.2 and for each $\mathrm{D}, \mathrm{D}' \in \mathscr{P}$ define the kernel

$$\mathfrak{A}^{\chi}_{\mathrm{D},\mathrm{D}'}(\boldsymbol{x}, \boldsymbol{y}) := \chi_{\mathrm{D}}(\boldsymbol{x}) |\boldsymbol{x} - \boldsymbol{y}|^{-\frac{1}{2}} \chi_{\mathrm{D}'}(\boldsymbol{y}) \qquad \forall \boldsymbol{x}, \boldsymbol{y} \in \mathbb{R}^2 \text{ with } \boldsymbol{x} \neq \boldsymbol{y}.$$

It follows that

$$\langle \mathscr{A}^{\chi}_{\mathrm{D},\mathrm{D}'}(u), v\rangle_{C^\infty(\mathbb{R}^2)^*\times C^\infty(\mathbb{R}^2)} = \int_{\partial\Omega}\int_{\partial\Omega} \mathfrak{A}^{\chi}_{\mathrm{D},\mathrm{D}'}(\boldsymbol{x}, \boldsymbol{y}) u(\boldsymbol{x}) v(\boldsymbol{y})\, d\boldsymbol{x} d\boldsymbol{y}.$$

In other words, the integral operator $\mathscr{A}^{\chi}_{\mathrm{D},\mathrm{D}'}$ is generated by the kernel $\mathfrak{A}^{\chi}_{\mathrm{D},\mathrm{D}'}(\boldsymbol{x}, \boldsymbol{y})$.

9. CONTINUITY ESTIMATES FOR RIESZ POTENTIALS ON POLYGONAL BOUNDARIES

Consider Notation 9.2. In view of Equation (9.6), the continuity properties of the mapping $\mathscr{A}$ can be established by analysing the localisations $\mathscr{A}^{\chi}_{\mathrm{D},\mathrm{D}'}$ for each $\mathrm{D},\mathrm{D}' \in \mathscr{P}$. More precisely, in order to prove Theorem 9.8, it suffices to establish the following result.

Proposition 9.1 (Continuity of the Localisations)**.** Let the finite cover $\mathscr{P}$ and partition of unity functions $\{\chi_{\mathrm{D}}\}_{\mathrm{D}\in\mathscr{P}} \in C^{\infty}(\mathbb{R}^2)$ be fixed as in Notation 9.1, let $\mathrm{D},\mathrm{D}' \in \mathscr{P}$ be any two disks and let the operator $\mathscr{A}^{\chi}_{\mathrm{D},\mathrm{D}'} \colon C^{\infty}(\mathbb{R}^2) \to C^{\infty}(\mathbb{R}^2)^*$ be defined as in Notation 9.2. Then there exists a constant $C_{\mathrm{D},\mathrm{D}'} > 0$ such that for all $u, v \in C^{\infty}(\mathbb{R}^2)$ it holds that

$$\left|\langle \mathscr{A}^{\chi}_{\mathrm{D},\mathrm{D}'}(u), v\rangle_{C^{\infty}(\mathbb{R}^2)^*\times C^{\infty}(\mathbb{R}^2)}\right| \leq C_{\mathrm{D},\mathrm{D}'}\|u\|_{L^2(\partial\Omega)}\|v\|_{H^{-\frac{1}{2}}(\partial\Omega)}. \tag{9.7}$$

Clearly, Theorem 9.8 will follow from a simple density argument once Proposition 9.1 has been proved. Unfortunately, the proof of Proposition 9.1 is non-trivial for the case where $\mathrm{D} = \mathrm{D}'$ and D contains a corner of $\partial\Omega$. For all other choices of the disks D and D' however, the estimate (9.7) can be easily established.

Proof of Proposition 9.1 when $\mathrm{D} \neq \mathrm{D}'$ ***or*** D ***is without a corner.*** Let $\mathrm{D},\mathrm{D}' \in \mathscr{P}$ be any two disks and let $\mathfrak{A}^{\chi}_{\mathrm{D},\mathrm{D}'}(\boldsymbol{x},\boldsymbol{y})$ denote the integral kernel as defined in Remark 9.9. Notice that if $\overline{\mathrm{D}} \cap \overline{\mathrm{D}}' = \emptyset$, the inequality (9.7) is clearly satisfied since $\mathfrak{A}^{\chi}_{\mathrm{D},\mathrm{D}'} \in C^{\infty}(\mathbb{R}^2 \times \mathbb{R}^2)$. Therefore, it suffices to consider the case

$$\overline{\mathrm{D}} \cap \overline{\mathrm{D}}' \neq \emptyset \text{ and } \overline{\mathrm{D}} \cap \overline{\mathrm{D}}' \text{ does not contain any corner of } \partial\Omega. \tag{9.8}$$

We now show that under this condition, the continuity property (9.7) follows from the continuity properties of Riesz potentials in flat spaces, as discussed in [194, Chapter V]. Indeed, under Condition (9.8), there exists a straight infinite line $\Sigma \subset \mathbb{R}^2$ such that $\Gamma_{\mathrm{D}} \cap \Gamma_{\mathrm{D}'} \subset \Sigma$. Let $\psi \in C^{\infty}(\mathbb{R}^2)$ be a cut-off function with the property that $\psi = 1$ on a neighbourhood $V_{\Gamma_{\mathrm{D}}\cap\Gamma_{\mathrm{D}'}}$ of $\Gamma_{\mathrm{D}} \cap \Gamma_{\mathrm{D}'}$ and $\psi = 0$ on $\partial\Omega \setminus \Sigma$. We define the functions $\psi_{\mathrm{D}} := \psi\chi_{\mathrm{D}}$ and $\psi_{\mathrm{D}'} := \psi\chi_{\mathrm{D}'}$, and we define the integral kernel

$$\mathfrak{A}^{\psi}_{\mathrm{D},\mathrm{D}'}(\boldsymbol{x},\boldsymbol{y}) := \psi_{\mathrm{D}}(\boldsymbol{x})|\boldsymbol{x}-\boldsymbol{y}|^{-\frac{1}{2}}\psi_{\mathrm{D}'}(\boldsymbol{y}) \qquad \forall \boldsymbol{x},\boldsymbol{y} \in \mathbb{R}^2 \text{ with } \boldsymbol{x} \neq \boldsymbol{y}.$$

It follows that for all $u, v \in C^{\infty}(\mathbb{R}^2)$ we can write

$$\begin{aligned}\langle \mathscr{A}^{\chi}_{\mathrm{D},\mathrm{D}'}(u), v\rangle_{C^{\infty}(\mathbb{R}^2)^*\times C^{\infty}(\mathbb{R}^2)} &= \langle (\mathscr{A}^{\chi}_{\mathrm{D},\mathrm{D}'} - \mathscr{A}^{\psi}_{\mathrm{D},\mathrm{D}'})u, v\rangle_{C^{\infty}(\mathbb{R}^2)^*\times C^{\infty}(\mathbb{R}^2)} \\ &\quad + \langle \mathscr{A}^{\psi}_{\mathrm{D},\mathrm{D}'}(u), v\rangle_{C^{\infty}(\mathbb{R}^2)^*\times C^{\infty}(\mathbb{R}^2)},\end{aligned} \tag{9.9}$$

$$\text{where} \quad \langle \mathscr{A}^{\psi}_{\mathrm{D},\mathrm{D}'}(u), v\rangle_{C^{\infty}(\mathbb{R}^2)^*\times C^{\infty}(\mathbb{R}^2)} := \int_{\partial\Omega\times\partial\Omega} \mathfrak{A}^{\psi}_{\mathrm{D},\mathrm{D}'}(\boldsymbol{x},\boldsymbol{y})v(\boldsymbol{x})u(\boldsymbol{y})d\boldsymbol{x}d\boldsymbol{y}.$$

We now estimate each term of the right hand side above. In order to estimate the first term, we recall that the partition of unity functions χ_{D} and $\chi_{\mathrm{D}'}$ are supported in the disks D and D' respectively so the integral kernel $\mathfrak{A}^{\chi}_{\mathrm{D},\mathrm{D}'} - \mathfrak{A}^{\psi}_{\mathrm{D},\mathrm{D}'}$ can only be singular on the set $\mathrm{D}\cap\mathrm{D}' \times \mathrm{D}\cap\mathrm{D}'$. On the other hand, the definition of the cutoff function $\psi \in C^{\infty}(\mathbb{R}^2)$

implies that $\psi_{\mathrm{D}}(\boldsymbol{y})\psi_{\mathrm{D}'}(\boldsymbol{x})$ coincides with $\chi_{\mathrm{D}}(\boldsymbol{y})\chi_{\mathrm{D}'}(\boldsymbol{x})$ on the neighbourhood $V_{\Gamma_{\mathrm{D}}\cap\Gamma_{\mathrm{D}'}}$ of $\Gamma_{\mathrm{D}}\cap\Gamma_{\mathrm{D}'}$. We can therefore conclude that $\mathfrak{A}^{\chi}_{\mathrm{D},\mathrm{D}'} - \mathfrak{A}^{\psi}_{\mathrm{D},\mathrm{D}'}$ is infinitely smooth on $\partial\Omega\times\partial\Omega$, and as a consequence there exists a constant $C_{\mathrm{D},\mathrm{D}'} > 0$ such that for all $u, v \in C^{\infty}(\mathbb{R}^2)$ it holds that

$$\left|\langle(\mathscr{A}^{\chi}_{\mathrm{D},\mathrm{D}'} - \mathscr{A}^{\psi}_{\mathrm{D},\mathrm{D}'})u, v\rangle_{C^{\infty}(\mathbb{R}^2)^*\times C^{\infty}(\mathbb{R}^2)}\right| \leq C^{1}_{\mathrm{D},\mathrm{D}'}\|u\|_{L^2(\partial\Omega)}\|v\|_{H^{-\frac{1}{2}}(\partial\Omega)}. \tag{9.10}$$

Next, observe that $(\partial\Omega\times\partial\Omega)\cap\mathrm{supp}(\mathfrak{A}^{\psi}_{\mathrm{D},\mathrm{D}'}) = (\Sigma\times\Sigma)\cap\mathrm{supp}(\mathfrak{A}^{\psi}_{\mathrm{D},\mathrm{D}'})$. Consequently, the second term in (9.9) can be written as

$$\langle\mathscr{A}^{\psi}_{\mathrm{D},\mathrm{D}'}(u), v\rangle_{C^{\infty}(\mathbb{R}^2)^*\times C^{\infty}(\mathbb{R}^2)} = \int_{\Sigma\times\Sigma}\mathfrak{A}^{\psi}_{\mathrm{D},\mathrm{D}'}(\boldsymbol{x},\boldsymbol{y})v(\boldsymbol{x})u(\boldsymbol{y})d\sigma(\boldsymbol{x},\boldsymbol{y}).$$

Thus, according to the continuity properties of Riesz potentials from [194, Chapter V], there exist constants $C_{\Sigma}, \tilde{C}_{\mathrm{D},\mathrm{D}'} > 0$ such that

$$\begin{aligned}\left|\langle\mathscr{A}^{\psi}_{\mathrm{D},\mathrm{D}'}(u), v\rangle_{C^{\infty}(\mathbb{R}^2)^*\times C^{\infty}(\mathbb{R}^2)}\right| &\leq C_{\Sigma}\|\psi_{\mathrm{D}}u\|_{L^2(\Sigma)}\|\psi_{\mathrm{D}'}v\|_{H^{-\frac{1}{2}}(\Sigma)}\\ &= C_{\Sigma}\|\psi_{\mathrm{D}}u\|_{L^2(\partial\Omega)}\|\psi_{\mathrm{D}'}v\|_{H^{-\frac{1}{2}}(\partial\Omega)}\\ &\leq C_{\Sigma}\tilde{C}_{\mathrm{D},\mathrm{D}'}\|u\|_{L^2(\partial\Omega)}\|v\|_{H^{-\frac{1}{2}}(\partial\Omega)}.\end{aligned} \tag{9.11}$$

In the inequality above we have used the fact that $\mathrm{supp}(\psi_{\mathrm{D}})\cap\Sigma = \mathrm{supp}(\psi_{\mathrm{D}})\cap\partial\Omega$ so that $\|\psi_{\mathrm{D}}u\|_{L^2(\Sigma)} = \|\psi_{\mathrm{D}}u\|_{L^2(\partial\Omega)}$ and $\|\psi_{\mathrm{D}'}v\|_{L^2(\Sigma)} = \|\psi_{\mathrm{D}'}v\|_{L^2(\partial\Omega)}$. Combining the bounds (9.10)-(9.11) with Equation (9.9), we obtain that the continuity estimate (9.7) indeed holds in the case (9.8). This shows that Proposition 9.1 holds for all disks $\mathrm{D}, \mathrm{D}' \in \mathscr{P}$ such that either $\mathrm{D} \neq \mathrm{D}'$ or D does not include a corner of the polygonal boundary $\partial\Omega$. □

It therefore remains to prove Proposition 9.1 in the case when $\mathrm{D} = \mathrm{D}'$ and the disk D contains a corner of $\partial\Omega$. As mentioned previously, this proof is non-trivial and requires a careful study of the Riesz kernel in the presence of corners.

9.3.2 Description of the operator at corners

Throughout this subsection, we assume that $\mathrm{D} \in \mathscr{P}$ is a disk that contains a corner $\boldsymbol{c} \in \partial\Omega$. Our goal is now to study in more detail the operator $\mathscr{A}^{\chi}_{\mathrm{D},\mathrm{D}}$ defined through Notation 9.2. To this end, we first introduce a precise parameterisation of the neighbouring edges of the corner $\boldsymbol{c} \in \partial\Omega$.

Definition 9.10 (Geometric description of corners)**.** Let $\boldsymbol{c} \in \partial\Omega$ be a corner of the polygonal domain Ω. We denote by $\boldsymbol{e}_{\pm} \in \mathbb{R}^2$ the two unit vectors tangent to $\partial\Omega$ at $\boldsymbol{c}$ with the convention that both unit vectors $\boldsymbol{e}_{\pm}$ point outwards from the corner $\boldsymbol{c}$. Moreover, we define the rays $\Gamma_{\pm} \subset \mathbb{R}^2$ and the cone $\Gamma \subset \mathbb{R}^2$ as

$$\Gamma_{\pm} := \{\boldsymbol{c} + t\,\boldsymbol{e}_{\pm},\quad t > 0\} \qquad \text{and} \qquad \Gamma := \overline{\Gamma}_{-}\cup\overline{\Gamma}_{+},$$

and we observe that $\mathrm{D}\cap\partial\Omega = \mathrm{D}\cap\Gamma$.

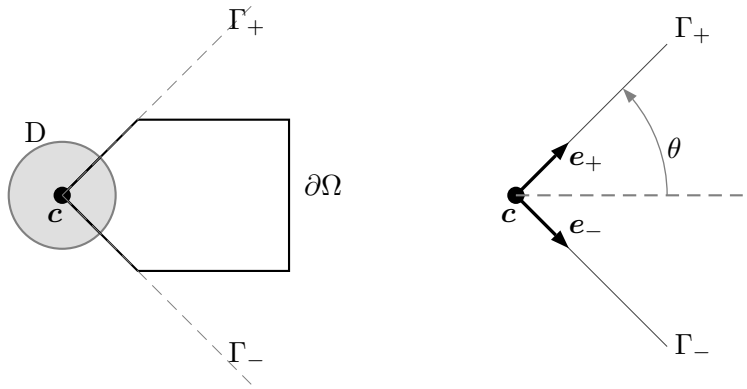

Figure 9.3: An example of a corner $\boldsymbol{c} \in \partial\Omega$ with unit vectors $\boldsymbol{e}_\pm \in \mathbb{R}^2$ describing the neighbouring edges.

Definition 9.11 (Riesz potential on corners)**.** Let $\boldsymbol{c} \in \partial\Omega$ be a corner of the polygonal domain Ω and let the cone Γ be defined as in Definition 9.10. We define the operator $\mathscr{A}_\Gamma \colon C^\infty_{\mathrm{comp}}(\mathbb{R}^2) \to C^\infty_{\mathrm{comp}}(\mathbb{R}^2)^*$ as the mapping with the property that for all $u, v \in C^\infty_{\mathrm{comp}}(\mathbb{R}^2)$ it holds that

$$\langle \mathscr{A}_\Gamma(u), v \rangle_{C^\infty_{\mathrm{comp}}(\mathbb{R}^2)^* \times C^\infty_{\mathrm{comp}}(\mathbb{R}^2)} := \int_{\Gamma\times\Gamma} \frac{u(\boldsymbol{y})v(\boldsymbol{x})}{\sqrt{|\boldsymbol{x}-\boldsymbol{y}|}}\, d\boldsymbol{x}d\boldsymbol{y}, \tag{9.12}$$

and we say that $\mathscr{A}_\Gamma$ is the Riesz potential operator associated with the cone Γ.

Recalling Notation 9.2 concerning the localisations of the Riesz potential on the polygonal boundary $\partial\Omega$, we immediately observe that

$$\langle \mathscr{A}^\chi_{\mathrm{D,D}}(u), v \rangle_{C^\infty(\mathbb{R}^2)^* \times C^\infty(\mathbb{R}^2)} = \langle \mathscr{A}_\Gamma(\chi_{\mathrm{D}} u), \chi_{\mathrm{D}} v \rangle_{C^\infty_{\mathrm{comp}}(\mathbb{R}^2)^* \times C^\infty_{\mathrm{comp}}(\mathbb{R}^2)} \quad \forall u, v \in C^\infty(\mathbb{R}^2).$$

In order to deduce the continuity estimate (9.7) in Proposition 9.1 for $\mathscr{A}^\chi_{\mathrm{D,D}}$, it therefore suffices to study in detail the operator $\mathscr{A}_\Gamma$. To this end, we first introduce some additional notation.

Notation: Let $u \in C^\infty(\mathbb{R}^2)$ be arbitrary and let the unit vectors $\boldsymbol{e}_\pm \subset \mathbb{R}^2$ be defined as in Definition 9.10. We define functions $u_\pm \colon \mathbb{R}_+ \to \mathbb{R}$, $[u] \colon \mathbb{R}_+ \to \mathbb{R}$ and $\{u\} \colon \mathbb{R}_+ \to \mathbb{R}$ as mappings with the property that for all $t \in \mathbb{R}_+$ it holds that

$$[u](t) := \frac{1}{\sqrt{2}}\big(u_+(t) - u_-(t)\big) \quad \text{and} \quad \{u\}(t) := \frac{1}{\sqrt{2}}\big(u_+(t) + u_-(t)\big), \tag{9.13}$$

where $u_\pm(t) := u(\boldsymbol{c} + t\boldsymbol{e}_\pm)$. Using Notation (9.13), we will now demonstrate that the Riesz potential $\mathscr{A}_\Gamma$ on the cone Γ can be written as a combination of multiplicative convolution operators associated with certain kernels.

Definition 9.12. Let $\boldsymbol{c} \in \partial\Omega$ be a corner of the polygonal domain Ω, let the arcs $\Gamma_\pm$ and the cone Γ be defined as in Definition 9.10, and let $\theta \in (0,\pi)$ be such that 2θ is the opening angle of the cone Γ. Then for each $\alpha \in [0,\pi)$ we define the kernel $\mathfrak{K}_\alpha$ as

$$\mathfrak{K}_\alpha(\tau) := \frac{1}{(4\sin^2(\alpha) + (\sqrt{\tau} - 1/\sqrt{\tau})^2\ )^{1/4}}, \tag{9.14}$$

and for each $u \in C^\infty_{\text{comp}}(\mathbb{R}^2)$ we define the operators $\mathscr{A}^\pm_\Gamma(u)\colon \mathbb{R}_+ \setminus \{1\} \to \mathbb{R}$ as mappings with the property that for all $t > 0$ it holds that

$$\mathscr{A}^\pm_\Gamma(u)(t) := t^{-1/4} \int_0^\infty \big(\ \mathfrak{K}_0(t/s) \pm \mathfrak{K}_\theta(t/s)\ \big) u(s) s^{-1/4}\, ds. \tag{9.15}$$

Consider the setting of Definition 9.12. Notice that we can view the mappings $\mathscr{A}^\pm_\Gamma$ as operators acting from $C^\infty_{\text{comp}}(\mathbb{R}_+)$ to $C^\infty_{\text{comp}}(\mathbb{R}_+)^*$.

Lemma 9.13 (Riesz potential on corners)**.** *Let $\boldsymbol{c} \in \partial\Omega$ be a corner of the polygonal domain Ω, let the cone Γ be defined as in Definition 9.10, let $\theta \in (0,\pi)$ be such that 2θ is the opening angle of the cone Γ, let the operator $\mathscr{A}_\Gamma\colon C^\infty_{\text{comp}}(\mathbb{R}^2) \to C^\infty_{\text{comp}}(\mathbb{R}^2)^*$ be defined as in Definition 9.11 and let the operators $\mathscr{A}^\pm_\Gamma\colon C^\infty_{\text{comp}}(\mathbb{R}^2) \to C^\infty_{\text{comp}}(\mathbb{R}^2)^*$ be defined as in Definition 9.12. Then for all $u, v \in C^\infty_{\text{comp}}(\mathbb{R}^2)$ it holds that*

$$\langle \mathscr{A}_\Gamma(u), v\rangle_{C^\infty_{\text{comp}}(\mathbb{R}^2)^* \times C^\infty_{\text{comp}}(\mathbb{R}^2)} = \int_0^\infty \mathscr{A}^+_\Gamma(\{u\})(t)\{v\}(t)\, dt + \int_0^\infty \mathscr{A}^-_\Gamma([u])(t)[v](t)\, dt. \tag{9.16}$$

Proof. The proof follows from a direct calculation in two steps. First, we simplify the integral kernel associated with the Riesz potential. To this end, let $\boldsymbol{x} \in \Gamma_+$ and $\boldsymbol{y} \in \Gamma_-$ denote two distinct points. There exist real numbers $s, t > 0$ such that $\boldsymbol{x} = \boldsymbol{c} + t\boldsymbol{e}_+$ and $\boldsymbol{y} = \boldsymbol{c} + s\boldsymbol{e}_-$. It follows that

$$\frac{1}{\sqrt{|\boldsymbol{x}-\boldsymbol{y}|}} = \frac{1}{|t\boldsymbol{e}_+ - s\boldsymbol{e}_-|^{\frac{1}{2}}}.$$

Obviously, we have $\boldsymbol{e}_- \cdot \boldsymbol{e}_+ = \cos(2\theta)$ and thus $|s\boldsymbol{e}_+ - t\boldsymbol{e}_-|^2 = (s-t)^2 + 4st\sin^2(\theta)$. We therefore obtain

$$\begin{aligned}\frac{1}{\sqrt{|\boldsymbol{x}-\boldsymbol{y}|}} &= \frac{1}{|(s-t)^2 + 4st\sin^2(\theta)|^{1/4}} = \frac{1}{|(\sqrt{s}/\sqrt{t} - \sqrt{t}/\sqrt{s})^2 + 4\sin^2(\theta)|^{1/4}}\, \frac{1}{(st)^{1/4}} \\ &= \mathfrak{K}_\theta(s/t)\frac{1}{(st)^{1/4}}.\end{aligned} \tag{9.17}$$

A similar result can be deduced for pairs of points $\boldsymbol{x}', \boldsymbol{y}' \in \boldsymbol{e}_+$ or $\boldsymbol{x}', \boldsymbol{y}' \in \boldsymbol{e}_-$ by setting $\theta = 0$.

Next, observe that by Definition 9.11 we have

$$\langle \mathscr{A}_\Gamma(u), v\rangle_{C^\infty(\mathbb{R}^2)^* \times C^\infty(\mathbb{R}^2)} = \int_{\Gamma\times\Gamma} \frac{u(\boldsymbol{y})v(\boldsymbol{x})}{\sqrt{|\boldsymbol{x}-\boldsymbol{y}|}}\, d\boldsymbol{x}d\boldsymbol{y}$$

$$= \int_{\Gamma_+\times\Gamma_+} \frac{u(\boldsymbol{y})v(\boldsymbol{x})}{\sqrt{|\boldsymbol{x}-\boldsymbol{y}|}}\,d\boldsymbol{x}d\boldsymbol{y} + \int_{\Gamma_-\times\Gamma_-} \frac{u(\boldsymbol{y})v(\boldsymbol{x})}{\sqrt{|\boldsymbol{x}-\boldsymbol{y}|}}\,d\boldsymbol{x}d\boldsymbol{y}$$
$$+ \int_{\Gamma_+\times\Gamma_-} \frac{u(\boldsymbol{y})v(\boldsymbol{x})}{\sqrt{|\boldsymbol{x}-\boldsymbol{y}|}}\,d\boldsymbol{x}d\boldsymbol{y} + \int_{\Gamma_-\times\Gamma_+} \frac{u(\boldsymbol{y})v(\boldsymbol{x})}{\sqrt{|\boldsymbol{x}-\boldsymbol{y}|}}\,d\boldsymbol{x}d\boldsymbol{y}.$$

Using the parameterisations of the rays $\Gamma_\pm$ and Equation (9.17) we therefore obtain

$$\langle \mathscr{A}_\Gamma(u), v\rangle_{C^\infty(\mathbb{R}^2)^*\times C^\infty(\mathbb{R}^2)} = \int_{\mathbb{R}_+\times\mathbb{R}_+} \mathfrak{K}_0(t/s)\big(\, u_+(s)v_+(t) + u_-(s)v_-(t)\,\big)\frac{dsdt}{(st)^{1/4}}$$
$$+ \int_{\mathbb{R}_+\times\mathbb{R}_+} \mathfrak{K}_\theta(t/s)\big(\, u_+(s)v_-(t) + u_-(s)v_+(t)\,\big)\frac{dsdt}{(st)^{1/4}}. \tag{9.18}$$

The result now follows by using the 'jump' and 'average' functions $[u], \{u\}, [v]$ and $\{v\}$ introduced through Equation (9.13) together with elementary algebra. □

Lemma 9.13 suggests that in order to further analyse the operator $\mathscr{A}_\Gamma$, it suffices to pursue a close examination of the operators $\mathscr{A}_\Gamma^\pm$. These are multiplicative convolutions and the natural tool to study such operators is the Mellin transform.

9.4 Recap on Mellin Transform

There are few references in the literature that provide an overview of the Mellin transform and its use to characterise weighted Sobolev spaces on the positive real line. Additionally, the precise conventions on the definition of the Mellin transform often vary across different references. The goal of the current section is to fix notation, summarise the main properties of the Mellin transform and provide a self-contained and consistent exposition on its connection to weighted Sobolev spaces. Most of the subsequent results are standard and can, for instance, be found in [55, 142, 179]. We follow the convention of [110].

9.4.1 Definition of the Mellin transform

Definition 9.14 (Mellin Transform)**.** Let $u \in C_0^\infty(\mathbb{R}_+)$. We define the Mellin transform of u, denoted $\hat{u} = \mathscr{M}(u)$, as the mapping with the property that for all $\lambda \in \mathbb{C}$ it holds that

$$\mathscr{M}u(\lambda) = \hat{u}(\lambda) := \int_0^{+\infty} u(r)r^{-\lambda}dr/r. \tag{9.19}$$

Morera's theorem [179, Chapter 10] implies that for any function $u \in C_0^\infty(\mathbb{R}_+)$, the Mellin transform $\hat{u} \in \mathcal{H}(\mathbb{C})$, i.e., the Mellin transform of any $u \in C_0^\infty(\mathbb{R}_+)$ is an analytic function in the whole complex plane $\mathbb{C}$.

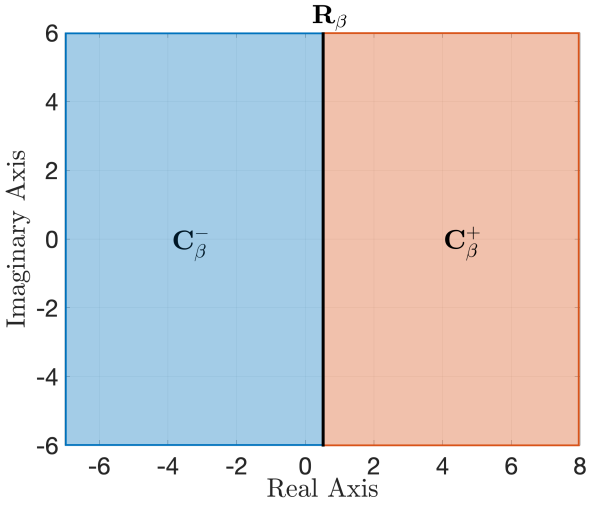

Figure 9.4: Visual Representation of the sets $\mathbb{R}_\beta$, $\mathbb{C}_\beta^+$, and $\mathbb{C}_\beta^-$ for $\beta = \frac{1}{2}$.

There is a close relationship between the Mellin and Fourier transform. Indeed, denoting by $S(\mathbb{R})^*$ the space of tempered distributions and by $\mathcal{F}\colon S(\mathbb{R})^* \to S(\mathbb{R})^*$ the Fourier transform, it is a simple exercise to show that for all $u \in C_0^\infty(\mathbb{R}_+)$ and all $\lambda \in \mathbb{C}$ it holds that

$$\mathscr{M}u(\imath\lambda) = \mathscr{F}u(\exp(\cdot))(\lambda). \tag{9.20}$$

Equation 9.20 allows us to transport any result from classical Fourier theory to the framework of the Mellin transform using the so-called Euler change of variables, i.e., using the map $t \mapsto \exp(t)$. In particular, we have a counterpart to the well-known Parseval theorem.

Lemma 9.15 (Parseval's Theorem for the Mellin Transform)**.** *For all $u \in C_0^\infty(\mathbb{R}_+)$ and all $\beta \in \mathbb{R}$ it holds that*

$$\int_0^\infty |u(r)|^2 r^{-2\beta} dr/r = \frac{1}{2\imath\pi} \int_{\beta-\imath\infty}^{\beta+\imath\infty} |\hat{u}(\lambda)|^2 d\lambda.$$

Notation: Let $\beta \in \mathbb{R}$. For clarity of exposition, we define the sets

$$\begin{aligned}\mathbb{R}_\beta &:= \{\lambda \in \mathbb{C},\ \Re e\{\lambda\} = \beta\},\\ \mathbb{C}_\beta^+ &:= \{\lambda \in \mathbb{C},\ \Re e\{\lambda\} > \beta\},\\ \mathbb{C}_\beta^- &:= \{\lambda \in \mathbb{C},\ \Re e\{\lambda\} < \beta\}.\end{aligned}$$

Lemma 9.15 in particular allows us to extend the domain of definition of the Mellin transform. Indeed, we introduce the following family of weighted Lebesgue spaces.

Definition 9.16 (Weighted Lebesgue spaces)**.** Let $\beta \in \mathbb{R}$. We define the Hilbert space $\mathcal{L}^2_\beta(\mathbb{R}_+)$ as the completion of $C_0^\infty(\mathbb{R}_+)$ with respect to the norm

$$\|u\|^2_{\mathcal{L}^2_\beta(\mathbb{R}_+)} := \int_0^\infty |u(r)|^2 r^{-2\beta} dr/r.$$

We now have the following result which follows from a classical density argument.

Lemma 9.17. *For every $\beta \in \mathbb{R}$, the Mellin transform extends as an isometric isomorphism from $\mathcal{L}^2_\beta(\mathbb{R}_+)$ onto $L^2(\mathbb{R}_\beta)$.*

9.4.2 The inversion formula and connections to Hardy spaces

Notation: Let $\beta \in \mathbb{R}$. We define the spaces $\mathcal{L}^2_\beta(0,1)$ and $\mathcal{L}^2_\beta(1,\infty)$ as

$$\mathcal{L}^2_\beta(1,\infty) := \left\{ u\colon (1,\infty) \to \mathbb{C} \text{ such that } \|u\|^2_{\mathcal{L}^2_\beta(1,\infty)} := \int_1^\infty |u(r)|^2 r^{-2\beta} dr/r < \infty \right\},$$
$$\mathcal{L}^2_\beta(0,1) := \left\{ u\colon (0,1) \to \mathbb{C} \text{ such that } \|u\|^2_{\mathcal{L}^2_\beta(0,1)} := \int_0^1 |u(r)|^2 r^{-2\beta} dr/r < \infty \right\}.$$

Next, we introduce the so-called Hardy spaces which are intimately connected to the Mellin transform.

Definition 9.18 (Hardy Spaces)**.** Let $\beta \in \mathbb{R}$. Then we define the Hilbert spaces $\mathfrak{H}^+(\mathbb{R}_\beta)$ and $\mathfrak{H}^-(\mathbb{R}_\beta)$ as the sets

$$\mathfrak{H}^+(\mathbb{R}_\beta) := \{u \in \mathcal{H}(\mathbb{C}^+_\beta),\ \sup_{\alpha>\beta} \|u\|^2_{L^2(\mathbb{R}_\alpha)} < \infty\},$$
$$\mathfrak{H}^-(\mathbb{R}_\beta) := \{u \in \mathcal{H}(\mathbb{C}^-_\beta),\ \sup_{\alpha<\beta} \|u\|^2_{L^2(\mathbb{R}_\alpha)} < \infty\},$$

together with the norms

$$\|u\|^2_{\mathfrak{H}^+(\mathbb{R}_\beta)} := \sup_{\alpha>\beta} \|u\|^2_{L^2(\mathbb{R}_\alpha)},$$
$$\|u\|^2_{\mathfrak{H}^-(\mathbb{R}_\beta)} := \sup_{\alpha<\beta} \|u\|^2_{L^2(\mathbb{R}_\alpha)}.$$

We have the following connection between the Hardy spaces defined through Definition 9.18 and the Mellin transform.

Lemma 9.19. *Let $\beta \in \mathbb{R}$. The Mellin transform maps isomorphically the spaces $\mathcal{L}^2_\beta(1,\infty)$ and $\mathcal{L}^2_\beta(0,1)$ onto the Hardy spaces $\mathfrak{H}^+(\mathbb{R}_\beta)$ and $\mathfrak{H}^-(\mathbb{R}_\beta)$ respectively.*

Proof. The proof follows by combining the classical Paley-Wiener theorem [179, Theorem 19.2] for the Fourier transform with Equation 9.20. □

Two remarks are now in order.

Remark 9.20. Using the inverse Fourier transform together with Equation 9.20, we can also deduce an inversion formula for the Mellin transform. Indeed, let $u \in \mathcal{L}^2_\beta(1,\infty)$ and let $\hat{u} = \mathscr{M}(u)$. Then for all $\alpha \geq \beta$ it holds that

$$u(r) = \frac{1}{2\imath\pi} \int_{\alpha-\imath\infty}^{\alpha+\imath\infty} \hat{u}(\lambda) r^\lambda d\lambda \tag{9.21}$$

where the integral should be understood in the sense of Fourier (see [179, Theorem 9.13] or [79, Proposition 22.1.6]). Similarly, if $v \in \mathcal{L}^2_\beta(0,1)$ and $\hat{v} = \mathscr{M}(v)$, then the inversion formula (9.21) holds for all $\alpha \leq \beta$.

Remark 9.21. Let $\alpha, \beta \in \mathbb{R}$ with $\alpha < \beta$. A direct calculation shows that

$$\mathcal{L}^2_\beta(0,1) \subset \mathcal{L}^2_\alpha(0,1) \qquad \text{and} \qquad \mathcal{L}^2_\alpha(1,\infty) \subset \mathcal{L}^2_\beta(1,\infty).$$

We can therefore deduce that $\mathcal{L}^2_\alpha(\mathbb{R}_+) \cap \mathcal{L}^2_\beta(\mathbb{R}_+) = \mathcal{L}^2_\alpha(1,\infty) \oplus \mathcal{L}^2_\beta(0,1)$ and hence the Mellin transform maps $\mathcal{L}^2_\alpha(\mathbb{R}_+) \cap \mathcal{L}^2_\beta(\mathbb{R}_+)$ onto $\mathfrak{H}^+(\mathbb{R}_\alpha) \oplus \mathfrak{H}^-(\mathbb{R}_\beta)$ which should be understood as a space of function that are analytic into the strip $\alpha < \Re e\{\lambda\} < \beta$.

9.4.3 Norm characterisation using the Mellin transform

It is well known that the Fourier Transform can be used to derive an alternative characterisation of the classical Sobolev norms in Euclidean spaces $\mathbb{R}^n$, $n \in \mathbb{N}$ (see, e.g., [50]). A similar characterisation of both the classical and weighted Sobolev norms on $\mathbb{R}_+$ can be accomplished using the Mellin transform. Indeed, we recall from the Parseval identity for Mellin transforms (Lemma 9.15) that for all $\phi \in C^\infty_0(\mathbb{R}_+)$ it holds that

$$\|\phi\|^2_{L^2(\mathbb{R}_+)} := \int_{-\frac{1}{2}-\imath\infty}^{-\frac{1}{2}+\imath\infty} |\widehat{\phi}(\lambda)|^2 \, d\lambda, \quad \text{and} \quad \|x^{-\frac{1}{2}}\phi\|^2_{L^2(\mathbb{R}_+)} := \int_{-\imath\infty}^{+\imath\infty} |\widehat{\phi}(\lambda)|^2 \, d\lambda.$$

Moreover, we have the following result due to Costabel and Stephan [44].

Lemma 9.22 ([44, Lemma 2.3])**.** *There exists a constant $C_2 > 1$ such that for all $\phi \in C^\infty_0(\mathbb{R}_+)$ it holds that*

$$\frac{1}{C_2} \int_{-\imath\infty}^{+\imath\infty} \frac{|\lambda|^2}{1+|\lambda|} |\widehat{\phi}(\lambda)|^2 \, d\lambda \leq |\phi|_{H^{\frac{1}{2}}(\mathbb{R}_+)} \leq C_2 \int_{-\imath\infty}^{+\imath\infty} \frac{|\lambda|^2}{1+|\lambda|} |\widehat{\phi}(\lambda)|^2 \, d\lambda.$$

Lemma 9.22 therefore allows us to obtain characterisations of the norms on $H^{\frac{1}{2}}(\mathbb{R}_+)$ and $W^{\frac{1}{2}}_0(\mathbb{R}_+)$ in terms of the Mellin transform. Furthermore, Lemma 9.22 also allows us to deduce a characterisation of the norm on the dual space $\widetilde{H}^{-\frac{1}{2}}(\mathbb{R}_+)$.

Lemma 9.23 ([44, Corollary 2.4])**.** *Let $C_2 > 0$ be the constant obtained in Lemma 9.22. Then for all $\psi \in C^\infty_0(\mathbb{R}_+)$ it holds that*

$$\|\psi\|_{\widetilde{H}^{-\frac{1}{2}}(\mathbb{R}_+)} \leq C_2 \int_{-\imath\infty}^{+\imath\infty} \frac{1+|\lambda|}{|\lambda|^2} |\widehat{\psi}(\lambda)|^2 \, d\lambda.$$

9.5 Detailed study of Mellin symbols of Riesz potentials

Throughout this section, we assume the setting of Sections 9.2-9.4. We recall that our final aim is to obtain a proof of Theorem 9.8, which establishes appropriate continuity

estimates for the Riesz potential on the polygonal boundary $\partial\Omega$. As demonstrated in Section 9.3.1, the key step in obtaining this proof is the analysis of the Riesz potential on corner points of the polygonal domain Ω, and as discussed in Section 9.3.2, the analysis at corner points can be carried out by studying in detail the Riesz potential $\mathscr{A}_\Gamma$ on an infinite cone Γ with vertex at a corner point $\boldsymbol{c} \in \partial\Omega$.

In Lemma 9.13, we obtained an explicit expression for the operator $\mathscr{A}_\Gamma$ as a combination of the multiplicative convolution operators $\mathscr{A}_\Gamma^\pm$ associated with the integral kernel $\mathfrak{K}_\alpha, \alpha \in [0,\pi)$ defined through Equation (9.14). The goal of this section is to analyse in detail the Mellin transform of the kernel $\mathfrak{K}_\alpha$. The motivation for this analysis comes from the following lemma.

Lemma 9.24. *Let $\boldsymbol{c} \in \partial\Omega$ be a corner of the polygonal domain Ω, let the cone Γ be defined as in Definition 9.10, let $\theta \in (0,\pi)$ be such that 2θ is the opening angle of the cone Γ, let $u \in C_0^\infty(\mathbb{R}^2)$ be arbitrary and let the operators $\mathscr{A}_\Gamma^\pm(u)\colon \mathbb{R}_+ \setminus \{1\} \to \mathbb{R}$ be defined as in Definition 9.12. Then for all $\lambda \in \mathbb{C}$ it holds that*

$$\widehat{\mathscr{A}_\Gamma^\pm(u)}(\lambda) = \Big(\widehat{\mathfrak{K}_0}(\lambda+1/4) \pm \widehat{\mathfrak{K}_\theta}(\lambda+1/4)\Big)\,\widehat{u}(\lambda-1/2). \tag{9.22}$$

Proof. The proof follows by a direct calculation. Indeed, using the definition of the Mellin transform we obtain that for all $\lambda \in \mathbb{C}$ it holds that

$$\begin{aligned}\widehat{\mathscr{A}_\Gamma^\pm(u)}(\lambda) &= \int_0^\infty \int_0^\infty \left(\mathfrak{K}_0(t/s) \pm \mathfrak{K}_\theta(t/s)\right) u(s) s^{\frac{3}{4}} t^{-\lambda-1/4}\, \frac{ds}{s}\frac{dt}{t} \\ &= \int_0^\infty \left(\int_0^\infty \left(\mathfrak{K}_0(t/s) \pm \mathfrak{K}_\theta(t/s)\right) t^{-\lambda-1/4}\, \frac{dt}{t}\right) u(s) s^{\frac{3}{4}} \frac{ds}{s}.\end{aligned}$$

Using the change of variables $w := t/s$, we further obtain

$$\begin{aligned}\widehat{\mathscr{A}_\Gamma^\pm(u)}(\lambda) &= \int_0^\infty \left(\int_0^\infty \left(\mathfrak{K}_0(w) \pm \mathfrak{K}_\theta(w)\right) w^{-\lambda-1/4}\, \frac{dw}{w}\right) u(s) s^{-\lambda+1/2} \frac{ds}{s}, \\ &= \int_0^\infty \left(\mathfrak{K}_0(w) \pm \mathfrak{K}_\theta(w)\right) w^{-\lambda-1/4}\, \frac{dw}{w} \int_0^\infty u(s) s^{-\lambda+1/2} \frac{ds}{s},\end{aligned}$$

so that

$$\widehat{\mathscr{A}_\Gamma^\pm(u)}(\lambda) = \Big(\widehat{\mathfrak{K}_0}(\lambda+1/4) \pm \widehat{\mathfrak{K}_\theta}(\lambda+1/4)\Big)\,\widehat{u}(\lambda-1/2).$$

□

Our first result establishes the analyticity of the Mellin transform of the kernel $\mathfrak{K}_\alpha, \alpha \in [0,\pi)$ on a strip in the complex plane.

Proposition 9.2. Let $\alpha \in [0,\pi)$, and let the integral kernel $\mathfrak{K}_\alpha$ be defined through (9.14). Then the Mellin transform $\widehat{\mathfrak{K}_\alpha}(\lambda)$ is well defined and analytic in the strip $|\Re e\{\lambda\}| < 1/4$.

Proof. We first consider the case $\alpha \in (0, \pi)$, i.e., we assume $\alpha \neq 0$. From (9.14), we have that the kernel $\mathfrak{K}_\alpha$ is given by

$$\mathfrak{K}_\alpha(\tau) = \frac{1}{(4\sin^2(\alpha) + (\sqrt{\tau} - 1/\sqrt{\tau})^2\ )^{1/4}} \qquad \forall \tau \in \mathbb{R}_+ \setminus \{1\}.$$

Notice that $\mathfrak{K}_\alpha(\tau)$ has no singularity at $\tau = 1$, which will be relevant later. Next, simple algebra yields that the kernel $\mathfrak{K}_\alpha$ can equivalently be written as

$$\mathfrak{K}_\alpha(\tau) = \frac{\tau^{1/4}}{(1 - (2\cos(2\alpha)\tau - \tau^2)\ )^{1/4}} \qquad \forall \tau \in \mathbb{R}_+ \setminus \{1\}.$$

Consequently, using the generalised binomial series we obtain the existence of some $\delta_0 > 0$ such that for all $0 < \tau < \delta_0$ we have the absolutely convergent series expansion

$$\mathfrak{K}_\alpha(\tau) = \tau^{1/4} \sum_{n=0}^{+\infty} \frac{1}{n!} \frac{\Gamma(n + 1/4)}{\Gamma(1/4)} \big(2\cos(2\alpha)\tau - \tau^2\big)^n. \tag{9.23}$$

For clarity, this series expansion can be further written as

$$\mathfrak{K}_\alpha(\tau) = \tau^{1/4} + \sum_{n=1}^{+\infty} \kappa_{\alpha,n} \tau^{n+1/4},$$

where each coefficient $\kappa_{\alpha,n},\ n \in \mathbb{N}$ is independent of τ and the series on the right hand side is again absolutely convergent for all $0 < \tau < \delta_0$. A direct calculation therefore reveals that $\mathfrak{K}_\alpha \in \mathcal{L}^2_{1/4-\epsilon}(0, 1)$ for every $\epsilon > 0$.

In a similar fashion, using the fact that for all $\tau > 0, \tau \neq 1$ we can deduce the existence of $\delta_\infty > 0$ such that for all $\tau > \delta_\infty$ we have the absolutely convergent asymptotic expansion

$$\mathfrak{K}_\alpha(\tau) = \tau^{-1/4} + \sum_{n=1}^{+\infty} \kappa_{\alpha,n} \tau^{-n-1/4}.$$

As a consequence, we can use once again a direct calculation to conclude that $\mathfrak{K}_\alpha \in \mathcal{L}^2_{-1/4+\epsilon}(1, \infty)$ for every $\epsilon > 0$. In view of Lemma 9.19 and Remark 9.21, it therefore holds that $\widehat{\mathfrak{K}}_\alpha(\lambda)$ is well defined and analytic in the strip $|\Re e\{\lambda\}| < 1/4$ as claimed.

Next, we consider the case $\alpha = 0$. In this case, the kernel $\mathfrak{K}_0$ can be written as

$$\mathfrak{K}_0(\tau) = \frac{\tau^{\frac{1}{4}}}{\sqrt{|\tau - 1|}} \qquad \forall \tau \in \mathbb{R}_+ \setminus \{1\}.$$

Notice that in contrast to the case $\alpha \neq 0$, the kernel $\mathfrak{K}_0$ has an integrable singularity at $\tau = 1$ which causes some additional difficulties. In order to deal with these difficulties we introduce a smooth cutoff function $\Psi \in C_0(\mathbb{R}_+)$ such that $\Psi = 1$ in a neighbourhood

of $\tau = 1$ and such that Ψ is supported in the interval $\left(\frac{1}{2}, \frac{3}{2}\right)$. It follows that we can write for all $\tau \in \mathbb{R}_+ \setminus \{1\}$:

$$\mathfrak{K}_0(\tau) = \underbrace{\Psi(\tau)\mathfrak{K}_0(\tau)}_{:=\mathfrak{M}_0(\tau)} + \underbrace{(1-\Psi(\tau))\mathfrak{K}_0(\tau)}_{:=\mathfrak{Z}_0(\tau)}.$$

The second term in the above decomposition is now smooth. Moreover, for all $\tau \in \mathbb{R}_+ \setminus \left(\frac{1}{2}, \frac{3}{2}\right)$ it holds that $\mathfrak{Z}_0(\tau) = \mathfrak{K}_0(\tau)$. As a consequence, we can apply our previous asymptotic estimates to obtain that $\widehat{\mathfrak{Z}}_0(\lambda)$ is well defined and analytic in the strip $|\Re e\{\lambda\}| < 1/4$.

As for the first term, we see that the function $\mathfrak{M}_0$ is integrable with compact support. Moreover, we recall from Equation (9.20) that for any $\lambda \in \mathbb{C}$, the Mellin transform $\widehat{\mathfrak{M}_0}(-\imath\lambda)$ is simply the composition of the Fourier transform and the Euler change of variables applied to $\mathfrak{M}_0$. In other words, the Mellin transform $\widehat{\mathfrak{M}_0}$ can be viewed as the Fourier transform of a compactly supported tempered distribution. As a consequence, we obtain from the Paley-Wiener-Schwartz theorem for compactly supported tempered distributions (see, e.g., [101, Theorem 7.1.14]) that $\widehat{\mathfrak{M}_0}$ extends as an entire function, i.e., $\widehat{\mathfrak{M}_0} \in \mathcal{H}(\mathbb{C})$. Due to the linearity of the Mellin transform, we can conclude that $\widehat{\mathfrak{K}}_0(\lambda)$ is well defined and analytic in the strip $|\Re e\{\lambda\}| < 1/4$. □

We now demonstrate that the Mellin transform of the integral kernel $\mathfrak{K}_\alpha$ can, in fact, be extended analytically to the entire complex plane $\mathbb{C}$, except for a countable number of points. In order to prove this result, we first require a preparatory lemma.

Lemma 9.25. *Let $\phi \in C^\infty(\mathbb{R})$ be a cut-off function satisfying $\phi(\tau) = 0$ for $\tau > 1/2$ and $\phi(\tau) = 1$ for $\tau < 1/4$. Then the Mellin transform $\widehat{\phi}(\lambda)$ is analytic on the entire complex plane $\mathbb{C}$ except at $\lambda = 0$ where it admits a simple pole. Furthermore for all $\mu \in \mathbb{R}$ and all $p \geq 0$ it holds that*

$$\lim_{\xi \to \infty} |\xi|^p \hat{\phi}(\mu \pm \imath\xi) = 0. \tag{9.24}$$

Proof. The definition of ϕ implies that $\phi \in \mathcal{L}^2_{-\epsilon}(0,1)$ for every $\epsilon > 0$. Lemma 9.19 therefore implies that $\widehat{\mathfrak{K}}_\alpha(\lambda)$ is well-defined and analytic for $\Re e\{\lambda\} < 0$. Furthermore, for any such $\lambda \in \mathbb{C}$ we have, using integration by parts, that

$$\begin{aligned} \hat{\phi}(\lambda) &= \int_0^\infty \phi(r) r^{-\lambda} dr/r = \frac{1}{\lambda}\int_0^\infty \Upsilon(r) r^{-\lambda} dr/r \\ &= \widehat{\Upsilon}(\lambda)/\lambda \quad \text{where} \quad \Upsilon(r) := r\partial_r \phi(r) \end{aligned} \tag{9.25}$$

Since $\operatorname{supp}(\partial_r \phi) \subset [\frac{1}{4}, \frac{1}{2}]$ by assumption we have that $\Upsilon \in C_0^\infty(\mathbb{R}_+)$. This implies in particular (see Section 9.4.1) that the Mellin transform $\widehat{\Upsilon}(\lambda)$ is analytic in the entire complex plane $\mathbb{C}$ and therefore $\widehat{\phi}(\lambda)$ is analytic on the entire complex plane $\mathbb{C}$ except at $\lambda = 0$ where it has a simple pole.

Next we demonstrate the validity of the decay condition (9.24). To this end, let $g\colon \mathbb{R} \to \mathbb{R}$ be defined as $g(t) := \Upsilon(\exp(t))\ \forall t \in \mathbb{R}$, and let $\lambda = \xi + \imath\mu \in \mathbb{C}$. Obviously,

$g \in C_0^\infty(\mathbb{R})$ and thus any order derivative of g is an integrable function on $\mathbb{R}$. The Riemann-Lebesgue lemma (see, e.g., [180, Chapter 5]) therefore implies that for any fixed $\mu \in \mathbb{R}$ and all $p \geq 0$ it holds that

$$\lim_{\xi \to \pm\infty} |\xi|^p \mathscr{F}(g)(\xi + \imath\mu) = 0,$$

where $\mathscr{F}(g)$ denotes the Fourier transform of g. The decay condition (9.24) now follows using the equivalence between the Fourier transform and the Mellin transform given by Equation 9.20. □

Proposition 9.3. Let $\alpha \in [0, \pi)$, and let the integral kernel $\mathfrak{K}_\alpha$ be defined by (9.14). Then the Mellin transform of the kernel $\mathfrak{K}_\alpha$ can be extended as an analytic function defined on $\mathbb{C} \setminus \mathfrak{S}$ where $\mathfrak{S} = (+1/4 + \mathbb{N}) \cup (-1/4 - \mathbb{N})$. Moreover $\widehat{\mathfrak{K}}_\alpha(\lambda)$ admits a simple pole at each point of $\mathfrak{S}$, and its residue at $\lambda = \pm 1/4$ does not depend on α.

Proof. As in the proof of Proposition 9.2, we will first consider the case $\alpha \in (0, \pi)$, i.e., we assume $\alpha \neq 0$. Let $\phi \in C^\infty(\mathbb{R})$ be a cut-off function satisfying $\phi(\tau) = 0$ for $\tau > 1/2$, and $\phi(\tau) = 1$ for $\tau < 1/4$ as described in Lemma 9.25, and let $Q \geq 2$ be a natural number. We define for all $\tau > 0$

$$\begin{aligned} \Phi_Q(\tau) &:= \left(\tau^{1/4} + \textstyle\sum_{q=1}^{Q-1} \kappa_{\alpha,q} \tau^{q+1/4} \right) \phi(\tau), \\ \mathrm{R}_Q(\tau) &:= \mathfrak{K}_\alpha(\tau) - \Phi_Q(\tau) - \Phi_Q(1/\tau). \end{aligned} \tag{9.26}$$

It is a simple exercise to prove that for any function $v \in C_0^\infty(\mathbb{R}_+)$, if we define $v_\sharp(\tau) := v(1/\tau)$ then we have $\hat{v}_\sharp(\lambda) = \hat{v}(-\lambda)$. Consequently, from Equation (9.26) we obtain that

$$\widehat{\mathfrak{K}_\alpha}(\lambda) = \widehat{\mathrm{R}_Q}(\lambda) + \widehat{\Phi_Q}(\lambda) + \widehat{\Phi_Q}(-\lambda). \tag{9.27}$$

We now analyse the behaviour of the Mellin transforms of the two functions Φ_Q and R_Q. To this end, we define the sets $\mathfrak{S} := (+1/4 + \mathbb{N}) \cup (-1/4 - \mathbb{N})$ and $\mathbb{B}_Q := \{\lambda \in \mathbb{C} \colon |\Re e\{\lambda\}| < Q + 1/4\}$. A direct calculation yields that

$$\widehat{\Phi_Q}(\lambda) = \hat{\phi}(\lambda - 1/4) + \sum_{q=1}^{Q-1} \kappa_{\alpha,q} \hat{\phi}(\lambda - q - 1/4). \tag{9.28}$$

Using Lemma 9.25, we deduce that the Mellin transform $\widehat{\Phi_Q}(\lambda)$ is well-defined and analytic for all $\lambda \in \mathbb{C} \setminus \mathfrak{S}$. Moreover, $\widehat{\Phi_Q}$ admits a simple pole at each point of $\mathfrak{S}$ and its residue at $\lambda = 1/4$ does not depend on α.

Furthermore, using the same arguments involving series expansions in neighbourhoods of $\tau = 0$ and $\tau \to \infty$ as in the proof of Proposition 9.2, we obtain that

$$\mathrm{R}_Q \in \mathcal{L}^2_{Q+1/4-\epsilon}(0,1) \quad \text{and} \quad \mathrm{R}_Q \in \mathcal{L}^2_{-Q-1/4+\epsilon}(1,\infty) \qquad \forall \epsilon > 0$$

As a consequence the Mellin transform $\widehat{\mathrm{R}_Q}(\lambda)$ is well defined and analytic for all $\lambda \in \mathbb{B}_Q$.

In view of Equation (9.27), we therefore conclude that the Mellin transform $\widehat{\mathfrak{K}_\alpha}(\lambda)$ is analytic for all $\lambda \in \mathbb{B}_Q \setminus \mathfrak{S}$, admits a simple pole for any $\lambda \in \mathbb{B}_Q \cap \mathfrak{S}$ and has residue at $\lambda = \pm 1/4$ that does not depend on α. Since Q can be chosen arbitrary large, the proof for the case $\alpha \in (0, \pi)$ now follows.

It remains to consider the case $\alpha = 0$ when the kernel $\mathfrak{K}_0$ has a singularity at $\tau = 1$. This special case can be dealt with following the approach presented in the proof of Proposition 9.2. Indeed, we introduce a smooth cutoff function $\Psi \in C_0(\mathbb{R}_+)$ such that $\Psi = 1$ in a neighbourhood of $\tau = 1$ and such that Ψ is supported in the interval $\left(\frac{1}{2}, \frac{3}{2}\right)$. Next, we write the kernel $\mathfrak{K}_0$ as

$$\mathfrak{K}_0(\tau) = \Psi(\tau)\mathfrak{K}_0(\tau) + (1 - \Psi(\tau))\mathfrak{K}_0(\tau) \qquad \forall \tau \in \mathbb{R}_+ \setminus \{1\}.$$

As argued in the proof of Proposition 9.2, the Paley-Wiener-Schwartz theorem (see [101, Theorem 7.1.14]) implies that the Mellin transform $\widehat{\Psi\mathfrak{K}_0}$ of the first term is holomorphic in the entire complex plane. Moreover, the second term in the above decomposition is smooth and for all $\tau \in \mathbb{R}_+ \setminus (\frac{1}{2}, \frac{3}{2})$ it holds that $(1 - \Psi(\tau))\mathfrak{K}_0(\tau) = \mathfrak{K}_0(\tau)$. Thus, the same asymptotic arguments that were used to establish the proof in the case $\alpha \in (0, \pi)$ can be applied in this case as well. □

Proposition 9.3 has a straightforward corollary concerning the decay properties of the Mellin transform of the integral kernel $\mathfrak{K}_\alpha, \alpha \in (0, \pi)$ on vertical lines in the complex plane.

Corollary 9.26. *Let $\alpha \in (0, \pi)$, i.e., $\alpha \neq 0$, and let the integral kernel $\mathfrak{K}_\alpha$ be defined by (9.14). Then the Mellin transform of the kernel $\mathfrak{K}_\alpha$ satisfies*

$$\lim_{\xi \to +\infty} |\widehat{\mathfrak{K}_\alpha}(\mu \pm \imath\xi)|^2 |\xi|^{2p} = 0 \quad \forall \mu \in \mathbb{R},\ \forall p \geq 0.$$

Proof. Let $p \geq 0$ be a non-negative integer and consider the proof of Proposition 9.3. Due to the decomposition (9.27), it suffices to show that there exists $Q \geq 2$ such that

$$\lim_{\xi \to +\infty} |\widehat{\Phi_Q}(\mu \pm \imath\xi)|^2 |\xi|^{2p} = 0 \quad \forall \mu \in \mathbb{R},\ \forall p \geq 0 \quad \text{and} \tag{9.29a}$$

$$\lim_{\xi \to +\infty} |\widehat{\mathrm{R}_Q}(\mu \pm \imath\xi)|^2 |\xi|^{2p} = 0 \quad \forall \mu \in \mathbb{R},\ \forall p \geq 0. \tag{9.29b}$$

The decay condition (9.29a) can be deduced for all $Q \geq 2$ using the decay condition (9.24) established in Lemma 9.25 together with the expression (9.28) for the Mellin transform $\widehat{\Phi_Q}$. In order to establish the decay condition (9.29b), we recall the earlier argument presented in the proof of Proposition 9.3 involving the Riemann-Lebesgue lemma (see, e.g., [180, Chapter V]) to prove the decay condition (9.24). In view of this argument, it is sufficient to establish that there exists $Q \geq 2$ such that the function $\mathrm{R}_Q \in C^\infty(\mathbb{R}_+)$ and the p^{th} derivative of R_Q is an integrable function on $\mathbb{R}_+$.

Let $Q \geq 2$. Notice that if $\alpha \in (0, \pi)$ then Equation (9.14) implies that $\mathfrak{K}_\alpha \in C^\infty(\mathbb{R}_+)$. Moreover, since the cutoff function $\phi \in C^\infty(\mathbb{R})$, the relation (9.26) implies that $\Phi_Q \in C^\infty(\mathbb{R}_+)$ from which we can deduce that $\mathrm{R}_Q \in C^\infty(\mathbb{R}_+)$.

It therefore remains to prove that for some choice of $Q \geq 2$, the p^{th} derivative of R_Q is an integrable function on $\mathbb{R}_+$. Thus, it suffices to show that for some choice of $Q \geq 2$ we have

$$\lim_{\tau \to 0} \left(\frac{d^p}{d\tau^p} \mathrm{R}_Q \right)(\tau) = \lim_{\tau \to \infty} \left(\frac{d^p}{d\tau^p} \mathrm{R}_Q \right)(\tau) = 0.$$

We first consider the limit $\tau \to 0$. Using the relation (9.26) and the definition of the cutoff-function ϕ we see that

$$\mathrm{R}_Q(\tau) = \mathfrak{K}_\alpha(\tau) - \Big(\tau^{1/4} + \sum_{q=1}^{Q-1} \kappa_{\alpha,q} \tau^{q+1/4} \Big) \phi(\tau) = \sum_{q=Q}^{\infty} \kappa_{\alpha,q} \tau^{q+1/4} \qquad \text{if } 0 < \tau \ll 1/4.$$

Consequently, if we pick $Q \geq p$, we deduce that $\lim_{\tau \to 0} \left(\frac{d^p}{d\tau^p} \mathrm{R}_Q \right)(\tau) = 0$ as required. In a similar fashion, we see that

$$\mathrm{R}_Q(\tau) = \mathfrak{K}_\alpha(\tau) - \Big(\tau^{-1/4} + \sum_{q=1}^{Q-1} \kappa_{\alpha,q} \tau^{-q-1/4} \Big) \phi(\tau) = \sum_{q=Q}^{\infty} \kappa_{\alpha,q} \tau^{-q-1/4} \qquad \text{if } \tau \gg 2,$$

where the second equality follows from the asymptotic expansion of the kernel $\mathfrak{K}_\alpha$ obtained in the proof of Proposition 9.2. It therefore follows that $\lim_{\tau \to \infty} \left(\frac{d^p}{d\tau^p} \mathrm{R}_Q \right)(\tau) = 0$. This completes the proof. □

Corollary 9.26 does not hold for the limiting case $\alpha = 0$ since the kernel $\mathfrak{K}_0$ is singular at $\tau = 1$. On the other hand, this singularity is integrable and a careful look at the proof of Proposition 9.2 suggests that $\mathfrak{K}_0 \in L^1_{\text{loc}}(\mathbb{R}_+)$. Determining the decay rate of $\widehat{\mathfrak{K}_0}(\lambda)$ for large imaginary values of λ then arises as a natural question that we shall examine in detail now.

Proposition 9.4. Let the integral kernel $\mathfrak{K}_0$ be defined by (9.14). Then the Mellin transform of the kernel $\mathfrak{K}_0$ satisfies

$$\lim_{\xi \to +\infty} |\widehat{\mathfrak{K}_0}(\mu \pm \imath\xi)|^2 |\xi| < \infty \quad \forall \mu \in \mathbb{R}.$$

Proof. We begin by recalling from Proposition 9.3 that the Mellin transform $\widehat{\mathfrak{K}_0}(\lambda)$ is well defined for all $\lambda \in \mathbb{C} \setminus \mathfrak{S}$ where $\mathfrak{S} = (+1/4 + \mathbb{N}) \cup (-1/4 - \mathbb{N})$. For any such λ we will write $\lambda = \mu + \imath\xi$.

Next, let $0 < \epsilon < 1/4$ and let $\Psi \in C^\infty_0(\mathbb{R}_+)$ be a smooth cutoff function with compact support away from the origin such that $\Psi(r) \equiv 1$ for all $r \in (1-\epsilon, 1+\epsilon)$. We consider the decomposition (c.f., the proof of Proposition 9.2)

$$\mathfrak{K}_0(r) = \underbrace{\Psi(r)\mathfrak{K}_0(r)}_{:=\mathfrak{M}_0(r)} + \underbrace{(1-\Psi(r))\mathfrak{K}_0(r)}_{\mathfrak{Z}_0(r)} \qquad \forall r > 0,\ r \neq 1$$

In other words, we have decomposed the kernel $\mathfrak{K}_0$ as the sum of two terms, the first of which is singular at $r = 1$ but has compact support on $\mathbb{R}_+$, while the second is smooth.

Due to the linearity of the Mellin transform, it suffices to show that

$$\lim_{\xi\to+\infty} |\widehat{\mathfrak{M}_0}(\mu \pm \imath\xi)|^2\,|\xi| < \infty \quad \forall \mu \in \mathbb{R} \qquad \text{and} \tag{9.30}$$

$$\lim_{\xi\to+\infty} |\widehat{\mathfrak{Z}_0}(\mu \pm \imath\xi)|^2\,|\xi| < \infty \quad \forall \mu \in \mathbb{R}. \tag{9.31}$$

Since $\mathfrak{Z}_0 \in C^\infty(\mathbb{R}_+)$, the same argument involving the Riemann-Lebesgue lemma that we used to prove Corollary 9.26 yields that

$$\lim_{\xi\to+\infty} |\widehat{\mathfrak{Z}_0}(\mu \pm \imath\xi)|^2|\xi|^{2p} = 0 \quad \forall \mu \in \mathbb{R}, \forall p \geq 0. \tag{9.32}$$

Consequently, it remains to prove the decay condition (9.30). To this end, we observe that the definition of the kernel $\mathfrak{M}_0$ given by Equation (9.14), the definition of the Mellin transform, and the Euler change of variables together imply that

$$\widehat{\mathfrak{M}_0}(\mu \pm \imath\xi) = \int_{-\infty}^{\infty} \frac{e^{t(1/4-\mu)}}{\sqrt{|e^t-1|}} \Psi(e^t) e^{-\imath t\xi}\,dt. \tag{9.33}$$

In other words, we have written the Mellin transform $\widehat{\mathfrak{M}_0}$ as the Fourier transform of a compactly supported function that is singular at $t = 0$. Consequently, in order to determine the decay behaviour of $\widehat{\mathfrak{M}_0}$, we have to analyse precisely the nature of this singularity at $t = 0$. To this end, we define the function $h\colon \mathbb{R} \to \mathbb{R}$ as

$$h(t) := \begin{cases} \sqrt{\dfrac{|t|}{|e^t-1|}} & \text{if} \quad t \neq 0, \\ 1 & \text{if} \quad t = 0. \end{cases}$$

A direct computation reveals that $h \in C^2(\mathbb{R})$ and we have the following Taylor expansion at $t = 0$:

$$h(t) = 1 - \frac{1}{4}t + r_2(t)t^2,$$

where the function $r_2\colon \mathbb{R} \to \mathbb{R}$ is the second order Taylor remainder. This computation suggests that we can rewrite the integral in Equation (9.33) as

$$\begin{aligned}
\widehat{\mathfrak{M}_0}(\mu \pm \imath\xi) &= \int_{-\infty}^{\infty} \frac{e^{t(1/4-\mu)}}{\sqrt{|e^t-1|}} \Psi(e^t) e^{-\imath t\xi}\,dt = \int_{-\infty}^{\infty} \frac{1}{\sqrt{|t|}} h(t) e^{t(1/4-\mu)} \Psi(e^t) e^{-\imath t\xi}\,dt \\
&= \int_{-\infty}^{\infty} \frac{1}{\sqrt{|t|}} e^{t(1/4-\mu)} \Psi(e^t) e^{-\imath t\xi}\,dt - \int_{-\infty}^{\infty} \frac{1}{\sqrt{|t|}} \left(\frac{1}{4}t\right) e^{t(1/4-\mu)} \Psi(e^t) e^{-\imath t\xi}\,dt \\
&+ \int_{-\infty}^{\infty} \frac{1}{\sqrt{|t|}} \left(r_2(t)t^2\right) e^{t(1/4-\mu)} \Psi(e^t) e^{-\imath t\xi}\,dt.
\end{aligned}$$

Consequently, defining for each $\mu \in \mathbb{R}$ the functions

$$h_1^\mu(t) := \frac{1}{\sqrt{|t|}} e^{t(1/4-\mu)} \Psi(e^t), \quad h_2^\mu(t) := \frac{1}{\sqrt{|t|}} \left(\frac{1}{4}t\right) e^{t(1/4-\mu)} \Psi(e^t) \quad \text{and}$$

$$h_3^\mu(t) := \frac{1}{\sqrt{|t|}} \left(r_2(t)t^2\right) e^{t(1/4-\mu)} \Psi(e^t),$$

we see that

$$\widehat{\mathfrak{M}_0}(\mu \pm \imath\xi) = \mathscr{F}(h_1^\mu)(\xi) + \mathscr{F}(h_2^\mu)(\xi) + \mathscr{F}(h_3^\mu)(\xi).$$

It is now easy to see that the functions h_2^μ and h_3^μ both have weak derivatives in $L^1(\mathbb{R})$. We can therefore conclude from the Riemann-Lebesgue lemma that

$$\lim_{|\xi|\to\pm\infty} |\mathscr{F}(h_2^\mu)(\xi)|\,|\xi| < \infty \quad \text{and} \quad \lim_{|\xi|\to\pm\infty} |\mathscr{F}(h_3^\mu)(\xi)|\,|\xi| < \infty. \tag{9.34}$$

Let us therefore consider the Fourier transform of the function h_1^μ. We observe that this Fourier transform can be decomposed as

$$\mathscr{F}(h_1^\mu)(\xi) = \int_{-\infty}^{\infty} \underbrace{\frac{1}{\sqrt{|t|}} \left(e^{t(1/4-\mu)}\Psi(e^t) - 1\right)}_{:=h_4^\mu(t)} e^{-\imath t\xi}\, dt + \mathscr{F}\left(\frac{1}{\sqrt{|t|}}\right)(\xi).$$

Here, the last term should be understood as the Fourier transform of a tempered distribution and is explicitly given by

$$\mathscr{F}\left(\frac{1}{\sqrt{|t|}}\right)(\xi) = \sqrt{\frac{2\pi}{|\xi|}}.$$

Additionally, using the fact that the cutoff function $\Psi(e^t) \equiv 1$ for all t in a neighbourhood of $t = 0$ and the series expansion of the exponential function, we obtain that the function h_4^μ also has weak derivative in $L^1(\mathbb{R})$. We can therefore conclude that

$$\lim_{|\xi|\to\pm\infty} |\mathscr{F}(h_1^\mu)(\xi)| \sqrt{|\xi|} = \sqrt{2\pi}. \tag{9.35}$$

Combining now the estimates (9.32), (9.34) and (9.35), we obtain that for all $\mu \in \mathbb{R}$ it holds that

$$\begin{aligned}
\lim_{\xi\to+\infty} |\widehat{\mathfrak{K}}_0(\mu \pm \imath\xi)| \sqrt{|\xi|} &\leq \lim_{\xi\to+\infty} |\widehat{\mathfrak{M}_0}(\mu \pm \imath\xi)| \sqrt{|\xi|} + \lim_{\xi\to+\infty} |\widehat{\mathfrak{Z}_0}(\mu \pm \imath\xi)| \sqrt{|\xi|} \\
&\leq \lim_{|\xi|\to\pm\infty} \left|\mathscr{F}(h_1^\mu)(\xi) + \mathscr{F}(h_2^\mu)(\xi) + \mathscr{F}(h_3^\mu)(\xi)\right| \sqrt{|\xi|} \\
&= \sqrt{2\pi},
\end{aligned}$$

and consequently for all $\mu \in \mathbb{R}$ it holds that

$$\lim_{\xi\to+\infty} |\widehat{\mathfrak{K}}_0(\mu \pm \imath\xi)|^2 \,|\xi| \leq 2\pi < \infty,$$

as claimed. □

We conclude this section by stating two corollaries that follow from the results stated above. These corollaries will be used to conclude the analysis of the Riesz potential on corners of the polyhedral domain Ω that we began in Section 9.3.

Corollary 9.27. *Let $\alpha \in [0,\pi)$ and let the integral kernel $\mathfrak{K}_\alpha$ be defined by (9.14). Then the Mellin transform of the kernel $\mathfrak{K}_\alpha$ satisfies*

$$\sup_{\xi\in\mathbb{R}} \frac{|\widehat{\mathfrak{K}}_\alpha(\mu+\imath\xi)|^2|\xi|^2}{1+|\xi|} < \infty \;\forall \mu \in \mathbb{R}.$$

Proof. Given any $\lambda \in \mathbb{C}$, we write $\lambda = \mu + \imath\xi$. In view of Corollary 9.26 and Proposition 9.4, it suffices to show that for any $\mu \in \mathbb{R}$ and any bounded set $K \subset \mathbb{R}$ it holds that

$$\sup_{\xi\in K} |\widehat{\mathfrak{K}}_\alpha(\mu+\imath\xi)|^2|\xi|^2 < \infty. \tag{9.36}$$

We recall from Proposition 9.3 that the Mellin transform $\widehat{\mathfrak{K}}_\alpha$ can be extended as an analytic function defined on $\mathbb{C}\setminus\mathfrak{S}$ where $\mathfrak{S} = (+1/4+\mathbb{N})\cup(-1/4-\mathbb{N})$ and furthermore that $\widehat{\mathfrak{K}}_\alpha(\lambda)$ admits a simple pole at each point of $\mathfrak{S}$. Consequently, the mapping

$$\widehat{\mathfrak{K}}_\alpha^{\text{extend}}(\mu+\imath\xi) := \widehat{\mathfrak{K}}_\alpha(\mu+\imath\xi)\,\xi,$$

can be extended as a continuous function for all $\xi, \mu \in \mathbb{R}$. The estimate (9.36) therefore follows. □

Corollary 9.28. *Let $\alpha \in [0,\pi)$ and let the integral kernel $\mathfrak{K}_\alpha$ be defined by (9.14). Then the Mellin transform of the kernel $\mathfrak{K}_\alpha$ satisfies*

$$\sup_{\lambda\in\pm 1/4+\imath\mathbb{R}} |\widehat{\mathfrak{K}}_0(\lambda) - \widehat{\mathfrak{K}}_\alpha(\lambda)| < +\infty \quad \textit{and} \tag{9.37}$$

$$\sup_{\lambda\in\imath\mathbb{R}} |\widehat{\mathfrak{K}}_\alpha(\lambda)| < +\infty \tag{9.38}$$

Proof. The estimate (9.38) follows by combining Proposition 9.3, which establishes that $\widehat{\mathfrak{K}}_\alpha(\lambda)$ is analytic for $\lambda \in \imath\mathbb{R}$ together with Corollary 9.26 and Proposition 9.4 which demonstrate that $\lim_{\xi\to\infty} |\widehat{\mathfrak{K}}_\alpha(\pm\imath\xi)| = 0$ for any $\alpha \in [0,\pi)$.

In order to establish Estimate (9.37), we recall from Proposition 9.3 that the Mellin transform $\widehat{\mathfrak{K}}_\alpha(\lambda)$ has a simple pole at $\lambda = \pm 1/4$ with residue that is independent of α. Consequently, the mapping $\widehat{\mathfrak{K}}_0(\pm 1/4+\imath\xi) - \widehat{\mathfrak{K}}_\alpha(\pm 1/4+\imath\xi)$ can be extended as an analytic function for all $\xi \in \mathbb{R}$. Using once again Corollary 9.26 and Proposition 9.4 to establish the decay behaviour for $\xi \to \infty$ yields the required result. □

9.6 Application to Corner Operators

Throughout this section, we assume the settings of Sections 9.2-9.5. Our goal now is to complete the proof of Theorem 9.8 using the tools and results developed in the previous sections.

Proof of Theorem 9.8. We have shown in Section 9.3.1 that the proof of Theorem 9.8 follows from a density argument if we can establish Proposition 9.1 which concerns continuity estimates for the localised operator $\mathscr{A}^{\chi}_{\mathrm{D},\mathrm{D}'}\colon C^{\infty}(\mathbb{R}^2) \to C^{\infty}(\mathbb{R}^2)^*$ defined through Notation 9.2. We further recall that we have already established in Section 9.3.1, the proof of Proposition 9.1 for cases when the disks $\mathrm{D} = \mathrm{D}'$ or the disk D does not contain a corner of the polyhedral boundary $\partial\Omega$. It therefore remains to prove the continuity estimate (9.7) for the case when $\mathrm{D} = \mathrm{D}'$ and D contains a corner $\boldsymbol{c} \in \partial\Omega$.

Subsequently, in Section 9.3.2, we introduced through Definition 9.11 the Riesz potential on the corner $\boldsymbol{c} \in \partial\Omega$, denoted $\mathscr{A}_{\Gamma}\colon C^{\infty}_{\mathrm{comp}}(\mathbb{R}^2) \to C^{\infty}_{\mathrm{comp}}(\mathbb{R}^2)^*$, and we introduced through Definition 9.12 for any $u \in C^{\infty}_{\mathrm{comp}}(\mathbb{R}^2)$, the mappings $\mathscr{A}^{\pm}_{\Gamma}(u)\colon \mathbb{R}_+ \setminus \{1\} \to \mathbb{R}$. We further deduced that for all $u, v \in C^{\infty}(\mathbb{R}^2)$ we have

$$\langle \mathscr{A}^{\chi}_{\mathrm{D},\mathrm{D}}(u), v\rangle_{C^{\infty}(\mathbb{R}^2)^*\times C^{\infty}(\mathbb{R}^2)} = \langle \mathscr{A}_{\Gamma}(\chi_{\mathrm{D}}u), \chi_{\mathrm{D}}v\rangle_{C^{\infty}_{\mathrm{comp}}(\mathbb{R}^2)^*\times C^{\infty}_{\mathrm{comp}}(\mathbb{R}^2)}. \tag{9.39}$$

where the disk D contains a corner $\boldsymbol{c} \in \partial\Omega$ and $\chi_{\mathrm{D}} \in C^{\infty}(\mathbb{R}^2)$ denotes the partition of unity function associated with D as fixed in Notation 9.1.

We will now apply the results on the Mellin transform of the integral kernels $\mathfrak{K}_{\alpha}$, $\alpha \in [0, \pi)$ from Section 9.5 to Equation (9.39) in order to derive the required continuity estimate (9.7) when D contains a corner $\boldsymbol{c} \in \partial\Omega$. We proceed in two steps: First we prove some estimates concerning the operators $\mathscr{A}^{\pm}_{\Gamma}$ introduced through Definition 9.12. In the second step, we use these estimates to prove the continuity estimate (9.7). For ease of notation, throughout this proof, we will frequently use $C > 0$ to refer to a general constant that may change from step-to-step. Additionally, it will be useful to recall from Equation (9.22) in Lemma 9.24 that we have the relation

$$\widehat{\mathscr{A}^{\pm}_{\Gamma}(u)}(\lambda) = \Big(\widehat{\mathfrak{K}_0}(\lambda + 1/4) \pm \widehat{\mathfrak{K}_{\theta}}(\lambda + 1/4)\Big)\, \widehat{u}(\lambda - 1/2).$$

Step 1) Pick an arbitrary $v \in C^{\infty}_{\mathrm{comp}}(\mathbb{R}_+)$. Using the Mellin transform characterisation of the L^2 norm and $H^{\frac{1}{2}}$ norm given by Lemmas 9.15 and 9.22 respectively and applying Corollary 9.27, we obtain the existence of a constant $C > 0$ such that

$$\begin{aligned} |\mathscr{A}^{\pm}_{\Gamma}(v)|^2_{H^{\frac{1}{2}}(\mathbb{R}_+)} &= \frac{1}{2\imath\pi}\int_{-\imath\infty}^{+\imath\infty} \frac{|\lambda|^2}{1+|\lambda|} |\widehat{\mathfrak{K}}_0\big(\lambda + 1/4\big) \pm \widehat{\mathfrak{K}}_{\alpha}\big(\lambda + 1/4\big)|^2 \big|\hat{v}(\lambda - \frac{1}{2})\big|^2 d\lambda \\ &\leq \frac{C}{2\imath\pi}\int_{-\imath\infty}^{+\imath\infty} \big|\hat{v}(\lambda - \frac{1}{2})\big|^2 d\lambda = C\|v\|^2_{L^2(\mathbb{R}_+)} \end{aligned} \tag{9.40}$$

By a density argument we conclude that the above estimate actually holds for all $v \in L^2(\mathbb{R}_+)$.

Similarly, for any smooth function $\chi \in C^{\infty}_{\mathrm{comp}}(\mathbb{R}_+)$, using Lemma 9.15 and Corol-

lary 9.28 yields the existence of constants $C_\chi, C'_\chi, C''_\chi > 0$ such that

$$\begin{aligned}\|\chi\mathscr{A}_\Gamma^{\pm}(\chi v)\|^2_{L^2(\mathbb{R}_+)} &\leq C_\chi\|\mathscr{A}_\Gamma^{\pm}(\chi v)\|^2_{\mathcal{L}^2_{-1/4}(\mathbb{R}_+)}\\ &= \frac{C_\chi}{2\imath\pi}\int_{-\imath\infty}^{+\imath\infty}|\widehat{\mathfrak{K}}_0(\lambda)\pm\widehat{\mathfrak{K}}_\alpha(\lambda)|^2|\widehat{\chi v}(\lambda-3/4)|^2d\lambda\\ &\leq \frac{C'_\chi}{2\imath\pi}\int_{-\imath\infty}^{+\imath\infty}|\widehat{\chi v}(\lambda-3/4)|^2d\lambda = C'_\chi\|\chi v\|^2_{\mathcal{L}^2_{-\frac{3}{4}}(\mathbb{R}_+)}\\ &\leq C''_\chi\|\chi v\|^2_{L^2(\mathbb{R}_+)}\end{aligned} \tag{9.41}$$

Note that the constants involved in the estimate above do depend on χ but not on v. Hence, by a density argument, Estimate (9.41) also holds for any $v \in L^2(\mathbb{R}_+)$. Finally, applying Corollary 9.28 yields a constant $C > 0$ such that

$$\begin{aligned}\|\mathscr{A}_\Gamma^{-}(v)\|^2_{\mathcal{L}^2_0(\mathbb{R}_+)} &= \frac{1}{2\imath\pi}\int_{-\imath\infty}^{+\imath\infty}|\widehat{\mathfrak{K}}_0(\lambda+1/4)-\widehat{\mathfrak{K}}_\alpha(\lambda+1/4)|^2|\hat{v}(\lambda-\frac{1}{2})|^2d\lambda\\ &\leq \frac{C}{2\imath\pi}\int_{-\imath\infty}^{+\imath\infty}|\hat{v}(\lambda-\frac{1}{2})|^2d\lambda = C\|v\|^2_{L^2(\mathbb{R}_+)}.\end{aligned} \tag{9.42}$$

Step 2) For the sake of conciseness, we shall write χ instead of χ_{D}. With this convention, Equation (9.39) yields the existence of a constant $C > 0$ such that

$$C\|\mathscr{A}^{\chi}_{\mathrm{D,D}}(u)\|^2_{H^{\frac{1}{2}}(\partial\Omega)} \leq \|\chi\mathscr{A}_\Gamma(\chi u)\|^2_{H^{\frac{1}{2}}(\Gamma)} \quad \text{for any } u \in C^\infty(\mathbb{R}^2).$$

To deal with the norm $\|\cdot\|_{H^{\frac{1}{2}}(\Gamma)}$, we now invoke [44, Lemma 2.12] and [89] where the authors proved that there exists a constant $c > 0$ such that for any $v \in H^{\frac{1}{2}}(\Gamma)$ it holds that

$$c\,\|v\|^2_{H^{\frac{1}{2}}(\Gamma)} \leq \|\{v\}\|^2_{H^{\frac{1}{2}}(\mathbb{R}_+)} + \|[v]\|^2_{\widetilde{H}^{\frac{1}{2}}(\mathbb{R}_+)}. \tag{9.43}$$

Since, on the other hand, Lemma 9.13 implies that $\{\mathscr{A}_\Gamma(u)\} = \mathscr{A}_\Gamma^+(\{u\})$ and $[\mathscr{A}_\Gamma(u)] = \mathscr{A}_\Gamma^-([u])$, we conclude the existence of a constant $C > 0$ such that for any $u \in L^2(\partial\Omega)$ it holds that

$$\begin{aligned}\|\mathscr{A}^{\chi}_{\mathrm{D,D}}(u)\|^2_{H^{\frac{1}{2}}(\partial\Omega)} &\leq C\|\chi\mathscr{A}_\Gamma(\chi u)\|^2_{H^{\frac{1}{2}}(\Gamma)}\\ &\leq \|\chi\mathscr{A}_\Gamma^+(\chi\{u\})\|^2_{H^{\frac{1}{2}}(\mathbb{R}_+)} + \|\chi\mathscr{A}_\Gamma^-(\chi[u])\|^2_{\widetilde{H}^{\frac{1}{2}}(\mathbb{R}_+)}.\end{aligned} \tag{9.44}$$

In order to bound the first term on the right hand side of Inequality (9.44), we will make use of the estimates (9.40)-(9.41)-(9.42). To this end, we recall the Mellin transform characterisation of the L^2 norm and $H^{\frac{1}{2}}$ norm given by Lemmas 9.15 and 9.22 respectively. A straightforward calculus then shows that there exists a constant $\widetilde{C}_\chi > 0$ that depends on χ such that for all $u \in C^\infty(\mathbb{R}^2)$ we have

$$\widetilde{C}_\chi\|\chi\mathscr{A}_\Gamma^+(\chi\{u\})\|^2_{H^{\frac{1}{2}}(\mathbb{R}_+)} \leq |\mathscr{A}_\Gamma^+(\chi\{u\})|^2_{H^{\frac{1}{2}}(\mathbb{R}_+)} + \|\chi\mathscr{A}_\Gamma^+(\chi\{u\})\|^2_{L^2(\mathbb{R}_+)}. \tag{9.45}$$

Combining Estimate (9.45) with (9.40) and (9.41) therefore yields the existence of a constant $\widehat{C}_\chi > 0$ that depends on χ such that for all $u \in C^\infty(\mathbb{R}^2)$ it holds that

$$\|\chi \mathscr{A}_\Gamma^+(\chi\{u\})\|_{H^{\frac{1}{2}}(\mathbb{R}_+)} \leq \widehat{C}_\chi \|\chi\{u\}\|_{L^2(\mathbb{R}_+)}.$$

In order to bound the second term in Estimate 9.44, we appeal to Lemma 9.6 to deduce the existence of a constant $\overline{C}_\chi > 0$ that depends on χ such that for all $u \in C^\infty(\mathbb{R}^2)$ it holds that

$$\overline{C}_\chi \|\chi \mathscr{A}_\Gamma^-(\chi[u])\|^2_{\widetilde{H}^{\frac{1}{2}}(\mathbb{R}_+)} \leq \|\mathscr{A}_\Gamma^-(\chi[u])\|^2_{W_0^{\frac{1}{2}}(\mathbb{R}_+)} = \|\mathscr{A}_\Gamma^-(\chi[u])\|^2_{\mathcal{L}_0^2(\mathbb{R}_+)} + |\mathscr{A}_\Gamma^-(\chi[u])|^2_{H^{\frac{1}{2}}(\mathbb{R}_+)}.$$

Moreover, from Estimate (9.42) we deduce that for any $u \in C^\infty(\mathbb{R}^2)$ we have

$$\|\mathscr{A}_\Gamma^-(\chi[u])\|_{\mathcal{L}_0^2(\mathbb{R}_+)} \leq C \|\chi[u]\|_{L^2(\mathbb{R}_+)}.$$

Combining these remarks with Estimate (9.44) finally yields a constant $\breve{C}_\chi > 0$ that depends on χ such that

$$\|\mathscr{A}^\chi_{\mathrm{D,D}}(u)\|^2_{H^{\frac{1}{2}}(\partial\Omega)} \leq \breve{C}_\chi \|u\|^2_{L^2(\partial\Omega)} \quad \forall u \in C^\infty(\mathbb{R}^2).$$

The required continuity estimate (9.7) now follows.

□

9.7 Conclusion

In this chapter, we established the continuity of the Riesz potential as a mapping from $L^2(\partial\Omega)$ to $H^{\frac{1}{2}}(\partial\Omega)$ for polygonal boundaries $\partial\Omega$ in two spatial dimensions. Although similar mapping properties for the Riesz potential have been established on flat spaces and smooth surfaces in two spatial dimensions, the presence of corners prevents a straightforward extension to polygonal boundaries. In order to prove our main result, we first showed that the analysis of the Riesz potential on polygonal boundaries can be carried out using Mellin transforms. Subsequently, we undertook a detailed analysis of the Mellin symbols of the Riesz potential on corners, which allowed us to deduce the required continuity property.

An important application of our result is in the analysis of non-overlapping domain decomposition methods for the Helmholtz equation. In contrast to classical Schwarz methods for the Laplace equation, the exact choice of transmission conditions (represented by a so-called transmission operator) on the interface of neighbouring subdomains determines the convergence rate of the iterative procedure. Moreover, many standard choices for the transmission operator in the literature (see, e.g., [49, 72, 109]) lead to *algebraic* rates of convergence. One approach to circumventing this slow rate of convergence was suggested in the work of Collino et al. [40, Theorem 7] who provided sufficient

conditions on the transmission operator under which the convergence rate of the iterative procedure can be proven to be *geometric*. Based on this result, Collino et al. proposed the use of Riesz potentials to construct the transmission operator on the interfaces of neighbouring subdomains.

Unfortunately, while the Riesz potential can be shown to satisfy the assumptions of [40, Theorem 7] in the case of smooth interfaces (see [41]), no such proof exists for non-smooth interfaces. Our work therefore represents a first step at overcoming this deficiency for polygonal interfaces in two spatial dimensions. A natural extension of our work is to consider next the case of polyhedral boundaries in three spatial dimensions, which will be the subject of future work.

10

Summary and Outlook

We have presented in this dissertation several results pertaining to the analysis of boundary integral equations and domain decomposition methods. Our results can be divided into three broadly independent categories.

In the first part of this dissertation (Chapters 2-5), we presented the numerical analysis of a second-kind boundary integral equation that describes the electrostatic interaction between an arbitrary number N of dielectric spherical particles undergoing mutual polarisation. Our main contribution was to prove that under appropriate geometrical assumptions, the three key physical quantities of interest, namely, the induced surface charge on each dielectric particle, the total electrostatic energy of the system and the electrostatic forces acting on each particle can be approximated with linear scaling in accuracy, i.e., given a system composed of N particles, it requires only $\mathcal{O}(N)$ computations to approximate each of these quantities up to a given and fixed relative error. Although N-body problems have long been studied by both mathematicians and practitioners, there are very few references in the literature concerning how the accuracy and computational cost of the proposed numerical algorithms scale with the number of objects N when one has to approximate the solution to a partial differential or boundary integral equation. To the best of our knowledge, the work presented in Part I of this dissertation is the first attempt at obtaining precise estimates in terms of N for the accuracy and computational cost of solving a N-body boundary integral equation. Although we have answered several important questions pertaining to such a scalability analysis, many challenges and open questions remain. For instance,

- In this dissertation, we considered the case of *spherical* dielectric particles that carried charge distributions only on their surfaces. A natural extension is to consider particles of arbitrary shape carrying volumetric charge densities in their interiors. Another obvious extension is to consider cases involving external electric fields.
- The analysis performed in this dissertation was limited to boundary integral operators derived from the Laplace differential operator. Many electrostatic phenomena (see, e.g., the linearised Poisson-Boltzman model) involve more general differential operators and an obvious next step is to extend our analysis to such settings.

- Scattering problems for wave propagation sometimes consist of geometrical configurations with a large number of obstacles. A more challenging task therefore is to attempt an extension of our analysis to the Helmholtz equation. This is a significantly more difficult undertaking since the underlying differential operator in this case is indefinite so many of the core ingredients of our analysis no longer hold and alternative approaches must be considered.

In the second part of the dissertation (Chapters 6-8), we presented some results on the scalability analysis of the parallel Schwarz domain decomposition method (PSM) for geometric configurations wherein subdomains are completely embedded in the interior of the global domain and an arbitrary number of subdomains have a common overlap. Our main contribution was to develop a systematic framework that allowed us to bound the norm of the Schwarz iteration operator for such geometrical configurations and to establish a sharp lower bound on the number of PSM iterations required to observe the first infinity norm contraction in the error. While the scalability properties of the parallel Schwarz method in the classical setting, i.e., for a fixed computational domain, are well understood, it is less clear how the PSM scales for problems in which both the size of the global domain and the number of subdomains is increasing. The first attempt at answering this question was made by Ciaramella and Gander in a series of articles [28, 29, 30] but their analysis was limited to cases where each subdomain in the domain decomposition had access to the global boundary and at most only two subdomains had a common overlap. The work we have presented in Part II of this dissertation is the first attempt at developing a systematic framework to tackle the general case, i.e., when many subdomains in the domain decomposition are embedded in the interior of the global domain and an arbitrary number of subdomains can overlap. Naturally, many open questions remain to be answered:

- In this dissertation, we were able to obtain a bound on the *number* of PSM iterations required to observe an infinity norm contraction in the error but we were unable to deduce precise estimates on the contraction factor itself. While this is an extremely challenging task, numerical experiments indicate that the contraction factor is strongly dependent on the problem geometry. We therefore feel that a better understanding of the scaling of the PSM cannot be obtained unless there are quantitative estimates of the contraction factor similar to those obtained by Ciaramella and Gander.
- Our analysis was limited to the case of the Laplace equation. An important task is to extend our results to the case of a general advection–reaction–diffusion equation.

In the third part of this dissertation (Chapter 9), we analysed the continuity properties of the so-called Riesz potential on polygonal boundaries $\partial\Omega$. Our main contribution was to prove that the Reisz potential extends as a bounded linear map from $L^2(\partial\Omega)$ to $H^{\frac{1}{2}}(\partial\Omega)$. Such a continuity estimate is well known to hold on flat spaces, i.e., on $\mathbb{R}^n$ as well as on smooth surfaces but our work here is the first extension to polygonal, a priori non-smooth boundaries in $\mathbb{R}^2$. Equipped with this result, it is possible to devise

a non-overlapping domain decomposition method for the Helmholtz equation in two dimensions with *guaranteed* exponential convergence (see [40, 41]). An important next step is therefore to obtain a similar continuity result for the Riesz potential on polyhedral boundaries in three spatial dimensions, which is expected to be considerably more technical.

Bibliography

[1] Agullo, E., Bramas, B., Coulaud, O., Darve, E., Messner, M. & Takahashi, T. (2014). Task-based FMM for multicore architectures. *SIAM Journal on Scientific Computing*, **36**, 66–93. 106

[2] Antoine, X., Geuzaine, C. & Ramdani, k. (2010). *Computational Methods for Multiple Scattering at High Frequency with Applications to Periodic Structures Calculations*, 73–108. Bentham Science Publishing. 47

[3] Appel, A.W. (1985). An efficient program for many-body simulation. *SIAM Journal on Scientific and Statistical Computing*, **6**, 85–103. 33

[4] Atkinson, K.E. (1967). The numerical solution of Fredholm integral equations of the second kind. *SIAM Journal on Numerical Analysis*, **4**. 47, 79, 81

[5] Atkinson, K.E. (1972). The numerical solution of Fredholm integral equations of the second kind with singular kernels. *Numerische Mathematik*, **19**, 248–259. 47

[6] Atkinson, K.E. (1997). *The numerical solution of integral equations of the second kind*, vol. 4 of *Cambridge Monographs on Applied and Computational Mathematics*. Cambridge University Press, Cambridge. 47

[7] Atkinson, K.E. & Han, W. (2009). *Theoretical numerical analysis*, vol. 39 of *Texts in Applied Mathematics*. Springer, Dordrecht, 3rd edn. 24, 27, 42, 47

[8] Axler, S., Bourdon, P. & Ramey, W. (2001). *Harmonic function theory*, vol. 137 of *Graduate Texts in Mathematics*. Springer-Verlag, New York, 2nd edn. 131

[9] Barnes, J. & Hut, P. (1986). A hierarchical O (N log N) force-calculation algorithm. *Nature*, **324**, 446. 33

[10] Barros, K. & Luijten, E. (2014). Dielectric effects in the self-assembly of binary colloidal aggregates. *Physical Review Letters*, **113**, 017801. 33

[11] Barros, K., Sinkovits, D. & Luijten, E. (2014). Efficient and accurate simulation of dynamic dielectric objects. *The Journal of Chemical Physics*, **140**, 064903. 34

[12] Bartlett, P. & Campbell, A.I. (2005). Three-dimensional binary superlattices of oppositely charged colloids. *Physical Review Letters*, **95**, 128302. 33

[13] Bartlett, R.J. & Stanton, J.F. (2007). *Applications of Post-Hartree–Fock methods: A tutorial*, 65–169. John Wiley & Sons, Ltd. 153

[14] Blanchard, P., Bramas, B., Coulaud, O., Darve, E., Dupuy, L., Etcheverry, A. & Sylvand, G. (2015). ScalFMM: A generic parallel fast multipole library. In *SIAM Conference on Computational Science and Engineering (SIAM CSE)*. 106, 144

[15] Boateng, H.A. & Krasny, R. (2013). Comparison of treecodes for computing electrostatic potentials in charged particle systems with disjoint targets and sources. *Journal of Computational Chemistry*, **34**, 2159–2167. 33

[16] Boles, M.A. & Talapin, D.V. (2015). Many-body effects in nanocrystal superlattices: Departure from sphere packing explains stability of binary phases. *Journal of the American Chemical Society*, **137**, 4494–4502. 33, 34

[17] Born, M. & Jordan, P. (1925). Zur Quantenmechanik. *Zeitschrift für Physik*, **34**, 858–888. 153

[18] Born, M., Heisenberg, W. & Jordan, P. (1926). Zur Quantenmechanik. II. *Zeitschrift für Physik*, **35**, 557–615. 153

[19] Borsuk, M. & Kondratiev, V. (2006). *Elliptic boundary value problems of second order in piecewise smooth domains*, vol. 69 of *North-Holland Mathematical Library*. Elsevier Science B.V., Amsterdam. 221

[20] Boubendir, Y., Antoine, X. & Geuzaine, C. (2012). A quasi-optimal non-overlapping domain decomposition algorithm for the Helmholtz equation. *Journal of Computational Physics*, **231**, 262–280. 217, 218

[21] Brezis, H. (2010). *Functional analysis, Sobolev spaces and partial differential equations*. Springer-Verlag New York. 14, 52

[22] Cancès, E., Mennucci, B. & Tomasi, J. (1997). A new integral equation formalism for the polarizable continuum model: Theoretical background and applications to isotropic and anisotropic dielectrics. *The Journal of Chemical Physics*, **107**, 3032–3041. 154, 157, 158

[23] Cancès, E., Maday, Y. & Stamm, B. (2013). Domain decomposition for implicit solvation models. *Journal of Chemical Physics*, **139**, 054111. 158, 163, 164, 165, 166, 210, 211

[24] Chan, T.F. & Mathew, T.P. (1994). Domain decomposition algorithms. *Acta Numerica*, **3**, 61–143. 160

[25] Chaouqui, F., Ciaramella, G., Gander, M.J. & Vanzan, T. (2018). On the scalability of classical one-level domain-decomposition methods. *Vietnam Journal of Mathematics*, **46**, 1053–1088. 161, 165, 166, 169, 197

[26] Cheng, H., Greengard, L. & Rokhlin, V. (1999). A fast adaptive multipole algorithm in three dimensions. *Journal of Computational Physics*, **155**, 468–498. 33

[27] Chipman, D.M. (2000). Reaction field treatment of charge penetration. *The Journal of Chemical Physics*, **112**, 5558–5565. 157

[28] Ciaramella, G. & Gander, M.J. (2017). Analysis of the parallel Schwarz method for growing chains of fixed-sized subdomains: Part I. *SIAM Journal on Numerical Analysis*, **55**, 1330–1356. 165, 169, 194, 197, 205, 246

[29] Ciaramella, G. & Gander, M.J. (2018). Analysis of the parallel Schwarz method for growing chains of fixed-sized subdomains: Part II . *SIAM Journal on Numerical Analysis*, **56 (3)**, 1498–1524. 165, 187, 192, 194, 197, 198, 202, 205, 246

[30] Ciaramella, G. & Gander, M.J. (2018). Analysis of the parallel Schwarz method for growing chains of fixed-sized subdomains: Part III . *Electronic Transactions on Numerical Analysis*, **49**, 201–243. 161, 165, 197, 198, 205, 246

[31] Ciaramella, G. & Höfer, R. (2019). Non-geometric convergence of the classical alternating Schwarz method. *to appear in Proceedings of the 25th International Conference on Domain Decomposition Methods, St. John's, Canada*. 204

[32] Ciaramella, G., Hassan, M. & Stamm, B. (2019). On the scalability of the parallel Schwarz method in one-dimension. *to appear in the Proceedings of the 25th International Conference on Domain Decomposition Methods, St. John's, Canada, arXiv:1912.10971*. 167

[33] Ciaramella, G., Hassan, M. & Stamm, B. (2020). On the scalability of the Schwarz method. *SMAI journal of Computational Mathematics*, **6**, 33–68. 167

[34] Claeys, X. (2011). A single trace integral formulation of the second kind for acoustic scattering. Tech. Rep. 2011-14, ETH, Seminar of Applied Mathematics Research. 47

[35] Claeys, X. & Hiptmair, R. (2013). Multi-trace boundary integral formulation for acoustic scattering by composite structures. *Communications on Pure and Applied Mathematics*, **66**, 1163–1201. 47

[36] Claeys, X., Hiptmair, R., Jerez-Hanckes, C. & Pintarelli, S. (2014). Novel multitrace boundary integral equations for transmission boundary value problems. In A. Fokas & B. Pelloni, eds., *Unified Transform for Boundary Value Problems*, chap. 7, 227–258, Society for Industrial and Applied Mathematics, Philadelphia, PA. 47

[37] Claeys, X., Hiptmair, R. & Spindler, E. (2015). A second-kind Galerkin boundary element method for scattering at composite objects. *BIT. Numerical Mathematics*, **55**, 33–57. 47

[38] Claeys, X., Hiptmair, R. & Spindler, E. (2017). Second kind boundary integral equation for multi-subdomain diffusion problems. *Advances in Computational Mathematics*, **43**, 1075–1101. 47

[39] Clercx, H.J.H. & Bossis, G. (1993). Many-body electrostatic interactions in electrorheological fluids. *Physical Review E*, **48**, 2721–2738. 34

[40] Collino, F., Ghanemi, S. & Joly, P. (2000). Domain decomposition method for harmonic wave propagation: a general presentation. *Computer methods in applied mechanics and engineering*, **184**, 171–211. 217, 218, 219, 243, 244, 247

[41] Collino, F., Joly, P. & Lecouvez, M. (2019). Exponentially convergent non overlapping domain decomposition methods for the Helmholtz equation. *ESAIM: Mathematical Modelling and Numerical Analysis, Forthcoming article*. 220, 244, 247

[42] Corona, E. & Veerapaneni, S. (2018). Boundary integral equation analysis for suspension of spheres in Stokes flow. *Journal of Computational Physics*, **362**, 327–345. 134

[43] Costabel, M. (2007). Some historical remarks on the positivity of boundary integral operators. In *Boundary element analysis*, vol. 29 of *Lecture Notes in Applied and Computational Mechanics*, 1–27, Springer, Berlin. 48

[44] Costabel, M. & Stephan, E. (1985). Boundary integral equations for mixed boundary value problems in polygonal domains and galerkin approximation. *Mathematical models and methods in mechanics, Banach Center Publications, Volume 15*, 175–251. 220, 221, 231, 242

[45] Costabel, M. & Stephan, E. (1985). A direct boundary integral equation method for transmission problems. *Journal of Mathematical Analysis and Applications*, **106**, 367–413. 47

[46] Cramer, C.J. & Truhlar, D.G. (2008). A universal approach to solvation modeling. *Accounts of Chemical Research*, **41**, 760–768. 154

[47] Dahirel, V., Jardat, M., Dufrêche, J.F. & Turq, P. (2007). New coarse-graining procedure for the dynamics of charged spherical nanoparticles in solution. *The Journal of Chemical Physics*, **126**, 114108. 34

[48] Dehnen, W. (2000). A very fast and momentum-conserving tree code. *The Astrophysical Journal Letters*, **536**, L39–L42. 33

[49] Després, B. (1991). *Méthodes de décomposition de domaine pour les problèmes de propagation d'ondes en régime harmonique. Le théorème de Borg pour l'équation de Hill vectorielle.* Ph.D. thesis, Université de Paris IX (Dauphine), Paris, thèse. 160, 217, 218, 243

[50] Di Nezza, E., Palatucci, G. & Valdinoci, E. (2012). Hitchhiker's guide to the fractional Sobolev spaces. *Bulletin des Sciences Mathématiques*, **136**, 521–573. 14, 54, 231

[51] Dirac, P. (1981). *The principles of quantum mechanics*. No. 27 in The International series of monographs on physics, Oxford University Press, Inc., New York, 4th edn. 153

[52] Dobnikar, J., Chen, Y., Rzehak, R. & Von Grünberg, H. (2002). Many-body interactions in colloidal suspensions. *Journal of Physics: Condensed Matter*, **15**, S263–S268. 33

[53] Doerr, T.P. & Yu, Y.K. (2006). Electrostatics of charged dielectric spheres with application to biological systems. *Physical Review E*, **73**. 33

[54] Dolean, V., Jolivet, P. & Nataf, F. (2015). *An introduction to domain decomposition methods: Algorithms, theory, and parallel implementation*, vol. 144. SIAM, Philadelphia, PA. 160

[55] Duren, P.L. (1970). Theory of H^p spaces. New York and London: Academic Press. 228

[56] Echenique, P. & Alonso, J.L. (2007). A mathematical and computational review of Hartree–Fock SCF methods in quantum chemistry. *Molecular Physics*, **105**, 3057–3098. 153

[57] Efstathiou, G., Davis, M., White, S.D. & Frenk, C.S. (1985). Numerical techniques for large cosmological N-body simulations. *The Astrophysical Journal Supplement Series*, **57**, 241–260. 33

[58] Eiermann, M. & Ernst, O. (2001). Geometric aspects of the theory of Krylov subspace methods. *Acta Numerica*, **10**, 251–312. 89

[59] Eisenstat, S., Elman, H. & Schultz, M. (1983). Variational iterative methods for nonsymmetric systems of linear equations. *SIAM Journal on Numerical Analysis*, **20**, 345–357. 89

[60] Ejtehadi, M.R., Avall, S.P. & Plotkin, S.S. (2004). Three-body interactions improve the prediction of rate and mechanism in protein folding models. *Proceedings of the National Academy of Sciences*, **101**, 15088–15093. 33

[61] Elman, H. (1982). *Iterative methods for large, sparse, nonsymmetric systems of linear equations*. Ph.D. thesis, Yale University New Haven, Conn. 89

[62] Elschner, J. (1992). The double layer potential operator over polyhedral domains. I. Solvability in weighted Sobolev spaces. *Applicable Analysis. An International Journal*, **45**, 117–134. 47, 48

[63] Elschner, J. (1992). The double layer potential operator over polyhedral domains. II. Spline Galerkin methods. *Mathematical Methods in the Applied Sciences*, **15**, 23–37. 47

[64] Evans, L.C. (2010). *Partial differential equations*, vol. 19 of *Graduate Studies in Mathematics*. American Mathematical Society, Providence, Rhode Island, 3rd edn. 14

[65] Fabes, E.B., Jodeit, M. & Rivière, N.M. (1978). Potential techniques for boundary value problems on C^1-domains. *Acta Mathematica*, **141**, 165–186. 48, 61

[66] Feynman, R.P., Leighton, R.B. & Sands, M. (1964). *The Feynman lectures on physics. Vol. 2: Mainly electromagnetism and matter*. Addison-Wesley Publishing Co., Inc., Reading, Mass.-London. 7, 116

[67] Fischer, B. (2011). *Polynomial based iteration methods for symmetric linear systems*. Society for Industrial and Applied Mathematics. 89, 96

[68] Folland, G.B. (1995). *Introduction to partial differential equations*. Princeton University Press, Princeton, NJ, 2nd edn. 14, 62, 130, 162

[69] Foulkes, W.M., Mitas, L., Needs, R.J. & Rajagopal, G. (2001). Quantum monte carlo simulations of solids. *Reviews of Modern Physics*, **73**, 33–83. 153

[70] Freed, K.F. (2014). Perturbative many-body expansion for electrostatic energy and field for system of polarizable charged spherical ions in a dielectric medium. *The Journal of Chemical Physics*, **141**, 034115. 34

[71] Gander, M.J. (2006). Optimized Schwarz methods. *SIAM Journal on Numerical Analysis*, **44**, 699–731. 160

[72] Gander, M.J. (2008). Schwarz methods over the course of time. *Electronic Transactions on Numerical Analysis*, **31**, 228–255. 158, 160, 207, 217, 243

[73] Gander, M.J. (2019). Does the partition of unity influence the convergence of Schwarz methods? *to appear in Proceedings of the 25th International Conference on Domain Decomposition Methods, St. John's, Canada*. 209

[74] Gander, M.J. & Zhao, H. (2002). Overlapping Schwarz waveform relaxation for the heat equation in N dimensions. *BIT Numerical Mathematics*, **42**, 779–795. 160, 166, 167, 171

[75] Gander, M.J., Halpern, L. & Nataf, F. (2000). *Optimized Schwarz Methods*, 15–27. 12th International Conference on Domain Decomposition Methods, Springer International Publishing, iD: unige:8285. 160

[76] Gander, M.J., Magoules, F. & Nataf, F. (2002). Optimized Schwarz methods without overlap for the Helmholtz equation. *SIAM Journal on Scientific Computing*, **24**, 38–60. 160, 217, 218

[77] Ganesh, M. & Hawkins, S. (2009). A high-order algorithm for multiple electromagnetic scattering in three dimensions. *Numerical Algorithms*, **50**, 469. 47

[78] Ganesh, M. & Hawkins, S. (2011). An efficient algorithm for simulating scattering by a large number of two dimensional particles. *ANZIAM Journal. Electronic Supplement*, **52**, 139–155. 47

[79] Gasquet, C. & Witomski, P. (1999). *Fourier analysis and applications. Filtering, numerical computation, wavelets. Translated from the French by R. Ryan.*, vol. 30. New York, NY: Springer. 231

[80] Gatto, P., Lipparini, F. & Stamm, B. (2017). Computation of forces arising from the polarizable continuum model within the domain-decomposition paradigm. *The Journal of Chemical Physics*, **147**, 224108. 116, 163

[81] Geng, W. & Krasny, R. (2013). A treecode-accelerated boundary integral Poisson–Boltzmann solver for electrostatics of solvated biomolecules. *Journal of Computational Physics*, **247**, 62–78. 33

[82] Gilbarg, D. & Trudinger, N.S. (2001). *Elliptic partial differential equations of second order*. Classics in Mathematics, Springer-Verlag, Berlin, reprint of the 1998 edition. 14

[83] Gilson, M.K., Davis, M.E., Luty, B.A. & McCammon, J.A. (1993). Computation of electrostatic forces on solvated molecules using the Poisson-Boltzmann equation. *The Journal of Physical Chemistry*, **97**, 3591–3600. 116

[84] Greenbaum, A. (1997). *Iterative methods for solving linear systems*, vol. 17 of *Frontiers in Applied Mathematics*. Society for Industrial and Applied Mathematics (SIAM), Philadelphia, PA. 96

[85] Greengard, L. (1988). *The rapid evaluation of potential fields in particle systems*. ACM Distinguished Dissertations, MIT Press, Cambridge, MA. 33

[86] Greengard, L. (1990). The numerical solution of the N-body problem. *Computers in Physics*, **4**, 142–152. 33

[87] Greengard, L. & Rokhlin, V. (1987). A fast algorithm for particle simulations. *Journal of Computational Physics*, **73**, 325–348. 33, 62, 105

[88] Griffiths, D.J. (2017). *Introduction to Electrodynamics*. Cambridge University Press, 4th edn. 116

[89] Grisvard, P. (1967). Caractérisation de quelques espaces d'interpolation. *Archive for Rational Mechanics and Analysis*, **25**, 40–63. 242

[90] Grisvard, P. (2011). *Elliptic Problems in Nonsmooth Domains*. Society for Industrial and Applied Mathematics. 221

[91] Grzybowski, B.A., Winkleman, A., Wiles, J.A., Brumer, Y. & Whitesides, G.M. (2003). Electrostatic self-assembly of macroscopic crystals using contact electrification. *Nature Materials*, **2**, 241. 33, 39

[92] Gubernatis, J., Kawashima, N. & Werner, P. (2016). *Quantum Monte Carlo Methods: Algorithms for Lattice Models*. Cambridge University Press. 153

[93] Haibing, W. & Jijun, L. (2013). On decomposition method for acoustic wave scattering by multiple obstacles. *Acta Mathematica Scientia. Series B. English Edition*, **33**, 1–22. 47

[94] Harbrecht, H., Wendland, W.L. & Zorii, N. (2012). On Riesz minimal energy problems. *Journal of Mathematical Analysis and Applications*, **393**, 397–412. 222

[95] Harbrecht, H., Wendland, W. & Zorii, N. (2014). Riesz minimal energy problems on $C^{k-1,1}$-manifolds. *Mathematische Nachrichten*, **287**, 48–69. 222

[96] Hassan, M. & Stamm, B. (2019). An integral equation formulation of the N-body dielectric spheres problem. Part I: Numerical Analysis. *to appear in ESAIM:M2AN, arXiv:1902.01315*. 36, 53

[97] Hassan, M. & Stamm, B. (2019). An integral equation formulation of the N-body dielectric spheres problem. Part II: Complexity Analysis. *arXiv preprint arXiv:1911.07258*. 36

[98] Hassan, M. & Stamm, B. (2020). A linear scaling in accuracy numerical method for computing the electrostatic forces in the N-body dielectric spheres problem. *accepted for publication in Communications in Computational Physics, arXiv:2002.01579*. 36

[99] Heisenberg, W. (1925). Über quantentheoretische Umdeutung kinematischer und mechanischer Beziehungen. *Zeitschrift für Physik*, **33**, 875–893. 153

[100] Hockney, R.W. & Eastwood, J.W. (1988). *Computer simulation using particles*. CRC Press. 33

[101] Hörmander, L. (2003). *The analysis of linear partial differential operators I: Distribution theory and Fourier analysis*. Springer-Verlag, Berlin Heidelberg, 2nd edn. 234, 236

[102] Houston, P. & Süli, E. (2001). hp-adaptive discontinuous Galerkin finite element methods for first-order hyperbolic problems. *SIAM Journal on Scientific Computing*, **23**, 1226–1252. 55, 127

[103] Houston, P., Schwab, C. & Süli, E. (2000). Stabilized hp-finite element methods for first-order hyperbolic problems. *SIAM Journal on Numerical Analysis*, **37**, 1618–1643. 55, 127

[104] Houston, P., Schwab, C. & Süli, E. (2002). Discontinuous hp-finite element methods for advection-diffusion-reaction problems. *SIAM Journal on Numerical Analysis*, **39**, 2133–2163. 55

[105] Hsiao, G.C. & Wendland, W.L. (2008). *Boundary integral equations*, vol. 164 of *Applied Mathematical Sciences*. Springer-Verlag, Berlin. 24, 27, 29, 42, 47, 48

[106] Hynninen, A.P., Christova, C.G., Van Roij, R., Van Blaaderen, A. & Dijkstra, M. (2006). Prediction and observation of crystal structures of oppositely charged colloids. *Physical Review Letters*, **96**. 33

[107] Illingworth, C.J. & Domene, C. (2009). Many-body effects and simulations of potassium channels. *Proceedings of the Royal Society A: Mathematical, Physical and Engineering Sciences*, **465**, 1701–1716. 33

[108] Jahnke, H. (2003). *A history of analysis*, vol. 24 of *History of mathematics*. American Mathematical Society. 159

[109] Japhet, C., Nataf, F. & Rogier, F. (2001). The optimized order 2 method: Application to convection–diffusion problems. *Future Generation Computer Systems*, **18**, 17–30. 217, 218, 243

[110] Jeanquartier, P. (1979). Transformation de Mellin et développement asymptotiques. *L'Enseignement Mathématique*, **25**, 285–308. 228

[111] Kantorovich, L.V. & Krylov, V.I. (1958). *Approximate methods of higher analysis*. Translated from the 3rd Russian edition by C. D. Benster, Interscience Publishers, Inc., New York; P. Noordhoff Ltd., Groningen. 192, 202, 204

[112] Klamt, A. & Schüürmann, G. (1993). COSMO: a new approach to dielectric screening in solvents with explicit expressions for the screening energy and its gradient. *Journal of the Chemical Society, Perkin Transactions 2*, 799–805. 154, 157, 158

[113] Knebe, A., Green, A. & Binney, J. (2001). Multi-level adaptive particle mesh (MLAPM): A code for cosmological simulations. *Monthly Notices of the Royal Astronomical Society*, **325**, 845–864. 33

[114] Koch, W. & Holthausen, M.C. (2001). *A chemist's guide to density functional theory*. John Wiley & Sons, Ltd. 153

[115] Kohn, W., Becke, A.D. & Parr, R.G. (1996). Density functional theory of electronic structure. *The Journal of Physical Chemistry*, **100**, 12974–12980. 153

[116] Kostiainen, M.A., Hiekkataipale, P., Laiho, A., Lemieux, V., Seitsonen, J., Ruokolainen, J. & Ceci, P. (2013). Electrostatic assembly of binary nanoparticle superlattices using protein cages. *Nature Nanotechnology*, **8**, 52. 33

[117] Kramers, H.A. & Heisenberg, W. (1925). Über die streuung von strahlung durch atome. *Zeitschrift für Physik*, **31**, 681–708. 153

[118] Kress, R. (2014). *Linear integral equations*, vol. 82 of *Applied Mathematical Sciences*. Springer, New York, 3rd edn. 24, 27, 42

[119] Labanowski, J.K. & Andzelm, J.W. (1991). *Density functional methods in chemistry*. Springer-Verlag, New York. 153

[120] Lecouvez, M. (2015). *Iterative methods for domain decomposition without overlap with exponential convergence for the Helmholtz equation*. Thèse, Ecole Polytechnique. 220

[121] Lee, V., Waitukaitis, S., Miskin, M. & Jaeger, H. (2015). Direct observation of particle interactions and clustering in charged granular streams. *Nature Physics*, **11**, 733. 39

[122] Li, P., Johnston, H. & Krasny, R. (2009). A cartesian treecode for screened coulomb interactions. *Journal of Computational Physics*, **228**, 3858–3868. 33

[123] Li, Y., Zhang, X. & Cao, D. (2013). Self-assembly of patterned nanoparticles on cellular membranes: effect of charge distribution. *The Journal of Physical Chemistry B*, **117**, 6733–6740. 34

[124] Liang, Y., Hilal, N., Langston, P. & Starov, V. (2007). Interaction forces between colloidal particles in liquid: Theory and experiment. *Advances in Colloid and Interface Science*, **134**, 151–166. 33

[125] Liesen, J. & Tichý, P. (2004). Convergence analysis of Krylov subspace methods. *GAMM Mitt. Ges. Angew. Math. Mech.*, **27**, 153–173. 88, 96, 102

[126] Lindgren, E.B., Stamm, B., Chan, H.K., Maday, Y., Stace, A.J. & Besley, E. (2017). The effect of like-charge attraction on aerosol growth in the atmosphere of Titan. *Icarus*, **291**, 245–253. 128

[127] Lindgren, E.B., Stace, A.J., Polack, E., Maday, Y., Stamm, B. & Besley, E. (2018). An integral equation approach to calculate electrostatic interactions in many-body dielectric systems. *Journal of Computational Physics*. 34, 35, 36, 56, 88, 106, 128

[128] Lindgren, E.B., Stamm, B., Maday, Y., Besley, E. & Stace, A.J. (2018). Dynamic simulations of many-body electrostatic self-assembly. *Philosophical Transactions of the Royal Society A: Mathematical, Physical and Engineering Sciences*, **376**. 39, 90, 115, 128

[129] Lindgren, E.B., Quan, C. & Stamm, B. (2019). Theoretical analysis of screened many-body electrostatic interactions between charged polarizable particles. *The Journal of chemical physics*, **150**, 044901. 128

[130] Linse, P. (2008). Electrostatics in the presence of spherical dielectric discontinuities. *The Journal of Chemical Physics*, **128**, 214505. 34

[131] Lions, J.L. & Magenes, E. (1972). *Non-homogeneous boundary value problems and applications. Vol. I*. Springer-Verlag, New York-Heidelberg, translated from the French by P. Kenneth, Die Grundlehren der mathematischen Wissenschaften, Band 181. 54

[132] Lions, P.L. (1988). On the Schwarz alternating method. I. In *First International Symposium on Domain Decomposition Methods for Partial Differential Equations (Paris, 1987)*, 1–42, SIAM, Philadelphia, PA. 158, 161, 164, 218

[133] Lions, P.L. (1989). On the Schwarz alternating method. II. Stochastic interpretation and order properties. In *Second International Symposium on Domain Decomposition Methods for Partial Differential Equations (Los Angeles, 1988)*, 47–70, SIAM, Philadelphia, PA. 161, 164, 166, 192, 202, 204

[134] Lions, P.L. (1990). On the Schwarz alternating method. III: A variant for nonoverlapping subdomains. In *Third International Symposium on Domain Decomposition Methods for Partial Differential Equations (Houston, 1989)*, 202–223, SIAM, Philadelphia, PA. 160, 161

[135] Lipparini, F., Stamm, B., Cances, E., Maday, Y. & Mennucci, B. (2013). Fast domain decomposition algorithm for continuum solvation models: Energy and first derivatives. *Journal of Chemical Theory and Computation*, **9**, 3637–3648. 158, 163, 211

[136] Lipparini, F., Lagardère, L., Scalmani, G., Stamm, B., Cancès, E., Maday, Y., Piquemal, J., Frisch, M.J. & Mennucci, B. (2014). Quantum calculations in solution for large to very large molecules: A new linear scaling QM/continuum approach. *Journal of Physical Chemistry Letters*, **5**, 953–958. 177, 209, 210, 212

[137] Lipparini, F., Scalmani, G., Lagardère, L., Stamm, B., Cancès, E., Maday, Y., Piquemal, J., Frisch, M.J. & Mennucci, B. (2014). Quantum, classical, and hybrid QM/MM calculations in solution: General implementation of the ddCOSMO linear scaling strategy. *Journal of Chemical Physics*, **141**, 184108. 116, 163, 211

[138] Lotan, I. & Head-Gordon, T. (2006). An analytical electrostatic model for salt screened interactions between multiple proteins. *Journal of Chemical Theory and Computation*, **2**, 541–555. 34

[139] Löwen, H. & Kramposthuber, G. (1993). Optimal effective pair potential for charged colloids. *EPL (Europhysics Letters)*, **23**. 33

[140] Lu, B., Zhang, D. & McCammon, A. (2005). Computation of electrostatic forces between solvated molecules determined by the Poisson–Boltzmann equation using a boundary element method. *The Journal of Chemical Physics*, **122**, 214102. 116

[141] Magnasco, V. (2013). Chapter 16– Post-Hartree-Fock methods. In V. M., ed., *Elementary molecular quantum mechanics*, 681 – 722, Elsevier, Oxford, second edition edn. 153

[142] Marcati, C. (2018). *Discontinuous hp finite element methods for elliptic eigenvalue problems with singular potentials*. Ph.D. thesis, Sorbonne Université, thèse. 228

[143] Mathew, T. (1998). Uniform convergence of the Schwarz alternating method for solving singularly perturbed advection-diffusion equations. *SIAM Journal on Numerical Analysis*, **35**, 1663–1683. 166, 167

[144] Maxwell, J.C. (1865). VIII. a dynamical theory of the electromagnetic field. *Philosophical transactions of the Royal Society of London*, 459–512. 6

[145] Maz'ya, V.G. (1991). Boundary integral equations. In *Analysis, IV*, vol. 27 of *Encyclopaedia of Mathematical Sciences*, 127–222, Springer, Berlin. 47

[146] McCarty, L.S., Winkleman, A. & Whitesides, G.M. (2007). Electrostatic self-assembly of polystyrene microspheres by using chemically directed contact electrification. *Angewandte Chemie International Edition*, **46**, 206–209. 33, 39

[147] McLean, W. (2000). *Strongly elliptic systems and boundary integral equations*. Cambridge University Press. 14, 24, 27, 42, 131, 135

[148] Mennucci, B. & Cammi, R. (2008). *Continuum solvation models in chemical physics: From theory to applications*. John Wiley & Sons, Ltd. 154

[149] Mennucci, B., Cancès, E. & Tomasi, J. (1997). Evaluation of solvent effects in isotropic and anisotropic dielectrics and in ionic solutions with a unified integral equation method: theoretical bases, computational implementation, and numerical applications. *The Journal of Physical Chemistry B*, **101**, 10506–10517. 157

[150] Mennucci, B., Cammi, R. & Tomasi, J. (1998). Excited states and solvatochromic shifts within a nonequilibrium solvation approach: A new formulation of the integral equation formalism method at the self-consistent field, configuration interaction, and multiconfiguration self-consistent field level. *The Journal of chemical physics*, **109**, 2798–2807. 154, 157, 158

[151] Merrill, J.W., Sainis, S.K. & Dufresne, E.R. (2009). Many-body electrostatic forces between colloidal particles at vanishing ionic strength. *Physical Review Letters*, **103**, 138301. 33

[152] Messina, R. (2002). Image charges in spherical geometry: Application to colloidal systems. *The Journal of Chemical Physics*, **117**, 11062–11074. 33, 34

[153] Messner, M., Bramas, B., Coulaud, O. & Darve, E. (2012). Optimized M2L kernels for the Chebyshev interpolation based fast multipole method. *arXiv preprint arXiv:1210.7292*. 106

[154] Miertuš, S., Scrocco, E. & Tomasi, J. (1981). Electrostatic interaction of a solute with a continuum. A direct utilizaion of ab initio molecular potentials for the prevision of solvent effects. *Chemical Physics*, **55**, 117–129. 154, 157

[155] Müller, C. (1969). *Foundations of the mathematical theory of electromagnetic waves*. Revised and enlarged translation from the German. Die Grundlehren der mathematischen Wissenschaften, Band 155, Springer-Verlag, New York-Heidelberg. 47

[156] Nachtigal, N., Reddy, S. & Trefethen, L. (1992). How fast are nonsymmetric matrix iterations? *SIAM Journal on Matrix Analysis and Applications*, **13**, 778–795. 89

[157] Nahin, P.J. (1992). Maxwell's grand unification. *IEEE Spectrum*, **29**. 6

[158] Neumann, J. (2018). *Mathematical foundations of quantum mechanics*. Princeton University Press, Princeteon, New Jersey. 153

[159] Newton, I. (1687). Philosophiæ Naturalis Principia Mathematica. 33

[160] Niko, Y., Kawauchi, S. & Konishi, G. (2013). Solvatochromic Pyrene analogues of Prodan exhibiting extremely high fluorescence quantum yields in apolar and polar solvents. *Chemistry – A European Journal*, **19**, 9760–9765. 154

[161] Pacheco, P. (2011). *An introduction to parallel programming*. Morgan Kaufmann, Boston. 165

[162] Panofsky, W.K. & Phillips, M. (1962). *Classical electricity and magnetism*. Second edition. Addison-Wesley Series in Physics, Addison-Wesley Publishing Co., Inc., Reading, Mass.-London. 116

[163] Parr, R.G. (1980). Density functional theory of atoms and molecules. In *Horizons of quantum chemistry*, 5–15, D. Reidel Publishing Company, Dordrecht, Holland. 153

[164] Patel, S., Mackerell Jr., A. & Brooks, C.L. (2004). CHARMM fluctuating charge force field for proteins: II Protein/solvent properties from molecular dynamics simulations using a nonadditive electrostatic model. *Journal of Computational Chemistry*, **25**, 1504–1514. 33

[165] Pohl, H.A. (1986). Giant polarization in high polymers. *Journal of Electronic Materials*, **15**, 201–203. 90

[166] Poincaré, H. (1890). Sur le problème des trois corps et les équations de la dynamique. *Acta Mathematica*, **13**, A3–A270. 33

[167] Pollack, G. & Stump, D. (2002). *Electromagnetism*. Addison Wesley, San Francisco. 116

[168] Procházka, K., Šindelka, K., Wang, X., Limpouchová, Z. & Lísal, M. (2016). Self-assembly and co-assembly of block polyelectrolytes in aqueous solutions. Dissipative particle dynamics with explicit electrostatics. *Molecular Physics*, **114**, 3077–3092. 34

[169] Pulay, P. (1980). Convergence acceleration of iterative sequences. The case of SCF iteration. *Chemical Physics Letters*, **73**, 393–398. 164, 211, 267

[170] Qin, J., Li, J., Lee, V., Jaeger, H., de Pablo, J. & Freed, K. (2016). A theory of interactions between polarizable dielectric spheres. *Journal of Colloid and Interface Science*, **469**, 237–241. 34

[171] Qiu-Dong, W. (1990). The global solution of the n-body problem. *Celestial Mechanics and Dynamical Astronomy*, **50**, 73–88. 33

[172] Quan, C. & Stamm, B. (2017). Meshing molecular surfaces based on analytical implicit representation. *Journal of Molecular Graphics and Modelling*, **71**, 200–210. 155

[173] Quan, C., Stamm, B. & Maday, Y. (2018). A domain decomposition method for the polarizable continuum model based on the solvent excluded surface. *Mathematical Models and Methods in Applied Sciences*, **28**, 1233–1266. 158, 210, 212

[174] Quan, C., Stamm, B. & Maday, Y. (2019). A domain decomposition method for the Poisson–Boltzmann solvation models. *SIAM Journal on Scientific Computing*, **41**, B320–B350. 154, 158

[175] Quarteroni, A. & Valli, A. (1999). *Domain Decomposition Methods for Partial Differential Equations*. Oxford University Press, Oxford, UK. 160

[176] Rappé, A.K., Casewit, C.J., Colwell, K.S., Goddard III, W.A. & Skiff, W.M. (1992). UFF, a full periodic table force field for molecular mechanics and molecular dynamics simulations. *Journal of the American Chemical Society*, **114**, 10024–10035. 154, 155, 210, 265

[177] Ristenpart, W.D., Aksay, I.A. & Saville, D.A. (2003). Electrically guided assembly of planar superlattices in binary colloidal suspensions. *Physical Review Letters*, **90**, 128303. 33

[178] Rokhlin, V. (1983). Solution of acoustic scattering problems by means of second kind integral equations. *Wave Motion. An International Journal Reporting Research on Wave Phenomena*, **5**, 257–272. 47

[179] Rudin, W. (1987). *Real and complex analysis*. McGraw-Hill Book Co., New York, 3rd edn. 228, 230, 231

[180] Rudin, W. (1991). *Functional analysis*. New York, NY: McGraw-Hill, 2nd edn. 235, 236

[181] Saad, Y. (1981). Krylov subspace methods for solving large unsymmetric linear systems. *Mathematics of Computation*, **37**, 105–126. 89

[182] Saad, Y. (2003). *Iterative methods for sparse linear systems*. Society for Industrial and Applied Mathematics, Philadelphia, PA, 2nd edn. 89, 144

[183] Saad, Y. & Schultz, M. (1986). GMRES: A generalized minimal residual algorithm for solving nonsymmetric linear systems. *SIAM Journal on Scientific and Statistical Computing*, **7**, 856–869. 88, 144, 164

[184] Sagui, C. & Darden, T.A. (1999). Molecular dynamics simulations of biomolecules: Long-range electrostatic effects. *Annual Review of Biophysics and Biomolecular Structure*, **28**, 155–179. 33, 116

[185] Sauter, S. & Schwab, C. (2010). *Boundary Element Methods*. Springer-Verlag, Berlin. 14, 20, 21, 22, 23, 24, 27, 29, 41, 42, 43, 44, 47, 48, 62, 157, 220

[186] Scalmani, G. & Frisch, M.J. (2010). Continuous surface charge polarizable continuum models of solvation. I. General formalism. *The Journal of Chemical Physics*, **132**, 114110. 158

[187] Schrödinger, E. (1982). *Collected papers on wave mechanics*, vol. 302. AMS Chelsea Publishing. 153

[188] Schwartz, L. (1966). *Théorie des distributions*. Publications de l'Institut de Mathématique de l'Université de Strasbourg, No. IX-X. Nouvelle édition, entiérement corrigée, refondue et augmentée, Hermann, Paris. 16

[189] Schwarz, H.A. (1870). Ueber einen Grenzübergang durch alternirendes Verfahren. *Vierteljahrsschrift der Naturforschenden Gesellschaft in Zürich*, **15**, 272–286. 159, 264

[190] Shevchenko, E.V., Talapin, D.V., Kotov, N.A., O'brien, S. & Murray, C.B. (2006). Structural diversity in binary nanoparticle superlattices. *Nature*, **439**, 55. 33

[191] Shubin, M.A. (2001). *Pseudodifferential operators and spectral theory*. Second edition. Translated from the Russian by S. I. Andersson, Springer-Verlag, Berlin. 219

[192] Soh, S., Liu, H., Cademartiri, R., Yoon, H.J. & Whitesides, G. (2014). Charging of multiple interacting particles by contact electrification. *Journal of the American Chemical Society*, **136**, 13348–13354. 39

[193] Stamm, B., Cancès, E., Lipparini, F. & Maday, Y. (2016). A new discretization for the polarizable continuum model within the domain decomposition paradigm. *The Journal of chemical physics*, **144**, 054101. 158

[194] Stein, E.M. (1970). *Singular integrals and differentiability properties of functions*. Princeton Mathematical Series, No. 30, Princeton University Press, Princeton, N.J. 219, 222, 224, 225

[195] Steinbach, O. (2008). *Numerical approximation methods for elliptic boundary value problems: Finite and boundary elements*. Springer-Verlag, New York. 24, 27, 42

[196] Steinbach, O. & Wendland, W.L. (2001). On C. Neumann's method for second-order elliptic systems in domains with non-smooth boundaries. *Journal of Mathematical Analysis and Applications*, **262**, 733–748. 47, 48

[197] Sundman, K.F. (1913). Mémoire sur le problème des trois corps. *Acta mathematica*, **36**, 105–179. 33

[198] Szabo, A. & Ostlund, N.S. (1989). *Modern quantum chemistry: Introduction to advanced electronic structure theory*. McGraw-Hill Publishing Company, New York. 153

[199] Tomasi, J. & Persico, M. (1994). Molecular interactions in solution: An overview of methods based on continuous distributions of the solvent. *Chemical Reviews*, **94**, 2027–2094. 157

[200] Tomasi, J., Cancès, E., Pomelli, C.S., Caricato, M., Scalmani, G., Frisch, M.J., Cammi, R., Basilevsky, M.V., Chuev, G.N. & Mennucci, B. (2007). *Modern theories of continuum models*, chap. 1, 1–123. John Wiley & Sons, Ltd. 154, 156

[201] Toselli, A. & Widlund, O. (2005). *Domain decomposition methods—algorithms and theory*, vol. 34 of *Springer Series in Computational Mathematics*. Springer-Verlag, Berlin. 158, 160, 161

[202] van der Vaart, A., Bursulaya, B.D., Brooks, C.L. & Merz, K.M. (2000). Are many-body effects important in protein folding? *The Journal of Physical Chemistry B*, **104**, 9554–9563. 33

[203] van Roij, R. & Hansen, J.P. (1997). Van der Waals–like instability in suspensions of mutually repelling charged colloids. *Physical Review Letters*, **79**. 33

[204] Verchota, G. (1984). Layer potentials and regularity for the Dirichlet problem for Laplace's equation in Lipschitz domains. *Journal of Functional Analysis*, **59**, 572–611. 48

[205] Vico, F., Greengard, L. & Gimbutas, Z. (2014). Boundary integral equation analysis on the sphere. *Numerische Mathematik*, **128**, 463–487. 134

[206] Von Petersdorff, T. (1989). Boundary integral equations for mixed Dirichlet, Neumann and transmission problems. *Mathematical Methods in the Applied Sciences*, **11**, 185–213. 47

[207] Walker, H.F. & Ni, P. (2011). Anderson acceleration for fixed-point iterations. *SIAM Journal on Numerical Analysis*, **49**, 1715–1735. 211, 267

[208] Wen, P., Gao, Z., Zhang, R., Li, A., Zhang, F., Li, J., Xie, J., Wu, Y., Wu, M. & Guo, K. (2017). A-π-D-π-A carbazole derivatives with remarkable solvatochromism and mechanoresponsive luminescence turn-on. *Journal of Materials Chemistry C*, **5**, 6136–6143. 154

[209] Xu, Z. (2013). Electrostatic interaction in the presence of dielectric interfaces and polarization-induced like-charge attraction. *Physical Review E*, **87**, 013307. 34

[210] Yap, E.H. & Head-Gordon, T. (2013). Calculating the bimolecular rate of protein–protein association with interacting crowders. *Journal of Chemical theory and Computation*, **9**, 2481–2489. 33

[211] York, D.M. & Karplus, M. (1999). A smooth solvation potential based on the conductor-like screening model. *The Journal of Physical Chemistry A*, **103**, 11060–11079. 158

[212] Zhang, D., Gonzalez-Mozuelos, P. & Olvera de la Cruz, M. (2010). Cluster formation by charged nanoparticles on a surface in aqueous solution. *The Journal of Physical Chemistry C*, **114**, 3754–3762. 34

List of Figures

List of Tables

Declaration

I, Muhamamd Hassan declare that this thesis and the work presented in it are my own and has been generated by me as the result of my own original research. I do solemnely swear that:

1. This work was done wholly or mainly while in candidature for the doctoral degree at this faculty and university;
2. Where any part of this thesis has previously been submitted for a degree or any other qualification at this university or any other institution, this has been clearly stated;
3. Where I have consulted the published work of others or myself, this is always clearly attributed;
4. Where I have quoted from the work of others or myself, the source is always given. This thesis is entirely my own work, with the exception of such quotations;
5. I have acknowledged all major sources of assistance;
6. Where the thesis is based on work done by myself jointly with others, I have made clear exactly what was done by others and what I have contributed myself;
7. Parts of this work have been published before as
   - X. Claeys, M. Hassan, and B. Stamm. **Continuity estimates for Riesz potentials on polygonal boundaries**, *under preparation.*
   - B. Bramas, M. Hassan, and B. Stamm. **An Integral Equation Formulation of the N-Body Dielectric Spheres Problem. Part II: Complexity Analysis**, *under review at ESAIM:M2AN*, arXiv preprint arXiv:1911.07258 (2019).
   - M. Hassan, and B. Stamm. **A Linear Scaling in Accuracy Numerical Method for Computing the Electrostatic Forces in the N-Body Dielectric Spheres Problem**, *accepted for publication in Communications in Computational Physics*, arXiv prepint arXiv:2002.01579 (2020).
   - M. Hassan and B. Stamm. **An Integral Equation Formulation of the N-Body Dielectric Spheres Problem. Part I: Numerical Analysis**, *to appear in ESAIM:M2AN*, arXiv preprint arXiv:1902.01315 (2019).
   - G. Ciaramella, M. Hassan and B. Stamm. **On the Scalability of the Schwarz Method**, *The SMAI Journal of Computational Mathematics*, Volume 6 (2020) , pp. 33-68.
   - G. Ciaramella, M. Hassan and B. Stamm. **On the Scalability of the Parallel Schwarz Method in One Dimension**, to appear in *The Proceedings of the 25th International Domain Decomposition Conference.*

Hassan
(01/07/2020)